



CM<P 2025 | Kharkiv, Ukraine

V INTERNATIONAL CONFERENCE

CONDENSED MATTER & LOW TEMPERATURE PHYSICS 2025

Abstracts book

2th – 6th June 2025
Kharkiv, Ukraine (Online)



B. Verkin ILTPE of NASU





**V International Conference
Condensed Matter and Low Temperature Physics
CM<P 2025**

**Book
of
abstracts**

Kharkiv, B. Verkin ILTPE of NASU, 2025

UDK 538.9

H 88

Hurova D.E., Dolbin A.V., Shevchenko S.N. (editors) V International Conference “Condensed Matter and Low Temperature Physics” 2025. Book of abstracts. – Kharkiv: B. Verkin ILTPE of NASU, 2025. – 294 p.

ISBN 978-617-95455-9-7

This book collects 228 peer-reviewed reports presented at the V International Conference “Condensed Matter and Low Temperature Physics” 2025. These materials present the studies of modern aspects of condensed matter and low temperature physics including electronic properties of conducting and superconducting systems, magnetism and magnetic materials, optics, photonics and optical spectroscopy, quantum liquids and quantum crystals, cryocrystals, nanophysics and nanotechnologies, biophysics and physics of macromolecules, materials science, theory of condensed matter physics, technological peculiarities of the instrumentation for physical experiments, and related fields.

The book will be useful to undergraduate, postgraduate students, and researchers in the field of condensed matter physics.

Ця книга зібрала 228 доповідей, представлених на V Міжнародній конференції “Condensed Matter and Low Temperature Physics” 2025 року. Дані матеріали представляють дослідження у галузі сучасних аспектів фізики конденсованого середовища та низьких температур, у тому числі електронні властивості провідних та надпровідних систем, магнетизм, оптику, фотоніку та оптичну спектроскопію, квантові рідини та квантові кристали, кріокристали, нанофізику та нанотехнології, біофізику та фізику макромолекул, матеріалознавство, теорію фізики конденсованих середовищ, технологічні особливості обладнання для фізичних експериментів та суміжні галузі.

Книга призначена для студентів, аспірантів та дослідників у галузі фізики конденсованого стану.

***Recommended to publish by Scientific Council of B. Verkin Institute for Low Temperature Physics and Engineering of the National Academy of Sciences of Ukraine
(protocol № 5, 16.04.2025)***

**Published by B. Verkin ILTPE of NASU
ISBN 978-617-95455-9-7**

**© D. Hurova, A. Dolbin, S. Shevchenko,
2025
© O. Konotop, O. Bludov, R. Basnukaeva,
2025
© B. Verkin ILTPE of NASU, 2025**

PROGRAM COMMITTEE

Chair: Prof. Alexander Dolbin, Corr. Member NASU, ILTPE (Kharkiv, Ukraine)
Vice-chair: Prof. Sergey Shevchenko, ILTPE NASU (Kharkiv, Ukraine)
Prof. Yurii Naidyuk, Corr. Member NASU, ILTPE NASU (Kharkiv, Ukraine)
Prof. Oleksandr Kordyuk, Full Member NASU, IMP NASU (Kyiv, Ukraine)
Prof. Leonid Pastur, Full Member NASU, ILTPE NASU (Kharkiv, Ukraine)
Prof. Viktor Chabanenko, DonFTI NASU (Kyiv, Ukraine)
Dr. Alexey Fedorchenco, ILTPE NASU (Kharkiv, Ukraine)
Dr. Alexander Yu. Glamazda, ILTPE NASU (Kharkiv, Ukraine)
Dr. Mykola Glushchuk, ILTPE NASU (Kharkiv, Ukraine)
Dr. Volodymyr P. Gnedilov, ILTPE NASU (Kharkiv, Ukraine)
Prof. Andrzej Jezowski, INTiBS PAN (Wroclaw, Poland)
Dr. Oleksandr Kalinenko, ILTPE NASU (Kharkiv, Ukraine)
Prof. Gennadii Kamarchuk, ILTPE NASU (Kharkiv, Ukraine)
Prof. Yuriy Kolesnichenko, ILTPE NASU (Kharkiv, Ukraine)
Prof. Konstantin Nemchenko, V.N.Karazin KNU (Kharkiv, Ukraine)
Prof. Pavel Pal-Val, ILTPE NASU (Kharkiv, Ukraine)
Prof. Elena Savchenko, ILTPE NASU (Kharkiv, Ukraine)
Dr. Victor Slavin, ILTPE NASU (Kharkiv, Ukraine)
Prof. Svyatoslav Sokolov, ILTPE NASU (Kharkiv, Ukraine)
Prof. Andrzej Szewczyk, IF PAN (Warsaw, Poland)
Prof. Yevgen Syrkin, ILTPE NASU (Kharkiv, Ukraine)
Dr. Andrii Terekhov, ILTPE NASU (Kharkiv, Ukraine)

ORGANIZING COMMITTEE

Chair: Dr. Diana Hurova
Vice-chair: Dr. Oleksii Konotop
Vice-chair (treasurer): Dr. Vusal Geidarov
Secretary: Dr. Yuliya Savina

Dr. Razet Basnukaeva
Dr. Ivan Bondar
Dr. Valentin Koverya
Dr. Oleksandr Leha

Dr. Yevhen Petrenko
PhD St. Tymofii Piddubnyi
Dr. Sergii Poperezhai

CONFERENCE PROGRAM

Time is specified for the Time Zone UTC/GMT+3, Eastern European Time

MONDAY, 2nd of JUNE

9:50-10:00

Opening Remarks

**Acting Director of the B. Verkin ILTPE of NAS of Ukraine
Corresponding Member of NAS of Ukraine
Prof. Alexander Dolbin
and
Chair of Organizing Committee Dr. Diana Hurova**

PLENARY LECTURES OF INVITED SPEAKERS

Chair Dr. Valentin Koverya

10:00-10:30	Bias-driven quantum matter	50
	Pedro Ribeiro <i>Instituto Superior Técnico, Universidade de Lisboa, Lisbon, Portugal</i>	
10:30-11:00	Fractional conductances in the strongly interacting one-dimensional system	46
	V. Kagalovsky <i>Shamoon College of Engineering, Beer-Sheva, Israel</i>	

ELECTRONIC PROPERTIES OF CONDUCTING AND SUPERCONDUCTING SYSTEMS

Chair Dr. Valentin Koverya

11:00-11:12	Influence of As₂O₃ vapor pressure on phase formation and superconducting properties of Tl-1223 HTS	69
	I. R. Metskhvarishvili ^{1,2} , Melita Menelaou ³ , D. L. Surmanidze ^{1,4} , T. E. Lobzhanidze ⁴ , A. D. Tchankvetadze ^{1,4} , B. G. Bendeliani ¹ , G. N. Dgebuadze ¹ , V. M. Gabunia ^{1,5} , M. R. Metskhvarishvili ⁶ , D. A. Jishiashvili ^{1,7}	
	¹ <i>Ilia Vekua Sukhumi Institute of Physics and Technology, Tbilisi, Georgia</i>	
	² <i>Georgian Technical University, Tbilisi, Georgia</i>	
	³ <i>Cyprus University of Technology, Limassol, Cyprus</i>	
	⁴ <i>Ivane Javakhishvili Tbilisi State University, Tbilisi, Georgia</i>	
	⁵ <i>Petre Melikishvili Institute of Physical and Organic Chemistry, Tbilisi, Georgia</i>	
	⁶ <i>“Talga” Institute of Georgian Technical University, Tbilisi, Georgia</i>	
	⁷ <i>V. Chavchanidze Institute of Cybernetics of the Georgian Technical University, Tbilisi, Georgia</i>	

11:12-11:24	Current driven depinning of elastic vortex filaments in superconductors with columnar pinning sites	70
	O. S. Hrechykha ¹ , A. L. Kasatkin ² , V. P. Tsvitkovskiy ²	
	¹ <i>Kyiv Academic University, Kyiv, Ukraine</i>	

²*G.V. Kurdyumov Institute for Metal Physics, NAS of Ukraine, Kyiv, Ukraine*

11:24-11:36	Eigenspectrum of extraordinary Josephson plasma waves in cylindrical layered superconductors	71
	<u>Yu. O. Averkov</u> ¹ , O. Yu. Averkov ² , E. N. Odarenko ³ , A. A. Shmat'ko ² , V. A. Yampol'skii ^{1,2}	
	¹ <i>O.Ya. Usikov Institute for Radiophysics and Electronics of NAS of Ukraine, Kharkiv, Ukraine</i>	
	² <i>V.N. Karazin Kharkiv National University, Kharkiv, Ukraine</i>	
	³ <i>Kharkiv National University of Radio Electronics, 14 Nauky Ave., Kharkiv, Ukraine</i>	
11:36-11:48	Semantic segmentation of ARPES spectra for electronic dispersion analysis	72
	<u>Yu. V. Pustovit</u> , M.O. Ohloblia	
	<i>Taras Shevchenko National University of Kyiv, Kyiv, Ukraine</i>	
11:48-12:00	Bulk-to-surface oxygen vacancy diffusion in ITO: a possible superconductivity mechanism	73
	<u>O. Feia</u> ^{1,2,3} , D. Menesenko ¹ , A. Parra ⁴ , A. Shapovalov ^{1,2} , A. Aliev ⁴	
	¹ <i>Kyiv Academic University, Kyiv, Ukraine</i>	
	² <i>G.V. Kurdyumov Institute for Metal Physics, NAS of Ukraine, Kyiv, Ukraine</i>	
	³ <i>Leibniz Institute for Solid State and Materials Research, Dresden, Germany</i>	
	⁴ <i>A.G. MacDiarmid NanoTech Institute, University of Texas at Dallas, Richardson, USA</i>	
12:00-12:12	Peculiarities of the behavior of fluctuation conductivity and pseudogap in untwined $\text{YBa}_2\text{Cu}_3\text{O}_{7-\delta}$ single crystals under electron irradiation with an energy of 2.5 MeV	74
	<u>M. V. Shytov</u> ¹ , K. Rogacki ² , L. V. Bludova ¹ , E. V. Petrenko ¹ , Yu. A. Kolesnichenko, A. L. Solovjov ^{1,2,3} , A. Sedda ³ , E. Lähderanta ³ , R. V. Vovk ⁴	
	¹ <i>B.Verkin Institute for Low Temperature Physics and Engineering, Kharkiv, Ukraine</i>	
	² <i>Institute for Low Temperatures and Structure Research, Wroclaw, Poland</i>	
	³ <i>Lappeenranta University of Technology, Lappeenranta, Finland</i>	
	⁴ <i>V.N. Karazin Kharkiv National University, Kharkiv, Ukraine</i>	
12:12-12:24	Polar crosstalk effects and negative capacitance state in dense ferroelectric nanocomposite films	75
	<u>O. V. Bereznykov</u> ¹ , O. S. Pylypchuk ¹ , S. E. Ivanchenko ² , D. O. Stetsenko ¹ , E. A. Eliseev ² , A. N. Morozovska ¹	
	¹ <i>Institute of Physics of NAS of Ukraine, Kyiv, Ukraine</i>	
	² <i>Frantsevich Institute for Problems in Materials Science, Kyiv, Ukraine</i>	
12:24-12:36	Machine learning analysis of bilayer splitting in multiband superconductors	76
	<u>K. H. Bohachov</u> ^{1,2} , A. A. Kordyuk ^{1,2,3}	
	¹ <i>G.V. Kurdyumov Institute for Metal Physics, Kyiv, Ukraine</i>	
	² <i>Kyiv Academic University, Kyiv, Ukraine</i>	
	³ <i>Leibniz Institute for Solid State and Materials Research, Dresden, Germany</i>	
12:36-12:48	Study of the effect of magnetic field on the temperature dependence of the pseudogap in optimally doped $\text{YBa}_2\text{Cu}_3\text{O}_{7-\delta}$ films	77
	<u>A. S. Kolisnyk</u> ¹ , M. V. Shytov ¹ , E. V. Petrenko ¹ , A. V. Terekhov ¹ , L. V. Bludova ¹ , K. Rogacki ² , A. L. Solovyov ^{1,2}	
	¹ <i>B.Verkin Institute for Low Temperature Physics and Engineering, Kharkiv, Ukraine</i>	
	² <i>Institute for Low Temperatures and Structure Research, Wroclaw, Poland</i>	
12:48-13:00	Anomalous behaviour of the temperature dependencies of the upper critical fields in $(\text{Dy}_{1-x}\text{Er}_x)\text{Rh}_{3.8}\text{Ru}_{0.2}\text{B}_4$ ($x=0, 0.2, 0.4$)	78
	<u>V. M. Yarovi</u> ¹ , A. V. Terekhov ¹ , A. P. Kazakov ² , P. M. Fesenko ³ , I. V. Zolochevskii ¹ , L. O. Ishchenko ¹	
	¹ <i>B.Verkin Institute for Low Temperature Physics and Engineering, Kharkiv, Ukraine</i>	
	² <i>Institute for Low Temperatures and Structure Research, Wroclaw, Poland</i>	
	³ <i>National Technical University "Kharkiv Polytechnic Institute", Kharkiv, Ukraine</i>	

- 13:00-13:12 Quantum reflectometry: effective capacitance of two- and multi-level systems 80**
O. Y. Kitsenko^{1,2}, S. N. Shevchenko¹
¹*B.Verkin Institute for Low Temperature Physics and Engineering, Kharkiv, Ukraine*
²*V.N. Karazin Kharkiv National University, Kharkiv, Ukraine*

- 13:12-13:24 Magnetoresistance of Bi_{88.08}Mn_{11.92} in magnetic fields up to 90 kOe 79**
V. M. Yarovyj¹, A. V. Terekhov¹, K. Rogacki², A. L. Solovjov^{1,2}
¹*B.Verkin Institute for Low Temperature Physics and Engineering, Kharkiv, Ukraine*
²*Institute for Low Temperatures and Structure Research, Wroclaw, Poland*

13:25-14:20

BREAK

MAGNETISM AND MAGNETIC MATERIALS

Chair Dr. Yuliya Savina

- 14:20-14:32 Electric field effect on superluminal-like magnons propagation in insulating antiferromagnets 101**
O. O. Boliasova^{1,2}, V. N. Krivoruchko³
¹*Kyiv Academic University, Kyiv, Ukraine*
²*G.V. Kurdyumov Institute for Metal Physics, NAS of Ukraine, Kyiv, Ukraine*
³*Donetsk Institute for Physics and Engineering named after O.O. Galkin, Kyiv, Ukraine*
- 14:32-14:44 Magnetic properties of the S = ½ spatially anisotropic triangular quantum magnet Cu(tn)Cl₂ 102**
A. Darwich, R. Tarasenko, M. Orendáč, A. Orendáčová
Institute of Physics, P. J. Šafárik University, Košice, Slovakia
- 14:44-14:56 Cu(en)(sal)Cl – a novel spin-½ 2D Heisenberg quantum magnet with ferromagnetic exchange interactions on the square lattice 103**
I. Kozin, R. Tarasenko, V. Tkáč, A. Orendáčová, E. Čižmár, M. Orendáč
Institute of Physics, P. J. Šafárik University, Košice, Slovakia
- 14:56-15:08 Confinement effects on the weak-field magnetic susceptibility of a two-dimensional electron gas 104**
J. Kumar
Aalto University, Department of Applied Physics, Espoo, Finland
- 15:08-15:20 Current-driven dynamics of vertical Bloch lines on a domain wall in magnetic films 105**
R. Teslia¹ and O. Kolezhuk^{1,2}
¹*V.G. Baryakhtar Institute of Magnetism of the NAS of Ukraine, Kyiv, Ukraine*
²*Institute of Physics, Johannes Gutenberg-University, Mainz, Germany*
- 15:20-15:32 Electric-field-driven fractional parametric resonance in spintronic nanostuctures 106**
R. V. Verba¹, A. Grimaldi², D. V. Slobodianik¹, G. Finocchio²
¹*V.G. Baryakhtar Institute of Magnetism of the NAS of Ukraine, Kyiv, Ukraine*
²*Department of Engineering, University of Messina, Messina, Italy*

PLENARY LECTURES OF INVITED SPEAKERS

Chair Dr. Yuliya Savina

- 15:35-16:05 AC Hanle effect and spin wave generation on a single F/N interface** 39
 (08:35 UTC-4) Ya. B. Bazaliy
University of South Carolina, Columbia, SC, USA

16:05-16:30 BREAK

- 16:30-17:00 Microwave electrodynamics of spin-triplet superconductor UTe₂** 38
 (09:30 UTC-4) Arthur Carlton-Jones¹, Nicholas P. Butch^{1,2}, Johnpierre Paglione¹, and Steven M. Anlage¹
¹*Maryland Quantum Materials Center, University of Maryland, College Park, USA*
²*NIST Center for Neutron Research, National Institute of Standards and Technology, Gaithersburg, Maryland, USA*

17:00-18:30 POSTER SESSION (1, 2, 3 AND 4 SECTIONS)

Chairs Dr. Diana Hurova, Dr. Yuliya Savina

17:00-17:45 Stage 1 (P1-P28)

17:45-18:30 Stage 2 (P29-P56)

ELECTRONIC PROPERTIES OF CONDUCTING AND SUPERCONDUCTING SYSTEMS

- P1 Broadband and resonant spectroscopy of thin film resonators from disordered superconductors** 81
M. Baránek¹, P. Neilinger^{1,2}, D. Manca^{1,2}, O.G. Turutanov^{1,3}, M. Grajcar^{1,2}
¹*Comenius University Bratislava, Bratislava, Slovakia*
²*Institute of Physics, Slovak Academy of Sciences, Bratislava, Slovakia*
³*B.Verkin Institute for Low Temperature Physics and Engineering, Kharkiv, Ukraine*
- P2 Detection of Villari effect in FeSe_{1-x}S_x (x=0.075)** 82
I. V. Bilych¹, K. R. Zhekov¹, G. A. Zvyagina¹, V. D. Fil, D. V. Fil^{2,3}
¹*B.Verkin Institute for Low Temperature Physics and Engineering, Kharkiv, Ukraine*
²*Institute for Single Crystals, NAS of Ukraine, Kharkiv, Ukraine*
³*V.N. Karazin Kharkiv National University, Kharkiv, Ukraine*
- P3 Study of structural, mechanical, electronic and thermodynamic properties of the N₂CaNa full-Heusler alloy using DFT approach** 83
 E. B. Ettah¹, M. E. Ishaje¹, K. A. Minakova², V. A. Sirenko³, I. S. Bondar³
¹*Cross River University of Technology, Calabar, Nigeria*
²*National Technical University “Kharkiv Polytechnic Institute”, Kharkiv, Ukraine*
³*B.Verkin Institute for Low Temperature Physics and Engineering, Kharkiv, Ukraine*
- P4 Differential shot noise and Fano factor in mesoscopic junctions with inhomogeneous superconductors** 84
V. Dmytrenko¹, E. Zhitlukhina^{1,2}, P. Seidel³
¹*O.O. Galkin Donetsk Institute for Physics and Engineering, Kyiv, Ukraine*
²*Comenius University Bratislava, Bratislava, Slovakia*
³*Institut für Festkörperfphysik, Friedrich-Schiller-Universität Jena, Jena, Germany*

P5	Anomalies of dissipative and kinetic properties of the high-entropy alloy Al_{0.5}CoCuCrNiFe below ~300 K	85
	<u>V. A. Frolov</u> , N. A. Azarenkov, E. V. Karaseva, V. S. Klochko, A. V. Korniets, V. I. Sokolenko, V. S. Okovit, A. V. Poida	
	<i>National Science Center “Kharkiv Institute of Physics and Technology”, Kharkiv, Ukraine</i>	
P6	Optical and transport properties of NbN thin films revisited	86
	<u>S. Kern</u> ¹ , P. Neilinger ^{1,2} , M. Poláčková ¹ , M. Baránek ¹ , T. Plecenik ¹ , T. Roch ¹ , and M. Grajcar ^{1,2}	
	¹ <i>Comenius University Bratislava, Bratislava, Slovakia</i>	
	² <i>Institute of Physics, Slovak Academy of Sciences, Bratislava, Slovakia</i>	
P7	Spin-dependent resonant tunneling through a magnetic quantum dot coupled to superconducting and ferromagnetic leads: F-mQD-S system	87
	<u>E. A. Koshina</u> , V. N. Krivoruchko	
	<i>O.O. Galkin Donetsk Institute for Physics and Engineering, Kyiv, Ukraine</i>	
P8	Properties of a metal-dielectric-metal point junction before and after electrical breakdown of a dielectric nanolayer	88
	<u>V. P. Koverya</u> , A. V. Krevsun, S. I. Bondarenko	
	<i>B.Verkin Institute for Low Temperature Physics and Engineering, Kharkiv, Ukraine</i>	
P9	Electronic properties of the boundary between hexagonal and Lieb lattices	89
	<u>I. V. Kozlov</u> , Yu. A. Kolesnichenko	
	<i>B.Verkin Institute for Low Temperature Physics and Engineering, Kharkiv, Ukraine</i>	
P10	Point-contact spectroscopy features of MoRe superconducting alloy	90
	<u>I. Martynenko</u> ^{1,2} , V. Tarenkov ^{2,3} , V. Krivoruchko ³ , A. Shapovalov ^{1,2} , O. Kalenyuk ^{1,2} , E. Zhitlukhina ^{3,4} , M. Belogolovskii ^{2,4}	
	¹ <i>G.V. Kurdyumov Institute for Metal Physics, NAS of Ukraine, Kyiv, Ukraine</i>	
	² <i>Kyiv Academic University, Kyiv, Ukraine</i>	
	³ <i>O.O. Galkin Donetsk Institute for Physics and Engineering, Kyiv, Ukraine</i>	
	⁴ <i>Comenius University Bratislava, Bratislava, Slovakia</i>	
P11	Analysis of the influence of vortex dynamics on the possibility of an avalanche-like transition of a microwave nonlinear HTS transmission line into a dissipative state	91
	<u>S. I. Melnyk</u>	
	<i>O.Ya. Usikov Institute for Radiophysics and Electronics, Kharkiv, Ukraine</i>	
P12	Features of vortex dynamics in the description of microwave absorption by a thin HTSC disk	92
	<u>S. I. Melnyk</u> , N. T. Cherpak	
	<i>O.Ya. Usikov Institute for Radiophysics and Electronics, Kharkiv, Ukraine</i>	
P13	Electron transport in pressed VO₂ samples: Mott hopping vs percolation behavior	93
	<u>E. Yu. Beliayev</u> ¹ , <u>I. G. Mirzoiev</u> ¹ , V. A. Horielyi ¹ , A. V. Terekhov ¹ , I. A. Chichibaba ²	
	¹ <i>B.Verkin Institute for Low Temperature Physics and Engineering, Kharkiv, Ukraine</i>	
	² <i>National Technical University “Kharkiv Polytechnic Institute”, Kharkiv, Ukraine</i>	
P14	Hydrostatic pressure effect on the pseudogap in slightly doped Y_{0.77}Pr_{0.23}Ba₂Cu₃O_{7-δ} single crystals	94
	<u>E. V. Petrenko</u> ¹ , L. V. Bludova ¹ , A. S. Kolisnyk ¹ , A. Sedda ² , E. Lähderanta ² , R. V. Vovk ³ , A. L. Solovjov ^{1,2,4}	
	¹ <i>B.Verkin Institute for Low Temperature Physics and Engineering, Kharkiv, Ukraine</i>	
	² <i>Lappeenranta University of Technology, Lappeenranta, Finland</i>	
	³ <i>V.N. Karazin Kharkiv National University, Kharkiv, Ukraine</i>	
	⁴ <i>Institute for Low Temperatures and Structure Research, Wroclaw, Poland</i>	

P15	Visualization of critical current oscillations in a doubly connected superconducting structure without Josephson junctions	95
	<u>A. G. Sivakov</u> , A. S. Pokhila, A. E. Kolinko	
	<i>B.Verkin Institute for Low Temperature Physics and Engineering, Kharkiv, Ukraine</i>	
P16	Precise tuning of superconducting and physical properties of Mo_{1-x}Si_x thin films for photon detector applications	96
	<u>O. V. Zraichenko</u> ¹ , O. O. Leha ¹ , V. Yu. Lyakhno ^{1,2} , S. V. Bengus ¹ , M. Yu. Mikhailov ³	
	¹ <i>B.Verkin Institute for Low Temperature Physics and Engineering, Kharkiv, Ukraine</i>	
	² <i>G.V. Kurdumov Institute for Metal Physics, NAS of Ukraine, Kyiv, Ukraine</i>	
	³ <i>Delft University of Technology, Delft, The Netherlands</i>	
P17	Resistive switching and diode effect in conductivity of TiTe₂ point contacts	97
	<u>O. E. Kvitnitskaya</u> ^{1,2} , L. Harnagea ³ , D. V. Efremov ² , B. Büchner ^{2,4} , Yu. G. Naidyuk ¹	
	¹ <i>B.Verkin Institute for Low Temperature Physics and Engineering, Kharkiv, Ukraine</i>	
	² <i>Leibniz Institute for Solid State and Materials Research, Dresden, Germany</i>	
	³ <i>Institute for Solid State Research, Dresden, Germany</i>	
	⁴ <i>Institute of Solid State and Materials Physics and Würzburg-Dresden Cluster of Excellence ct.qmat, Technische Universität Dresden, Dresden, Germany</i>	

MAGNETISM AND MAGNETIC MATERIALS

P18	Antiferromagnetic resonance in CuCrP₂S₆ layered crystal	107
	<u>O. Bludov</u> ¹ , Yu. Savina ¹ , V. Pashchenko ¹ , M. Kobets ¹ , K. Glukhov ² , Yu. Vysochanskii ²	
	¹ <i>B.Verkin Institute for Low Temperature Physics and Engineering, Kharkiv, Ukraine</i>	
	² <i>Institute for Solid State Physics and Chemistry, Uzhhorod National University, Uzhhorod, Ukraine</i>	
P19	Tunable magnetic properties of layered double hydroxides: between cluster glass and canonical spin glass	108
	<u>A. V. Fedorchenco</u> ¹ , E. L. Fertman ¹ , I. P. Kobzar ¹ , Yu. G. Pashkevich ² , E. Čízmár ³ , V. Tkáč ³ , R. Tarasenko ³ , A. Feher ³ , M. Holub ⁴ , A. N. Salak ⁵	
	¹ <i>B.Verkin Institute for Low Temperature Physics and Engineering, Kharkiv, Ukraine</i>	
	² <i>O.O. Galkin Donetsk Institute for Physics and Engineering, Kyiv, Ukraine</i>	
	³ <i>Institute of Physics, P.J. Šafárik University in Košice, Košice, Slovakia</i>	
	⁴ <i>Synchrotron SOLEIL, L'Orme des Merisiers, St Aubin BP48, Gif sur Yvette Cedex, France</i>	
	⁵ <i>CICECO – Aveiro Institute of Materials, University of Aveiro, Aveiro, Portugal</i>	
P20	Raman studies of two-compound spin-liquid candidate (Na_{1-x}Li_x)₂IrO₃	109
	<u>A. Glamazda</u> ^{1,4} , V. Gnezdilov ^{1,2} , P. Lemmens ^{2,3} , P. Gegenwart ⁵	
	¹ <i>B.Verkin Institute for Low Temperature Physics and Engineering, Kharkiv, Ukraine</i>	
	² <i>Institute for Condensed Matter Physics, TU-Braunschweig, Braunschweig, Germany</i>	
	³ <i>Laboratory for Emerging Nanometrology and International Graduate School of Metrology, TU-Braunschweig, Braunschweig, Germany</i>	
	⁴ <i>V. N. Karazin Kharkiv National University, Kharkiv, Ukraine</i>	
	⁵ <i>Institute of Physics, University of Augsburg, Augsburg, Germany</i>	
P21	Low temperature thermodynamic of spin model formed by XX chains coupled via Ising spins	110
	<u>E. V. Ezerskaya</u> , <u>A. O. Kabatova</u>	
	<i>V. N. Karazin Kharkiv National University, Kharkiv, Ukraine</i>	

P22	High-pressure study of magnetic and magnetic resonance properties of rare-earth paramagnet KEr(MoO₄)₂	111
	K. Kutko ¹ , <u>V. Khrustalyov</u> ¹ , T. Sakurai ² , H. Ohta ² , S. Kimura ³ , H. Nojiri ³ , and D. Kamenskyi ⁴	
	¹ <i>B.Verkin Institute for Low Temperature Physics and Engineering, Kharkiv, Ukraine</i>	
	² <i>Molecular Photoscience Research Center, Kobe University, Kobe, Japan</i>	
	³ <i>Institute for Materials Research, Tohoku University, Sendai, Japan</i>	
	⁴ <i>Institute of Physics, University of Augsburg, Augsburg, Germany</i>	
P23	Magnetic properties of the Heisenberg–Ising model of nanomagnets on the base of transition metal polymeric complexes	112
	E. V. Ezerskaya, <u>S. Ye. Kononenko</u>	
	<i>V. N. Karazin Kharkiv National University, Kharkiv, Ukraine</i>	
P24	Estimation of magnetic characteristics of Ni-Zn ferrite prepared by hydroxide precipitation method	113
	O. I. Tovstolytkin ¹ , A. F. Kravets ^{1,2} , <u>S. M. Konoplyuk</u> ¹	
	¹ <i>Institute of Magnetism of the NAS of Ukraine, Kyiv, Ukraine</i>	
	² <i>Nanostructure Physics division, Royal Institute of Technology, Stockholm, Sweden</i>	
P25	Pressure effects on magnetic properties of LaMnO₃ and YMnO₃	114
	<u>A.A. Lyogenkaya</u> , A. S. Panfilov, G. E. Grechnev, and V. A. Pashchenko	
	<i>B.Verkin Institute for Low Temperature Physics and Engineering, Kharkiv, Ukraine</i>	
P26	Effect of magnetic field orientation on the behavior of linear dichroism in YIG:Co epitaxial film	115
	<u>O. V. Myoslavská</u> , Yu. M. Kharchenko, M. F. Kharchenko	
	<i>B.Verkin Institute for Low Temperature Physics and Engineering, Kharkiv, Ukraine</i>	
P27	About the nature of incommensurate phase in double Jahn-Teller rare-earth molybdates	116
	Yu. M. Kharchenko, K. V. Kutko, <u>N. M. Nesterenko</u>	
	<i>B.Verkin Institute for Low Temperature Physics and Engineering, Kharkiv, Ukraine</i>	
P28	Investigation of magnetic structure by spin-polarized scanning tunneling microscopy in ErB₄ tetraboride	117
	<u>O. Onufriienko</u> ¹ , D. Volavka ² , S. Gabáni ¹ , K. Flachbart ¹ , G. Pristáš ¹ , K. Siemensmeyer ³ , K. Prokeš ³ , N. Shitsevalova ⁴	
	¹ <i>Centre of Low Temperature Physics, Institute of Experimental Physics, Košice, Slovakia.</i>	
	² <i>Centre of Low Temperature Physics, Faculty of Science, P.J. Safarik University, Košice, Slovakia.</i>	
	³ <i>Helmholtz Zentrum für Materialien und Energie, Berlin, Germany.</i>	
	⁴ <i>Institute for Problems of Materials Science, Kiev, Ukraine.</i>	
P29	Comparative analysis of Raman and IR spectra in LiCoPO₄ and LiNiPO₄ magnetoelectrics	118
	<u>A. V. Peschanskii</u> ¹ , V. P. Gnezdilov ¹ , and A. Yu. Glamazda ^{1,2}	
	¹ <i>B.Verkin Institute for Low Temperature Physics and Engineering, Kharkiv, Ukraine</i>	
	² <i>V. N. Karazin Kharkiv National University, Kharkiv, Ukraine</i>	
P30	Manifestation of spiral magnetic phase in optical absorption spectra of NdFe₃(BO₃)₄ crystal	119
	<u>V. G. Piryatinskaya</u> , V. V. Slavin, I. S. Kachur, V. S. Kurnosov	
	<i>B.Verkin Institute for Low Temperature Physics and Engineering, Kharkiv, Ukraine</i>	
P31	Dynamic cluster magnetic subsystems in diluted magnetic semiconductor Ge_{1-x-y}Sn_xMn_yTe	120
	V. E. Slyanko ¹ , L. Kilanski ² , M. Arciszewska ² , V. I. Ivanov ¹	
	¹ <i>Chernivtsi Branch of Frantsevych Institute for Problems of Materials Science, Chernivtsi, Ukraine</i>	
	² <i>Institute of Physics, Polish Academy of Sciences, Warsaw, Poland</i>	

P32	Thermal conductivity of the Dy_xY_{1-x}(PO₃)₃ phosphate glasses	121
	<u>V. Stadnyk</u> ¹ , V. Tkáč ¹ , M. Tokarčík ¹ , P. Baloh ² , R. Tarasenko ¹ , E. Čižmár ¹ , M. Orendáč ¹ , A. Orendáčová ¹ , J. Holubová ³ , E. Černošková ³ , Z. Černošek ³ , and A. Feher ¹	
	¹ <i>Institute of Physics, P. J. Šafárik University in Košice, Košice, Slovakia</i>	
	² <i>International Institute for Carbon-Neutral Energy Research, Kyushu University, Fukuoka, Japan</i>	
	³ <i>University of Pardubice, Pardubice, Czech Republic</i>	
P33	Nonreciprocity of surface magnetoelastic waves in a ferromagnetic bilayer with noncollinear layer magnetizations	122
	<u>L. I. Ushii</u> ¹ , A. N. Slavin ² , R. V. Verba ¹	
	¹ <i>V.G. Baryakhtar Institute of Magnetism of the NAS of Ukraine, Kyiv, Ukraine</i>	
	² <i>Department of Physics, Oakland University, Rochester, Michigan, USA</i>	

OPTICS, PHOTONICS AND OPTICAL SPECTROSCOPY

P34	Optical properties of “left-handed” media based on a cubic lattice of metallic nanodimers	140
	<u>L. O. Abramenco</u> ¹ , A. V. Korotun ^{1,2} , V. M. Matiushyn ¹	
	¹ <i>National University Zaporizhzhia Politechnic, Zaporizhzhia, Ukraine</i>	
	² <i>G.V. Kurdyumov Institute for Metal Physics of the NAS of Ukraine, Kyiv, Ukraine</i>	
P35	Two-photon interaction in a superconducting circuit with SQUID-mediated coupling	141
	E. V. Stolyarov ¹ , <u>V. L. Andriichuk</u> ² , and A. M. Sokolov ²	
	¹ <i>Institute of Physics of the National Academy of Sciences, Kyiv, Ukraine</i>	
	² <i>Bogolyubov Institute for Theoretical Physics, Kyiv, Ukraine</i>	
P36	The effect of spatial dispersion on optical phenomena in spherical metallic nanoparticles	142
	R. Yu. Korolkov ¹ , <u>O. Yu. Berezhnyi</u> ¹ , A. V. Korotun ^{1,2}	
	¹ <i>National University Zaporizhzhia Politechnic, Zaporizhzhia, Ukraine</i>	
	² <i>G.V. Kurdyumov Institute for Metal Physics of the NAS of Ukraine, Kyiv, Ukraine</i>	
P37	Improvement of quantum efficiency of photodetectors by introducing plasmonic nanoparticles	143
	<u>D. V. Demianenko</u> ¹ , V. I. Reva ¹ , A. V. Korotun ^{1,2} , E.V. Stegantsev ³	
	¹ <i>National University Zaporizhzhia Politechnic, Zaporizhzhia, Ukraine</i>	
	² <i>G.V. Kurdyumov Institute for Metal Physics of the NAS of Ukraine, Kyiv, Ukraine</i>	
	³ <i>Zaporizhzhia National University, Zaporizhzhia, Ukraine</i>	
P38	Masking of nanoparticles with the help of multilayer cylindrical coatings	144
	R. Yu. Korolkov ¹ , A. V. Korotun ^{1,2} , V. M. Matiushyn ¹ , <u>R. V. Fliahin</u> ¹	
	¹ <i>National University Zaporizhzhia Politechnic, Zaporizhzhia, Ukraine</i>	
	² <i>G.V. Kurdyumov Institute for Metal Physics of the NAS of Ukraine, Kyiv, Ukraine</i>	
P39	Atomic structure calculations of singly ionized vanadium	145
	<u>S. V. Gedeon</u> , V. Yu. Lazur, V. I. Kazakov	
	<i>Department of Theoretical Physics, Uzhhorod National University, Uzhhorod, Ukraine</i>	
P40	Threshold conditions analysis of microlaser configuration with gold film and DBR	146
	S. S. Herasymov	
	<i>Kharkiv National University of Radio Electronics, Kharkiv, Ukraine</i>	

P41	Self-stabilization of microwave current in a superconducting resonator for photon detection	147
	O. Kalenyuk^{1,2}, S. Futimsky^{1,2}, I. Martynenko¹, A. Shapovalov^{1,2}	
	<i>¹G.V. Kurdyumov Institute for Metal Physics of the NAS of Ukraine, Kyiv, Ukraine</i>	
	<i>²Kyiv Academic University, Kyiv, Ukraine</i>	
P42	Absorption cross-section of toroidal metallic nanoparticles	148
	A. V. Korotun^{1,2}	
	<i>¹National University Zaporizhzhia Politechnic, Zaporizhzhia, Ukraine</i>	
	<i>²G.V. Kurdyumov Institute for Metal Physics of the NAS of Ukraine, Kyiv, Ukraine</i>	
P43	Width of the line of the surface plasmonic resonance in metal-dielectric nanocups	149
	V. I. Reva¹, R. O. Malysh¹, R. Yu. Korolkov¹, A. V. Korotun^{1,2}, I. M. Titov¹	
	<i>¹National University Zaporizhzhia Politechnic, Zaporizhzhia, Ukraine</i>	
	<i>²G.V. Kurdyumov Institute for Metal Physics of the NAS of Ukraine, Kyiv, Ukraine</i>	
P44	Plasmonic capacitance of the gap between two closely spaced spherical metal nanoparticles	150
	H. V. Moroz¹, A. V. Korotun^{1,2}, V. P. Kurbatsky¹	
	<i>¹National University Zaporizhzhia Politechnic, Zaporizhzhia, Ukraine</i>	
	<i>²G.V. Kurdyumov Institute for Metal Physics of the NAS of Ukraine, Kyiv, Ukraine</i>	
P45	Tensor of electric field enhancement in the vicinity of a metallic triangular equilateral nanoprism	151
	N. I. Pavlyshche	
	<i>National University Zaporizhzhia Politechnic, Zaporizhzhia, Ukraine</i>	
P46	The role of donor-acceptor defect complexes in the recombination of non-equilibrium carriers in cadmium iodide	152
	M. Rudka	
	<i>National University “Lviv polytechnic”, Lviv, Ukraine</i>	
P47	Electrical controlled multi-spectral light slowing in metasurface with graphen/dielectric/metal sandwich microresonators	153
	Yu. N. Savin	
	<i>O.Ya. Usykov Institute for Radiophysics and Electronics, Kharkiv, Ukraine</i>	
P48	Overheating of metallic nanoparticles under excitation of plasmonic resonances on their surface	154
	R. Yu. Korolkov¹, M. A. Shvydkyi¹, A. V. Korotun^{1,2}, I. M. Titov¹	
	<i>¹National University Zaporizhzhia Politechnic, Zaporizhzhia, Ukraine</i>	
	<i>²G.V. Kurdyumov Institute for Metal Physics of the NAS of Ukraine, Kyiv, Ukraine</i>	
P49	Signatures of disorder in the heat capacity of Nd-doped LAO laser materials	155
	V. Sokolenko, D. Szewczyk, N. Miniajlik-Gaweł, P. Dereń	
	<i>Institute for Low Temperatures and Structure Research, Wroclaw, Poland</i>	
P50	Effect of molecular impurity N₂ on photoluminescence and structure of fullerite C₆₀ during diffusion intercalation and chemical sorption	156
	V. N. Zoryansky, P.V. Zinoviev, N.N. Galtsov and Yu.O. Semerenko	
	<i>B.Verkin Institute for Low Temperature Physics and Engineering, Kharkiv, Ukraine</i>	
P50_1	Optical and electrical characteristics of FeS₂ thin films obtained in gas discharge	134
	E. Svitlichnyi¹, A. Molnar²	
	<i>¹Institute of Electron Physics of NAS of Ukraine, Uzhgorod, Ukraine</i>	
	<i>²Uzhgorod National University, Uzhgorod, Ukraine</i>	

P50_2	Obtaining of FeS₂ thin films on glass substrates in gas discharge plasma	135
	E. Svitlichnyi ¹ , A. Minya ² , M. Pop ² , R. Gritsak ² , M. Feldii ²	
	¹ <i>Institute of Electron Physics of NAS of Ukraine, Uzhgorod, Ukraine</i>	
	² <i>Uzhgorod National University, Uzhgorod, Ukraine</i>	

QUANTUM LIQUIDS AND QUANTUM CRYSTALS, CRYOCRYSTALS

P51	Scattering amplitude of C₆₀ fullerite in the ordered phase. Theory and calculations	162
	N. A. Aksanova ¹ , D. E. Hurova ² , V. Kinzhbalo ³ , N. N. Galtsov ²	
	¹ <i>V. N. Karazin Kharkiv National University, Kharkiv, Ukraine</i>	
	² <i>B.Verkin Institute for Low Temperature Physics and Engineering, Kharkiv, Ukraine</i>	
	³ <i>Institute for Low Temperatures and Structure Research, Wroclaw, Poland</i>	
P52	Correlation between the thermal conductivity plateau and the hump in heat capacity of polymer and composite materials	163
	<u>Yu. V. Horbatenko</u> , O. A. Korolyuk, A. I. Krivchikov, M. S. Barabashko	
	<i>B.Verkin Institute for Low Temperature Physics and Engineering, Kharkiv, Ukraine</i>	
P53	The substrate nanoroughness analysis by surface electrons over helium film	164
	V. A. Nikolaenko	
	<i>B.Verkin Institute for Low Temperature Physics and Engineering, Kharkiv, Ukraine</i>	
P54	Phase transitions in large atomic clusters. Computer modeling	165
	<u>M. Ratner</u> , V. V. Yanovsky	
	<i>Institute for Single Crystals of NAS of Ukraine, Kharkiv, Ukraine</i>	
P55	Thermal conductivity of nanostructured thin films and a composite material based on PbTe and PbSe	166
	<u>V. V. Sagan</u> , Yu. V. Horbatenko, O. A. Korolyuk, O. O. Romantsova, A. I. Krivchikov	
	<i>B.Verkin Institute for Low Temperature Physics and Engineering, Kharkiv, Ukraine</i>	
P56	Multi-channel heat transfer in CO₂ solutions with N₂O and Xe impurities	167
	<u>V. V. Sagan</u> , O. A. Korolyuk, A. I. Krivchikov, V. A. Konstantinov, Yu. V. Horbatenko	
	<i>B.Verkin Institute for Low Temperature Physics and Engineering, Kharkiv, Ukraine</i>	

TUESDAY, 3rd of JUNE

PLENARY LECTURES OF INVITED SPEAKERS

<i>Chair</i>	<i>Dr. Maksym Barabashko</i>	
10:00-10:30	Chirality induced spin selectivity: what is it, what do we really know and understand?	52
	Jan M. van Ruitenbeek	
	<i>Huygens-Kamerlingh Onnes Laboratory, Leiden University, Leiden, the Netherlands</i>	

- 10:30-11:00 Phonon thermal conductance of 3D conductors of rectangular cross-section in the ballistic regime** 49

J. Amrit¹, K. Nemchenko², Ye. Nemchenko², S. Rogova², A. Tonkonozhenko², T. Vikhtinskaya²

¹LISN, Université Paris-Saclay, CNRS, Orsay, France

²V.N.Karazin Kharkiv National University, Kharkiv, Ukraine

NANOPHYSICS AND NANOTECHNOLOGIES

Chair Dr. Maksym Barabashko

- 11:00-11:12 Low-temperature heat capacity of thermally expanded graphite: contribution of ZA flexural phonons** 171

M. S. Barabashko¹, A. I. Krivchikov^{1,2}, A. Jeżowski², D. Szewczyk², Yu. Horbatenko¹, O. Romantsova^{1,2}, G. Dovbeshko^{2,3}, Yu. Sementsov⁴

¹B.Verkin Institute for Low Temperature Physics and Engineering, Kharkiv, Ukraine

²Institute for Low Temperatures and Structure Research, Wrocław, Poland

³Institute of Physics, NAS of Ukraine, Kyiv, Ukraine

⁴Chuiko Institute of Surface Chemistry, NAS of Ukraine, Kyiv, Ukraine

- 11:13-11:24 Nanotechnology for future systems and equipment for improved survivability** 172

L. N. Illyashenko^{1, 2, 3}, N. N. Kolchigin², O. G. Nerukh³

¹National Academy of the National Guard of Ukraine, Zolochiv, Lviv Region, Ukraine

²V. N. Karazin Kharkiv National University, Kharkiv, Ukraine

³Kharkiv National University of Radio Electronics, Kharkiv, Ukraine

- 11:25-11:36 Dual hydrophobic/hydrophilic properties: a biomimetic microstructure taken from *Salvinia* leaf** 173

N. M. Kizilova

V. N. Karazin Kharkiv National University, Kharkiv, Ukraine

- 12:37-11:48 TbO_{2-x} nanoparticles with pro-oxidant properties and ROS-dependent luminescence of Tb³⁺ ions** 174

M. I. Lapan¹, V. V. Seminko, P. O. Maksimchuk, K. O. Hubenko, V. K. Klochkov, S. L. Yefimova

Institute for Scintillation Materials of NAS of Ukraine, Kharkiv, Ukraine

- 11:49-12:00 Raman spectroscopy of multilayer rhombohedral graphite** 175

S. I. Menshykova¹, S. I. Khaldeev, V. Mantena, P. Hakonen, M. Kumar, J. T. Mäkinen
Department of Applied Physics, Aalto University, Aalto, Finland

- 12:00-12:12 Dynamics and structure of quasi-2D hybrid materials** 176

Y. M. Trotskyi¹, E. S. Syrkin¹, V. O. Lykah²

¹B.Verkin Institute for Low Temperature Physics and Engineering, Kharkiv, Ukraine

²National Technical University “Kharkiv Polytechnic Institute”, Kharkiv, Ukraine

- 12:13-12:25 Enhancement of nematic ordering in cyanobiphenyl liquid crystals induced by resorcinol: novel insights on supramolecular arrangement in hydrogen-bonded liquid crystals** 177

P. V. Vashchenko¹, D. S. Sofronov², L. N. Lisetski¹

¹Institute for Scintillation Materials of NAS of Ukraine, Kharkiv, Ukraine

²Institute for Single Crystals of NAS of Ukraine, Kharkiv, Ukraine

12:25-13:20

BREAK

PLENARY LECTURES OF INVITED SPEAKERS

Chair *Dr. Vlada Pashynska*

- 13:20-13:50 Physicochemical properties of hazardous carbon smoke nanoparticles with heavy metals**

41

G. I. Dovbeshko^{1,2}, T. O. Borisova^{1,2}, O. Bezkrovnyi², O. P. Gnatyuk^{1,2}, A. S. Tolochko¹, V. V. Boiko^{1,2}, W. Strek²

¹*Institute of Physics of NAS of Ukraine, Kyiv, Ukraine*

²*Institute for Low Temperatures and Structure Research, Wroclaw, Poland*

- 13:50-14:20 Spectroscopic features of single-walled carbon nanotube films as biosensor elements**

44

A. Glamazda and V. Karachevtsev

B.Verkin Institute for Low Temperature Physics and Engineering, Kharkiv, Ukraine

BIOPHYSICS AND PHYSICS OF MACROMOLECULES

Chair *Dr. Vlada Pashynska*

- 14:20-14:32 Peculiarities of a nanocomposite of molybdenum disulfide with cysteine amino acid as revealed by laser desorption/ionization mass spectrometry**

197

M. V. Kosevich¹, V. S. Shelkovsky¹, O. A. Boryak¹, P. O. Kuzema², V. A. Karachevtsev¹

¹*B.Verkin Institute for Low Temperature Physics and Engineering, Kharkiv, Ukraine*

²*Chuiko Institute of Surface Chemistry, Kyiv, Ukraine*

- 14:32-14:44 Characteristic features of lipid domains formed by the mechanism of binding depending on surroundings - "preferential binding": results of computer simulation**

198

R. Ye. Brodskii¹, O. V. Vashchenko²

¹*Institute for Single Crystals of NAS of Ukraine, Kharkiv, Ukraine*

²*Institute for Scintillation Materials of NAS of Ukraine, Kharkiv, Ukraine*

- 14:44-14:56 Anticancer drugs interactions with the drug delivery nanostructures: mass spectrometry insight**

199

V. A. Pashynska¹, M. V. Kosevich¹, O. A. Boryak¹, I. M. Voloshin¹, P. O. Kuzema², V. A. Karachevtsev¹

¹*B.Verkin Institute for Low Temperature Physics and Engineering, Kharkiv, Ukraine*

²*Chuiko Institute of Surface Chemistry, Kyiv, Ukraine*

- 14:56-15:08 Cellular approach to the zeta potential of aqueous-salt albumin solutions**

200

O. D. Stoliaryk¹, A. A. Guslisty², O. V. Khorolskyi³

¹*Odesa I. I. Mechnikov National University, Odesa, Ukraine*

²*Family Medicine Center Amedika LLC, Odesa, Ukraine*

³*Poltava V. G. Korolenko National Pedagogical University, Poltava, Ukraine*

- 15:08-15:20 Thermal profiles of unloaded liposomes and liposomes with MoS₂ nanoparticles**

201

M. V. Olenchuk, Eu. O. Andreev, Yu. M. Barabash, G. I. Dovbeshko

Institute of Physics of NAS of Ukraine, Kyiv, Ukraine

- 15:20-15:32 Nanohybrids of uracil with graphene and noble metal nanoclusters**

202

T. Piddubnyi¹, S. Stepanian¹, L. Adamowicz²

¹*B.Verkin Institute for Low Temperature Physics and Engineering, Kharkiv, Ukraine*

²*Department of Chemistry and Biochemistry, University of Arizona, Tucson, USA*

15:32-15:44	Functionalization of transition metal dichalcogenides by organic polymers studied by mass spectrometry	203
	<u>V. G. Zobnina</u> ¹ , V. S. Shelkovsky ¹ , O. A. Boryak ¹ , P. O. Kuzema ² , M. V. Kosevich ¹ , V. A. Karachevtsev ¹	
	¹ <i>B.Verkin Institute for Low Temperature Physics and Engineering, Kharkiv, Ukraine</i>	
	² <i>Chuiko Institute of Surface Chemistry, Kyiv, Ukraine</i>	
15:44-15:56	Fluorescent voltage sensors for neuronal activity monitoring	204
	A. G. Bulova	
	<i>B.Verkin Institute for Low Temperature Physics and Engineering, Kharkiv, Ukraine</i>	

16:00-16:30

BREAK

PLENARY LECTURES OF INVITED SPEAKERS

Chair *Dr. Diana Hurova*

16:30-17:00	THz-driven magnetic switching and dynamical coupling in rare-earth orthoferrites with non-Kramers ions: theory and experiment	57
	<u>N. R. Vovk</u> ¹ , O. Y. Kovalenko ¹ , E. V. Ezerskaya ² , R. V. Mikhaylovskiy ¹	
	¹ <i>Lancaster University, Bailrigg, Lancaster, United Kingdom</i>	
	² <i>V. N. Karazin Kharkiv National University, Kharkiv, Ukraine</i>	
17:00-17:30	Extremes of ultralow temperatures and high magnetic fields: opportunities for exploring quantum materials	47
(10:00 UTC-4)	Mark W. Meisel	
	<i>Department of Physics and MagLab High B/T Facility, University of Florida, Gainesville, USA</i>	

17:30-19:00

POSTER SESSION (5, 6, 7, 8 AND 9 SECTIONS)

Chairs *Dr. Diana Hurova, Dr. Sergii Poperezhai*

17:30-18:15 **Stage 1 (P57-P87)**

18:15-19:00 **Stage 2 (P88-P117)**

NANOPHYSICS AND NANOTECHNOLOGIES

P57	The role of incomplete ionization in radial p-n junction structures at low temperatures	178
	<u>J. Sh. Abdullayev</u> ¹ , I. B. Sapaev ^{1, 2}	
	¹ <i>National Research University TIIAME, Tashkent, Uzbekistan</i>	
	² <i>Western Caspian University, Baku, Azerbaijan</i>	
P58	Dimensional effects in the thermal expansion of carbon fiber reinforced plastic at low temperatures	179
	N. A. Vinnikov, A. V. Dolbin, V. B. Esel'son, V. G. Gavrilko, <u>R. M. Basnukaeva</u> , E. M. Grytsiuk, L. M. Buravtseva	
	<i>B.Verkin Institute for Low Temperature Physics and Engineering, Kharkiv, Ukraine</i>	

P59	Vibrational characteristics of graphene-based materials and hexagonal modification of niobium dichalcogenide: stability, low-dimensional peculiarities and peculiarities of phonon expansion and localization	180
	K. A. Minakova ¹ , V. A. Sirenko ¹ , I. S. Bondar ² , I. G. Mirzoiev ²	
	¹ <i>National Technical University "Kharkiv Polytechnic Institute", Kharkiv, Ukraine</i>	
	² <i>B.Verkin Institute for Low Temperature Physics and Engineering, Kharkiv, Ukraine</i>	
P60	Low-temperature thermodynamics of branched spin-1/2 system formed by XX chains connected through Ising spins	181
	K. S. Dzhenzherova, E. V. Ezerskaya, V. O. Kovalenko	
	<i>V.N. Karazin Kharkiv National University, Kharkiv, Ukraine</i>	
P61	Effect of dispersion in various liquid crystal matrices on the excitonic properties of cyanine dye J-aggregates	182
	S. S. Hrankina ^{1,2} , O. M. Samoilov ¹ , I. I. Grankina ¹ , L. N. Lisetski ¹ , S. L. Yefimova ¹ , O. V. Sorokin ¹	
	¹ <i>Institute for Scintillation Materials of NAS of Ukraine, Kharkiv, Ukraine</i>	
	² <i>Kharkiv National Medical University, Kharkiv, Ukraine</i>	
P62	Physical sorption of aluminum in carbon honeycomb structures: models and experiment	183
	M. A. Kabanenko ¹ , V. O. Hamalii ¹ , Y. A. Mastrikov ² , E. A. Kotomin ² , N. V. Krainyukova ¹	
	¹ <i>B.Verkin Institute for Low Temperature Physics and Engineering, Kharkiv, Ukraine</i>	
	² <i>Institute of Solid State Physics, University of Latvia, Riga, Latvia</i>	
P63	Selective sorption of argon in carbon honeycombs of different sizes	184
	M. A. Kabanenko, V. O. Hamalii, N. V. Krainyukova	
	<i>B.Verkin Institute for Low Temperature Physics and Engineering, Kharkiv, Ukraine</i>	
P64	Magnetic properties of two finite spin-1/2 XX chains connected through two Ising spins	185
	K. S. Dzhenzherova, E. V. Ezerskaya, <u>V. O. Kovalenko</u>	
	<i>V.N. Karazin Kharkiv National University, Kharkiv, Ukraine</i>	
P65	Inter-strip coupling effects in graphene-based metasurface	186
	K. S. Kuznetsova ¹ , Z. E. Eremenko ¹ , V. A. Pashynska ^{1,2}	
	¹ <i>O.Ya. Usykov Institute for Radiophysics and Electronics, Kharkiv, Ukraine</i>	
	² <i>B.Verkin Institute for Low Temperature Physics and Engineering, Kharkiv, Ukraine</i>	
P66	Information recording medium based on tunnel magnetic transitions	187
	M. M. Krupa	
	<i>V.G. Baryakhtar Institute of Magnetism of the NAS of Ukraine, Kiev, Ukraine</i>	
P67	Spin-boson model with time-dependent coupling to a selected vibrational mode	188
	V. O. Leonov, Ye. V. Shevchenko, V. I. Teslenko, E. G. Petrov	
	<i>Bogolyubov Institute for Theoretical Physics of NAS of Ukraine, Kyiv, Ukraine</i>	
P68	Resonances in a chain of bimetallic nanoparticles on a dielectric substrate	189
	M. S. Maniuk ¹ , A. V. Korotun ^{1,2} , V. P. Kurbatsky ¹	
	¹ <i>National University Zaporizhzhia Politechnic, Zaporizhzhia, Ukraine</i>	
	² <i>G.V. Kurdyumov Institute for Metal Physics, Kyiv, Ukraine</i>	
P69	Fetal bovine serum-mediated enhancement of cerium oxide-based luminescent sensors for hydrogen peroxide detection	190
	Ye. Neuhodov ¹ , P. Maksimchuk ¹ , G. Grygorova ¹ , A. Onishchenko ² , N. Kavok ¹ , G. Dudetskaya ¹ , Yu. Kot ³ , S. Yefimova ¹ , V. Seminko ¹	
	¹ <i>Institute for Scintillation Materials of NAS of Ukraine, Kharkiv, Ukraine</i>	
	² <i>Kharkiv National University of Radio Electronics, Kharkiv, Ukraine</i>	
	³ <i>School of Biology, V. N. Karazin Kharkiv National University, Kharkiv, Ukraine</i>	

P70	Magnetic and magnetotransport properties of modified by cobalt carbon nanotubes	191
	I. Ovsienko ¹ , D. Shpylka ¹ , T. Len ¹ , L. Matzui ¹ , A. Sedda ² , E. Lähderanta ^{2,3,4} , A. Terekhov ⁴ , I. Mirzoiev ⁴	
	¹ Taras Shevchenko National University of Kyiv, Kyiv, Ukraine	
	² Lappeenranta University of Technology, Lappeenranta, Finland	
	³ Institute for Low Temperatures and Structure Research, Wroclaw, Poland	
	⁴ B.Verkin Institute for Low Temperature Physics and Engineering, Kharkiv, Ukraine	
P71	Josephson junctions with barrier from semiconductor doped by metal	192
	V. E. Shaternik, A. P. Shapovalov	
	G.V. Kurdyumov Institute for Metal Physics, Kyiv, Ukraine	
P72	Dielectric properties of layer crystals and nanostructures based on them	193
	B. O. Seredyuk ¹ , M. S. Karkulovska ² , N. K. Tovstyuk ² , O. Y. Mykytiuk ³ .	
	¹ National Army Academy named after Hetman Petro Sahaidachnyi, Lviv, Ukraine	
	² Institute of Mathematics and Applied Physics, Lviv Polytechnic National University, Lviv, Ukraine	
	³ Bukovinian State Medical University, Chernivtsi, Ukraine	

BIOPHYSICS AND PHYSICS OF MACROMOLECULES

P73	The effect of mutations on the binding affinity of macrolides with ribosomal proteins: a molecular docking approach	205
	N. V. Khmil ^{1,2} , V. G. Kolesnikov ¹	
	¹ O.Ya. Usykov Institute for Radiophysics and Electronics, Kharkiv, Ukraine	
	² Kharkiv National University of Radio Electronics, Kharkiv, Ukraine	
P74	Analysis of low-temperature electron transport in a composite film of reduced graphene oxide with molybdenum disulfide	206
	N. V. Kurnosov, A. M. Plokhotnichenko, V. A. Karachevtsev	
	B.Verkin Institute for Low Temperature Physics and Engineering, Kharkiv, Ukraine	
P75	Mass spectrometry and Raman spectroscopy characterization of the bactericidal nanofiber mats with incorporated antibiotics	207
	V. A. Pashynska ¹ , A. M. Plokhotnichenko ¹ , A. Yu. Glamazda ¹ , P. O. Kuzema ² , V. A. Karachevtsev ¹	
	¹ B.Verkin Institute for Low Temperature Physics and Engineering, Kharkiv, Ukraine	
	² Chuiko Institute of Surface Chemistry, Kyiv, Ukraine	
P76	Peculiarities of interaction of the sulfur-containing antiviral drug lamivudine with molybdenum disulfide	208
	T. Piddubnyi ¹ , S. Stepanian ¹ , L. Adamowicz ²	
	¹ B.Verkin Institute for Low Temperature Physics and Engineering, Kharkiv, Ukraine	
	² Department of Chemistry and Biochemistry, University of Arizona, Tucson AZ, USA	
P77	On the features of multi-charged meso-porphyrin binding to nucleic acids	209
	O. A. Ryazanova	
	B.Verkin Institute for Low Temperature Physics and Engineering, Kharkiv, Ukraine	
P78	Mass spectrometric probing of C60 with MoS₂ composite produced in aqueous medium	210
	V. S. Shelkovsky ¹ , M. V. Kosevich ¹ , O. A. Boryak ¹ , P. O. Kuzema ² , A. V. Dolbin ¹ , N. A. Vinnikov ¹ , S. V. Cherednichenko ¹ , V. A. Karachevtsev ¹	
	¹ B.Verkin Institute for Low Temperature Physics and Engineering, Kharkiv, Ukraine	
	² Chuiko Institute of Surface Chemistry, Kyiv, Ukraine	

P79	Experimental and theoretical study of the binding of native DNA to MoS₂ nanoflakes	211
	<u>E. Usenko¹</u> , A. Glamazda ^{1,2} , V. Valeev ¹ , I. Voloshin ¹ , S. Petrushenko ² , S. Stepanian ¹ , L. Adamowicz ³ , V. Karachevtsev ¹	
	¹ <i>B. Verkin Institute for Low Temperature Physics and Engineering, Kharkiv, Ukraine</i>	
	² <i>V. N. Karazin Kharkiv National University, Kharkiv, Ukraine</i>	
	³ <i>Department of Chemistry and Biochemistry, University of Arizona, Tucson AZ, USA</i>	
P80	The impact of the outer membrane and general porins on cyanide diffusion in gram-negative bacteria	212
	<u>V. Yakovliev</u> , B. Lev	
	<i>Bogolyubov Institute for Theoretical Physics, Kyiv, Ukraine</i>	
<hr/> <hr/> <hr/> MATERIALS SCIENCE <hr/> <hr/>		
P81	Structural and optical study of undoped and Ag-doped Sb₂S₃ polycrystals and thin films	221
	<u>Y. M. Azhniuk¹</u> , V. V. Lopushansky ¹ , A. I. Pogodin ² , M. J. Filep ³ , I. M. Voynarovych ¹ , V. M. Kryshenik ¹ , A. V. Gomonnai ¹	
	¹ <i>Institute of Electron Physics, Uzhhorod, Ukraine</i>	
	² <i>Uzhhorod National University, Uzhhorod, Ukraine</i>	
	³ <i>Ferenc Rákóczi II Transcarpathian Hungarian Institute, Berehovo, Ukraine</i>	
P82	Optical properties and transition temperatures of multiple structures of amorphous ice mixed with CO₂	226
	<u>N. N. Chigambayeva</u> , A. Y. Nurmukan	
	<i>Al-Farabi Kazakh National University, Almaty, Kazakhstan</i>	
P83	Change of structure of polyimide PM-A after low temperature deformation	227
	V. G. Geidarov	
	<i>B. Verkin Institute for Low Temperature Physics and Engineering, Kharkiv, Ukraine</i>	
P84	Classical and fractal models of chalcogenide glasses viscoelasticity	228
	<u>A. A. Horvat</u> , A. A. Molnar, V. V. Minkovich	
	<i>Uzhhorod National University, Uzhhorod, Ukraine</i>	
P85	The microstructure and low-temperature mechanical properties of ultrafine-grained copper: effect of deformation and annealing	229
	<u>T. Hryhorova¹</u> , S. Shumilin ¹ , P. Zabrodin ^{1,2} , D. Drozdenko ³	
	¹ <i>B. Verkin Institute for Low Temperature Physics and Engineering, Kharkiv, Ukraine</i>	
	² <i>Institute of Theoretical and Applied Mechanics, Prague, Czech Republic</i>	
	³ <i>Charles University, Faculty of Mathematics and Physics, Prague, Czech Republic</i>	
P86	The low-temperature plasticity and deformation microstructure of SPD Al-Li alloy	230
	<u>T. Hryhorova¹</u> , S. Shumilin ¹ , P. Zabrodin ^{1,2} , D. Drozdenko ³	
	¹ <i>B. Verkin Institute for Low Temperature Physics and Engineering, Kharkiv, Ukraine</i>	
	² <i>Institute of Theoretical and Applied Mechanics, Prague, Czech Republic</i>	
	³ <i>Charles University, Faculty of Mathematics and Physics, Prague, Czech Republic</i>	
P87	Peculiarities of the electronic and elastic properties of indium selenide in different structural modifications	231
	<u>O. I. Korolov</u> , L. Yu. Kharkhalis, K. E. Glukhov	
	<i>Institute for Physics and Chemistry of Solid State, Uzhhorod National University, Uzhhorod, Ukraine</i>	

P88	The role of internal stresses in the realisation of dislocation-diffusion viscous flow of eutectic alloys under the conditions of superplasticity	232
	<u>V. F. Korshak</u> ¹ , Y. O. Shapovalov ² , P. P. Pal-Val ²	
	¹ <i>V. N. Karazin Kharkiv National University, Kharkiv, Ukraine</i>	
	² <i>B.Verkin Institute for Low Temperature Physics and Engineering, Kharkiv, Ukraine</i>	
P89	Photo- and thermostimulated phase transformations in Ge₂Sb₂Se_{5-x}Tex glasses	233
	<u>V. M. Kryshenik</u> ¹ , S. M. Hasynets ¹ , Y. M. Azhniuk ¹ , M. J. Filep ² ,	
	V. V. Lopushansky ¹ , O. O. Gomonna ³ , V. Y. Loya ¹ , A. V. Gomonna ¹	
	¹ <i>Institute of Electron Physics, Uzhhorod, Ukraine</i>	
	² <i>Ferenc Rákóczi II Transcarpathian Hungarian Institute, Berehovo, Ukraine</i>	
	³ <i>Uzhhorod National University, Uzhhorod, Ukraine</i>	
P90	Study of the sensory response of porous films with fluorescent dyes to microconcentrations of acetone and ammonia	234
	<u>Ya. P. Lazorenko</u> ¹ , V. P. Mitsai ²	
	¹ <i>G.V. Kurdyumov Institute for Metal Physics, Kyiv, Ukraine</i>	
	² <i>V.G. Baryakhtar Institute of Magnetism, Kyiv, Ukraine</i>	
P91	Experimental studies of hydrogen-palladium interaction in the α-region of the Pd-H diagram	235
	O. M. Liubymenko	
	<i>State higher education institution "Donetsk National Technical University", Drohobych, Ukraine</i>	
P92	The influence of hydrogen diffusion on electrical resistivity of amorphous metallic alloys	236
	A. Grib, <u>V. Makharynskyi</u>	
	<i>V. N. Karazin Kharkiv National University, Kharkiv, Ukraine</i>	
P93	Modification of electrophysical parameters of CuInP₂S₆ crystals by betta, gamma and neutron irradiation	237
	<u>A. Molnar</u> ¹ , A. Haysak ¹ , I. Haysak ¹ , D. Gál ²	
	¹ <i>Uzhhorod National University, Uzhhorod, Ukraine</i>	
	² <i>HUN-REN WIGNER Research Center for Physics, Budapest, Hungary</i>	
P94	Estimation of the thermal conductivity of porous silicon using molecular dynamics and machine learning methods	238
	V. V. Kuryliuk, <u>O. Ya. Olikh</u>	
	<i>Taras Shevchenko National University of Kyiv, Kyiv, Ukraine</i>	
P95	Prediction of isomorphous substitutions of strontium or barium by sodium and actinides for their immobilization in molybdates with a scheelite-type structure	239
	<u>S. V. Radio</u> , E. I. Get'man	
	<i>Vasyl' Stus Donetsk National University, Vinnytsia, Ukraine</i>	
P96	Low-temperature thermal properties of carbon-based nanomaterials: exploration of graphene oxide and fullerene composites	240
	<u>O. O. Romantsova</u> ^{1,2} , D. Szewczyk ² , A. Jeżowski ² , Yu. Horbatenko ¹ , M. Vinnikov ¹ ,	
	S. Cherednichenko ¹ , A. I. Krivchikov ^{1,2}	
	¹ <i>B.Verkin Institute for Low Temperature Physics and Engineering, Kharkiv, Ukraine</i>	
	² <i>Institute of Low Temperatures and Structure Research, Wroclaw, Poland</i>	
P97	The effect of the vanadium content on the microhardness of CoCrFeNiMnV_x high-entropy alloys in the temperature range of 77-293 K	241
	<u>H. V. Rusakova</u> ¹ , L. S. Fomenko ¹ , S. V. Lubenets ¹ , M. A. Tikhonovsky ² ,	
	I. F. Kislyak ² , E. D. Tabachnikova ¹ , Yi Huang ³ , and Terence G. Langdon ⁴	
	¹ <i>B.Verkin Institute for Low Temperature Physics and Engineering, Kharkiv, Ukraine</i>	
	² <i>National Science Center "Kharkiv Institute of Physics and Technology", Kharkiv, Ukraine</i>	
	³ <i>Faculty of Science and Technology, Bournemouth University, Poole, Dorset, UK</i>	
	⁴ <i>Department of Mechanical Engineering, University of Southampton, Southampton, UK</i>	

P98	The effect of low temperatures on the rheological properties of amorphous and amorphous-crystalline polymers	242
	V. D. Natsik, <u>H. V. Rusakova</u> , V. A. Lototskaya	
	<i>B.Verkin Institute for Low Temperature Physics and Engineering, Kharkiv, Ukraine</i>	
P99	Investigation of low-temperature dislocation structure and dynamics in the high-entropy alloy Al_{0.5}CoCrCuFeNi	243
	Yu. Semerenko ¹ , V. Natsik ¹ , N. Galtsov ¹ , D. Hurova ¹ , V. Zoryansky ¹ , E. Tabachnikova ¹ , T. Bednarchuk ² , Yu. Lipovska ³	
	¹ <i>B.Verkin Institute for Low Temperature Physics and Engineering, Kharkiv, Ukraine</i>	
	² <i>Institute of Low Temperatures and Structure Research, Wroclaw, Poland</i>	
	³ <i>National Science Center "Kharkiv Institute of Physics and Technology", Kharkiv, Ukraine</i>	
P100	Comparative analysis of mechanical properties and microstructure of coarse-grained and nanostructured nonequiatomical medium-entropy alloys Fe₄₀Mn₄₀Co₁₀Cr₁₀ and Fe₅₀Mn₃₀Co₁₀Cr₁₀ in the temperature range of 4.2–300 K	244
	S. E. Shumilin ¹ , T. V. Hryhorova ¹ , S. N. Smirnov ¹ , Yu. O. Semerenko ¹ , I. V. Kashuba ¹ , Yu. O. Shapovalov ¹ , E. D. Tabachnikova ¹ , M. A. Tikhonovsky ² , Y. Huang ³ , T. G. Langdon ⁴	
	¹ <i>B.Verkin Institute for Low Temperature Physics and Engineering, Kharkiv, Ukraine</i>	
	² <i>National Science Center "Kharkiv Institute of Physics and Technology", Kharkiv, Ukraine</i>	
	³ <i>Faculty of Science and Technology, Bournemouth University, Poole, Dorset, UK</i>	
	⁴ <i>Department of Mechanical Engineering, University of Southampton, Southampton, UK</i>	
P101	On the influence of surface roughness of polymer kapton-H on momentum transfer in supersonic flow of atomic oxygen plasma	245
	V. A. Shuvalov, G. S. Kochubei, Yu. P. Kuchugurnyi, D. K. Voronovskyi, B. V. Yurkov	
	<i>Institute of Technical Mechanics, Dnipro, Ukraine</i>	
P102	Strain rate dependent deformation behavior of Ti-Nb alpha-alloys at low temperatures	246
	V. A. Moskalenko, <u>R. V. Smolianets</u>	
	<i>B.Verkin Institute for Low Temperature Physics and Engineering, Kharkiv, Ukraine</i>	
P103	Study of pore distribution in activated carbon by low-temperature nitrogen adsorption	247
	V. M. Vashchynskyi	
	<i>Lviv Polytechnic National University, Lviv, Ukraine</i>	
P104	Impact of electromagnetic radiation from spark discharge on the dielectric properties of Cd_{1-x}Zn_xTe crystals within the low-frequency region	248
	O. Chugai, S. Kulish, <u>Yu. Voloshyn</u> , S. Sulyma	
	<i>National Aerospace University "Kharkiv Aviation Institute", Kharkiv, Ukraine</i>	
P105	Formation energies of point defects in Ti-doped YAG crystals: first-principles calculations	249
	M. Y. Vovsianiker, D. V. Fil	
	<i>Institute for Single Crystals of NAS of Ukraine, Kharkiv, Ukraine</i>	
P106	The temperature dependences of resistivity of spinel-nanocarbon-epoxy composites	250
	O. Yakovenko ¹ , L. Matzui ¹ , L. Vovchenko ¹ , L. Kaykan ² , J. Mazurenko ^{1, 2, 3} , D. Zaiatc ¹ , K. Dubyk ¹ , D. Shpylka ¹	
	¹ <i>Taras Shevchenko National University of Kyiv, Kyiv, Ukraine</i>	
	² <i>G.V. Kurdyumov Institute for Metal Physics, Kyiv, Ukraine</i>	
	³ <i>Institute of Experimental Physics SAS, Košice, Slovak Republic</i>	

THEORY OF CONDENSED MATTER PHYSICS

P107	Modeling of metal strengthening during severe plastic deformation <u>O. V. Khomenko</u> , A. P. Chopov, K. P. Khomenko, M. S. Holubnycha <i>Sumy State University, Sumy, Ukraine</i>	268
P108	Theory of Bose-Einstein condensation with pair correlations within successive iteration method <u>M. Bulakhov</u> ^{1,2} , <u>A.S. Peletinskii</u> ^{1,2} ¹ <i>Akhiezer Institute for Theoretical Physics, Kharkiv, Ukraine</i> ² <i>National Science Center "Kharkiv Institute of Physics and Technology", Kharkiv, Ukraine</i>	269
P109	General collisionless kinetic approach to studying excitations in arbitrary-spin quantum atomic gases <u>M. Bulakhov</u> ¹ , A. S. Peletinskii ¹ , and Yu. V. Slyusarenko ^{1,2} ¹ <i>Akhiezer Institute for Theoretical Physics, Kharkiv, Ukraine</i> ² <i>Lviv Polytechnic National University, Lviv, Ukraine</i>	270
P110	Fluctuation pinning/depinning as a result of transmutation of diffusive gas-fluctuation modes into opposite propagating ones at the formation of two non-Hermitian topological phases originated by gas scattering on impurity center <u>S. P. Lukyanets</u> , O. V. Kliushnichenko <i>Institute of Physics of NAS of Ukraine, Kyiv, Ukraine</i>	271
P111	Quasiclassical energy spectra of the Boussinesq breathers in anharmonic crystals <u>O. V. Charkina</u> , M. M. Bogdan <i>B.Verkin Institute for Low Temperature Physics and Engineering, Kharkiv, Ukraine</i>	272
P112	Breathers dumping by extended moving domain walls in highly dispersive nonlinear systems <u>O. V. Charkina</u> ¹ , Igor Poltavskyi ² , Anton Charkin-Gorbulin ² , M. M. Bogdan ¹ ¹ <i>B.Verkin Institute for Low Temperature Physics and Engineering, Kharkiv, Ukraine</i> ² <i>University of Luxembourg, Luxembourg City, Luxembourg</i>	273
P113	Interface phonon spectrum and electron-phonon interaction in GaN/AlGaN nanostructures <u>Ju. O. Seti</u> ¹ , I. V. Boyko ² ¹ <i>Lviv Polytechnic National University, Lviv, Ukraine</i> ² <i>Ternopil Ivan Puluj National Technical University, Ternopil, Ukraine</i>	274

TECHNOLOGIES AND INSTRUMENTATION FOR PHYSICAL EXPERIMENTS

P114	Methodology of multichannel study of cryoeffect <i>in vitro</i> <u>V. Yu. Globa</u> ¹ , G. O. Kovalov ¹ , M. O. Chyzh ¹ , G. V. Shustakova ² , Ed. Yu. Gordiyenko ² , Yu. V. Fomenko ² ¹ <i>Institute for Problems of Cryobiology and Cryomedicine, Kharkiv, Ukraine</i> ² <i>B.Verkin Institute for Low Temperature Physics and Engineering, Kharkiv, Ukraine</i>	285
P115	Theoretical aspects and engineering approaches to energy-saving liquid atomization technologies <u>P. E. Trofymenko</u> , O. V. Khomenko, <u>M. V. Naida</u> , D. T. Lohvynenko <i>Sumy State University, Sumy, Ukraine</i>	286

P116	Quantum point-contact sensors for the emotion state detection in real time	287
	M. Romanov¹, D. Harbuz¹, V. Belan¹, O. Pospelov², L. Kamarchuk³, V. Gudimenko¹ and G. Kamarchuk¹	
	¹ <i>B. Verkin Institute for Low Temperature Physics and Engineering, Kharkiv, Ukraine</i>	
	² <i>National Technical University "Kharkiv Polytechnic Institute", Kharkiv, Ukraine</i>	
	³ <i>SI "Institute for Children and Adolescents Health Care" of NAMS of Ukraine, Kharkiv, Ukraine</i>	
P117	Relevance of metrological documentation development for heat flux calculations in ultracold neutron converters	288
	A. K. Sauleyeva¹, Ye. S. Korshikov¹, K. Turlybekuly², V. V. Nesvizhevsky³	
	¹ <i>Institute of Experimental and Theoretical Physics, al-Farabi Kazakh National University, Almaty, Kazakhstan</i>	
	² <i>Institute of Nuclear Physics, Ministry of Energy of the Republic of Kazakhstan, Almaty, Kazakhstan</i>	
	³ <i>European Centre for Neutron Research "Institut Max von Laue – Paul Langevin", Grenoble, France</i>	

WEDNESDAY, 4th of JUNE

PLENARY LECTURES OF INVITED SPEAKERS

<i>Chair</i>	<i>Dr. Oleksii Konotop</i>	
10:00-10:30	Mass-selected matrix isolation spectroscopy of astrochemically relevant aromatic cations in solid neon	58
	Yu-Jong Wu^{1,2}	
	¹ <i>National Synchrotron Radiation Research Center, Hsinchu, Taiwan</i>	
	² <i>National Yang Ming Chiao Tung University, Hsinchu, Taiwan</i>	
10:30-11:00	Radiolysis products and delayed desorption from methane-doped cryogenic matrices studied by emission spectroscopy methods	53
	M. A. Bludov, I. V. Khyzhniy, S. A. Uyutnov, E. V. Savchenko	
	<i>B. Verkin Institute for Low Temperature Physics and Engineering, Kharkiv, Ukraine</i>	

QUANTUM LIQUIDS AND QUANTUM CRYSTALS, CRYOCRYSTALS

<i>Chair</i>	<i>Dr. Oleksii Konotop</i>	
11:00-11:12	Creating of bounded Majorana pairs in superconducting net of quantum nanowires in SmMnO_{3+δ}	159
	F. N. Bukhanko	
	<i>Donetsk Institute for Physics and Engineering named after O.O. Galkin, Kyiv, Ukraine</i>	
11:12-11:25	The influence of second sound resonances on the vibrations of a quartz tuning fork in a superfluid solution of ³He in ⁴He	160
	V. K. Chagovets, V. E. Syvokon, S. S. Sokolov	
	<i>B. Verkin Institute for Low Temperature Physics and Engineering, Kharkiv, Ukraine</i>	
11:25-11:38	Peculiarities of growth of close packed phases in large substrate-free rare gas clusters	161
	O. P. Konotop, O. G. Danylchenko	
	<i>B. Verkin Institute for Low Temperature Physics and Engineering, Kharkiv, Ukraine</i>	

PLENARY LECTURES OF INVITED SPEAKERS

Chair *Dr. Oleksii Konotop*

- 11:40-12:10 Structural evolution and thermal properties of SiOC glass derived from polymer: influence of atmosphere and porosity**

55

D. Szewczyk¹, M. Casseta², M. Biesuz²

¹*Institute for Low Temperature and Structure Research, Wroclaw, Poland*

²*Department of Industrial Engineering, University of Trento, Trento, Italy*

12:10-13:00

BREAK

PLENARY LECTURES OF INVITED SPEAKERS

Chair *Dr. Sergii Poperezhai*

- 13:00-13:30 Exploring topological and quantum transport properties of topological crystalline insulator (111) Pb_{1-x}Sn_xSe thin films grown by MBE**

56

Valentine V. Volobuev^{1,2}

¹*International Research Centre MagTop, Institute of Physics, Warsaw, Poland*

²*National Technical University “Kharkiv Polytechnic Institute”, Kharkiv, Ukraine*

OPTICS, PHOTONICS AND OPTICAL SPECTROSCOPY

Chair *Dr. Sergii Poperezhai*

- 13:30-13:42 Resonant frequency intersection of toroidal modes in all-dielectric metasurface with hexagonal unit cell**

125

O. A. Breslavets¹, Z. E. Eremenko^{1,2}

¹*O.Ya. Usikov Institute for Radiophysics and Electronics Kharkiv, Ukraine*

²*Leibniz Institute for Solid State and Materials Research, Dresden, Germany*

- 14:42-13:54 Combined optical effects in unconventional multilayer metamaterial structures**

126

A. F. Bukhanko

Donetsk Institute for Physics and Engineering named after O.O. Galkin, Kyiv, Ukraine

- 13:54-14:06 Enhancement of optical chiral sensing with subwavelength gratings**

127

O. Demianyk¹, S. Polevoy², V. Tuz¹, O. Yermakov^{1,3}

¹*V.N. Karazin Kharkiv National University, Kharkiv, Ukraine*

²*O.Ya. Usikov Institute for Radiophysics and Electronics Kharkiv, Ukraine*

³*Leibniz Institute of Photonic Technology, Jena, Germany*

- 14:06-14:18 Experimental determination of emission cross sections for electron-induced processes in a supersonic argon jet**

128

Yu. S. Doronin, A. A. Tkachenko, V. L. Vakula, G. V. Kamarchuk

B.Verkin Institute for Low Temperature Physics and Engineering, Kharkiv, Ukraine

14:18-14:30	Engineering plasmon canalization for resonant plasmonic metasurfaces	129
	<u>A. Hrinchenko</u> ¹ , S. Polevoy ² , O. Demianyk ¹ , O. Yermakov ^{1,3}	
	¹ <i>V.N. Karazin Kharkiv National University, Kharkiv, Ukraine</i>	
	² <i>O.Ya. Usikov Institute for Radiophysics and Electronics Kharkiv, Ukraine</i>	
	³ <i>Leibniz Institute of Photonic Technology, Jena, Germany</i>	
14:30-14:42	Optical scattering for ground combat capabilities	130
	<u>O. G. Nerukh</u> ¹ , <u>L. N. Illyashenko</u> ²	
	¹ <i>Kharkiv National University of Radio Electronics, Kharkiv, Ukraine</i>	
	² <i>National Academy of the National Guard of Ukraine, Zolochiv, Lviv Region, Ukraine</i>	
14:42-14:54	Control of Brewster's angle with plasmonic metasurfaces	131
	<u>O. Mankovska</u> ¹ , T. Shudra ² , A. Hrinchenko ³ , O. Yermakov ^{3,4}	
	¹ <i>Ivan Franko National University of Lviv, Lviv, Ukraine</i>	
	² <i>School "Basis", Kyiv, Ukraine</i>	
	³ <i>V.N. Karazin Kharkiv National University, Kharkiv, Ukraine</i>	
	⁴ <i>Leibniz Institute of Photonic Technology, Jena, Germany</i>	
14:54-15:06	Features of oxazine laser dyes in solvents of different polarity and proton donor activity	132
	<u>V. V. Maslov</u> ¹ , I. M. Pritula ²	
	¹ <i>O.Ya. Usikov Institute for Radiophysics and Electronics Kharkiv, Ukraine</i>	
	² <i>Institute for Single Crystals of NAS of Ukraine, Kharkiv, Ukraine</i>	
15:06-15:18	Aggregation features of cyanine dyes in a liquid crystalline environment	133
	<u>I. Yu. Ropakova</u> ^{1,2} , O. M. Samoilov ¹ , O. V. Sorokin ¹ , L. N. Lisetski ¹ , S. L. Yefimova ¹	
	¹ <i>Institute for Scintillation Materials of NAS of Ukraine, Kharkiv, Ukraine</i>	
	² <i>Dipartimento di Scienza dei Materiali, Università degli Studi Milano-Bicocca, Milano, Italy</i>	

15:20-16:00**BREAK****PLenary Lectures of Invited Speakers**Chair *Dr. Sergii Poperezhai*

16:00-16:30	OCT versus (and in complementarity with) X-ray biomedical imaging	42
	<u>V.-F. Duma</u> ¹⁻³ and R.-A. Erdelyi ¹	
	¹ <i>Polytechnic University of Timisoara, Timisoara, Romania</i>	
	² <i>Aurel Vlaicu University of Arad, Arad, Romania</i>	
	³ <i>National University of Science and Technology POLITEHNICA Bucharest, Bucharest, Romania</i>	

OPTICS, PHOTONICS AND OPTICAL SPECTROSCOPYChair *Dr. Sergii Poperezhai*

16:30-16:42	The influence of electron irradiation on the emission spectra of glucose and fructose in a gas discharge plasma	136
	<u>Yu. Bandurin, E. Svitlichnyi</u> <i>Institute of Electron Physics of NAS of Ukraine, Uzhhorod, Ukraine</i>	

16:42-16:54	Increasing the sensitivity of a surface plasmon resonance biosensor based on the Kretschmann configuration using Ti₃C₂T_x-MXene nanomaterial	138
	R. S. Terekhov¹, Z. E. Eremenko^{1,2}, S. M. Kulish³	
	¹ <i>O.Ya. Usikov Institute for Radiophysics and Electronics Kharkiv, Ukraine</i>	
	² <i>Leibniz Institute of Photonic Technology, Jena, Germany</i>	
	³ <i>National Aerospace University "Kharkiv Aviation Institute", Kharkiv, Ukraine</i>	
16:56-17:08	Dielectric metasurfaces for light control: polarizer, collector, demultiplexer and anti-reflector	139
	A. Ovcharenko¹, S. Polevoy², K. Nemchenko¹, V. Tuz¹, O. Yermakov^{1,3}	
	¹ <i>V.N. Karazin Kharkiv National University, Kharkiv, Ukraine</i>	
	² <i>O.Ya. Usikov Institute for Radiophysics and Electronics Kharkiv, Ukraine</i>	
	³ <i>Leibniz Institute of Photonic Technology, Jena, Germany</i>	
17:08-17:20	Study of gas-discharge plasma properties in mixtures of inert gases with selenium vapor	137
	A. General, E. Svitlichnyi	
	<i>Institute of Electron Physics of NAS of Ukraine, Uzhhorod, Ukraine</i>	

WORKSHOP: OPPORTUNITIES AND TECHNOLOGIES FOR RESEARCHERS

Chair Dr. Diana Hurova

17:25-17:55	LabsArena.com: connecting researchers, laboratories, and manufacturers to unlock new opportunities and boost global research	65
	R. M. Basnukaeva, B. O. Postolnyi	
	<i>LabsArena.com</i>	
17:55-18:25	Nanofabrication of Josephson junctions	66
	Maryna Dryhailo^{1,2}	
	¹ <i>CEA-Leti, Grenoble, France</i>	
	² <i>Université Grenoble-Alpes, Saint-Martin-d'Hères, France</i>	

THURSDAY, 5th of JUNE

PLENARY LECTURES OF INVITED SPEAKERS

Chair Dr. Yevhen Petrenko

10:00-10:40	Variations on a theme of Aharonov and Bohm	37
	Michael Berry	
	<i>University of Bristol, Bristol, United Kingdom</i>	
10:40-11:10	Low-temperature phase transitions in hybrid organic-inorganic halo-bismuthates (III) and halo-antimonates (III)	38
	A. Gągor	
	<i>Institute for Low Temperatures and Structure Research, Wroclaw, Poland</i>	

MATERIALS SCIENCE

Chair *Dr. Yevhen Petrenko*

11:10-11:22	Study of the thermal conductivity of pressed nanocarbon materials at low temperatures	215
	<u>D. Sokolov</u> ^{1,2} , K. Vorobieva ¹ , O. Vorobyova ^{1,2}	
	¹ <i>Al-Farabi Kazakh National University, Almaty, Kazakhstan</i>	
	² <i>Almaty Technological University, Almaty, Kazakhstan</i>	
11:22-11:34	Truncated Coulomb potential for planar channeling	216
	<u>M. V. Bondarenco</u> ^{1,2} , N. S. Moskvitin ^{1,2}	
	¹ <i>NSC Kharkov Institute of Physics and Technology of NAS of Ukraine, Kharkiv, Ukraine</i>	
	² <i>V.N. Karazin Kharkov National University, Kharkiv, Ukraine</i>	
11:34-11:46	The ordering of defects controlled by the symmetry of the CdI₂ crystal lattice: justification and experimental confirmation	217
	<u>N. Tovstyuk</u> ¹ , M. Rudka ¹ , O. Bilenka ¹ , F. Ivashchyshyn ¹ , M. Karkuliovskaya ¹ , B. Seredyuk ²	
	¹ <i>Lviv Polytechnic National University, Lviv, Ukraine</i>	
	² <i>Hetman Petro Sahaidachnyi National Army Academy, Lviv, Ukraine</i>	
11:46-11:58	Up-conversion and luminescent properties of SiO₂-CaF₂:Pr³⁺ nanoceramics	218
	<u>O. Bezkrovna</u> ^{1,2} , R. Lisiecki ¹ , P. J. Dereń ¹	
	¹ <i>Institute of Low Temperature and Structure Research, Wrocław, Poland</i>	
	² <i>Institute for Single Crystals of NAS of Ukraine, Kharkiv, Ukraine</i>	
11:58-12:10	Connection of cryogenic pipelines made of different metals by bimetallic adapters	225
	L. M. Lobanov, <u>A. G. Bryzgalin</u> , E. D. Pekar, N. A. Pashin, O. L. Mikhodui, L. M. Malakhova	
	<i>E. O. Paton Electric Welding Institute, Kyiv, Ukraine</i>	
12:10-12:22	Study of structural, electronic, optical, and thermodynamic properties of RbGeI₃ perovskite using DFT	215
	T. Abera	
	<i>Wachemo University, Hossana, Ethiopia</i>	
12:22-12:34	Low-temperature ultrasonic investigations of CoCrFeMnNi high-entropy alloy doped with vanadium	221
	V. S. Klochko, <u>A. V. Korniets</u> , V. I. Sokolenko, I. V. Kolodiy, O. O. Kondratov, I. F. Kislyak, Yu. S. Lipovska, M. A. Tikhonovsky, T. M. Tikhonovska	
	<i>National Science Center "Kharkiv Institute of Physics and Technology" Kharkiv, Ukraine</i>	
12:34-12:46	Particularity of relaxation of mechanical properties of polyimide films of the Kapton H type at different strain rates after long-term exposure at environmental conditions	222
	V. A. Lototskaya	
	<i>B.Verkin Institute for Low Temperature Physics and Engineering, Kharkiv, Ukraine</i>	
12:46-12:58	Energetics of carbon-related defects in YAG and their role in controlling the concentration of anion and cation vacancies	223
	<u>K. V. Hermash</u> ¹ , D. V. Fil ^{1,2}	
	¹ <i>Institute for Single Crystals of NAS of Ukraine, 60 Nauky Avenue, Kharkiv, Ukraine</i>	
	² <i>V.N. Karazin Kharkov National University, Kharkiv, Ukraine</i>	

12:58-13:10	Investigation of electrophysical properties, phase diagrams and charge carrier transfer in $\text{Bi}_{1-x}\text{Sm}_x\text{FeO}_3$ nanopowders	224
	<u>V. O. Kolupaiev, A. N. Morozovska, V. N. Poroshin, and O. S. Pylypchuk</u>	
	<i>Institute of Physics of NAS of Ukraine, Kyiv, Ukraine</i>	
13:10-14:00	BREAK	
<i>Chair</i>	<i>Dr. Denys Laptiev</i>	
14:00-14:30	Wave phenomena in Josephson junction ladders: breathers, flat bands and more	59
	<u>Y. Zolotaryuk</u>	
	<i>Bogolyubov Institute for Theoretical Physics, Kyiv, Ukraine</i>	
14:30-15:00	Studying the properties of spin systems and their quantum states using quantum programming	45
	<u>Kh. P. Gnatenko</u>	
	<i>Ivan Franko National University of Lviv, Lviv, Ukraine</i>	
<hr/> THEORY OF CONDENSED MATTER PHYSICS <hr/>		
<i>Chair</i>	<i>Dr. Denys Laptiev</i>	
15:00-15:12	Density of states and differential entropy in graphene in crossed magnetic and in-plane electric fields	253
	<u>Andrii A. Chaika, Yelizaveta Kulynych, D. O. Oriekhov, and Sergei G. Sharapov</u>	
	<i>Bogolyubov Institute for Theoretical Physics, Kyiv, Ukraine</i>	
15:12-15:24	On inhomogeneous equilibrium states in single-sublattice high-spin magnets	254
	<u>M. Yu. Kovalevsky</u>	
	<i>National Science Center "Kharkiv Institute of Physics and Technology" Kharkiv, Ukraine</i>	
15:24-15:36	Flexo-sensitive ferrons in Van der Waals ferrielectrics at low temperatures	255
	<u>Oleksii V. Bereznykov¹, Anna N. Morozovska¹, Eugene. A. Eliseev²,</u>	
	<u>Mykola Ye. Yelisieiev³, Guo-Dong Zhao⁴, Yujie Zhu⁵, Venkatraman Gopalan⁴,</u>	
	<u>Long-Qing Chen⁴, Jia-Mian Hu⁵, and Yulian M. Vysochanskii⁶</u>	
	¹ <i>Institute of Physics, National Academy of Sciences of Ukraine, Kyiv, Ukraine</i>	
	² <i>Frantsevich Institute for Problems in Materials Science, Kyiv, Ukraine</i>	
	³ <i>Institute of Semiconductor Physics, Kyiv, Ukraine</i>	
	⁴ <i>Pennsylvania State University, University Park, PA, USA</i>	
	⁵ <i>University of Wisconsin-Madison, Madison, WI, USA</i>	
	⁶ <i>Institute of Solid-State Physics and Chemistry, Uzhhorod University, Uzhhorod, Ukraine</i>	
15:36-15:48	Measurement-induced phase transitions in the Lipkin-Meshkov-Glick spin model	256
	<u>P. O. Kofman^{1,2}, N. Samos¹, P. Ribeiro^{1,3}</u>	
	¹ <i>Instituto Superior Tecnico, Universidade de Lisboa, Lisbon, Portugal</i>	
	² <i>B.Verkin Institute for Low Temperature Physics and Engineering, Kharkiv, Ukraine</i>	
	³ <i>Beijing Computational Science Research Center, Beijing, China</i>	
15:48-16:00	Maximization of squeezing and amplification in open quantum systems in the Jaynes-Cummings model by means of Holstein-Primakoff transformations	257
	<u>R. T. Oysiannikov¹, D. I. Bondar², K. Jacobs^{3,4}, A. G. Sotnikov¹</u>	
	¹ <i>NSC «Kharkiv Institute of Physics and Technology», Kharkiv Ukraine</i>	
	² <i>Tulane University, New Orleans, Louisiana, United States</i>	
	³ <i>United States Army Research Laboratory, Adelphi, Maryland, USA</i>	
	⁴ <i>University of Massachusetts at Boston, Boston, Massachusetts, USA</i>	

16:00-16:12	Interaction-induced directional tunneling through asymmetric potential barriers in the Fermi-Hubbard lattice model	258
	<u>S. S. Litvinova¹, A. G. Sotnikov^{1,2}</u>	
	¹ <i>V.N. Karazin Kharkiv National University, Kharkiv, Ukraine</i>	
	² <i>Akhiezer Institute for Theoretical Physics, Kharkiv, Ukraine</i>	
16:12-16:24	Application of Kolmogorov-Arnold-network-based neural quantum states for continuous many-body systems	259
	<u>M. O. Luhanko¹, I. V. Lukin², D. I. Bondar³, A. G. Sotnikov^{1,2}</u>	
	¹ <i>V.N. Karazin Kharkiv National University, Kharkiv, Ukraine</i>	
	² <i>Akhiezer Institute for Theoretical Physics, Kharkiv, Ukraine</i>	
	³ <i>Tulane University, New Orleans, Louisiana, United States</i>	
16:24-16:36	Comparison of viscoelastic properties of fluorosubstituted aliphatic alcohols using an artificial neural network	260
	<u>O. V. Khorolskyi¹, A. M. Hetalo¹, Ye. G. Rudnikov^{2,3}</u>	
	¹ <i>Poltava V. G. Korolenko National Pedagogical University, Poltava, Ukraine</i>	
	² <i>Taras Shevchenko National University of Kyiv, Kyiv Ukraine</i>	
	³ <i>National Technical University of Ukraine "Igor Sikorsky Kyiv Polytechnic Institute", Kyiv, Ukraine</i>	
16:36-16:48	The effect of inelastic scattering on the resonant peak in a binary alloy type model	261
	<u>D. A. Dobushovskyi, A. M. Shvaika</u>	
	<i>Institute for Condensed Matter Physics of NAS of Ukraine, Lviv, Ukraine</i>	

16:50-17:30**BREAK****PLENARY LECTURES OF INVITED SPEAKERS**

Chair Dr. Yevhen Petrenko

17:30-18:00	Controlling quantum coherence in diluted spin systems	60
(10:30 UTC-4)	I. Chiorescu	
	<i>Florida State University, Tallahassee, Florida, USA</i>	
18:00-18:30	Novel quantum dynamics with superconducting qubits	51
(08:00 UTC-7)	Pedram Roushan	
	<i>Google Quantum AI, Santa Barbara, USA</i>	
18:30-19:00	Radiation physics and chemistry in low temperature molecular ices: applications to astrochemistry and astrobiology	48
(08:30 UTC-7)	<u>Duncan V. Mifsud¹, Péter Herczku¹, Zuzana Kaňuchová², Béla Sulik¹, Gergő Lakatos^{1,3}, Richárd Rácz¹, Sándor Biri¹, Sergio Ioppolo⁴, Zoltán Juhász¹, and Nigel J. Mason^{1,5}</u>	
	¹ <i>HUN-REN Institute for Nuclear Research, Debrecen, Hungary</i>	
	² <i>Slovak Academy of Sciences, Tatranska Lomnica, Slovakia</i>	
	³ <i>University of Debrecen, Debrecen, Hungary</i>	
	⁴ <i>University of Aarhus, Aarhus, Denmark</i>	
	⁵ <i>University of Kent, Canterbury, United Kingdom</i>	

FRIDAY, 6th of JUNE

PLENARY LECTURES OF INVITED SPEAKERS

Chair *Dr. Oleksii Konotop*

- 10:00-10:30 Local surface properties as guides to chemical reactivity in nanostructured systems** 40

Tore Brinck

KTH Royal Institute of Technology, Stockholm, Sweden

- 10:30-11:00 On collective phenomena in one-dimensional networks of threshold-type memristors** 54

V. A. Slipko¹, Yu. V. Pershin²

¹*Institute of Physics, Opole University, Opole, Poland*

²*Department of Physics and Astronomy, University of South Carolina, Columbia, SC, USA*

TECHNOLOGIES AND INSTRUMENTATION FOR PHYSICAL EXPERIMENTS

Chair *Dr. Oleksii Konotop*

- 11:00-11:12 Global perturbations of the ionosphere during the geospace storm on September 11-21, 2024** 277

L. F. Chernogor, V. O. Bessarabova

V. N. Karazin Kharkiv National University, Kharkiv, Ukraine

- 11:12-11:24 Analysis of total electron content disturbances in the ionosphere on May 10–11, 2024, caused by high solar activity** 278

L. F. Chernogor, R. M. Kovalov, M. B. Shevelev

V. N. Karazin Kharkiv National University, Kharkiv, Ukraine

- 11:24-11:36 Highly informative format for comprehensive analysis of space weather conditions** 279

L. F. Chernogor, D. R. Kulyk

V. N. Karazin Kharkiv National University, Kharkiv, Ukraine

- 11:36-11:48 Amorphous Mo_{1-x}Si_x films for quantum systems applications** 280

O. O. Leha¹, V. Yu. Lyakhno^{1,2}, I. O. Martynenko², S. V. Bengus¹,
O. G. Turutanov^{3,1}

¹*B.Verkin Institute for Low Temperature Physics and Engineering, Kharkiv, Ukraine*

²*G.V. Kurdyumov Institute for Metal Physics, Kyiv, Ukraine*

³*Comenius University, Bratislava, Slovakia*

- 11:48-12:00 Method of detonation velocity measuring of the condensed explosives** 281

E. D. Pekar, A. G. Bryzgalin, N. A. Pashin, S. D. Ventsev, L. M. Malakhova
E.O. Paton Electric Welding Institute, Kyiv, Ukraine

- 12:00-12:12 System spectral analysis of infrasonic wave disturbances caused by the Tonga supervolcano eruption on January 15, 2022** 282

L. F. Chernogor¹, O. I. Liashchuk², N. M. Tilichenko¹, M. B. Shevelev¹

¹*V. N. Karazin Kharkiv National University, Kharkiv, Ukraine*

²*National Center for Control and Testing of Space Means of the State Space Agency of Ukraine, Horodok, Zhytomyr region, Ukraine*

12:12-12:24	Global response of total electron content of ionosphere during powerful geospacer storm on November 4-5, 2023	283
	<u>M. Yu. Tkachenko</u> , L. F. Chernogor	
	<i>V. N. Karazin Kharkiv National University, Krarkiv, Ukraine</i>	
12:24-12:36	Computer modeling of a nitrogen-cooled cryopanel	284
	<u>O. Vorobyova</u> ^{1,2} , D. Sokolov ^{1,2} , Ye. Korshikov ¹	
	¹ <i>Al-Farabi Kazakh National University, Almaty, Kazakhstan</i>	
	² <i>Almaty Technological University, Almaty, Kazakhstan</i>	

PLENARY LECTURES OF INVITED SPEAKERS

Chair *Dr. Oleksii Konotop*

12:40-13:10	New ionic conductors based on salts of hypodiphosphoric acid, H₄P₂O₆	61
	<u>Vasyl Kinzhylalo</u>	
	<i>Institute for Low Temperatures and Structure Research, Wroclaw, Poland</i>	

13:10-13:40	BREAK
--------------------	--------------

THEORY OF CONDENSED MATTER PHYSICS

Chair *Dr. Denys Laptiev*

13:40-13:52	Two-qubit detector of microwave photons	262
	<u>O. A. Ilinskaya</u> , S. N. Shevchenko	
	<i>B.Verkin Institute for Low Temperature Physics and Engineering, Kharkiv, Ukraine</i>	
13:52-14:04	Implementing signal processing algorithms using the adiabatic-impulse model	263
	<u>O. V. Ivakhnenko</u> ^{1,2} , D. O. Shendryk ^{1,3} , S. N. Shevchenko ¹ , and F. Nori ^{2,4}	
	¹ <i>B.Verkin Institute for Low Temperature Physics and Engineering, Kharkiv, Ukraine</i>	
	² <i>Center for Quantum Computing, RIKEN, Wakoshi, Saitama, Japan</i>	
	³ <i>Ruhr-Universität Bochum, Germany</i>	
	⁴ <i>Physics Department, University of Michigan, Ann Arbor, MI, USA</i>	

14:04-14:16	Tunneling transport in semiconductor nanostructures considering the presence of a weak time-dependent electromagnetic field: Lewis-Riesenfeld approach	264
	<u>I. V. Boyko</u> ¹ , Ju. O. Seti ²	
	¹ <i>Ternopil Ivan Puluj National Technical University, Ternopil, Ukraine</i>	
	² <i>Lviv Polytechnic National University, Lviv, Ukraine</i>	

14:16-14:28	The fluxon interaction with the dipole impurity in the Josephson transmission line	265
	<u>Ivan. O. Starodub</u> , Yaroslav Zolotaryuk	
	<i>Bogolyubov Institute for Theoretical Physics of the NAS of Ukraine, Kviv, Ukraine</i>	

14:28-14:40	Longitudinal Josephson effect in two-layer systems with electron-hole pairing	266
	<u>S. I. Shevchenko</u> , <u>O. M. Konstantynov</u>	
	<i>B.Verkin Institute for Low Temperature Physics and Engineering, Kharkiv, Ukraine</i>	

14:40-14:48	Dynamics of small fluctuations in Boltzmann kinetics	267
	<u>A. I. Sokolovsky</u> , S. F. Lyagushyn	
	<i>Oles Honchar Dnipro National University, Dnipro, Ukraine</i>	

15:00-15:30

Closing Remarks
Acting Director of the B. Verkin ILTPE of NAS of Ukraine
Corresponding Member of NAS of Ukraine
Prof. Alexander Dolbin
and
Chair of Organizing Committee Dr. Diana Hurova

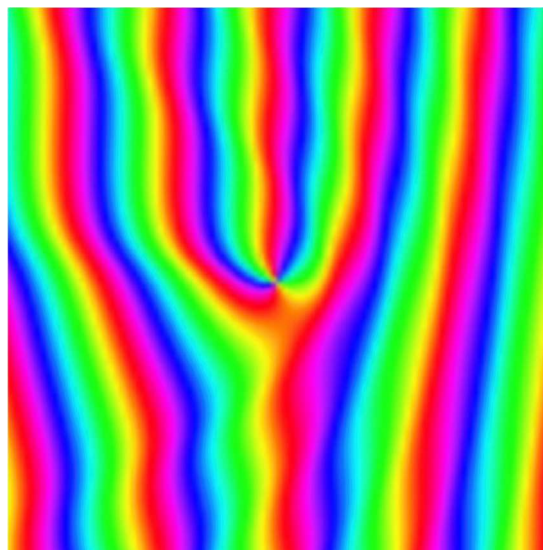
PLENARY LECTURES OF INVITED SPEAKERS

Variations on a theme of Aharonov and Bohm

Michael Berry

*University of Bristol, Beacon House,
Queens Road, Bristol, BS8 1QU, United Kingdom
asymptotico@bristol.ac.uk*

The Aharonov-Bohm effect (AB) concerns the role in quantum physics of the magnetic vector potential of an impenetrable line of magnetic flux. Its partial anticipation by Ehrenberg and Siday, in terms of interference, was an approximation whose wavefunction was not single valued, and whose connection with the single valued AB wave involves topology: ‘whirling waves’ winding round the flux. AB is a fine illustration of idealization in physics. There are four AB effects, depending on whether the waves and the flux are classical or quantum. In the classical-classical case, many details of the AB wavefunction have been explored experimentally in ripples scattered by a water vortex, where the flow velocity of the water corresponds to the vector potential. The AB wave possesses a phase singularity, and there is a similar phenomenon in general interferometers. Gauge-invariant AB streamlines exhibit extraordinary sub-wavelength structure. Connections between the AB wave and the Cornu spiral describing edge diffraction lead to extremely accurate approximations.



Microwave electrodynamics of spin-triplet superconductor UTe₂

Arthur Carlton-Jones,¹ Nicholas P. Butch,^{1,2} Johnpierre Paglione,¹ and Steven M. Anlage¹

¹*Maryland Quantum Materials Center, Physics Department, University of Maryland, College Park, MD 20742, USA*

²*NIST Center for Neutron Research, National Institute of Standards and Technology, Gaithersburg, Maryland 20899, USA*

e-mail: anlage@umd.edu website: <https://anlage.umd.edu>

The complex surface impedance is a well-established tool to study the super- and normal-fluid responses of superconductors. Fundamental properties of the superconductor, such as the pairing mechanism, Fermi surface, and topological properties, also influence the surface impedance [1]. We explore the microwave surface impedance of spin-triplet UTe₂ single crystals as a function of temperature using resonant cavity perturbation measurements (Fig. 1) employing a novel multi-modal analysis to gain insight into these properties. We determine a composite surface impedance of the crystal for each mode using resonance data combined with the independently measured normal state dc resistivity tensor [2]. The normal state surface impedance reveals the weighting of current flow directions in the crystal of each resonant mode. For UTe₂, we find an isotropic $\Delta\lambda(T) \sim T^\alpha$ power-law temperature dependence for the magnetic penetration depth for $T \leq T_c/3$ with $\alpha < 2$, which is inconsistent with a single pair of point nodes on the Fermi surface under weak scattering. We also find a similar power-law temperature dependence for the low-temperature surface resistance $R_s(T) \sim T^{\alpha_R}$ with $\alpha_R < 2$. We observe a strong anisotropy of the residual microwave loss across these modes, with some modes showing loss below the universal line-nodal value, to those showing substantially more. We compare to predictions for topological Weyl superconductivity in the context of the observed isotropic power-laws, and anisotropy of the residual loss.

Acknowledgement: Work supported by NSF-DMR/2004386, and ARO/FSDL under grant W911NF-24-1-0153.

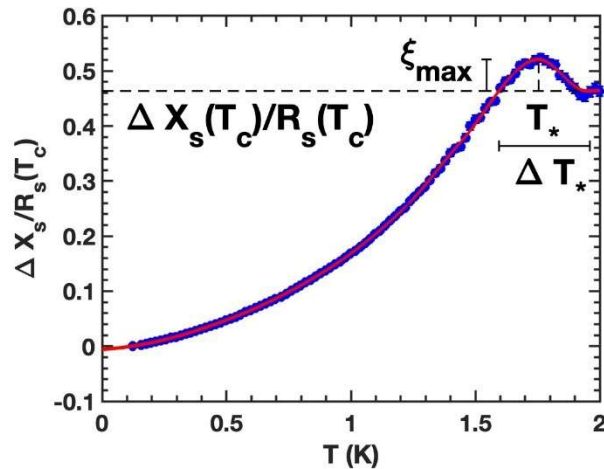


Fig. 1 Examination of surface reactance peak $X_s(T)$ below T_c in UTe₂ single crystal B39 measured at 6.77 GHz. The plot utilizes only raw frequency shift and quality factor data from a temperature-dependent cavity perturbation experiment [1]. The outcome is an assumption-free estimation of the quasiparticle relaxation time $\omega\tau$ at temperature T_* [2].

[1] Seokjin Bae, et al., “Anomalous normal fluid response in a chiral superconductor,” Nature Communications 12:2644 (2021). <https://doi.org/10.1038/s41467-021-22906-6>.

[2] Arthur Carlton-Jones, et al., “Revealing isotropic sub-gap excitations in UTe₂ through complex microwave surface impedance,” arXiv:2502.07955.

AC Hanle effect and spin wave generation on a single F/N interface

Ya. B. Bazaliy

*Department of Physics and Astronomy, University of South Carolina,
712 Main St., Columbia, SC 29208, USA
e-mail: bazaliy@mailbox.sc.edu*

It is known [1] that ac spin current flowing through an F/N/F spin valve in the absence of magnetic field produces results reminiscent of the Hanle effect, with current frequency playing the role of the external magnetic field. Here we study the combination of two effects with ac current and magnetic field both present. In such "alternating current Hanle effect", interesting effects are observed already at a single F/N interface. In particular, a resonance-like dependence of interface voltage was predicted [1]. Here we show that in addition, the field-induced precession of electron spins in the normal part of the structure leads to the generation of spin torque on a single F/N interface. This torque excites magnetic dynamics in the F-layer, which, in turn, provides some back-action on current propagation. We solve self-consistent equations for spin current, electric current and magnetization, coupled by the non-linear boundary conditions at the interface. The non-linearity leads to voltage rectification, much like it happens in the F/N/F spin diode [2]. On top of that, ac Hanle effect is predicted to produce spin waves propagating into the depth of the F-layer, with a possibility of detection far away from the interface.

- [1] D. Kochan, M. Gmitra, and J. Fabian, "Theory of the ac Spin-Valve Effect", Phys. Rev. Lett. 107, 176604 (2011).
- [2] Ya. B. Bazaliy, "Alternating current Hanle effect as poor man's paramagnetic resonance", Phys. Rev. B 109, 224427 (2024).
- [3] A. A. Tulapurkar, Y. Suzuki, A. Fukushima, H. Kubota, H. Maehara, K. Tsunekawa, D. D. Djayaprawira, N. Watanabe, and S. Yuasa, "Spin-torque diode effect in magnetic tunnel junctions", Nature 438, 339 (2005).

Local surface properties as guides to chemical reactivity in nanostructured systems

Tore Brinck

*Department of Chemistry, CBH, KTH Royal Institute of Technology,
SE-100 44 Stockholm, Sweden
e-mail: tore@kth.se*

The molecular electrostatic potential computed on a surface defined by constant electron density is widely used for analysis and prediction of non-covalent interactions, such as halogen and hydrogen bonding [1]. We have recently shown that the surface electrostatic potential (VS(r)) can be an effective tool also for the analysis of chemical interactions within extended systems, such as nanoparticles and crystalline surfaces. In particular, we have found that the well-known nanostructural effects in gold catalysis can be rationalized from VS(r) [2, 3]. The catalytic activity in nanostructured systems is often explained by an increased binding affinity for Lewis bases at low-coordinated sites, such as corners of nanoparticles, and the reason is that these sites have a high surface electrostatic potential. A similar mechanism also explains the increased reactivity at defects on crystalline metal surfaces. Several examples will be presented on the effects of metal defects on the VS(r). I will also show that the variation of VS(r) with geometric and elemental surface structure can be used as guide in the development of heterogenous electrocatalysts. The VS(r) plays an integral role in the ligand binding in electrochemical reactions of ions and polar molecules and often determines reaction selectivity [4-6].

Two other DFT-based surface properties, the average local ionization energy and the local electron attachment energy, will also be introduced which are better than VS(r) for analyzing strong interactions that lead to the formation of covalent bonds [1, 3]. I will emphasize similarities with the well-known d-band model for metallic systems, but also demonstrate how these properties extend the predictive domain to insulators and semi-conductors and allow for the prediction of local reactivity in large nanostructured systems.

- [1] T. Brinck, and J.H. Stenlid, *Adv. Theory Simul.* 2, 1800149 (2019).
<http://dx.doi.org/10.1002/adts.201800149>.
- [2] J.H. Stenlid, and T. Brinck, *J. Am. Chem. Soc.* 139, 11012 (2017).
<http://pubs.acs.org/doi/full/10.1021/jacs.7b05987>.
- [3] J.H. Stenlid, A.J. Johansson, and T. Brinck, *Phys. Chem. Chem. Phys.* 21, 17001 (2019).
<http://dx.doi.org/10.1039/C9CP03099A>.
- [4] S. Choi, C. Liu, D.H. Seo, S.W. Im, R.M. Kim, J. Jo, J.W. Kim, G.-S. Park, M. Kim, T. Brinck, and K.T. Nam, *Nano Lett.* 24, 4528 (2024). <https://doi.org/10.1021/acs.nanolett.4c00413>.
- [5] J.J. Wang, H.T.D. Bui, X. Wang, Z. Lv, H. Hu, S. Kong, Z. Wang, L. Liu, W. Chen, H. Bi, M. Yang, T. Brinck, J. Wang, and F. Huang, *J. Am. Chem. Soc.* 147, 8012 (2025).
<https://doi.org/10.1021/jacs.5c00837>.
- [6] J.J. Wang, H.T.D. Bui, H. Hu, S. Kong, X. Wang, H. Zhu, J. Ma, J. Xu, Y. Liu, L. Liu, W. Chen, H. Bi, M. Yang, F. Huang, T. Brinck, and J. Wang, *Adv. Mater.* n/a, 2418451 (2025).
<https://doi.org/10.1002/adma.202418451>.

Physicochemical properties of hazardous carbon smoke nanoparticles with heavy metals

G. I. Dovbeshko^{1,2}, T. O. Borisova^{1,2}, O. Bezkrovnyi², O. P. Gnatyuk^{1,2}, A. S. Tolochko¹, V. V. Boiko^{1,2}, W. Strek²

¹*Institute of Physics, National Academy of Sciences of Ukraine,
46 Nauky Ave, Kyiv, 03028, Ukraine*

²*Institute for Low Temperatures and Structure Research, Polish Academy of Sciences,
P.O. Box 1410, 50-950 Wroclaw, Poland
e-mail: matinelli@gmail.com*

In modern situation in Ukraine with huge artillery shelling and missile attacks, a large amount of pollution consisting of carbon particles with heavy metals and remains of organic molecules are formed. This is why modeling these particles and collecting them is important for understanding how they affect human health.

Earlier a method for obtaining nanohybrids based on carbon particles was developed in the Palladin Institute of Biochemistry NAS of Ukraine and applied for biochemical tasks [1]. Here it was used to obtain carbon hybrids with Fe ions of different valence (3+ and 2+).

Methods of optical and luminescent spectroscopy, dynamic light scattering (DLS), elemental analysis and TEM microscopy were applied. Experiments have shown that the particles formed by burning wood and then adding metal ions are a carbon core modified with various functional groups and metals.

The luminescent spectroscopy data showed that carbon particles with Fe of both valences are similar to luminescent spectra of carbon quantum dots with specific features. Size of particles are registered in wide regions from nm to tens of μm . Different molecular groups belonging to hazard aromatic molecules was observed also. The data obtained allow us to conclude about the potential toxicity of these nanoparticles for human health not only in Ukraine, but also on the entire European continent.

ACKNOWLEDGMENTS

This work was supported by the Polish Academy of Sciences in collaboration with U.S. National Academy of Sciences within the “Long-term program to support Ukrainian research teams”, Project “War_derived air pollution nanohybrids composed of carbon-containing smoke nanoparticles and metal compounds: FTIR/Raman spectroscopic, fluorescent and membrane-active properties, their potential neurotoxicity and its prevention”. Project PAN.BFB.S. BWZ.380.022.2023.

- [1] N. Krisanova, N. Pozdnyakova, A. Pastukhov, M. Dudarenko, A. Tarasenko, A. Borysov, M. Driuk, A. Tolochko, O. Bezkrovnyi, K. Paliienko, R. Sivko, O. Gnatyuk, G. Dovbeshko, T. Borisova Food and Chemical toxicity, 193, 115009, (2024). <https://doi.org/10.1016/j.fct.2024.115009>.

OCT versus (and in complementarity with) X-ray biomedical imaging

V.-F. Duma¹⁻³ and R.-A. Erdelyi¹

¹*Faculty of Electronics, Telecommunications, and Information Technology,*

Polytechnic University of Timisoara, Bd. Vasile Parvan nr. 2, Timisoara 300223, Romania

²*3OM Optomechatronics Group, Faculty of Engineering, Aurel Vlaicu University of Arad,*

Str. Elena Dragoi no. 2, 310177 Arad, 3 Vasile Milea Ave, Arad 310131, Romania

³*National University of Science and Technology POLITEHNICA Bucharest, Center of Research and Development for Mechatronics, Splaiul Independentei 313, Sector 6, Bucharest, Romania*

e-mail: virgil.duma@upt.ro

We have been approaching comparisons between Optical Coherence Tomography (OCT) and a range of other high-end imaging methods, both for the biomedical field and for Non-Destructive Testing (NDT) in industry. The present report presents one of these directions of work, with a focus on Dental Medicine, regarding the assessment of the capabilities of various types of radiographies (as X-ray imaging is the gold standard in the field) and OCT, the latter based on low coherence laser interferometry [1]. We utilized an in-house developed Swept Source (SS) OCT system with a 1310 nm center wavelength. Two types of modern X-ray units were also utilized: Planmeca ProMax 3D Plus (Planmeca, Helsinki, Finland) and Gendex Oralix (Danaher Corporation, Washington DC, USA). OCT has in general a low penetration depth (of 1 to 1.5 mm) and a resolution from 2 μm [2] to the most common of 10 to 15 μm [1,3,4], which is much better than the one that characterizes X-ray imaging in Dentistry - from 150 μm to 75 μm , the latter for Cone Beam-Computed Tomography (CBCT). Therefore, these two methods have contradictory parameters, with a high penetration depth but a lower resolution for all types of radiographies (panoramic, intraoral, CBCT, and cephalometric), especially since a limited radiation dose must be employed in investigating living tissue, according to the ALARA (as-low-as-possible radiation dose) protocol.

The presentation is centered on two of our recent studies:

(1) The first one explored all the possible medical conditions within the oral cavity and divided them in two categories, based on which is the most appropriate investigating method: X-ray imaging or OCT [3]. Thus, the explored medical conditions were divided in: (i) those that require large Fields-of-View (FOV) and high penetration depths, therefore must be investigated only with radiography, e.g., bone fractures, scaffolds, or inflammatory processes; (ii) those that require high resolutions must be investigated with OCT, e.g., issues of the dentine, enamel or soft tissue; (iii) those that are best investigated in a complementarity of X-ray imaging and OCT, e.g., periodontitis, orthodontics, fillings, or dental crowns. Quantitative assessments were demonstrated to require OCT, except for periodontitis and bone assessments. For the most common condition, i.e., cavities, radiographies give errors of even 50%, while OCT provide a good precision.

(2) The second study further demonstrated the synergy of OCT and radiographies as, for the first time to our knowledge, an OCT-based optimization method of X-ray imaging for Dentistry was developed [4]. This *ex vivo* optimization determines the necessary X-ray parameters (i.e., anode voltage, current, exposure time, and radiation dose) by observing with OCT small conditions (e.g., early cavities of fillings) and then increasing the X-ray tube parameters until the targeted dental details become visible. This method was developed both for panoramic radiographies and CBCT. It demonstrates the necessary trade-off between the resolution and the radiation dose.

Acknowledgement: This work was supported by the Romanian IPCEI (Important Project of Common European Interest) on microelectronics, via Continental Automotive Romania.

[1] W. Drexler, et al, J. Biomed. Opt. 19, 071412 (2014). <https://doi.org/10.1117/1.jbo.19.7.071412>.

[2] A. Cogliati, et al., Opt. Express 24, 13365 (2016). <http://dx.doi.org/10.1364/OE.24.013365>.

[3] R.-A. Erdelyi, et al., Materials 13, 4825 (2020). <https://doi.org/10.3390/ma13214825>.

[6] R.-A. Erdelyi, V.-F. Duma, et al. Sensors 21, 4554 (2021). <https://doi.org/10.3390/s21134554>.

Low-temperature phase transitions in hybrid organic-inorganic halo-bismuthates (III) and halo-antimonates (III)

A. Gągor

*Institute for Low Temperatures and Structure Research, Polish Academy of Sciences,
P.O. Box 1410, 50-950 Wrocław, Poland
e-mail: login@inbox.com*

Hybrid organic-inorganic compounds exhibit a range of desirable physicochemical properties, including polarity, ferroelectricity, photovoltaic activity, luminescence, and multiferroicity. This, in combination with facile synthesis and processing, cost-effectiveness, and highly tunable structural parameters make them suitable for applications including solar cells, LEDs, detectors, sensors, scintillators, or nonlinear optical devices [1-2].

Organic-inorganic hybrids integrate the structural rigidity, optical and electronic properties of inorganic components with the flexibility and tunability of organic molecules and crystallize in multiple crystal forms. The most extensively studied are perovskites of ABX_3 formula, where oxygen atoms are replaced by larger ligands (e.g., halides, formates, cyanates), allowing larger molecular cations to fit within crystal cavities at A sites. In contrast, layered A_2BX_4 structures or lower-dimensional inorganic frameworks incorporate molecular spacers without constraints from the inorganic substructure.

A common characteristic of these compounds is their strong temperature dependence, leading to polymorphic phase transitions. Structural complexity, including modulated phases and intricate phase sequences, arises from short-range intermolecular forces, anionic unit flexibility, steric effects, and thermally activated cation dynamics. Hydrogen bonding at the organic-inorganic interface induces distortions of anionic components during molecular ordering, making low-temperature ‘order-disorder’ transitions crucial for phase symmetry and packing.

This contribution, based on single-crystal x-ray diffraction, dielectric spectroscopy, and thermal properties (DSC, DTA, TG), examines the molecular mechanisms underlying phase transitions in halo-antimonates (III) and halo-bismuthates (III) crystallizing with small polar molecules and adopting discrete zero-dimensional and one-dimensional anionic substructures. A common characteristic of discussed materials is their ferroic (ferroelectric or ferroelastic) low-temperature arrangement preceded by a sequence of structural phase-transitions.

The research was supported by the National Science Centre as part of the OPUS 22 project (No. 2021/43/B/ST5/01172).

- [1] B. Saparov, D.B. Mitzi, Chem. Rev. 116, 4558–4596, (2016).
- [2] Y. Han, S. Yue, B.B. Cui, Adv. Sci. 8, 2004805, (2021).

Spectroscopic features of single-walled carbon nanotube films as biosensor elements

A. Glamazda and V. Karachevtsev

*B. Verkin Institute for Low Temperature Physics and Engineering of NAS of Ukraine,
47 Nauky Ave., Kharkiv, 61103, Ukraine
glamazda@ilt.kharkov.ua*

In recent years, studying the physical properties of new multifunctional low-dimensional crystalline materials has been one of the most relevant topics in modern solid-state physics. In these materials, the structural low-dimensionality or the limited propagation of magnetic, electronic, or phonon excitations leads to stimulating of quantum phenomena that are not inherent in bulk materials. Single-walled carbon nanotubes (SWNTs) are 1D nanostructures with unique mechanical, optical, and electronic properties. Their practical applications can be expanded by functionalizing their surfaces with a variety of organic and biological compounds. The alignment of SWNTs in a chosen direction, or the creation of a spatial network of nanotubes, will contribute to increasing the efficiency of energy or charge transfer between neighboring nanotubes. The alignment can be achieved in several ways, and mechanical stretching of polymer films to create a selected direction is the simplest and most effective method. The polymer film plays the role of the protective dielectric layer between neighboring nanotubes, preventing them from sticking together.

The present work is devoted to a review of our activities aimed at creating films of SWNTs in complexes with biological and organic molecules.

The present work was partially supported by the Thematic Program of the Wolfgang Pauli Institute, Ukraine “Mathematics for Biology and Medicine”.

Studying the properties of spin systems and their quantum states using quantum programming

Kh. P. Gnatenco

*Professor Ivan Vakarchuk Department for Theoretical Physics,
Ivan Franko National University of Lviv, 12 Drahomanov St. Lviv, 79005, Ukraine
e-mail: khrystyna.gnatenco@gmail.com*

We propose algorithms for studying the characteristics of evolutionary quantum states of spin systems, as well as the properties of these systems, using quantum programming.

For a system of spins described by the Ising model, we have detected energy levels, the velocity of quantum evolution, and the geometric characteristics of evolutionary quantum states using quantum computations on IBM's quantum simulators and quantum computers [1-3].

The energy levels of the systems have been determined using an original algorithm proposed in [3]. This algorithm is noise-resistant and enables the determination of energy levels for spin systems with arbitrary types of interactions.

The evolutionary states of spin systems governed by the Ising model can be represented as graphs and considered quantum graph states. These states are multi-qubit entangled states that have widespread applications in quantum computing. For these states, we have established a relationship between the properties of spin systems and their quantum states with graph characteristics. Specifically, we show that the geometric characteristics of evolutionary quantum states are related to the sum of the products of edge weights forming triangles and squares, as well as the sum of the weighted degrees of nodes [1]. The geometric measure of entanglement of a qubit with other qubits in quantum graph state is linked to the outdegree and indegree of the corresponding vertex in the graph, weights of ingoing and outgoing arcs with respect to the vertex representing the qubit [2]. To calculate the geometric measure of entanglement its relation with the mean spin obtained in [4] was considered.

Based on the obtained results, we also propose a quantum algorithm for solving the partition problem. This problem involves dividing a set of numbers into two subsets such that the total sum of the numbers in each subset is as close to equal as possible.

- [1] Kh. P. Gnatenco, to appear in Eur. Phys. J. Plus (2025) <http://dx.doi.org/10.1140/epjp/s13360-025-06172-9>, arXiv:2408.01511.
- [2] Kh. P. Gnatenco, Physics Letters A 521, 129815 (2024). <https://doi.org/10.1016/j.physleta.2024.129815>.
- [3] Kh. P. Gnatenco, H. P. Laba, V. M. Tkachuk, Eur. Phys. J. Plus 137(4), 522 (2022). <https://doi.org/10.1140/epjp/s13360-022-02753-0>.
- [4] A. M. Frydryszak, M. I. Samar, V. M. Tkachuk, Eur. Phys. J. D 71 (9), (2017). <https://doi.org/10.1140/epjd/e2017-70752-3>.

Fractional conductances in the strongly interacting one-dimensional system

V. Kagalovsky

*Shamoon College of Engineering, Beer-Sheva, 8410802 Israel
e-mail: victork@sce.ac.il*

This research considers a strongly interacting one-dimensional system with N channels. We study the conditions necessary for the coexistence of various perturbations. The neutrality requirement restricts the most general interaction (beyond forward-scattering quadratic terms in the Lagrangian), meaning that each term in the Hamiltonian conserves the number of particles. To become relevant and open a gap, the perturbation has to represent a new field, and new fields must preserve the form of Lagrangian. Another constraint (formulated by Haldane) is on the type of perturbations allowed to coexist. If particular relevant perturbations freeze some combinations of the fields, it is natural to define a new basis containing these frozen combinations. The matrix describing the transition from the original basis to a new one consisting of frozen and conducting fields defines the physics of the Luttinger liquid, in particular, the properties of the remaining conducting channels. The conductance (in e^2/h units) of the remaining free fields can be presented as the difference between the initial conductance of all N channels and the conductance eliminated by K compatible relevant perturbations that freeze K corresponding fields. The variety of possible combinations of the relevant perturbations provides a variety of possible fractional conductances experimentally observed in GaAs/AlGaAs heterostructures [1-3].

- [1] Y. Gul, S. N. Holmes, M. Myronov, S. Kumar, M. Pepper, J. Phys. Condens. Matter 2018, 30, 09LT01.
- [2] S. Kumar, M. Pepper, S. N. Holmes, H. Montagu, Y. Gul, D. A. Ritchie, I. Farrer, Phys. Rev. Lett. 2019, 122, 086803.
- [3] S. Kumar, M. Pepper, Appl. Phys. Lett. 2019, 119, 110502.

Extremes of ultralow temperatures and high magnetic fields: opportunities for exploring quantum materials

Mark W. Meisel

*Department of Physics and MagLab High B/T Facility,
University of Florida, Gainesville, FL 32611-8440, USA
meisel@ufl.edu*

The mission of the MagLab High B/T Facility (HBT) at the University of Florida is to provide users a safe, welcoming, and unique atmosphere for performing research in high magnetic fields and at ultralow temperatures with an ultra-quiet electromagnetic interference environment. This combination of parameters, which are not commonly available in the home institutions of users, is available for the investigation and characterization of a wide-variety of quantum phenomena and devices. Proposals for using the MagLab HBT Facility, or any of the other MagLab Facilities, may be submitted online [1], and due to the unique techniques and expertise required to explore this frontier of parameter space, potential new users are encouraged to contact an appropriate MagLab scientist in advance of submitting a proposal.

An overview of the MagLab HBT instrumentation and techniques will be given along with some examples of recent, ongoing, and future studies/directions. Specifically, one challenge is cooling the electrons in quantum devices with reduced dimensionality to extremely low temperatures due to the weakening of the electron-phonon coupling, which also then requires further reduction of external heat leaks from electromagnetic interference and noise. The use of pure 3He immersion cells with integrated sintered heat exchanges, which also provide signal filtering, will be described.

This presentation is presented on behalf of the MagLab HBT group consisting of faculty scientists Chao Huan, Rasul Gazizulin, and Sangyun Lee; staff engineer Chris Ollmann; postdoctoral associate Nicolas Silva, and graduate student Alex M. Donald. The National High Magnetic Field Laboratory (MagLab) is supported by the National Science Foundation (NSF) through cooperative agreement DMR-2128556 and the state of Florida.

- [1] National High Magnetic Field Laboratory User Facilities, “Find the User Facility to Meet Your Research Needs”, <https://nationalmaglab.org/user-facilities/>.
- [2] J. Adams, M. Lewkowitz, C. Huan, N. Masuhara, D. Candela, N.S. Sullivan, “Dynamics of 3He in one dimension in the Luttinger liquid limit”, Phys. Rev. B 106, 195402 (2022), <https://doi.org/10.1103/PhysRevB.106.195402>.
- [3] M. Zheng, R. Makaju, R. Gazizulin, A. Levchenko, S. Addamane, D. Laroche, “Tunable contributions from rectification and momentum transfer to 1D Coulomb Drag”, (2024), <https://arxiv.org/abs/2408.12737>.
- [4] M. Zheng, R. Makaju, R. Gazizulin, A. Levchenko, S. Addamane, D. Laroche, “Quasi-1D Coulomb drag in the nonlinear regime”, APS Global Physics Summit, MAR-X20/8 (2025), <https://summit.aps.org/events/MAR-X20/82>, and <https://arxiv.org/abs/2410.17569>.
- [5] M. Zic, C. Huan, N. Silva, Y. Li, M. Meisel, I. Fisher, “Ultralow temperature phase diagram near the quantum critical point in the model nematic insulator TmVO₄”, APS Global Physics Summit, MAR-S26/2 (2025), <https://summit.aps.org/events/MAR-S26/2>.
- [6] A. Donald, R. Gazizulin, A. Duque, C. Jia, S. Li, N. Silva, C. Huan, C. Ollmann, M. Meisel, R. Haley, R. Schanen, “Novel application of adiabatic demagnetization refrigeration”, APS Global Physics Summit, MAR-W26/13 (2025), <https://summit.aps.org/events/MAR-W26/13>.

Radiation physics and chemistry in low temperature molecular ices: applications to astrochemistry and astrobiology

Duncan V. Mifsud¹, Péter Herczku¹, Zuzana Kaňuchová², Béla Sulik¹, Gergő Lakatos^{1,3}, Richárd Rácz¹, Sándor Biri¹, Sergio Ioppolo⁴, Zoltán Juhász¹, and Nigel J. Mason^{1,5}

¹HUN-REN Institute for Nuclear Research, Debrecen H-4026, Hungary

²Slovak Academy of Sciences, Tatranska Lomnicá SK-059 60, Slovakia

³University of Debrecen, Debrecen H-4032, Hungary

⁴University of Aarhus, Aarhus DK-8000, Denmark

⁵University of Kent, Canterbury CT2 7NH, United Kingdom

e-mail: mifsud.duncan@atomki.hu

The interstellar medium (ISM) is molecular in nature, although it puzzled early astronomers and spectroscopists as to how molecules can form in such low-temperature environments that are characterized by high radiation dose rates. Today, it is widely recognized that molecules (including complex organic molecules that may have contributed to the emergence of life) can be formed on the surfaces of or within nano- to microscale ices adsorbed on the surfaces of cosmic dust grains [1]. Among the many drivers of such chemistry, one of the most important is radiation in the form of galactic cosmic rays and stellar winds. Radiation-driven chemistry in ices is also relevant to a number of outer Solar System bodies (e.g., Europa, Enceladus, Pluto); where surface ices are processed through continual exposure to the solar wind [2].

In this presentation, an overview of the astrochemistry laboratory facilities at the HUN-REN Institute for Nuclear Research (Atomki) in Debrecen, Hungary, will be provided [3,4]; along with examples of how the set-ups there can be used to probe the chemistry and physics occurring during the irradiation of low-temperature (>20 K) astrophysical ice analogues. Following this, the topic of ‘sulfur astrochemistry’ will be introduced, along with a major contemporary problem in this field known as the Depleted Sulfur Problem; which refers to the as-yet unexplained observation that the measured quantity of sulfur in the diffuse ISM is in agreement with its expected cosmic abundance, but in the dense ISM it is depleted by up to three orders of magnitude [5]. Following the suggestion that refractory forms of sulfur adsorbed to interstellar dust grains could be a major sink of this element in the dense ISM [6,7], we have performed experiments in which sulfur-rich astrophysical icy grain mantle analogues were prepared by depositing various neat ices (i.e., O₂, CO, CO₂, and H₂O) onto elemental sulfur. These analogues were then irradiated with 1 MeV He⁺ ions at 20 K to determine whether new, sulfur-containing molecules could be formed and what implications this would have for sulfur chemistry in the dense ISM. Some experiments were also repeated at higher temperature (i.e., 70 K) so as to compare the simulated interstellar chemistry with chemistry occurring on the surfaces of sulfur-rich icy bodies in the outer Solar System, such as Jupiter’s moon Europa.

- [1] HM Cuppen, H Linnartz, and S Ioppolo, Annu. Rev. Astron. Astrophys. 62, 243 (2024).
- [2] RL Hudson and MH Moore, J. Geophys. Res. Planet. 106, 33275 (2001).
- [3] P Herczku, DV Mifsud, S Ioppolo, et al. Rev. Sci. Instrum. 92, 084501 (2021).
- [4] R Rácz, STS Kovács, G Lakatos, et al. Rev. Sci. Instrum. 95, 095105 (2024).
- [5] DV Mifsud, Z Kaňuchová, P Herczku, et al. Space Sci. Rev. 217, 14 (2021).
- [6] M Kama, O Shorttle, AS Jermyn, et al. Astrophys. J. 885, 114 (2019).
- [7] S Cazaux, H Carrascosa, GM Muñoz Caro, et al. Astron. Astrophys. 657, A100 (2022).

Phonon thermal conductance of 3D conductors of rectangular cross-section in the ballistic regime

J. Amrit¹, K. Nemchenko², Ye. Nemchenko², S. Rogova², A. Tonkonozhenko², T. Vikhtinskaya²

¹LISN, Université Paris-Saclay, CNRS, 91405, Orsay, France

²V.N.Karazin Kharkiv National University, 61022, Kharkiv, Ukraine

e-mail: egor.nemchenko@karazin.ua

This report presents the study of the thermal conductivity of three-dimensional dielectric thermal conductors with the rectangular cross-section operating in the ballistic regime of phonon propagation. The analysis employs the radiative approximation, wherein phonons are emitted by a heater and cooler maintained at a fixed temperatures, and their interaction with the conductor walls is treated as fully diffusive. The proposed methodology is based on the solution of definite integral equation [1] and allows deriving the explicit analytical equation for the thermal conductivity for any ratios between the length, width and the thickness of the conductor.

The results turn-out to be contrasted with those obtained from the widely accepted linear gradient approach, where external sources impose a fixed temperature gradient [2, 3]. The distinction between these results becomes particularly evident when considering the concept of the "mean free path" of a phonon Λ , a key parameter in the expression $\kappa = \frac{1}{3} C V \Lambda$ for the thermal conductivity coefficient related to the effective velocity V and heat capacity C . For example, for the case of a very long conductor with a rectangular cross-section with sides a and b , we obtain from the general result

$$\Lambda = \frac{3}{2} \frac{ab}{(a+b)} + \frac{3}{4} \left\{ b \ln \left(\frac{a + \sqrt{a^2 + b^2}}{b} \right) + a \ln \left(\frac{b + \sqrt{a^2 + b^2}}{a} \right) + \frac{1}{3} \frac{-(a^2 + b^2)^{3/2} + a^3 + b^3}{ab} \right\}. \quad (1)$$

This expression differs from the result of Refs [2, 3] by the presence of the first term, which is close in order of magnitude to the second term. The physical distinction between these terms stems from the fact that, although the temperature dependence approaches a linear profile as the conductor length L increases, deviations from the linear dependence near both ends persist with a magnitude on the order of $\sqrt{a^2 + b^2}/L$. These deviations generate an additional phonon flux, also on the order of $\sqrt{a^2 + b^2}/L$. At the same time, the phonon flux associated with the linear gradient, given by the second term, is formally a similarly small value on the order of $\sqrt{a^2 + b^2}/L$. Consequently, both contributions appeared to be of the same order of magnitude. In order to compare these terms, we can consider the case of the square cross-section ($b = a$), when the maximum closeness of these terms is achieved and expression (1) simplifies to

$$\Lambda = \frac{3}{2} a \left(\frac{1}{2} + \ln(1 + \sqrt{2}) - \frac{\sqrt{2} - 1}{3} \right) = \frac{3}{2} a \cdot (0.5 + 0.743). \quad (2)$$

Then, in the report, we compare the theoretical predictions with experimental data, underscoring the importance of accounting for the experimental methodology in interpreting and reconciling the observed results with the theoretical framework.

This work was supported by the project “Remote Research Grants for Ukrainian Researchers” that has received funding through the EURIZON project, which is funded by the European Union under grant agreement No.871072.

[1] J. Amrit, K. Niemchenko, Ye. Niemchenko, S. Rogova, T. Vikhtynska, FNT 51, 41(2025). <https://doi.org/10.1063/10.0034642>.

[2] H. B. G. Casimir, Physica V, 495 (1938). [https://doi.org/10.1016/S0031-8914\(38\)80162-2](https://doi.org/10.1016/S0031-8914(38)80162-2).

[3] H.J. Maris, S. Tamura, Phys. Rev. B 85, 054304(2012) <https://doi.org/10.1103/PhysRevB.85.054304>.

Bias-driven quantum matter**Pedro Ribeiro**

*Instituto Superior Técnico, Universidade de Lisboa
Av. Rovisco Pais, Lisbon, 1049-001, Portugal
e-mail: ribeiro.pedro@tecnico.ulisboa.pt*

This talk presents recent works on the phases of correlated quantum systems under applied bias conditions. I will first discuss a bias-driven transverse field Ising chain coupled to magnetic thermal reservoirs, where increasing the magnetization bias leads to a discontinuous jump in the magnetic order parameter, accompanied by a divergence in the correlation length. Next, I will examine the fate of the quasicondensed state of hard-core bosons in one dimension within an open-system setup, where two macroscopic leads are maintained at different chemical potentials. Finally, I will present a scenario involving the breakdown of a Mott insulator induced by chemical pressure in a paradigmatic model of interacting spinless fermions on a chain coupled to metallic leads. In this case, we find various current-carrying non-equilibrium phases, as well as instances of hysteretic behavior, sharp current onset, and negative differential conductance.

Novel quantum dynamics with superconducting qubits

Pedram Roushan

Google Quantum AI, Santa Barbara, USA
e-mail: pedramr@google.com

In recent years, superconducting qubits have emerged as a leading platform for quantum simulation, particularly for studying quantum dynamics on Noisy Intermediate-Scale Quantum (NISQ) processors. I will discuss some of our work within this broad area of research.

In a recent study [1], we directly image the dynamics of charges and strings in (2+1)-dimensional lattice gauge theories. We identify two distinct regimes within the confining phase: in the weak confinement regime, the string exhibits strong transverse fluctuations, while in the strong confinement regime, these fluctuations are significantly suppressed. In another study [2], we observe a novel form of localization in quantum many-body systems in one and two dimensions. Despite the absence of disorder, energy perturbations do not spread, even when both the evolution operator and initial states are fully translationally invariant.

These results demonstrate that NISQ processors—in the absence of fully developed quantum computers—are invaluable tools for probing non-equilibrium physics, offering critical insights into complex quantum dynamics.

[1] Cochran et al., arxiv.org/abs/2409.17142.

[2] Gyawali et al., arxiv.org/abs/2410.06557.

Chirality induced spin selectivity: what is it, what do we really know and understand?

Jan M. van Ruitenbeek

*Huygens-Kamerlingh Onnes Laboratory, Leiden University,
Niels Bohrweg 2, Leiden, the Netherlands
e-mail: ruitenbeek@physics.leidenuniv.nl*

Two decades ago, Ron Naaman [1,2] and collaborators demonstrated a surprising effect for electron transmission through a monolayer of chiral molecules: The chirality (left- or right handed structure) of the molecules produces a pronounced spin polarization for electrons that are transmitted through these molecules. The sign of the spin polarization is determined by the sign of the chirality. Even more surprising results appeared in later years, showing that the direction of the magnetization of a thin film is controlled by the chirality, and more.

Such effects, collectively known as CISS (chirality controlled spin polarization) pose one of the most interesting and challenging problems in nanoscience. I will present a concise overview of the most important experiments, with special attention on those experiments that have been done at the single-molecule level. I will discuss the fundamental questions these experiments raise, and to what extent partial answers have been formulated.

In this overview I will focus on fundamental problems that these experiments confront us with, in terms of apparent violation of Onsager's relations and time-reversal symmetry breaking.

- [1] K. Ray, S. P. Ananthavel, D. H. Waldeck, R. Naaman, Asymmetric scattering of polarized electrons by organized organic films of chiral molecules, *Science* 283 (5403), 814-816 (1999).
- [2] R. Naaman, D. H. Waldeck, Chiral-induced spin selectivity effect, *The Journal of Physical Chemistry Letters*, 3 (16), 2178 (2012).

Radiolysis products and delayed desorption from methane-doped cryogenic matrices studied by emission spectroscopy methods

M. A. Bludov, I. V. Khyzhniy, S. A. Uyutnov, E. V. Savchenko

B. Verkin Institute for Low Temperature Physics and Engineering of NAS of Ukraine,
47 Nauky Ave., Kharkiv, 61103, Ukraine
e-mail: savchenko@ilt.kharkov.ua

The phenomenon of delayed explosive desorption is of fundamental importance and the ongoing interest to this phenomenon is connected with its possible role in the distribution of matter between gas and solid phase in dense molecular clouds, viz. existence of complex organic molecules (COMs) in the gas phase of these interstellar objects (see e.g. [1] and references therein). Delayed explosive desorption is a non-thermal process based on the conversion of energy released in chemical reactions between radiation-induce reagents into the kinetic energy of the reaction products as well as environmental particles. Attention to this phenomenon in solid methane is also due to a problem in the operation of cryogenic methane neutron moderators [2]. Most existing studies are based on infrared absorption and mass spectroscopy methods in combination with different irradiation techniques.

We have developed a new approach using a complex of emission methods – optical emission spectroscopy (OES), nonstationary luminescence (NsL) and desorption (NsD), measurements of stimulated currents (TSEE) and the total particle yield. Ar matrices doped with methane from 0.1 to 10 % were exposed to a low-energy electron beam. Along with radiative fragments of CH₄ photolysis: H, H₂, CH, and C detected in our previous study [3] new products were found – C₂ molecules and C₃ clusters. C₂ molecules were detected by the Swan molecular system ($d^3\Pi_g \rightarrow a^3\Pi_u$), and C₃ clusters by the $A^1\Pi_u - X^1\Sigma_g^+$ and $^3\Pi_u - X^1\Sigma_g^+$ transitions. Also observed were two bands tentatively assigned to CH₂. In the presence of O atoms CO molecules were formed. The energy transfer by free excitons of the matrix resulted in the population of the $d^3\Delta_i$ state and we observed successive transitions: $d^3\Delta_i - a^3\Pi$ (Triplet system) and $a^3\Pi - X^1\Sigma^+$ (Cameron bands). The selected radiolysis products as well as the total yield of desorbed particles were monitored in a correlated manner. Three channels of energy transfer to dopant and radiolysis products were analyzed: by free charge carriers, free excitons and photons from the “intrinsic source” provided by emission of the self-trapped excitons. Experiments performed using the NsL and NsD methods, as well as TSEE recordings, revealed the contributions of charged and neutral channels to the formation of radiolysis products. Monitoring of optical emissions (H atom, CH₃ radicals via CH [4] and C₂ molecules), particle ejection, and temperature revealed a nonmonotonic behavior of optical yields with a strong luminescence flash after almost an hour of exposure, which correlated with explosive pulse of particle ejection and temperature. The connection of this phenomenon with the processes of energy transfer and radical-radical recombination is discussed.

- [1] Ch. Zhu, A. Bergantini, S.K. Singh, M.J. Abplanalp and R.I. Kaiser, *Astrophys. J.* 920, 73 (2021). <https://doi.org/10.3847/1538-4357/ac116a>.
- [2] O. Kirichek, C.R. Lawson, G.L. Draper, D.M. Jenkins, D.J. Haynes and S. Lilley, *Journal of Neutron Research*, 22, 281 (2020), <https://doi.org/10.3233/JNR-190132>.
- [3] M. Bludov, I. Khyzhniy, S. Uyutnov, E. Savchenko, *Methane*, 2(4), 372 (2023); <https://doi.org/10.3390/methane2040025>
- [4] E. Savchenko, I. V. Khyzhniy, S. A. Uyutnov, M. A. Bludov, and V. E. Bondybey, *J. Mol. Structure*, 1221, 128803 (2020), <https://doi.org/10.1016/j.molstruc.2020.128803>.

On collective phenomena in one-dimensional networks of threshold-type memristors

V. A. Slipko¹, Yu. V. Pershin²

¹*Institute of Physics, Opole University, Opole 45-052, Poland*

²*Department of Physics and Astronomy, University of South Carolina,
Columbia, SC 29208 USA
e-mail: vslipko@uni.opole.pl*

Memristors have recently gained significant attention for their applications in neuromorphic computing, enabling energy-efficient and hardware-based implementations of neural networks. Their ability to mimic synaptic plasticity and store analog information makes them promising candidates for next-generation artificial intelligence and machine learning architectures. In this context, we explore the unique dynamical properties of one-dimensional (1D) memristive networks, which, despite their morphological simplicity, represent an important class of memory networks characterized by strong interactions among their components. This study focuses on key dynamical aspects of 1D memristive networks composed of realistic threshold-type memristive devices.

First, we introduce and analyze two fundamental switching regimes in memristive networks: accelerated and decelerated switching under the application of a slowly increasing voltage [1]. In the accelerated regime, an increase in memristance leads to a higher voltage across the device, speeding up the switching process. Conversely, in the decelerated regime, a decrease in memristance reduces the voltage across the device, potentially slowing or halting the switching process if the voltage drops below the threshold. These regimes depend on device connection polarity and applied voltage.

Second, using both analytical techniques and numerical simulations, we reveal a remarkable phenomenon of switching synchronization in 1D networks [2]. When memristive devices with different switching rates are connected in series with the same polarity, they exhibit coherent switching behavior despite their individual differences. Specifically, when a network combines fast- and slow-switching memristive systems, the fast-switching devices "wait" for the slower ones to switch. We show that it is possible to solve exactly the system of N coupled equations describing the dynamical behavior of a memristive network, even in the general case of arbitrary distributions of switching rates and threshold voltages. At long times, the memristance of individual devices decreases linearly with time at a rate proportional to the total network memristance.

Third, we introduce the concept of metastable memristive lines, where memristors are maintained in a quasi-equilibrium state just below their threshold voltage [3]. These lines can transmit information through switching fronts propagating across the network, similar to signal transmission in conventional transmission lines. This property enables the implementation of Boolean logic operations using coupled metastable memristive lines.

The findings demonstrate that 1D memristive networks can perform a triad of essential functionalities: information processing, storage, and transfer [4]. These results provide fundamental insights into the dynamics of memristive networks and may pave the way for novel computing paradigms based on memristive architectures.

- [1] Yuriy V. Pershin, Valeriy A. Slipko, and Massimiliano Di Ventra, Phys. Rev. E 87, 022116 (2013). <https://doi.org/10.1103/PhysRevE.87.022116>.
- [2] Valeriy A. Slipko, Yuriy V. Pershin, Phys. Rev. E 96, 062213 (2017). <https://doi.org/10.1103/PhysRevE.96.062213>.
- [3] Valeriy A. Slipko, Yuriy V. Pershin, Phys. Rev. E 95, 042213 (2017). <https://doi.org/10.1103/PhysRevE.95.042213>.
- [4] V.A. Slipko, Y.V. Pershin, (2019). In: Chua, L., Sirakoulis, G., Adamatzky, A. (eds) Handbook of Memristor Networks. Springer, Cham. https://doi.org/10.1007/978-3-319-76375-0_33.

Structural evolution and thermal properties of SiOC glass derived from polymer: influence of atmosphere and porosity

D. Szewczyk¹, M. Cassetta², M. Biesuz²

¹*Institute for Low Temperature and Structure Research, Polish Academy of Sciences,
50-420 Wroclaw, Poland*

²*Department of Industrial Engineering, University of Trento, 38123 Trento, Italy
e-mail: d.szewczyk@intibs.pl*

The transformation of a methyl-siloxane polymer into a SiOC glass in Ar and CO₂ atmospheres was investigated, focusing on structural, microstructural, mechanical, and thermal properties. During pyrolysis, a transient microporosity emerges at 700°C, consisting of voids inherited from the parent polymer (~0.8 nm) and additional pores (~1.2 nm) formed during ceramization. In CO₂, the lower viscosity of the SiO₂-like matrix promotes rapid pore relaxation, whereas in Ar, the presence of carbidic carbon increases viscosity, stabilizing the porosity. By 800°C, interconnected pores are fully closed, and further heating leads to a progressive reduction in pore size and volume, resulting in a denser SiOC structure in Ar at 1250°C.

The amorphous network evolves with temperature, with the correlation length stabilizing at 2.7–2.9 nm from 900°C onward, significantly lower than that of typical silica glass. The correlation length, ξ , representing the distance over which the short-range order of the amorphous structure is lost, was derived from the combination of calorimetric Boson peak data and elastic property measurements. This analysis highlights the influence of atomic-scale structural rearrangements on the macroscopic properties of the material.

Finally, the structural and microstructural changes directly influence the nanomechanical and thermal properties. The indentation modulus, hardness, and thermal conductivity increase monotonically between 700 and 1250°C, with higher values observed in Ar. The lower thermal conductivity of SiOC processed in CO₂ is attributed to the presence of the free carbon phase, which disrupts heat transfer in the glass network [1].

Acknowledgments:

This work was partially funded by the National Science Centre Poland, grant no. UMO/2024/53/B/ST3/02514.

- [1] M. Biesuz, A. Abebe, L. Karacasulu, S. Mariazzi, R.S. Brusa, D. Szewczyk, N. Pugno, G. Sero, M. Butterling, M.O. Liedke, A. Wagner, M. Cassetta, G.D. Soraru, “From polymer to SiOC glass: structure, microstructure, mechanical and thermal properties”, submitted to Journal of the American Ceramic Society.

Exploring topological and quantum transport properties of topological crystalline insulator (111) $\text{Pb}_{1-x}\text{Sn}_x\text{Se}$ thin films grown by MBE

Valentine V. Volobuev^{1,2}

¹ International Research Centre MagTop, Institute of Physics, Polish Academy of Sciences,
Aleja Lotników 32/46, PL-02668 Warsaw, Poland

² National Technical University “KhPI”, Kyrpychova Str. 2, 61002 Kharkiv, Ukraine
e-mail: volobuev@magtop.ifpan.edu.pl

Topological crystalline insulators (TCIs) are promising materials for next-generation electronics and spintronics, offering unique quantum properties crucial for fundamental condensed matter physics. TCIs, such as those found in the tin chalcogenide family, possess topological states (TSs) protected by mirror plane symmetry, which can be tuned through external perturbations like temperature, composition, strain, and electric or magnetic fields. While most previous studies focused on bulk TCI crystals cleaved along the (001) plane, the (111) surface remains relatively unexplored.

In this study, we investigate (111)-oriented $\text{Pb}_{1-x}\text{Sn}_x\text{Se}$ TCIs in the form of thin epilayers synthesized by molecular beam epitaxy (MBE) technique. This low-dimensional form exhibits novel physical properties unattainable in bulk materials. We present results on their growth, structural characterization, transport properties, and electronic structure using angle-resolved photoemission spectroscopy (ARPES).

By varying temperature and Sn content, we drive the system through a topological-to-normal insulator transition. Magnetoresistance measurements reveal that weak antilocalization (WAL) persists even in topologically trivial thin films [1], challenging the notion that WAL is a signature of a topological phase. Moreover, spin-resolved ARPES (SR-ARPES) confirms the presence of helical spin polarization in both topological and trivial phases, a phenomenon previously thought to be exclusive to topological insulators. Additionally, we explore the effects of transition metal deposition on the TCI surface, demonstrating how it induces a band gap opening via surface composition changes rather than magnetism [2].

Furthermore, we fabricated $\text{Pb}_{1-x}\text{Sn}_x\text{Se}$ TCI quantum wells (QWs) confined by $\text{Pb}_{1-y}\text{Eu}_y\text{Se}$ barriers on one side and by vacuum on the other and show via ARPES studies how the Rashba effect can be induced and controlled using quantum well asymmetry [3]. Sandwiching $\text{Pb}_{1-x}\text{Sn}_x\text{Se}$ TCI QWs between two equivalent barriers, we achieve a high-quality two-dimensional hole gas, confirmed by low-field Shubnikov-de Haas oscillations (SdHO). WAL and universal conductance fluctuations (UCF) indicate strong spin-orbit coupling and long phase coherence times. At high magnetic fields, quantum Hall effect plateaus and near-zero longitudinal resistance emerge. A four-band $k \cdot p$ model was employed to interpret our findings and allowed to obtain the topological phase diagram with alternating normal insulator – quantum spin hall insulator phases [4]. Our results suggest that precise tuning of Sn content and carrier densities can enable robust topologically protected edge transport without the need for an external magnetic field, paving the way for novel quantum device applications.

- [1] A. Kazakov, W. Brzezicki, T. Hyart, V. V. Volobuev, T. Dietl, Phys. Rev. B 103, 245307 (2021). <http://dx.doi.org/10.1103/PhysRevB.103.245307>.
- [2] B. Turowski, A. Kazakov, V. V. Volobuev, Appl. Surf. Sci. 610, 155434 (2023). <http://dx.doi.org/10.1016/j.apsusc.2022.155434>.
- [3] R. Rechciński, M. Galicka, M. Simma, V. V. Volobuev, et al., Adv. Funct. Mater. 31, 2008885 (2021). <http://dx.doi.org/10.1002/adfm.202008885>.
- [4] A. Kazakov, V. V. Volobuev, Chang-Woo Cho, Benjamin A. Piot, et al., arXiv:2501.02302 (2025). <https://www.arxiv.org/abs/2501.02302>.

THz-driven magnetic switching and dynamical coupling in rare-earth orthoferrites with non-Kramers ions: theory and experiment

N. R. Vovk¹, O. Y. Kovalenko¹, E. V. Ezerskaya², R. V. Mikhaylovskiy¹

¹ Department of Physics, Lancaster University, Bailrigg, Lancaster, United Kingdom

² Department of Physics, V. N. Karazin Kharkiv National University, Kharkiv 61022, Ukraine

e-mail: m.vovk1@lancaster.ac.uk

The rare-earth orthoferrite (REO) material class has been attracting significant attention since its discovery in the 1940s due to its unique magnetic properties, such as spin reorientation phase transitions (SRPT), strong magneto-optical effects, high-frequency spin dynamics, high-harmonic generation, strong magneto-elastic effects, multiferroicity, and as a novel platform in antiferromagnetic spintronics. Recent advancements in the development of THz time-domain spectroscopy (THz-TDS) techniques allowed the study of various types of excitations, including spin dynamics, by directly interacting with atomic spins using THz radiation. Regarding the REOs an interesting idea was to use intense THz fields to achieve control over nonlinear SRPT and switch of iron spins due to the changing crystalline magnetic anisotropy via R subsystem, driven by laser pulses [1,2]. This raises the question regarding the exchange interaction between rare-earth and iron orbitals in a non-equilibrium state. Moreover, different scenarios for dynamic coupling are possible depending on the type of rare-earth ion.

To address this issue, we have formulated a theoretical model [3] based on the microscopic approach [4] to elucidate the magnetic switching in REOs with non-Kramers ions subjected to strong THz excitation [1–2]. Using the archetypical orthoferrite $TmFeO_3$ as a model system, we investigated the static properties of the R and Fe subsystems across the SRPT. Employing an adiabatic approximation, we determined the resonance frequencies for the Fe and R magnetic sub-lattices as a function of temperature, aligning our findings with experimental data from [1–2]. We then performed numerical modelling to accurately describe the behaviour of its anisotropy functions vs temperature. Through numerical modelling, we described the behaviour of anisotropy functions relative to temperature, identified threshold fields for spin switching—whether via Zeeman mechanisms or anisotropy-driven torques altered through the R-subsystem—and estimated the energy dissipation during the switching process, achieving excellent correlation with experimental values [3].

Furthermore, we extended our model to interpret recent experimental results showing the signatures of magnetic analogue of Jahn-Teller effect in $TbFeO_3$, a unique member of the orthoferrite family. $TbFeO_3$ exhibits a cross-over (i.e. equality) of the frequencies of the antiferromagnetic resonance mode and atomic-like mode of Tb, which leads to their dynamical repulsion and avoided crossing effect. In this regard, the adiabatic approximation is no longer valid. The coupling is so strong that the frequency of the low-lying hybrid mode is pushed to zero. Despite this unique phase diagram, the coupled dynamics of spins and rare-earth orbitals in $TbFeO_3$ have not yet been studied. Using our model, we managed to model dynamics between interacting Fe and Tb magnetic subsystems, and to fit it with an excellent match to our experimental findings.

- [1] S. Baierl, M. Hohenleutner, T. Kampfrath, A. K. Zvezdin, A. V. Kimel, R. Huber, and R. V. Mikhaylovskiy, Nat. Photonics 10, 715 (2016).
- [2] S. Schlauderer, C. Lange, S. Baierl, T. Ebnet, C. P. Schmid, D. C. Valovcin, A. K. Zvezdin, A. V. Kimel, R. V. Mikhaylovskiy, and R. Huber, Nature 569, 383 (2019).
- [3] N. R. Vovk, E. V. Ezerskaya, and R. V. Mikhaylovskiy, Phys. Rev. B 111, 64411 (2025).
- [4] A. K. Zvezdin, V. M. Matveev, A. A. Mukhin, Rare-Earth Ions in Magnetically Ordered Crystals, Nauka (Moscow, 1985).

Mass-selected matrix isolation spectroscopy of astrochemically relevant aromatic cations in solid neon

Yu-Jong Wu^{1,2}

¹*National Synchrotron Radiation Research Center, Hsinchu, Taiwan*

²*Department of Applied Chemistry and Institute of Molecular Science,
National Yang Ming Chiao Tung University, Hsinchu, Taiwan*
e-mail: yjwu@nsrrc.org.tw

The recent discovery of cyano-substituted aromatic molecules such as benzonitrile in the interstellar medium has sparked significant interest in astrochemistry [1]. The ionic forms of these molecules, particularly cations, are believed to play pivotal roles in astrophysical environments exposed to vacuum UV radiation, potentially contributing to unidentified infrared bands and diffuse interstellar bands. However, existing information regarding the molecular structures, vibrational frequencies, and electronic transitions of these ions has primarily been obtained through photoelectron spectroscopy. These techniques often introduce fragmentation, limit spectral resolution, and yield data that cannot be directly compared with astronomical observations.

In this work, we have employed our newly-built mass-selected matrix isolation system to record IR and UV-visible absorption spectra of carbon-based aromatic cations and anions, including benzonitrile, isolated in solid neon matrices. Our measurements provide the first comprehensive IR absorption data for benzonitrile ions ($C_6H_5CN^+$ and $C_6H_5CN^-$) [2], significantly enhancing our understanding of their intrinsic vibrational structures. Furthermore, the measured frequencies for the benzonitrile cation demonstrate marked deviations from previous gas-phase data, underlining the advantages of the matrix isolation environment. For benzonitrile anions, our results validate theoretical predictions and confirm that the ground electronic state is valence-bound. Moreover, we extended our investigations to include other astrochemically relevant ions such as aniline ($C_6H_5NH_2^+$) [3] and carbon dioxide (CO_2^+) [4] cations. These studies highlight the effectiveness and adaptability of our method for characterizing transient ionic species and their electronic transitions, thus underscoring its potential as a powerful tool in astrochemical research.

- [1] G. Wenzel, I. R. Cooke, P. B. Changala et al., *Science* 386, 810 (2024), and references therein.
- [2] W.-J. Huang, S. L. Chou, C.-H. Chin, S.-Y. Lin, and Y.-J. Wu, submitted (2025).
- [3] S.-L. Chou, W.-J. Huang, C.-H. Chin, S.-Y. Lin, H.-F. Chen, and Y.-J. Wu, *J. Mol. Struct.* 1316, 139051 (2024).
- [4] W.-J. Huang, S.-L. Chou, S.-Y. Lin, H.-F. Chen, and Y.-J. Wu, *Low Temp. Phys.* 50, 733 (2024).

Wave phenomena in Josephson junction ladders: breathers, flat bands and more

Y. Zolotaryuk

*Bogolyubov Institute for Theoretical Physics of NAS of Ukraine,
Vul. Metrologichna 14-B, Kyiv, 03143, Ukraine
e-mail: yzolo@bitp.kyiv.ua*

Ladders of inductively coupled small Josephson junctions (JJs) support a number of non-trivial wave phenomena. Spatially localized excitations known as intrinsic localized modes or discrete breathers have no analog in the continuum limit. These excitations are whirling states which persist under a spatially homogeneous force due to the bias current. Their existence has been confirmed experimentally [1]. The stability analysis of these solutions is used to interpret the measured patterns in the I-V characteristics [2].

The dispersion law for the Josephson plasmons in the quasi-one-dimensional multiladder-like arrays that consists of the finite number of N rows ($N > 1$) in Y direction and is infinite in X direction has $2N - 1$ branches [3]. Among these branches there is an N -fold completely flat degenerate one that coincides with the Josephson plasma frequency. The remaining $N - 1$ branches have a standard Josephson plasmon dispersion law typical for parallel 1D JJ arrays. Application of the uniform dc bias on the top of each vertical column of junctions lifts the degeneracy and only one flat branch remains unchanged. The rest of the previously flat branches become weakly dispersive. The parameter range where the flatness of these branches is maximal has been discussed. The density of states of the Josephson plasma waves has a δ -function term due to the flat band and $3N - 2$ singularities [4]. The spatial distribution of the amplitudes of the plasmon wave is expressed through the orthogonal polynomials that are similar but not identical to the Chebyshev polynomials.

Topological solitons known as fluxons or Josephson vortices exist in arrays of Josephson junctions. Comparison between fluxons in ladders and simple 1D JJ arrays is performed including the respective I-V characteristics.

- [1] P. Binder, D. Abraimov, A. V. Ustinov, S. Flach, and Y. Zolotaryuk, Phys. Rev. Lett. 84, 745 (2000). <https://doi.org/10.1103/PhysRevLett.84.745>.
- [2] A. E. Miroshnichenko, S. Flach, M. Fistul, Y. Zolotaryuk and J. B. Page, Phys. Rev. E 64, 066601 (2001). <https://doi.org/10.1103/PhysRevE.64.066601>.
- [3] D.V. Bukatova and Y. Zolotaryuk, J. Phys.: Condens. Matter 34, 175402 (2022). <https://doi.org/10.1088/1361-648X/ac4f7f>.
- [4] D.V. Bukatova, I. O. Starodub and Y. Zolotaryuk, arXiv:2412.07071 [cond-mat. supr-con] (2024). <https://arxiv.org/abs/2412.07071>.

Controlling quantum coherence in diluted spin systems

I. Chiorescu

*Florida State University, Physics Dept and the National High Magnetic Field Laboratory,
1800 East Paul Dirac Drive, Tallahassee, Florida 32310, USA
e-mail: ichiorescu@fsu.edu*

Recently we have demonstrated experimentally the implementation of a novel and universal method to increase the decoherence time of spins qubits [1] in systems with different anisotropies / symmetries / spin-orbit coupling and type of element. The method is based on Floquet engineering of spin qubits quasi-energies by adding a second microwave drive with a frequency commensurate to that of the main Rabi drive. Qualitatively, the increase in coherence time can be linked to dynamical sweet spots (level repulsion) in quasi-energy spectra. Quantitatively, we add insight using numerical simulations [2] aiming to clarify the actual physical processes that take place in the bath surrounding the qubit. We are also exploring the potential use of spin systems as quantum memories [3] and to that effect, we have performed spectroscopic and pulsed studies of S=7/2 Gd ions placed on a coplanar stripline superconducting resonator. In the weak coupling limit, continuous-wave spectroscopy of the cavity resonance perturbation allows us to detect the forbidden electro-nuclear transition of the 155,157Gd isotopes by applying a static field almost perpendicular to crystal c-axis [4]. By increasing the coupling of the spin ensemble to the resonator we observe spin-cavity dressed states with a large mode splitting of ~150 MHz. Numerical simulations based on Dicke model shows a strong hybridization of the first excited level in the presence of a photon and the second excited level with no photon as well as a strong perturbation of the spin ground state generated by photons.

- [1] S. Bertaina, H. Vezin, H. De Raedt, and I. Chiorescu, Scientific Reports 10, 1 (2020).
- [2] H. De Raedt; S. Miyashita; K. Michielsen; H. Vezin, S.U. Bertaina; I. Chiorescu, European Physical Journal B 95 (9), 158 (2022).
- [3] M. Blencowe, Nature 468, 44 (2010).
- [4] G. Franco-Rivera; J.R. Cochran; S. Miyashita, S.U. Bertaina, I. Chiorescu, Physical Review Applied 19, 024067 (2023).

New ionic conductors based on salts of hypodiphosphoric acid, $H_4P_2O_6$

Vasyl Kinzhbalo

Institute for Low Temperatures and Structure Research, Polish Academy of Sciences,
Okólna 2, 50-422 Wrocław, Poland
e-mail: v.kinzhbalo@intibs.pl

The European Union has adopted the green transition, setting an ambitious goal of achieving climate neutrality by 2050. Its main reason is the desire to move from an economy based on exhaustible natural resources to one based on renewable sources of electricity. One of the most important challenges related to achieving this goal is the development of electricity storage infrastructure based on rechargeable batteries. Paradoxically, this requires a significant amount of natural resources, in particular lithium and graphite. Due to limited lithium deposits, using the much more abundant sodium, especially in stationary power sources, seems to be a reasonable alternative.

Ionic conductors are solids capable of conducting electricity through the diffusion of ions. They are an essential component of all-solid-state batteries and, in contrast to typical gel or liquid electrolytes, provide much higher energy densities. Therefore, the search for new sodium ion-conducting materials is one of the main tasks in the development of new sodium ion batteries.

Hypodiphosphoric acid, $(HO)_2OP-PO(OH)_2$, $H_4P_2O_6$, is less-known acid of phosphorus, the analogue of diphosphoric(V) acid, $H_4P_2O_7$, with a direct P–P bond [1]. It is mainly obtained by oxidation of red phosphorus by $NaClO_2$, H_2O_2 or other oxidizing agents with further neutralization by $NaOH$ to produce sparingly soluble sodium salts. The free acid is then obtained on ion-exchange resins. It is unstable in water solution and slowly undergoes hydrolytic disproportionation to give a mixture of H_3PO_3 and H_3PO_4 . In contrast to other phosphates, salts of hypodiphosphoric acid were studied to a substantially smaller extent. Therefore, the studies on sodium hypodiphosphates, their crystal structure, thermal stability and ionic conductivity were undertaken.

As a result of a systematic study, a series of 14 sodium hypodiphosphates was obtained. Their crystal structures were determined with the use of single-crystal and powder X-ray and 3D electron diffraction techniques [2]. The crystals structures of anhydrous salts of $Na(H_3P_2O_6)$ (α and β), $Na_2(H_2P_2O_6)$ (α and β), $Na_3(HP_2O_6)$ (α and β) and $Na_4(P_2O_6)$ composition were analyzed with the use of SoftBV software to determine the sodium ion conductivity pathways (Fig. 1), energetic barriers and ionic conductivity-temperature dependencies [3]. The experimental determination of an ac ionic conductivity was carried out for the two best candidates: α - $Na_2(H_2P_2O_6)$ and $Na_4(P_2O_6)$, for which the ion conductivity-crystal structure relation was discussed.

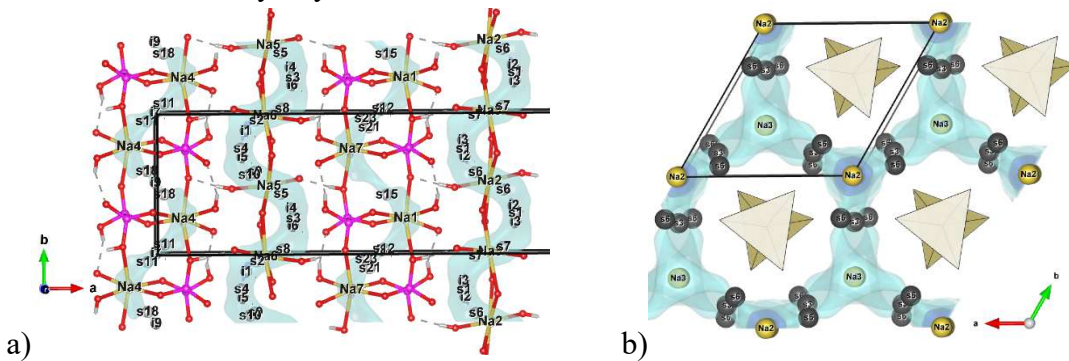


Fig. 1. The ion migration routes in (a) α - $Na_2(H_2P_2O_6)$ and (b) $Na_4(P_2O_6)$.

- [1] V. Kinzhbalo, M. Otręba, K. Ślepokura and T. Lis, Wiad. Chem. 75, 423 (2021).
- [2] V. Kinzhbalo, J. Wojciechowski, P. Szklarz, A. Piecha-Bisiorek, M. Otręba, M. Siczek and K. Ślepokura, J. Mater. Chem. C. 12, 11347 (2024). <https://doi.org/10.1039/D4TC01216J>.
- [3] L. L. Wong, K. C. Phuah, R. Dai, H. Chen, W. S. Chew and S. Adams, Chem. Mater. 33, 625 (2021). <https://doi.org/10.1021/acs.chemmater.0c03893>.

WORKSHOP:
OPPORTUNITIES AND TECHNOLOGIES FOR RESEARCHERS

LabsArena.com: connecting researchers, laboratories, and manufacturers to unlock new opportunities and boost global research

R. M. Basnukaeva, B. O. Postolnyi

LabsArena.com
e-mail: razet@labsarena.com

Access to research equipment and services remains one of the biggest challenges researchers face worldwide. Half of scientists around the globe struggle to find the necessary equipment, while 72% of equipment manufacturers, laboratories, and service providers have the capacity and willingness to support more users [1]. This mismatch leads to delays and diminished research quality, unrealized innovations and projects, limited training opportunities, constrained manufacturing, and slowed R&D progress. LabsArena.com bridges this gap by offering an innovative digital platform that connects researchers, laboratories, and manufacturers to streamline research, R&D, and manufacturing processes. It provides a collaborative research equipment-sharing platform and marketplace, facilitating easy searching, sharing, and selling of scientific equipment, consumables, and services. By democratizing access to research infrastructure, LabsArena.com ensures that researchers — regardless of their location, financial resources, or institutional affiliations — can access the scientific equipment and resources needed to advance their research. The platform promotes greater efficiency in the collective use of scientific equipment and expands the horizons of scientific collaboration, both within Ukraine and globally. Additionally, it highlights the contributions of Ukrainian equipment manufacturers, increasing their visibility on the international stage. LabsArena.com also streamlines cataloging of Ukrainian research infrastructure by organizing existing and available equipment for research, featuring an easily navigable filter system, detailed information about laboratories, and reviews.

Recognizing the urgent need for international support, LabsArena.com responded swiftly in the early days of Russia’s full-scale invasion of Ukraine by launching an initiative to assist Ukrainian scientists and students in securing research positions abroad [2]. This effort successfully connected numerous researchers with international organizations, enabling them to continue their research in a safe environment.

To explore all opportunities for researchers and stay updated, visit [LabsArena.com](https://www.labsarena.com) and follow its social media channels [3-6].

- [1] <https://cordis.europa.eu/project/id/824173/results>.
- [2] <https://labsarena.com/support-ua/>.
- [3] <https://labsarena.com/>.
- [4] <https://www.linkedin.com/company/labsarena>.
- [5] <https://instagram.com/labsarena>.
- [6] <https://www.facebook.com/LabsArena/>.

Nanofabrication of Josephson junctions

Maryna Dryhailo^{1,2}

¹*CEA-Leti, 17 Avenue des Martyrs, Grenoble, 38000, France*

²*Université Grenoble-Alpes, 621 Avenue Centrale, Saint-Martin-d'Hères, 38400, France
e-mail: maryna.dryhailo@cea.fr*

Josephson junctions are among the key components of quantum computing devices. These devices consist of two superconducting plates and a thin insulating barrier. The low dimensionality of Josephson junctions calls for careful selection of materials and fabrication conditions.

The nanofabrication process consists of the following steps [1, 2]:

- Deposition of material onto the silicon wafer. A layer of material is created to form the first superconducting plate.
- Lithography. Selective patterning of the deposited material, creating a plate of the correct shape.
- Etching. The native oxides and other possible contamination are removed from the surface of the plate.
- Controlled oxidation. Plate is exposed to high-quality oxygen, growing the insulating layer.

For the fabrication of the second superconducting plate, steps 1-3 are repeated.

Nowadays, it is common to experiment with different materials used in the process, as well as the fabrication conditions at each of the steps. The aim of these experiments is to maximize the performance of the Josephson junction while minimizing its size [3, 4].

- [1] Shen, D., Zhu, R., Xu, W. et al. Character and fabrication of Al/Al₂O₃/Al tunnel junctions for qubit application. Chin. Sci. Bull. 57, 409–412 (2012). <https://doi.org/10.1007/s11434-011-4821-4>.
- [2] Bal, M. et al. Overlap junctions for superconducting quantum electronics and amplifiers. Appl. Phys. Lett. 15 March 2021; 118 (11): 112601. <https://doi.org/10.1063/5.0048621>.
- [3] Zheng, Y., Li, S., Ding, Z. et al. Fabrication of Al/AlOx/Al junctions with high uniformity and stability on sapphire substrates. Sci Rep 13, 11874 (2023). <https://doi.org/10.1038/s41598-023-39052-2>.
- [4] McFadden, A.P., Goswami, A., Zhao, T. et al. Fabrication and characterization of low-loss Al/Si/Al parallel plate capacitors for superconducting quantum information applications. npj Quantum Inf 11, 11 (2025). <https://doi.org/10.1038/s41534-025-00967-5>.

**ELECTRONIC PROPERTIES OF CONDUCTING AND
SUPERCONDUCTING SYSTEMS**

Influence of As_2O_3 vapor pressure on phase formation and superconducting properties of Tl-1223 HTS

I. R. Metskhvarishvili^{1,2}, Melita Menelaou³, D. L. Surmanidze^{1,4}, T. E. Lobzhanidze⁴,
A. D. Tchankvetadze^{1,4}, B. G. Bendeliani¹, G. N. Dgebuadze¹, V. M. Gabunia^{1,5},
M. R. Metskhvarishvili⁶, D. A. Jishiashvili^{1,7}

¹*Ilia Vekua Sukhumi Institute of Physics and Technology, Laboratory of Cryogenic Technique and Technologies, Mindeli St. 7, 0186 Tbilisi, Georgia*

²*Georgian Technical University, Faculty of Informatics and Control Systems, Department of Microprocessor and Measurement Systems, Kostava St. 77, 0175 Tbilisi, Georgia*

³*Department of Mechanical Engineering and Materials Science and Engineering, Cyprus University of Technology, Limassol 3036, Cyprus*

⁴*Ivane Javakhishvili Tbilisi State University, Faculty of Exact and Natural Sciences, Department of Chemistry, Chavchavadze Ave. 3, 0179 Tbilisi, Georgia*

⁵*Petre Melikishvili Institute of Physical and Organic Chemistry of the Iv. Javakhishvili Tbilisi State University, Jikia str 5, 0186, Tbilisi, Georgia*

⁶*“Talga” Institute of Georgian Technical University, Zurab Anjaparidze 5, 0186 Tbilisi, Georgia*

⁷*V. Chavchanidze Institute of Cybernetics of the Georgian Technical University,
Zurab Anjaparidze 5, Tbilisi 0186, Georgia
e-mail: i.metskhvarishvili@gtu.ge*

The formation of the non-substituted Tl-1223 phase under ambient pressure is a complex process. As a result, various elements are commonly used as additives or substituents in during the synthesis of Tl-based superconductors. This approach facilitates the formation of the superconducting phase, enhances critical temperature (T_c), introduces effective pinning centres, and enhances critical current density (J_c). The present work focuses on utilizing materials whose transition temperature to steam (boiling point) is lower than Tl_2O_3 oxide. By adopting this method, we can control the vapor pressure of thallium (Tl) in a sealed quartz tube, enabling sintering at high ambient pressures. In the study, we used arsenic trioxide (As_2O_3) as a dopant, as its boiling point is lower than that of Tl_2O_3 . This approach allowed us to regulate, Tl vapor pressure within the sealed quartz tube, facilitating sintering at high ambient pressures.

The synthesis of $\text{TlBa}_2\text{Ca}_2\text{Cu}_3\text{O}_{8+\delta}$ samples was carried out using a two-step method. In the first stage, $\text{Ba}_2\text{Ca}_2\text{Cu}_3\text{O}_x$ precursors were prepared using the *in-situ* polymerization method. In the second stage, Tl_2O_3 and As_2O_3 were added simultaneously, thoroughly mixed and pressed into pellets. The final sintering process was performed in closed quartz tubes under 1 atm of oxygen pressure.

The resulting samples were characterized by X-ray powder diffraction patterns, obtained on a Dron-3 + PC diffractometer with $\text{CuK}\alpha$ radiation. The morphology and structure were analyzed using an FEI Quanta FEG 600 scanning electron microscope (SEM) equipped with an energy dispersive spectrometer (EDS) from Oxford Instruments (AztecOne). Superconducting properties, including both linear and nonlinear susceptibility, were also examined.

Our results demonstrate that even a small amount of arsenic effectively controls the thallium vapor pressure, promoting the formation of high- T_c phase and enhancing both the critical temperature (T_c) and current density (J_c).

This research PHDF-24-1841 has been supported by Shota Rustaveli National Science Foundation of Georgia (SRNSFG).

Current driven depinning of elastic vortex filaments in superconductors with columnar pinning sites

O. S. Hrechykha¹, A. L. Kasatkin², V. P. Tsvitkovskiy²

¹Kyiv Academic University, 36 Vernadsky blvd., Kyiv 03142, Ukraine

²G.V. Kurdyumov Institute for Metal Physics, NAS of Ukraine,
36 Vernadsky blvd., Kyiv 03142, Ukraine
e-mail: alkas1951@gmail.com

The problem of an elastic Abrikosov vortex filament depinning from a columnar defect under the action of the switched-on transport current is considered in the framework of Lagrangian classical mechanics. This problem is explored for a superconducting plate of thickness $d > 2\lambda$ (λ is the London penetration depth) loaded by non-stationary and non-uniformly distributed transport current, flowing in the surface Meissner layer. The conditions for the occurrence of instability of the pinned state of the vortex are investigated and the corresponding depinning critical current density at which the vortex filament starts its escape from the columnar defect is studied employing the numerical solution of the dynamic equation for an elastic vortex string, which is settled in the pinning potential well of a columnar defect and exerted to the action of switched on (at some moment t_0) an inhomogeneous Lorentz force, concentrated near the surface within the screening layer of width λ . This dynamic equation may be written as follows [1]:

$$P \frac{\partial^2 s}{\partial z^2} + \phi_0 j(z, t) - \frac{\partial U_p}{\partial s} = \eta \frac{\partial s}{\partial t} ; \quad j(z, t) = \Theta(t - t_0) j_0 \frac{\cosh(z/\lambda)}{\cosh(d/2\lambda)} ; \quad (1)$$

where P is the vortex line tension; $U_p(s)$ is the pinning potential created by the columnar defect (we use the Lorentzian form for $U_p(s)$ [2]); η is viscosity coefficient for the vortex filament; $\Theta(t - t_0)$ is the Heaviside step function. The 3D graph for the solution of Eq.(1) at a current higher than the critical value is shown in Fig.1.

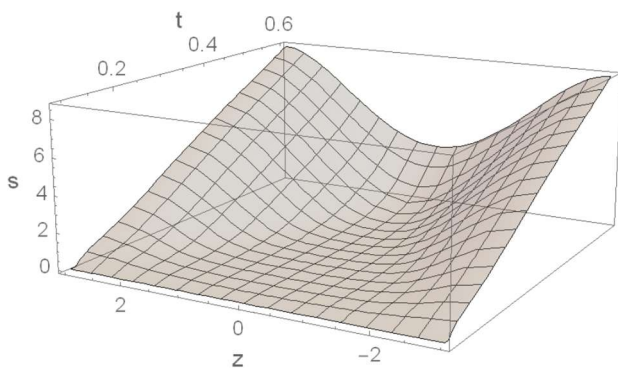


Fig.1. 3D graph of the pinned vortex filament escape from a columnar defect at current higher than the depinning critical value

One can see that the depinning process for a flexible vortex filament starts at the plate's surface ($z = \pm 3$) and then the vortex detachment wave propagates from the surface to the specimen center. It worth noticing that the vortex depinning process in this case has a definite duration, which can noticeably affect on electromagnetic response of a superconductor.

For instance, it can cause a delay in a switching-on of the resistive state at the pulse current loading of this type superconductor.

We have determined the time for the vortex depinning process and its dependencies on the sample thickness and the transport current value. Also, we have calculated numerically the average critical current density and its dependence on the plate thickness d .

[1] W.-K. Kwok, U. Welp, A. Glatz, A.E. Koshelev, K.J. Kihlstrom, and G.W. Crabtree, Rep. Prog. Phys., 79, 116501 (2016). <https://doi.org/10.1088/0034-4885/79/11/116501>.

[2] E. A. Pashitskii and V. I. Vakaryuk, Low Temp. Phys. 28, 11 (2002). <https://doi.org/10.1063/1.1449179>.

Eigenspectrum of extraordinary Josephson plasma waves in cylindrical layered superconductors

Yu. O. Averkov¹, O. Yu. Averkov², E. N. Odarenko³, A. A. Shmat'ko², V. A. Yampol'skii^{1,2}

¹*O.Ya. Usikov Institute for Radiophysics and Electronics of NAS of Ukraine,
 12 Acad. Proskury St., Kharkiv, 61085, Ukraine*

²*V.N. Karazin Kharkiv National University, 4 Svobody Sq., Kharkiv, 61022, Ukraine*

³*Kharkiv National University of Radio Electronics, 14 Nauky Ave., Kharkiv, 61166, Ukraine
 e-mail: yuriyaverkov@gmail.com*

In the present study, we investigate the eigenspectrum of extraordinary Josephson plasma waves (EJPWs) in an infinitely long layered superconductor of the cylindrical configuration, excluding the retardation effect. The superconductor occupies an ideally conducting waveguide with radius ρ_0 , where its layers are oriented in perpendicular to the waveguide's axis (the z -axis). Solving the wave equation for the vector potential of EJPWs in the linear approximation for the Josephson current, we obtain the following dispersion equation for EJPWs:

$$\omega = \omega_J \sqrt{1 + \frac{\lambda_c^2 \mu_{ns}^2}{\rho_0^2 (1 + q_z^2 \lambda_{ab}^2)}}, \quad (1)$$

where μ_{ns} are the roots of the n -th order Bessel function of the first kind, $J_n(\mu_{ns}) = 0$. Fig. 1 presents the dispersion curves of EJPWs, which are electric-type ones, plotted for the following structural parameters: $\rho_0 = 0.25$ cm, $\omega_J = 2\pi \cdot 10^{12}$ s⁻¹, $\lambda_{ab} = 5 \cdot 10^{-5}$ cm, $\lambda_c = 10^{-2}$ cm.

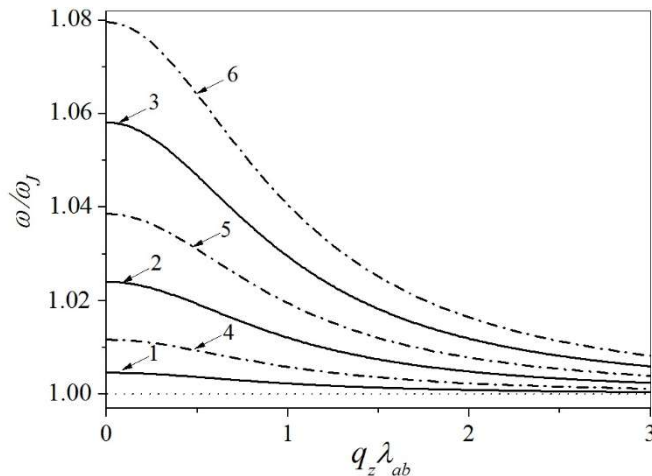


Fig. 1. Dispersion curves of EJPWs.

Here, ω and q_z denote the wave frequency and longitudinal wave vector, respectively. The values λ_{ab} and λ_c are the London penetration depths across and along the layers, respectively, while ω_J is the Josephson plasma frequency. Curves 1, 2 and 3 correspond to $n = 0$ and $s = 1, 2$ and 3 , respectively. Curves 4, 5 and 6 correspond to $n = 1$ and $s = 1, 2$ and 3 , respectively. The dotted line represents the dimensionless Josephson plasma frequency, $\omega/\omega_J = 1$, which serves as the asymptotic limit of the dispersion curves for large longitudinal wave numbers q_z . As seen from Fig. 1, for a fixed azimuthal mode index n , the eigenwave frequencies increase with the radial mode index s . Moreover, all dispersion curves exhibit negative dispersion, suggesting the possibility of absolute instability when the studied structure interacts with a tubular beam of charged particles.

Semantic segmentation of ARPES spectra for electronic dispersion analysis

Yu. V. Pustovit, M.O. Ohloblia

*Faculty of Radiophysics, Electronics and Computer Systems of Taras Shevchenko National University of Kyiv, 4g Hlushkova Avenue, Kyiv, 03127, Ukraine
e-mail: jura.pustvit@gmail.com*

We address the problem of extracting electronic band dispersion from angle-resolved photoemission spectroscopy (ARPES) spectra as a semantic segmentation task. The goal is to find the map between the broadened and distorted experimental dispersion and the corresponding “bare” electronic dispersion. Each pixel of the image is assigned to one of two possible classes. The first class represents the electronic dispersion pixel, and the other one is the “background” (broadening, distortion of the dispersion by intrinsic and extrinsic processes, noises, and influence of the apparatus function).

To solve semantic segmentation task approaches based on the DeepLabV3 [1] and U-Net with attention mechanism [2] models are used. Both neural networks are trained with a generated data set that consists of 10 thousand examples using a supervised learning approach. The training data set of the neural network consists of pairs of images: as the input - the generated spectra, which can contain up to 3 zones and the desired output corresponding labeled image (segmentation map), where each pixel within an image is assigned to a specific label. The input image has dimensions $128 \times 128 \times 1$, while the output has dimensions $128 \times 128 \times 2$.

The one-particle spectral function is used to simulate the detected experimental one-band spectra

$$A(k, \omega) = \frac{\Sigma''(k, \omega)}{((\omega - \varepsilon(k) - \Sigma'(k, \omega))^2 + \Sigma''(k, \omega)^2)},$$

where $\varepsilon(k) = mk^2 + l$ is the bare electronic dispersion, $\Sigma'(k, \omega) = \alpha\omega$ and $\Sigma''(k, \omega) = \beta\omega^2 + Imp$ - real and imaginary part of the quasiparticle’ self-energy. α, β, m, k, Imp are parameters chosen randomly in a wide range of values. The multiband spectra are generated as the sum of several one-band spectra with different parameters.

We calculated the IoU and Dice coefficient metrics on 2000 generated examples to evaluate the performance of the neural networks. For the DeepLabV3 the mean values are 0.76 (for IoU) and 0.64 (Dice coefficient) for U-Net 0.89 (for IoU) and 0.803 (Dice coefficient).

Experimentally obtained ARPES spectra of Fe(Se,Te), YBCO, and BiSe₃ were processed with two neural networks. The results demonstrated the possibility of extracting dispersion in a wide range of energies for spectra similar to the training set examples (Fe(Se,Te)), as well as in cases where the spectra differed dramatically (YBCO, BiSe₃). As demonstrated a key advantage of the proposed approach is its ability to eliminate the need for spectra denoising before processing, as well as its robustness to noise.

- [1] L.-C. Chen, Y. Zhu, G. Papandreou, F. Schroff, H. Adam Encoder-Decoder with Atrous Separable Convolution for Semantic Image Segmentation. In: Ferrari, V., Hebert, M., Sminchisescu, C., Weiss, Y. (eds) Computer Vision – ECCV 2018. ECCV 2018. Lecture Notes in Computer Science, vol 11211. Springer, Cham. https://doi.org/10.1007/978-3-030-01234-2_49.
- [2] O. Oktay, J. Schlemper, L. Folgoc, M. Lee, M. Heinrich, K. Misawa, K. Mori, S. McDonagh, N. Y Hammerla, B. Kainz, B. Glocker, D. Rueckert- Attention U-Net: Learning Where to Look for the Pancreas - Medical Imaging with Deep Learning, Amsterdam, 4-6 July 2018.

Bulk-to-surface oxygen vacancy diffusion in ITO: a possible superconductivity mechanism

O. Feia^{1,2,3}, D. Menesenko¹, A. Parra⁴, A. Shapovalov^{1,2}, A. Aliev⁴

¹*Kyiv Academic University, 36 Vernadsky blvd., Kyiv 03142, Ukraine*

²*G.V. Kurdyumov Institute for Metal Physics, NAS of Ukraine,
36 Vernadsky blvd., Kyiv 03142, Ukraine*

³*Leibniz Institute for Solid State and Materials Research, Dresden, Germany*

⁴*A.G. MacDiarmid NanoTech Institute, University of Texas at Dallas, Richardson, TX75080 USA
e-mail: feyaolkodmi@gmail.com*

Electrochemically reduced indium-tin oxide (ITO) films offer a promising platform for quantum technologies, combining tunable superconductivity with optical transparency across the visible, NIR, and mid-IR regions. Understanding the electrochemical processes at the ITO surface and the dimensionality of the resulting superconducting state is essential for developing quantum devices that harness electromagnetic wave interactions. We have explored three approaches to modulating charge density in ITO films to potentially induce superconductivity: (1) heterovalent atom doping, (2) electrochemical intercalation, and (3) synthesis of oxygen-deficient ITO films [1].

Among these methods, electrochemical intercalation induced a two-dimensional superconducting state at the ITO surface. Using density functional theory, we modeled possible surface states following electrochemical intercalation. Simulations of ion migration into the bixbyite structure of ITO indicated that inserting H⁺ and Mg²⁺ cations requires minimum energies of -0.5 eV and -0.67 eV, respectively [2]. When negative potential is applied to the ITO film, the positively charged H⁺ and Mg²⁺ layer attracts free electrons to the surface. These electrons reduce In³⁺ and Sn⁴⁺ cations, weakening their bonding energy with oxygen atoms. The strong electrical potential of the double layer can locally extract O²⁻ anions, which then react with H⁺ and Mg²⁺ in the electrolyte to form water or precipitated MgO at the bottom of the vial. Our simulations show that the most promising mechanism for surface superconductivity is the migration of oxygen atoms from bulk to surface, which flattens the surface bands near the Fermi level.

This research of transparent superconductors is supported by the NATO Science for Peace and Security Programme, project SPS G6082 and NASA Early Stage Innovations (ESI23) project 0015. This work was also partially supported by the Ministry of Education and Science of Ukraine under contract No. M/83-2024

[1] A. Parra et al., IEEE Trans. Appl. Supercond. 35, 1 (2025).
<https://doi.org/10.1109/TASC.2025.3530326>.

[2] D. Menesenko et al., Low Temp. Phys. 50, 688 (2024). <https://doi.org/10.1063/10.0027926>.

Peculiarities of the behavior of fluctuation conductivity and pseudogap in untwined $\text{YBa}_2\text{Cu}_3\text{O}_{7-\delta}$ single crystals under electron irradiation with an energy of 2.5 MeV

**M. V. Shytov¹, K. Rogacki², L. V. Bludova¹, E. V. Petrenko¹, Yu. A. Kolesnichenko,
A. L. Solovjov^{1,2,3}, A. Sedda³, E. Lähderanta³, R. V. Vovk⁴**

¹*B.Verkin Institute for Low Temperature Physics and Engineering of NAS of Ukraine,
47 Nauky Ave., Kharkiv, 61103, Ukraine*

²*Institute for Low Temperatures and Structure Research, of PAS, Wroclaw 50-422, Poland*

³*Lappeenranta University of Technology, School of Engineering Science,
53850 Lappeenranta, Finland*

⁴*Physics Department, V.N. Karazin Kharkiv National University,
4 Svobody Sq., Kharkiv, 61022, Ukraine
e-mail: shytovnikita@gmail.com*

To study various properties of high-temperature superconductors (HTSC), including the yet unknown superconducting (SC) pairing, we used electrons with an energy of 2.5 MeV, which effectively displace all the atoms in the YBCO crystal and allow for the controlled formation of numerous defects in the CuO_2 planes by gradually increasing the irradiation dose φ from $\varphi_1=0$ to $\varphi_{12}=23 \cdot 10^{19} \text{ e/cm}^2$. This leads to an increase in the scattering rate of normal charge carriers, resulting in a linear increase in resistivity, a linear decrease in T_c , and a metal-insulator transition at high φ . But, the interaction of the radiation with another type of charge carriers, the so-called local pairs (LPs), which occur in HTSCs below the pseudogap (PG) opening temperature T^* and are believed to transport charge without dissipation, is less obvious. To clarify the issue, we studied, for the first time, the temperature dependences of fluctuation conductivity (FLC) $\sigma'(T)$ and PG $\Delta^*(T)$ in untwined YBCO single crystals under irradiation. It is believed that at small φ the linear decrease in T_c is due to the LPs pair-breaking mechanism of the Abrikosov-Gorkov (AG). Whereas at large φ the Emery-Kivelson (EK) mechanism of quantum fluctuations of the order parameter should operate [1]. It was shown that our radiation dose φ_3 exactly corresponds to the AG-EK crossover. And it is at φ_3 that the features on $\sigma'(T)$ and $\Delta^*(T)$ are observed. At small φ , both $\sigma'(T)$ and $\Delta^*(T)$ exhibit a shape typical of well-structured YBCO. Near T_c , $\sigma'(T)$ is described by the Aslamazov-Larkin (AL) theory for 3D systems, and then a crossover to the 2D Maki-Thompson (MT) fluctuations follows. However, at φ_3 , everything changes dramatically. Now, above the 3D-2D crossover temperature T_0 , unexpectedly, the 2D fluctuations are described by the 2D AL theory, and $\sigma'(T)$ decreases sharply. This decrease in $\sigma'(T)$ leads to the observed sharp increase and unusual shape of $\Delta^*(T)$ in the high-temperature region, exceeding the values at φ_2 . At φ_4 , the shape of $\sigma'(T)$ does not change, but $\Delta^*(T)$ decreases sharply and acquires a completely unusual shape, which was not present in our database. But the most surprising result is obtained at the highest $\varphi_5 = 5.6 \cdot 10^{19} \text{ e/cm}^2$, when both $\sigma'(T)$ and $\Delta^*(T)$ again show curves typical of well-structured YBCO. This result can be explained only if we assume that the more defects, the more isotropic the sample is [2]. And such an isotropic crystal is perceived by LPs as a defect-free sample. Thus, our analysis within the local pair model allows not only to rationally explain the obtained results, but also confirms the existence of paired fermions in the form of LPs in HTSCs at $T \leq T^*$.

- [1] F. Rullier-Albenque, H. Alloul, and R. Tourbot, Phys. Rev. Lett. 91, 047001 (2003). <https://doi.org/10.1103/PhysRevLett.91.047001>.
- [2] A. L. Solovjov, L. V. Omelchenko, E. V. Petrenko, et al. Low Temp. Phys. 48, 700 (2022). <https://doi.org/10.1063/10.0013294>.

Polar crosstalk effects and negative capacitance state in dense ferroelectric nanocomposite films

**O. V. Bereznykov¹, O. S. Pylypchuk¹, S. E. Ivanchenko², D. O. Stetsenko¹, E. A. Eliseev²,
A. N. Morozovska¹**

¹*Institute of Physics, National Academy of Sciences of Ukraine,
46 Nauky Ave., 03028 Kyiv, Ukraine*

²*Frantsevich Institute for Problems in Materials Science, National Academy of Sciences of Ukraine,
3, str. Omeliana Pritsaka, 03142 Kyiv, Ukraine
e-mail: alexber36@gmail.com*

The temperature dependence of the dielectric permittivity and dielectric loss tangent of dense nanocomposites with BaTiO₃ nanoparticles (volume fraction 38.7% and 70%) was investigated from -200°C to +200°C. The obtained results were compared with the results of a pure polymer matrix that does not contain nanoparticles. The analysis showed that the addition of nanoparticles leads to an increase in the dielectric permittivity by more than 2 and 5 times, respectively.

For the theoretical calculation of the dielectric permittivity of these composites, the model of a binary mixture of an effective medium was used. The results demonstrate good agreement with experimental data. However, the proposed model still has a certain discrepancy with experiment, which requires evolving a more perfect model.

Also, modeling was carried out to explain the dielectric permittivity behavior in the dense composites, the effective model approximation (EMA) for the effective dielectric mixture and the finite element modelling (FEM) are used. The results of this simulation showed that the domain structure of the particles leads to the fact that the electric field is concentrated near the surface of the nanoparticles. Surface effects determine the distribution of the electric field, demonstrating stronger crosstalk in denser composites. For nanocomposites with 70 vol. % nanoparticles, it was theoretically obtained on the hysteresis curve for polarization extremum points, which we associate with the appearance of the negative capacitance state.

Acknowledgements. O.V.B. and D.O.S. acknowledge the Target Program of the National Academy of Sciences of Ukraine, Project No. 5.8/25-II “Energy-saving and environmentally friendly nanoscale ferroics for the development of sensorics, nanoelectronics and spintronics”. The work of A.N.M., O.S.P. and E.A.E. are funded by the National Research Foundation of Ukraine (grant N 2023.03/0132 “Manyfold-degenerated metastable states of spontaneous polarization in nanoferroics: theory, experiment and perspectives for digital nanoelectronics” and N 2023.03/0127 “Silicon-compatible ferroelectric nanocomposites for electronics and sensors”).

Machine learning analysis of bilayer splitting in multiband superconductors

K. H. Bohachov^{1, 2}, A. A. Kordyuk^{1, 2, 3}

¹*G.V. Kurdyumov Institute for Metal Physics, NAS of Ukraine,
36 Vernadsky blvd., Kyiv 03142, Ukraine*

²*Kyiv Academic University, 36 Vernadsky blvd., Kyiv 03142, Ukraine*

³*Leibniz Institute for Solid State and Materials Research,
IFW Dresden, D-01171, Dresden, Germany
e-mail: bogachov.kyrylo@gmail.com*

Unraveling the coherent and incoherent components in photoemission spectra of strongly correlated systems is a formidable task, complicated by the interplay of numerous factors. We employ Convolutional Neural Networks (CNNs) to explore bilayer splitting in superconducting cuprates, a longstanding problem in condensed matter physics. Training CNNs on modeled spectra, we validate the presence of bilayer splitting across all doping levels (Fig. 1), revealing that its magnitude persists even in the underdoped regime — contrary to prior assumptions. This machine learning approach offers a powerful tool for analyzing electronic properties in correlated superconductors, with implications for future studies of high-T_c materials [1].

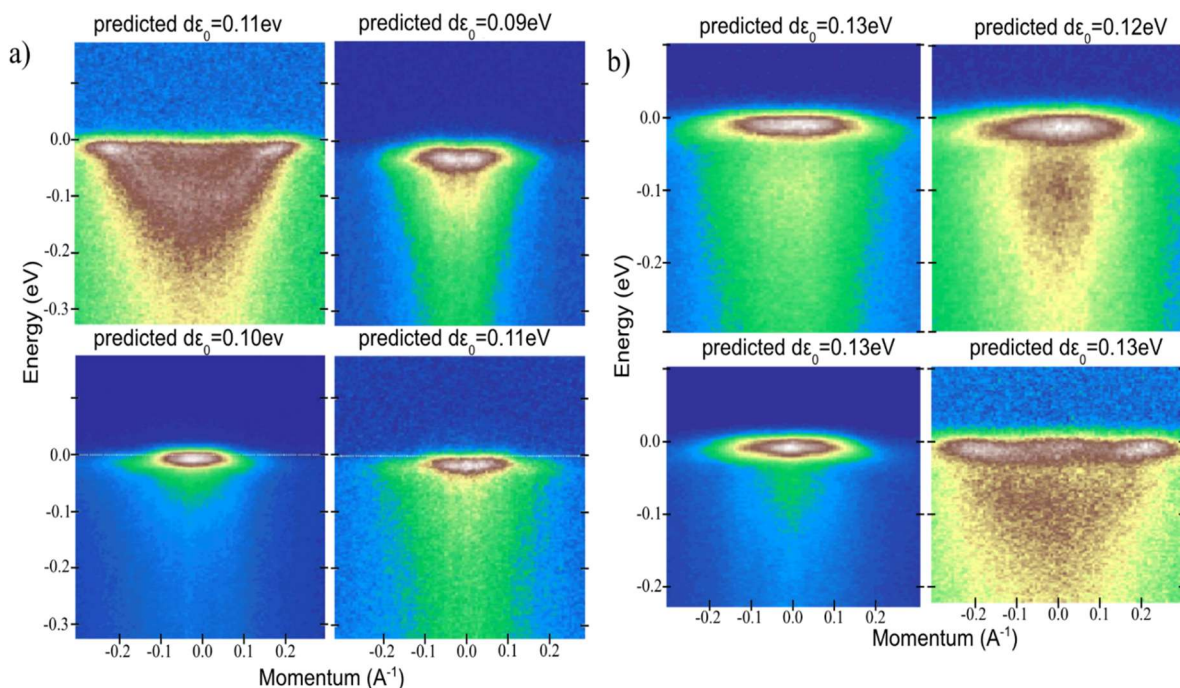


Figure 1. Prediction of bilayer splitting from real data using a hierarchical dual-model approach: (a) optimally doped regime, (b) severely underdoped regime.

- [1] K. H. Bohachov, A. A. Kordyuk, Disentangling Coherent and Incoherent Effects in Superconductor Photoemission Spectra via Machine Learning. arXiv:2412.11129 (2024). <https://doi.org/10.48550/arXiv.2412.11129>.

Study of the effect of magnetic field on the temperature dependence of the pseudogap in optimally doped $\text{YBa}_2\text{Cu}_3\text{O}_{7-\delta}$ films

**A. S. Kolisnyk¹, M. V. Shytov¹, E. V. Petrenko¹, A. V. Terekhov¹, L. V. Bludova¹,
K. Rogacki², A. L. Solovyov^{1,2}**

¹*B.Verkin Institute for Low Temperature Physics and Engineering of NAS of Ukraine,
47 Nauky Ave., Kharkiv, 61103, Ukraine*

²*Institute for Low Temperatures and Structure Research, of PAS, Wroclaw 50-422, Poland
e-mail: kubandrey606@gmail.com*

Despite nearly four decades having passed since the discovery of high-temperature superconductors (HTSCs) in 1986, there is still no unified theory explaining the mechanism of superconducting (SC) pairing at temperatures above 100 K. In fact, this remains a significant challenge in modern solid-state physics, particularly in the context of discovering new materials with critical temperatures (T_c) approaching room temperature. One of the possible keys to understanding this mechanism in HTSCs is the study of the pseudogap, which opens in cuprate HTSCs within the temperature range $T^* > T > T_c$ [1].

For the first time in this work the temperature dependence of the pseudogap $\Delta^*(T)$ in thin $\text{YBa}_2\text{Cu}_3\text{O}_{7-\delta}$ (YBCO) films [2] with a critical temperature $T_c = 88.8$ K ($B = 0$) under the influence of a magnetic field B up to 9 T, oriented parallel to the c -axis was studied. As the magnetic field increases, the low-temperature maximum near $T_0 > T_c$, below which the fluctuation conductivity is transformed from the 2D Maki-Thompson (2D-MT) regime to the 3D Aslamazov-Larkin (3D-AL) regime, gradually smears out and disappears at $B > 0.5$ T. Accordingly, above the Ginzburg temperature T_G , which defines the region of critical fluctuations, a minimum of $\Delta^*(T_{\min})$ forms in fields $B > 0.5$ T, becoming more pronounced with increasing B . It was established that for different B values, the shape of the pseudogap $\Delta^*(T)$ in the range $T^* > T_{\text{pair}} > T_c$ exhibits a broad maximum at the BEC–BCS crossover temperature $T_{\text{pair}} \approx 140$ K, which is typical for YBCO films and single crystals. However, the magnitude of $\Delta^*(T_{\text{pair}})$ remains constant regardless of the magnetic field, while T_{pair} shifts toward lower temperatures as B increases. The obtained data are in good agreement with the results of [1].

Analysis of the behavior of the BCS ratio $2\Delta(0)/k_B T_c = 2\Delta^*(T_G)/k_B T_c$ [1] revealed interesting features: in fields B from 0 to 1 T, despite a nearly threefold increase in the coherence length $\xi_c(0)$, the value of $2\Delta^*(T_G)/k_B T_c$ remains almost unchanged. However, unexpectedly, for $B \geq 6$ T, an increase of approximately 10% in $2\Delta^*(T_G)/k_B T_c$ is observed suggesting the increase of the SC pairing mechanism. Since the field does not affect $R(T)$ at high T , the detected anomalies can be explained by the interaction of the field with local pairs that emerge in HTSCs at $T < T^*$ [1].

- [1] A. L. Solovjov and V. M. Dmitriev, Low Temp. Phys. 35, 169 (2009).
<https://doi.org/10.1063/1.3081150>.
- [2] E. V. Petrenko, K. Rogacki, A. V. Terekhov, L. V. Bludova, Yu. A. Kolesnichenko, M. V. Shytov, D. M. Sergeyev, E. Lähderanta, and A. L. Solovjov, Low Temp. Phys. 50, 299 (2024).
<https://doi.org/10.1063/10.0025295>.

Anomalous behaviour of the temperature dependencies of the upper critical fields in $(\text{Dy}_{1-x}\text{Er}_x)\text{Rh}_{3.8}\text{Ru}_{0.2}\text{B}_4$ ($x=0, 0.2, 0.4$)

**V. M. Yarovyi¹, A. V. Terekhov¹, A. P. Kazakov², P. M. Fesenko³,
I. V. Zolochevskii¹, L. O. Ishchenko¹**

¹*B. Verkin Institute for Low Temperature Physics and Engineering of NAS of Ukraine,
47 Nauky Ave., Kharkiv, 61103, Ukraine*

²*Institute for Low Temperatures and Structure Research, Polish Academy of Sciences,
P.O. Box 1410, 50-950 Wroclaw, Poland*

³*National Technical University “Kharkiv Polytechnic Institute”,
2 Kyrpychova str., Kharkiv, 61002, Ukraine
e-mail: yarovyi@ilt.kharkov.ua*

Triplet superconductivity is a fascinating and unconventional state of superconductivity. It should be noted that triplet superconductors are expected to be widely used in spintronics in the future. In such materials, the electric current not only flows without scattering, but also is also fully spin-polarized below the transition to the superconducting state. Besides, triplet superconductivity is a necessary component for the artificial creation of Majorana states, which would be stable for a long time and resistant to external influences, and based on which qubits for quantum computers are expected to be created. Unlike conventional singlet superconductivity, where Cooper pairs are formed by electrons with opposite spins, triplet superconductivity involves pairs of electrons with parallel or mixed spin states. In addition, in such superconductors, the electrons in the Cooper pair are coupled by spin fluctuations rather than by phonons as in conventional superconductors. This may indicate that potential candidates for triplet superconductors are magnetic ones in which superconductivity and magnetism coexist.

Rare earth borides of rhodium are convenient objects for studying aspects of the coexistence of superconductivity and long-range magnetic ordering. Previously, we studied the superconducting compounds $\text{Dy}_{1-x}\text{Y}_x(\text{Rh},\text{Ru})_4\text{B}_4$, where several intriguing phenomena were observed. These include the Wolleben effect, the coexistence of superconductivity with ferri- or ferromagnetism, and most notably, signatures of triplet superconductivity [1,2,3].

The aim of this work was to study in detail the behavior of the temperature dependences of the upper critical field in $(\text{Dy}_{1-x}\text{Er}_x)\text{Rh}_{3.8}\text{Ru}_{0.2}\text{B}_4$ ($x = 0, 0.2, 0.4$) compounds and describe unusual phenomena that have been observed and may indicate the presence of unusual superconductivity.

In this work a detailed analysis of the behavior of the temperature dependences of the upper critical fields $H_{c2}(T)$ in the compounds $(\text{Dy}_{1-x}\text{Er}_x)\text{Rh}_{3.8}\text{Ru}_{0.2}\text{B}_4$ ($x = 0, 0.2, 0.4$) has been carried out. It is found that the $H_{c2}(T)$ in $(\text{Dy}_{0.8}\text{Er}_{0.2})\text{Rh}_{3.8}\text{Ru}_{0.2}\text{B}_4$ has an inflection point at 3 kOe, which may be related to the low-temperature magnetic ordering, while a more exotic mechanism caused by the transition from ordinary singlet to triplet superconductivity is not excluded. For the first time, the experimental $H_{c2}(T)$ dependences of $(\text{Dy}_{1-x}\text{Er}_x)\text{Rh}_{3.8}\text{Ru}_{0.2}\text{B}_4$ ($x = 0, 0.2, 0.4$) compounds have been fitted within the framework of Werthamer-Helfand-Hohenberg theory (WHH) with the Maki parameter $\alpha > 0$, indicating that spin-paramagnetic effects due to magnetic exchange interactions play an essential role in suppressing superconductivity in these compounds.

- [1] V. M. Dmitriev, A. V. Terekhov, A. Zaleski, E. N. Khatsko, P. S. Kalinin, A. I. Rykova, A. M. Gurevich, S. A. Glagolev, E. P. Khlybov, I. E. Kostyleva, and S. A. Lachenkov, *Low Temp. Phys.* 38, 154 (2012). <https://doi.org/10.1063/1.3681903>.
- [2] L. F. Rybaltchenko, E. V. Khristenko, L. A. Ishchenko, A. V. Terekhov, I. V. Zolochevskii, T. V. Salenkova, E. P. Khlybov, and A. J. Zaleski, *Low Temp. Phys.* 38, 1106 (2012). <https://doi.org/10.1063/1.4769209>.
- [3] A. V. Terekhov, I. V. Zolochevskii, L. A. Ischenko, A. N. Bludov, A. Zaleski, E. P. Khlybov, and S. A. Lachenkov, *Low Temp. Phys.* 45, 1241 (2019). <https://doi.org/10.1063/10.0000202>.

Magnetoresistance of $\text{Bi}_{88.08}\text{Mn}_{11.92}$ in magnetic fields up to 90 kOe

V. M. Yarovyj¹, A. V. Terekhov¹, K. Rogacki², A. L. Solovjov^{1,2}

¹*B.Verkin Institute for Low Temperature Physics and Engineering of NAS of Ukraine,
47 Nauky Ave., Kharkiv, 61103, Ukraine*

²*Institute for Low Temperatures and Structure Research, Polish Academy of Sciences,
P.O. Box 1410, 50-950 Wroclaw, Poland
e-mail: yarovyj@ilt.kharkov.ua*

Bismuth exhibits unique electronic properties that make it an intriguing material for modern condensed matter physics and quantum technology. Recent studies have indicated that specific electrons in bismuth can be regarded as massive Dirac fermions. It has also been shown that bismuth can be used in a relatively new area of modern electronics – valleytronics, which uses the valley degree of freedom to carry quantum information in multivalley semiconductors or semimetals, including bismuth. It is suggested that valley-based quantum qubits may be possible in the future.

Studies in our group have shown that Bi-Mn solid solutions containing low amounts of manganese exhibit colossal positive anisotropic magnetoresistance and unusual temperature dependence of electrical resistance in magnetic field [1].

This study aims to investigate the evolution of the $R(H)$ behavior in magnetic fields as the manganese content increases. We have measured the electrical resistivity in magnetic fields up to 90 kOe at 5 K, 80 K, 150 K and 300 K, plotted the field dependence of the magnetoresistance $MR = ([R(H) - R(0)]/R(0)) * 100\%$ for the configurations $\mathbf{H} \parallel \mathbf{I}$ and $\mathbf{H} \perp \mathbf{I}$ for $\text{Bi}_{88.08}\text{Mn}_{11.92}$ solid solutions. Further, the comparison with the $\text{Bi}_{95.69}\text{Mn}_{3.69}\text{Fe}_{0.62}$ with lower manganese content was made.

Detailed analysis of the magnetoresistance for $\text{Bi}_{88.08}\text{Mn}_{11.92}$ showed that the magnetoresistance is positive in the whole field region. The maximum MR values are $\approx 3161\%$ for $\mathbf{H} \perp \mathbf{I}$ and $\approx 379\%$ for $\mathbf{H} \parallel \mathbf{I}$ in a field of 90 kOe. At the same time, our previous studies for $\text{Bi}_{95.69}\text{Mn}_{3.69}\text{Fe}_{0.62}$ with a lower manganese content reveal the maximum MR values are $\approx 3877\%$ for $\mathbf{H} \perp \mathbf{I}$ and $\approx 742\%$ for $\mathbf{H} \parallel \mathbf{I}$ in a field of 90 kOe.

It is assumed that the primary factor contributing to the difference in magnetoresistance between the $\text{Bi}_{88.08}\text{Mn}_{11.92}$ and $\text{Bi}_{95.69}\text{Mn}_{3.69}\text{Fe}_{0.62}$ is the influence of the internal magnetism of α -BiMn phase inclusions on the behavior of charge carriers (electrons and holes) within the bismuth matrix.

- [1] A. V. Terekhov, K. Rogacki, V. M. Yarovyj, Z. D. Kovalyuk, E. Lähderanta, E. V. Khristenko, A. L. Solovjov, Low Temp. Phys. 50, 543 (2024). <https://doi.org/10.1063/10.0026270>.

Quantum reflectometry: effective capacitance of two- and multi-level systems

O. Y. Kitsenko^{1,2}, S. N. Shevchenko¹

¹*B.Verkin Institute for Low Temperature Physics and Engineering of NAS of Ukraine,
47 Nauky Ave., Kharkiv, 61103, Ukraine*

²*V.N. Karazin Kharkiv National University, 4 Svobody Sq., Kharkiv, 61022, Ukraine
e-mail: kitsenko.sasha1212@gmail.com*

When a classical resonator is coupled to a quantum system, its capacitance, inductance, and resistance are modified [1-3]. We investigate this effect using a superconducting island (Fig. 1a) and double quantum dot (Fig 1b) as examples, exploring how a two-level system interacts with classical electric circuits and how it can be effectively replaced by an impedance that is directly measurable. Furthermore, we extend our study to quantum multilevel systems.

To define the effective capacitance, we quantize the system and apply perturbation theory. We show that quantum capacitance originates from the curvature of energy levels, while tunneling capacitance appears when relaxation [1, 2] or resonant microwave driving occurs [3]. Additionally, we analyze how the quantum and tunneling capacitance of a superconducting island depend on relaxation times and how microwave driving influences the effective capacitance.

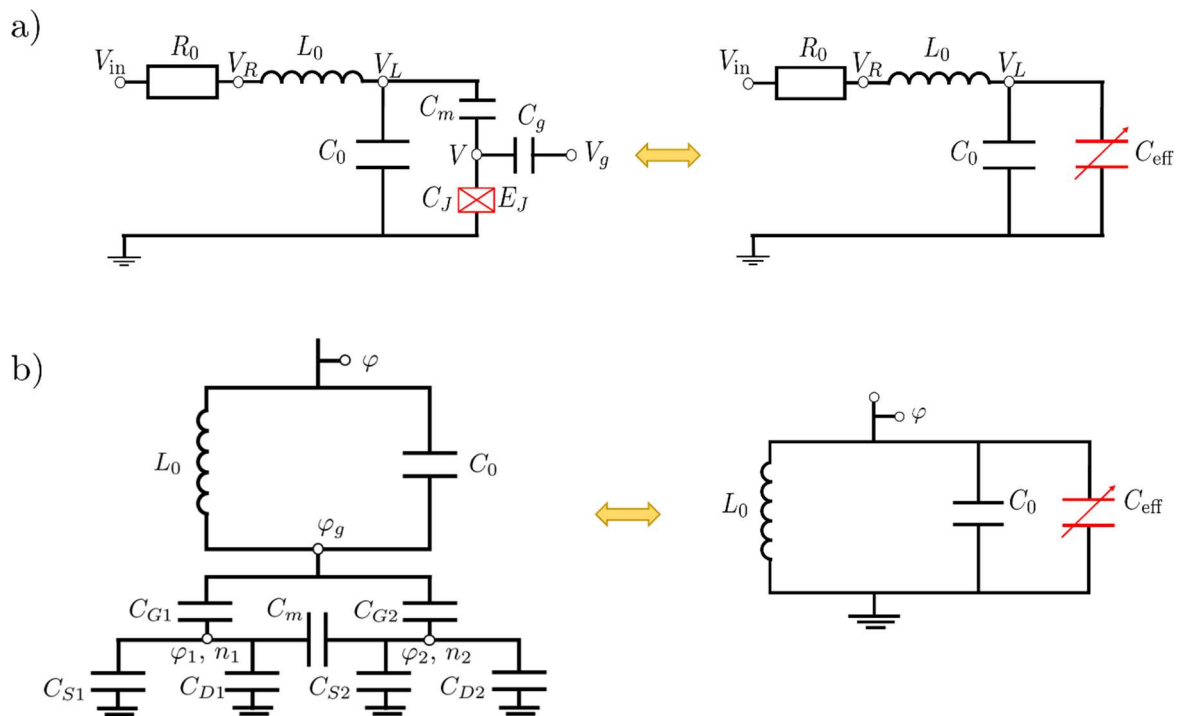


Fig.1 Examples of a single electron transistor [2] (a) and a double quantum dot [1] (b) coupled with classical LC circuit and respective equivalent circuits containing effective capacitances. The effective capacitance includes both quantum and tunneling capacitances.

[1] R. Mizuta, R. M. Oxtoa, A. C. Betz, M. F. Gonzalez-Zalba, , Phys. Rev. B 95, 045414 (2017). <https://doi.org/10.1103/PhysRevB.95.045414>.

[2] T. Duty, G. Johansson, K. Bladh, D. Gunnarsson, C. Wilson, P. Delsing, Phys. Rev. Lett. 95, 206807 (2005). <https://doi.org/10.1103/PhysRevLett.95.206807>.

[3] S. N. Shevchenko, A. N. Omelyanchouk, E. Ilichev, Low Temp. Phys. 38, 283 (2012). <https://doi.org/10.1063/1.3701717>.

Broadband and resonant spectroscopy of thin film resonators from disordered superconductors

M. Baránek¹, P. Neilinger^{1,2}, D. Manca^{1,2}, O.G. Turutanov^{1,3}, M. Grajcar^{1,2}

¹*Dept. of Experimental Physics, Faculty of Mathematics, Physics and Informatics, Comenius University Bratislava, Mlynská Dolina F1, 842 48 Bratislava, Slovakia*

²*Institute of Physics, Slovak Academy of Sciences, Dúbravská cesta 9, 84511 Bratislava, Slovakia*

³*B.Verkin Institute for Low Temperature Physics and Engineering of NAS of Ukraine,*

47 Nauky Ave., Kharkiv, 61103, Ukraine

e-mail: martin.baranek@fmph.uniba.sk

The technique of non-contact broadband transmission line and resonant flip-chip spectroscopy is utilized to probe resonances of mm-sized square resonators fabricated from strongly disordered molybdenum carbide films in the GHz frequency range [1]. The temperature dependence of the resonances was modelled by the surface impedance of the thin films via the complex conductivity of disordered superconductors [2], which reflects the Dynes superconducting density of states of these superconductors. The obtained Dynes broadening parameters from broadband spectroscopy relate reasonably well to those known from scanning tunnelling spectroscopy measurements. The eigenmodes of the 2D resonator were visualized by EM model in Sonnet software. The resonant spectroscopy was performed on a high quality niobium resonator, with significant drop in resonance quality with nonlinear behavior when the probing resonator frequency tunes to the strongly temperature dependent resonance frequency of MoC film. The system was modelled by lumped element approximation of inductively coupled resonators with nonlinear inductance and yields qualitative agreement with the experimental data. The nonlinear response can be utilized in e.g. parametric amplifiers. The bare MoC thin films, due to their high disorder, can be utilized e.g. as tunable superconducting filters with small dimensions.

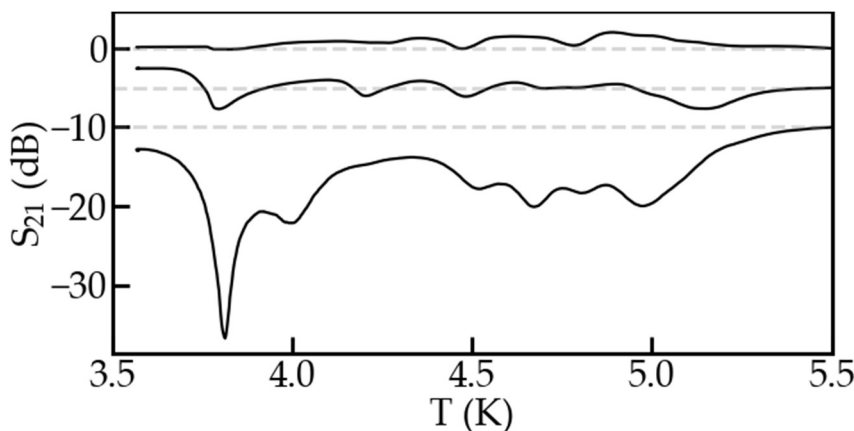


Figure: Temperature sweep of transmission coefficient S_{21} for 3, 6 and 9 GHz, with visible resonance dips. The values are offset by 5dB for each frequency.

This work was supported by the QuantERA grant SiUCs and by the project skQCI No. 101091548, founded by the European Union (DIGITAL) and the Recovery and Resilience Plan of the Slovak Republic. O.G.T. has been funded by the EU NextGenerationEU through the Recovery and Resilience Plan for Slovakia under the project No. 09I03-03-V01-00031. M.G. acknowledges support from Slovak Research and Development Agency under the contracts APVV-20-0425.

[1] M. Baránek et al., To be published. (preprint: <https://doi.org/10.48550/arXiv.2102.13483>)

[2] M. Žemlička et al., Phys. Rev. B 92, 224506 (2015).

<https://doi.org/10.1103/PhysRevB.92.224506>.

Detection of Villari effect in FeSe_{1-x}S_x (x=0.075)

I. V. Bilych¹, K. R. Zhekova¹, G. A. Zvyagina¹, V. D. Fil², D. V. Fil^{2,3}

¹*B.Verkin Institute for Low Temperature Physics and Engineering of NAS of Ukraine,
47 Nauky Avenue, Kharkiv, 61103, Ukraine*

²*Institute for Single Crystals, NAS of Ukraine, 60 Nauky Avenue, Kharkiv, 61072, Ukraine*

³*V.N. Karazin Kharkiv National University, 4 Svobody Square, Kharkiv, 61022, Ukraine
e-mail: bilich@ilt.kharkov.ua*

Recently, our experiments on acoustoelectric transformation (AET), see for example [1], showed that superconducting chalcogenides FeSe_{1-x}S_x demonstrate the strong AET signal that increases rapidly below the structural transformation temperature ($T_s < 90\text{K}$), and decreases almost to zero at the superconducting transition point. The specificity of the behavior of the AET signal can only be explained by the presence of piezomagnetic interaction in these compounds. Although it was considered that the structural and nematic phase transition observed in iron-based chalcogenides at T_s is not accompanied by long-range magnetic ordering, the registration of the AET signal, which we associate with the existence of piezomagnetism, indicates that a hidden magnetic order is realized in the orthorhombic FeSe_{1-x}S_x compounds, caused, for example, by the ordering of magnetoelectric quadrupoles. Importantly, such ordering breaks the time-reversal symmetry required for the occurrence of a piezoelectric response.

In piezomagnets, an elastic wave propagating in the sample excites oscillations of the magnetic moment in it, which cause oscillations of the electric field. At the free surface of the sample, these oscillations are transformed into an emitted plane electromagnetic wave, which is registered by a loop antenna. A measurement of the amplitude and phase of the AET signal at different orientations of the antenna, different polarization of the elastic mode, and in the presence of the external magnetic field make it possible to study the qualitative and quantitative characteristics of magnetoelastic effects.

This work is devoted to the study of magnetoelastic interactions in single crystals of FeSe_{1-x}S_x (x=0.075) in an external magnetic field. The rotation diagrams were studied in the absence and in an external magnetic field, which give the dependence of the amplitude and phase of the signal on the angle of rotation of the antenna. It was found that in the magnetic field, the plane of polarization of the emitted electromagnetic wave rotates, and the sign of the rotation angle corresponds to the sign of the applied magnetic field. This behavior can naturally be explained by the fact that in the presence of a magnetic field, an elastic deformation induces an additional magnetic moment directed along the other axis of the crystal.

The physical mechanism of the studied feature is that the elastic deformation leads to the appearance of a non-diagonal component of the magnetic susceptibility and to the generation of an additional alternating magnetic moment perpendicular to the external magnetic field and to the elastic displacement. The observed features are interpreted as a manifestation of the Villari effect, that is, a change in magnetization under the action of elastic deformation.

A phenomenological description of the experimental results is given. The observed effect indicates that the symmetry of the low-temperature phase FeSe_{1-x}S_x belongs to the triclinic syngony. The value of the piezomagnetic modulus in FeSe_{1-x}S_x is estimated. The results obtained can be considered as direct confirmation of the violation of time reversal symmetry in single crystals FeSe_{1-x}S_x. That is, the presence of piezomagnetism in FeSe_{1-x}S_x crystals indicates the existence of hidden magnetic order with an odd order parameter relative to the spin variables.

- [1] V. D. Fil, D. V. Fil, G. A. Zvyagina, K. R. Zhekova, I. V. Bilich, D. A. Chareev, M. P. Kolodyazhnaya, A. Bludov, and E. Nazarova, Phys. Rev. B 104, 094424 (2021). <https://doi.org/10.1103/PhysRevB.104.094424>.

Study of structural, mechanical, electronic and thermodynamic properties of the N₂CaNa full-Heusler alloy using DFT approach

E. B. Ettah¹, M. E. Ishaje¹, K. A. Minakova², V. A. Sirenko³, I. S. Bondar³

¹*Department of Physics, Cross River University of Technology, Calabar, Nigeria*

²*Department of Physics, National Technical University “Kharkiv Polytechnic Institute”,
2 Kyrpychova str., Kharkiv, 61002, Ukraine*

³*B.Verkin Institute for Low Temperature Physics and Engineering of NAS of Ukraine,
47 Nauky Ave., Kharkiv, 61103, Ukraine
e-mail: ibondar@ilt.kharkov.ua*

Heusler alloys, intermetallic compounds with flexible electronic, magnetic, and mechanical properties, have gained attention for their use in high-performance applications, particularly in spintronics. Full-Heusler alloys, characterized by their X₂YZ formula, incorporate transition metals and main-group elements and are known for their tunable properties. One such property is half-metallicity, where one spin channel is metallic, and the other is semiconducting. N₂CaNa, a relatively unknown full-Heusler alloy, has been proposed for advanced applications due to its theoretical half-metallicity and thermal stability, making it attractive for spintronic devices and materials requiring tailored thermal and mechanical resilience.

This study explores the structural, electronic, mechanical, and thermodynamic properties of the full-Heusler alloy N₂CaNa using density functional theory (DFT) to assess its potential in advanced applications such as spintronics and related fields. DFT calculations enable investigation of atomic structure and electronic interactions from first principles, providing accurate predictions of stability, electronic band structure, and thermodynamic behavior [1].

The DFT calculations were performed using the Vienna Ab initio Simulation Package (VASP), chosen for its efficient plane-wave basis set and projector augmented wave (PAW) method. The Perdew-Burke-Ernzerhof (PBE) generalized gradient approximation (GGA) was applied for the exchange-correlation function, with an energy cutoff of 500 eV ensuring accurate wavefunction representation. Quantum ESPRESSO was also utilized for specific thermodynamic calculations. Structural optimization was achieved using the third-order Birch-Murnaghan equation of state, refining lattice constants and minimizing energy. Electronic band structure and DOS were analyzed to explore the alloy's electronic characteristics. Mechanical properties were derived from elastic constants, bulk modulus, and shear modulus values, while thermodynamic properties were assessed using Debye and Einstein models to predict stability across temperatures.

Results for the structural analysis establish structural stability with a minimum formation energy of 29.9 eV. The compound is mechanically stable and ductile, as verified by the Pugh criterion with a B/G ratio of 4.766. The electronic band structure revealed half-metallicity, with metallic behavior in the majority spin channel and a narrow bandgap (~5.08 eV) in the minority channel. This feature enables N₂CaNa to conduct spin-polarized electrons, a valuable property for spintronics where data is processed via electron spin rather than charge. The DOS analysis corroborated these findings, showing significant contributions from nitrogen 2p, calcium 2s, and sodium 4p orbitals near the Fermi level. The hybridization of these atomic states enhances N₂CaNa's potential in spin-based electronic applications and facilitating efficient data storage and processing.

The results demonstrate potential N₂CaNa for applications in spintronics, structural engineering, and other fields requiring materials with tailored properties.

- [1] E.B. Ettah, K.A. Minakova, M.E. Ishaje et al., Low Temp. Phys. 49, 1389 (2023).
<https://doi.org/10.1063/10.0021371>.

Differential shot noise and Fano factor in mesoscopic junctions with inhomogeneous superconductors

V. Dmytrenko¹, E. Zhitlukhina^{1,2}, P. Seidel³

¹*O.O. Galkin Donetsk Institute for Physics and Engineering of NAS of Ukraine,
46 Nauky Ave., Kyiv, 03028, Ukraine*

²*Centre for Nanotechnology and Advanced Materials, Faculty of Mathematics, Physics and
Informatics, Comenius University Bratislava, Mlynská dolina, Bratislava, 84248, Slovak Republic*

³*Institut für Festkörperphysik, Friedrich-Schiller-Universität Jena,
5 Helmholtzweg, Jena, 07743, Germany
e-mail: dmitrenko_v@ukr.net*

Measurements of the differential shot-noise characteristics arising from out-of-equilibrium current fluctuations in mesoscopic systems is a powerful tool to probe the nature of current carrying excitations in quantum systems [1]. While differential conductance-vs-voltage $G(V)$ curves provide information on the average probability of the quasiparticles transmission from source to drain, shot noise has proven invaluable for understanding their charge and the transport statistics for the structures under study. Unlike mesoscopic devices with normal electron reservoirs, shot noise can be enhanced in devices with superconducting leads due to Andreev reflection processes occurring at the interface between the normal metal (N) and the superconductor (S). Therefore, combined studies of the differential shot noise $S_I(V)$ and the Fano factor $F(V)$, defined as the ratio of average current fluctuations to the average current, can be used as an extremely effective way to characterize hybrid N/S-based systems.

Using the simplest approximations, the most important of which is the homogeneity of the superconductor, the famous BTK theory, see Ref. [2], explained in principle the shape of the $G(V)$ curves for N/I/S trilayers with an insulating barrier I and made it possible to calculate corresponding noise properties. In this contribution, we take a step further and develop a methodology of obtaining $G(V)$, $S_I(V)$, and $F(V)$ transport characteristics for five-layer N/I₁/S₁/I₂/S₂ heterostructures, remaining at the same time within the framework of the BTK approximations. Its main idea based on the methods of scattering theory is to interpret the charge transmission across the multilayer as a sequence of an infinite number of interface scattering events, sequentially increasing the number of layers and applying the formula for a double-barrier system at each stage [2].

Numerical calculations show fundamental differences between the results expected for single- and two-barrier junctions. New features that are absent in the BTK theory include the appearance of a significant $G(V)$ dip in the voltage range between the two gaps and the ratio of the zero-bias conductance to that at voltages above the larger gap, which can significantly exceed the value of two expected from the BTK approach. These results show that point-contact spectroscopy, providing direct information on the amplitude and symmetry of the superconducting order parameter and offering versatility in probing various regions of superconductors could also be a source of information about the spatial variation of the order parameter. In the latter case, respective noise characteristics complement associated differential conductance data, which is crucial for understanding complex superconducting systems.

Elena Zhitlukhina acknowledges support of the EU NextGenerationEU through the Recovery and Resilience Plan for Slovakia under Project 09I03-03-V01-00140. This work was supported by the German-Ukrainian collaborative project “Controllable quantum-information transfer in superconducting networks” (DFG project SE 664/21-1, No. 405579680).

- [1] K. Kobayashi and M. Hasgisa, *J. Phys. Soc. Jpn.* **90**, 102001 (2021). <https://doi.org/10.7566/JPSJ.90.102001>
- [2] M. Belogolovskii and E. Zhitlukhina, in *Comprehensive Guide to Superconductivity*, ed. R. Morrow (Nova, New York, Hauppauge 2021), Chapter 2. ISBN: 978-1-53618-901-8.

Anomalies of dissipative and kinetic properties of the high-entropy alloy $\text{Al}_{0.5}\text{CoCuCrNiFe}$ below ~ 300 K

**V. A. Frolov, N. A. Azarenkov, E. V. Karaseva, V. S. Klochko,
A. V. Korniets, V. I. Sokolenko, V. S. Okovit, A. V. Poida**

National Science Center "Kharkiv Institute of Physics and Technology", Kharkiv, 61108, Ukraine
e-mail: vsokol@kipt.kharkov.ua

Attention to anomalies of the dissipative properties of the high-entropy alloy (HEA) $\text{Al}_{0.5}\text{CoCuCrNiFe}$ below ~ 300 K was first drawn in [1], where a resonance of internal friction Q^{-1} was reported in range of ~ 260 -160 K with $T_{\max} \approx 230$ K. The Koiwa–Hasiguti' resonance of the dislocations thermally torn away from point defects was assumed [2] as the mechanism. Later, the anomalies of the absolute thermopower S and electrical resistance R were discovered in same alloy in a partially overlapping range of ~ 210 -170 K. They were explained [3] by the electron-hole transformations (conversion) of one type charge carriers into another (electrons into holes and vice versa). It was of interest to determine the presence of the correlations between the two phenomena. The practical aspect also important: the alloy is considered as promising for use at low temperatures, where the anomalous interval is located. These two motives initiated further study of dissipative and kinetic anomalies of the $\text{Al}_{0.5}\text{CoCuCrNiFe}$ alloy below ~ 300 K. The studies were performed on the same samples. As a tool for studying the dissipative features, the temperature dependences of the velocity v and attenuation β of longitudinal ultrasonic (US) waves of ~ 50 MHz were measured. In order to identificate the kinetic anomalies, the temperature dependences of the absolute thermopower S and electrical resistance R were measured. It was found that β anomalously increases with decreasing T in the range of ~ 240 -120 K, reaching a maximum of $\sim 100\%$ at $T_{\max\beta} \approx 180$ K. The energy activation of this maximum is close to the energy of Bordoni' relaxation resonance. The velocity $v(T)$ demonstrates a deflection in the same range indicating a "softening" of the coefficients controlling the sound passage. The $S(T)$ and $R(T)$ dependences demonstrate the presence of the same anomalous interval of ~ 240 -120 K, in which all their features correlate strong with corresponding features of the $\beta(T)$ dependence. The anomalies of the $S(T)$ -curve are most pronounced. They identified as a consequences of a crossover of the latent conversions of charge carriers. According to S -data, the hole carriers concentration into the anomalous interval is increased compare to value at $T \sim 300$ K. The peak temperature of the thermoelectric anomaly is $T_{\max S} \approx 190$ K. Here, the hole-carriers subsystem has maximum addition. Take notice that $T_{\max S}$ almost coincides with $T_{\max\beta} \approx 180$ K. The ohmic data confirm the presence of an increased of hole carriers concentration in the anomalous interval, although the ohmic conversion effect itself is small. Thus, both kinetic data indicate strictly correlates of the increase of US attenuation with an increased of hole charge carriers concentration. Conclusion. Since in the studies of internal friction [1] the sample was subjected by mechanical action initiated resonance in the dislocation system, but the kinetic data free this factor, one conclude that explanations [2] and [3] are not contradictory, especially taking into account the enormous discrepancy (~ 40 K) between the temperatures of the maximum manifestations of the Koiwa-Hashiguchi' resonance and discovered ultrasonic resonance correlating strong with (caused by?) electron-hole conversion. The question remains open what the reasons of such a strong attenuation β itself in latter case. Two reasons are under consideration 1) the Bordoni' relaxation resonance; 2) electron-hole ultrasonic resonance, consisting in a change in the ratio between electron and hole components of the spontaneous magnetization.

- [1] Yu. O. Semerenko, O. D. Tabachnikova et al., Metallofiz. Nov. Tekhn. 37, 1527 (2015).
- [2] Yu. O. Semerenko, V. D. Natsik, Low Temp. Phys. 46, 78 (2020).
<https://doi.org/10.1063/10.0000367>.
- [3] V. N. Voyevodin, V. A. Frolov, E. V. Karaseva et al., Funct. Mater. 28, 683 (2021).
<https://doi.org/10.15407/fm28.04.683>.

Optical and transport properties of NbN thin films revisited

**S. Kern¹, P. Neilinger^{1,2}, M. Poláčková¹, M. Baránek¹, T. Plecenik¹, T. Roch¹, and
M. Grajcar^{1,2}**

¹*Department of Experimental Physics, Comenius University, SK-84248 Bratislava, Slovakia*

²*Institute of Physics, Slovak Academy of Sciences, Dúbravská cesta, SK-84511 Bratislava, Slovakia*

e-mail: samuel.kern@fmph.uniba.sk

Highly disordered NbN thin films exhibit promising superconducting and optical properties [1]. Despite extensive study, significant disagreement persists with regards to some of their electronic properties persist.

First, the characterization of the disorder in NbN is obtained from transport and Hall effect measurements. This is done via the Ioffe-Regel parameter $k_F l$, where k_F is the Fermi wave vector and l is the electron mean free path. It is well known that $k_F l \sim 1$ can be obtained in thin NbN films, and such highly disordered films are approaching metal-insulator transition [2]. Alternatively, this criterion can be expressed via electron scattering rate in energy units $\hbar\Gamma$, which is comparable to the Fermi energy. Therefore, in highly disordered metals, $\hbar\Gamma$ is expected to be a couple eV.

Second, analysis of the optical conductivity of disordered ultrathin NbN films, obtained from spectroscopic ellipsometry by the standard Drude-Lorentz model, gives $\hbar\Gamma$ an order of magnitude lower [3].

We argue that this discrepancy arises from neglecting the presence of quantum corrections to conductivity in the IR range. To resolve this matter, we suggest a modification to the Drude-Lorentz model, incorporating quantum corrections. The parameters obtained from the modified model are consistent with transport and superconducting measurements. The revisited values describing conduction electrons, which differ significantly from commonly adopted ones, are the electron relaxation rate, $\hbar\Gamma \approx 1.8$ eV, the Fermi velocity $v_F \approx 0.7 \cdot 10^6$ m·s⁻¹, and the electron density of states $N(E_F) = 2$ states of both spins/eV/V_{fu}.

This work was supported by the project skQCI No. 101091548, founded by the European Union (DIGITAL) and the Recovery and Resilience Plan of the Slovak Republic and the Operational Program Integrated Infrastructure for the projects: Advancing University Capacity and Competence in Research, Development and Innovation (ACCORD, ITMS2014 + :313021X329). M.G. acknowledges support from Slovak Research and Development Agency under the contracts APVV-20-0425.

- [1] L. Toth, *Transition Metal Carbides and Nitrides* (Elsevier, Amsterdam, The Netherlands, 2014).
- [2] S. P. Chockalingam, M. Chand, J. Jesudasan, V. Tripathi, and P. Raychaudhuri, Phys. Rev. B 77, 214503 (2008). <https://doi.org/10.1103/PhysRevB.77.214503>.
- [3] A. Semenov, B. Günther, U. Böttger, H.-W. Hübers, H. Bartolf, A. Engel, A. Schilling, K. Ilin, M. Siegel, R. Schneider *et al.*, Phys. Rev. B 80, 054510 (2009). <https://doi.org/10.1103/PhysRevB.80.054510>.

Spin-dependent resonant tunneling through a magnetic quantum dot coupled to superconducting and ferromagnetic leads: F-mQD-S system

E. A. Koshina, V. N. Krivoruchko

*O.O. Galkin Donetsk Institute for Physics and Engineering of NAS of Ukraine,
 46 Nauky Ave., Kyiv, 03028, Ukraine
 e-mail: elena.koshina1@gmail.com*

Various theoretical proposals exist to transform states induced by magnetic nanoparticles inside a superconducting gap into Majorana fermion states. The main challenge in this route is conclusive proof and undoubtedly distinguishing between topologically trivial subgap Andreev bound states (ABS) and topologically nontrivial magnetically polarized Majorana bound states. This motivated us to investigate nonequilibrium electrons tunneling through a ferromagnetic metal–magnetic quantum dot–s-wave superconductor (F-mQD-SC) nanostructure [1]. Special attention is devoted to analyzing the implications of the spin-splitting electron levels in the dot on the tunneling process and the system’s conductance characteristics. Using Keldysh Green’s function method, the expressions for tunnel current and probability of the Andreev reflection (AR) versus energy are derived and studied. In contrast to a system with non-magnetic QD, where the differential conductance exhibits a series of peaks with equal intervals, the conductance of the F-mQD-SC system demonstrates a more complicated pattern. This property originates from the splitting levels of the mQD by an effective (external and proximity-induced) magnetic field and, if the energy levels of the mQD are not equal spacing, the series of peaks will be much more complicated. We find that the system’s resonant ARs conductance exhibits different kinds of peaks depending on a spin splitting of the mQD levels, the spin polarization magnitude of the F-lead current, the gate voltage, and an external magnetic field magnitude. The nanostructure’s conductance versus a bias voltage exhibits extra peaks which at some combination of its parameters can mimic ones expected for Majorana modes in a topological superconducting state. We found that a series of additional peaks appeared due to energy levels spin-splitting in the mQD by the external magnetic field. I.e., for distinguishing between trivial and topological zero-bias conductance peculiarities arising from the coalescence of ABS, the magnetic field effect on the peak position is important (see Fig.1). We suggest the

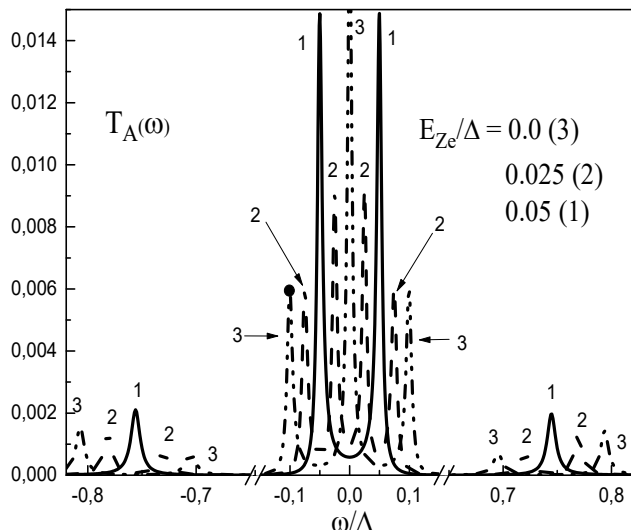


Fig.1. The resonant AR probability $T_A(\omega)$ vs the energy ω when the F-lead current spin polarization is fixed $P=0.1$, the mQD has two states $\epsilon_1^0 = 0.3\Delta$ and $\epsilon_2^0 = -0.5\Delta$, the gate voltage $V_g = 0.25\Delta$, the Zeeman energy $E_{Ze} = 0.05\Delta$ (1), 0.025Δ (2), 0 (3), the linewidths $\Gamma_{F0} = \Gamma_S = 0.01$.

presented results will be useful to determine whether the topological or non-topological superconducting phase is induced in F-mQDs-SC nanostructures.

- [1] V. N. Krivoruchko and E. A. Koshina. Low Temp. Phys. 49, 1015 (2023).
<https://doi.org/10.1063/10.0020593>.

Properties of a metal-dielectric-metal point junction before and after electrical breakdown of a dielectric nanolayer

V. P. Koverya, A. V. Krevsun, S. I. Bondarenko

B.Verkin Institute for Low Temperature Physics and Engineering of NAS of Ukraine,
47 Nauky Ave., Kharkiv, 61103, Ukraine
e-mail: koverya@ilt.kharkov.ua

The work is a continuation of the research of an original and straightforward method of creating Josephson junctions during electrical breakdown of a dielectric nanolayer [1, 2]. Unlike junctions we have previously studied, the considered one is formed by mechanical point pressing of a U-shaped wire with a diameter of about 50 microns. The wire made of an InSn alloy (cathode) is closely positioned to the surface of an oxide nanolayer on the Nb film (anode). The breakdown method is similar to that described in [1, 2]. At 300K, the structure and electrical properties of the junction were studied before and after electrical breakdown of the oxide with a thickness ranging from 15 to 60 nm. Before breakdown, the capacitance of the junction with an oxide thickness of 15 nm with a corresponding current-voltage characteristic (CVC) were measured. The CVC shape indicates a semiconductor type of oxide. During the short breakout time, two simultaneous processes occur. First, the wire cathode melts at the point of contact over an area of about $6 \mu\text{m}^2$. Second, an InSn nanobridge is formed inside of the oxide with a length, equal to the thickness of the oxide. The resistance obtained (at oxide thicknesses of 30–60 nm) is close to that one of nanobridges during breakdown between film electrodes [1, 2]. The electric field strength of the breakdown of oxide with a thickness of 15 nm and the resistance of the formed bridges were found to be significantly greater in comparison with those for oxide thicknesses of 30-60 nm. Critical values of breakdown current ($1-2 \mu\text{A}$) and the minimum value of capacitor capacitance ($10^{-3} \mu\text{F}$) at which oxide breakdown does not occur have been determined. For the first time, it was discovered that the CVC of bridges with a length of 15 nm consists of an initial linear and two nonlinear sections (Fig. 1). Two phase transitions explain the dynamics observed: the solid bridge turns into liquid (starting at 15 mA) and then evaporates (at 34 mA) due to overheating of the bridge by the transport current.

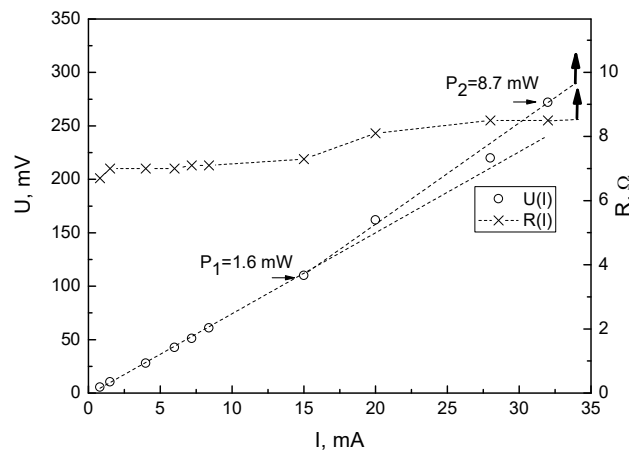


Fig. 1. Current-voltage characteristic of the junction and the dependence of the junction resistance on the current $R(I)$.

- [1] S. I. Bondarenko, A. V. Krevsun, V. P. Koverya, A. G. Sivakov, R. S. Galushkov, Low Temp. Phys. 48, 741 (2022). <https://doi.org/10.1063/10.0013310>.
- [2] A. V. Krevsun, S. I. Bondarenko, V. P. Koverya, Low Temp. Phys. 49, 83 (2023). <https://doi.org/10.1063/10.0016479>.

Electronic properties of the boundary between hexagonal and Lieb lattices

I. V. Kozlov, Yu. A. Kolesnichenko

*B.Verkin Institute for Low Temperature Physics and Engineering of NAS of Ukraine,
47 Nauky Ave., Kharkiv, 61103, Ukraine
e-mail: kozlov@ilt.kharkov.ua*

A boundary of two media with different topological order can be characterized by series of properties, the existence of which the existence of which is associated with the difference in the nature of the two materials. The well-known example is the surface conductivity of topological insulators. In the present study, the boundary between a conventional Dirac conductor and a conductor with Dirac cone without Berry phase in the electron energy spectrum is considered. A similar system can be implemented on the boundary between hexagonal and Lieb lattices [1]. The geometry of the problem was chosen based on considerations of maximum similarity of the classical electron energy spectrum of both conductors. As was shown earlier and first presented at the previous conference, in such system specific edge states appear that implement a continuous transition between two types of topological conductors. Despite a number of interesting theoretical properties, this system cannot be considered simple for experimental research. Thus, it is of interest to search for and calculate characteristics that are most convenient for observation, which is the goal of the presented study.

As part of this task, the contribution to magnetization appearing from the orbital magnetism of edge states is obtained. The dependences of the local density of states $\rho(\mathbf{r}, E)$ and current density $\mathbf{j}(\mathbf{r}, E)$ were calculated numerically. The first is similar to the value considered by the authors in the work [2] for systems of a different nature. The numerical calculation recurrently uses the previously obtained analogue of the area quantization rule and quasi-classical wave functions. These dependencies can be useful in studying edge states using STM. The contribution of edge states to the Hall conductivity also attracted attention. Its existence is guaranteed by an additional twofold degeneracy of the Landau levels in the hexagonal lattice, which is absent in the Lieb lattice and can be considered a natural manifestation of the theorem [3] on the even number of cone points in usual Dirac conductors.

- [1] Elliott H. Lieb, Phys. Rev. Lett. 62, 1201 (1989).
<https://doi.org/10.1103/PhysRevLett.62.1927.5>.
- [2] I. V. Kozlov, Yu. A. Kolesnichenko, Low Temp. Phys. 43, 855 (2017).
<https://doi.org/10.1063/1.4995636>.
- [3] H. B. Nielsen, M. Ninomiya, Physics Letters 105B, 219 (1981).
[https://doi.org/10.1016/0370-2693\(81\)91026-1](https://doi.org/10.1016/0370-2693(81)91026-1).

Point-contact spectroscopy features of MoRe superconducting alloy

I. Martynenko^{1,2}, V. Tarenkov^{2,3}, V. Krivoruchko³, A. Shapovalov^{1,2}, O. Kalenyuk^{1,2}, E. Zhitlukhina^{3,4}, M. Belogolovskii^{2,4}

¹*G.V. Kurdyumov Institute for Metal Physics, NAS of Ukraine, 03142, Kyiv, Ukraine*

²*Kyiv Academic University, 03142, Kyiv, Ukraine*

³*O.O. Galkin Donetsk Institute for Physics and Engineering of NAS of Ukraine,
46 Nauky Ave., Kyiv, 03028, Ukraine*

⁴*Centre for Nanotechnology and Advanced Materials, Faculty of Mathematics, Physics and
Informatics, Comenius University Bratislava, 84248, Bratislava, Slovak Republic*

e-mail: i.martynenko@kau.edu.ua

The development of quantum devices (SQUIDs, Rapid Single Flux Quantum, RSFQ) is of great interest nowadays, and superconductors are the basis for creating these devices. Creating and improving the superconducting properties of superconductors is the key to creating and improving these devices. Our MoRe alloy under study is a low-temperature superconducting alloy that has high anti-corrosion properties, resistance to mechanical stress, and is also resistant to thermal cycling. To improve the properties of MoRe, we used the mechanical method of surface treatment HPT (high-pressure torsion) [1]. The treatment consists in fixing the sample (1 mm thick) between two anvils, one of which made 5 revolutions relative to the other under a pressure of $P = 20$ kbar. The analysis of the processing result was carried out on an optical microscope after etching the sample in 35% HNO_3 , and an elongated coarse-grained structure was found before HPT treatment, and after HTP treatment, the orientation of the grains corresponded to an anisotropic pattern with a decrease in the size of these grains.

One of the methods for studying the fundamental characteristics of superconductors is point-contact spectroscopy, which is based on the Andreev reflection effect at the interface between a superconductor and a conventional metal. Due to the very small contact plane of the order tens of nanometers and larger, almost all incident electrons with energy below the energy gap Δ undergo Andreev reflections, which are theoretically described by solving the Bogolyubov-de Gennes equations. An Ag needle was used as a conventional metal, which created an N/S contact with a small area. The obtained differential conductivities of the contact before and after MoRe treatment revealed changes. Interpretation of the curves according to the Blonder-Tinkham-Klapwick model gave values $\Delta_1 = 0.81$ meV, and $\Delta_2 = 1.62$ meV, before and after HPT, respectively. The ratio of the energy band gap to the critical temperature from the BSC theories has a universal value of $2\Delta/kT_c = 3.52$, which is sensitive to the strength of the electron-phonon interaction. In our case, $2\Delta_1/kT_c = 2.1$ before HTP, which corresponds to the depletion of the superconducting phase on the sample surface, and $2\Delta_2/kT_c = 4.2$ after HTP, the value not only returns to the typical one but also increases, thereby indicating the presence of a strong electron-phonon coupling after treatment. The increase in the electron-phonon interaction in our samples after HTP treatment is associated with the loss of crystallinity and their subsequent amorphisation. This is based on the theory of phonon-mediated superconductivity in amorphous materials with strong bonding [2]. The increase in the strength of the electron-phonon interaction is controlled by the growing role of low-frequency transverse phonon excitations.

This work was supported by the National Academy of Sciences of Ukraine through the research program No. 0125U000295 (G.V. Kurdyumov Institute for Metal Physics).

[1] T. Nishizaki, S. Lee, Z. Horita, T. Sasaki and N. Kobayashi, Physica C 493, 132 (2013). <https://doi.org/10.1016/j.physc.2013.03.046>.

[2] M. Baggio, C. Setty, and A. Zacccone, Phys. Rev. B 101, 214502 (2020). <https://doi.org/10.1103/PhysRevB.101.214502>.

Analysis of the influence of vortex dynamics on the possibility of an avalanche-like transition of a microwave nonlinear HTS transmission line into a dissipative state

S. I. Melnyk

O.Ya. Usikov Institute for Radiophysics and Electronics NAS of Ukraine,
12, Ac. Proskury st., Kharkiv, 61085, Ukraine
e-mail: melnyksergiy72@gmail.com

In an experimental study of the properties of a microwave (MW) transmission line of the coplanar waveguide type based on high-temperature superconductors (HTS) at certain values of the input power P_{in} and direct current (DC) I_{dc} , the effect of strong (abrupt) changes in MW losses at a certain waveguide temperature $T < T_c$, where T_c is the critical temperature, was discovered [1].

The nature of the studied behavior of the MW loss dependencies allows us to consider the abrupt changes in the properties of a nonlinear HTS transmission line as a "catastrophe" of the "fold" type and to use the methodological and mathematical apparatus of the "catastrophe" theory to describe it [2].

It was shown that taking into account the fourth-degree term in the expansion of the dependence of the HTS properties on current and changing the sign of the quadratic term allows us to qualitatively explain the experimentally observed effects.

$$R_1(t) \approx R_{11} \left[1 - \frac{I(t)^2}{I_{0R}^2} + \frac{I(t)^4}{I_{0R}^4} \right]$$

In [3], an approximation of existing nonlinearity models for the case of strong and weak currents by a fourth-degree polynomial is proposed. However, positive values of both nonlinear terms do not provide the occurrence of a "fold" type feature. Therefore, we can assume the presence of an additional physical factor that provides the occurrence of an inflection point on the $R_1(I)$ dependence. Such a factor may be a feature of the vortex structure dynamics in a microwave field, which is not taken into account in the previously considered models.

The description of the vortex dynamics arising in HTS thin-film under the influence of an alternating magnetic field is usually carried out within the framework of the phenomenological model proposed by Bean. It gives good agreement with the experiment for frequencies up to 100 kHz, but cannot be directly used for the case of a MW field and additional direct current.

In this report, we analyzed the possibility of such a generalization of the Bean model, as well as the possibility of the influence of the vortex structure dynamics on the nature of the nonlinear $R_1(I)$ dependence. In particular, the asymmetry of the vortex density distribution and its possible hysteresis dynamics in the presence of DC are described. Preliminary analytical estimates of the effect under consideration are made and the results of numerical modeling are presented.

The work was performed within the framework of Agreement No 4.5/25-II on Jan. 1, 2025 between National Academy of Sciences (NAS) of Ukraine and O. Ya. Usikov IRE of NAS of Ukraine.

- [1] N. Cherpak, A. Lavrinovich, A. Gubin, S. Vitusevich, IEEE Trans. on Appl. Supercond. 26, 1501204 (2016). <https://doi.org/10.1109/TASC.2016.2537138>.
- [2] S. I. Melnyk, S. S. Melnyk, A. A. Lavrinovich, N. T. Cherpak, Low Temp. Phys. 46, 358 (2020). <https://doi.org/10.1063/10.0000867>.
- [3] S. M. H. Javadzadeh, F. Farzaneh, M. Fardmanesh, Phys. C Supercond. 486, 37 (2013) <https://doi.org/10.1016/j.physc.2013.01.012>.

Features of vortex dynamics in the description of microwave absorption by a thin HTSC disk

S. I. Melnyk, N. T. Cherpak

*O.Ya. Usikov Institute for Radiophysics and Electronics NAS of Ukraine,
12, Ac. Proskury st., Kharkiv, 61085, Ukraine
e-mail: melnyksergiy72@gmail.com*

The study of the dynamics of the vortex structure caused by the action of the perpendicular alternating magnetic fields on high-temperature superconductor (HTS)-based film structures has a long history. The most complete review of the models used for this and an analysis of their compliance with the experimental results obtained is given in [1]. All existing models, one way or another, are generalizations of the phenomenological Bean model, in which the mechanism of the emergence and movement of vortices is not considered. In fact, this implies a quasi-stationary state of the vortex structure, which adequately describes the dynamics of the distribution of the magnetic field up to frequencies of about 100 kHz. In this regard, the applicability of the obtained results to the MW range is questionable. Models of absorption of the microwave (MW) field by a vortex structure formed by an additional large constant magnetic field have also been analyzed in sufficient detail [2]. They consider the absorption mechanism associated with the oscillatory motion of pinned or free vortices, the distribution of which is specified by a large constant component of the field.

However, in the case of only MW action of perpendicular orientation on a thin HTSC disk, the vortices do not have time to move over sufficiently large distances, and the dynamics of their radial distribution is apparently associated with reorientation or annihilation mechanisms. We analyzed the correspondence of this hypothesis and the Bean model, and developed a corresponding numerical model.

The obtained results of the analysis are of particular interest in connection with the previously discovered strange feature of the response of the thin $\text{FeSe}_{1-x}\text{Te}_x$ film in a perpendicular MW field [3]. It is completely absent for a parallel orientation of the film. And, most surprisingly, this feature manifested itself only in the films of $\text{FeSe}_{1-x}\text{Te}_x$ superconductors and did not manifest itself in the films of other type II superconductors. It was hypothesized that with perpendicular orientation, two competing mechanisms of MW energy dissipation in the film may take place, one of which leads to an increase in energy dissipation caused by magnetic vortices with the MW field, and the other to a decrease due to the emergence of Majorana bound states with zero energy [4].

The work was performed within the framework of Agreement No 4.5/25-II on Jan. 1, 2025 between National Academy of Sciences (NAS) of Ukraine and O. Ya. Usikov IRE of NAS of Ukraine.

- [1] D. V. Shantsev, Y. M. Galperin, and T. H. Johansen, Phys. Rev. B 60, 13112 (1999) <https://doi.org/10.1103/PhysRevB.60.13112>.
- [2] O. Dobrovolskiy, (2024). Fast Dynamics of Vortices in Superconductors. In T. Chakraborty (Ed.), Encyclopedia of Condensed Matter Physics (Vol. 2, pp. 735-754). Elsevier. <https://doi.org/10.1016/B978-0-323-90800-9.00015-9>.
- [3] Y. Wu, A. A. Barannik, L. Sun, Y.-S. He, N. T. Cherpak, The unusual microwave response of chalcogenide $\text{FeSe}_{1-x}\text{Te}_x$ film compared to other superconductors, Condensed Matter & Low Temperature Physics: II Intern. Advanced Study Conference, June 6-12 (2021).
- [4] N. T. Cherpak, A. A. Barannik, Y. S. He, L. Sun, Y. Wu, S. I. Melnyk, Possible manifestation of topological superconductivity and Majorana bound states in the microwave response of thin $\text{FeSe}_{1-x}\text{Te}_x$ film, arXiv:2312.11155 (2023). <https://doi.org/10.48550/arXiv.2312.11155>.

Electron transport in pressed VO₂ samples: Mott hopping vs percolation behavior

E. Yu. Beliayev¹, I. G. Mirzoiev¹, V. A. Horielyi¹, A. V. Terekhov¹, I. A. Chichibaba²

¹B.Verkin Institute for Low Temperature Physics and Engineering of NAS of Ukraine,
 47 Nauky Ave., Kharkiv, 61103, Ukraine

²National Technical University “Kharkiv Polytechnic Institute”,
 2 Kyrpychova str., Kharkiv, Ukraine
 e-mail: beliayev@ilt.kharkov.ua

Vanadium dioxide is a transition metal oxide that exhibits a sharp metal-insulator transition (MIT) near 340 K, making it a key material for electronic and functional applications. However, when VO₂ is synthesized in a nanopowder form and compressed into bulk samples, the influence of structural disorder and interparticle effects significantly alters its electrical transport behavior. In this study, we investigate the temperature-dependent conductivity of compressed VO₂ nanopowders to distinguish between Mott variable-range hopping (VRH) and percolation-driven transport mechanisms. VO₂ powders (Fig. 1) were synthesized hydrothermally [1] and characterized using scanning electron microscopy (SEM) and X-ray diffraction (XRD), confirming the presence of monoclinic VO₂ (M) and high-temperature tetragonal VO₂ (B) polymorphs. The pressed samples were analyzed in a temperature range of 78–700 K using a 4-probe DC method. Electrical measurements reveal a decrease in resistivity with temperature, without a pronounced conductivity jump typically observed in VO₂ single crystals (Fig. 2).

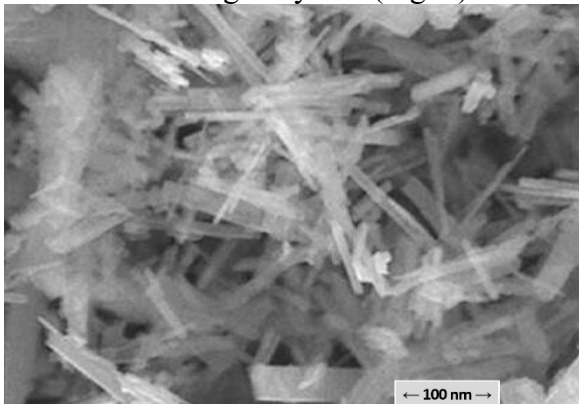


Fig. 1. SEM image for synthesized VO₂ nanoparticles.

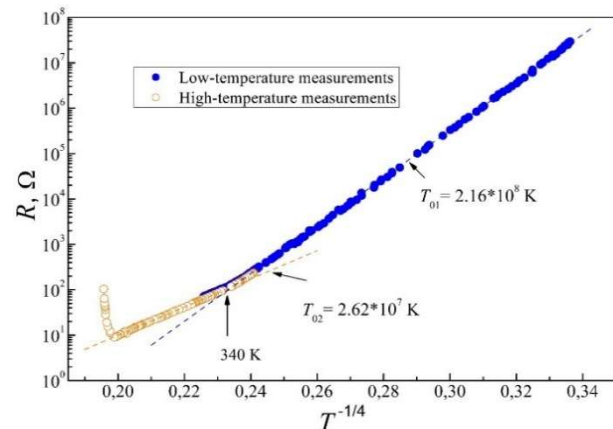


Fig. 2. $\ln R \propto T^{-1/4}$ plot for VO₂ pressed powder sample.

The temperature dependence of resistance followed a Mott Variable Range Hopping (VRH) behavior with a characteristic $R(T) \propto \exp(T_0/T)^{-1/4}$ scaling, indicative of electron localization. However, analysis of the localization length ζ and the density of states at the Fermi level $N(E_F)$ [2] suggests that Mott's model alone does not fully describe electron transport. Instead, the observed conductivity changes were strongly influenced by percolation effects arising from interparticle barriers and anisotropic current paths within the compressed granular structure. A transition between different conduction regimes occurs around the MIT temperature, where the material exhibits a shift in the percolation network, altering electronic pathways. The presence of insulating grain boundaries (e.g., minor V₂O₅ inclusions) and variations in particle connectivity contribute to the suppression of a sharp MIT signature. The obtained results highlight the interplay between Mott VRH hopping and percolation conduction in disordered VO₂ nanopowder systems, emphasizing the importance of considering percolation effects in nanostructured oxide materials.

[1] Y. V. Petukhova, O. M. Osmolowskaya, M. G. Osmolowsky, J. Phys. Conf. Ser. 643, 012121 (2015); <https://doi.org/10.1088/1742-6596/643/1/012121>.

[2] J.-P. Pouget, Comptes Rendus. Phys. 22(1), 37 (2021). <https://doi.org/10.5802/crphys.74>.

Hydrostatic pressure effect on the pseudogap in slightly doped $\text{Y}_{0.77}\text{Pr}_{0.23}\text{Ba}_2\text{Cu}_3\text{O}_{7-\delta}$ single crystals

E. V. Petrenko¹, L. V. Bludova¹, A. S. Kolisnyk¹, A. Sedda², E. Lähderanta², R. V. Vovk³, A. L. Solovjov^{1,2,4}

¹*B.Verkin Institute for Low Temperature Physics and Engineering of NAS of Ukraine,
47 Nauky Ave., Kharkiv, 61103, Ukraine*

²*Lappeenranta University of Technology, School of Engineering Science,
Lappeenranta, Finland*

³*Physics Department, V.N. Karazin Kharkiv National University,
4 Svobody Square, Kharkiv, 61022, Ukraine*

⁴*Institute for Low Temperatures and Structure Research, of PAS, Wroclaw 50-422, Poland
e-mail: petrenko@ilt.kharkov.ua*

The pseudogap (PG) state, which is opened in cuprate high-temperature superconductors (HTSCs) below the characteristic temperature $T^* \gg T_c$, is one of the most mysterious and simultaneously interesting phenomena in modern solid state physics [1]. It is well established that in HTSCs, the PG is observed when the charge carrier concentration varies between slightly doped (SD) and optimally doped levels. Understanding the PG physics would definitely shed more light on the mechanism of superconducting pairing in HTSCs, which is also not fully clarified yet. The $\text{YBa}_2\text{Cu}_3\text{O}_{7-\delta}$ cuprate is believed to be the most reliable material for studying the PG [1], especially when high pressures is applied [2]. In our work, for the first time, we carried out the analysis of the influence of hydrostatic pressure up to 1.1 GPa on the temperature dependence of pseudogap $\Delta^*(T)$ of the SD $\text{Y}_{0.77}\text{Pr}_{0.23}\text{Ba}_2\text{Cu}_3\text{O}_{7-\delta}$ single crystals. It is shown that the pressure effect on T_c and resistivity $\rho(T)$ is different. Under pressure $\rho(T)$ decreases, while T_c increases, which is associated with the redistribution of charge carriers in the CuO_2 planes. It was shown that under pressure the $\Delta^*(T)$ increases with a rate $d\ln\Delta^*/dP = 0.9 \text{ GPa}^{-1}$, which is most likely due to a decrease in the frequencies of the phonon spectrum of the superconductor when pressure is applied. It is revealed that without pressure, a “magnetic” maximum occurs on the $\Delta^*(T)$ at high temperatures, followed by a linear section with a positive slope, limited by the temperatures of structural transition T_s and spin density wave ordering T_{SDW} . At $P = 1.1 \text{ GPa}$, the maximum disappears (Fig.1). The transition of $\Delta^*(T)$ into the superconducting state below the temperature T_{01} , that limits the superconducting fluctuations from above, happens in a usual way (insert to Fig.1).

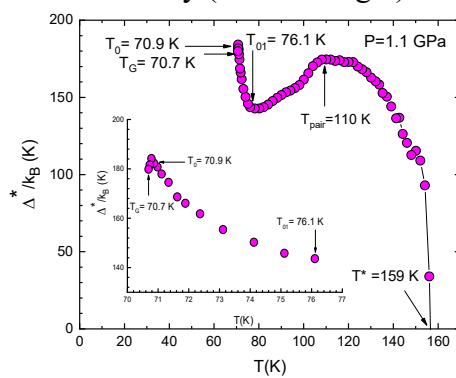


Fig. 1. Pseudogap temperature dependence of the $\text{Y}_{0.77}\text{Pr}_{0.23}\text{Ba}_2\text{Cu}_3\text{O}_{7-\delta}$ single crystal under the pressure of 1.1 GPa. The inset shows the same dependence in the vicinity of the superconducting transition.

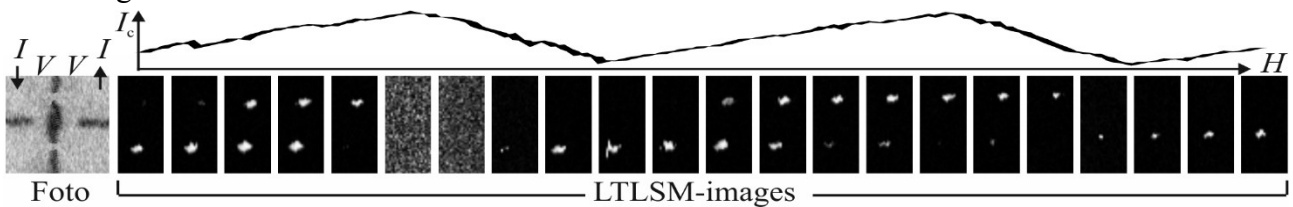
- [1] A. L. Solovjov, V. M. Dmitriev, Low Temp. Phys. 32, 576 (2006). <https://doi.org/10.1063/1.2215374>.
- [2] A. L. Solovjov, L. V. Omelchenko et al, Current Applied Physics 16, 931-938 (2016). <https://doi.org/10.1016/j.cap.2016.05.014>.

Visualization of critical current oscillations in a doubly connected superconducting structure without Josephson junctions

A. G. Sivakov, A. S. Pokhila, A. E. Kolinko

*B.Verkin Institute for Low Temperature Physics and Engineering of NAS of Ukraine,
47 Nauky Ave., Kharkiv, 61103, Ukraine
e-mail: sivakov@ilt.kharkov.ua*

Various oscillation effects in doubly connected superconductors manifest themselves in such systems as thin-walled cylinders and narrow rings in the form of the Little-Parks effect or in loops with two parallel Josephson junctions due to the interference of critical transport currents. Oscillations of both types are periodic in the flux of the external magnetic field, with a period equal to Φ_0 . Recently, the possibility of creating “interferometers” that do not contain artificial Josephson contacts and have microscopic doubly connected elements whose linear dimensions do not exceed the coherence length has attracted considerable interest from experimenters. However, experiments on wide tin films with a rectangular macroscopic hole have convincingly demonstrated [1] that the “microscopic nature” of a doubly connected superconducting system is not a necessary condition for observing oscillations of the critical transport current. In this case, the oscillation effect is associated with the addition of the transport current to the circulating current, the magnitude of which is determined by the magnetic field and the inductance of the structure. Since the oscillation effect does not follow from the direct algebraic addition of the critical current of the circuit with the circulating current in the magnetic field (the circulating current is added in one arm and subtracted in the other), additional considerations are needed to explain the effect. In order to determine how the critical state is reached in individual arms of the “interferometer”, we used the technique of low-temperature scanning laser microscopy (LTLSM) [2]. The applicability of the technique became possible due to the macroscopic dimensions of the structure. The experiment consisted of scanning a DC SQUID type structure with a focused laser probe at fixed values of the external magnetic field. The constant transport current was set lower than the current of return to the superconducting state on the current-voltage characteristic. While the magnetic field changes, the circulating current changes sign and amplitude, so the operating point for the current sometimes approaches and sometimes moves away from the constant value of the local critical current. The intensity of the laser probe was modulated in time, so the magnitude of the voltage response was greater the closer the operating point was to the critical current, since the sample was in a resistive state for most of the modulation period. The beam intensity amplitude was selected to be sufficient to suppress the maximum difference between the critical current and the circulating current. The beam intensity was modulated at a frequency of 100 kHz, and the voltage response signal was recorded using a lock-in amplifier. The results showed that, depending on the external magnetic field, the critical current of each bridge oscillates with a period equal to the quantum of magnetic flux and an amplitude equal to the circulating current. The critical current of the entire structure achieves alternately in one or another bridge when the transport current coincides with the direction of the circulating current in it.



- [1] A. G. Sivakov, A. S. Pokhila, A. M. Glukhov, S. V. Kuplevakhsky, A. N. Omelyanchouk. Low Temp. Phys. 40, 408 (2014). <https://doi.org/10.1063/1.4876229>.
- [2] A. P. Zhuravel, A. G. Sivakov, O. G. Turutanov, A. N. Omelyanchouk, S. M. Anlage etc. Low Temp. Phys. 32, 592 (2006)). <https://doi.org/10.1063/1.2215376>.

Precise tuning of superconducting and physical properties of $\text{Mo}_{1-x}\text{Si}_x$ thin films for photon detector applications

O. V. Zraichenko¹, O. O. Leha¹, V. Yu. Lyakhno^{1,2}, S. V. Bengus¹, M. Yu. Mikhailov³

¹*B.Verkin Institute for Low Temperature Physics and Engineering of NAS of Ukraine,
47 Nauky Ave., Kharkiv, 61103, Ukraine*

²*G.V. Kurdyumov Institute for Metal Physics, NAS of Ukraine,
36 Vernadsky blvd., Kyiv 03142, Ukraine*

³*Department of Imaging Physics, Delft University of Technology, 2628 CN Delft, The Netherlands
e-mail: zraichenko@ilt.kharkov.ua*

MoSi-based structures are promising for single-photon detection at microwave and millimeter-wave frequencies, where conventional photon counters lose efficiency [1]. Their integration into superconducting circuits enables the development of frequency-tunable photon detectors and low-noise parametric amplifiers.

A significant set of materials have already been tested as base materials in the development of optical photon detectors. Large gap amplitude for traditional SNSPD (like NbN [2]) materials is efficient in the single-photon detection regime only in a limited frequency range of the InfraRed domain. Extending detection to longer wavelengths, which are useful for applications such as long-distance quantum communications, remains a challenge. The quantum efficiency of the detectors depends on the crystalline phase of the NbN and defects on the substrate surface. Beside this, commonly used methods for producing such films by reactive magnetron sputtering involve obtaining equilibrium compounds and are poorly amenable to varying the coating composition [3]. To increase the quantum efficiency or extend frequency range the reduction of the thickness of the superconducting film or fabricating films with more disordered structure is proposed. Such amorphous superconductors as MoGe [4], MoC [5] and WSi [6], as well as MoSi, were suggested as alternatives to NbN.

Our technological capabilities enable precise tuning of the normal resistance value of the MoSi superconducting film by controlling its thickness and composition. Films were produced by DC magnetron sputtering from two separate sources within argon gas so we can modify content of film composition. We present the results of four-point resistance measurements in cryostat cooled down to the temperature of the liquid helium for films with thickness down to 4 nm. The film thickness was controlled by tuning the sputtering time according to the previously defined sputtering rate of 10-25 nm/min.

Our goal was the preparation of thin amorphous films with high T_c and high sheet resistance. The results are promising and elaborate technology should enable us to produce superconducting structures which could interfere with quantum coherent objects.

- [1] Yu. P. Korneeva, M. Yu. Mikhailov, Yu. P. Pershin, *et al.*, *Supercond. Sci. Technol.* 27 (2014). <https://doi.org/10.1088/0953-2048/27/9/095012>.
- [2] A. Semenov, B. Günther, U. Böttger, *et al.*, *Phys. Rev. B* 80, 054510 (2009). <https://doi.org/10.1103/PhysRevB.80.054510>.
- [3] Y. Pan, H. Zhou, X. Zhang, *et al.*, *Opt. Express* 30, 40044-40052 (2022). <https://doi.org/10.1364/OE.472378>.
- [4] V. B. Verma, A. E. Lita, M. R. Vissers, *et al.*, *Appl. Phys. Lett.* 105, 022602 (2014). <https://doi.org/10.1063/1.4890277>.
- [5] M. Trgala, M. Žemlička, P. Neilinger, *et al.*, *Applied Surface Science*, 312, 216 (2014). <https://doi.org/10.1016/j.apsusc.2014.05.200>.
- [6] X. Zhang, A. Engel, Q. Wang, *et al.*, *Phys. Rev. B* 94, 174509 (2016) <https://doi.org/10.1103/PhysRevB.94.174509>.

Resistive switching and diode effect in conductivity of TiTe_2 point contacts

**O. E. Kvitnitskaya^{1,2}, L. Harnagea³, D. V. Efremov², B. Büchner^{2,4},
 Yu. G. Naidyuk¹**

¹*B.Verkin Institute for Low Temperature Physics and Engineering of NAS of Ukraine,
 47 Nauky Ave., Kharkiv, 61103, Ukraine*

²*Leibniz Institute for Solid State and Materials Research, IFW Dresden, 01069 Dresden, Germany*

³*Institute for Solid State Research, IFW Dresden, D-01171 Dresden, Germany*

⁴*Institute of Solid State and Materials Physics and Würzburg-Dresden Cluster of Excellence*

ct.qmat, Technische Universität Dresden, 01062 Dresden, Germany

e-mail: kvitnitskaya@yahoo.com

We have measured the $I(V)$ and $dV/dI(V)$ characteristics of TiTe_2 -based point contacts (PCs) from room to helium temperatures. The features indicating the emergence of charge density wave (CDW) were detected. They are represented by the symmetrical with respect to $V=0$ humps in $dV/dI(V)$ around ± 150 mV at liquid helium temperatures, which disappear above 150 K, similar to the case of the sister CDW compound TiSe_2 [1]. Applying higher voltages above 200 mV, we observed a resistive switching in TiTe_2 PCs from a metallic-like low-resistance state to non-metallic type high-resistance state with a change of resistance by an order of magnitude (Fig.1). A unique diode-like effect was registered in “soft” TiTe_2 PCs with hysteretic $I(V)$ at the negative voltage on TiTe_2 (Fig.2). The discovery of the resistive switching and diode effect adds TiTe_2 to transition-metal dichalcogenides, which could be useful in the development of non-volatile ReRAM memory and other upcoming nanotechnologies.

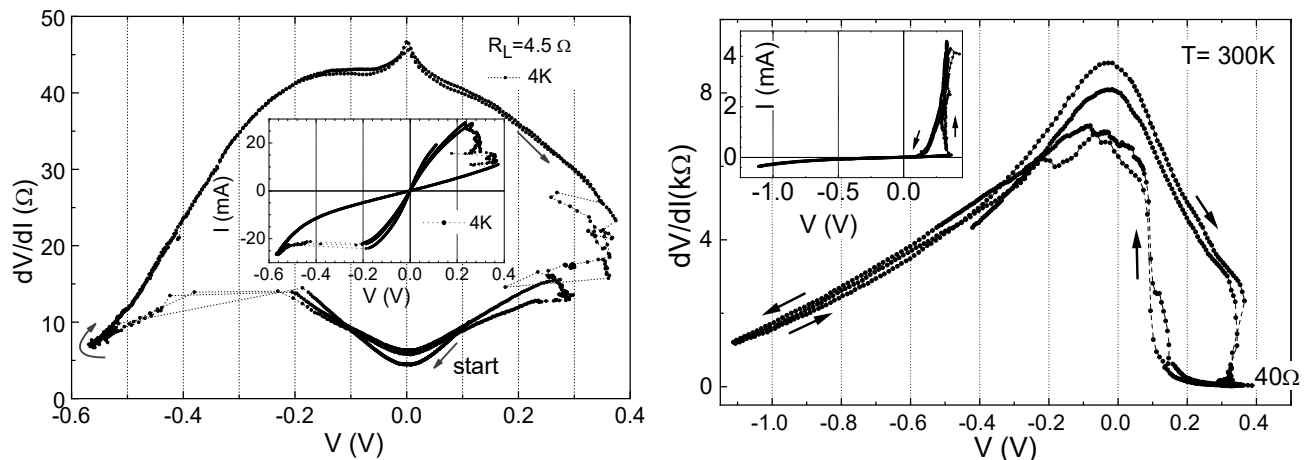


Fig.1. Resistive switching in $dV/dI(V)$ for $\text{TiTe}_2\text{-Ag}$ hard PC by clockwise sweeping of bias voltage. Inset: $I(V)$ curve for this PC.

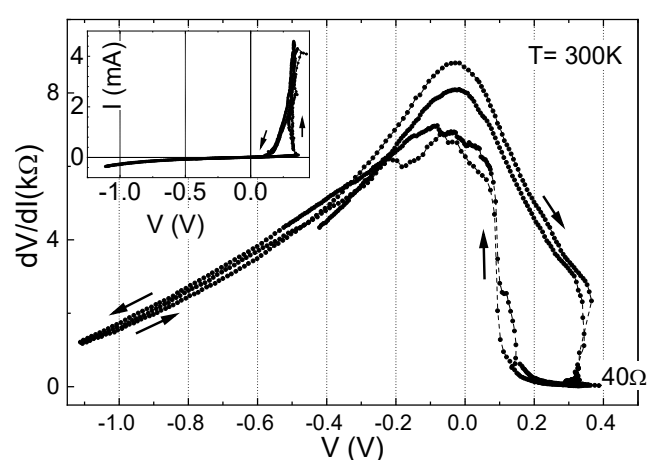


Fig.2. $dV/dI(V)$ and $I(V)$ curve (inset) for TiTe_2 “soft” PC at 300K with diode-like effect.

[1] D.L. Bashlakov, O.E. Kvitnitskaya, S. Aswartham, Y. Shemerliuk, H. Berger, D.V. Efremov, B. Büchner, Yu.G. Naidyuk, Low Temp. Phys. 49, 834 (2023). <https://doi.org/10.1063/10.0019694>.

MAGNETISM AND MAGNETIC MATERIALS

Electric field effect on superluminal-like magnons propagation in insulating antiferromagnets

O. O. Boliasova^{1,2}, V. N. Krivoruchko³

¹*State Research Institution «Kyiv Academic University»*

36 Academician Vernadsky Boulevard, 03142, Kyiv, Ukraine,

²*G. V. Kurdyumov Institute for Metal Physics of the N.A.S. of Ukraine*

36 Academician Vernadsky Boulevard, Kyiv, 03142, Ukraine

³*Donetsk Institute for Physics and Engineering named after O.O. Galkin of the NAS of Ukraine,*

46 Nauki Avenue, Kyiv, 03028, Ukraine

e-mail: ol.boliasova@gmail.com

The unique characteristic of magnetization dynamics - fast speed, up to terahertz, and distinct (right-handed and left-handed) spin waves (SWs) polarization - give grounds to consider antiferromagnets (AFMs) as a perspective material platform for the realization of a variety of high-density and fast-speed magnonic devices. This makes the effective methods to control magnetization dynamics in AFMs relevant for study as a potential area of information technology in magnonics. An external electric field has been considered recently as one of the alternative and efficient solutions to control SW characteristics. The effect of an external electric field on SW dynamics is due to the induced additional topological phase, the so-called Aharonov-Casher phase, which manifested as a shift in the dispersion of SW [1]. In addition to frequency, attenuation length and group velocity are important characteristics for practical applications. This phenomenon can be used to create, e.g., field-effect transistors [2]. The SW group velocity is crucial for transferring information between different computational components. Previous estimations of the group velocity ranged from 10 to 100 km/s [3,4]. Recent research has revealed the so-called superluminal-like magnon propagation up to 650 km/s [5].

We study the topological AC effect on magnetization dynamics in two-sublattice easy-axis dielectric AFMs. In the analytical calculation based on Landau-Lifshitz-Gilbert equations, we got expressions for frequency, attenuation length, and group velocity of the right-handed and left-handed polarization SWs. Our findings suggest that in dielectric AFM, with typical magnetic characteristics the group velocity could be around 300 km/s. The maximum group velocity is shifted at a distance $\pm k_0$ along the wave vector, which is proportional to the applied electric field and depends on the exchange energy and spin-orbit coupling in the AFM. This implies that the electric field control of SW dynamics provides a new direction for spin-based device development and opens a new way of SW steering in a variety of high-density THz magnonic devices.

This work was partially supported by the National Academy of Sciences of Ukraine through the research program No. 0121U110080.

- [1] Y. Aharonov and A. Casher, Topological Quantum Effects for Neutral Particles. Phys. Rev. Lett. 53, 319 (1984); <https://doi.org/10.1103/PhysRevLett.53.319>.
- [2] R. Cheng, M. W. Daniels, J.-G. Zhu, and D. Xiao, Antiferromagnetic spin wave field-effect transistor, Sci. Rep. 6, 24223 (2016); <https://doi.org/10.1038/srep24223>.
- [3] R.V. Ovcharov, B.A. Ivanov, J. Åkerman, and R.S. Khymyn, Emission of fast-propagating spin waves by an antiferromagnetic domain wall driven by spin current, Phys. Rev. B 109, L140406 (2024). <https://doi.org/10.1103/PhysRevB.109.L140406>.
- [4] O. Gomonay, T. Jungwirth, and J. Sinova, High antiferromagnetic domain wall velocity induced by Néel spin-orbit torques. Phys. Rev. Lett. 117, 017202 (2016). <https://doi.org/10.1103/PhysRevLett.117.017202>.
- [5] K. Lee, DK. Lee, D. Yang, et al., Superluminal-like magnon propagation in antiferromagnetic NiO at nanoscale distances. Nat. Nanotechnol. 16, 1337 (2021). <https://doi.org/10.1038/s41565-021-00983-4>.

Magnetic properties of the $S = \frac{1}{2}$ spatially anisotropic triangular quantum magnet $\text{Cu}(\text{tn})\text{Cl}_2$

A. Darwich, R. Tarasenko, M. Orendáč, A. Orendáčová

*Institute of Physics, P. J. Šafárik University, Park Angelinum 9, 04001 Košice, Slovakia
e-mail: ali.darwich@student.upjs.sk*

The model of the spin-1/2 Heisenberg antiferromagnet (HAF) on the square lattice with the nearest-neighbors (NN) coupling J became a paradigmatic model of low-dimensional magnetism [1]. Most of the theoretical studies of the model have been focused on the quasi-one-dimensional region ($J'/J > 1$) due to the possibility of rich experimental response. Previous studies [2] of powdered $\text{Cu}(\text{tn})\text{Cl}_2$ ($\text{tn} = \text{C}_3\text{H}_{10}\text{N}_2$) identified the compound as a candidate for the spin-1/2 HAF $J - J'$ model with $J'/J < 0.6$. The effective intralayer coupling has been estimated $J/kB \sim 3 \text{ K}$. The extreme weakness of interlayer interactions has been manifested by the absence of the specific heat λ -like anomaly associated with the phase transition to magnetic long-range order (LRO) down to 60 mK . To understand the origin of the strong magnetic two dimensionality, first-principle calculations of exchange couplings were performed. The first-principle calculations introduced a concept of quasi-2D magnetic lattice in $\text{Cu}(\text{tn})\text{Cl}_2$, comprising 2D arrays of magnetic chains with relatively strong intrachain coupling. Recent thermodynamic and structural studies of $\text{Cu}(\text{tn})\text{Cl}_2$ revealed a structural phase transition at about 160 K associated with the removing of the carbon disorder in tn rings present in the high-temperature phase with $Pnma$ symmetry. The thermodynamic data was analyzed within magnetic models based on the results of first-principle calculations. Interestingly, the real interlayer coupling is a few orders of magnitude weaker than its theoretically predicted counterpart. While zero-field specific heat is in excellent agreement with the model of a rectangular lattice, its failure in the description of the susceptibility data suggests the importance of other weaker intralayer interactions. Apparently, $\text{Cu}(\text{tn})\text{Cl}_2$ belongs to a few quantum magnets with extremely weak interlayer interactions of the order of dipolar coupling between nearly ordered magnetic layers. The application of magnetic field leads to inducing phase transitions which, despite monocrystalline samples, are accompanied by very broad specific heat anomalies. Since the exchange coupling parameters strongly depend on the position of the tn group, the observed broadening may be associated with the gradual modulation of tn positions in the incommensurate modulated crystal structure leading to the decomposition of the lattice into many sublattices with more or less different exchange couplings.

- [1] U. Schollwöck, J. Richter, D. J. J. Farnell, and R. F. Bishop, Quantum Magnetism (Springer, Berlin, 2004).
- [2] A. Orendáčová, E. Cižmár, L. Sedláčková, J. Hanko, M. Kajnaková, M. Orendáč, A. Feher, J. S. Xia, L. Yin, D. M. Pajerowski, M. W. Meisel, V. Zeleňák, S. Zvyagin, and J. Wosnitza, Phys. Rev. B 80, 144418 (2009), DOI: <https://doi.org/10.1103/PhysRevB.80.144418>.

Cu(en)(sal)Cl – a novel spin-½ 2D Heisenberg quantum magnet with ferromagnetic exchange interactions on the square lattice

I. Kozin, R. Tarasenko, V. Tkáč, A. Orendáčová, E. Čižmár, M. Orendáč

*Institute of Physics, Faculty of Science, P.J. Šafárik University in Košice,
Park Angelinum 9, 040 01 Košice, Slovakia
e-mail: illia.kozin@student.upjs.sk*

Low-dimensional magnetic systems based on spin-1/2 Cu²⁺ ions are well-known thanks to their unconventional magnetic properties, which originate from the particular geometrical coordination of localized magnetic moments and quantum fluctuations. In this work, we introduce unique thermal and magnetic properties of the metal-organic complex Cu(en)(sal)Cl (*en* = ethylenediamine = C₂H₈N₂; *sal* = 2-hydroxybenzoic acid = salicylic acid = C₇H₆O₃). A square-like layered framework in the *bc* plane was formed in this compound, with two distinct ligand coordination: one is an axially elongated CuN₄Cl₂ unit from two *en* ligands, and the other is a CuO₄Cl₂ unit from a pair of asymmetrically bound *sal* anions.

The experimental study of heat capacity was carried out by means of Physical Property Measurement System with ³He insert down to 0.38 K in magnetic fields up to 9 T. Magnetic phase transition was observed at $T_C = 0.82$ K, indicating a presence of ferromagnetic long-range order. Also, the experimental data were compared with the theoretical model for spin ½ Heisenberg 2D ferromagnet on a square lattice [1], showing a good agreement and revealing an exchange interaction value J/k_B to be about 2 K.

Magnetization and susceptibility measurements were performed by using a Quantum Design SQUID magnetometer MPMS over the temperature (from 0.38 K to 300 K) and magnetic fields (up to 5 T) ranges. Ferromagnetic phase at $T_C = 0.82$ K from heat capacity measurements was also validated by a divergence of zero-field cooling (ZFC) and field cooling (FC) magnetization curves in external field of 100 mT. In addition, ferromagnetic hysteresis was observed at 0.5 K confirming long-range magnetic order below T_C . The susceptibility and effective magnetic moment analyses yielded values of a *g*-factor of 2.20, a Curie-Weiss temperature of $\theta_{CW} \approx 4$ K and an exchange interaction of $J/k_B \approx 1.9$ K. Last but not the least, high-temperature experimental data were compared with relevant theoretical models and predictions for a spin-1/2 Heisenberg isotropic 2D square lattice with ferromagnetic exchange [1,2], showing a good overall agreement.

The financial support of projects VEGA 1/0132/22, APVV-18-0197, APVV-22-0172 and APVV-23-0006 is acknowledged.

[1] G. A. Baker, H. E. Gilbert, J. Eve and G. S. Rushbrooke, Physics Letters A 25 (3), 207–209 (1967). [https://doi.org/10.1016/0375-9601\(67\)90860-2](https://doi.org/10.1016/0375-9601(67)90860-2).

[2] F. Suzuki, N. Shimata and C. Ishii, Journal of the Physical Society of Japan 63 (4), 1539–1547 (1994) <https://doi.org/10.1143/jpsj.63.1539>.

Confinement effects on the weak-field magnetic susceptibility of a two-dimensional electron gas

J. Kumar

Aalto University, Department of Applied Physics, Konemiehentie 1, Espoo, Finland
e-mail: jishad.kumar@aalto.fi

Modern techniques can restrict the motion of an electron gas to a two-dimensional plane, say in GaAs-AlGaAs heterojunctions, without posing any conceptual challenges. However, confining such a low-dimensional system whose linear dimension is comparable to or less than the cyclotron radius to a finite volume introduces new energy scales in the problem and leads to modifications in the Landau susceptibility. Explicit spin-orbit coupling (SOC), albeit small compared to other involved characteristic energies, via Rashba [1] or Dresselhaus [2] interactions produces a splitting of the otherwise degenerate energy bands around the Fermi level. This may significantly affect the thermodynamic [3] and the transport properties [4] of lowdimensional systems. We study the weak-field magnetic susceptibility of two-dimensional electron gas under isotropic parabolic, anisotropic, and Gaussian confinements. The asymmetric (anisotropic) confinement, in semiconductor quantum dot structures, restricts the motion of the charge carriers. They are quite popular in the field of elliptical quantum dots. In semiconductors, impurity is considered very important in maneuvering the system's properties. Gaussian confinement potential is a pure mathematical representation of such impurity potentials. We found that susceptibility strongly depends on the boundary confinement and removal of the boundary results in a singularity. We show that a field-dependent susceptibility emerges when the confinement is Gaussian, in contrast to the canonical case of a field-independent susceptibility. We also show that the weak-field susceptibility is independent of the anisotropy parameter as well as the spin-orbit coupling for the anisotropic confinement model. For all the other models, the susceptibility vanishes for large spin-orbit coupling [5]. We also found the de-Haas van Alphen oscillations of the magnetic susceptibility, at very low temperatures and very strong magnetic fields, depend significantly on the depth and the range of the confining potential for Gaussian confinement [6].

This work was supported by the Academy of Finland through its QTF Center of Excellence program (Project No. 312298)

- [1] E.I. Rashba, Sov. Phys. Solid State 2 (1960) 1109.
- [2] G. Dresselhaus, Phys. Rev. 100 (1955) 580. DOI: <https://doi.org/10.1103/PhysRev.100.580>
- [3] L. E. Diaz-Sanchez et al., Phys. Rev. Lett. 99 (2007) 165504 DOI: <https://doi.org/10.1103/PhysRevLett.99.165504>; F. Gao et al., Physica E 40 (2008) 1454 DOI: <https://doi.org/10.1016/j.physe.2007.09.039>; J. Lian et al., Phys. Rev. A 86 (2012) 063620 DOI: <https://doi.org/10.1103/PhysRevA.86.063620>.
- [4] M. A. Manya et al., Phys. Rev. B 105 (2022) 165421 DOI: <https://doi.org/10.1103/PhysRevB.105.165421>.
- [5] Jishad Kumar, Tapio Ala-Nissila, submitted.
- [6] Jishad Kumar, Tapio Ala-Nissila, submitted.

Current-driven dynamics of vertical Bloch lines on a domain wall in magnetic films

R. Teslia¹ and O. Kolezhuk^{1,2}

¹*V.G. Baryakhtar Institute of Magnetism of the NAS of Ukraine, 03142 Kyiv, Ukraine*

²*Institute of Physics, Johannes Gutenberg-University Mainz, D-55128 Mainz, Germany*

e-mail: rroman200187@gmail.com

Topologically nontrivial magnetic textures are promising as information carriers in data storage and processing devices [1]. One of the oldest candidates is vertical Bloch lines (VBLs) in ferromagnets (FMs), with field-controlled and current-controlled memory schemes proposed. However, ferromagnetic dynamics impose significant limitations on processing speed: typically, achievable VBL speeds in FMs do not exceed a few hundred m/s.

Recently, the electrical creation and manipulation of “meron-antimeron pairs” (essentially the same topological textures as VBLs) localized on 180-degree domain walls in CuMnAs has been reported [2]. Another recent work proposed an antiferromagnetic memory scheme with a VBL driven by spin-polarized current [3], with VBL velocities potentially reaching the range of several km/s. However, in the analysis of the VBL motion under the action of the current in [3], the term in the interaction [4], which relates the angular variable (describing the rotation of the Neel vector in the wall) and the displacement of the wall center, was neglected.

To fill this gap, we have performed the analysis of the VBL/vortex motion under the action of a current in an antiferromagnetic domain wall, taking into account this interaction term. Since the motion of the VBL along the wall always causes a local transverse displacement of the wall, the pinning of the wall in the transverse direction significantly affects the vortex dynamics. Our preliminary studies show that, depending on the parameters of the problem, the dependence of the vortex velocity on the current strength can be non-monotonic and exhibit a maximum at a particular current strength, similar to the well-known phenomenon of Walker breakdown in ferromagnets.

- [1] B. Göbel, I. Mertig, and O. A. Tretiakov, Beyond skyrmions: Review and perspectives of alternative magnetic quasiparticles, *Physics Reports* 895, 1 (2021). <https://dx.doi.org/10.1016/j.physrep.2020.10.001>.
- [2] O. J. Amin, S. F. Poole, S. Reimers, L. X. Barton, A. Dal Din, F. Maccherozzi, S. S. Dhesi, V. Novák, F. Krizek, J. S. Chauhan, R. P. Campion, A. W. Rushforth, T. Jungwirth, O. A. Tretiakov, K. W. Edmonds, and P. Wadley, Antiferromagnetic half-skyrmions electrically generated and controlled at room temperature, *Nature Nanotechnology* 18, 849 (2023). <https://dx.doi.org/10.1038/s41565-023-01386-3>.
- [3] R. Ovcharov, B. Ivanov, J. Åkerman, and R. Khymyn, Antiferromagnetic Bloch line driven by spin current as room-temperature analogue of a fluxon in a long josephson junction, *Phys. Rev. Appl.* 20, 034060 (2023). <https://dx.doi.org/10.1103/PhysRevApplied.20.034060>.
- [4] R. Cheng and Q. Niu, Dynamics of antiferromagnets driven by spin current, *Phys. Rev. B* 89, 081105 (2014). <https://dx.doi.org/10.1103/PhysRevB.89.081105>.

Electric-field-driven fractional parametric resonance in spintronic nanostuctures

R. V. Verba¹, A. Grimaldi², D. V. Slobodianiuk¹, G. Finocchio²

¹*V. G. Baryakhtar Institute of Magnetism of the NAS of Sciences of Ukraine,
03142, 36-b Akad. Vernadskogo blvd., Kyiv, Ukraine.*

²*Department of Engineering, University of Messina,
Piazza Pugliatti, 1 - 98122 Messina, Italy
e-mail: verry@ukr.net*

Spin-torque diodes based on magnetic tunnel junctions (MTJs) are nanoscale devices with significant potential for applications in microwave technology and beyond. In addition to spin-transfer torque (STT) effect and tunnel magnetoresistance, MTJs enable for the effective utilization of surface and interface phenomena to control the ferromagnetic state and induce resonant modes within the device. A particular research interest is paid to the effect of voltage-controlled magnetic anisotropy (VCMA), which appears to be one of the most efficient mechanisms for magnetization manipulation [1].

In current work, we predict a fractional parametric resonant response in passive spintronic diode both theoretically and by means of micromagnetic simulations. Fractional resonance can occur when a diode is excited simultaneously by STT and VCMA in zero field, as well as solely by VCMA if the static magnetization is tilted by a small bias magnetic field. These resonances take place at the frequencies f_0/n , where f_0 is linear (ferromagnetic resonance) frequency and $n = 2, 3, 4, \dots$ (Fig. 1), which differs MTJ behavior from common Mathieu parametric oscillator; the latter demonstrates higher-order parametric resonances at $2f_0/n$ [2]. The physics behind our observations is the combined influence of parametric VCMA pumping and linear force, enabled by STT or VCMA in a tilted magnetization state.

The investigated resonance mechanism has the potential to expand the operational frequency range of spintronic detectors, making them more versatile. Additionally, it can be effectively utilized for frequency multiplication, enabling the generation of higher harmonic signals, as well as for the development of compact and efficient demodulation schemes in advanced spintronic communication and signal processing systems.

This work was partially supported by Verhovna Rada of Ukraine grant for young scientists No. 0124U003904.

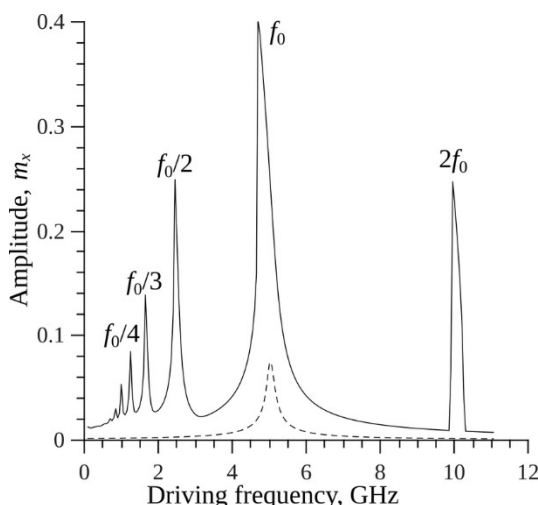


Fig. 1. Resonance spectra of a CoFeB MTJ with 1 nm thick elliptic (100 nm x 40 nm) free layer having perpendicular ground state; dashed line – no VCMA drive (linear STT resonance), solid line – 100 mT VCMA drive in a tilted state (in-plane field $B_x = 5$ mT). Simulation parameters: saturation magnetization $M_s = 800$ kA/m, surface perpendicular anisotropy $K_s = 0.43$ mJ/m², Gilbert damping parameter $\alpha_G = 0.02$.

[1] S. Miwa, et al., J. Phys. D 52, 063001 (2018), <http://doi.org/10.1088/1361-6463/aaef18>.

[2] D. K. Arrowsmith et al., Meccanica 34, 401 (1999), <http://doi.org/10.1023/A:1004727920844>.

Antiferromagnetic resonance in CuCrP₂S₆ layered crystal

O. Bludov¹, Yu. Savina¹, V. Pashchenko¹, M. Kobets¹, K. Glukhov², Yu. Vysochanskii²

¹*B.Verkin Institute for Low Temperature Physics and Engineering of NAS of Ukraine,
 47 Nauky Ave., Kharkiv, 61103, Ukraine*

²*Institute for Solid State Physics and Chemistry, Uzhhorod National University,
 54 Voloshyn Str., Uzhhorod, 88000, Ukraine
 e-mail: bludov@ilt.kharkov.ua*

The van der Waals layered materials $M^I M^{III} P_2 X_6$ ($M^I = Cu, Ag$; $M^{III} = Cr, V$; $X = S, Se$) represent a class of 2D multiferroic semiconductors that simultaneously possess antiferroelectric and antiferromagnetic orders below certain temperature [1,2]. In these materials, Cu ions spontaneously move away from the center atomic plane, giving rise to nontrivial electric dipole moment perpendicular to the layer. In addition, their magnetic ordering originates from indirect exchange interaction between Cr or V ions. The presence of multiferroicity in such materials is important for potential applications as sensor of magnetic field or in the nonvolatile storage devices controlled by external electric or magnetic fields.

The copper chromium thiophosphate CuCrP₂S₆ crystallizes in a layered two-dimensional structure which is formed by double sheets of sulfur atoms sandwiching the metal cations and P–P groups which occupy the octahedral voids defined by the sulfur atoms. At room temperature the crystal structure has a space group of $C2/c$. At $T_c = 150$ K crystal undergoes phase transition into antiferroelectric phase with Pc space group. Antiferromagnetic ordering of Cr³⁺ ions (Cu¹⁺ is nonmagnetic) appears below $T_N = 31$ K.

Antiferromagnetic resonance (AFMR) investigations have been carried out by means of a homemade multifrequency spectrometer with a resonator (17–142 GHz, at 4.2 K, up to 7 T). Additional magnetic measurements have been carried out by using a SQUID magnetometer MPMS–XL5 QD (2–300 K, up to 5 T).

The obtained results are discussed within the framework of a model for an antiferromagnet with two magnetic anisotropy axes for Cr³⁺ ion with $S = 3/2$ and $g = 2$.

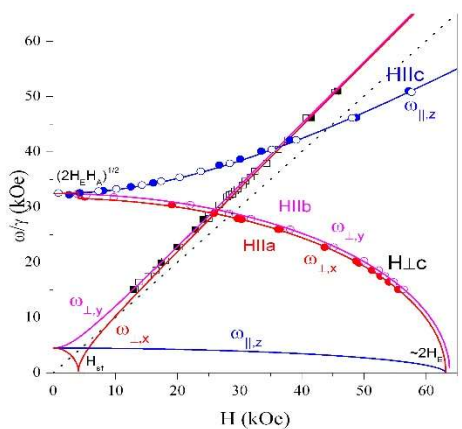


Fig. 1. The frequency-field dependences of AFMR spectrum of CuCrP₂S₆ for 4.2 K. Symbols are experimental data, solid lines – results of calculations in framework of a model for an antiferromagnet with two magnetic anisotropy axes.

[1] R. Brec, Solid State Ionics 22, 3, (1986); M. S. Dresselhaus (Ed.), “Intercalation in Layered Materials”, Springer Science+Business Media New York (1986). (R. Brec, “Review on Structural and Chemical Properties of Transition Metal Phosphorus Trisulfides MPS₃”, pp 93–124. doi:10.1007/978-1-4757-5556-5_4).

[2] M. Susner, M. Chyasnichyus, M. McGuire, P. Ganesh, P. Maksymovych, Adv. Mater., 1602852, (2017). doi: 10.1002/adma.201602852.

Tunable magnetic properties of layered double hydroxides: between cluster glass and canonical spin glass

A. V. Fedorchenko¹, E. L. Fertman¹, I. P. Kobzar¹, Yu. G. Pashkevich², E. Čižmár³, V. Tkáč³, R. Tarasenko³, A. Feher³, M. Holub⁴, A. N. Salak⁵

¹*B. Verkin Institute for Low Temperature Physics and Engineering of NAS of Ukraine,
47 Nauky Ave., Kharkiv, 61103, Ukraine*

²*O. Galkin Donetsk Institute for Physics and Engineering, NAS of Ukraine,
46 Pr. Nauki, Kyiv, 03028 Ukraine*

³*Institute of Physics, Faculty of Science, P.J. Šafárik University in Košice,
041 54 Košice, Slovakia*

⁴*Synchrotron SOLEIL, L'Orme des Merisiers, St Aubin BP48, Gif sur Yvette Cedex 91192, France*

⁵*Department of Materials and Ceramic Engineering, CICECO – Aveiro Institute of Materials,
University of Aveiro, 3810-193 Aveiro, Portugal
e-mail: fedorchenko.alexey@gmail.com*

Layered double hydroxides (LDH) represent a class of two-dimensional materials with remarkable chemical flexibility, allowing for precise control over their composition and properties. These materials are characterized by mixed-metal hydroxide layers intercalated with anions and water molecules, which influence their structural and functional behavior. The ability to tune the divalent-to-trivalent cation ratio, modify the interlayer anion species, and control basal spacing renders LDH highly versatile for various applications, including magnetism-related functionalities. The interplay between the chemical composition of hydroxide layers and intercalated anions has been shown to affect the structural organization and magnetic ordering, leading to complex magnetic behaviors in LDH containing transition metal cations.

The study of Co-Al LDH with varying cobalt-to-aluminum ratios demonstrates that these materials exhibit frequency-dependent magnetic properties indicative of cluster spin glass behavior. The temperature-dependent ac magnetic susceptibility measurements reveal a deviation from conventional long-range ferromagnetic ordering, suggesting the presence of magnetic clusters with constrained interactions. The observed magnetic relaxation phenomena, analyzed using the Vogel-Fulcher model, confirm the cluster glass-like state of these materials, with relaxation parameters aligning with those reported for spin glass-like systems. The Mydosh parameter values indicate that some Co-Al LDH are close to the canonical spin glasses, hinting at the presence of small-sized magnetic clusters in the hydroxide layers.

The results suggest that the structural and compositional features of LDH significantly influence their low-temperature magnetic phenomena. The observed cluster glass behavior appears to be a consequence of both cation distribution within hydroxide layers and interlayer anion effects. While the general classification of Co-Al LDH as cluster spin glasses is supported by the experimental data, subtle structural differences may lead to variations in magnetic interactions and relaxation dynamics. Further investigations employing advanced structural characterization techniques, such as high-resolution electron diffraction and X-ray microscopy are necessary to elucidate the microscopic nature of cluster formation and its impact on the macroscopic magnetic properties of LDH. This work highlights the potential of LDH as tunable magnetic materials and emphasizes the importance of understanding cationic and anionic arrangements in shaping their functional characteristics.

This work was supported by the EU H2020 project European Microkelvin Platform (EMP), grant agreement No. 824109. The research at the P.J. Šafárik University was supported by the Slovak Research and Development Agency under grant Nos. APVV-22-0172 and APVV-SK-PT-18-0019 and by the Scientific Grant Agency of the Ministry of Education, Science, Research and Sport of the Slovak Republic under grant No. 1/0132/22.

Raman studies of two-compound spin-liquid candidate $(\text{Na}_{1-x}\text{Li}_x)_2\text{IrO}_3$

A. Glamazda^{1,4}, V. Gnezdilov^{1,2}, P. Lemmens^{2,3}, P. Gegenwart⁵

¹*B. Verkin Institute for Low Temperature Physics and Engineering of NAS of Ukraine,
47 Nauky Ave., Kharkiv, 61103, Ukraine*

²*Institute for Condensed Matter Physics, TU-Braunschweig, D-38106 Braunschweig, Germany*

³*Laboratory for Emerging Nanometrology and International Graduate School of Metrology, TU-
Braunschweig, D-38106 Braunschweig, Germany*

⁴*V. N. Karazin Kharkiv National University, 4 Svobody sq., Kharkiv, 61022, Ukraine*

⁵*Experimental Physics VI, Center for Electronic Correlations and Magnetism, Institute of Physics,
University of Augsburg, 86159 Augsburg, Germany
e-mail: glamazda@ilt.kharkov.ua*

The purposeful search for real crystalline compounds in which the Kitaev spin-liquid state can be realized and their study has recently been one of the urgent tasks of solid-state physics and magnetism. The prospect of the possible implementation of these materials in the field of quantum computers and quantum communications makes these efforts relevant. The present work was aimed at obtaining important information about the structure of the ground and low-energy excited states of the magnetic subsystem in the crystals of the two-dimensional alkali metal iridate family and the manifestation of spin-liquid properties in this structure, in particular, magnetic excitations with fractional torque and flux visions. Raman light scattering in a Mott insulator with spin-orbit interaction in a cellular lattice, the system $(\text{Na}_{1-x}\text{Li}_x)_2\text{IrO}_3$ ($x = 0 - 0.2$), was carried out. New data on the temperature behavior, as well as the doping dependence of the phonon line parameters (intrinsic energy, intensity and width) and their spectral shape were obtained. A quasi-critical behavior of the phonon system with the replacement of sodium by lithium in the $(\text{Na}_{1-x}\text{Li}_x)_2\text{IrO}_3$ system was revealed, which is associated with the displacement of oxygen in the IrO_6 octahedra, which in turn leads to a significant variation of spin correlations. The detected anomalies in the phonon spectra correlate with the features of magnetic excitations, which indicates a strong coupling of the lattice and magnetic subsystems in $(\text{Na}_{1-x}\text{Li}_x)_2\text{IrO}_3$. The obtained results are important for understanding the influence of the lattice topology on the spin and, as a consequence, the formation of the spin-liquid state in materials - candidates for Kitaev physics.

Low temperature thermodynamic of spin model formed by XX chains coupled via Ising spins

E. V. Ezerskaya, A. O. Kabatova

*V. N. Karazin Kharkiv National University, 4 Svoboda Sq, Kharkiv, 61022, Ukraine
e-mail: kabatova@ukr.net*

Low temperature thermodynamics of model spin system formed by open finite spin-1/2 XX chains coupled through Ising spins- S into periodical structure via one intermediate lattice site with the same number and two first and last sites of each XX chains was theoretically studied. The model Hamiltonian has the following form

$$\begin{aligned} \hat{\mathbf{H}} = & -\sum_{l=1}^L \left[g_0 \mu_B H \sigma_l^z + (\sigma_l^z + \sigma_{l+1}^z) (J_0 S_{l,n_0}^z + J_1 S_{l,1}^z + J_2 S_{l,N}^z) \right. \\ & \left. + \sum_{n=1}^N g \mu_B H S_{l,n}^z + J \sum_{n=1}^{N-1} (S_{l,n}^x S_{l,n+1}^x + S_{l,n}^y S_{l,n+1}^y) \right]. \end{aligned} \quad (1)$$

Periodic boundaries are supposed for Ising decorating spins:

$$\sigma_{L+1}^z \rightarrow \sigma_1^z, S_{L+1,i}^z \rightarrow S_{1,i}^z, i = 1, n_0, N$$

Spin operators σ_l^z in (1) can be substituted by quantum numbers, which are additional L discrete parameters. The Hamiltonian can be rewritten in the following block form:

$$\hat{\mathbf{H}} = \sum_{l=1}^L \mathbf{H}(\sigma_l, \sigma_{l+1}),$$

where $\mathbf{H}(\sigma_l, \sigma_{l+1})$ is the Hamiltonians of finite spin-1/2 XX chains with the effective “impurity” spins ($S = 1/2$) at both ends and at one of the intermediate sites n_0 . Spin-1/2 XX chain is well known example of exact solvable spin model [1, 2]. This permits us to use standard transfer-matrix technique for numerical simulation of the model thermodynamics. For the Hamiltonian under consideration the transfer-matrix is the 2x2 matrix if Ising spins $S = 1/2$.

The field and temperature dependencies of the main magnetic characteristics like magnetization, specific heat, the field dependencies of $\langle \sigma_l^z \rangle$, and the pairwise correlation functions for the nearest neighboring decorating spins $\langle \sigma_l^z \sigma_{l+1}^z \rangle$ were calculated numerically. For the case of the large values of the g-factor in XX chains and antiferromagnetic Ising interaction, simple analytical calculations indicate that the pair correlation functions for neighbor Ising spins can take zero value at some critical fields. This behavior is associated with additional degeneracy of the exact energy spectrum. Field dependence of magnetization demonstrates two intermediate plateaus for strong AF and FM Ising interactions at very low temperatures. We found numerically three maxima behavior of zero field temperature dependence of specific heat at some values of model parameters.

We acknowledge support by IEEE via “Magnetism in Ukraine Initiative” (STCU project No. 9918).

- [1] E. Lieb, T. Schultz, D. Mattis, Ann. Phys. 16, 407 (1961). DOI: 10.1016/0003-4916(61)90115-4.
- [2] A. A. Zvyagin, Quantum Theory of One-Dimensional Spin Systems, Cambridge Scientific Publishers, Cambridge, 2010.

High-pressure study of magnetic and magnetic resonance properties of rare-earth paramagnet $\text{KEr}(\text{MoO}_4)_2$

K. Kutko¹, V. Khrustalyov¹, T. Sakurai², H. Ohta², S. Kimura³, H. Nojiri³, and D. Kamenskyi⁴

¹*B.Verkin Institute for Low Temperature Physics and Engineering of NAS of Ukraine,
 47 Nauky Ave., Kharkiv, 61103, Ukraine*

²*Molecular Photoscience Research Center, Kobe University, 657 – 8501 Kobe, Japan*

³*Institute for Materials Research, Tohoku University, 980-8577 Sendai, Japan*

⁴*Experimental Physics V, Center for Electronic Correlations and Magnetism,
 Institute of Physics, University of Augsburg, 86159 Augsburg, Germany*

e-mail: khrustalyov@ilt.kharkov.ua

Recently, we reported a remarkably strong magnetostrictive response of the insulator paramagnet $\text{KEr}(\text{MoO}_4)_2$, observed in magnetic field about 14.6 T ($H \parallel b$) [1]. A high lattice sensitivity to the applied magnetic field together with a giant rotational magnetocaloric effect reported in this compound earlier [2] provide great perspectives for applications in cryogenic and magnetic technologies.

For better understanding the microscopic mechanism behind the strong magnetostrictive response we investigate the effect of hydrostatic pressure (up to 2 GPa) on the magnetic and resonant properties of $\text{KEr}(\text{MoO}_4)_2$ single crystal. In this work we use SQUID and ESR techniques to study the evolution of magnetization and the electronic transitions in Er^{3+} ion in magnetic field under different pressure on the sample. Fig.1a shows the magnetic field dependencies of the magnetic moment of $\text{KEr}(\text{MoO}_4)_2$ at different values of hydrostatic pressure, when the magnetic field applied along the “easy” axis of the crystal ($H \parallel c$). At $P \approx 0.85$ GPa the magnetic moment decreases abruptly as shown in Fig 1b. Such feature may indicate at significant changes in local environment of the magnetic ion.

High-field EPR measurements under applied hydrostatic pressure performed at several frequencies between 90 and 150 GHz also reveal some peculiarities which can be caused by structural modification. At $P \approx 0.85$ GPa the EPR spectra exhibit significant changes, the feature in magnetic field $\mu_0 H_{\text{cr}} = 14.6$ T is disappear and two new low magnetic field branches arise.

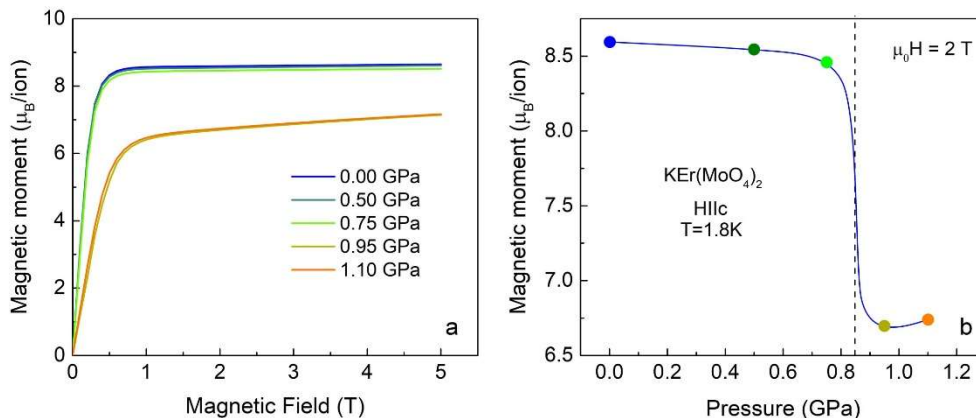


Figure 1. (a) The magnetic field dependence of magnetic moment of $\text{KEr}(\text{MoO}_4)_2$ at $H \parallel c$ and $T = 1.8$ K for different hydrostatic pressure; (b) the dependence of magnetic moment vs. pressure ($H \parallel c$, $\mu_0 H = 2$ T, $T = 1.8$ K). By dashed line denoted the pressure critical value 0.85 GPa.

[1] B. Bernath et al, Adv. Electron. Mater. 8, 2100770 (2022).
<https://doi.org/10.1002/aelm.202100770>

[2] V. Tkac et al, Phys. Rev. B 92, 024406 (2015). <https://doi.org/10.1103/PhysRevB.92.024406>

Magnetic properties of the Heisenberg–Ising model of nanomagnets on the base of transition metal polymeric complexes

E. V. Ezerskaya, S. Ye. Kononenko

V. N. Karazin Kharkiv National University, 4 Svoboda Sq, Kharkiv, 61022, Ukraine
e-mail: semen.kononenko@student.karazin.ua

This work is devoted to the theoretical study of mixed spin model built from two Ising spin-1/2 rings, which are decorated by three-spin fragments with XXZ Heisenberg interaction.

The corresponding Hamiltonian has following form:

$$\hat{H} = -\sum_{l=1}^L \left[g_1 \mu_B H \sigma_{l,1}^z + g_3 \mu_B H \sigma_{l,3}^z + J_1 (\sigma_{l,1}^z + \sigma_{l+1,1}^z) S_{l,1}^z + J_3 (\sigma_{l,3}^z + \sigma_{l+1,3}^z) S_{l,3}^z + \sum_{n=1}^3 g \mu_B H S_{l,n}^z + J \sum_{n=1}^2 (S_{l,n}^x S_{l,n+1}^x + S_{l,n}^y S_{l,n+1}^y + \gamma S_{l,n}^z S_{l,n+1}^z) \right].$$

Translational symmetry: $\sigma_{l+1,1}^z = \sigma_{l,1}^z$, $\sigma_{l+1,3}^z = \sigma_{l,3}^z$ is supposed. This structure is similar to cylinder. Z-projections of all Ising spins are a good quantum numbers for the Hamiltonian.

We performed numerical simulation of the model's low-temperature properties using transfer matrix method. Thermodynamic characteristics such as magnetization and heat capacity of presented model were calculated for different L and various coupling parameters. We also studied $\langle S_{l,i}^z \rangle$, $i = 1, 2, 3$, $\langle \sigma_{l,1}^z \rangle$, $\langle \sigma_{l,3}^z \rangle$ and two particle correlators for different pairs of spins. For the case of big g-factors on XXZ chains and antiferromagnetic Ising interactions nearest neighbor Ising spin correlators are equal to zero at some fixed values of magnetic field. This behavior is associated with additional degeneration of the energy levels.

Also, for some modifications of the above model with additional Ising coupling terms $-\sum_{l=1}^L [J_{21}(\sigma_{l,1}^z + \sigma_{l+1,1}^z) + J_{23}(\sigma_{l,3}^z + \sigma_{l+1,3}^z)] S_{l,2}^z$ unusual temperature behavior of magnetic susceptibility and specific heat like pseudo-phase transition [1, 2] are found numerically (Fig. 1).

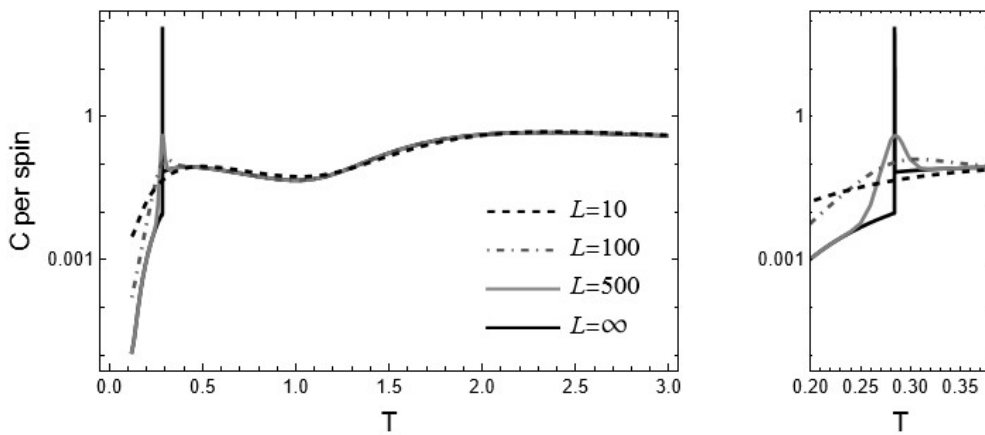


Fig1. Temperature dependence of heat capacity at $\mu_B H / J = 0.47$, $J_1 / J = J_2 / J = -12$, $J_{21} / J = -1$, $J_{23} / J = 0.5$, $\gamma = -1$.

We acknowledge support by IEEE via “Magnetism in Ukraine Initiative” (STCU project No. 9918).

- [1] T. Hutak, T. Krokhmalskii, O. Rojas, S.M. de Souza, O. Derzhko, Physics Letters A 387, 127020 (2021). DOI: 10.1016/j.physleta.2020.127020.
- [2] A. A. Zvyagin, V. V. Slavin, Phys Rev. B 109, 214438 (2024). DOI: 10.1103/PhysRevB.109.214438.

Estimation of magnetic characteristics of Ni-Zn ferrite prepared by hydroxide precipitation method

O. I. Tovstolytkin¹, A. F. Kravets^{1,2}, S. M. Konoplyuk¹

¹ Institute of Magnetism of the NAS of Ukraine, 36-b Vernadsky Blvd., Kyiv 03142, Ukraine

² Nanostructure Physics division, Royal Institute of Technology,
SE-100 44 Stockholm 10691, Sweden
e-mail: ksm@imag.kiev.ua

In recent years, fast growing automotive, aerospace, telecommunication, robotics industries show great demand for electronic components, in which soft ferrites play important roles as core in inductors, transformers, electromagnetic interference suppressors, as material for antenna rods, sensors, phase shifters and in many other applications. Ni-Zn ferrites [1] represent class of soft spinel ferrites with superior magnetic permeability, ultralow electric losses and excellent corrosion resistivity.

In this work, the hydroxide precipitation method [2] was adopted for preparation of bulk polycrystalline Ni-Zn ferrite compound. The XRD and magnetic methods were employed for characterization of sintered specimens. The XRD analysis showed that the samples exhibited single spinel phase, however thermomagnetic examination revealed that magnetic structure is not homogeneous and consists of magnetic clusters separated by nonmagnetic layers, which weakly interact at low temperatures and switch into the superparamagnetic regime at higher temperatures. The average size and magnetic moments of these clusters calculated from magnetic hysteresis loop indicated their multidomain structure. The effective magnetic anisotropy constant was determined by LAS method [3] and its temperature dependence was analyzed.

- [1] P. Thakur, S. Taneja, D. Chahar, B. Ravelo, and A. Thakur, Jmmm 530, 167925 (2021). <https://doi.org/10.1016/j.jmmm.2021.167925>.
- [2] A. I. Tovstolytkin, M. M. Kulyk, V. M. Kalita, S. M. Ryabchenko, V. O. Zamorskyi, O. P. Fedorchuk, S.O. Solopan, and A. G. Belous, Jmmm, 473, 422 (2019). <https://doi.org/10.1016/j.jmmm.2018.10.075>.
- [3] E. C. Devi, and I. Soibam, Journal of Superconductivity and Novel Magnetism, 32, 1293 (2019). <https://doi.org/10.1007/s10948-018-4823-4>.

Pressure effects on magnetic properties of LaMnO₃ and YMnO₃

A.A. Lyogenkaya, A. S. Panfilov, G. E. Grechnev, and V. A. Pashchenko

*B.Verkin Institute for Low Temperature Physics and Engineering of NAS of Ukraine,
47 Nauky Ave., Kharkiv, 61103, Ukraine
e-mail: lyogenkaya@ilt.kharkov.ua*

LaMnO₃ and YMnO₃ compounds are members of the manganite family and both demonstrate a variety of intriguing properties, including the colossal magnetoresistance effect. This is primarily owing to the fascinating coexistence and interplay between orbital, charge, and spin degrees of freedom in these materials.

At ambient conditions, LaMnO₃ is an insulator with an orthorhombic perovskite structure. At zero pressure and below the Néel temperature ($T_N \approx 140$ K), LaMnO₃ adopts an A-type antiferromagnetic (AFM) order characterized by spin plane alternation along the c-axis. Competition between in-plane ferromagnetic (FM) interactions in the (001) layers and interplane AFM interactions leads to a mixed AFM-FM ground state.

In contrast, the hexagonal compound YMnO₃ is a multiferroic with antiferromagnetic ordering and a Néel temperature of 80 K. The transition from the paraelectric to the ferroelectric phase is accompanied by structural distortions, including tilting of the oxygen bipyramids surrounding the Mn ions and bending of the intermediate Y layers.

The magnetic properties of these compounds are being studied extensively. Recent studies show that their temperature-dependent magnetic susceptibility follows the Curie-Weiss law, with an effective magnetic moment close to the spin-only value for the Mn³⁺ ion ($S = 2$). This behavior of $\chi(T)$ allows us to investigate the effect of pressure on the susceptibility, providing information on the pressure dependence of Curie temperature Θ and the volume dependence of the exchange interaction between the magnetic moments of Mn.

In this report, we present the first experimental study of the hydrostatic pressure effect on the magnetic susceptibility of LaMnO₃ and YMnO₃ in the paramagnetic phase. Using the Curie-Weiss law to describe the temperature dependence of the susceptibility, we determined the magnitude of the pressure effect by analyzing the pressure dependence of the paramagnetic Curie temperature. The obtained derivatives $d\Theta/dP$ allowed us to estimate the magnetic Grüneisen parameter $\gamma_m = -(d\ln|\Theta|/d\ln V)$. Despite significant differences in the crystal structure and Θ values between the two compounds, their γ_m values are virtually identical. The estimated value $\gamma_m \approx 4$ closely matches the average value of 10/3 observed in a wide range of magnetic insulators with superexchange interactions, emphasizing the dominant role of superexchange interactions in the magnetism of the studied manganites.

Effect of magnetic field orientation on the behavior of linear dichroism in YIG:Co epitaxial film

O. V. Myoslavskaya, Yu. M. Kharchenko, M. F. Kharchenko

*B.Verkin Institute for Low Temperature Physics and Engineering of NAS of Ukraine,
47 Nauky Ave., Kharkiv, 61103, Ukraine
e-mail: olga.miloslav@gmail.com*

Known for its photo-magnetic properties, cobalt-doped iron-yttrium garnet (YIG:Co) continues to attract the attention of researchers, in particular, due to the discovered ability to control magnetic states by the action of pulsed polarized femtosecond laser radiation [1] and the prospects for technological use of the discovered photo-magnetic properties of this material. Here presented are the results of spectral studies of optical linear dichroism induced by a magnetic field applied to a YIG:Co film at different angles relative to the crystallographic axis [100]. The $\text{Y}_2\text{CaFe}_{3.9}\text{Co}_{0.1}\text{GeO}_{12}$ film with a thickness of 5.8μ was grown by the method of liquid phase epitaxy on a transparent single-crystal $\text{Gd}_3\text{Ga}_5\text{O}_{12}$ plate with a developed surface parallel to the (001) crystallographic plane. The magnetic field $H = 8.6$ kOe was directed in the (001) plane of the film at different angles to the [100] axis. Measurements were made in the spectral range from ~ 550 nm to ~ 750 nm. The light beam was directed along the normal to the film surface, $k \parallel [001]$. The orientation of the field relative to the [100] crystallographic axis was changed by rotating the sample around the [001] axis. The temperature of the film was ~ 50 K. According to data [2], at temperatures around 50 K the easy magnetization axis of YIG:Co film is directed along [001].

The detected magnetic linear dichroism (MLD) changes are especially noticeable in the wavelength range, where, according to [3], electronic transitions are observed in cobalt ions Co^{2+} , Co^{3+} , which occupy the sites with octahedral and tetrahedral symmetry. The observed well-defined dependence of the MLD on the field orientation not only confirms the strong anisotropy of cobalt ions, but also provides an opportunity to better understand the role of Co^{2+} and Co^{3+} ions in the formation of magnetic anisotropy in YIG:Co and changes in the magnetic states of doped YIG:Co films under the influence of external factors.

- [1] T. Zalewski, A. Maziewski, and A. Stupakiewicz Appl. Phys. Lett. 123, 032402 (2023). <http://doi:10.1063/5.0157894>
- [2] M. Tekielak, A. Stupakiewicz, A. Maziewski and J. M. Desvignes, J. Magn. Magn. Mater. 254–255, 562 (2003). [http://doi.org/10.1016/S0304-8853\(02\)00881-8](http://doi.org/10.1016/S0304-8853(02)00881-8)
- [3] Z. Simsa, J. Simsova, P. Gornert, A. Maziewski, Acta Ph. Pol. A76, 277 (1989).

About the nature of incommensurate phase in double Jahn-Teller rare-earth molybdates

Yu. M. Kharchenko, K. V. Kutko, N. M. Nesterenko

*B.Verkin Institute for Low Temperature Physics and Engineering of NAS of Ukraine,
47 Nauky Ave., Kharkiv, 61101 Ukraine
e-mail: nesterenko@ilt.kharkov.ua*

According to the study of temperature and magnetic field (up to 7 T) dependences of optical absorption and birefringence spectra, the ordering of the cooperative Jahn-Teller effect (CJTE) type in the layered double rare-earth molybdate $K\text{Dy}(\text{MoO}_4)_2$ occurs through an intermediate phase [1]. Near the CJTE temperature, the intermediate (incommensurate) phase (IP) exists between temperatures $T_1 = 11.5$ K and $T_2 = 14.3$ K. The aim of this work was to carry out a symmetry analysis of possible structural changes during the CJTE-type phase transition through IP in a series of isostructural layered compounds of double molybdates $M\text{Re}(\text{MoO}_4)_2$ ($M = K, Cs; \text{Re} = Dy, Er, Tm$).

The symmetry analysis, proposed here, taking into account the interaction of the electronic degrees of freedom of rare-earth ions (RE) with rotations of "rigid" tetrahedral anions $(\text{MoO}_4)^{2-}$, shows that an incommensurate phase can arise with mutual shifts of the RE layers which are parallel to the ac plane. Since the unit cell of the isostructural series of double molybdates in the initial rhombic phase contains two energetically equivalent RE layers [2], the specificity of the arising IP, apparently, requires taking into account the dynamics of mutual shifts of the rare-earth layers. The similarity structures of a number of RE molybdates and the proximity of their parameters in the RE layers permit us to conclude that IP can also arise in other RE compounds that undergo CJET.

An applied external magnetic field leads to energy non-equivalence of two adjacent RE layers connected by a two-fold axis in a rhombic unit cell [3]. As a result of a low-temperature phase transition observed in compounds at 5 T under the same conditions, a decrease in symmetry of the unit cell is possible. The issue of changing the crystal symmetry under the influence of an external magnetic field in $K\text{Er}(\text{MoO}_4)_2$ in the fields up to 15 T [4] is also discussed.

- [1] Yu.N. Kharchenko, Low Temp. Phys. 22, 306 (1996). <https://doi.org/10.1063/10.0033975>.
- [2] S. Chong, S. Perry, B. J. Riley and Z. J. Nelson, Acta Crystallogr., Sec. E 76, 1871 (2020). <https://doi.org/10.1107/S205698902001542X>.
- [3] V. I. Kut'ko, Low Temp. Phys. 31, 1 (2005). <https://doi.org/10.1063/1.1820349>.
- [4] B. Bernáth, K. Kutko, S. Wiedmann, at el, Adv. Electron. Mater. 8, 2100770 (2022). <https://doi.org/10.1002aelm.202100770>.

Investigation of magnetic structure by spin-polarized scanning tunneling microscopy in ErB₄ tetraboride.

**O. Onufriienko¹, D. Volavka², S. Gabáni¹, K. Flachbart¹, G. Pristáš¹, K. Siemensmeyer³,
K. Prokeš³, N. Shitsevalova⁴**

¹ Centre of Low Temperature Physics, Institute of Experimental Physics,
Slovak Academy of Sciences, Košice, Slovakia.

²Centre of Low Temperature Physics, Faculty of Science, P.J. Safarik University, Košice, Slovakia.

³Helmholtz Zentrum für Materialien und Energie, Berlin, Germany.

⁴Institute for Problems of Materials Science, Ukraine Academy of Science, Kiev, Ukraine.
e-mail: onufriienko@saske.sk

Rare earth tetraborides (REB₄) are known as 2D frustrated magnets on the Shastry-Sutherland lattice (SSL), where they form a structure of squares and equilateral triangles [1]. Moreover, at a critical magnetic fields and/or critical temperatures, these materials can transform from the antiferromagnetic to the ferrimagnetic state.

In this work, we compare the topography of the atomic structure with the possible topography of spin states in ErB₄ using a scanning tunneling microscope (STM). Measurements were performed at temperature of 1.2 K and in zero magnetic field as well as above the critical magnetic field of 2 T, using non-magnetic gold (Au) and a modified spin-polarized antiferromagnetic chromium (Cr) tips. The Fourier transformation of the topography at zero magnetic field with Au-tip reveals a lattice constant of $a \approx 7.02 \text{ \AA}$, which closely matches the value of 7.057 Å for ErB₄ [2]. At the same time, increasing the magnetic field above the critical value did not show any changes in the surface structure of the sample. Replacing the Au-tip by a Cr one, even at zero field, revealed magnetic stripes on the sample surface. The width of observed stripe domains of $\approx 21.41 \text{ \AA}$ was measured in the Fourier transformation of the topography, corresponding to a three-lattice constants-wide stripe. Moreover, the direction of the magnetic stripes is slightly rotated with respect to the atomic structure of the sample. However, scanning the topography at magnetic fields above the critical values, where the sample goes to the ferrimagnetic state, did not show any changes in the magnetic structure. This may be due to the insufficient sensitivity of our STM electronics and to small changes in the electronic state of the sample associated with the transition from the antiferromagnetic to the ferrimagnetic state.

Further studies of similar systems are required with upgrades of the measuring equipment.

Acknowledgements

This work was supported by projects APVV-23-0226, VEGA 2/0034/24, DAAD-SAS-2023-02. Liquid nitrogen for experiments was sponsored by U.S. Steel Košice, s.r.o.

[1] S. Gabani, K. Flachbart, K. Siemensmeyer, T. Mori, Journal of Alloys and Compounds, 821 (2020), 153201. <https://doi.org/10.1016/j.jallcom.2019.153201>.

[2] L. Ye, T. Suzuki, and J. G. Checkelsky, Phys. Rev. B, 95 (2017), 174405. <https://doi.org/10.1103/PhysRevB.95.174405>.

Comparative analysis of Raman and IR spectra in LiCoPO₄ and LiNiPO₄ magnetoelectrics

A. V. Peschanskii¹, V. P. Gnezdilov¹, and A. Yu. Glamazda^{1,2}

¹*B.Verkin Institute for Low Temperature Physics and Engineering of NAS of Ukraine,
47 Nauky Ave., Kharkiv, 61103, Ukraine*

²*V.N. Karazin Kharkiv National University, 4 Svobody Sq., 61022, Kharkov, Ukraine
e-mail: peschansky@ilt.kharkov.ua*

The olivine-type lithium orthophosphates LiMPO₄ ($M=\text{Fe}^{2+}$, Mn^{2+} , Co^{2+} , and Ni^{2+}) family have intriguing magnetoelectric properties. The present work is dedicated to the Raman studies of the LiCoPO₄ single crystal possessing the highest magnetoelectric coefficient among the above-mentioned crystals of the LiMPO₄ family. The performed analysis of taken Raman spectra in the different polarization configurations has revealed a number of additional phonon lines upon transition to a magnetically ordered state: 192.2, 230.0, 237.5, and 333.5 cm⁻¹ (Figs. 1a, 1c); 541.4 cm⁻¹ (Fig. 1b); 1031.5 cm⁻¹ (Fig. 1d). A revealed effect can be explained in terms of two scenarios: 1) the unit-cell multiplication below T_N ; 2) IR phonon leakage due to the magneto-electric effect.

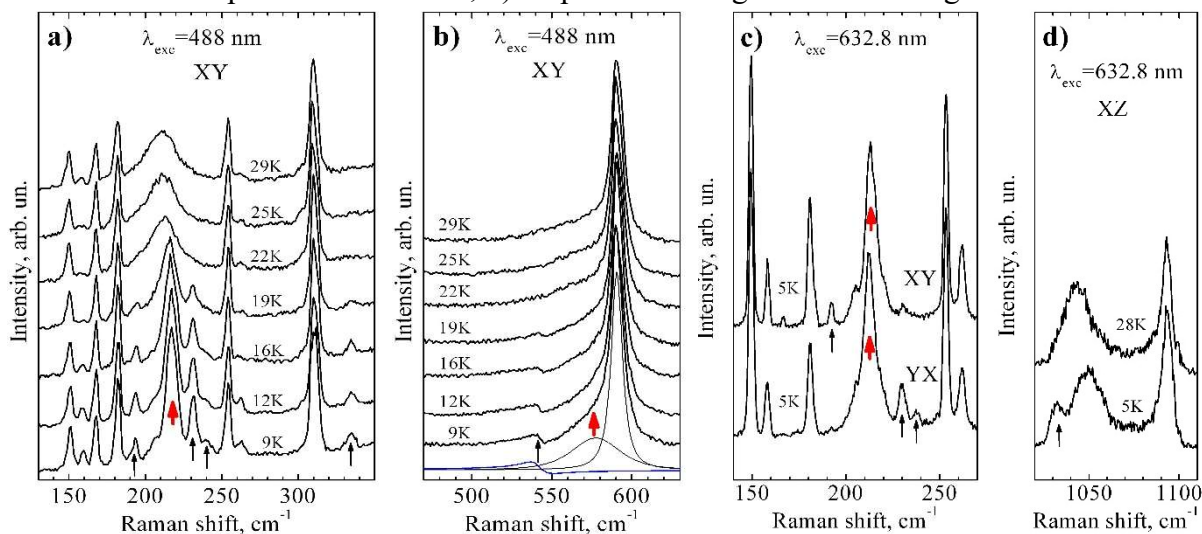


Fig. 1. Temperature dependent polarized Raman spectra taken in: a), b), c) – (YX, YX) B_{1g} ; d) – (XZ) B_{2g} modes. Spectral resolution: a), b) – 3.0 cm^{-1} ($\lambda_{\text{exc}} = 488 \text{ nm}$); c), d) – 1.8 cm^{-1} ($\lambda_{\text{exc}} = 632.8 \text{ nm}$). Thin arrows are related to the additional phonon lines. The thick arrows mark electronic excitations.

The assumption about the presence of the unit-cell multiplication contradicts the available X-ray and neutron diffraction data. There are no data on low-temperature IR phonons for LiCoPO₄ to verify the second scenario. The performed analysis of our Raman spectra of LiCoPO₄ [1] and LiNiPO₄ [2] allowed us to find the empirical dependences of the frequency positions of phonon lines on the ionic radius and atomic vibration types. Having performed the comparative analysis of obtained abovementioned Raman data and IR spectra of LiNiPO₄ ($T=30 \text{ K}$) [3], we calculated the frequency positions of the IR phonons in LiCoPO₄. The results obtained are in good agreement with the frequency positions of additional phonons observed in Raman spectrum.

The work was partially supported by the Thematic Program of the Wolfgang Pauli Institute "Mathematics–Magnetism–Materials" and IEEE program "Magnetism for Ukraine 2024/25".

- [1] V. I. Fomin, V. P. Gnezdilov, V. S. Kurnosov, A. V. Peschanskii, et. al., Low. Temp. Phys., 25, 829 (1999). <https://doi.org/10.1063/1.593827>.
- [2] V. I. Fomin, V. P. Gnezdilov, V. S. Kurnosov, A. V. Peschanskii, et. al., Low Temp. Phys. 28, 203 (2002). <https://doi.org/10.1063/1.1468525>.
- [3] M. S. Radionov, S. A. Klimin, A. Yu. Glamazda, A. V. Peschanskii, Low Temp. Phys. 48, 246 (2022). <https://doi.org/10.1063/10.0009544>.

Manifestation of spiral magnetic phase in optical absorption spectra of $\text{NdFe}_3(\text{BO}_3)_4$ crystal

V. G. Piryatinskaya, V. V. Slavin, I. S. Kachur, V. S. Kurnosov

*B.Verkin Institute for Low Temperature Physics and Engineering of NAS of Ukraine,
 47 Nauky Ave., Kharkiv, 61103, Ukraine
 e-mail: piryatinskaya@ilt.kharkov.ua*

$\text{NdFe}_3(\text{BO}_3)_4$ belongs to the family of rare-earth ferroborates which are of interest due to their nontrivial magnetic properties. The crystal structure of $\text{NdFe}_3(\text{BO}_3)_4$ is described by the space symmetry group $R\bar{3}2$. At $T_N \approx 30$ K the crystal orders into easy-plane collinear antiferromagnetic structure. Below $T_{IC} \approx 13.5$ –16 K, the magnetic structure transforms to a long-period spiral propagating along C_3 axis; orientation of all magnetic moments remains parallel to the basal plane.

We study optical absorption spectra of $\text{NdFe}_3(\text{BO}_3)_4$ in the region of the transition $^4I_{9/2} \rightarrow ^2H_{11/2}$ in Nd^{3+} (C-group) in the temperature range 6–32 K. We obtain the temperature dependences of the integral intensities of exchange splitting components of lines C5 (15971 cm^{-1}) and C6 (15997 cm^{-1}). For π -polarization, the intensity behavior can be described in terms of thermoactivation model (Fig. 1) where intensities are determined by thermal populations of the lowest and excited sublevels of the Nd^{3+} ground doublet. On the contrary, the temperature dependences of intensities in σ -spectra significantly differ from the thermoactivation one (Fig. 1).

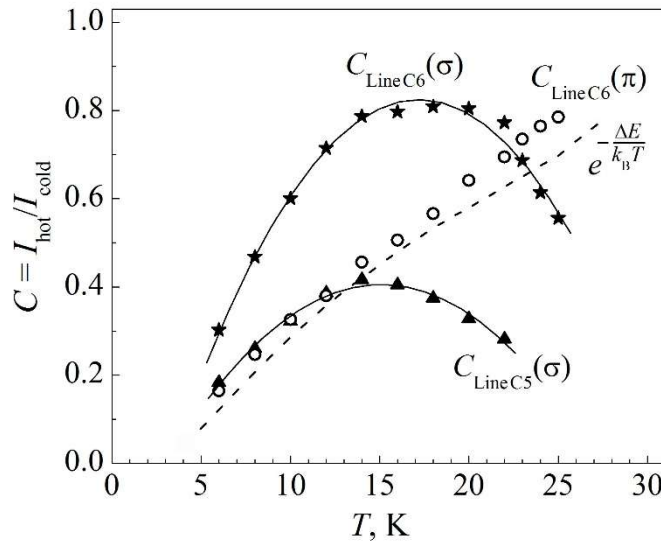


Fig. 1. The ratio of integral intensities of the "hot" and "cold" components of absorption lines C5 and C6 of the optical transition $^4I_{9/2} \rightarrow ^2H_{11/2}$ (C-group) in $\text{NdFe}_3(\text{BO}_3)_4$ spectra depending on temperature. Dash line corresponds to thermoactivation model. Solid curves are the results of fitting the experimental data by the theoretic model.

We associate the unusual temperature dependences of lines intensities with the transition from collinear magnetic structure to long-period spiral in the considered temperature range. Due to the fact that Nd^{3+} moments lie in the basal plane in the whole temperature range $T < T_N$, π -spectra are non-sensitive to this phase transition. In σ -spectra, the rotation of magnetic moments in the basal plane results in a change of probability of optical transitions. We assume that this rotation can be caused by Dzyaloshinskii–Moriya interaction between Nd^{3+} and Fe^{3+} ions. To describe the temperature behavior of lines intensity we propose theoretical model which takes into account the Dzyaloshinskii–Moriya interaction. The calculations show good agreement between the experimental and theoretical data.

Dynamic cluster magnetic subsystems in diluted magnetic semiconductor $\text{Ge}_{1-x-y}\text{Sn}_x\text{Mn}_y\text{Te}$

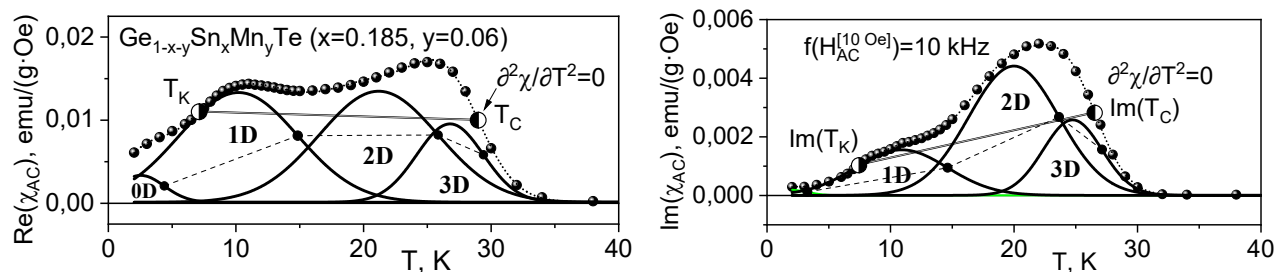
V. E. Slynko¹, L. Kilanski², M. Arciszewska², V. I. Ivanov¹

¹ Chernivtsi Branch of Frantsevych Institute for Problems of Materials Science, NASU,
5 Iryny Vilde St., Chernivtsi, 58001, Ukraine

² Institute of Physics, Polish Academy of Sciences,
Aleja Lotników 32/46, PL-02668 Warsaw, Poland
e-mail: slynko.vasily@gmail.com

Diluted magnetic semiconductors (DMS) based on $\text{A}^{\text{IV}}\text{B}^{\text{VI}}$ compounds doped with magnetic impurities are of considerable scientific and practical interest [1]. They are promising materials for spin electronics and convenient objects for fundamental research in the field of magnetism.

We have synthesized a series of $\text{Ge}_{1-x-y}\text{Sn}_x\text{Mn}_y\text{Te}$ samples of various compositions. Detailed studies of their magnetic properties have been carried out. The temperature dependences of the dynamic magnetic susceptibility $\text{Re}(\chi_{\text{AC}})(T)$ of some samples contain two peaks: the left (lower temperature) and the right (higher temperature). When the frequency of the external magnetic field H_{AC} changes, the right peak in the $\text{Re}(\chi_{\text{AC}})(T)$ dependences shifts, while the left one remains stationary. Fitting the experimental $\text{Re}(\chi_{\text{AC}})(T)$ dependences with Gaussian curves revealed four types of dynamic cluster magnetic subsystems of different spatial dimensions (0D, 1D, 2D, 3D). Dynamic magnetic clusters arise due to thermal vibrations of the crystal lattice containing ions of magnetic impurities and can be likened to standing waves, the size and structure of which provide long-range RKKY interaction (Ruderman–Kittel–Kasuya–Yosida) via charge carriers [2].



It was found that in $\text{Ge}_{1-x-y}\text{Sn}_x\text{Mn}_y\text{Te}$ the phases of spin glass (SG) and cluster glass (CG) always coexist with the ferromagnetic (FM) phase, which is proved by the presence of magnetic hysteresis loops down to the lowest measurement temperatures of ~ 2 K.

By analogy with the *Curie temperature* T_c (which is determined at the inflection point on the right wing of the $\text{Re}(\chi_{\text{AC}})(T)$, where $\partial^2\chi/\partial T^2=0$), the concept of the *Kilanski temperature* T_K is introduced, for which the same condition ($\partial^2\chi/\partial T^2=0$) is satisfied on the left wing of the $\text{Re}(\chi_{\text{AC}})(T)$ dependence. The distance between T_K and T_c is a convenient measure for determining the temperature range of magnetic transformations accompanied by the presence of magnetic hysteresis loops. Thanks to it, the symmetry between the two types of magnetic disordering becomes obvious: low-temperature (spin-glass) and high-temperature (paramagnetic) [3].

- [1] A. Khaliq et al., Journal of Alloys and Compounds 968, 171893-1-12 (2023). <https://doi.org/10.1016/j.jallcom.2023.171893>.
- [2] J. Stöhr, and H. C. Siegmann, Magnetism: From Fundamentals to Nanoscale Dynamics. – Springer-Verlag Berlin Heidelberg, 2006. – P. 290-293. – 821 p. – ISBN 978-3540302827.
- [3] I. Georgescu, Nature Reviews Physics 5, 80 (2023). <https://doi.org/10.1038/s42254-023-00554-7>.

Thermal conductivity of the $Dy_x Y_{1-x} (PO_3)_3$ phosphate glasses

**V. Stadnyk¹, V. Tkáč¹, M. Tokarčík¹, P. Baloh², R. Tarasenko¹, E. Čižmár¹, M. Orendáč¹,
A. Orendáčová¹, J. Holubová³, E. Černošková³, Z. Černošek³ and A. Feher¹**

¹*Institute of Physics, Faculty of Science, P. J. Šafárik University in Košice, Park Angelinum 9, 041
54 Košice, Slovakia*

²*International Institute for Carbon-Neutral Energy Research, Kyushu University (I2CNER),
744 Motooka, Nishi-ku, Fukuoka 819-0395, Japan*

³*Department of General and Inorganic Chemistry, Faculty of Chemical Technology,
University of Pardubice, Studentská 573, 532 10 Pardubice, Czech Republic
e-mail: vladyslav.stadnyk@student.upjs.sk*

This work presents an experimental study of phosphate glasses doped with rare earth elements to investigate their behaviour at low temperatures (LT). We study how the magnetic subsystem influences on thermal transport by choosing Dy^{3+} as the magnetic ion and Y^{3+} as the non-magnetic analogue. The study of magnetic properties considers the effect of the crystal electric field on Dy^{3+} ions, which is strongly affected by the disordered atomic structure inherent to amorphous materials.

We have performed a low-temperature study of magnetically doped phosphate glasses of composition $Dy_x Y_{1-x} (PO_3)_3$ via specific heat measurements from $T = 0.4$ K to $T = 20$ K and using the thermal conductivity from room temperature down to $T = 2$ K. Experiments were conducted on $Dy_x Y_{1-x} (PO_3)_3$ glasses with six samples containing varying Dy concentrations ($x = 0\%, 0.01\%, 0.1\%, 1\%, 10\%$ and 100%). The heat capacity shows a characteristic maximum at low temperatures, known as boson peak (BP), associated with the presence of excessive low-frequency vibrational states. Well-visible BP is observed in $x = 0\%$ sample at $T = 12$ K [1], while C_p in $x \neq 0\%$ samples is affected by the onset of Schottky maximum. Thermal conductivity measurements showed typical glass-like behaviour: a plateau in $k(T)$ between $T \approx 5$ and 20 K. Below 5 K is observed onset on $k(T) \sim T^2$ and a slight increase of $k(T)$ above $T = 15$ K. Magnetic Dy^{3+} ions influence phonon transport, likely via phonon scattering on magnetic excitations and disorder. Thermal conductivity demonstrates a non-linear dependence on composition. The highest value is observed for the $x = 100\%$ sample, while the minimal one corresponds to $x = 1\%$. The results confirm that Dy-doped phosphate glasses display universal low-temperature glassy behaviour.

Acknowledgements:

The work was supported by the Slovak Research and Development Agency Projects APVV-22-0172.

- [1] P. Baloh et al., Journal of Magnetism and Magnetic Materials 588 (2023) 171415.
<https://doi.org/10.1016/j.jmmm.2023.171415>.

Nonreciprocity of surface magnetoelastic waves in a ferromagnetic bilayer with noncollinear layer magnetizations

L. I. Ushii¹, A. N. Slavin², R. V. Verba¹

¹*V.G. Baryakhtar Institute of Magnetism of the NAS of Ukraine,
36-B Vernadskogo blvd., Kyiv 03142, Ukraine*

²*Department of Physics, Oakland University,
318 Meadow Brook Rd., Rochester, Michigan 48309, USA
e-mail: ushiy@ukr.net*

Nonreciprocity of surface acoustic waves (SAWs) in a microwave frequency band is a very attractive feature, which would drastically enhance functionality of microwave SAW electronics devices. Due to symmetry of fundamental laws of mechanics, pure acoustic waves in solids are reciprocal, and nonreciprocity of their frequency and/or losses can be induced only by a coupling to excitations of another nature. The most promising way to induce SAW nonreciprocity is the utilization of magnetoelastic interaction of SAW with spin waves (SWs) propagating in hybrid magnetoelastic heterostructures [1,2].

Recent works have shown that ultimate isolation of counter-propagating hybridized SAW/SW is achieved in heterostructures consisting of a synthetic antiferromagnet – ferromagnetic (FM) bilayer with antiferromagnetic RKKY interlayer coupling – placed on top of a piezoelectric acoustic waveguide [3-4]. Fabrication of such structures is quite complex and could be a bottleneck in the overall simple SAW electronics technology.

In this work, we study in details a more practical and technologically simpler system based on an FM bilayer, where the layers are coupled by only dipole-dipole interaction, placed on a top of piezoelectric crystal. In contrast to previous works [5-6], in which SAW nonreciprocity was observed due to occasionally weakly noncollinear magnetization of the layers, we propose to fabricate FM layers with intentionally noncollinear in-plane anisotropy. A weak in-plane anisotropy of just 1-2 mT magnitude, which can be easily induced by FM layer growth in a magnetic field, is shown to be enough for supporting noncollinear magnetizations of the layers and, thus, SW nonreciprocity. We formulate requirements for the relative orientation of the layer's magnetizations and wave propagation direction necessary to realize an efficient SAW microwave isolator, and demonstrate examples of SAW transmission characteristics which prove the possibility of achieving an isolation exceeding 50 dB for a submillimeter-long FM bilayer with insertion losses of just a few decibels more than those of a pure SAW device. In addition to relative fabrication simplicity, the proposed magnetoelastic heterostructure exhibits a reasonable robustness in respect to deviations in the anisotropy axes and/or bias field directions, which is an important benefit for device mass production.

- [1] M. Weiler et al., Phys. Rev. Lett. 106, 117601 (2011). <https://doi.org/10.1103/PhysRevLett.106.117601>.
- [2] R. Verba, et al., Phys. Rev. Applied 9, 064014 (2018). <https://doi.org/10.1103/PhysRevApplied.9.064014>.
- [3] R. Verba, V. Tiberkevich, and A. Slavin, Phys. Rev. Applied 12, 054061 (2019). <https://doi.org/10.1103/PhysRevApplied.12.054061>.
- [4] H. Matsumoto, et al., Appl. Phys. Express 15, 063003 (2022). <https://doi.org/10.35848/1882-0786/ac6da1>.
- [5] P. J. Shah et al., Sci. Adv. 6, eabc5648 (2020). <https://doi.org/10.1126/sciadv.abc5648>.
- [6] D. A. Bas et al, Phys. Rev. Appl. 18, 044003 (2022). <https://doi.org/10.1103/PhysRevApplied.18.044003>.

OPTICS, PHOTONICS AND OPTICAL SPECTROSCOPY

Resonant frequency intersection of toroidal modes in all-dielectric metasurface with hexagonal unit cell

O. A. Breslavets¹, Z. E. Eremenko^{1,2}

¹*O.Ya. Usikov Institute for Radiophysics and Electronics of NAS of Ukraine,
12 Ac. Proskura St., Kharkiv, 61085, Ukraine*

²*Leibniz Institute for Solid State and Materials Research,
Helmholtzstraße 20, 01069 Dresden, Germany
e-mail: alex.breslavets@gmail.com*

Nowadays, the development of metasurfaces with enhanced functionality, compactness, and simplified fabrication is driving advancements in THz technologies [1]. Recent studies have investigated all-dielectric metasurface (ADM) cluster designs for exciting toroidal modes. Hexagonal clusters were selected for their crucial role in topological photonics and their ability to support net toroidal dipole moments. The toroidal dipole moment vectors differ: toroidal (TO) has co-directional vectors, while anti-toroidal (ATO) has opposite ones [2].

Our ADM consists of a hexagonal unit cell with 18 disks arranged as 6 trimers (each is 3 disk with one disk of different height), modeled in COMSOL Multiphysics. In a metasurface with a hexagonal elementary supercell, natural oscillations exist but remain unexcited when all disk heights are identical, making them «dark» modes. To excite these oscillations, we need to break the symmetry of the hexagonal structure. This analysis applies to eigenmodes fields and toroidal dipole moments, while the supercell symmetry defines possible magnetic groups. For a given trimer eigenmode, the toroidal dipole moment dominates and emerges under dark or bright incident field excitations. Accessing the dark state requires symmetry breaking in hexagonal clusters.

According to the group theory we examined two symmetry breaking configurations, $C_s^{(1)}$ (z -axis asymmetrical) and C_{6v} (z -axis symmetrical) [3], enabling toroidal resonances through disk height variations. Numerical simulations evaluated eigenfrequencies, quality factors (Q-factors), and electromagnetic field distributions in a resonant ADM. Due to symmetry breaking, toroidal modes arise from confined magnetic fields, forming toroidal vector rotation in each trimer plane.

The ADMs period is $2p = 2296$ nm. Disk resonators have radius of $r_d = 170$ nm and height of $h_d = 149$ nm. The substrate and disks are made of silicon and taken without losses. A key finding is the TO and ATO frequency intersection: for $C_s^{(1)}$, it occurs at $\Delta h_d/h_d = -0.44$, and for C_{6v} at $\Delta h_d/h_d = -0.3$. These intersections yield vastly different Q-factors — of the order of 10^3 for $C_s^{(1)}$ and 10^9 for C_{6v} . At this point, the Q-factor depends on symmetry breaking type, enabling precise tuning of the resonant electromagnetic properties.

Our THz-range model is adaptable across broader frequencies. Metasurfaces become crucial for beam splitters and ultra-narrow-band absorbers as optical devices shrink, where high-Q resonances are key. ADMs with toroidal modes enable applications in optical rectifiers, electro-optic modulators, artificial magnetism, antennas, microwave circuits, absorbers, switches, and sensors. They also aid in studying physical phenomena, developing multiferroic materials, and analyzing complex systems with 3D symmetries and quasi-bound states in photonic crystal slabs.

- [1] D. Hao, J. Liu, P. Zou, Y. Zhang, R. Moro and L. Ma, *Laser Photonics Rev.* 18, 2301210 (2024). <https://doi.org/10.1002/lpor.202301210>.
- [2] T. Wu, A. B Evlyukhin and V. R Tuz, *Journal of Physics D: Applied Physics* 57, 50, 505301 (2024). <https://dx.doi.org/10.1088/1361-6463/ad7bc6>.
- [3] V. Dmitriev, S. D. S. Santos, A. B. Evlyukhin, A. S. Kuprianov and V. R. Tuz, *Phys. Rev. B* 103, 165402 (2021). <https://doi.org/10.1103/PhysRevB.103.165402>.

Combined optical effects in unconventional multilayer metamaterial structures

A. F. Bukhanko

*Donetsk Institute for Physics and Engineering Named after O.O. Galkin,
National Academy of Sciences of Ukraine, 46 Nauki ave, Kyiv, 03028, Ukraine
e-mail: metatem@ukr.net*

In this study, we present a theoretical investigation of the polaritons propagation in an unconventional multilayer metamaterials. An interesting example of metamaterials arises if the extreme material parameters are combined with anisotropy. These artificial structures exhibit a combination of electromagnetic characteristics that are not observed in natural media. The iso-frequency surface for such metamaterials differs significantly from a sphere or an ellipsoid. For example, tensor diagonal elements with opposite signs result in a hyperbolic iso-frequency surface for the extraordinary polarization. In recent years, significant theoretical and experimental research efforts have been dedicated to artificial materials with unconventional properties [1-5].

Taking into account boundary conditions for tangential electromagnetic field components and using Maxwell equations, we derived a set of equations in order to describe the eigenmodes and wave normal surface equation for an unconventional multilayer metamaterial. On this basis, the conditions for the existence of surface waves were investigated in the approximation of extreme material parameters. Dispersion dependences were obtained for the eigenmodes of such a structure, which were studied graphically. The conditions are found for the unusual effects in an unconventional multilayer metamaterials with extreme material parameters, in particular with tensors with zero diagonal elements or with diagonal elements with an opposite sign.

The results obtained could potentially be useful for the control of an electromagnetic wave dispersion and propagation characteristics in an unconventional multilayer metamaterial.

- [1] Vladimir R Tuz, Journal of Magnetism and Magnetic Materials. 419, 559 (2016) <http://dx.doi.org/10.1016/j.jmmm.2016.06.070>
- [2] V. I. Fesenko, I.V. Fedorin, Vladimir R. Tuz, Optics Letters. 41, 2093 (2016). <http://dx.doi.org/10.1364/OL.41.002093>
- [3] Vladimir R. Tuz, I. V. Fedorin, and V. I. Fesenko, Modal phenomena of surface and bulk polaritons in magnetic-semiconductor superlattices, in Surface Waves. Chap. 6, 99 (IntechOpen, Rijeka 2018) <http://dx.doi.org/10.5772/intechopen.71837>
- [4] Nguyen Pham Quynh Anh and Nguyen N. Hieu, Journal of Nonlinear Optical Physics & Materials. 2350012 -1 (2023). <http://dx.doi.org/10.1142/S0218863523500121>.
- [5] W. Freeman, J. Appl. Phys. 129, 085110 (2021) <https://doi.org/10.1063/5.0030845>.

Enhancement of optical chiral sensing with subwavelength gratings

O. Demianyk¹, S. Polevoy², V. Tuz¹, O. Yermakov^{1,3}

¹*V.N. Karazin Kharkiv National University, 4, Svobody Square, Kharkiv 61022, Ukraine.*

²*O. Ya. Usikov Institute for Radiophysics and Electronics of the NASU,
12, Proskura st., Kharkiv 61085, Ukraine.*

³*Leibniz Institute of Photonic Technology, 9 Albert-Einstein-Straße, Jena, 07745, Germany.
e-mail: o.demianyk@gmail.com*

Chirality is used to describe an object that is not superposable on its mirror image. Despite having the same chemical structure, most chiral molecules show significant differences in biological activity, being the poison or the drug depending on the handedness. The main difficulty during the measurement of chiral substances is the need to detect extremely weak chiroptical signals from a small concentration of molecules.

First, we consider the thin gold film of 50-nm thickness at the quartz substrate. Exciting a surface plasmon-polariton via the prism coupling in the attenuated total internal reflection regime (Kretschmann configuration [1]) with a plane TM-polarized wave, we study the reflection spectra [2]. In this case, the small response in the TE-polarization emerges due to the mixing of electric and magnetic fields. As a result, there is the angular difference between the spectral resonances in right- and left-handed circular polarized waves due to the presence of chiral substance.

Then, we replace a gold thin film by a gold subwavelength grating to enhance the sensitivity of the chiroptical sensor. We observe the enhancement of the chiral sensitivity by about two orders of magnitude. The observed improvement is explained by the appearance of the Rayleigh anomaly, which arises due the subwavelength grating structure. This anomaly occurs under specific conditions where a diffracted wave originates and propagates tangentially along the grating surface. At this point, the diffracted wave becomes an evanescent wave. As a result, the coupling between the evanescent wave strongly localized at the edges of grating and the chiral substance leads to the significant amplification of the chiroptical response.

Thus, we demonstrate that the structuring of the thin plasmonic film leads to the multifold enhancement of the chiral sensing. The results obtained open new opportunities for the optical sensing of the polarization-sensitive molecules in the real-time regime.

[1] E. Kretschmann and H. Raether, Zeitschrift für Naturforschung A 23(12), 2135-2136 (1968).

DOI: <https://doi.org/10.1515/zna-1968-1247>

[2] S. Droulias and L. Bougas, ACS Photonics 6, 1485 (2019).

DOI: <https://doi.org/10.1021/acspophotonics.9b00137>.

Experimental determination of emission cross sections for electron-induced processes in a supersonic argon jet

Yu. S. Doronin, A. A. Tkachenko, V. L. Vakula, G. V. Kamarchuk

*B. Verkin Institute for Low Temperature Physics and Engineering of NAS of Ukraine,
47 Nauky Ave., Kharkiv, 61103, Ukraine
e-mail: doronin@ilt.kharkov.ua*

Electron-excited supersonic jets of noble gases are compact intense sources of vacuum ultraviolet (VUV) radiation. In atomic jets, VUV radiation is primarily produced by resonance transitions between the ground and excited states of atoms and ions. In jets containing clusters, the contribution to the VUV radiation flux provided by the continua emitted by the neutral (Rg_2^*) and charged excimer complexes (Rg_4^+)^{*} formed in the clusters becomes dominant as the number and size of clusters in the jet increase.

For the practical use of such VUV sources and the development of methods for their application, data on absolute fluxes and spectral characteristics of the radiation are required. Using an absolute calibration of a gas-jet source of VUV radiation at a fixed pressure $P_0 = 0.2$ MPa and temperature $T_0 = 300$ K of argon at the nozzle inlet for the energy of colliding electrons of 1000 eV, we have estimated the emission cross sections $\sigma(\lambda)$ for the argon Ar I resonance lines ($\lambda=1048$ Å, $\lambda=1067$ Å) and for the maximum of the so-called second excimer continuum ($\lambda=1270$ Å).

It was found that the cross sections $\sigma = 10 \cdot 10^{-18}$ cm² for the resonance line 1048 Å and $\sigma = 5.9 \cdot 10^{-18}$ cm² for the resonance line 1067 Å significantly exceed the previously measured emission cross sections for argon atoms in gas [1]. This can be explained by the contribution of metastable states and free electrons to the intensity of the resonance lines. At the same time, this contribution is higher for the less energetic line $\lambda=1067$ Å. The emission cross section for the second excimer continuum emitted by the clusters, $\sigma(\lambda=1270$ Å) = $2.1 \cdot 10^{-16}$ cm², indicates efficient conversion of the electron beam energy into the emission of this continuum.

[1] J M Ajello, G K James, B Franklin and S Howell J. Phys. B: At. Mol. Opt. Phys. 23, 4355 (1990). DOI 10.1088/0953-4075/23/23/017.

Engineering plasmon canalization for resonant plasmonic metasurfaces

A. Hrinchenko¹, S. Polevoy², O. Demianyk¹, O. Yermakov^{1,3}

¹ *V. N. Karazin National University, 4 Svobody sq., Kharkiv, 61022, Ukraine*

² *O. Ya. Usikov Institute for Radiophysics and Electronics NASU,*

12 Akademika Proskura, Kharkiv, 61085, Ukraine

³ *Leibniz Institute of Photonic Technology, 9 Albert-Einstein-Straße, Jena, 07745, Germany.*

e-mail: artitus1509@gmail.com

Hyperbolic metasurfaces are known for their dispersion and polarization properties, such as negative refraction, hyperlensing, enhanced spontaneous emission, etc [1]. The surface waves localized at hyperbolic metasurfaces are called hyperbolic plasmon-polaritons and exhibit a lot of potential applications for planar technologies [2].

In this work, we analyze the dependencies of the spectral positions of the resonances and spectral bandwidth of hyperbolic regime for the metasurfaces based on square arrays of the nanodisks [3] and rectangular nanopatches [4]. Namely, we study the resonant characteristics of metasurfaces by varying the size of the nanoparticles, the degree of stretching (anisotropy) and the period of the metasurface from the isotropic to extreme anisotropic cases.

Surface plasmons typically propagate radially in all directions, losing a significant portion of their energy during the directional signal transferring. Typical values of the signal amplitude reaching the receiver usually do not exceed 0.1% of the signal amplitude at the source output, and this significantly limits the use of surface plasmons in practical applications. To solve this problem, we demonstrate the one special regime as plasmon canalization, which is characterized by a flat isofrequency contour and the self-collimated unidirectional propagation of surface wave. In this case, the signal transmission efficiency is close to the maximum, that is, the signal amplitude at the source output and at the receiver input are approximately the same, which makes it possible to ensure highly efficient signal transmission with minimal losses. The canalization takes place in the vicinity of one of the resonances highlighting the relevance of the metasurface engineering for the in-plane optical signal transferring.

- [1] O. Takayama, and A. V. Lavrinenko, *J. Opt. Soc. Am. B: Opt. Phys.* 36(8), 38–48 (2019). <https://doi.org/10.1364/JOSAB.36.000F38>.
- [2] J. S. Gomez-Diaz, and A. Alu, *ACS Photonics* 3(12), 2211–2224 (2016). <https://doi.org/10.1021/acsphotonics.6b00645>.
- [3] A. Hrinchenko, and O. Yermakov, *J. Phys. D: Appl. Phys.* 56(46), 465105 (2023). <https://doi.org/10.1088/1361-6463/acefde>.
- [4] A. Hrinchenko, S. Polevoy, O. Demianyk, and O. Yermakov, *J. Appl. Phys.* 135(22), 223102 (2024). <https://doi.org/10.1063/5.0213515>.

Optical scattering for ground combat capabilities

O. G. Nerukh¹, L. N. Illyashenko²

¹*Kharkiv National University of Radio Electronics,
14 Nauky Ave. 14, Kharkiv, 61166, Ukraine*

²*National Academy of the National Guard of Ukraine,
2 Sichovyh Strilciv Str., Zolochiv, Lviv Region, 80700, Ukraine
e-mail: mila.illyashenko@gmail.com*

Electromagnetics has found a lot of applications in various fields of research and industry. Among others are applications for health and life sciences, agriculture and food industry, manufacturing and quality control, however due to appearance of war the military applications start to be very important. It is time to improve the military compatibilities across all five military domains including land, sea, air, space and information. The field is extremely broad, and in this work, we will mostly focus on electromagnetic scattering for ground combat applications, understanding that light is also electromagnetic wave. Then the methods, developed to study electromagnetic effects are also applicable to study scattering, propagation, interference, diffraction of light, and give a lot of opportunities to investigate optical scattering. Among methods, applicable to study optical scattering, integral equation methods are very attractive [1]. While such methods are divided on two categories, such as the domain discretization methods and the boundary discretization methods, the methods of the second category [2] are more attractive to study optical scattering. The methods are also divided on low frequency, medium frequency and high frequency methods, having in mind that high frequency means that size of the scatterer is equal to high number of wavelengths. However optical waves give possibility to study small scatterers, and when it seems that low frequency is expected, small scatterers appear electromagnetically big due to the chosen material, that leads to the use of medium frequency methods [3, 4, 5], and each of them is useful, depending on other aspects, such as shape of the scatterer [3], orientation of the scatterers with respect to each other [4] and to the source of illumination [4, 5], as well as with respect to minimization of the computer resources such as time and memory to obtain accurate solution [5]. Now land forces must be a mix of light, medium, and heavy forces. Land assets and platforms need sufficient mobility, protection, and concealment capabilities to ensure their own security, including increased firepower incorporating flexible payloads. Optical scattering applications in this work are developed for upgrade and development of Main Battle Tank, Infantry Fighting Vehicle and Armoured Personnel Carrier, enabled to operate in all environmental conditions and to face novel threats, such as small Unmanned Aerial Systems using swarming techniques.

- [1] A. Nerukh, T. Benson, *Non-Stationary Electromagnetics: An Integral Equations Approach* (Jenny Stanford Publishing, New York 2018).
- [2] G.C. Hsiao and W.L. Wendland, Boundary integral equations, vol. 164. in Applied Mathematical Sciences (Springer, Cham, Switzerland, 2021) doi: 10.1007/978-3-030-71127-6.
- [3] L. Illyashenko, Spectral Boundary Integral Equation method for electromagnetic research with different geometrical configurations. (DIPED, Tbilisi, Georgia), DOI:10.1109/DIPED63529.2024.10706201.
- [4] U. Koch, J. Niegemann, Ch. Hafner and J. Leuthold, MMP Simulation of Plasmonic Particles on Substrate Under E-Beam Illumination, In The Generalized Multipole for Light Scattering (Springer, Cham, Switzerland, 2018). DOI: 10.1007/978-3-319-74890-0_6.
- [5] E. Iscan, V. Tabatadze, Solution of 3D Electromagnetic Diffraction Problem by PEC Circular Double Disks Using the Method of Auxiliary Sources, (DIPED, Tbilisi, Georgia). DOI: 10.1109/DIPED63529.2024.10706053.

Control of Brewster's angle with plasmonic metasurfaces

O. Mankovska¹, T. Shudra², A. Hrinchenko³, O. Yermakov^{3,4}

¹*Ivan Franko National University of Lviv, 1 Universytetska St, Lviv, 79000, Ukraine*

²*School "Basis", 12-B Kozhumyatska Street, Kyiv, 04071, Ukraine*

³*V. N. Karazin Kharkiv National University, 4 Svobody Square, Kharkiv, 61022, Ukraine*

⁴*Leibniz Institute of Photonic Technology, 9 Albert-Einstein-Straße, Jena, 07745, Germany*

e-mail: oksana.mmankovska@gmail.com

The polarization of incident light may be tuned with the Brewster effect that is widely used in photography, microscopy and optical coatings. The Brewster angle demonstrating zero-reflection is usually observed for transverse-magnetic (TM) polarized light, but the recent studies discover the generalized Brewster effect in transverse-electric (TE) polarization using nanostructures [1]. Here, we discover the way to control the Brewster angle both in the TM and TE polarization by using two-dimensional (2D) plasmonic materials and nanostructures.

We derive the analytical expressions connecting the Brewster angle in TM and TE polarization and the surface conductivity of the two-dimensional sheet at the interface between two isotropic dielectric media. The two-dimensional sheet may be represented by the 2D materials (graphene, hexagonal boron nitride, transition metal dichalcogenide monolayers, etc.), nanostructures and metasurfaces, and it is described by the surface conductivity. We describe the impact of surface conductivity of 2D layer on the shift of the TM Brewster angle in the angular reflection spectrum [2]. Then, we demonstrate the TE Brewster angle, which cannot be observed in non-magnetic media without 2D layer. Finally, we verify the analytical results by the full-wave numerical simulation and provide the real designs of plasmonic metasurfaces based on gold nanodisks adjusting the Brewster angle in TM and TE polarizations.

The results obtained open new opportunities for the planar polarization optics and related devices including polarization transformers, optical isolators, antireflection coatings and biodetectors.

[1] X. Lin, Y. Shen, I. Kaminer, H. Chen, and M. Soljačić, Phys. Rev. A, 94(2), 023836 (2016).
<https://doi.org/10.1103/PhysRevA.94.023836>.

[2] O. Yermakov, Phys. Rev. A, 109, L031502 (2024).
<https://doi.org/10.1103/PhysRevA.109.L031502>.

Features of oxazine laser dyes in solvents of different polarity and proton donor activity

V. V. Maslov¹, I. M. Pritula²

¹*O.Ya. Usikov Institute for Radiophysics and Electronics of NAS of Ukraine,
12, Ac. Proskury St., Kharkiv, 61085, Ukraine*

²*Institute for Single Crystals of NAS of Ukraine
60, Nauky Ave., Kharkiv, 61072, Ukraine
e-mail: maslov@ire.kharkov.ua*

The spectral, fluorescent, and laser characteristics of two oxazine dyes Cresyl Violet 670 (CV670) and Oxazine720 (Ox720) in solvents of different polarity and proton donor activity were investigated and analyzed in order to expand the possibilities of creating active photonic elements for the red spectral region, including sensors for biomedical research, based on them.

The absorption spectra of these dyes in methanol (Met), acetonitrile (AcN) and dimethyl sulfoxide (DMSO) were recorded with a Lambda 35 spectrophotometer (Perkin-Elmer), and the fluorescence ones – on a Cary Eclipse fluorescence spectrometer (Varian). The fluorescence decay curves of the dye solutions were recorded and the lifetimes τ_f were measured with a FluoTime 200 lifetime fluorometer (PicoQuant). The laser characteristics of the dyes were studied on the setup [1] when their solutions were excited by radiation of rhodamine 6G laser with a wavelength of 588 nm and output energy of up to 100 mJ. The fluorescence quantum yields of the dyes Q in AcN and DMSO were calculated from their recorded fluorescence spectra and the known value of this quantity in methanol. From the measured values of fluorescence decay times τ_f and the obtained values of its quantum yield Q , the constants of radiative $k^r = Q/\tau_f$ and non-radiative $k^{nr} = (1-Q)/\tau_f$ transitions were calculated.

The peculiarity of the behavior of the oxazine dyes in polar and aprotic AcN and DMSO in comparison with the earlier studied laser dyes DCM and LD1 [1,2] was manifested in the fact that oxazine dyes turned out to be sensitive to the proton-acceptor properties of these solvents [3]. As a result of producing deprotonated forms of CV670 and Ox720 in AcN and DMSO in the ground state, a short-wavelength band appears in the absorption spectra of these dyes, which is shifted from the main one by approximately 115 nm. At the same time, for solutions in DMSO, for which the parameter β_1 [3], that characterizes its proton-accepting ability, is approximately twice as large as for AcN, the fluorescence decay curve of solutions becomes non-exponential and consists of two exponents, one of which, the short-term one, describes the fluorescence quenching created by the deprotonated forms of oxazine molecules. In this case, the quantum yield Q decreases, and the constant of non-radiative transitions k^{nr} increases.

Note that with increasing concentration of the dyes to values $C_d \geq 200$ mcM used in laser solutions, as well as with the addition of a small amount of acid $C_a \sim 50$ mcM, the effect of producing the deprotonated form of the oxazine dye decreases or disappears. This is manifested in the absence of a short-wavelength absorption band, an increase in the fluorescence quantum yield and the constant of radiative transitions, and a decrease in the non-radiative ones. In this case, the fluorescence decay curve becomes exponential

- [1] V. V. Maslov, O. M. Bezkravna and I. M. Pritula, Funct. Mater. 29, 488 (2022). <https://doi.org/10.15407/fm29.04.488>.
- [2] V. V. Maslov, Funct. Mater. 19, 226 (2012). <http://functmaterials.org.ua/contents/19-2/fm192-15.pdf>.
- [3] C. Laurence, S. Mansour, D. Vuluga, et al., J. Org. Chem. 86, 4143 (2021). <https://pubs.acs.org/doi/abs/10.1021/acs.joc.0c02964>.

Aggregation features of cyanine dyes in a liquid crystalline environment

I. Yu. Ropakova^{1,2}, O. M. Samoilov¹, O. V. Sorokin¹, L. N. Lisetski¹, S. L. Yefimova¹

¹Institute for Scintillation Materials of NAS of Ukraine, 60 Nauky Ave., Kharkiv 61072, Ukraine

²Dipartimento di Scienza dei Materiali, Università degli Studi Milano-Bicocca,

via R. Cozzi 55, 20125, Milano, Italy

e-mail: adelma@ukr.net

In recent years, the use of liquid crystals as host matrices for incorporating various inorganic and organic nanoparticles has been increasing, playing a crucial role in both fundamental research and the development of novel composite nanomaterials. These materials hold promising applications in optoelectronics, particularly in display technologies, lasers, sensors, and optical data storage systems. However, when it comes to luminescent dopants, they often face the challenge of fluorescence quenching due to molecular aggregation or interactions with the liquid crystal (LC) matrix. Cyanine dye J-aggregates, which exhibit high optical anisotropy and reduced non-radiative quenching, are promising candidates for the creation of such materials.

In our previous work, we successfully demonstrated the formation of J-aggregates of the cyanine dye TDBC in a nematic LC matrix (5CB) [1]. One of the key findings was the significant enhancement of the photo- and physical stability of J-aggregates compared to aqueous solutions, confirming the relevance and potential of such systems. This study serves as a logical continuation of the previous work: we investigated the formation of molecular aggregates of organic dyes in a different type of LC matrix—cholesteric (M5).

We conducted a comparative analysis of two methods for introducing dyes into the LC matrix: direct addition of dry dye powder and prior dissolution in chloroform, water, or DMF, followed by solvent evaporation. The second method was found to lead to residual impurities in the system, which can significantly affect the material properties. In contrast, the first method ensures high reproducibility of aggregate formation and stability of luminescent characteristics.

We examined the aggregation behavior of several cyanine dyes, including PIC, its amphiphilic derivative amphi-PIC, a modification with hydrocarbon tails of length C9, and TDBC. Our results showed that all dyes, except for TDBC, either did not form aggregates in the M5 LC matrix at all or did so randomly and irreproducibly. However, for TDBC, we observed consistently reproducible results, making this dye particularly promising. As a result, only TDBC was selected for further experiments on the study of optical and electro-optical properties.

The influence of dye concentration on the formation of H- and J-aggregates in the LC matrix was studied. We demonstrated the possibility of a transition between different types of aggregates depending on the concentration, providing a means to control their optical properties.

Evaluation of the electro-optical characteristics revealed that the presence of J-aggregates in the LC matrix makes the Freedericksz transition more abrupt, which could be useful for the development of tunable optical elements. Photostability studies demonstrated a significant improvement in the stability of J-aggregates in LC matrices compared to aqueous solutions, attributed to the reduced exposure of dye molecules to oxygen and other oxidizing agents. As expected, photostability in the M5 LC matrix was higher than in water and was also found to be higher than in the 5CB matrix. Furthermore, an increase in fluorescence lifetime and enhanced quantum yield were observed, indicating reduced non-radiative losses in these systems.

The results highlight the potential of cyanine J-aggregates in liquid crystalline materials for the development of stable, highly anisotropic luminescent media with tunable optical and electro-optical properties.

[1] I. I. Grankina, O. M. Samoilov et. al. Optical Materials Express, Vol. 13, 6, pp. 1741-1751 (2023) <https://doi.org/10.1364/OME.491678>.

Optical and electrical characteristics of FeS₂ thin films obtained in gas discharge

E. Svitlichnyi¹, A. Molnar²

¹*Institute of Electron Physics of NAS of Ukraine*

Universitetska str., 21, Uzhgorod, 88017, Ukraine

²*Uzhgorod National University, Voloshin str. 56, 88000 Uzhgorod, Ukraine*

e-mail: bercheni14@gmail.com

Iron disulfide FeS₂ (pyrite) is a non-toxic material, and due to its wide distribution on Earth, it has the prospect of becoming a low-cost alternative for creating high-efficiency solar cells. This is facilitated both by its environmental friendliness and optical properties close to optimal for efficient conversion of radiation energy: the bandgap energy is 0.95 eV, and the optical absorption coefficient is more significant than 10⁵ cm⁻¹ at energy $h\nu > 1.4$ eV [1]. Iron and sulfur can form sulfides with different stoichiometric compositions and structures during film fabrication, which affects the material properties. Considering the complex zone structure [2,3], FeS₂ thin films with a wide range of intrinsic absorption (from 1 to 3.8 eV) are obtained [4]. Depending on their optical properties, they can be used in solar cells as a photoactive absorbing layer or as a frontal translucent layer in heterostructures.

This paper presents the results of the study of electrical and optical properties of FeS₂ thin films obtained by sputtering in gas discharge plasma at temperatures from 250 to 350 °C. To study electrical and optical properties, film samples were used on quartz glass substrates of 11 × 11 mm.

Transmission spectra of thin films were recorded using a spectrometer based on an MS 7504i spectral monochromator. A hydrogen source was used as an emission source.

Silver paste electrodes were applied to the sputtered FeS₂ films to investigate the temperature dependence of conductivity. The sample resistance was recorded using a GoodWill LCR-819 impedance meter at 1 kHz. The temperature control process was carried out by an automated computer-aided temperature regulation system [5] in the range of 290-400 K. Based on the obtained data; we can conclude that there are two mechanisms of electrical conductivity in the investigated interval; the first one from 290 to 380, and the second one above 380 K.

- [1] B. Rezig, H. Dahman, M. Kenzari. Renewable Energy 2, 125 (1992).
DOI: [https://doi.org/10.1016/0960-1481\(92\)90098-N](https://doi.org/10.1016/0960-1481(92)90098-N).
- [2] J. Hu, Y. Zhang, M. Law, R. Wu. J. Am. Chem. Soc. 134, 32, 13216 (2012).
DOI: <https://doi.org/10.1021/ja3053464>.
- [3] P. Xiao, X.-L. Fan, L. M. Liu, W.-M. Lau. Phys. Chem. Chem.Phys. 16, 24 466 (2014).
- [4] A.K. Abass, Z.A. Ahmed, R.E. Tahir. Phys. Status Solisi A 97,243 (1986).
- [5] A.A. Molnar. Scientific Herald of Uzhhorod University. Series "Physics", 2, 101(1998).

Obtaining of FeS₂ thin films on glass substrates in gas discharge plasma

E. Svitlichnyi¹, A. Minya², M. Pop², R. Gritsak², M. Feldii²

¹*Institute of Electron Physics of NAS of Ukraine*

Universitetska str., 21, Uzhgorod, 88017, Ukraine

²*Uzhgorod National University, Voloshin str. 56, 88000 Uzhgorod, Ukraine*

e-mail: bercheni14@gmail.com

Among the wide variety of methods for applying films of various materials onto dielectric and metallic surfaces [1], there is currently no universal method that can be singled out; each method has its own specific advantages and disadvantages.

The main methods for obtaining homogeneous thin films include thermal deposition of the material, magnetron sputtering, and chemical and electrochemical deposition methods. However, after the films are applied, chemical and thermal treatments are often necessary to improve their adhesion to the substrate, which can lead to uncontrolled changes in their physical properties. Thus, the search for alternative, simpler, and less resource-intensive methods of film deposition remains relevant. The aim of this work was to develop a methodology for depositing thin FeS₂ films on dielectric substrates (quartz glass).

In our experiments we used a universal gas discharge chamber which consist of quartz tube 15 cm long, vacuum gasket, dielectric flanges, universal high-voltage inputs, Fe electrodes with adjustable interelectrode distance, heating element(optional) and pins for fixation. For sputtering we will use chalcogens located in the interelectrode space. Due the experiments, the voltage on the high-voltage rectifier was up to 5 kV, the average discharge current was up to 1 A, and the frequency of the pumping pulses was up to 10 kHz. Helium was used as a buffer gas, the pressure of which was 30 Torr. Crystalline sulfur was in the gas discharge chamber. The temperature of the mixture during the operation of the installation did not exceed 350 °C.

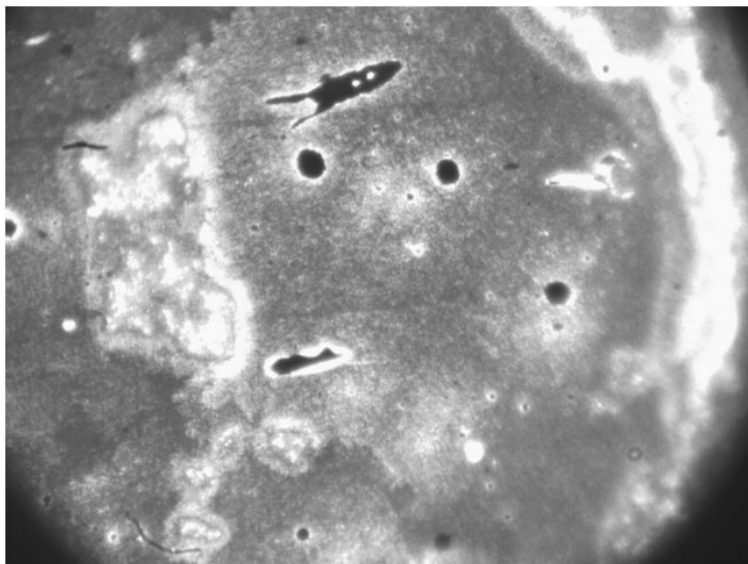


Fig. 1. Image of a quartz glass substrate with a FeS₂ film at 10x increase

A device and a method for applying FeS₂ films to the surface of dielectric glass substrates has been proposed and developed. The resulting thin FeS₂ films on dielectric substrates (quartz glass) without noticeable destruction of their surface are shown in Fig. 1.

[1] Martinu L., Poitras D. Plasma deposition of optical films and coatings. J. Vac. Sci. Technol. A. - 2000. - Vol. 18, No 6. - P. 2619-2645. DOI: <https://doi.org/10.1116/1.1314395>.

The influence of electron irradiation on the emission spectra of glucose and fructose in a gas discharge plasma.

Yu. Bandurin, E. Svitlichnyi

*Institute of Electron Physics of NAS of Ukraine
Universitetska str., 21, Uzhhorod, 88017, Ukraine
e-mail: bercheni14@gmail.com*

Monosaccharides are the basic building blocks of carbohydrates and play a key role in biological processes. They are the simplest carbohydrates, consisting of carbon, hydrogen and oxygen with the general formula $C_x(H_2O)_y$. They are divided into aldoses and ketoses, which differ in chemical structure. Common natural carbohydrates are found in many fruits, berries, milky plant juice, and whey.

The study of monosaccharides in a gas discharge can be used to solve several tasks:

1. Composition Analysis: Investigating monosaccharides in a gas discharge allows for the accurate determination of their composition and concentration in various samples, such as food products, biological fluids, and more.

2. Reaction Studies: Gas discharge can be used to study the processes of interaction between monosaccharide molecules and electrons or ions.

3. Mechanism Investigation: Gas discharge can be utilized to examine the mechanisms of fragmentation or transformation of monosaccharide molecules under the influence of high temperatures or other factors, which is important for understanding their behavior under different conditions. So, the study of monosaccharides in gas discharge opens up new possibilities for the analysis and understanding of their properties and behavior in different contexts.

In Fig. 1, the emission spectrum of glucose and fructose is presented in the wavelength range of 200-800 nm. During the experiment, the voltage on the high-voltage rectifier was 1 kV, with a discharge current of 0.08 A and a pulse frequency of 4 kHz. Helium was used as the buffer gas, with a pressure of 30 Torr. The temperature of the mixture during the measurements was 114 °C.

From the presented spectrum, we can see that in the wavelength range of 415-441.8 nm, there is an emission of an intense band from the CH molecule (system transitions $A^2\Delta-X^2\Pi$).

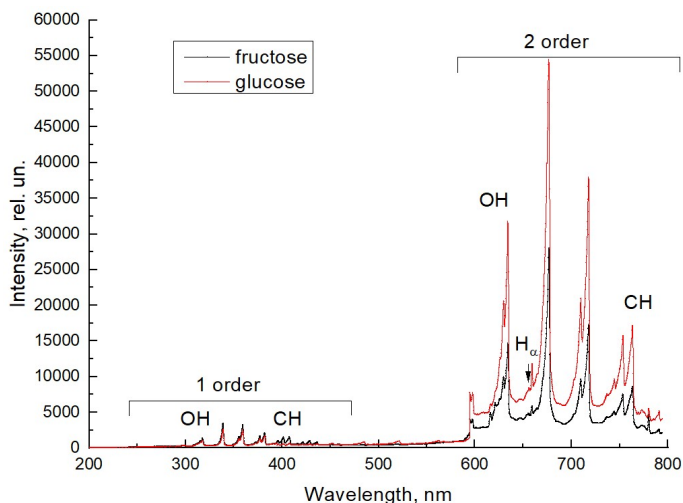


Fig. 1, the emission spectrum of glucose and fructose

The main contribution to emission in a rather wide band at $\lambda = 307$ nm is related to the excited OH radical. In addition, a detailed investigation of the emission spectrum of OH radical [1] makes it possible to also identify transitions in this system with vibrational levels 1–0. Maybe we have detected a weak radiation of the spectral lines H_α ($\lambda = 656,3$ nm). The spectral line H_β of the hydrogen atom ($\lambda = 486,13$ nm) is absent in the spectra. This indicates a small number of excited hydrogen atoms in the fragmentation channels of monosaccharide molecules.

[1] C. G. Pariger, C. M. Helstern, B. S. Jordan, D. M. Surmick and R. Splinter, *Molecules* **25**, 988 (2020). DOI: <https://doi.org/10.3390/molecules25040988>.

Study of gas-discharge plasma properties in mixtures of inert gases with selenium vapor

A. General, E. Svitlichnyi

*Institute of Electron Physics of NAS of Ukraine
Universitetska str., 21, Uzhhorod, 88017, Ukraine
e-mail: bercheni14@gmail.com*

The chalcogens are the chemical elements in group 16 of the periodic table [1]. This group is also known as the oxygen family. Group 16 consists of the elements oxygen (O), sulfur (S), selenium (Se), tellurium (Te), and the radioactive elements polonium (Po) and livermorium (Lv). [2] Often, oxygen is treated separately from the other chalcogens, sometimes even excluded from the scope of the term "chalcogen" altogether, due to its very different chemical behavior from sulfur, selenium, tellurium, and polonium.

The relevance of studying selenium in a gas discharge is determined by its industrial applications in various fields, including electronics, photodetectors, and solar cells. Understanding its behavior in gas discharges can contribute to the improvement of technologies. Additionally, selenium is an important trace element, but in high concentrations, it can be toxic. Researching its interactions in plasma may aid in the development of purification and disposal methods. Gas discharges and plasma technologies are significant areas of focus in physics and chemistry. Studying the behavior of selenium under these conditions may lead to new discoveries in the field of plasma chemistry and physics.

Therefore, in the presented work, gas discharge structures were developed and manufactured for the first time, which create low-temperature plasma through the excitation of barrier discharge at atmospheric pressure using working mixtures of helium-selenium and argon-selenium.

The results of the first measurements of the spectral characteristics of the emission of a mixture of selenium vapor with argon and helium in a gaseous pulse-periodic discharge in the ultraviolet and visible spectral regions were obtained.

In the experiments, the voltage on the high-voltage rectifier was up to 5 kV, the average discharge current was up to 0.8 A, and the frequency of the pumping pulses was up to 5 kHz. Argon and helium were used as a buffer gas, the pressure of which was 30 Torr. The temperature of the mixture during the operation of the installation did not exceed 450 °C.

The time-integrated emission characteristics of the discharge were recorded using the MS 7504i spectrometer. The MS 7504i also included two optical radiation detectors: a HS 101H CCD camera and an R928 photomultiplier. Recording information from these detectors and its analysis was carried out using a personal computer.

Based on the results of the work performed, it has been established that the main mechanism for the formation of excited selenium molecules is the energy transfer from metastable atoms of an inert gas to selenium molecules and atoms. The obtained experimental data allowed for the creation of a low-temperature plasma source based on selenium vapor, which may find practical applications in physical electronics, medicine, and lighting technology.

- [1] House, James E.; House, James Evan (2008). Inorganic chemistry. Amsterdam Heidelberg: Elsevier Academic Press. p. 523. ISBN 978-0-12-356786-4.
- [2] Emsley, John (2011). Nature's Building Blocks: An A-Z Guide to the Elements (New ed.). New York, NY: Oxford University Press. pp. 375–383, 412–415, 475–481, 511–520, 529–533, 582. ISBN 978-0-19-960563-7.

Increasing the sensitivity of a surface plasmon resonance biosensor based on the Kretschmann configuration using $\text{Ti}_3\text{C}_2\text{T}_x$ -MXene nanomaterial.

R. S. Terekhov¹, Z. E. Eremenko^{1,2}, S. M. Kulish³

¹*O. Ya. Usikov Institute for Radio Physics and Electronics of the NAS of Ukraine,
12 Academician Proskura St., Kharkiv, 61085, Ukraine*

²*Leibniz Institute for Solid State and Materials Research,
Helmholtzstraße 20, 01069 Dresden, Germany*

³*National Aerospace University "Kharkiv Aviation Institute", NAU "KhAI",
17 Vadym Manka St., Kharkiv, 61000, Ukraine
e-mail: r.s.terekhov@gmail.com*

Modern biosensor technologies play a key role in the high-precision analysis of biomolecular interactions, providing fast and highly sensitive measurements. One of the most promising areas is the use of optical phenomena to detect changes at the molecular level. The surface plasmon resonance (SPR) method allows recording variations in the refractive index near a metal nanostructured surface, thus enabling the detection of various pathogens in the environment, the concentration of an active substance, etc. However, traditional SPR biosensors (e.g., Kretschmann, Otto configuration) have limited sensitivity and do not eliminate nonspecific protein binding [2]. The $\text{Ti}_3\text{C}_2\text{T}_x$ nanomaterial (MXene) improves the Kretschmann configuration due to its porous structure and the possibility of surface modification. The high electrical conductivity [3] of MXene does not interfere with the excitation of plasmon polaritons, and its porous structure and the possibility of modification [4] allow us to effectively solve the problem of nonspecific adsorption to the biosensor surface.

In this work, a two-layer biosensor structure consisting of a silver layer and a $\text{Ti}_3\text{C}_2\text{T}_x$ -MXene layer was proposed. A BK-7 glass prism is used to fix the angle of incidence of light. Measurements are performed at a wavelength of the probing laser of 633 nm. The finite element method is used to model the structure of the biosensor.

The results of our research include: the optimal geometry of the structure materials, which achieves minimum reflection at the resonance point and maximum Q-factor: 55 nm - silver layer, 2.98 nm - MXene layer; increased sensitivity of the biosensor by 10% compared to the SPR biosensor based on the Kretschmann configuration; established a relative measurement error of approximately 3% when studying samples of real biological tissues of the human body.

- [1] A. Keshavarz, S. Zangenehzadeh, and A. Hatef, "Optimization of surface plasmon resonance-based biosensors for monitoring hemoglobin levels in human blood," *Appl Nanosci*, vol. 10, no. 5, pp. 1465–1474, May 2020, doi: 10.1007/s13204-020-01252-x.
- [2] C. Liu, F. Hu, W. Yang, J. Xu, and Y. Chen, "A critical review of advances in surface plasmon resonance imaging sensitivity," *TrAC Trends in Analytical Chemistry*, vol. 97, pp. 354–362, Dec. 2017, doi: 10.1016/j.trac.2017.10.001.
- [3] C. Qiao, H. Wu, X. Xu, Z. Guan, and W. Ou-Yang, "Electrical Conductivity Enhancement and Electronic Applications of 2D $\text{Ti}_3\text{C}_2\text{T}_x$ MXene Materials," *Adv Materials Inter*, vol. 8, no. 24, p. 2100903, Dec. 2021, doi: 10.1002/admi.202100903.
- [4] Y. Pei et al., "Ti₃C₂T_x MXene for Sensing Applications: Recent Progress, Design Principles, and Future Perspectives," *ACS Nano*, vol. 15, no. 3, pp. 3996–4017, Mar. 2021, doi: 10.1021/acsnano.1c00248.

Dielectric metasurfaces for light control: polarizer, collector, demultiplexer and anti-reflector

A. Ovcharenko¹, S. Polevoy², K. Nemchenko¹, V. Tuz¹, O. Yermakov^{1,3}

¹*V. N. Karazin Kharkiv National University, 4 Svobody Square, Kharkiv 61022, Ukraine.*

²*O. Ya. Usikov Institute for Radiophysics and Electronics of the NASU,
12, Proskura st., Kharkiv 61085, Ukraine.*

³*Leibniz Institute of Photonic Technology, 9 Albert-Einstein-Straße, Jena 07745, Germany.
e-mail: oe.yermakov@gmail.com*

Two-dimensional (2D) materials present exceptional opportunities in light emission, energy harvesting, light-matter interactions and optical biosensing. The specific interest is raised by the artificially engineered 2D micro- and nanostructures, which enable on-demand optical properties, opening avenues for diverse applications such as lensing, holography, imaging, polarimetry, and biosensing. The rapid advancement of 2D nanostructures introduces new challenges in their precise design and novel functional implementations. In this work, we focus on dielectric metasurfaces representing periodic arrays of subwavelength scatterers as a key platform for addressing these challenges.

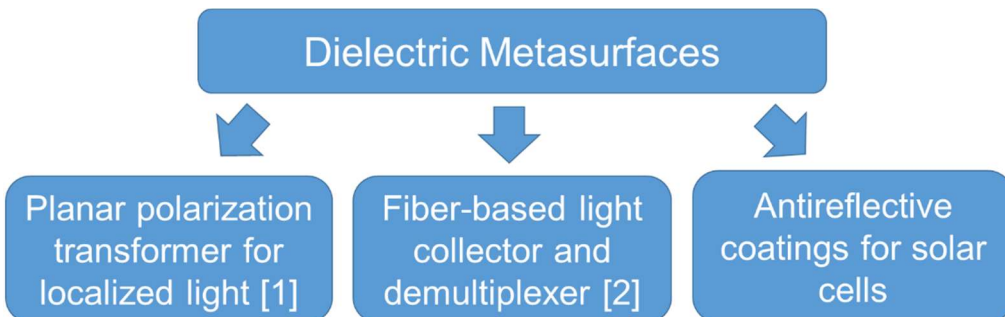


Figure 1. The applications of dielectric metasurfaces discussed in this work.

Namely, we consider three cases:

- 1) Ceramic metasurfaces in the microwave range operating as the ultrathin platform for the polarization control of localized light [1]. As an illustrative example, we demonstrate the planar linear-to-circular polarizer of guided waves.
- 2) Polymer metasurfaces in the near-infrared range created at the fiber tip for the efficient light collection and angular demultiplexing [2]. As an illustrative example, we demonstrate the coupling of light into the nanostructured multicore single-mode fiber.
- 3) Silicon metasurfaces in the visible and near-infrared ranges act as the broadband antireflective coatings for silicon solar cells. As an illustrative example, we demonstrate the suppression of light reflection with a metasurface based on the inverse design optimization.

O.Y. acknowledges the support of the Alexander von Humboldt Foundation within the framework of the Humboldt Research Fellowship for postdoctoral researchers and the American Physical Society's IRTAP-Ukraine program supporting physicists impacted by the Russian invasion of Ukraine.

[1] R. Li, S. Polevoy, V. Tuz, and O. Yermakov, *Physical Review Applied*, 23(1), 014084 (2025).
<https://doi.org/10.1103/PhysRevApplied.23.014084>.

[2] O. Yermakov et al., *Nature Communications*, 16(1), 2294 (2025).
<https://doi.org/10.1038/s41467-025-57440-2>.

Optical properties of “left-handed” media based on a cubic lattice of metallic nanodimers

L. O. Abramenko¹, A. V. Korotun^{1,2}, V. M. Matiushyn¹

¹*National University Zaporizhzhia Politechnic, 64 University Str., Zaporizhzhia, 69063, Ukraine*

²*G.V. Kurdyumov Institute for Metal Physics of the NAS of Ukraine,*

36 Academician Vernadsky Blvd., Kyiv, 03142, Ukraine

e-mail: andko@zp.edu.ua

As is well known, a “left-handed” medium is a material in which the real parts of both the dielectric permittivity and the magnetic permeability are simultaneously negative. It has been established that one type of “left-handed” medium is a composite based on a cubic lattice of metallic nanodimers. Provided that the wavelength of light is much larger than the size of the unit cell of the nanocomposite, the collective response of “left-handed” medium can be approximated by the response of a certain homogeneous “effective” medium. In this case, the nanocomposite under consideration can be characterized by effective dielectric permittivity and magnetic permeability, the expressions for which take the following form

$$\epsilon_{\text{eff}} = \epsilon_m \left(1 + 3\beta \frac{\frac{R^3}{\alpha(\omega)} - \frac{1}{\epsilon_m} \left(\frac{R}{d} \right)^3}{\left(\frac{R^3}{\alpha(\omega)} + \frac{1}{\epsilon_m} \left(\frac{R}{d} \right)^3 \right) \left(\frac{R^3}{\alpha(\omega)} - \frac{2}{\epsilon_m} \left(\frac{R}{d} \right)^3 \right) - \beta \frac{R^3}{\alpha(\omega)} - \frac{1}{\epsilon_m} \left(\frac{R}{d} \right)^3} \right); \quad (1)$$

$$\mu_{\text{eff}} = 1 + \beta \left(\frac{k_0 d}{2} \right)^2 \frac{1}{\frac{R^3}{\alpha(\omega)} - \frac{1}{\epsilon_m} \left(\frac{R}{d} \right)^3 - \frac{\beta}{3} \left(\frac{k_0 d}{2} \right)^2}, \quad (2)$$

where $\alpha(\omega)$ – polarizability of a nanoparticle in a dimer; ϵ_m – dielectric permittivity of the matrix; $k_0 = \omega/c$ – wavenumber in a vacuum, ω and c – frequency and speed of a light wave; R – radius of a nanoparticle in a dimer; d – distance between particles in a dimer; $\beta = 8\pi(R/l)^3$, l – edge length of the unit cell.

Since the polarizability of a spherical metallic nanoparticle

$$\alpha(\omega) = R^3 \frac{\tau(\omega) - \epsilon_m}{\tau(\omega) + 2\epsilon_m}, \quad (3)$$

and the dielectric function in Drude model

$$\tau(\omega) = \tau^\infty - \frac{\omega_p^2}{\omega(\omega + i\gamma_{\text{eff}})}, \quad (4)$$

where γ_{eff} – effective electron relaxation rate in the nanoparticle, material characteristics τ^∞ and ω_p – contribution of the crystal lattice to the dielectric permittivity and plasma frequency, so the width of the spectral interval, in which the considered nanocomposite is a “left-handed” medium, is determined by the relationships $\text{Re}\tau_{\text{eff}}(\mu_{\text{eff}}) < 0$, and depends on the size and material of the particle, the geometric parameters of the dimer and the unit cell.

Calculations have shown that the width of the desired spectral interval practically does not depend on the distance between particles in the dimer and the edge length of the unit cell, but is determined by the size and material of the nanoparticles.

Two-photon interaction in a superconducting circuit with SQUID-mediated coupling

E. V. Stolyarov¹, V. L. Andriichuk², and A. M. Sokolov²

¹*Institute of Physics of the National Academy of Sciences, pr. Nauky 46, Kyiv 03028, Ukraine*

²*Bogolyubov Institute for Theoretical Physics, National Academy of Sciences of Ukraine,
vul. Metrolohichna 14-b, Kyiv 03143, Ukraine
e-mail: valentyn.andriichuk@gmail.com*

In this work, we study interactions between a resonator and an rf SQUID (Superconducting QUantum Interference Device) coupled via a Josephson element. The latter is a symmetrical dc SQUID, which induces two-photon and other inductive interactions. By changing the SQUID magnetic bias, one can control two- and single-photon interaction rates [1]. In addition to the two-photon interaction mediated by the SQUID coupler, we consider cross-Kerr, linear, and optomechanical interactions. The rf SQUID in the circuit acts as an artificial atom—a phase qubit [2].

We focus on the regime of resonant two-photon interaction. We calculate the rates of relevant interactions, including renormalizations near the two-photon resonance. Our theory provides interpretations for these renormalizations and establishes conditions under which particular interactions can be neglected. Finally, we discuss the range of its validity.

E.V.S. acknowledges support from the National Research Foundation of Ukraine through the Project No. 2023.03/0165, Quantum correlations of electromagnetic radiation.

[1] E. V. Stolyarov, V. L. Andriichuk, A. M. Sokolov, arXiv:2412.05016 (2024)

[2] J. M. Martinis, Quant. Inf. Proc. 8, 81 (2009). DOI: <https://doi.org/10.1007/s11128-009-0105-1>.

The effect of spatial dispersion on optical phenomena in spherical metallic nanoparticles

R. Yu. Korolkov¹, O. Yu. Berezhnyi¹, A. V. Korotun^{1,2}

¹National University Zaporizhzhia Politechnic, 64 University Str., Zaporizhzhia, 69063, Ukraine

²G.V. Kurdyumov Institute for Metal Physics of the NAS of Ukraine,
36 Academician Vernadsky Blvd., Kyiv, 03142, Ukraine
e-mail: romankor@zp.edu.ua

In the last two decades, the hybrid nanostructures of the type “metallic nanoparticle – semiconductor quantum dot” have attracted the attention of many researchers due to the manifestation of unique optical effects in such structures, for example, exciton-plasmon Coulomb interaction. The study of the optical properties of such nanostructures relies on the consideration of the spatial dispersion (nonlocality) of the dielectric function of the metallic nanoparticle.

The relation for the nonlocal dielectric function has the form [1]

$$\tau_{NL}(\omega) = \left[\frac{1}{\tau_D(\omega)} + 3 \left(\frac{\omega_p R}{\beta u} \right)^2 I_{3/2}(u) K_{3/2}(u) \right]^{-1}, \quad (1)$$

where $u = R \sqrt{\omega_p^2 - \omega(\omega + i\gamma_{eff})}/\beta$; $\beta = \sqrt{3/5}v_F$, v_F is Fermi electron velocity, R is the radius of nanoparticle; ω_p is plasma frequency; Drude (local) dielectric function

$$\tau_D(\omega) = \tau^\infty - \frac{\omega_p^2}{\omega(\omega + i\gamma_{eff})}, \quad (2)$$

τ^∞ is the contribution of the crystal lattice into the dielectric function; γ_{eff} is effective relaxation rate, in which bulk and surface relaxation and the radiation damping make an additive contribution.

The calculations for the frequency dependencies of the real and imaginary parts of nonlocal dielectric function have been performed for silver nanoparticle with the radius $R = 10$ nm. The results of the calculations indicate that $\text{Re}\tau_{NL}(\omega)$ is alternating function, while $\text{Im}\tau_{NL}(\omega) > 0$ in the frequency range, which is under the consideration. In this respect the behavior of the function $\text{Re}(\text{Im})\tau_{NL}(\omega)$ is similar to the behavior of the function $\text{Re}(\text{Im})\tau_D(\omega)$. At the same time, in the optical frequency range (under $\hbar\omega \geq 1.56$ eV) $\text{Re}(\text{Im})\tau_{NL}(\omega) \approx \text{Re}(\text{Im})\tau_D(\omega)$. However, $\text{Re}\tau_{NL}(\omega)$ and $\text{Re}\tau_D(\omega)$ are significantly different in the infrared frequency range, and the differences between $\text{Im}\tau_{NL}(\omega)$ and $\text{Im}\tau_D(\omega)$ are essential only in the interval 0.7 eV $< \hbar\omega < 1.5$ eV. In addition, in the infrared spectral interval on the curves $\text{Re}(\text{Im})\tau_{NL}(\omega)$ and $\text{Re}(\text{Im})\tau_D(\omega)$ there are small amplitude oscillations due to the manifestation of kinetic effects.

[1] V. V. Datsyuk, Ukr. J. Phys. 56, 122 (2011).

Improvement of quantum efficiency of photodetectors by introducing plasmonic nanoparticles

D. V. Demianenko¹, V. I. Reva¹, A. V. Korotun^{1,2}, E.V. Stegantsev³

¹National University Zaporizhzhia Politechnic, 64 University Str., Zaporizhzhia, 69063, Ukraine

²G.V. Kurdyumov Institute for Metal Physics of the NAS of Ukraine,
 36 Academician Vernadsky Blvd., Kyiv, 03142, Ukraine

³Zaporizhzhia National University, 66 University Str., Zaporizhzhia, 69063, Ukraine
 e-mail: andko@zp.edu.ua

In recent years plasmonic nanoparticles have found wide application to improve the efficiency of photodetectors by increasing light extraction by amplifying local electric fields or directly converting absorbed photons into electrical energy by transferring hot charge carriers from plasmonic metals to semiconductor receptors. Hence, the problem connected with the influence of plasmonic effects in metallic nanoparticles on the physical and technical characteristics of photodetectors is actual.

The most important characteristic of photodetectors, in which the thickness of the semiconductor layer is significantly greater than the radius of the nanoparticle, is their quantum efficiency, defined by the relation

$$\eta = \frac{A}{8\epsilon_F} \frac{(\hbar\omega - e\varphi_B)^2}{\hbar\omega}, \quad (1)$$

where ϵ_F is Fermi energy; φ_B is the height of Schottky barrier at the interface “metal – semiconductor”; ω is the frequency of light, and the absorption coefficient at $\gamma_{\text{eff}} \ll \omega \ll \omega_p$ (in the working area of photodetectors – near infrared and visible regions) is determined by the formula

$$A = \frac{2\gamma_{\text{eff}}}{\omega_p}. \quad (2)$$

In formula (2) ω_p is plasma frequency, and the effective relaxation rate of electrons in spherical nanoparticle γ_{eff} is determined by the additive contribution of bulk relaxation, surface relaxation and radiation damping [1]

$$\gamma_{\text{eff}} = \gamma_{\text{bulk}} + \frac{\mathcal{K}}{\omega^2}, \quad (3)$$

where $\gamma_{\text{bulk}} = \text{const}$ for specific metal;

$$\mathcal{K} = \frac{1}{4} \omega_p^2 \frac{V}{R} \left[1 + \frac{V}{6\pi\sqrt{\epsilon_m(\epsilon^\infty + 2\epsilon_m)}} \left(\frac{\omega_p}{c} \right)^3 \right], \quad (4)$$

c is light velocity; ϵ_F is Fermi electron velocity; R and V are the radius and volume of nanoparticle; ϵ_m is dielectric permittivity of semiconductor medium; ϵ^∞ is the contribution of the crystal lattice into the dielectric function of metal.

The calculations have been performed for nanoparticles of different plasmonic metals in silicon matrix. It has been shown that the frequency dependence of the quantum efficiency has two extrema: the minimum in the near infrared region and the maximum in the visible region of the spectrum.

[1] A. V. Korotun, H. V. Moroz, R. Yu. Korolkov, Funct. Mater. 31, 119 (2024).
 DOI: <http://dx.doi.org/10.15407/fm31.01.119>.

Masking of nanoparticles with the help of multilayer cylindrical coatings

R. Yu. Korolkov¹, A. V. Korotun^{1,2}, V. M. Matiushyn¹, R. V. Fliahin¹

¹National University Zaporizhzhia Politechnic, 64 University Str., Zaporizhzhia, 69063, Ukraine

²G.V. Kurdyumov Institute for Metal Physics of the NAS of Ukraine,

36 Academician Vernadsky Blvd., Kyiv, 03142, Ukraine

e-mail: romankor@zp.edu.ua

The study of the possibility of creating invisible coatings of different geometries has been significantly developed after the publication of pioneering works [1, 2], in which it was proposed to use spatial transformation to realize the invisibility of material objects (the concept of “wave flotation”). One approach to achieving near-perfect invisibility is based on transformational optics and requires the use of materials with inhomogeneous and anisotropic dielectric and magnetic permittivities. This is impossible without the use of metamaterials, which, as a rule, have narrow bandwidths, high losses and other practical difficulties when used in the optical frequency range, and are therefore used in the microwave range. In this regard, an alternative approach, which consists in the reduction of scattering by plasmonic or dielectric layered structures, is actual.

It is known that the nanostructure does not contribute to the scattered field and does not absorb the energy of light wave if its absorption and scattering cross-sections are equal to zero, which is equivalent to the fact that the polarizability of the nanostructure is equal to zero. In turn, the polarizability can be found by solving the electrostatics boundary value problem, which for the three-layer cylindrical nanoparticle consists of Laplace equations for each layer and the space outside the nanostructure

$$\Delta\varphi_i = 0, (i = 1, 2, 3, 4) \quad (1)$$

where φ_i is the electrostatic potential in the i -th region of space, and boundary values

$$\begin{aligned} \varphi_1|_{r=a} &= \varphi_2|_{r=a}, \quad \varphi_2|_{r=b} = \varphi_3|_{r=b}, \quad \varphi_3|_{r=R} = \varphi_4|_{r=R}, \\ T_1 \frac{\partial \varphi_1}{\partial r}|_{r=a} &= T_2 \frac{\partial \varphi_2}{\partial r}|_{r=a}, \quad T_2 \frac{\partial \varphi_2}{\partial r}|_{r=b} = T_3 \frac{\partial \varphi_3}{\partial r}|_{r=b}, \quad T_3 \frac{\partial \varphi_3}{\partial r}|_{r=R} = T_4 \frac{\partial \varphi_4}{\partial r}|_{r=R}, \end{aligned} \quad (2)$$

the internal (masked) shell (region $0 < r \leq a$) has permittivity T_1 , the shielding shell (region $a < r \leq b$) and the shell, which compensates the scattering (region $b < r \leq R$) – permittivities T_2 and T_3 , and the entire nanostructure is placed in medium (region $r > R$) with permittivity T_4 . Here a , b and R are the radii of the first, second and third cylindrical regions, r is the current radial coordinate.

The results of the calculations show that the masking (electric field shielding) in the axis region of the cylindrical nanostructure is possible in two cases. The first case is shielding by the layer with quasi-zero permittivity ($T_2 \rightarrow 0$), which cannot be obtained from transformational optics because it corresponds to the excitation of resonant plasmon in the shielding layer (plasmonic masking). The second case – $|T_2| \rightarrow \infty$, which is predicted by transformational optics and corresponds to the presence of the dielectric permittivity singularity, can be realized with the help of natural materials.

[1] J. B. Pendry, D. Schurig, D. R. Smith, Science. 312, 1780 (2006).

DOI: <http://dx.doi.org/10.1126/science.1125907>.

[2] U. Leonhardt, Science. 312, 1777 (2006). <http://dx.doi.org/10.1126/science.1126493>.

Atomic structure calculations of singly ionized vanadium

S. V. Gedeon, V. Yu. Lazur, V. I. Kazakov

*Department of Theoretical Physics, Uzhhorod National University,
53 Voloshina str., Uzhhorod, 88000, Ukraine
e-mail: sergej.gedeon@uzhnu.edu.ua*

Atomic structure and spectroscopic properties of the neutral and ionized vanadium is of great interest to several fields of applied and fundamental science such as as astrophysics, plasma physics, fusion, and laser development. For example, in the recent work [1] the optical emission spectroscopy method was used to study of vanadium plasma in a cathodic-arc discharge in a nitrogen atmosphere. In the scope of that research, the spectral lines of neutral atoms and ions of the cathode material VI, VII, and VIII were observed in the discharge plasma.

Accurate atomic data for vanadium and its ions are required for the analysis of astrophysical and laboratory plasmas. In turn, theoretical calculations of most spectroscopic properties of complex atoms and ions require knowledge of wave functions.

To calculate the wave functions of the ground and lower excited states of vanadium ion VII we employed multi-configuration Hartree–Fock method (MCHF) [2] together with configuration interaction (CI) approach with non-orthogonal orbitals and *B*-splines as basis functions [3, 4]. This approach allows to take into account the term-dependence of valence orbitals, the effects of correlation and relaxation.

In present research we considered the ground and lower excited states of the VII ion which have electronic configurations $3d^4$, $3d^34s$, $3d^34p$ and $3d^24s^2$ and terms ${}^1S^{1,3,5}PDF^{1,3}GH^1I$ and ${}^{1,3,5}SPDF^{1,3}GH^1I^o$. Deep core orbitals $1s$, $2s$, and $2p$ were generated using the Hartree–Fock (HF) method for the ground state $3d^34s^2 {}^4F$ of neutral vanadium. Such approximation did not affect significantly the calculated excitation energy levels of VII, but will simplify further calculations of photoionization cross sections of vanadium. Sub-valence orbitals $3s$ and $3p$ together with valence $3d$, $4s$ and $4p$ orbitals were generated separately in term-average HF-calculations for each of principal electronic configurations of VII. Correlation orbitals $4l$ and $5l$ ($l = 0–4$) also were obtained in separate MCHF calculations for one of the terms for each of the selected configurations.

As a result, in scope of non-relativistic *LS* approximation, we obtained wave functions of the ground and 60 lower excited states of singly ionized vanadium. Calculated excitation energies are in satisfactory agreement with the averaged by fine structure levels experimental values recommended by NIST [5].

Resulting sets of the wave functions will be used in further atomic structure calculations of VII using the quasi-relativistic Breit–Pauli approximation in order to obtain data on transitions between levels, taking into account fine structure splitting. Also, they can be used in non-relativistic calculations of low-energy electron scattering by vanadium ion and photoionization processes.

- [1] Yu. V. Kovtun, A. S. Kuprin, A. N. Kuprin, S. A. Leonov, R. L. Vasilenko, and Yu. A. Besedin, J. Appl. Phys. 134, 243301 (2023). <https://doi.org/10.1063/5.0177931>.
- [2] C. F. Fischer, G. Tachiev, G. Gaigalas, and M. R. Godefroid, Comput. Phys. Commun. 176, 559 (2007). <https://doi.org/10.1016/j.cpc.2007.01.006>.
- [3] O. Zatsarinny and C. F. Fischer, Comput. Phys. Commun. 124, 247 (2000). [https://doi.org/10.1016/S0010-4655\(99\)00441-5](https://doi.org/10.1016/S0010-4655(99)00441-5).
- [4] O. Zatsarinny and C. F. Fischer, Comput. Phys. Commun. 180, 2041 (2009). <https://doi.org/10.1016/j.cpc.2009.06.007>.
- [5] A. Kramida, Yu. Ralchenko, J. Reader, and NIST ASD Team. NIST Atomic Spectra Database (ver. 5.10) (2022). Available: <https://physics.nist.gov/asd>.

Threshold conditions analysis of microlaser configuration with gold film and DBR

S. S. Herasymov

*Department of Physical Fundamentals of Electronic Engineering,
Kharkiv National University of Radio Electronics,
14 Nauky Ave., Kharkiv, 61166, Ukraine
e-mail: serhii.herasymov@nure.ua*

This work dedicated to the analysis of the threshold conditions for a layered microlaser model made of a gain-material cavity, sandwiched between gold film, and distributed Bragg reflector (DBR). The Lasing Eigenvalue Problem based on a source-free linear set of Maxwell equations is used for electromagnetic analysis. Within this approach, we look for a scalar function of electrical field component with the eigenvalues as real number pairs of a mode emission wavelength and correlated threshold values of the gain index.

Nowadays, the cutting edge microlaser research focus on a rare-earth ions active materials, due to its unique properties [1]. To facilitate the analysis of microlaser emission, we disregard all non-electromagnetic effects. This allows the use of the source-free linear Maxwell equations, along with appropriate boundary and radiation conditions, for further investigation of the electromagnetic field. This approach, known as the Lasing Eigenvalue Problem (LEP), is discussed in greater detail in [2, 3].

Within the LEP, the complex reflective index, ν of active medium is presented as known refractive index $\alpha_c = \text{Re}\nu > 0$ and unknown gain index threshold value $\gamma = -\text{Im}\nu > 0$. In addition, for such layered structure we apply the transmission matrix method (TMM) and obtain transcendental equation. The roots of this equation are LEP eigenvalues, namely a frequency and a threshold.

The Fig. 1 shows the color maps of laser eigenvalue modes for microlaser based on Nd crystal ($\epsilon=1.81$) with two quantities of pair ($N_{\text{DBR}}=2$ and $N_{\text{DBR}}=20$) in the distributed Bragg reflector made of TiO_2 and SiO_2 layers and gold film of 10 nm thickness. As one can see, the threshold gain index of modes (denoted by crosses) is dropped in the lower color map for the bigger number of DBR layers. That happened due to the mode is in the band gap of the DBR. Also, the blue stripes correspond to so-called “parasitic” modes caused by dielectric layers of DBR, so their number grows with the increase of the number of layers. Besides, the influence of the gold film thickness is investigated as well, and it shows a similar behavior, the thicker the film, the lower the threshold.

Overall, the parametric analysis of the LEP eigenvalues was presented. The impact or the superstrate gold film thickness and substrate DBR configuration are explained.

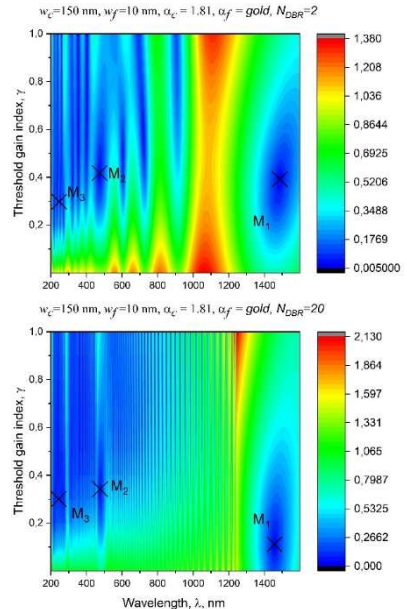


Fig. 1 Color map of laser eigenvalue modes on the plane of threshold gain index and wavelength

- [1] Z. Chen, G. et al., Progress in Materials Science 121, 100814, (2021). <https://doi.org/10.1016/j.pmatsci.2021.100814>.
- [2] S. S. Herasymov, O. S. Hnatenko, J. Nano-Electron. Phys. 16, 4, 04033 (2024). [https://doi.org/10.21272/jnep.16\(4\).04033](https://doi.org/10.21272/jnep.16(4).04033).

Self-stabilization of microwave current in a superconducting resonator for photon detection

O. Kalenyuk^{1,2}, S. Futimsky^{1,2}, I. Martynenko¹, A. Shapovalov^{1,2}

¹*Kurdyumov Institute for Metal Physics, NAS of Ukraine, 03142, Kyiv, Ukraine*

²*Kyiv Academic University, 03142, Kyiv, Ukraine*

e-mail: oleksii.kaleniuk@gmail.com

Photon detectors have found widespread applications in both scientific research and practical tasks. Highly sensitive photon detectors based on superconducting materials have been developed using kinetic-inductive and bolometric detection principles. The energy of absorbed photons is sufficient to break Cooper pairs in a superconductor, leading to a change in the concentration of superconducting pairs. Due to the inherent inertia of these pairs, this change affects the kinetic inductance of the superconducting film. Consequently, the inductance variation alters the resonant frequency of superconducting resonators, which form large two-dimensional arrays and are connected to a single microwave transmission line in microwave kinetic inductance detectors (MKIDs) [1].

Alternatively, the bolometric detection method relies on the transition of thin superconducting wires to a normal state upon photon absorption. This requires maintaining the current in the wire just below the critical current and detecting the emergence of resistance when a photon disrupts the superconducting state. However, implementing matrix detection using this approach necessitates a large number of wires for current supply and voltage measurement, significantly complicating the measurement and cooling systems.

We propose combining the principles of these two methods to create a matrix detector connected to a single transmission line. The proposed detector is based on a microstrip resonator with a central narrowing, analogous to a nanowire. Our measurements of such a niobium (Nb) resonator reveal a dip in the frequency response when the power entering the resonator exceeds the critical power $P_c < 10 \mu\text{W}$, for a narrowing width of 12 μm . Similar effects have been observed in other studies [2]. For instance, [3] demonstrates that the amplitude of the current at which the dip appears corresponds to the critical current. The dip exhibits a flat bottom, indicating self-stabilization of the resonator's wave impedance near the resonant frequency. Consequently, the current in the narrowing also self-stabilizes. Detection criteria may include the occurrence of a dip itself, as well as changes in its depth and the frequencies marking its onset and termination.

This research was carried out within the framework of the project 2023.04/0157 funded by the National Research Foundation of Ukraine «High-speed matrix kinetic detector of long-wave infrared radiation»

- [1] N. Boudou, A. Benoit, O. Bourrion, M. Calvo, F.-X. Désert, J. Macias-Perez, A. Monfardini, M. Roesch, “Kinetic inductance detectors for millimeter and submillimeter astronomy,” Comptes Rendus Physique 13, 62-70 (2012). DOI: <https://doi.org/10.1016/j.crhy.2011.10.008>.
- [2] C. Kurter, A. P. Zhuravel, A. V. Ustinov, and S. M. Anlage, “Microscopic examination of hot spots giving rise to nonlinearity in superconducting resonators,” Phys. Rev. B 84, 104515 (2011). DOI: <https://doi.org/10.1103/PhysRevB.84.104515>.
- [3] A. A. Kalenyuk, A. I. Rebikov, A. L. Kasatkin and V. M. Pan, Nonlinear HTS lumped elements in microwave transmission and resonance circuits”, 2010 International Kharkov Symposium on Physics and Engineering of Microwaves, Millimeter and Submillimeter Waves, Kharkiv, Ukraine. (2010).

Absorption cross-section of toroidal metallic nanoparticles

A. V. Korotun^{1,2}

¹*National University Zaporizhzhia Politechnic, 64 University Str., Zaporizhzhia, 69063, Ukraine*

²*G.V. Kurdyumov Institute for Metal Physics of the NAS of Ukraine,
36 Academician Vernadsky Blvd., Kyiv, 03142, Ukraine*

e-mail: andko@zp.edu.ua

Toroidal-shaped nanostructures have recently found increasing applications in nanooptics [1] and for the creation of the composites with toroidal inclusions, which have the properties of “left-handed” media. Moreover, such particles are used as nanoscale sensors, transformers and resonators [2]. Hence, the task of the studying the optical properties of metallic nanoparticles, which have toroidal shape, is an actual task.

The absorption cross-section of the considered nanoparticle is determined by the following relation due to the presence of axial symmetry

$$C_{\text{abs}} = \frac{\omega}{c} \sqrt{\epsilon_m} \operatorname{Im} \left(\frac{2}{3} \alpha_{\perp} + \frac{1}{3} \alpha_{\parallel} \right), \quad (1)$$

where ω and c are the frequency and velocity of light; ϵ_m is dielectric permittivity of the environment, and $\alpha_{\perp(\parallel)}$ are the diagonal components of the polarizability tensor of toroidal nanoparticle, which are given by the following formula in the frameworks of T-method

$$\alpha_{\perp(\parallel)} = \frac{\tau(\omega) - \epsilon_m}{4\pi\epsilon_m} \sum_l C_{\perp(\parallel)}^l \frac{\tau_l^{\perp(\parallel)} - \epsilon_m}{\tau_l^{\perp(\parallel)} - \tau(\omega)}. \quad (2)$$

In formula (2) $\tau(\omega)$ is dielectric function of nanoparticle material, which is determined by Drude formula; $\tau_l^{\perp(\parallel)}$ are the value of dielectric function at the frequencies of the transverse and longitudinal plasmonic resonances of multipolarity l , the summation is performed over all multipoles; $C_{\perp(\parallel)}^l$ are geometrical factors determined by volume integrals of electric field intensity

$$C_{\perp(\parallel)}^l = \frac{\int \mathcal{E}_{\perp}^l dV \int \mathcal{E}_{\parallel}^l dV}{\int (\mathcal{E}_{\perp}^l + \mathcal{E}_{\parallel}^l) dV}, \quad (3)$$

\mathcal{E}_{\perp}^l , $\mathcal{E}_{\parallel}^l$ are the transverse and longitudinal components of the intensities of electric field of multipolarity l .

The calculations for the frequency dependences of the absorption cross-section have been performed for toroidal nanoparticles of different materials and different sizes. It has been demonstrated the presence of two maxima of the absorption cross-section, which correspond to the dipole transverse and longitudinal resonances, while the higher multipole resonances are not manifested due to the smallness of the intensities of the fields of higher multipoles.

- [1] B. K. Bhowmik, K. M. Rohith, S. John, S. Prabhu and G. Kumar, New J. Phys. 26, 063024 (2024). <http://dx.doi.org/10.1088/1367-2630/ad570e>.
- [2] O. V. Kharissova, M. Garza Castañón, B. I. Kharisov, J. Mater. Res. 34, 3998 (2019). <http://dx.doi.org/10.1557/jmr.2019.370>.

Width of the line of the surface plasmonic resonance in metal-dielectric nanocups

V. I. Reva¹, R. O. Malysh¹, R. Yu. Korolkov¹, A. V. Korotun^{1,2}, I. M. Titov¹

¹National University Zaporizhzhia Politechnic, 64 University Str., Zaporizhzhia, 69063, Ukraine

²G.V. Kurdyumov Institute for Metal Physics of the NAS of Ukraine,
36 Academician Vernadsky Blvd., Kyiv, 03142, Ukraine
e-mail: revvi@zp.edu.ua

The nanoparticles of noble metals have unique optical properties due to the excitation of plasmonic resonances on their surfaces – collective oscillations of conduction electrons, excited by the electromagnetic wave incident on the particle [1]. It is known that the resonance spectra of metallic and metal-dielectric nanoparticles depend significantly on the details of their geometry. The synthesis of nanostructures with different shapes such as nanospheres, nanorods, nanocubes, nanocones, nanoprisms, nanorings and nanoshells allows tuning of resonance frequency from near-infrared to ultraviolet region [2]. The particles of the above-mentioned forms are symmetric, so only the plasmonic modes of the same multipolarity are mixed in them. The symmetry breaking removes this restriction and mixing (hybridization) of modes of the different multipolarity becomes possible. One form of nanoparticle with broken symmetry is nanocup, which consists of the dielectric core, only partially covered by metallic shell of the constant thickness. The advantage of these nanoparticles, except the broken symmetry, is also the possibility to influence the enhancement of local fields and anisotropic optical response by changing the height of nanocups and the size of the core and shell.

The width of the surface plasmonic resonance line of nanocups, as in the case of particles of other shapes [3], is determined by the effective electron relaxation rate in metallic shell, to which three mechanisms additively contribute: volume relaxation and surface relaxation, as well as radiation damping

$$\gamma_{\text{eff}} = \gamma_{\text{bulk}} + \gamma_{\text{surf}} + \gamma_{\text{rad}}. \quad (1)$$

It is shown that all components of the effective relaxation rate, and, correspondingly, the width of the surface plasmonic resonance line are determined by such a set of geometrical parameters as the external radius of nanocup R , $\beta_c = R_c/R$, where R_c is the radius of the dielectric core; $h = R_c/H$, where H is the height of nanocup. In the limiting case $H \rightarrow 2R$ the obtained results coincide with those for two-layer spherical nanoparticle of the type “dielectric core – metallic nanoshell”.

[1] A. O. Koval, A. V. Korotun, Yu. A. Kunytskyi, V. A. Tatarenko, and I. M. Titov, Electrodynamics of Plasmon Effects in Nanomaterials (Naukova Dumka, Kyiv 2021) (in Ukrainian).

[2] V. V. Kulish, J. Nano- Electron. Phys. 3, 105 (2011).

[3] A. V. Korotun, H. V. Moroz, R. Yu. Korolkov, Funct. Mater. 31, 119 (2024).

DOI: <http://dx.doi.org/10.15407/fm31.01.119>.

Plasmonic capacitance of the gap between two closely spaced spherical metal nanoparticles

H. V. Moroz¹, A. V. Korotun^{1,2}, V. P. Kurbatsky¹

¹*National University Zaporizhzhia Politechnic, 64 University Str., Zaporizhzhia, 69063, Ukraine*

²*G.V. Kurdyumov Institute for Metal Physics of the NAS of Ukraine,*

36 Academician Vernadsky Blvd., Kyiv, 03142, Ukraine

e-mail: garrymrz@zp.edu.ua

The production of high-energy capacitors based on nanoparticles of various geometries is important for storing electrical energy due to their high pulse power and insignificant charge leakage. The collection and storage of electromagnetic energy has practical application in such important areas of human activity as photovoltaics, communications, fiber optics, data storage and integrated optoelectronics. Nanoparticles of noble metals are of considerable interest from this point of view due to strong localization and large magnitude of electric field upon excitation of plasmon resonance [1].

When two spherical metal nanoparticles are located at a small distance from each other, the capacitance of the gap between them increases due to strong electromagnetic interaction, which leads to a change in the plasmon modes and the energy of the plasmon resonance. The capacitance of the gap between the nanoparticles, taking into account electron tunneling, is determined by the relation

$$C = \left(\frac{1}{C_c} + \frac{2}{C_Q} \right)^{-1}, \quad (1)$$

where the mutual capacitance of the metal spheres up to terms of the order of $(R/d)^2$ is

$$C_c \approx \pi \epsilon_0 \tau \frac{R^2}{d} \left(1 + \frac{R}{2d} \right), \quad (2)$$

and the quantum capacitance is

$$C_Q = \frac{4\pi R^2 \epsilon_0 \sqrt{\tau}}{\ell_{TF}}. \quad (3)$$

In formulas (2) and (3), ϵ_0 is the electric constant; R is the radius of the nanoparticle; d is the distance between centers of the particles; ℓ_{TF} is the screening length in a two-dimensional electron gas; $\tau(\omega)$ is the dielectric function determined by the Drude model.

Relations (1) – (3) allow us to determine the size and frequency dependences of the capacitance of the gap between closely spaced spherical metal nanoparticles.

- [1] A. Korotun, G. Moroz, R. Korolkov, I. Titov, 2023 IEEE XIIIth International Conference on Electronics and Information Technologies (ELIT) (Lviv, September 26-28, 2023), 320. DOI: <http://dx.doi.org/10.1109/ELIT61488.2023.10310803>.

Tensor of electric field enhancement in the vicinity of a metallic triangular equilateral nanoprism

N. I. Pavlyshche

*National University Zaporizhzhia Politechnic, 64 University Str., Zaporizhzhia, 69063, Ukraine
 e-mail: Pavlishchenazar@gmail.com*

Among metal nanoparticles of various shapes, triangular nanoprisms attract much attention due to their unique optical properties. Thus, near the surface of such nanoparticles, there is a significant amplification of electric fields, which makes them ideal candidates for the manufacture of sensitive elements of optical sensors. However, information on the optical properties of prismatic nanoparticles is practically not presented in the scientific literature, so the corresponding studies are relevant.

We will consider a metal nanoparticle in the form of a triangular equilateral prism located in a medium with the permittivity τ_m . Due to the symmetry of the nanoparticle under study, the field enhancement is described by a second-rank diagonal tensor, the components of which have the form

$$\mathcal{G}_{\perp(\parallel)} = \frac{\tau_1^{\perp(\parallel) 2} + \tau_2^{\perp(\parallel) 2}}{\left| L_{\perp(\parallel)} (\tau_1^{\perp(\parallel)} + \tau_m) + \tau_m \right|^2 + \left| L_{\perp(\parallel)} \tau_2^{\perp(\parallel)} \right|^2}, \quad (1)$$

where the real and imaginary parts of the dielectric function, according to the Drude theory, are

$$\tau_1^{\perp(\parallel)} = \tau^\infty - \frac{\omega_p^2}{\omega^2 + \gamma_{\text{eff}}^{\perp(\parallel) 2}}, \quad \tau_2^{\perp(\parallel)} = \frac{\omega_p^2 \gamma_{\text{eff}}^{\perp(\parallel)}}{\omega (\omega^2 + \gamma_{\text{eff}}^{\perp(\parallel) 2})}. \quad (2)$$

In formulas (1) and (2), $L_{\perp(\parallel)}$ and $\gamma_{\text{eff}}^{\perp(\parallel)}$ are the depolarization factors and effective electron relaxation rates determined within the framework of the equivalent oblate spheroid approach as functions of the effective aspect ratio [1]; τ^∞ and ω_p are the contribution of the crystal lattice to the dielectric function of the metal and the frequency of bulk plasmons, respectively.

Calculations of the dependences $\mathcal{G}_1(\omega)$ and $\mathcal{G}_2(\omega)$ were carried out for silver nanoprisms located in Teflon. It was found that the maxima of the frequency dependence curves experience a “blue” shift with an increase in the aspect ratio, accompanied by a decrease in the magnitude of the maximum. It should be noted that the “blue” shift is more significant for the longitudinal component of the electric field enhancement tensor.

- [1] N. I. Pavlyshche, A.V. Korotun and V. P. Kurbatsky, Low Temp. Phys. 51, 140 (2025).
 DOI: <https://doi.org/10.1063/10.0034657>.

The role of donor-acceptor defect complexes in the recombination of non-equilibrium carriers in cadmium iodide

M. Rudka

*National University "Lviv polytechnic", 12, Bandera str., Lviv, Ukraine
e-mail: mykola.m.rudka@lpnu.ua*

Layered CdJ₂ crystals have a structural type C6, in which the J anions form a close hexagonal packing, and half of the octahedral voids are occupied by Cd cations. The crystal matrix is built by parallel packing of sandwiches of the J-Cd-J type. The key feature of CdJ₂ is the manifestation in them at low temperatures ($T < 200$ K) of a selective band at the edge of the fundamental absorption at 3.24 eV. However, it is present only if the sample is illuminated in the direction of the main crystallographic axis C6. In the direction perpendicular to C6, another selective band can be observed at 3.21 eV. In cadmium iodide crystals activated by various kinds of impurities, the intensity of the selective band increases and can shift its position within 3.24 ... 3.19 eV. In such crystals, the intensity of low-temperature luminescence and photoconductivity also increase.

It is shown that the reason for the appearance of these bands is the generation of two different cationic donor-acceptor (DA) complexes of intrinsic defects of the type (Cd_i-V_{Cd}). The displacement of the nodal cadmium into the adjacent unfilled octahedral cavity in the J-Cd-J layer generates a (DA)₁ pair, the arm of which is perpendicular to C6, and the displacement into the van der Waals gap generates (DA)₂ pairs, the arm of which is parallel to C6. The significant advantage within the structural layer of the covalent bond over the ionic bond is the reason for the dominance of (DA)₁ and (DA)₂ pairs in the CdJ₂ crystals. Such a trimer - a DAD_i center of the type (Cd_i⁰-V_{Cd}⁻-Cd_i⁺), is specifically oriented relative to the C6 axis [1]. Spontaneous or stimulated displacement of the nodal cadmium at distances greater than the elementary lattice parameter CdJ₂ causes the decomposition of the layer molecule, the release of halogen in the form of gas, the movement of the cation into the van der Waals gap with its subsequent entry into the trimer or diffusion into the drains and coagulation. The decomposition of the CdJ₂ molecule generates a 1D vacancy of the layer molecule of the type (V_J-V_{Cd}-V_J), and their association gives 2D and 3D vacancies of the crystal layers. Activation of cadmium iodide with various impurities can improve the crystalline matrix by preventing the formation of vacancies in the layer molecules. At the same time, the concentration of intrinsic and impurity DA defect complexes increases [1], which can significantly increase both the intensity of the selective edge band and, correlated with this, the intensity of luminescence, photoconductivity, etc. Light from the fundamental absorption region of CdJ₂ crystals generates non-equilibrium charge carriers – electron-hole pairs – which can subsequently rapidly recombine or localize at donor and acceptor energy levels in the band gap of the material. The fundamental absorption edge of CdJ₂ at room temperature is at 3.2 eV and shifts to 3.5 eV with decreasing temperature to 77 K. At room temperature, the recombination of non-equilibrium charge carriers gives fast luminescence of low intensity, but with decreasing temperature below 200 K, the intensity of afterglow in the spectral range of 500 ... 650 nm increases rapidly, reaching a maximum quantum yield at temperatures of 80-110 K. It was established that the intense luminescence of such crystals in the specified spectral region is of donor-acceptor nature and is caused by the capture of non-equilibrium genetic electron-hole pairs (GEHP) on the associated DA and DAD_i complexes of structural defects with their subsequent radiative recombination. The decay of such GEHP and the capture of "fragments" on different DA centers cause the appearance of maxima on the curves of thermally stimulated luminescence and conductivity. This is also the reason for the increase in the lifetime of non-equilibrium carriers and, accordingly, the increase in the contribution of phosphorescence to the integral luminescence of crystals with decreasing temperature. Below 40 K, radiative recombination of non-equilibrium charge carriers also occurs in the form of exciton luminescence in the violet spectrum.

[1] Rudka M., et. al., Low Temp. Phys. 51, 43–48 (2025). DOI: <https://doi.org/10.1063/10.0034643>.

Electrical controlled multi-spectral light slowing in metasurface with graphen/dielectric/metal sandwich microresonators

Yu. N. Savin

*O.Ya. Usykov Institute for Radiophysics and Electronics, Academy of Sciences of Ukraine,
Acad. Proskury St.12, 61085, Kharkiv, Ukraine
e-mail: yuriyns49@gmail.com*

In recent years, electromagnetic metamaterials with multi-window plasmonic-induced transparency (multi-PIT) and multi-spectral slow-light properties of electromagnetic packets have attracted much attention. In particular, metasurfaces with multi-spectral slow-light properties may be of interest for optical information processing systems, since information can be stored and retrieved separately through multiple channels [1,2].

Nevertheless, it is still highly challenging to obtain three or more transparency windows with sufficiently large group delay and transparency bandwidth. In addition, most metamaterial-based slow-light devices are passive, which limits their practical applications. In this study, novel designed multi-PIT metasurfaces with near-field graphene/dielectric/metal sandwich resonators (GDMR) coupling system are numerically simulated, integrating the localized plasmon properties of graphene surface and metal surface, and their optical responses are studied.

The designed unit cell consists of metal stripline microresonators (as dipole antenna), one “bright” (strong interaction with external excitation) and two “dark” (weak interaction) GDMR on a crystal Al_2O_3 substrate with thin Si layer. The transmission and reflection optical spectra of metasurfaces are investigated numerically by COMSOL Multiphysics 5.6 software package. The metasurface is excited by a plane polarized electromagnetic wave in the terahertz range from 5 to 10 THz at normal incidence.

The excitation spectra of surface plasmon modes, depending on the Fermi energy of graphene, as well as the geometric parameters and thickness of the interlayer dielectric in the GDMRs, are determined. Multi-window optical transparency properties are investigated depending on sizes in individual GDMR, as well their localization in the unit cell and graphene Fermi energy. It has been found the asymmetry of the sizes of dark GDMRs leads to the excitation of an additional resonance (quadrupole mode) and thus the appearance of an additional transparency window in the transmission spectra.

The multi-window PIT effect is analyzed in framework of the classical coupled Lorentz for four oscillator model [3]. The dependence of the coupling constants, the decay rates on the Fermi energy in graphene are determined. The developed unit cell model allows dynamic control of its optical characteristics (group delay of the wave packet in each transparency window, bandwidth of the transparency windows and the corresponding refractive index) by manipulating the Fermi level of graphene via gate voltage in the GDMR.

Our work provides an efficient base to obtain the metamaterial structures with controlled multiple transparency windows and multispectral light slowing effect. We assumed the obtained numerical simulation results can be used in multi-frequency filtering, multi-band slow light and operation devices, highly-sensitive sensors.

- [1] J. Chen, O.A. Breslavets, Yu. N. Savin, A. S. Kupriianov, Z. E. Eremenko and V. R. Tuz, *J. Appl. Phys.* 135, 033103 (2024), <https://doi.org/10.1063/5.0179112>.
- [2] L. Zhu, F.-Y. Meng, J.-H. Fu, Q. Wu, J. Hua, *Optics Express*, 20, N4, 4494 (2012). <https://doi.org/10.1364/OE.20.004494>.
- [3] S. Yang, X. Xia, Z. Liu, E. Yiwen, Y. Wang, C. Tang, W. Li, J. Li, L. Wang, and C. Gu, *J. Phys.: Condens. Matter* 28, 445002 (2016). <https://doi.org/10.1088/0953-8984/28/44/445002>.

Overheating of metallic nanoparticles under excitation of plasmonic resonances on their surface

R. Yu. Korolkov¹, M. A. Shvydkyi¹, A. V. Korotun^{1,2}, I. M. Titov¹

¹*National University Zaporizhzhia Politechnic, 64 University Str., Zaporizhzhia, 69063, Ukraine*

²*G.V. Kurdyumov Institute for Metal Physics of the NAS of Ukraine,
36 Academician Vernadsky Blvd., Kyiv, 03142, Ukraine
e-mail: romankor@zp.edu.ua*

In recent years, thermoplasmonic phenomena in metallic nanoparticles of the different shapes and compositions have been actively investigated. This is associated with such practical applications of thermonanoplasmonics as photothermal therapy of malignant tumors, acceleration of some physical reactions, thermoplasmonic sensing of phase transformations taking place in nanoscale systems. Let us point out that the physical cause of the overheating is the rapid conversion of electromagnetic energy into thermal energy when light is absorbed. However, the studies of the overheating of nanoparticles of different geometry under the excitation of surface plasmonic resonances have hardly been carried out and are, therefore, actual.

Let us assume that plasmonic nanoparticle of arbitrary shape is located in the dielectric medium with the given dielectric permittivity. The overheating of nanoparticles, the value of which is determined by the expression [1], takes place under the excitation of surface plasmonic resonances

$$\Delta T = \frac{C_{\text{abs}} I_0}{4\pi\kappa\beta R_{\text{eq}}}, \quad (1)$$

where I_0 is the intensity of light incident on the nanoparticle; κ is environmental thermal conductivity coefficient; C_{abs} is absorption cross-section; β and R_{eq} are shape parameter and the equivalent radius of nanoparticle, R is the radius of sphere, d is diameter of cylinder / disk, l is the length of cylinder, h is the height of disk (Table. 1).

Table 1. Geometric parameters of nanoparticles

Parameter	Shape		
	Sphere	Cylinder	Disk
R_{eq}	R	$\frac{1}{2}\sqrt[3]{\frac{3}{2}d^2l}$	$\frac{1}{2}\sqrt[3]{\frac{3}{2}d^2h}$
β	1	$1 + 0.96587 \ln^2\left(\frac{l}{d}\right)$	$\exp\left\{0.040 - 0.0124 \ln\left(\frac{h}{d}\right) + 0.0677 \ln^2\left(\frac{h}{d}\right) - 0.00457 \ln^3\left(\frac{h}{d}\right)\right\}$

The calculations have been performed for spherical, cylindrical and disk-shaped nanoparticles of gold.

It has been found that the maximum overheating (at the frequency of surface plasmonic resonance) increases by approximately one order of magnitude under the variation of the shape of nanoparticles in the row “sphere → cylinder → disk”. The above fact indicates the feasibility of using spherical nanoparticles for photothermal therapy, since the overheating is minimal for them. At the same time, it is reasonable to use disk particles in photocatalysis because the reaction rate increases with increasing temperature, according to Arrhenius law.

[1] G. Baffou, Thermoplasmonics: Heating Metal Nanoparticles Using Light (Cambridge University Press 2017). <http://dx.doi.org/10.1017/9781108289801>.

Signatures of disorder in the heat capacity of Nd-doped LAO laser materials

V. Sokolenko, D. Szewczyk, N. Miniaj luk-Gaweł, P. Dereń

*Institute for Low Temperatures and Structure Research, Polish Academy of Sciences,
Okólna 2, 50-422 Wrocław, Poland
e-mail: v.sokolenko@intibs.pl*

We present low-temperature specific heat (C_p) of novel class of glass-ceramic materials prepared by aerodynamic levitation method and subsequent heat treatment. The proposed method allowed to obtain a uniquely patterned structure of amorphous and crystalline phase [1]. The investigation of thermal property compares two different samples, amorphous and ceramic one. The heat capacity measurements were performed in a wide temperature range in two series, 1st cooling from 25 K down to 1.8 K and 2nd heating from 1.8 K up to room temperature. Thermal relaxation method implemented in the Heat Capacity Option of commercial setup PPMS® was used to determine the heat capacity [2,3]

In both cases, the results indicate characteristic features of disordered materials, including a Boson peak near 16 K in the C_p/T^3 vs. T plot and an upturn of C_p/T^3 at low temperatures – connected to the presence of the linear term, shifting slightly depending on the sample. Comparative analysis revealed that the ceramic sample exhibits significantly higher disorder than the amorphous one, as evidenced by the intensity of two-level systems, which is nearly three times greater. The detailed analysis of the heat capacity data will be presented based on applying the soft potential model [4], while the Debye contribution allows estimation of the characteristic Debye temperature at the lowest temperatures.

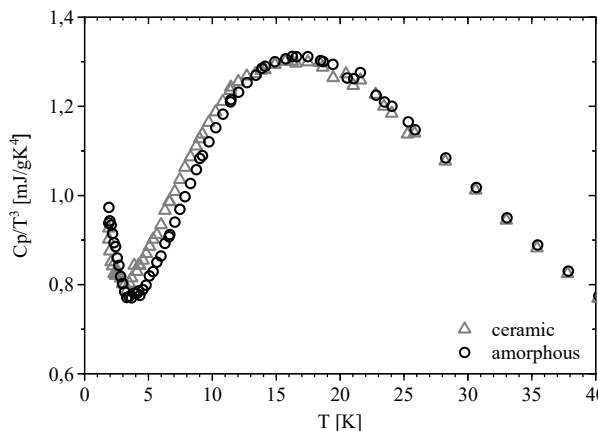


Figure 1 Comparison of Boson peak vicinity of both samples ceramic (triangles) and amorphous (circles).

- [1] N. Miniaj luk-Gaweł, B. Bondzior, A. Chudzynska, P.J. Deren Application of an aerodynamic levitation method to obtain LaAlO₃: Nd³⁺ glass ceramics, Journal of Alloys and Compounds, 1010, 177088 (2025) <https://doi.org/10.1016/j.jallcom.2024.177088>
- [2] J. C. Lashley, M. F. Hundley, A. Migliori, et al., Critical Examination of Heat Capacity Measurements Made on a Quantum Design Physical Property Measurement System, Cryogenics (Guildf). 43, 369 (2003). [http://dx.doi.org/10.1016/S0011-2275\(03\)00092-4](http://dx.doi.org/10.1016/S0011-2275(03)00092-4).
- [3] D. Szewczyk, A. Jeżowski, A. I. Krivchikov, and J. Ll. Tamarit, Influence of Thermal Treatment on Thermal Properties of Adamantane Derivatives, Low Temp. Phys. 41, 469 (2015). <http://dx.doi.org/10.1063/1.4922101>.
- [4] M. A. Ramos, Low-Temperature Thermal and Vibrational Properties of Disordered Solids (2022). <http://dx.doi.org/10.1142/q0371>.

Effect of molecular impurity N₂ on photoluminescence and structure of fullerite C₆₀ during diffusion intercalation and chemical sorption

V. N. Zoryansky, P.V. Zinoviev, N.N. Galtsov and Yu.O. Semerenko

*B. Verkin Institute for Low Temperature Physics and Engineering of NAS of Ukraine,
47 Nauky Ave., Kharkiv, 61103, Ukraine
e-mail: zoryansky@gmail.com*

Polycrystals of C₆₀ with an admixture of N₂ molecules were studied using X-ray diffractometry [1] and photoluminescence spectroscopy [2-4] in a wide temperature range (10-300 K). Saturation was carried out at various sorption temperatures (T_s) from 200 °C to 550 °C in a nitrogen atmosphere under a pressure of 30 atm. Consistent studies of the optical and structural characteristics of the C₆₀+N₂ complex, as well as their temperature behavior, were carried out. The kinetics of nitrogen sorption for different T_s and the efficiency of impurity diffusion were studied. The influence of the impurity on the orientational phase transition, the processes of glass state formation and the dynamics of electron excitation transfer were determined depending on the mechanism of interaction in the impurity-matrix system.

A combined analysis of experimental spectroscopy and diffractometry data showed the presence of an adsorption crossover at a sorption temperature of about 420 °C - a transition from the diffusion mechanism of filling intermolecular voids with an impurity (physisorption) to the chemical impurity-matrix interaction (chemisorption).

For solid solutions of C₆₀+N₂ (T_s<420 °C), curves of the increase in the lattice parameter from the saturation time were established and an increase in the luminescence of impurity glow centers ("deep X-traps") was shown, correlating with an increase in the concentration of octahedral voids of the C₆₀ lattice filled with N₂ molecules. The different dynamics of these processes indicate a significant gradient in impurity concentration over the penetration depth. In the case of extremely saturated solid solutions of C₆₀+N₂, as shown by the temperature dependences of the luminescence intensity and the lattice parameter, the temperature of formation of the glass state (T_g) decreases, but not as significantly as the temperature of the orientational phase transition (T_c). At the same time, in the case of chemical sorption of nitrogen (T_s>420 °C) in C₆₀, the orientational phase transition is completely suppressed, and the temperature boundaries of the glass transition processes are greatly blurred with a simultaneous significant increase in the volume of the cubic cell and thermal expansion of the crystals. Also, for this saturation mechanism, reformatting and a shift towards low energies with a significant inhomogeneous broadening of the luminescence spectrum were found, the primary analysis of which showed the presence of biazafullerite (C₅₉N)₂ in the resulting new multicomponent complex of nitrogen-containing substances. Significant changes in the behavior of the temperature dependence of the integrated radiation intensity indicate the presence of additional mechanisms of electron excitation transport in crystals with a new chemical composition. The quenching of photoluminescence at low temperatures observed here may be associated with the emergence of many additional Frenkel exciton capture centers with high efficiency of their nonradiative deactivation.

- [1] I. V. Legchenkova, K. A. Yagotintsev, N. N. Galtsov, V. V. Meleshko, Yu. E. Stetsenko, A. I. Prokhvatilov, Low Temp. Phys. 40 (8), 685 (2014). <https://doi.org/10.1063/1.4894316>.
- [2] P. V. Zinoviev, V. N. Zoryansky, V. V. Meleshko, Yu. E. Stetsenko, Low Temp. Phys. 41 (3), 236 (2015). <https://doi.org/10.1063/1.4915916>.
- [3] P. V. Zinoviev, V. N. Zoryansky, Low Temp. Phys. 47 (2), 173 (2021). <https://doi.org/10.1063/10.0003180>.
- [4] P. V. Zinoviev, V. N. Zoryansky, Low Temp. Phys. 48 (3), 268 (2022). <https://doi.org/10.1063/10.0009547>.

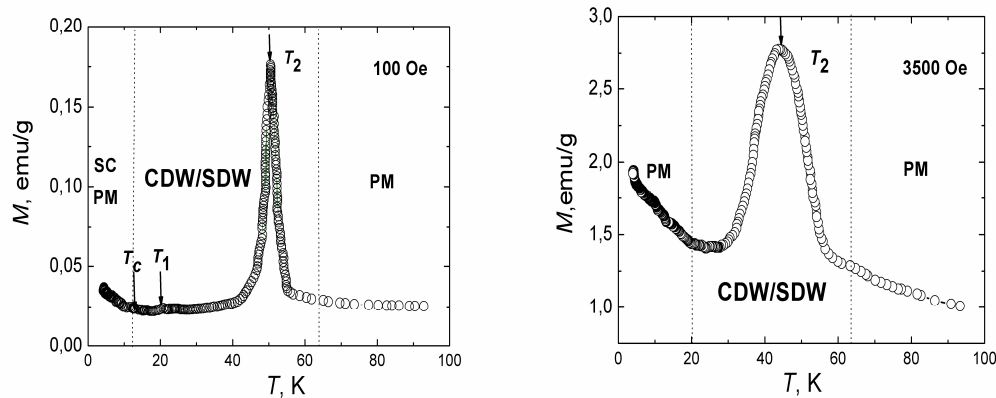
**QUANTUM LIQUIDS AND QUANTUM CRYSTALS,
CRYOCRYSTALS**

Creating of bounded Majorana pairs in superconducting net of quantum nanowires in $\text{SmMnO}_{3+\delta}$

F. N. Bukhanko

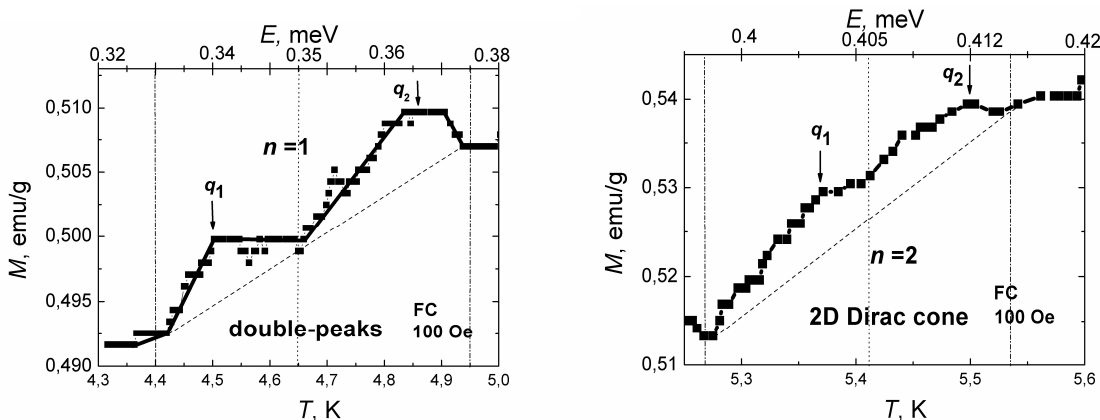
*Donetsk Institute for Physics and Engineering named after O.O. Galkin of NAS of Ukraine,
 46 Nauky ave., Kyiv, 03028, Ukraine
 e-mail: fnbukhanko@gmail.com*

In this work, the formation of a superconducting network of quantum nanowires in $\text{SmMnO}_{3+\delta}$ manganites in two hidden topological states CSL1 and CSL2 of a chiral quantum spin liquid was experimentally studied. It is believed that the states of bound pairs of Majorana fermions are trapped at the two ends of the quantum nanowire. The formation of nanofragments of 1D coupled charge and spin density waves with wave vectors $q_1 \parallel a$ and $q_2 \parallel b$ directions the crystal lattice in the magnetic fields $H \geq 100$ Oe indicates formation in ab planes of 2D quantum nanowires-like net. In the weak magnetic fields $H = 100$ Oe, 350 Oe and 1 kOe the continuous spectrum of the thermal excitations of bounded Majorana pairs in $\text{SmMnO}_{3+\delta}$ in interval temperature 4.2 - 12 K is divided into two low-energy Landau zones with numbers $n = 1$, $n = 2$, with two specific features of magnetization $M(T)$ in the shape of alternating double peaks and truncated Dirak cones.



(a)(b)

Fig.1. Charge/spin density wave state is realized in the form of a two-peak magnetization feature $M(T)$ (a). Spin density wave state is realized in the form of a wide peak magnetization feature $M(T)$ (b).



(a)(b)

Fig. 2. Excitation of bounded Majorana pairs in Landau zone with $n = 1$ (a). Excitation of bounded Majorana pairs in Landau zone $n = 2$ (b).

The influence of second sound resonances on the vibrations of a quartz tuning fork in a superfluid solution of ^3He in ^4He

V. K. Chagovets, V. E. Syvokon, S. S. Sokolov

*B.Verkin Institute for Low Temperature Physics and Engineering of NAS of Ukraine,
47 Nauky Ave., Kharkiv, 61103, Ukraine
e-mail: chagovets@ilt.kharkov.ua*

Quartz tuning forks, along with other oscillating bodies, turned out to be a convenient tool for studying various properties of superfluid ^4He and solutions of ^3He in ^4He . Their distinctive feature is high frequency stability, low intrinsic losses, good reproducibility of properties at low temperatures, insensitivity to a magnetic field and ease of use. The relationship between the properties of a liquid and the resonant frequency of a tuning fork and its losses can be established within the framework of a hydrodynamic model of an incompressible liquid with an accuracy of the geometric parameters of the tuning fork. However, in superfluid liquids, processes are possible that go beyond the incompressible liquid model, these are oscillations of the liquid density or the first sound and oscillations of temperature and entropy - the second sound. The emission of these sounds by a tuning fork leads to an increase in its losses and damping of oscillations. In addition, in an experimental cell with superfluid ^4He and solutions of ^3He in ^4He , resonances of the waves of the first and second sounds associated with the geometry of the cell can be excited under oscillations of the tuning fork. The occurrence of these resonances has a great influence on the operation of the tuning fork itself and its amplitude-frequency characteristic.

In Ref. [1], the calculation and analysis of the relationship between the natural oscillations of an open tuning fork and the resonances of the first sound modes arising in a cell with normal and superfluid ^4He and concentrated solutions of ^3He in ^4He were carried out. It was shown that in cases where the resonance frequency of the tuning fork and the frequency of the standing wave of the first sound coincide, a connection of oscillations arises, which leads to a distortion of the shape of the observed resonance line and complicates the interpretation of the experimental data.

In the case where the tuning fork is surrounded by a standard cylindrical body from the manufacturer, at relatively low frequencies, a situation arises when the dimensions of the body are so small that they do not allow the first sound wave to arise in helium. However, since the velocity of the second sound in superfluid ^4He and ^3He - ^4He solutions is significantly lower than that of the first, for a given frequency the wavelength of the second sound will be shorter, and a wave process will arise.

In the present work, the temperature dependence of the acoustic modes of the second sound, which can arise in a superfluid solution of ^3He in ^4He at oscillations of a quartz tuning fork limited by a body, is calculated. The calculated modes at given temperature are compared with the resonance curves of the quartz tuning fork obtained experimentally in a solution containing 15 % of ^3He in ^4He in the temperature range of 0.5 - 2.5 K at tuning fork excitation voltages of 0.1 and 1 V. It is shown that the amplitude-frequency characteristics of the tuning fork are significantly affected by the second-sound resonances that arise in a cylindrical resonator, which is the tuning fork body with a solution of ^3He in ^4He . The influence of the acoustic resonances decreases with increasing voltage exciting the tuning fork. The absence of distortions in the amplitude-frequency dependences of the tuning fork in a non-superfluid solution of 15 % ^3He in ^4He , where there is no second sound, convincingly shows that it is precisely this that is the cause of distortions in the superfluid solution.

[1]. V. K. Chagovets, V. E. Syvokon, and S. S. Sokolov, Fiz. Nyzk. Temp. 50, 973 (2024) [Low Temp. Phys. 50, 875 (2024)]. <https://doi.org/10.1063/10.0028633>.

Peculiarities of growth of close packed phases in large substrate-free rare gas clusters

O. P. Konotop, O. G. Danylchenko

*B.Verkin Institute for Low Temperature Physics and Engineering of NAS of Ukraine,
47 Nauky Ave., Kharkiv, 61103, Ukraine
konotop@ilt.kharkov.ua*

Interest in the study of structural transformations in nanoclusters, in particular, is caused by the need to obtain an answer to the question of how the non-crystalline structure of small icosahedral aggregations is transformed and the structure of massive solids is formed. At the same time, even large clusters with sizes of tens and hundreds of thousands of atoms can have a structure different from the solid state due to the significant contribution of surface energy to their total energy. One of the most intriguing effects discovered in free clusters of rare gases and not inherent in massive cryocrystals is the realization of a stable hcp structure in large clusters (more than 10^4 atoms per cluster).

The transformation from the fcc to the two-phase fcc-hcp structure with a change in the size of one-component Ar clusters and binary Ar-Kr clusters of equimolar component composition was previously studied in [1]. In present work, in order to check the correctness of the conclusions made in [1] regarding the mechanism of nucleation and growth of the hcp phase, and to research an influence of component mole fraction on the competition between two close packed phases, we performed THEED quantitative phase analysis of argon-krypton clusters in a wide range of component concentrations. The average cluster size \bar{N} ranged from $2 \cdot 10^3$ to $1 \cdot 10^5$ at./cl. (i.e. the average linear cluster size δ was varied from 60\AA to 200\AA). It was found that the threshold cluster size for the formation of fcc phase does not depend on the component composition and equals to $\delta \approx 90\text{\AA}$ ($\bar{N} \approx 1.1 \cdot 10^4$ at/cl). As clusters grow, the relative volume of hcp phase increases substantially to reach its maximum at $\delta \approx 150\text{--}160\text{\AA}$, ($\bar{N} \approx 4 \cdot 10^4$ at/cl). In the case of two-phased clusters having the same size, it was found that the volume of hcp phase in heterogeneous clusters significantly exceeds that in homogeneous ones, with the maximum fraction of hcp phase being at equimolar contents of argon and krypton.

At the same time, although in this range of cluster sizes the relative proportion of the fcc phase decreases, the absolute sizes of the fcc domains continue to increase. This result experimentally confirms the formation of two-phase fcc-hcp clusters in a supersonic jet, rather than single-phase fcc and hcp ones. The simultaneous growth of both close-packed phases also indicates a diffusion mechanism for the nucleation and growth of the hcp structure from the initial liquid phase.

- [1] O.G. Danylchenko, S.I. Kovalenko, O.P. Konotop, V.N. Samovarov, Low Temp. Phys. 40, 1083 (2014). <https://doi.org/10.1063/1.4904000>.

Scattering amplitude of C₆₀ fullerite in the ordered phase. Theory and calculations.

N. A. Aksanova¹, D. E. Hurova², V. Kinzhylalo³, N. N. Galtsov²

¹*V. N. Karazin Kharkiv National University, Kharkiv 61022, Ukraine*

²*B. Verkin Institute for Low Temperature Physics and Engineering of NAS of Ukraine,
47 Nauky Ave., Kharkiv, 61103, Ukraine*

³*Institute for Low Temperatures and Structure Research, Polish Academy of Sciences,
Wroclaw, 50-950, Poland
e-mail: aksanova@karazin.ua*

In solid fullerite, phase transitions occur with the temperature decreases, which are associated with a change in the rotational motion of the C₆₀ fullerene molecules. Thus, in the high-temperature phase (disordered phase) the C₆₀ molecules almost “freely” rotate. In the ordered phase, neighboring fullerene molecules rotate along one of the molecular axes, which is directed along the spatial diagonal of the cubic lattice. The low-temperature phase (orientation glass) is characterized by the relative orientations of the adjacent molecules and can still fluctuate between two distinct orientations when the C₆₀ molecules “freeze” in their orientations.

The rotational motion of the C₆₀ molecule is most clearly observed in the analysis of the set of X-ray diffraction patterns. This is revealed in the fact that in the entire region of existence of the solid phase of fullerite C₆₀, reflections from the cubic crystal structure are present, and there are no reflections from planes of the {h00} type.

In [1], the approach was proposed to describe the X-ray scattering amplitude of C₆₀ fullerite in the high-temperature phase, which made it possible to explain the reason for the absence of the {h00} type reflection in diffraction patterns.

In this work, using the approach for describing the scattering amplitude of solid nitrogen in the ordered phase [2, 3], a method was proposed for calculating the X-ray scattering amplitude of pure C₆₀ fullerite in the region of existence of the orientationally ordered phase.

- [1] P. A. Heiney, et al., Phys. Rev. Lett. 66, 2911 (1991). <https://doi.org/10.1103/PhysRevLett.66.2911>.
- [2] N. N. Galtsov, et al., Low Temp. Phys. 28, 365 (2002). <https://doi.org/10.1063/1.1480244>.
- [3] D. E. Hurova, et al., Low Temp. Phys. 49, 1184 (2023). <https://doi.org/10.1063/10.0020873>.

Correlation between the thermal conductivity plateau and the hump in heat capacity of polymer and composite materials

Yu. V. Horbatenko, O. A. Korolyuk, A. I. Krivchikov, M. S. Barabashko

*B.Verkin Institute for Low Temperature Physics and Engineering of NAS of Ukraine,
47 Nauky Ave., Kharkiv, 61103, Ukraine
e-mail: horbatenko@ilt.kharkov.ua*

Crystals and disordered systems exhibit fundamentally distinct heat transfer mechanisms, posing challenges in universally interpreting low-temperature anomalies in their thermal properties. In crystals, heat is primarily carried by the particle-like propagation of phonons, as described by the Peierls equation. In disordered systems, heat transfer involves an additional mechanism, by the coupling of vibrational modes. Currently, the thermal conductivity of amorphous composite materials is characterized by the sum of two distinct contributions:

$$\kappa(T) = \kappa_p + \kappa_c(1)$$

Here, term κ_p associated with the particle-like propagation of excitations, while κ_c denotes the "coherences" contribution, due to wave-like tunneling [1]. At low temperatures, the thermal conductivity of these materials exhibits a quadratic dependence, $\kappa = \beta T^2$, which saturates into a thermal conductivity plateau, κ_{pl} . In the high-temperature range, the "coherences" contribution, κ_c is well-described by a simple Arrhenius-type function:

$$\kappa_c = \kappa_0 \cdot \exp(-E/T)(2)$$

This behavior is observed for solid heterogeneous crystalline and amorphous materials [2]. Additionally, the maximum temperature, T_{max} (the "hump" in the reduced heat capacity, C/T^3), occurs within the temperature range of the thermal conductivity plateau, κ_{pl} . This phenomenon has been observed in glasses, amorphous solids of various compositions, and complex disordered crystals [3]. However, the correlation between the low-temperature behaviors of heat capacity and thermal conductivity near the plateau remains insufficiently understood and requires further theoretical investigation.

In this study we analyzed experimental data on the thermal conductivity and heat capacity of various polymer and composite materials, including epoxy resin, polyvinyl chloride, tetrahedrite $\text{Cu}_{10}\text{Zn}_2\text{Sb}_4\text{S}_{13}$, and PSN ceramic $\text{Pb}(\text{Sc}_{0.5}\text{Nb}_{0.5})\text{O}_3$. Key fitting parameters – κ_{pl} , β , κ_0 , and E were calculated to describe the temperature dependence of thermal conductivity in these composites. We propose a definition for the temperature of the thermal conductivity plateau T_{pl} , based on the parameters κ_{pl} and β . Furthermore, a linear correlation between T_{pl} was tested. A universal empirical relation was developed to describe the temperature dependence of thermal conductivity near the plateau ($0.01 \leq T/T_{max} \leq 2$):

$$\kappa(T/T_{pl})^{-1} = \beta^{-1}(T/T_{pl})^n + \kappa_{pl}^{-1}(3)$$

This relation offers a robust framework for understanding the thermal conductivity behavior of disordered solids in the vicinity of the thermal conductivity plateau.

Acknowledgement: this work supported by the National Research Foundation of Ukraine (Grant 2023.03/0012).

- [1] M. Simoncelli, N. Marzari, and F. Mauri, Nature Physics, 15, 809 (2019). <https://doi.org/10.1038/s41567-019-0520-x>.
- [2] Y. V. Horbatenko, et al., Low Temp. Phys. 50, 379 (2024). <https://doi.org/10.1063/10.0025621>.
- [3] A. I. Krivchikov, A. Jeżowski, Thermal conductivity of glasses and disordered crystals. In Low-Temperature Thermal and Vibrational Properties of Disordered Solids: A Half-Century of Universal “Anomalies” of Glasses (World Scientific Publishing Europe Ltd. 2023; pp. 69-112). <https://doi.org/10.1142/q0371>.

The substrate nanoroughness analysis by surface electrons over helium film

V. A. Nikolaenko

B.Verkin Institute for Low Temperature Physics and Engineering of NAS of Ukraine,
47 Nauky Ave., Kharkiv, 61103, Ukraine
e-mail: nikolaenko@ilt.kharkov.ua

Both the method and the tools for analyzing the substrate nanoroughness using surface electrons (SEs) over helium film are considered. The conductivity of SEs essential depends from the image field variation on surface substrate. The expression here is:

$$\delta V \approx -Q_d \frac{e^2}{4\pi\epsilon_0 Z} \frac{\pi\xi}{A} \left(\frac{A}{Z}\right)^{1/2} e^{-\frac{2\pi Z}{A}}$$

where, Q_d is the effective force of the electron image in the dielectric, ϵ_0 is the dielectric permittivity of vacuum and value Z is electron distance to the substrate; ξ and A are the effective amplitude and period of the inhomogeneities, respectively.

The experimental tools in details are shown on Figs 1, 2. The cell is situated in hermetic chamber like on Fig. 2.

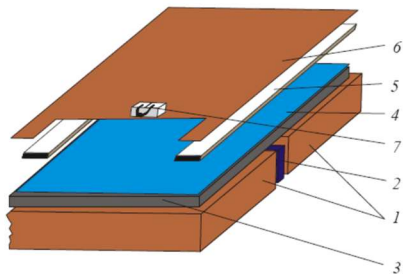


Fig.1. Measuring cell. Here 1-2 – the measurement electrodes, 3 – dielectric substrate, 4 – helium film, 5 – guard electrode, 6 – upper electrode, 7 – heat filament.

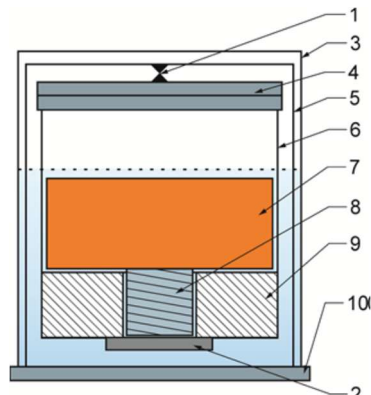


Fig.2. Device for analyzing of substrate nano-inhomogeneities. Here are 1 – the hinge, 2 – plumb, 3 – helium chamber, 4 – measuring cell, 5 – support frame, 6 – cylinder, 7 – plunger, 8 – movable coil, 9 – immobile coil, 10 – bottom of helium chamber.

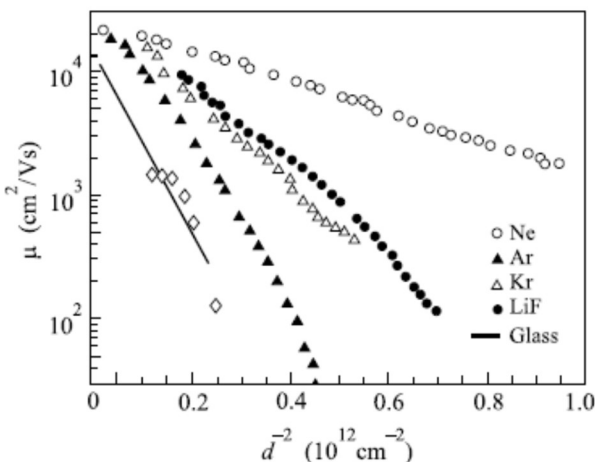


Fig.3. Dependences of electron mobility μ vs helium thickness d for some substrates.

So, here is considered a non-destructive method of analyzing the quality of substrate surfaces by measuring SE conductivity changes above a helium film at changing its thickness. The possibility to identify nanoroughness from some nanometers (for nonsaturated helium film) to 10^2 nanometers (at the saturated helium film) is demonstrated.

[1] Yu. Z. Kovdrya, F. F. Mende, and V. A. Nikolaenko, Phys. Nizk. Temp. 10, 1129 (1984). <https://doi.org/10.1063/10.0031200>.

Phase transitions in large atomic clusters. Computer modeling

M. Ratner, V. V. Yanovsky

*Institute for Single Crystals of NAS of Ukraine, 60 Nauky Ave., Kharkiv, 61001, Ukraine
e-mail: marinaratner2017@gmail.com*

The present work deals with computer modeling of phase transitions of Ar clusters in the size range of 2000-12000 atoms (mesoscopic range) and in temperature range of 20-85 K. Both solid-liquid phase transition and processes in solid clusters with intrinsic pore are considered.

Many properties of clusters are different from those of the bulk, like binding energies, thermodynamic functions, crystalline structure, optical, magnetic or chemical behavior (see e.g. [1-4]. Linking atomic and mesoscopic range become a challenging task, since the use of traditional modeling methods for small systems (Molecular Dynamics) as well as of macroscopic statistical physics are not suitable for this range of sizes (see e.g. [3]). For this purpose, modified Monte Carlo method was developed that mimics melting processes in real cluster, where cluster shells melt consecutively starting from the outer shell and moving towards the cluster center [2]. Moreover, the adjustable atom random displacement range was introduced, that grows when system is far from free energy minimum and decreases when system approaches global or local free energy minimum. The proposed method decreases exponentially required number of M.C. steps as cluster size grows.

The dependence of melting temperature on cluster size was obtained. It was shown that melting temperature approaches macroscopic solid argon value at cluster size $N_{cl} \sim 11000$. Melting temperature as function of cluster size shows peaks at “magic” cluster sizes, but this phenomenon becomes negligible at $N_{cl} \sim 6500$. Also, cluster volume fluctuations in the solid state were considered as a function of N_{cl} , and were shown to become negligibly small for sizes more than $N_{cl} \sim 9000$. The relation η of mean nearest neighbor distance for liquid and solid state was also considered as a function of cluster size. It was shown that transfer of melting process from “configurational” to “classical” type occurs at $N_{cl} \sim 9000$. The saturation values both for T_{melt} and η are close to literature values for macroscopic bodies. Size dependence of energy barrier between stable solid cluster state and metastable state with intrinsic pore is obtained.

Thus, it can be concluded that proposed by authors modified MC method adequately describes atomic clusters behavior in mesoscopic range of sizes. Three criteria, such as melting temperature, mean interatomic distance and cluster volume fluctuations are in accordance and show that cluster thermal properties become close to that of macroscopic body at size $N_{cl} \sim 11000$.

- [1] Z Wang, Y. Liu, Z. Zhang, (eds) Clusters. Handbook of Nanophase and Nanostructured Materials. (Springer, Boston, MA. 2003). https://doi.org/10.1007/0-387-23814-X_22.
- [2] B. M. Smirnov, Clusters and Small Particles: in Gases and Plasmas, (Springer-Verlag, NY 2000). <https://doi.org/10.1007/978-1-4612-1294-2>.
- [3] J. Pilla, G. Villani, C. Brangian. Philosophical Magazine B 79, 11 (1999). <https://doi.org/10.1080/13642819908223083>.
- [4] D. V. Chalin and S. B. Rochal, Phys. Rev. B. 107, 024102 (2023). <https://doi.org/10.1103/PhysRevB.107.024102>.

Thermal conductivity of nanostructured thin films and a composite material based on PbTe and PbSe

V. V. Sagan, Yu. V. Horbatenko, O. A. Korolyuk, O. O. Romantsova, A. I. Krivchikov

*B.Verkin Institute for Low Temperature Physics and Engineering of NAS of Ukraine,
47 Nauky Ave., Kharkiv, 61103, Ukraine
e-mail: sagan@ilt.kharkov.ua*

As the number of molecules in a unit cell increases or the degree of structural disorder rises, thermal conductivity in complex molecular crystals transitions from crystalline-like to glass-like behavior. In particular, in thin films of PbTe, PbSe, and the nanostructured composite PbTe–PbSe, experimental data on thermal conductivity exhibit glass-like behavior, characterized by a weak increase in thermal conductivity followed by saturation with increasing temperature [1].

The recently published unified theory of thermal transport in crystals and glasses [2] provides a theoretical framework for understanding these behaviors. Using a quantum mechanical approach, it offers a heat conduction expression that unifies crystalline-like and glass-like behaviors as limiting cases. This theory introduces two independent contributions to thermal conductivity: (i) a Peierls contribution (κ_P) associated with the particle-like propagation of phonon wave packets and (ii) a «coherence» contribution (κ_c) related to wave-like tunneling and loss of coherence between different vibrational eigenstates:

$$\kappa(T) = \kappa_P + \kappa_c \quad (1)$$

For amorphous materials above the plateau temperature, $\kappa_P(T)$ is assumed to be constant (κ_{pl}), while κ_c can be approximated by an Arrhenius-type function:

$$\kappa(T) = \kappa_{pl} + \kappa_0 \cdot \exp(-E/T) \quad (2)$$

where κ_0 represents the high-temperature limit of thermal conductivity, and E denotes the characteristic energy associated with dominant diffusive processes.

Experimental data on thermal conductivity for PbTe, PbSe (bulk samples), nanostructured thin films of PbTe, PbSe, and PbTe–PbSe nanocomposite [3] were analyzed. The crystal-like thermal conductivity of bulk samples is described using the equation:

$$k(T) = A/T + B \quad (3)$$

where A/T corresponds to phonon-phonon (three-phonon) scattering processes, and B accounts for short-wave excitations, attributed to diffusons.

The glass-like behavior of nanostructured thin films and the PbTe–PbSe nanocomposite is well described by Eq. (2).

This study effectively describes the temperature dependence of thermal conductivity in thin films of PbTe, PbSe, and the PbTe–PbSe nanostructured composite using the approach based on Eq. (2) in the temperature range of 70 to 300 K. The results show that the approximation (2) accurately fits the experimental data [3].

This research was supported by the National Research Foundation of Ukraine (Project № 2023.03/0012).

- [1] M. E. DeCoster, X. Chen, K. Zhang, C. M. Rost, E. R. Hoglund, J. M. Howe, T. E. Beechem, H. Baumgart, and P. E. Hopkins, *Adv. Funct. Mater.* 29, 1904073 (2019). <https://doi.org/10.1002/adfm.201904073>.
- [2] M. Simoncelli, N. Marzari, and F. Mauri, *Nat. Phys.* 15, 809 (2019). <https://doi.org/10.1038/s41567-019-0520-x>.
- [3] Yu. V. Horbatenko, V. V. Sagan, O. A. Korolyuk, O. O. Romantsova, and A. I. Krivchikov, *Low Temp. Phys.* 50, 379 (2024). <https://doi.org/10.1063/10.0025621>.

Multi-channel heat transfer in CO₂ solutions with N₂O and Xe impurities

V. V. Sagan, O. A. Korolyuk, A. I. Krivchikov, V. A. Konstantinov, Yu. V. Horbatenko

B.Verkin Institute for Low Temperature Physics and Engineering of NAS of Ukraine,
 47 Nauky Ave., Kharkiv, 61103, Ukraine
 e-mail: sagan@ilt.kharkov.ua

The low-thermal-conductivity (κ) crystals often display intriguing temperature (T) dependencies: a crystal-like $\kappa \propto T^{-1}$ behavior at intermediate temperatures, transitioning to a weaker, glasslike T -dependence at higher temperatures. Interestingly, in dynamically orientationally disordered (DOD) phases of molecular crystals, the isochoric thermal conductivity generally increases with temperature [1].

In this study, we propose that phonons retain their role but transport heat via multiple channels: (i) normal phonons governed by the Boltzmann transport equation (BTE), (ii) diffuson-like phonons, and (iii) diffuson-like excitations mediated by wave-like tunneling.

It is assumed that, taking into account all contributions, the general expression for thermal conductivity can be of the form:

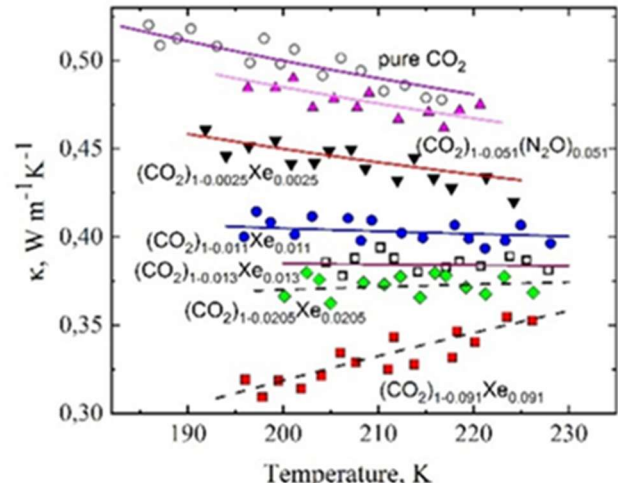
$$\kappa(T) = \kappa_{ph} + \kappa_{dif} + \kappa_C(T) = A/T + B + \kappa_0 \exp(-E/T)$$

where $\kappa_{ph} = A/T$ arises from phonon-phonon scattering, and $\kappa_{dif} = B$ accounts for temperature-independent diffusons contributions. Tunnel contribution «coherences» ($\kappa_C(T) = \kappa_0 * \exp(-E/T)$) follows an Arrhenius-type exponential dependence over a wide temperature range, where κ_0 is the pre-exponential factor, which represents the maximum tunneling heat transfer, and E denotes the dominant excitation energy and is expressed in Kelvin [2].

The isochoric thermal conductivity of CO₂ solutions with N₂O and Xe impurities has been analyzed, and it has been shown that it undergoes significant changes with an increase in impurity concentration. The results demonstrate that the multi-channel heat transfer mechanism effectively describes the deviation of isochoric thermal conductivity from the $1/T$ dependence, as well as the increase in thermal conductivity with rising temperature in DOD phases of molecular crystals and their solutions.

The transition from a crystal-like to a glass-like temperature dependence of $\kappa(T)$ in solid solutions of cryocrystals occurs gradually and can be interpreted as a continuous change in the parameters of the phonon contribution $\kappa_{ph}(T)$ and the tunneling «coherence» contribution $\kappa_C(T)$. The first two channels account for heat transfer by phonons (κ_{ph}) and diffusons (κ_{dif}), while the third channel describes the contribution of wave tunneling and the loss of coherence between different vibrational eigenstates ($\kappa_C(T)$).

This research was supported by the National Research Foundation of Ukraine (Project № 2023.03/0012).



[1] V. A. Konstantinov, Heat Transfer in Molecular Crystals, In Book: Heat Transfer - Theoretical Analysis, Experimental Investigations and Industrial Systems, Aziz Belmiloudi (Ed.), “InTech” Open Access Publisher, p.157-188 (2011). <https://doi.org/10.5772/13551>.

[2] Yu. V. Horbatenko, V. V. Sagan, O. A. Korolyuk, O. O. Romantsova, and A. I. Krivchikov, Low Temp. Phys. 50, 379 (2024). <https://doi.org/10.1063/10.0025621>.

NANOPHYSICS AND NANOTECHNOLOGIES

Low-temperature heat capacity of thermally expanded graphite: contribution of ZA flexural phonons

**M. S. Barabashko¹, A. I. Krivchikov^{1,2}, A. Jeżowski², D. Szewczyk², Yu. Horbatenko¹,
O. Romantsova^{1,2}, G. Dovbeshko^{2,3}, Yu. Sementsov⁴**

¹*B.Verkin Institute for Low Temperature Physics and Engineering of NAS of Ukraine,
47 Nauky Ave., Kharkiv, 61103, Ukraine*

²*Institute for Low Temperatures and Structure Research, Polish Academy of Sciences,
Okólna 2, 50-420 Wrocław, Poland*

³*Institute of Physics, NAS of Ukraine, Prospect Nauky, 46, Kyiv 03028, Ukraine*

⁴*Chuiko Institute of Surface Chemistry, NAS of Ukraine, General Naumov str. 17, Kyiv, 03164,
Ukraine*

e-mail: barabaschko@ilt.kharkov.ua

Graphite, an allotropic form of carbon, features a layered structure that gives rise to high anisotropy in its thermal properties. Thermally expanded graphite (TEG) is a category of powdered material with a graphite-like layered structure, produced through a thermal shock process applied to graphite intercalation compounds, followed by electrochemical hydrolysis. The decomposition and evaporation of the intercalant results in a significant exfoliation of the graphite-like structure. TEG is synthesized through chemical oxidation using potassium dichromate ($K_2Cr_2O_7$) in sulfuric acid (H_2SO_4), with the oxidant-to-graphite ratio significantly exceeding the stoichiometric value [1].

The specific heat of sets of thermally expanded graphite (TEG) with different density has been studied in the temperature range 2-300 K. Both high-frequency in-plane (LA and TA) and low-frequency transverse out-of-plane (ZA) acoustic vibrational modes contribute to the low-temperature heat capacity of TEG.

Below 10 K, changes in the density of TEG lead to significant variations in heat capacity. The temperature dependencies of low-temperature heat capacity below 5 K has been fitted by an equation: $C(T)=A_1T+A_3T^3$. The first term (A_1T) is associated with the quadratic dispersion of the ZA out-of-plane flexural long-wave transverse acoustic phonons $\omega \sim k^2$. The second term (A_3T^3) is related to the Debye phonon contribution to the phonon density of states of TEG. The behavior of the phonon heat capacity $C_{ph} = C - A_1T$, with a subtracted A_1T term, resembles the behavior observed in graphite. C_{ph}/T^3 is weakly temperature dependent below 3 K and decreases with increasing temperature. The observed behavior of C_{ph}/T^3 for TEG is related to the peculiar dynamics of the layered structure, which exhibits strong anisotropy in the interaction forces between carbon atoms. Similar behavior of C_{ph}/T^3 was observed for the single-walled carbon nanotubes (SWCNTs) and multi-walled carbon nanotubes (MWCNTs) [2].

Funding:

This work was partly supported by the National Research Foundation of Ukraine (Grant 2023.03/0012) and National Science Centre Poland (Grant 2022/45/B/ST3/02326).

- [1] N.V. Morozovsky, Y.M. Barabash, Y.V. Grebelna, M.T. Kartel, Y.I. Sementsov, G.I. Dovbeshko, Low Temperature Physics, 49(5), 553. (2023).
- [2] M.S. Barabashko, A.I. Krivchikov, A. Jeżowski, O. Bezkrovnyi, M.I. Bagatskii, V.V. Sumarokov, D. Szewczyk, Carbon Trends, 19, 100479 (2025).

Nanotechnology for future systems and equipment for improved survivability

L. N. Illyashenko^{1,2,3}, N. N. Kolchigin², O. G. Nerukh³

¹*National Academy of the National Guard of Ukraine,*

²*Sichovyh Strilciv Str., Zolochiv, Lviv Region, 80700, Ukraine*

²*V. N. Karazin Kharkiv National University, Svobody Sq. 4, Kharkiv, 61022, Ukraine*

³*Kharkiv National University of Radio Electronics, 14 Nauky Ave. 14, Kharkiv, 61166, Ukraine*

e-mail: mila.illyashenko@gmail.com

Technological developments have given rise to new methods and means for research, the academic world, and industry. Benefits of technological developments come with consequences: live of people may be in danger. The protective suits may be used to avoid problems when working in special environments. Nanotechnology offers a lot of solutions. When dealing with nanoparticles (NPs), it may be helpful to use metal NPs, in which localized surface plasmon resonances (LSPR) may appear. LSPR in NP results in strong scattering and/or absorption of light to be used for new developments in nanotechnology. NPs may be solid and layered. The last allow combining several materials in one NPs, providing a lot of new effects. While LSPR of single isolated NP depend strongly on shape, size and chosen material, a lot of effects arise when several NPs are clustered together. However, it is difficult to investigate all possible geometrical configurations of NPs, and a fast and reliable tool is needed. The Spectral Method appeared to be especially suitable to study NP, since nanosized objects have mostly smooth shapes. However, such a method was suitable only for single isolated object with the elliptical shape of the cross-section. The invention of the conformal mapping approach to generate parameterizations of various cross-section shapes by the leading author of this work brought benefits for nanotechnology since various shapes now may be investigated, proving fast and reliable results [1]. Conjunction of several mathematical methods by the leading author of this work resulted in the development of numerical simulation algorithms, which appeared as Spectral Galerkin Boundary Integral Equation (SBIE) Methods with analytical regularizations in terms of singularity subtraction improved by Fast Fourier Transform. Since LSPR depend on the NP orientation with respect to the light source and with respect to each other, in this work various new SBIE numerical simulation algorithms were developed to study clusters of NPs with powerful research made on Integral Equations [2] in combinations with new ideas following obtained already promising results for military application [3]. When such NPs are incorporated in fabric, the suit may not only protect a person against various threats, but also may monitor and guard the physical and mental condition of the user, continue to incorporate human enhancement technologies and adopt new advanced materials to exploit new opportunities for improved survivability in terms of protection, medical monitoring, concealment, deception, and camouflage, as well as for information exchange, for the development of flexible solar cells to recharge batteries, and for health treatment, including diagnostics and treatment of diseases and targeted drug delivery.

- [1] L. Illyashenko, Spectral Boundary Integral Equation method for electromagnetic research with different geometrical configurations. (DIPED, Tbilisi, Georgia),
- [2] A. Nerukh, T. Benson, Non-Stationary Electromagnetics: An Integral Equations Approach (Jenny Stanford Publishing, New York 2018). <https://doi.org/10.1201/9780429027734>
- [3] N.N. Kolchigin, M.N. Legenkiy, A.A. Maslovskiy, A. Demchenko, S. Vinnichenko, I. Vasilchenko, S. Rolenko, Yu. Devyatilov, V. Glebov, In Telecommunications and Radio Engineering (Begell House, 2018), DOI: 10.1615/telecomradeng.v77.i11.20.

Dual hydrophobic/hydrophilic properties: a biomimetic microstructure taken from *Salvinia* leaf

N. M. Kizilova

V.N Karazin Kharkiv National University, 4 Svobody sq., Kharkiv, 61022, Ukraine
e-mail: kizilova@karazin.ua

Nature demonstrates many types of smart surfaces with superomniphobic properties, self-cleaning, ice-phobic, super-adhesive, and other types of surfaces. In plants and animals, such surfaces possess multipurpose structures with different physical principles acting in synergy. The most famous of them are self-cleaning water-repelling lotus leaf, super-adhesive gecko feet, light-absorbing drag reducing butterfly wings, water-accumulating surfaces in desert beetles [1, 2], and others. Here a minimization of Gibbs free energy approach used for optimization of the micro-roughness based on the *Salvinia* leaves. This floating fern with a pillar-type coating of trichomes with a complex geometry and a combination of hydrophobic and hydrophilic properties designed for air accumulation during long tropical rainfalls (Fig.1). Its geometry was already proposed for gas capture, CO₂ storage, oil-water separation, and gas hydrate repelling [1]. The problem was not sufficiently studied for the ice-phobic roughness that is the aim of the study.

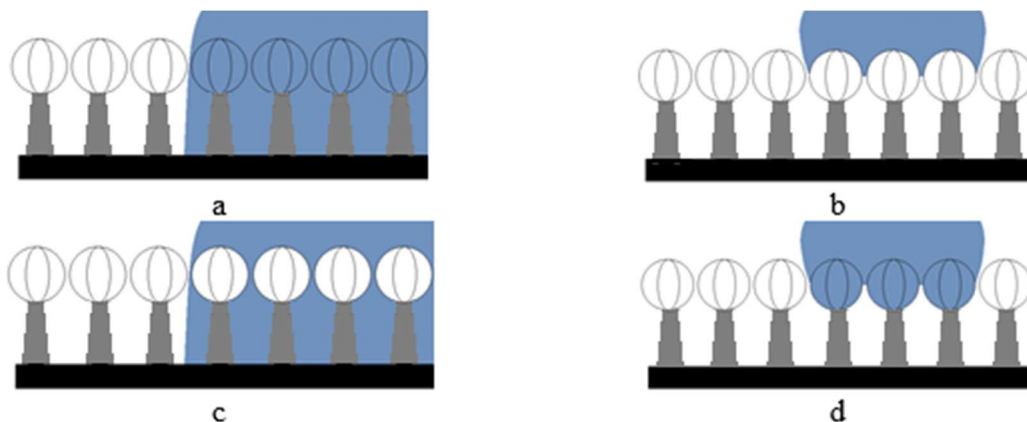


Figure 1: Water droplet on a salvinia-type microstructure in Wenzel (a), Cassie-Baxter (b), Wenzel/Cassie-Baxter (c) and Cassie-Baxter/Wenzel (d) states.

Geometry of trichomes was optimized by minimization of Gibbs surface energy, including the energy of interfaces A_{ij} and three-face contact lines L_{ijk} :

$$G = \sum_{i,j} \gamma_{ij} A_{ij} + \sum_{i,j,k} \kappa_{ijk} L_{ijk} + C = G(L, d_n, d_b, D, \theta) \rightarrow \min, \quad (1)$$

where γ_{ij} and κ_{ijk} are surface and line tensions, C is the surface- and line independent part, L, d_n, d_b, D are the height, neck, bottom and head diameters/ respectively; θ is the contact angle. The approach applied to a state with given constant temperature $T < 0$ C, pressure and number of moles (isobaric ensemble). The optimal geometry {L, d_n, d_b, D} was defined for different solids and fluids.

- [1] N. Kizilova, S. Kjelstrup and Z. Zhang Zhang, Nature-inspired pillar-type smart multipurpose coatings. Proceedings of 10th ECCOMAS Thematic Conference on Smart Structures and Materials. University of Patras, Greece. 507-518 (2023) doi: 10.7712/150123.9805.445538.
- [2] A.R. Parker and C.R. Lawrence, Water capture by a desert beetle, *Nature*, 414, 33–34 (2001).
- [3] D. Bedeaux, S. Kjelstrup and S. K. Schnell, *Nanothermodynamics. Theory and Applications*, World Scientific, Singapore (2024).

TbO_{2-x} nanoparticles with pro-oxidant properties and ROS-dependent luminescence of Tb³⁺ ions

**M. I. Lupan, V. V. Seminko, P. O. Maksimchuk, K. O. Hubenko, V. K. Klochkov,
S. L. Yefimova**

*Institute for Scintillation Materials, National Academy of Sciences of Ukraine, 61072,
60 Nauky Ave., Kharkiv, Ukraine
e-mail: nikita.lupan4@gmail.com*

Cerium oxide nanocrystals (CeO_{2-x}) are known for their antioxidant properties, determined by the variable valence of Ce ions. In addition to cerium, terbium and praseodymium also form a stable IV-valent oxide [1]. In this work, TbO_{2-x} nanoparticles were synthesized and studied — a material structurally identical to CeO_{2-x} but with pronounced pro-oxidant activity and ROS-sensitive luminescence of Tb³⁺.

TbO_{2-x} nanoparticles were obtained by hydrothermal precipitation synthesis followed by heat treatment and dispersion in an aqueous medium. The synthesized nanoparticles were studied by TEM, XRD, and XPS, TbO_{2-x} luminescence spectra were obtained. TEM images showed that the average particle size is 20.0 ± 1.4 nm. XRD revealed that the structure of the obtained samples corresponds to a fluorite-like FCC with a unit cell parameter of 5.23 Å. Using the Scherrer equation, the average nanocrystal size was calculated to be ~ 25 nm, which is consistent with TEM results. XPS analysis of the 3d and 4d levels of terbium showed that approximately 33% of surface and near-surface terbium has a valence state of 3+. The study of the 1s levels of oxygen showed that its spectrum consists of two bands: the 534.9 nm band (20%), attributed to oxygen in OH groups bound to the nanoparticle surface, and the 532.8 nm band (80%), corresponding to oxygen ions in the crystal lattice.

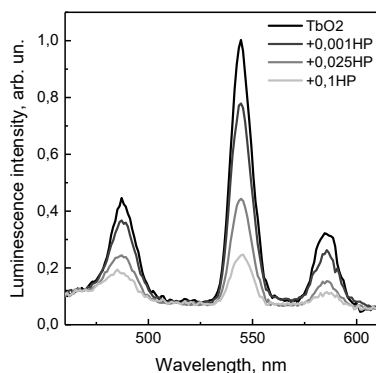
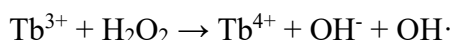


Fig. 1. Luminescence spectra of terbium oxide nanoparticles solutions with different concentrations of H₂O₂.

Luminescence measurements in the green spectrum show a standard set of peaks for trivalent terbium. The study of nanoparticle interactions with hydrogen peroxide indicates that adding higher concentrations of peroxide to the solution, as well as increasing the interaction time, leads to a decrease in Tb³⁺ luminescence intensity, which suggests oxidation of trivalent terbium upon interaction with hydrogen peroxide. Additionally, hydroxyl radical formation is observed upon interaction of the particles with hydrogen peroxide. These two results may indicate that the nanoparticles decompose hydrogen peroxide mostly via a Fenton-like reaction:



[1] E. van der Kolk and P. Dorenbos, Chem. Mater., 18 (15), 3458–3462 (2006).

Raman spectroscopy of multilayer rhombohedral graphite

S. I. Menshykova, S. I. Khaldeev, V. Mantena, P. Hakonen, M. Kumar, J. T. Mäkinen

*Department of Applied Physics, QTF Centre of Excellence, Aalto University,
P.O. Box 15100, FI-00076 Aalto, Finland
e-mail: svitlana.menshykova@aalto.fi*

Few-layer graphene continues to be an attractive material in the search for superconductivity due to its apparent simplicity and the availability of experimental control knobs. Recently, it was experimentally observed [1] that as few as two layers, twisted relative to each other by so-called “magic-angle” $\sim 1.1^\circ$, exhibits an intrinsic superconductive transition. Such twisting results in a moiré pattern that hosts flat bands near the Fermi energy [2,3], resulting in a relatively high critical temperature T_c . In bulkier samples flat bands have been observed in the rhombohedral graphite with ABC stacking (3R) [4].

Rhombohedral graphite, however, is unstable, as it has higher energy than the common Bernal graphite with AB stacking (2H). Natural graphite, for example, consists of mainly Bernal structure, with only about 15% of the 3R phase. A significant problem is that the metastable ABC phase easily relaxes to its Bernal counterpart, making sample preparation and subsequent measurements difficult tasks. Moreover, precise characterization of the stacking order of graphite remains a challenge.

Here, we aim to identify the stacking order in graphite and to determine the possible effect of thermal cycling on its constitution. We characterize the stacking order locally with Raman spectroscopy before and after thermal cycling in a dilution refrigerator (temperature range 30 mK to 300 K), and use atomic force microscopy to assess the morphology and thickness of the graphite flakes.

We perform Raman spectral imaging of more than a hundred flakes and find that the amount of ABC stacking in our natural graphite (origin: Madagascar) increases due to twisting during the exfoliation process. Besides pure Bernal and rhombohedral phases, we locate areas in which the width of the 2D peak in the Raman spectrum lies in between the pure states. In these areas, the amplitude of the spectral features corresponding to the M band is also found to vary in the same fashion. We interpret these changes in terms of the ratio between the Bernal and rhombohedral phases. We further show that the corresponding Raman spectral features in such areas can be reconstructed by summing the pure AB and ABC Raman spectra with fitted prefactor – i.e. that the two spectral features are additive. Finally, we confirm that thermal cycling within the studied range has no effect on the amount of the rhombohedral phase.

- [1] Y. Cao, V. Fatemi, S. Fang, K. Watanabe, T. Taniguchi, E. Kaxiras, and P. Jarillo-Herrero, Nature 556, 43 (2018). <https://doi.org/10.1038/nature26160>.
- [2] N.B. Kopnin, T.T. Heikkilä, and G.E. Volovik, Physical Review B 83, 220503 (2011).
- [3] S. Peotta and P. Törmä, Nature Communications 6, 8944 (2015).
- [4] H. Henck, J. Avila, Z. Ben Aziza, D. Pierucci, J. Baima, B. Pamuk, J. Chaste, D. Utt, M. Bartos, K. Nogajewski, B. A. Piot, M. Orlita, M. Potemski, M. Calandra, M. C. Asensio, F. Mauri, C. Faugeras, and A. Ouerghi, Phys. Rev. B 97, 245421 (2018).

Dynamics and structure of quasi-2D hybrid materials

Y. M. Trotskyi¹, E. S. Syrkin¹, V. O. Lykah²

¹*B.Verkin Institute for Low Temperature Physics and Engineering of NAS of Ukraine,
47 Nauky Ave., Kharkiv, 61103, Ukraine*

²*National Technical University “Kharkiv Polytechnic Institute”,
2 Kyrpychov St., Kharkiv, 61002, Ukraine
e-mail: trotskyi@ilt.kharkov.ua*

The pure graphene is a zero-gap semiconductor where bonding π and antibonding π^* bands touch in a single point at the Fermi energy level at the corner of the Brillouin zone. Close to the Dirac point, bands demonstrate a linear dispersion and as a result, exceptionally high mobility of electrons and holes ($15,000 \text{ cm}^2/\text{Vs}$ against Silicon with the carrier mobility of approximately $1,400 \text{ cm}^2/\text{Vs}$) [1]. The ability of graphene to adsorb gas molecules and therefore to increase the charge carrier concentration allows us to utilize this material as a highly sensitive gas sensor [2]. Moreover, the graphene layer with atoms or molecules adsorbed on its surface can be used in nanoscale electronics and bioelectronics devices.

In our report, we analyze the structure and interaction of benzene molecules adsorbed on a graphene monolayer. There exist two structures: 1) a high-symmetry (hollow) structure, where a benzene molecule is placed right above the graphene hexagon; 2) a low-symmetry (stack) structure, where a benzene molecule's center is positioned above one of Carbon atoms in graphene. The energy of interaction is -0.25 eV for the hollow structure and -0.3 eV for the stack structure, so the second one is an energetically stable interaction [4].

There exists a starlike set of six vectors and two types of star domains of the low-symmetry structure. The set of six vectors describe transitions from symmetric high energy state into the stable low symmetric position. The direction of benzene molecules' transitions is the same in some limited regions (domains) [4].

- [1] A.K. Geim and K.S. Novoselov, *Nature materials* 6.3, 183-191 (2007).
- [2] Schedin, Fredrik, et al., *Nature materials* 6.9, 652-655 (2007).
- [3] Alzahrani, Ali Zain, *Graphene Simulation* 1, 21-38 (2011).
- [4] V.A. Lykah, E.S. Syrkin, *Low Temperature Physics* 48 (4), 353-358 (2022).

Enhancement of nematic ordering in cyanobiphenyl liquid crystals induced by resorcinol: novel insights on supramolecular arrangement in hydrogen-bonded liquid crystals

P. V. Vashchenko¹, D. S. Sofronov², L. N. Lisetski¹

¹*Institute for Scintillation Materials of NAS of Ukraine, 60 Nauky Ave., Kharkiv, 61072, Ukraine*

²*Institute for Single Crystals of NAS of Ukraine, 60 Nauky Ave., Kharkiv, 61072, Ukraine*

e-mail: pv@isma.kharkiv.ua

In studies of liquid crystals (LC) as systems offering various examples of nano- and supramolecular structuring, a promising topical example are so-called hydrogen-bonded liquid crystals (HBLC). In a number of papers, mixtures of an alkylcyanobiphenyl and a carboxylic acid are studied, with interaction between cyano- and carboxylic groups giving rise to formation of nematic or smectic mesophases or enhancement of their thermal stability. However, there are but some rare examples of LC interaction with phenol-type compounds, resulting in eventual formation of CN...HO bonds affecting supramolecular ordering [1,2].

In our study, we used a set of dihydroxybenzenes (*o*-, *m*- and *p*-phenol diols, respectively, catechol (CA), resorcinol (RE), and hydroquinone (HQ) – used as non-mesogenic dopants (NMD) added to a classical nematic 4-pentyl-4'-cyanobiphenyl (5CB).

In all three cases, FTIR spectra measurements (LC samples sandwiched between two ZnSe crystals without spacers, with the distance between outer surfaces of the crystals fixed by a cell holder) clearly indicated formation of H-bonded complexes of similar nature. However, DSC studies showed that the effects of the three dihydroxybenzenes on the nematic-to-isotropic transition temperature, T_i , of 5CB were markedly different. HQ was poorly soluble in 5CB, causing an increase in T_i at ~1 % w/w, CA acted as a classical NMD, quickly decreasing T_i with concentration, while introduction of RE led to significant rise of T_i (by up to ~15°C) until ~12 % w/w (corresponding to 3:1 molar ratio), with a subsequent slight decrease at ~18 % w/w (2:1 molar ratio, i.e., the theoretical composition of an eventual complex). Higher RE concentrations retained the nematic phase, which became monotropic (i.e., revealed only on cooling) above ~14 % w/w RE.

A tentative explanation is proposed, with the hydrogen-bonded 2:1 5CB-RE complex affecting orientation of the adjacent dimerized 5CB molecules, re-arranging them into a 3:1 sterically favorable structure.

- [1] M. Pfletscher, S. Hölscher, C. Wölper, et al., *Chem. Mater.*, 29, 8462–8471 (2017). <https://dx.doi.org/10.1021/acs.chemmater.7b03182>.
- [2] R. Nandi, V. Jain, M. Devi, et al., *Colloids and Surfaces A: Physicochemical and Engineering Aspects*, 625, 126952 (2021). <https://doi.org/10.1016/j.colsurfa.2021.126952>.

The role of incomplete ionization in radial p-n junction structures at low temperatures

J. Sh. Abdullayev¹, I. B. Sapaev^{1, 2}

¹*National Research University TIIAME, Department of Physics and Chemistry,
Tashkent, Uzbekistan*

²*Western Caspian University, Scientific researcher, Baku, Azerbaijan
e-mail: j.sh.abdullayev6@gmail.com*

The planar p-n junction is a fundamental component of semiconductor devices [1]. In comparison, radial p-n homo- and heterojunction structures have been extensively explored through experimental investigations [2], computational modeling [3], and theoretical approaches, including the solution of the Poisson equation in cylindrical coordinates [4]. Radial p-n and p-i-n junctions represent a pivotal area of contemporary research in semiconductor physics. However, many studies have overlooked the effects of incomplete ionization—a phenomenon particularly significant at low temperatures, where donor and acceptor ions in the depletion region are not fully ionized.

This paper investigates the current mechanisms and electrophysical characteristics of radial p-n junction structures, with a focus on the role of incomplete ionization at low temperatures. We examine and compare the electrical behavior of radial p-n junctions based on submicron Silicon (Si), Gallium Arsenide (GaAs), and ⁴H Silicon Carbide (⁴H-SiC) structures, emphasizing the impact of dopant atom ionization at temperatures below 800 K. By solving the Poisson equation in cylindrical coordinates, analytical solutions were derived for radial structures with a core radius of $R=0.5 \mu\text{m}$. The analysis provides expressions for the ionization probability of dopant atoms, $P(T)$, over a temperature range of 4 K to 800 K, and the corresponding variation in space charge density, $\rho(T)$, with temperature. At low temperatures, not all donor and acceptor ions in the depletion region of the radial p-n junction are fully ionized. Analytical expressions were developed to determine the differences in the electric field and potential as functions of distance, comparing scenarios with and without the effects of incomplete ionization. The ionization probability $P(T)$, which estimates the degree of ionization of ions in the depletion region, depends on temperature, ionization energies, and doping concentrations. It is described by the following equations (1a) and (1b):

$$\text{In the p-region (core): } P(T) = \frac{1}{1 + \frac{g_A \cdot p_p}{\beta_p \cdot N_V(T)} \cdot \exp\left(\frac{\Delta E_A^{\text{eff}}(N_A, T)}{k \cdot T}\right)} \quad \text{for } r_p < r < R \quad (1a)$$

$$\text{In the n-region (shell): } P(T) = \frac{1}{1 + \frac{g_D \cdot n_n}{\beta_n \cdot N_C(T)} \cdot \exp\left(\frac{\Delta E_D^{\text{eff}}(N_D, T)}{k \cdot T}\right)} \quad \text{for } R < r < r_n \quad (2b)$$

here, k is the Boltzmann constant, g_A, g_D are the degeneracy factors, $N_C(T)$, $N_V(T)$ denote the effective density of conditions for the conduction and valence band edges, respectively. $\Delta E_D^{\text{eff}}(N_D, T)$, $\Delta E_A^{\text{eff}}(N_A, T)$ ionization energy of donor and acceptor ions, respectively.

- [1] Kanoun, O. (2000). IEEE Transactions on Instrumentation and Measurement, 49(4), 901–904. <https://doi.org/10.1109/19.863946>.
- [2] H. Xia, M. Luo, W. Wang et al. Light Sci Appl 11, 170 (2022).
- [3] J. Abdullayev, I. Sapaev, Physical Sciences and Technology. 11, 3-4, 39–48 (2024).
- [4] V.L. Borblik, SPQEO, 24 (4), pp. 419-424 (2021). <https://doi.org/10.15407/spqeo24.04.419>.

Dimensional effects in the thermal expansion of carbon fiber reinforced plastic at low temperatures

N. A. Vinnikov, A. V. Dolbin, V. B. Esel'son, V. G. Gavrilko, R. M. Basnukaeva,
E. M. Grytsiuk, L. M. Buravtseva

B.Verkin Institute for Low Temperature Physics and Engineering of NAS of Ukraine,
47 Nauky Ave., Kharkiv, 61103, Ukraine
e-mail: basnukaeva@ilt.kharkov.ua

Carbon fiber-reinforced composites are polymer-based materials in which carbon fibers are embedded within a polymer matrix (for instance, epoxy resin). These composites emerged relatively recently as a logical development of widely used glass fiber-based composites. Being lighter than fiberglass (with a density of fiberglass around 1.8 g/cm^3 , while carbon fiber-reinforced plastics have a density of about 1.45 g/cm^3), carbon fiber plastics significantly outperform fiberglass materials in several key properties: high strength and hardness, chemical inertness, thermal and electrical conductivity, superior fatigue resistance, and low creep deformation [1,2].

The thermal expansion behavior of carbon fiber-reinforced composite plastics (matrix: commercial carbon fiber TS36S, binder: EDT-10P) and composite plastics with a braided base was studied in this work in the temperature range of 160–293 K using high-sensitivity capacitive dilatometry. Over the entire temperature range, the thermal expansion of the composite materials is anisotropic, with thermal expansion coefficients measured along and perpendicular to the fiber direction differing by two orders of magnitude in absolute value and showing opposite signs. The negative thermal expansion along the fiber direction is likely due to the transverse thermal vibrations of the two-dimensional carbon planes that form the fiber structure. These unique thermal expansion properties further emphasize the advantages of carbon fiber-reinforced plastics, making them highly suitable for applications requiring dimensional stability under varying thermal conditions. Their combination of lightweight characteristics, high mechanical performance, and thermal stability underscores their superiority over traditional composite materials like fiberglass.

- [1] X. Huang, Materials, 2 (4), 2369–2403 (2009). <https://doi.org/10.3390/ma2042369>.
- [2] P.F. Aubourg, C. Crall, J. Hadley, R. D. Kaverman, D. M. Miller, Engineered Materials Handbook; ASM International, Vol. 4, pp 1027–1031 (1987).

Vibrational characteristics of graphene-based materials and hexagonal modification of niobium dichalcogenide: stability, low-dimensional peculiarities and peculiarities of phonon expansion and localization

K. A. Minakova¹, V. A. Sirenko¹, I. S. Bondar², I. G. Mirzoiev²

¹*Department of Physics, National Technical University Kharkiv Polytechnic Institute Kharkiv,
2 Kyrpychova str., Kharkiv, 61002, Ukraine*

²*B.Verkin Institute for Low Temperature Physics and Engineering of NAS of Ukraine,
47 Nauky Ave., Kharkiv, 61103, Ukraine
e-mail: ibondar@ilt.kharkov.ua*

The synthesis of new materials with unique low-temperature properties, characterized by pronounced anisotropy, led to the observation, generally made by neutron-diffraction methods, of completely new features of the vibrational characteristics of such systems.

This study explores of 2H-NbSe₂ and graphene-based materials compound in order to reveal the features of behavior near electron transitions in structures with honeycomb pattern of atoms in “sandwich” layers. The main research methods are X-ray and neutron scattering, combined with numerical simulations, to examine how temperature stability, defects, and crystal structure inhomogeneities affect the electronic and vibrational behavior of these nanostructures.

On the basis of experimental data on the study of temperature dependences of the lattice parameters of anisotropic layered compounds, the features of the phonon densities of states of the ultrathin films of niobium diselenide and graphene have been analyzed. It has been established that the relation of minima on the linear thermal expansion (LTEC) temperature dependences and maxima on the calculated dependences of the relations derived from the rms displacement allows one to extract (or verify) information on interatomic interactions in complex, strongly anisotropic crystal structures. Based on the analysis of temperature dependences of the rms amplitudes of the atomic oscillations in the direction normal to the plane of the film, the temperature stability intervals of the flat form of the nanoformations considered have been determined.

Low-temperature thermodynamics of branched spin-1/2 system formed by XX chains connected through Ising spins

K. S. Dzhenzherova, E. V. Ezerskaya, V. O. Kovalenko

*V.N. Karazin Kharkiv National University, 4 Svoboda Sq, Kharkiv, 61022, Ukraine
 e-mail: xa13346957@student.karazin.ua*

Low dimensional magnetism is of big interest for the theoretical study because of numerous experimental data related to really existing magnetic crystals formed by weakly interacting clusters, chains or planes.

We propose mesoscopic spin-ring model formed by finite spin-1/2 XX chains “pinned” periodically via additional Ising spins. The model Hamiltonian is

$$\hat{\mathbf{H}} = -\sum_{l=1}^L \left\{ \sum_{i=1}^2 \left[g_i \mu_B H \sum_{n=1}^{N_i} S_{i,l,n}^z + J_i \sum_{n=1}^{N_i-1} (S_{i,l,n}^x S_{i,l,n+1}^x + S_{i,l,n}^y S_{i,l,n+1}^y) \right] - g_0 \mu_B H \sigma_l^z + I_i (\sigma_l^z S_{i,l,1}^z + \sigma_{l+1}^z S_{i,l,N_i}^z) \right\} \quad (1)$$

The spin-1/2 XX chain is a well-known example of an exactly solvable spin system [1, 2]. Jordan-Wigner transformation [1] reduces its Hamiltonian to the ideal gas of spinless fermions even for the chain with any defects. Proposed model Hamiltonian may give new information about the well-known broken-chain effect in real quasi-one-dimensional magnetic materials [3, 4].

Special structure of model Hamiltonians, where Ising z -projections of the impurity spins are the good quantum numbers, permits us to use standard transfer-matrix technique for numerical simulation of the model thermodynamics.

Taking into account the periodicity, one can rewrite the Hamiltonian as

$$\hat{\mathbf{H}}(\sigma_1, \dots, \sigma_L) = \sum_{l=1}^L [\hat{\mathbf{H}}_1(\sigma_l, \sigma_{l+1}) + \hat{\mathbf{H}}_2(\sigma_l, \sigma_{l+1})], \quad \sigma_{L+1} \rightarrow \sigma_1.$$

Here

$$\begin{aligned} \hat{\mathbf{H}}_i(\sigma_l, \sigma_{l+1}) = & E_0^{(i)} + (g_i \mu_B H + I_i \sigma_l) a_{i,l,1}^\dagger a_{i,l,1} + (g_i \mu_B H + I_i \sigma_{l+1}) a_{i,l,N_i}^\dagger a_{i,l,N_i} + \\ & + g_i \mu_B H \sum_{n=2}^{N_i-1} a_{i,l,n}^\dagger a_{i,l,n} - \frac{J_i}{2} \sum_{n=1}^{N_i-1} (a_{i,l,n+1}^\dagger a_{i,l,n} + a_{i,l,n}^\dagger a_{i,l,n+1}); \quad i = 1, 2 \end{aligned} \quad (2)$$

is the Hamiltonian of finite spin-1/2 XX chain with two “impurities” at both ends in terms of spinless fermions.

By means of a standard transfer-matrix scheme, we obtained the exact partition function of the above system

$$Z = \text{Tr} T^L, \quad T(\sigma_l, \sigma_{l+1}) = \exp \left[-\frac{E_0(\sigma_l, \sigma_{l+1})}{T} \right] \prod_{\lambda_1} \left[1 + \exp \left(-\frac{\varepsilon_{\lambda_1}(\sigma_l, \sigma_{l+1})}{T} \right) \right] \prod_{\lambda_2} \left[1 + \exp \left(-\frac{\varepsilon_{\lambda_2}(\sigma_l, \sigma_{l+1})}{T} \right) \right].$$

We performed numerical simulation of the low-temperature thermodynamics, such as field and temperature dependences of magnetization and specific heat, field dependences of the pairwise correlation functions for the nearest neighboring decorating spins.

EVE acknowledges support by IEEE via “Magnetism in Ukraine Initiative” (STCU project No. 9918).

- [1] E. Lieb, T. Schultz, and D. Mattis, Ann. Phys. 16, 407 (1961).
- [2] A.A. Zvyagin, Quantum Theory of One-Dimensional Spin Systems, Cambridge Scientific Publishers, Cambridge, 2010. – 330 p.
- [3] A. Klumper and D.C. Johnston, Phys. Rev. Lett., 84, 4701 (2000).
- [4] Y. Liu, J.E. Drumheller and R.D. Willett, Phys. Rev., B52, 15327 (1995).

Effect of dispersion in various liquid crystal matrices on the excitonic properties of cyanine dye J-aggregates

S. S. Hrankina^{1,2}, O. M. Samoilov¹, I. I. Grankina¹, L. N. Lisetski¹, S. L. Yefimova¹, O. V. Sorokin¹

¹*Institute for Scintillation Materials of NAS of Ukraine, 60 Nauky Ave., Kharkiv 61072, Ukraine*

²*Kharkiv National Medical University, 4 Nauky Ave., 61022, Kharkiv, Ukraine*

e-mail: holdami@ukr.net

In recent years, liquid crystals (LCs) have gained increasing attention as host matrices for incorporating and dispersing various inorganic and organic nanoparticles. This trend is evident in both fundamental research and the development of novel composite nanomaterials. A particularly intriguing aspect of these studies involves organic substances that, while exhibiting poor solubility in LC matrices, cannot be treated as conventional non-mesogenic dopants. However, with specific techniques, these substances can be successfully introduced into the orientationally ordered LC structure, influencing both phase transitions and various physical properties. In this context, J - aggregates – spontaneously formed organic nanoparticles – have attracted significant interest for their potential interactions with liquid crystals as anisotropic, ordered fluids.

J - aggregates are low-dimensional molecular crystals formed by certain organic dyes, such as cyanines and perylene derivatives. Due to their excitonic electronic excitations and characteristic one- or two-dimensional structure, J - aggregates exhibit optical properties that differ significantly from those of individual molecules or bulk crystals.

Recently, we reported the formation of J - aggregates of the anionic cyanine dye TDBC in a nematic LC matrix 5CB along with an analysis of the optical-fluorescent and electro-optical properties of the resulting novel material [1]. The TDBC J - aggregates exhibited a relatively long lifetime and high photostability within the nematic matrix. Their presence significantly modified the electro-optical characteristics of the LC matrix, leading to a slight increase in the Fredericksz transition threshold. However, this was accompanied by an improvement in optical contrast. Notably, the formation of J - aggregates had only a minor impact on the molecular order of the LC structure [1].

In the present report, we aim to compare the spectroscopic properties of TDBC J - aggregates dispersed in the nematic 5CB matrix with those for dispersions in the cholesteric M5 matrix. A cholesteric LC is a type of liquid crystal with a helical structure, in which the director's orientation periodically changes in space along a defined axis. From a thermodynamic perspective, the cholesteric phase shares the same structure as the nematic phase, but its distinguishing feature is the spatial twisting of the director, which leads to the formation of a helical structure. Due to this liquid crystal structure, the arrangement and, consequently, the excitonic properties of the J - aggregates dispersed within it will differ from those of aggregates dispersed in a nematic matrix. This report is dedicated to discussing these differences.

[1] I.I. Grankina, O.M. Samoilov, N.A. Kasian, I.Yu. Ropakova, S.S. Hrankina, S.L. Yefimova, L.N. Lisetski, O.V. Sorokin, Opt. Mat. Express 13 (6), 1741 (2023). <http://dx.doi.org/10.1364/OME.491678>.

Physical sorption of aluminum in carbon honeycomb structures: models and experiment

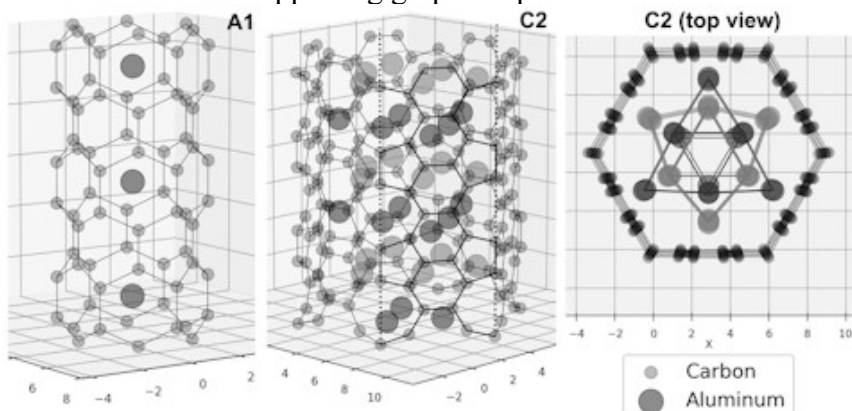
M. A. Kabanenko¹, V. O. Hamalii¹, Y. A. Mastrikov², E. A. Kotomin², N. V. Krainyukova¹

¹*B.Verkin Institute for Low Temperature Physics and Engineering of NAS of Ukraine,
47 Nauky Ave., 61103 Kharkiv, Ukraine*

²*Institute of Solid State Physics, University of Latvia, Kengaraga Str. 8, LV-1063 Riga, Latvia
e-mail: kabanenko@ilt.kharkov.ua*

The carbon honeycomb (CH) structures have demonstrated previously their high storage capacity with respect to inert and molecular gases (Kr, Xe, CO₂) due to physical absorption in their unique 3D cellular architecture [1-3] as well as their structural stability and diversity owing to different chiralities (armchair, zigzag) and wall widths [3,4]. However, it has been unclear how metal atoms will behave within the CH nanochannels.

In the present work we applied the DFT calculations to elucidate the role of a type of interatomic bonding in the anticipated uptake of aluminum in the CH channels. The theory showed that the single Al atoms put on defect-free graphene planes, constituents of the CH walls, can be successfully adsorbed with the bonding energies ~0.64 eV without any noticeable deformation of a graphene layer. If the Al configuration on graphene includes several neighboring atoms, Al atoms form a plane, which slightly moves away from a graphene surface. These results imply that the rather physical than chemical bonding is realized allowing for the relatively small bonding energies of Al on graphene and undisturbed supporting graphene planes.



We used these calculations in order to build the proper models for Al filling the CH channels of different chiralities (armchair as for the model A1 in the figure and zigzag as for the model C₂) to be compared with the electron diffraction experiments made on the CH films filled with aluminum at the room and elevated temperatures. For the thinner CH channels the behavior of Al atoms in CH channels is mainly driven only by adsorption of Al on graphene in the confined geometry, as it is shown for the model A1. We have also revealed that increasing the CH sizes results in the tendency to transform the Al clusters in a channel towards the bulk 3D structure as it is shown for the model C₂. We see in the latter case the typical HCP sequence ABAB.

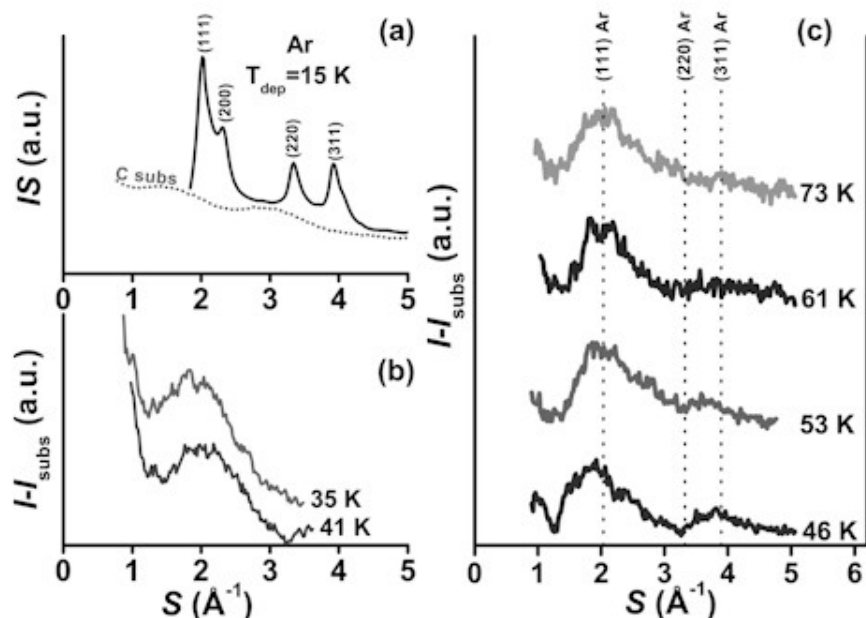
- [1] N.V. Krainyukova and E.N. Zubarev, Phys. Rev. Lett. 116, 055501 (2016).
<http://dx.doi.org/10.1103/PhysRevLett.116.055501>.
- [2] N.V. Krainyukova, Low Temp. Phys. 187, 90 (2017).
- [3] N.V. Krainyukova, B. Kuchta, L. Firlej and P. Pfeifer, Low Temp. Phys. 46, 219 (2020).
<http://dx.doi.org/10.1063/10.0000705>.
- [4] D.G. Diachenko and N.V. Krainyukova, Low Temp. Phys. 48, 232 (2022).
<http://dx.doi.org/10.1063/10.0009542>.

Selective sorption of argon in carbon honeycombs of different sizes

M. A. Kabanenko, V. O. Hamalii, N. V. Krainyukova

B.Verkin Institute for Low Temperature Physics and Engineering of NAS of Ukraine,
47 Nauky Ave., Kharkiv, 61103, Ukraine
e-mail: kabanenko@ilt.kharkov.ua

Carbon honeycomb (CH) cellular structures have been experimentally discovered and first reported in [1]. These structures are built from monolayer graphene nanoribbons joined in a 3-fold manner around the junction lines [1-3]. They are produced from graphite heated in vacuum up to the sublimation temperature when graphene patches are separated from graphite while preserving sp^2 bonds within the patches, and then either collide in vacuum forming 3-fold junction lines and/or deposit on substrates as upright standing graphene fragments. CHs have been proved to possess high absorption capacity for several gases Kr, Xe, CO₂ [1,2,4].



In the present study we have also found the high sorption capacity of CHs with respect to Ar investigated by transmission high energy electron diffraction. Figure (a) shows the diffraction pattern of the initial polycrystalline Ar deposited on CH films. Such films are then heated to temperatures close to the sublimation point of Ar in vacuum and kept at 3-4 degrees below this point. This process results in a high saturation of CHs with Ar that is well seen in the difference signal (figures (b) and (c)) between the Ar filled CH matrices and the diffraction curve for pure CHs (in figure (a)). At elevated temperatures (figure (c)) almost complete desorption of argon atoms captured in CHs occurs at temperatures more than twice higher than the sublimation point of argon in vacuum. This supports the physical absorption of argon with strong bonding in a carbon matrix. We analyze the effect of channel size on the sorption capacity and the structure of clusters formed inside the channels of different sizes in quest of realistic models describing Ar distributions in CHs.

- [1] N.V. Krainyukova and E.N. Zubarev, Phys. Rev. Lett. 116, 055501 (2016).
- [2] N.V. Krainyukova, Low Temp. Phys. 187, 90 (2017).
- [3] D.G. Diachenko and N.V. Krainyukova, Low Temp. Phys. 48, 232 (2022).
- [4] N.V. Krainyukova, B. Kuchta, L. Firlej and P. Pfeifer, Low Temp. Phys. 46, 219 (2020).

Magnetic properties of two finite spin-1/2 XX chains connected through two Ising spins

K. S. Dzhenzherova, E. V. Ezerskaya, V. O. Kovalenko

*V.N. Karazin Kharkiv National University, 4 Svoboda Sq, Kharkiv, 61022, Ukraine
 e-mail: kovalenko2020.8954539@student.karazin.ua*

The exactly solvable models like spin-1/2 XX chain attract much attention of theoreticians [1] for more than 60 years. This model is one of the theoretical instruments for checking the numerical results for more complicated spin systems, and also can be applied for description of the magnetic properties of some real compounds [2, 3].

We propose exactly solvable quantum model based on finite spin-1/2 XX chains with two bridging Ising spins, connecting XX chains at two intermediate lattice sites numbered $(1, n_1), (1, n_2), (2, n_3), (2, n_4)$. Model Hamiltonian has the form:

$$\hat{H} = -g_1 \mu_B H \sum_{n=1}^{N_1} S_{1,n}^z - J_1 \sum_{n=1}^{N_1-1} (S_{1,n}^x S_{1,n+1}^x + S_{1,n}^y S_{1,n+1}^y) - g_2 \mu_B H \sum_{n=1}^{N_2} S_{2,n}^z - J_2 \sum_{n=1}^{N_2-1} (S_{2,n}^x S_{2,n+1}^x + S_{2,n}^y S_{2,n+1}^y) - (1) \\ -g_{01} \mu_B H \sigma_1^z - g_{02} \mu_B H \sigma_2^z - J_{01} \sigma_1^z (S_{1,n_1}^z + S_{2,n_3}^z) + J_{02} \sigma_2^z (S_{1,n_2}^z + S_{2,n_4}^z).$$

Z-projections of Ising bridging spins commute with Hamiltonian (1) and are simply additional parameters $\sigma_1 = -S_1, \dots, S_1$, $\sigma_2 = -S_2, \dots, S_2$. This property permits us to consider Hamiltonian (1) as the Hamiltonians of two finite XX-chains with two effective impurity spins $S = 1/2$ at two intermediate lattice sites.

The peculiarities of field and temperature dependences of the thermodynamic characteristics of the model were investigated numerically. The behavior of the average z-projection of Ising spins and longitudinal Ising impurity spin-spin correlation functions at low temperatures have been studied numerically. It was shown that under certain conditions, the average z-spin projection for impurity spins may have the finite jumps and non-monotonic dependence on the magnetic field at very low temperatures (see Fig. 1(a, b)).

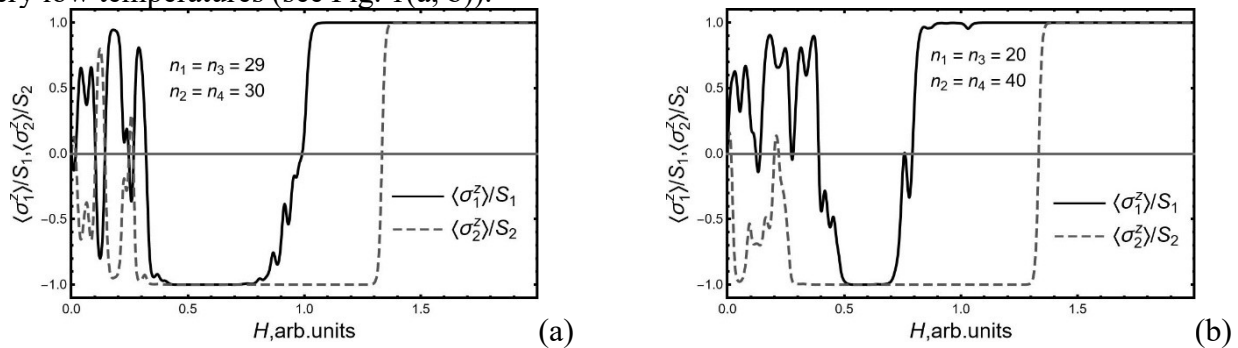


Fig. 1. $\langle \sigma_i^z \rangle / S_i$, $i=1,2$ as H at $g_1 = 1, g_2 = 2, g_{01} = 1, g_{02} = 1.5, J_1/J_2 = 2, J_{01}/J_2 = -1, J_{02}/J_2 = -2$

EVE acknowledges support by IEEE via “Magnetism in Ukraine Initiative” (STCU project No. 9918).

- [1] A.A. Zvyagin, Quantum Theory of One-Dimensional Spin Systems (Cambridge Scientific Publishers, Cambridge, 2010).
- [2] P.M. Duxbury, J. Oitmaa, M.N. Barber, A. van der Bilt, K.O. Joung, R.L. Carlin, Phys.Rev. B 24, 5149 (1981). DOI: <https://doi.org/10.1103/PhysRevB.24.5149>.
- [3] M. Kenzelmann, R. Coldea, D.A. Tennant, D. Visser, M. Hofmann, P. Smeibidl, Z. Tylczynski, Phys. Rev. B, 65, (2002). DOI: <https://doi.org/10.1103/PhysRevB.65.144432>.

Inter-strip coupling effects in graphene-based metasurface

K. S. Kuznetsova¹, Z. E. Eremenko¹, V. A. Pashynska^{1,2}

¹*Usikov Institute for Radiophysics and Electronics of the NAS of Ukraine,
12 Ac. Proskury Str., Kharkiv 61085, Ukraine*

²*B.Verkin Institute for Low Temperature Physics and Engineering of NAS of Ukraine,
47 Nauky Ave., Kharkiv, 61103, Ukraine*

Graphene-based metasurfaces have gained significant attention in recent years due to their unique and tunable optical and electronic properties, enabling precise control of plasmonic resonances that opens great possibilities for the development of sensors, absorbers, and other devices [1]. Precisely controlling surface plasmon interactions provided by the metasurface structural modifications is essential for optimizing device performance. We present a numerical study of a graphene-based metasurface integrated into a polymer and demonstrate its potential for biosensing applications. A unit cell of the metasurface consists of a thin silicon carbide (SiC) layer (thickness $t_d = 2.5 \mu\text{m}$) with a centrally positioned graphene strip with the short and long edges, $W = 0.4 \mu\text{m}$, $L = 6.36 \mu\text{m}$, respectively (Fig. 1). A gold backplane (thickness $t = 0.1 \mu\text{m}$) is positioned under SiC layer. The size along one axis is fixed ($P_1 = 7 \mu\text{m}$), while the distance between neighboring graphene strips (P) varies from 1 to 7 μm to evaluate coupling effects between graphene strips. Numerical modelling was performed in terahertz range by using COMSOL Multiphysics software to analyze the reflection coefficient S_{11} . Two resonance modes were observed at approximately $f_1 = 5 \text{ THz}$ and $f_2 = 15 \text{ THz}$ (Fig. 2). The intensity of the first resonance f_1 increased with the distance P decrease, while the second resonance f_2 remained nearly unchanged. Additional higher-order resonances were detected above 20 THz, which shifted with the P variations. Electric field distribution analysis revealed that for f_1 the maximum field concentration occurs at the narrow edges of the graphene strip W , indicating the excitation of localized surface plasmon (LSP) modes. At f_2 the electric field exhibited maximum concentration along both the short W and long L edges of the graphene strip, indicating the hybridization of surface plasmon-polariton (SPP) and LSP modes [2]. The field enhancement along the long edges suggests the contribution of propagating SPPs, while the concentration at the short edges corresponds to LSP excitation. The study results show that the f_1 resonance intensity is highly dependent on the P variations, confirming the presence of SPP interactions. The f_2 resonance exhibits minimal dependence on P , indicating a localized plasmonic nature. These findings demonstrate that tuning the inter-strip distance provides a mechanism for controlling terahertz plasmonic resonances of the metasurface. This tunability is particularly relevant for the development of reconfigurable plasmonic devices and highly sensitive biosensors operating in the terahertz frequency range [3].

[1] S. Ogawa, S. Fukushima, Sensors, 20, 12, 3563 (2020). <https://doi.org/10.3390/s20123563>.

[2] R. Alharbi, M. Irannejad, M. Yavuz, Sensors, 19, 4, 862 (2019).

[3] Q.H. Pan, J.R. Hong, G.H. Zhang, Y. Shuai, and H.P. Tan, Optics Express, 25, 14, 16400-16408 (2017). <https://doi.org/10.1364/OE.25.016400>.

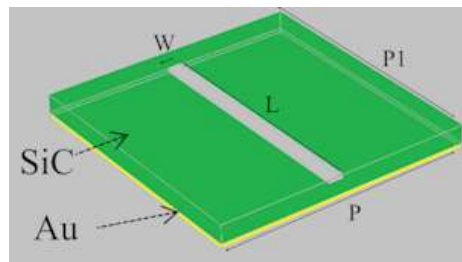


Fig. 1. The unit cell of the graphene-based metasurface, consisting of SiC layer with a centrally positioned graphene strip.

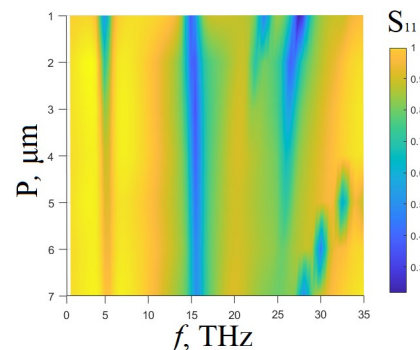


Fig. 2. The reflection coefficient S_{11} as a function of frequency and metasurface periodicity.

Information recording medium based on tunnel magnetic transitions

M. M. Krupa

*V.G. Baryakhtar Institute of Magnetism of the NAS of Ukraine,
03142, Kiev, bulv. Vernadskogo, 36-b, Ukraine
e-mail: lidermkyk@i.ua*

Although tunnel magnetic junctions (MTJs) have been studied for a long time, the prospect of practical use of MTJs has become relevant after registering a large change in resistance (TMR) and capacitance (TMC) in them when one of the magnetic electrodes is magnetized. In this report, we want to consider the mechanisms that can describe the TMR and TMC effects in tunnel magnetic junctions, as well as the schemes for constructing an information carrier based on MTJs and the principle of recording and reading information from such an information carrier.

The magnitude of the change in resistance and capacitance depends on the characteristics of the interface and the electronic structure of the contacting materials magnetic electrode/dielectric barrier nanolayer, but the effects themselves are due to the magnetoelectric effect that occurs at the interface between the dielectric and a spin-polarized metal, and which describes the response of the electric polarization of the electronic system to an applied magnetic field. In MTJs with antiparallel magnetized electrodes, the conductivity will depend on the characteristics of electron tunneling through the dielectric barrier layer and through additional energy barriers that arise in such contacts near each magnetic electrode. In such MTJs, an additional so-called spin capacitance appears, which arises due to spin-dependent diffusion of polarized electrons. Spin-dependent diffusion of polarized electrons leads to spatial separation of major and minor polarized electrons and changes in the characteristics of the dielectric constant in the magnetic metal/insulator interface region.

Record-high TMC and TMR values were obtained in MTJs in which magnesium oxide is used as an insulator. In Fe/MgO/Fe tunnel contacts, the TMC value reaches values of more than 400%, and the TMR value can be greater than TMR = 500%. Such high values of TMR and TMC can be obtained only with very good matching between the crystal lattice of the barrier nanolayer and the crystal lattice of the magnetic electrode, which is achieved when using epitaxial methods of obtaining such nanolayers. However, even with perfect matching of these lattices, significant temperature stresses will arise in the interface region, which can greatly reduce the values of the tunneling magnetic dependence and tunneling magnetoresistance.

We want to show that in MTJs with electrodes that have perpendicular anisotropy, high values of TMC and TMR can be obtained without epitaxy, which greatly simplifies their manufacturing technologies and may have good prospects for practical use in the development of spintronics elements.

Spin-boson model with time-dependent coupling to a selected vibrational mode

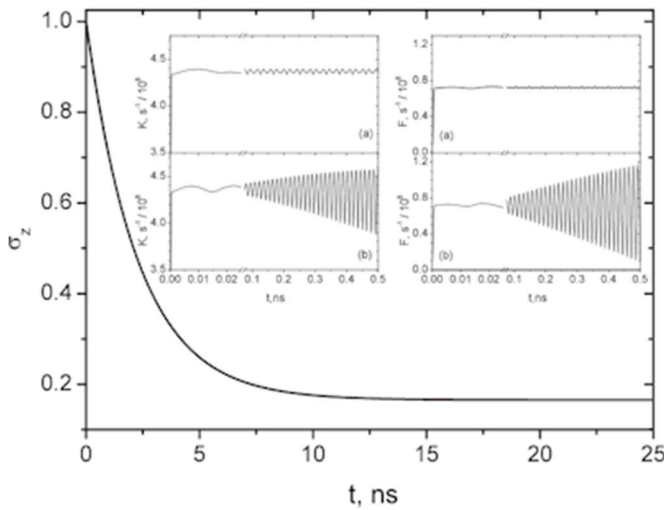
V. O. Leonov, Ye. V. Shevchenko, V. I. Teslenko, E. G. Petrov

*Bogolyubov Institute for Theoretical Physics of NAS of Ukraine,
14-b Metrolohichna str., Kyiv, 03143, Ukraine
e-mail: leogluck@gmail.com*

The master equation is derived for the state populations of a two-level system (TLS) that has a nonstationary coupling with one of the oscillation modes, while the coupling with other bath oscillation modes appears in a standard time-independent form. Using a transformation matrix of the form $R(t) = \sum_n S_n(t)|n\rangle\langle n|$ with $S_n(t) = \exp[\xi_n(t)b^+ - \xi_n^*(t)b] \times \exp \sum_j (\kappa_j/\hbar\omega_j)(b_j^+ - b_j)$,

we arrive at the Hamiltonian of the entire system SE, i.e. TLS + E (environment), in which transitions between TLS states are specified by a “phonon-dressed” transition operator $V_{12}(t) = V_{21}^*(t) = S_1(t)V_{12}S_2^*(t)$. The corresponding matrix $S_n(t)$ is specified in terms of the functions $\xi(t)$, which can be found by solving the equation $i \frac{d\xi_n(t)}{dt} = \omega_n \xi_n(t) - \kappa_n(t)$, in which $\kappa_n(t)$ is a coupling parameter containing stationary and time-dependent contributions. Having determined the probabilities of occupation of the TLS states $|n\rangle$, $n=1,2$, as $P_n(t) = \text{tr}(\rho_{SE}(t)|n\rangle\langle n|)$, where $\rho_{SE}(t)$ is the density matrix of the SE system and taking into account the fact that $P_1(t) + P_2(t) = 1$, we arrive at the following master equation for the difference in the occupation probabilities $\sigma_z(t) = P_1(t) - P_2(t)$:

$$\dot{\sigma}_z(t) = - \int_0^t g(t, t-\tau) \sigma_z(t-\tau) d\tau - \int_0^t f(t, t-\tau) d\tau$$



the process of hopping transitions between TLS states. When the frequency of the non-stationary coupling to the selected vibration mode matches the frequency of that mode, the fast stage of establishment of the quasi-stationary mode for the occupation probabilities exhibits resonant behavior over time. This is a direct demonstration of the role of nonstationary coupling in the dynamics of the behavior of state occupation probabilities within the spin-boson model.

Here, the functions $g(t, t-\tau)$ and $f(t, t-\tau)$ are specified by the couplings $\kappa_n(t)$ and hopping parameter $V \equiv V_{12} = V_{21}^*$ [1]. The Figure 1 shows one of the versions for establishing of a three-stage establishment for the probability of quasi-stationary occupancies caused by the coupling of TLS states with the phonon bath under conditions when one of the couplings has a periodic time dependence. Two fast stages are associated with stationary and non-stationary couplings of TLS states with environmental vibrations, and a slow stage with a scale of about 1 ns directly reflects

[1] E.G. Petrov, Ye.V. Shevchenko, V.O. Leonov, V.I. Teslenko, Ukr. J. Phys., 69, 522-561 (2024).

Resonances in a chain of bimetallic nanoparticles on a dielectric substrate

M. S. Maniuk¹, A. V. Korotun^{1,2}, V. P. Kurbatsky¹

¹National University Zaporizhzhia Politechnic, 64 University Str., Zaporizhzhia, 69063, Ukraine

²G.V. Kurdyumov Institute for Metal Physics of the NAS of Ukraine,

36 Academician Vernadsky Blvd., Kyiv, 03142, Ukraine

e-mail: andko@zp.edu.ua

Chains of plasmonic nanoparticles are currently being actively studied with a view to their use as a possible design for optical radiation waveguides. This application is associated with the propagation of plasmons in them with a transverse localization size significantly smaller than the wavelength of light. The scientific literature has already described studies of chains of monometallic nanoparticles of various shapes (spherical, prolate and oblate spheroids) [1]. One of the most important parameters of such systems is the frequency of the collective (chain) resonance. It is known that in the case of isolated nanoparticles, bimetallic nanoparticles are more effective in terms of plasmon resonance regulation due to the additional ability to change the core size and shell thickness [2]. Therefore, we should expect an expansion of such capabilities for controlling collective resonances in chains of bimetallic nanoparticles.

Let the chain under study be located on a dielectric substrate with permittivity T_d in a medium with permittivity T_m . The transverse component of the polarizability tensor of the chain under consideration is determined by the relation:

$$\alpha_{\perp}^{\text{chain}} = \frac{\alpha_{\perp}(\omega)}{1 - \frac{\alpha_{\perp}(\omega)}{d^3 T_m} \left(S_{\perp}^d + \frac{T_d - T_m}{T_d + T_m} S_{\perp}^i \right)}, \quad (1)$$

where d is the distance between particles in the chain; S_{\perp}^d and S_{\perp}^i are chain sums describing the interaction between particles in the chain and the interaction with the image dipoles; α_{\perp} is the polarizability of an isolated bimetallic nanoparticle.

The condition of collective resonance in the non-dissipative approximation is the equality to zero of the denominator of expression (1), from which we obtain a biquadratic equation for the resonance frequency ω_{res} with two real roots and two imaginary ones. The real roots are equal to the frequencies of collective (chain) resonance, which depend on the material of the nanoparticles, the substrate and the environment, the distance between the particles in the chain, the size of the core and the thickness of the particle shell.

- [1] M.S. Maniuk, A.V. Korotun, V.P. Kurbatsky, Low Temp. Phys. 51, 156 (2025).
<http://dx.doi.org/10.1063/10.0034659>.
- [2] A.V. Korotun, A.O. Koval, V.V. Pogosov, Ukr. J. Phys. 66, 518 (2021).
<http://dx.doi.org/10.15407/ujpe66.6.518>.

Fetal bovine serum-mediated enhancement of cerium oxide-based luminescent sensors for hydrogen peroxide detection

Ye. Neuhodov¹, P. Maksimchuk¹, G. Grygorova¹, A. Onishchenko², N. Kavok¹, G. Dudetskaya¹, Yu. Kot³, S. Yefimova¹, V. Seminko¹

¹*Yu.V.Malyukin Department of Nanostructured Materials, Institute for Scintillation Materials NAS of Ukraine, 60 Nauky Ave., Kharkiv, 61072, Ukraine*

²*Department of Physics, Kharkiv National University of Radio Electronics, 14 Nauky Ave., Kharkiv, 61166, Ukraine*

³*School of Biology, V. N. Karazin Kharkiv National University, 14 Svobody sq., Kharkiv, 61022, Ukraine
e-mail: pavel.maksimchuk@gmail.com*

Reactive oxygen species (ROS) such as hydrogen peroxide (HP), hydroxyl radicals and superoxide anions play a significant role in biological processes utilized by living cells as signaling molecules and immune agents. At the same time, an increase of the level of ROS within cells can trigger inflammation, DNA and protein damage, and even cell death [1]. Therefore, controlling the level of ROS in biological systems is a challenging task.

For luminescent HP sensing both organic molecules (such as dichlorodihydrofluorescein diacetate, dihydrorhodamine and Amplex Red (Invitrogen)) and inorganic NPs are used [2]. Inorganic HP sensors have an advantage of higher stability and reversibility compared to organic molecules. Another advantage of HP sensors based on doped NPs compared to organic sensors is the ability for time-resolved measurements providing the change of HP concentration in dynamics, while the organic sensors are non-reversible and therefore can detect the total amount of HP generated, but not the instantaneous HP concentration [3]. In this study Ce³⁺ luminescence intensity of cerium oxide NPs is used for monitoring the HP concentration.

Luminescent sensors based on the FBS-stabilized cerium oxide nanoparticles have a number of advantages when using for hydrogen peroxide sensing in biological media with high ionic strength. The fetal bovine serum both improves the colloidal stability of cerium oxide nanoparticles and stimulates Ce⁴⁺ → Ce³⁺ reduction leading to an increase in the intensity of Ce³⁺ luminescence of cerium oxide nanoparticles. FBS-stimulated increase in the luminescence intensity of NPs provides higher sensitivity to HP with linear concentration dependences from tens of μM to hundreds of mM. The luminescence sensors based on the FBS-stabilized cerium oxide nanoparticles are reversible due to Ce^{3+↔ Ce⁴⁺ regeneration ability in nanoceria and able for multi-use in biological media.}

Acknowledgments: This research was supported by National Research Foundation of Ukraine, Grant № 2023.03/0050.

- [1] B. Halliwell, J.M. Gutteridge, Free radicals in biology and medicine, fifth ed., Oxford University Press, Oxford, 2015.
- [2] M. Schäferling, D.B.M. Grögel, S. Schreml, Luminescent probes for detection and imaging of hydrogen peroxide, *Microchim. Acta*. 174 (2011) 1 – 18.
- [3] Y. Malyukin, V. Seminko, P. Maksimchuk, E. Okrushko, O. Sedyh, Y. Zorenko, Hydrogen peroxide sensing using Ce³⁺ luminescence of cerium oxide (CeO_{2-x}) nanoparticles, *Opt. Mater.* 85 (2018) 303 – 307. <https://doi.org/10.1016/j.optmat.2018.08.063>.

Magnetic and magnetotransport properties of modified by cobalt carbon nanotubes

I. Ovsiienko¹, D. Shpylka¹, T. Len¹, L. Matzui¹, A. Sedda², E. Lähderanta^{2, 3,4}, A. Terekhov⁴, I. Mirzoiev⁴

¹Taras Shevchenko National University of Kyiv, Departments of Physic,
 Volodymyrska Str., 64/13, 01601, Kyiv, Ukraine

²Lappeenranta University of Technology, School of Engineering Science,
 53850, Lappeenranta, Finland

³Institute for Low Temperatures and Structure Research, Polish Academy of Sciences,
 50-422 Wroclaw, Poland

⁴B.Verkin Institute for Low Temperature Physics and Engineering of NAS of Ukraine,
 47 Nauky Ave., 61103, Kharkiv, Ukraine
 e-mail: iaryna2002@gmail.com

The temperature and field dependences of magnetization and magnetoresistance in cobalt-modified multiwall carbon nanotubes (MWCNTs) are investigated. The modification of MWCNTs with cobalt (30% mass) has been performed by the method of metal reduction from aqueous salt solution. According to structural and phase investigations modified MWCNTs contain cobalt (ferromagnetic phase) and cobalt oxide (CoO) (antiferromagnetic phase with Neel temperature $T_N = 291$ K) particles up to 3 nm in size. Cobalt and cobalt oxide particles are distributed in internal cavity of MWCNTs and at the ends of tubes. The resistance and magnetization have been measured in the temperature interval from 3 K to 293 K and in the magnetic fields up to 2.2 T.

Figure presents the field dependences of magnetization (hysteresis loops) at different temperatures (a), the temperature dependence of magnetization in the modes of cooling in zero magnetic field (ZFC) and cooling in magnetic field (FC) (b) and magnetoresistance $\Delta\rho/\rho_0(B)$ ($T = 293$ K) at parallel mutual orientation of the magnetic field and current through specimen for bulk specimen of modified by Cobalt MWCNTs (c)

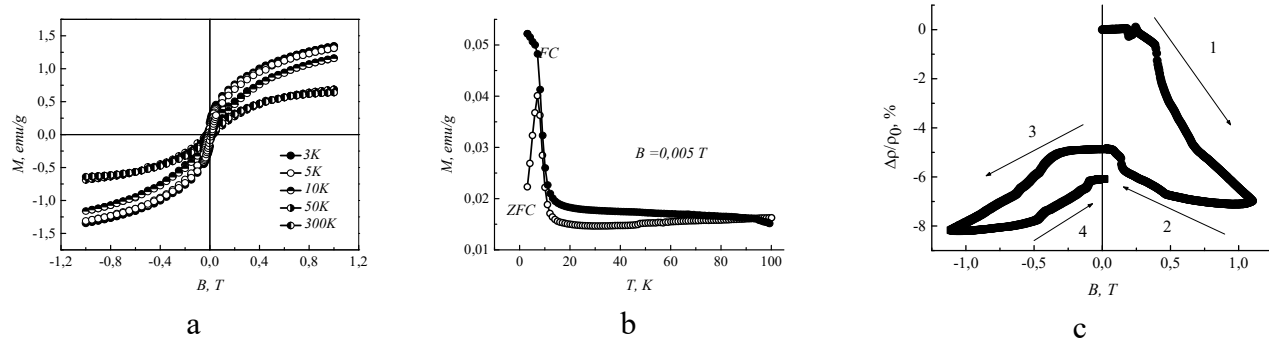


Fig. Dependences $M(B)$ at different temperatures (a), $M(T)$ for FC and ZFC modes (b) and field dependence of magnetoresistance $\Delta\rho/\rho_0(B)$ ($T = 293$ K) for bulk specimen of cobalt-modified MWCNTs. Arrows and numbers indicate the sequence of measurements

The $M(T)$ dependences for FC and ZFC modes, as shown in the figure, diverge indicating a superparamagnetic state of cobalt particles in the MWCNTs. The presence of cobalt particles in a superparamagnetic state is also evidenced by the absence of saturation in the hysteresis loops at low temperature. The $\Delta\rho/\rho_0(B)$ dependence at $T = 293$ K exhibits pronounced hysteresis, symmetrical to the magnetic field direction. This type of $\Delta\rho/\rho_0(B)$ dependence is characteristic for systems containing ferromagnetic and antiferromagnetic phases and is associated with the realization of the effect of the giant magnetoresistance due to exchange anisotropy that occurs between the layers of ferro- and antiferromagnets.

Josephson junctions with barrier from semiconductor doped by metal

V. E.Shaternik, A. P. Shapovalov

*G.V.Kurdyumov Institute for Metal Physics, 36 Vernadskii blvrd, 03142, Kyiv, Ukraine,
e-mail: Shaternikvolod@gmail.com*

Technologically, Josephson junctions are manufactured either in the form of thin-film superconductor-insulator (or metal)-superconductor structures or in the form of point contact of superconductors. The disadvantage of thin-film junctions is their relatively large capacity, which reduces the speed of these junctions and their operating frequencies. The point contacts junctions have an attractive negligible capacitance, but are mechanically unstable in operation. The aim objective of the study was to develop and manufacture Josephson junctions that would be free from the above-mentioned drawbacks. Currently, nanostructured Josephson heterostructures are considered to be one of the most promising, in which charge transport occurs through energy states localized in their amorphous semiconductor barriers.

Thin-film MoRe-Si(W)-MoRe junctions were fabricated by magnetron sputtering of targets in an argon atmosphere, followed by deposition of thin films through metal masks on polycrystalline aluminum oxide (polycor) substrates or on sapphire substrates.

The Si(W) barrier films were formed by sputtering a complex target consisting of a single-crystal silicon Si plate, on the surface of which tungsten W wires of 0.3 mm thickness and about 10 mm length were laid in the amount of 20–30 pieces. The manufactured thin amorphous MoRe films had a critical superconducting transition temperature $T_C \approx 9.1$ K.

The Si(W) barrier films had a thickness of several nanometers. But the study of transmission electron microscopy of thicker Si(W) films produced under the same technological conditions showed that clusters of amorphous tungsten W are formed in amorphous silicon films Si. A typical I-V characteristic of one of the MoRe-Si(W)-MoRe junctions is shown in Fig.1.

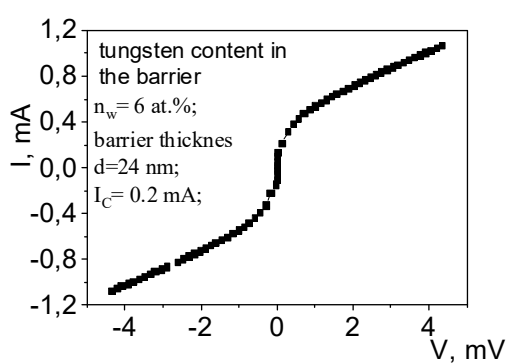


Fig.1. I-V characteristic of one of the MoRe-Si(W)-MoRe junctions.

The experimental I-V characteristics of the MoRe-Si(W)-MoRe junctions are compared with those calculated within the framework of the multiple Andreev reflection model [1]. It is shown that the junctions behave as having a set of barrier sections with high transparency close to unity.

It is emphasized that due to the use of barriers of a new type (semiconductor doped with metal), the specific capacitance and, consequently, the capacitance of thin-film Josephson tunnel junctions decreases by at least an order of magnitude, which is extremely important from the point of view of practical applications of these new type junctions. It is also emphasized that, although the created junctions may have a current-voltage characteristic

of S-N-S junctions, nevertheless, the well-known undesirable effect of proximity between these S and N layers does not occur in such junctions, which is also extremely important from the point of view of practical applications of these new type of Josephson junctions.

[1] M. Hurd, S. Datta, P.F. Bagwell, Physical Review B - Condensed Matter and Materials Physics 56, 11232 (1997). <https://doi.org/10.1103/PhysRevB.56.11232>.

Dielectric properties of layer crystals and nanostructures based on them

B. O. Seredyuk¹, M. S. Karkulovska², N. K. Tovstyuk², O. Y. Mykytiuk³.

¹*National Army Academy named after Hetman Petro Sahaidachnyi,
32 Herojiv Maidanu str., Lviv, 79032, Ukraine*

²*Institute of Mathematics and Applied Physics, Lviv Polytechnic National University,
12 Bandera str., Lviv, 790012, Ukraine*

³*Bukovinian State Medical University, 4 Teatral'na Sq., Chernivtsi, 58000, Ukraine
e-mail: b.seredyuk@gmail.com*

The paper examines the influence of the dimensionality of the crystal structure on the calculations of the frequency and dispersion dependence of the components of the dielectric function (or absorption coefficient and refractive index) for crystals of different dimensions in the random phase approximation.

The influence of the anisotropic environment on the dynamic and static components of the z -th component of the dielectric constant ε_{zz} is studied through the non-parabolic law of electron dispersion. It is shown that in one-dimensional systems ($\alpha=0$) in the static case ($\Omega=0$), the behavior of $\varepsilon_1(q)$, $\varepsilon_2(q)$ dependence and extrema on the corresponding curves are related to singularities in the real component of the polarization loop at $q=2k_F$ and $q=2(\pi-k_F)$. In the dynamic case ($\Omega \neq 0$), with increasing frequency, the dielectric function $\varepsilon_1(q, \Omega)$, decreases in magnitude, while in the frequency interval $\Omega < 2t$ it has a sign-changing character, and at $\Omega > 2t$ - oscillating, but without singularities, and a $\varepsilon_2(q, \Omega)$, decreasing function, which at $\Omega > 2t$ becomes zero because then $\text{Im}\Pi(q, \Omega)=0$.

Numerical calculations of the quasi-two-dimensional and three-dimensional cases ε_1 , ε_2 were carried out for the following positions of the Fermi energy level: i) $\varepsilon_F < 2t$, ii) $\varepsilon_F > 2t$. The frequency dependence of $\varepsilon_1(\Omega)$ and $\varepsilon_2(\Omega)$ was calculated for small ($q_x=q_y=0$, $q_z=0.01$), and ($q_x=q_y=q_z=0.01$), $\alpha=0.10$ eV, $t=0.01$ eV.

In the two-dimensional case ($t=0$), the sharp minimum of $\text{Re}\Pi$ ($\text{Re}\Pi=-7.42*10^{-2}$) is realized at $\Omega=1.5*10^{-3}$ eV. When we talk about the "anisotropy" of a chemical bond, it follows from the comparison of the dispersion curve in different directions of the inverse space.

The optical characteristics were also analyzed, namely the frequency dependence of the absorption coefficient (χ) and refractive index (n) for different values of the position of the Fermi level. They were obtained with the help of the found real and imaginary components of the dielectric constant due to the validity of the Kramers-Kroning relation in the entire frequency range. The obtained results were compared with experimental measurements of optical spectra of both crystals and films cadmium iodide at low temperatures.

BIOPHYSICS AND PHYSICS OF MACROMOLECULES

Peculiarities of a nanocomposite of molybdenum disulfide with cysteine amino acid as revealed by laser desorption/ionization mass spectrometry

M. V. Kosevich¹, V. S. Shelkovsky¹, O. A. Boryak¹, P. O. Kuzema², V. A. Karachevtsev¹

¹B. Verkin Institute for Low Temperature Physics and Engineering of the NAS of Ukraine,
47 Nauky Ave., Kharkiv, 61103, Ukraine

²Chuiko Institute of Surface Chemistry of the NAS of Ukraine,
17 General Naumov Str., Kyiv, 03164, Ukraine
e-mail: mvkosevich@gmail.com

Spectroscopic experimental techniques, including mass spectrometry, are invented to obtain scientific information on natural or artificial objects. Along with analytical identification of substances, modern mass spectrometry permits monitoring of various processes in the systems under study, which is relatively easy to achieve for the samples in the gas or liquid state. Reconstruction of events in the solid sample on the basis of its mass spectra is more sophisticated. In the present work we have applied laser desorption/ionization (LDI) mass spectrometry to exploration of molecular processes in nanomaterials composed of MoS₂ and amino acid cysteine (Cys). (MoS₂ + Cys) nanocomposite was produced by ultrasound treatment of an aqueous mixture of the two substances. Combination of inorganic and organic components is aimed at obtaining a nanomaterial with new properties. If this goal is successfully achieved, the mass spectrum of the nanocomposite must differ from the simple superposition of the spectra of individual components. The aim of the present investigation was to reveal what features of the LDI mass spectra of the (MoS₂ + Cys) nanocomposite reflect certain processes and interactions occurring in this system. The expectations are based on a possibility of interactions between sulfur atoms of MoS₂ and thiol group of cysteine.

LDI mass spectra of cysteine (C₃H₇NO₂S, m.w. 121 a.u.) contained protonated [Cys + H]⁺, cationized [Cys + Na]⁺, and deprotonated [Cys - H]⁻ molecules. LDI mass spectra of MoS₂ contained sets of clusters Mo_xS_yO_z⁻ (x=1-4, y=1-6, z=0-6) in the negative ion mode [1].

The main distinctive feature of LDI mass spectra of (MoS₂ + Cys) nanocomposite was the appearance of the peaks corresponding to cysteine covalent dimer (2Cys - 2H) bound by -S-S-disulfide bond, which is formed due to catalytic activity of MoS₂ [2] and was recorded as [(2Cys - 2H) + H]⁺, [(2Cys - 2H) + Na]⁺, [(2Cys - 2H) + K]⁺, and [(2Cys - 2H) - H]⁻ ions.

Physical adsorption of cysteine and its reduction product at the surface of MoS₂ nanosheets causes so-called shielding effect, which is reflected in suppression of sputtering of Mo_xS_yO_z⁻ clusters with x>2 under LDI.

Interaction of thiol group of cysteine with terminal sulfur atoms at the edges of MoS₂ sheets is reflected in cleavage of the sulfur atoms in complex with cysteine recorded as [Cys - H + S]⁺, [Cys - H + S]⁻ ions. Naked in this process, the terminal molybdenum atom can be cleaved from the nanosheet under LDI, which is reflected in appearance of Mo⁺ ion in the positive ion mode.

In nanotechnology, thiols, including cysteine, are applied for “healing” of S-vacancies defects at the MoS₂ surface [2]. In the case of insertion and incorporation of the sulfur atom of cysteine molecule into the surface layer of MoS₂, the laser pulse under LDI may cause thermal desorption of the remaining fragment of cysteine, which is recorded indeed as [Cys - SH]⁺ ion.

Thus, at least five distinctive features of the (MoS₂ + Cys) nanocomposite can be deduced from the analysis of its LDI mass spectra obtained both in the positive and negative ion modes.

This work was supported by the Grant 0123U100628 of the NAS of Ukraine.

- [1] O. A. Boryak, M. V. Kosevich, V. A. Pashynska, P. O. Kuzema, and V. A. Karachevtsev, *Him. Fiz. Tehnol. Poverhni* (2025) in press.
- [2] X. Chen, N. C. Berner, C. Backes, G. S. Duesberg, and A. R. McDonald, *Angew. Chem. Int. Ed.* 55, 5803 (2016). <https://doi.org/10.1002/anie.201510219>.

Characteristic features of lipid domains formed by the mechanism of binding depending on surroundings - "preferential binding": results of computer simulation

R. Ye. Brodskii¹, O. V. Vashchenko²

¹ Institute for Single Crystals of NAS of Ukraine, 60 Nauky Ave., Kharkiv, 61072, Ukraine

² Institute for Scintillation Materials of NAS of Ukraine, 60 Nauky Ave., Kharkiv, 61072, Ukraine
e-mail: r.brodskii@gmail.com

Formation of lipid domains as intrinsic feature of lipid membranes possesses large and still undisclosed regulatory potential in many living processes. At present, there is clearly a need for quantitative characterization of lipid domain patterns obtained in both experiments and simulations. Spontaneous dopant-driven formation of lipid domains was experimentally observed in a monolipid membrane for dopants with bimodal adsorption. An underlying mechanism of domains formation in such a case is dopant binding ‘like the surroundings’, i.e. preferential binding [1]. Basing on this mechanism, we developed a numerical model and obtained lipid domain patterns corresponding to various simulation parameters. The main simulation parameters were the binding probabilities ‘like the surroundings’ (p_{same}), ‘opposite to the surroundings’ (p_{other}) and to neat membrane (p_0). Among the relevant characteristic features of lipid domains formed, there were suggested domain size distribution, the average size $\langle s_L \rangle$ of the largest lipid domains [1] as well as the fraction v_{same} of cells surrounded by the same type cells.

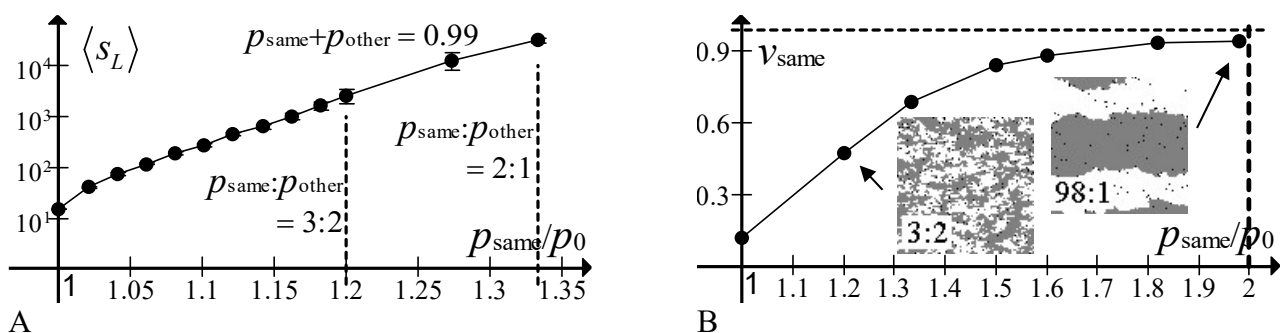


Fig. 1. A: The average size $\langle s_L \rangle$ of the largest lipid domains as a function of $p_{\text{same}} : p_0$ [1]. The mean values and the standard deviations over 10 generation are shown. B: The fraction v_{same} as a function of $p_{\text{same}} : p_0$. The dotted line corresponds to v_{same} value obtained for a single round large domain. Inset: typical membrane patterns for different $p_{\text{same}} : p_{\text{other}}$ ratios (signed on pictures).

The range of the simulation parameters was determined, where density of domain size distribution is power-law, $p(s) \propto s^{-k}$, where lower k values indicate greater portion of larger domains, and *vice versa*. However, even slight variations in $p_{\text{same}} : p_{\text{other}}$ ratio cause visually pronounced alterations in membrane dispersion accompanying with significant changes of $\langle s_L \rangle$ and v_{same} . Visually traced modifications of domain patterns correspond to changes in largest lipid domains. Fig. 1A shows $\langle s_L \rangle$ elevation by orders of magnitude under $p_{\text{same}} : p_{\text{other}}$ changes from 1 to 2. For clarity, the dependences were plotted as a function of $p_{\text{same}} : p_0$, where $p_0 = (p_{\text{same}} + p_{\text{other}})/2$ was taken. Highly dispersed membrane is characterized by low v_{same} values and behaves as a physically homogeneous medium, whereas low dispersion causes physical inhomogeneity. The dependence of v_{same} shown in Fig. 1B allows us to determine the threshold between these cases. Thus, the suggested set of the characteristic features provide an adequate description of the lipid domain patterns and the related membrane properties.

Anticancer drugs interactions with the drug delivery nanostructures: mass spectrometry insight

V. A. Pashynska¹, M. V. Kosevich¹, O. A. Boryak¹, I. M. Voloshin¹, P. O. Kuzema²,
V. A. Karachevtsev¹

¹*B. Verkin Institute for Low Temperature Physics and Engineering of the NAS of Ukraine,
47 Nauky Ave., Kharkiv, 61103, Ukraine*

²*Chuiko Institute of Surface Chemistry of the NAS of Ukraine, 17 General Naumov Str.,
Kyiv, 03164, Ukraine
e-mail: vlada.pashynska@gmail.com*

The biophysical aspect of the drug delivery problem is associated with the examining of molecular interactions of drug delivery nanostructures with the medicines molecules to be transported. It is important to elucidate whether the drug delivery system can be effectively uploaded by the drugs and whether the interaction of the medicine molecules with the delivery system elements does not change the drugs' activity that is definitely determined by chemical structure stability of the medicinal agent. Among the nanostructures promising for drug delivery the two-dimensional transition metal dichalcogenides, in particular MoS₂, are in the focus of the current research owing to their biocompatibility and unique physicochemical properties of MoS₂ 2D nanosheets. These properties provide the possibility of the nanomaterial utilization not only for the drugs transportation but also for photothermal therapy (PTT) of cancers. In our recent research we characterized MoS₂ nanostructures by the matrix-free laser desorption/ionization (LDI) mass spectrometry (MS) that confirmed the efficiency of this method for nanotechnological applications as well as for the study of interactions of MoS₂ with biologically active compounds [1].

In the current research the biophysical aspects of interactions within nanocomposites containing MoS₂ nanosheets and selected anticancer drugs doxorubicin (DOX), 6-thiopurine (TP), and 2-thioadenine (TA) were studied by LDI MS. The nanocomposites were obtained by two different ultrasound-treatment regimes (as described in [1]), which allowed evaluating the sonication conditions on the (MoS₂ + drug) nanocomposite production. Analysis of the mass spectra of samples of (MoS₂ + DOX) nanocomposite revealed the intensive peak of DOX molecular ion existence in the spectra that confirmed the DOX molecule stability within the composite. The molecular structure stability is crucial for DOX therapeutic activity preservation. The observed in the spectra changes in the MoS₂ characteristic peaks intensity distribution pointed to active exfoliating role of DOX in ultrasound technology of MoS₂ nanosheets production. The LDI mass spectra of nanocomposites of MoS₂ with anticancer thioderivatives of nucleobases (MoS₂ + TA) and (MoS₂ + TP) indicated that along with the presence in the mass spectra the molecular ions of TA and TP, the relative intensity of peaks of covalent dimers of thioderivatives was higher for the nanocomposite in comparison with the spectra of pure drugs. Moreover, in the positive ion spectrum of (MoS₂ + TP) sample there were molybdenum-containing peaks that can be attributed to the product of covalent interactions of MoS₂ or its oxidation products with the drug molecules. The results obtained testify to the idea that interaction of these sulfur containing anticancer drugs with nanostructures of MoS₂ (known as catalytically active material) can affect the chemical structure of the drug molecules and, consequently, their therapeutic activity.

This work was supported by the National Academy of Sciences of Ukraine (Grant 0123U100628). LDI mass spectrometric studies have been carried out using the equipment of the Center for collective use of scientific instruments/equipment "Mass spectrometry and liquid chromatography" of the National Academy of Sciences of Ukraine.

[1] O. Boryak, M. Kosevich, V. Pashynska, P. Kuzema, V. Karachevtsev; Him. Fiz. Tehnol. Poverhni., In press (2025).

Cellular approach to the zeta potential of aqueous-salt albumin solutions

O. D. Stoliaryk¹, A. A. Guslisty², O. V. Khorolskyi³

¹*Odesa I. I. Mechnikov National University,*

²*Dvoryanska Str., Odesa, 65082, Ukraine*

²*Family Medicine Center Amedika LLC,*

^{103b} *Semena Paliya Str., Odesa, 65123, Ukraine*

³*Poltava V. G. Korolenko National Pedagogical University,*

²*Ostrogradskogo Str., Poltava, 36003, Ukraine*

e-mail: khorolskiy.alexey@gmail.com

The research is devoted to the study of the properties of the zeta potential of human serum albumin. This electrostatic characteristic of the albumin macromolecule is determined by the distribution of charges inside and around the albumin macromolecule. For the calculation, a model is usually used in which the potential is related to the distribution of charges and is described by electrostatic equations and boundary conditions. Within the framework of this cellular approach, the zeta potential is found to be a function of the radius of the albumin macromolecules (r_a), the thickness of the diffuse layer (r_D), and the cell radius (r_c), in the case when the diffuse electric layers of neighboring albumin macromolecules overlap. Within the framework of this approach, in the work [1] it was shown that the zeta potential of human serum albumin is equal to:

$$\zeta_a \approx \frac{4\pi\sigma}{\varepsilon} r_D \left[\tanh\left(\frac{r_c - r_a}{r_n}\right) - \frac{r_D}{r_n} \tanh^2\left(\frac{r_c - r_a}{r_n}\right) + \dots \right],$$

Where σ is the surface charge density of the albumin macromolecule, ε is the dielectric permittivity of water.

It has been established that the asymmetry of the dependence of the zeta potential of albumin macromolecules on the difference ($pH - pH_0$) does not exceed 30%, where pH_0 is the value of the acid-base balance at the isoelectric point.

The study of the dependence of the zeta potential of albumin macromolecules on the pH of their aqueous solution revealed its similarity to the behavior of the magnetization of paramagnets as a function of magnetic field. The nature of the dependence of the zeta potential of albumin macromolecules on the pH of their aqueous-salt solutions has been determined, based on the equation of magnetization of paramagnets.

The similarity of the behavior of the zeta potential of albumin macromolecules and paramagnets in the vicinity of a singular point of 42°C gives grounds for the application of the theory of second-order phase transitions on the electrophysical properties of aqueous albumin solutions [2]. Near the singular point, the behavior of the zeta potential dependence as the pH function has a linear character. This region of linear dependence $\zeta_a(pH)$ coincides with the area of application of the Landau theory. Moreover, the existence of all living things coincides with the area of linear dependence of the zeta potential on pH [3]. We assume that all vital processes are on the border that separates the area of application of the Landau theory and the electrophysical properties of albumin.

[1] O. Stoliaryk, A. Guslisty, and O. Khorolskyi, Ukr. J. Phys. 68, 742 (2023). <https://doi.org/10.15407/ujpe68.11.742>.

[2] O. V. Khorolskyi, N. P. Malomuzh. Macromolecular sizes of serum albumins in its aqueous solutions. AIMS Biophysics. 7, 219 (2020). <https://doi.org/10.3934/biophys.2020017>.

[3] A. A. Guslisty, N. P. Malomuzh, and A. I. Fisenko. Optimal temperature for human life activity. Ukr. J. Phys. 63, 809 (2018). <https://doi.org/10.15407/ujpe63.9.809>.

Thermal profiles of unloaded liposomes and liposomes with MoS₂ nanoparticles

M. V. Olenchuk, Eu. O. Andreev, Yu. M. Barabash, G. I. Dovbeshko

*Institute of Physics of NAS of Ukraine,
46 Nauky Ave., Kyiv, 03028, Ukraine
e-mail: m.olenchuk@yahoo.com*

The study of cell temperature and thermogenesis is a complex but important task in biology and medicine. Innovative temperature measurement methods are split into three groups: localized contact, non-contact and global measurement methods. Each of them has their pros and cons. Contact methods affect the cells' local temperature and can damage the cells. Non-contact methods are not as accurate as contact methods. Global methods are the most accurate, but they do not give local temperature, but only global temperature. All methods combined offer new insights into the metabolic states of the cell and will expand our understanding of cellular thermodynamics.

A non-contact method for measuring the thermal profile of a sample was proposed. A device has been developed that measures in real time the change in infrared radiation of a sample when it is irradiated with visible light. In this case, both the intensity and time of exposure can be controlled.

Spatiotemporal variations in thermal profiles have been numerically studied for DOPC liposomes as a model system, DOPC liposomes with the addition of MoS₂ nanoparticles. The results obtained show that the greatest changes in ΔT occur for DOPC liposomes with the addition of MoS₂ nanoparticles. It was found that relaxation coefficients correlate with the thermophysical properties of the samples. The results obtained are useful for understanding the influence of environmental factors. These thermal profiles can be used in diagnosing cancer cells [1].

This work was supported by NRFU Project, No 2021.01/0229 “Biophysical characteristics of circulating metastatic cells as potential targets of antimetastatic therapy”.

- [1] M. M. Savitski, F. B. Reinhard, H. Franken, T. Werner, M. F. Savitski, D. Eberhard, D. Martinez Molina, R. Jafari, R.B. Dovega, S. Klaeger, B. Kuster, P. Nordlund, M. Bantscheff, G. Drewes, *Science* 346 (6205), 1255784 (2014). <https://doi.org/10.1126/science.1255784>.

Nanohybrids of uracil with graphene and noble metal nanoclusters

T. Piddubnyi¹, S. Stepanian¹, L. Adamowicz²

¹*B.Verkin Institute for Low Temperature Physics and Engineering of NAS of Ukraine,
47 Nauky Ave., Kharkiv, 61103, Ukraine*

²*Department of Chemistry and Biochemistry, University of Arizona, 85721 Tucson AZ, USA
e-mail: piddubnyi@ilt.kharkov.ua*

In this work, we present the results of a computational study of the structure, energetic and spectral properties of ternary complexes that include graphene, gold or silver nanoparticles and the uracil molecule. The calculations were performed using the quantum-mechanical DFT method with the density functional M06-2X. In the calculations, we used the Stuttgart RSC 1997 ECP basis set for gold and silver atoms and the 6-31+G* basis set for graphene and uracil. The graphene surface is represented by a fragment that includes 96 carbon atoms and is terminated by 24 hydrogen atoms. Silver and gold particles consist of 10 metal atoms. For clusters of this size, both flat and 3D stable structures are possible. Calculations of the structure of silver and gold particles demonstrated the existence of 15 stable structures for Au_{10} and 21 for Ag_{10} . Next, for the most stable metal particles, calculations of their binary complexes with graphene were performed. After that, a third component (uracil molecule) was added to the discovered graphene-metal particle structures. Totally we located 18 unique Gr- Ag_{10} -Ura and 20 Gr- Au_{10} -Ura structures and determined their relative stabilities and interaction energies between their components. The natural bond orbital (NBO) population analysis was performed to elucidate the nature of the interactions in the ternary complexes.

The complexes were shown to be stabilized by three types of intermolecular interactions: cation-p interactions between the graphene surface and gold or silver particles, coordination bonds between the atoms of the metal particles and the oxygen atoms of uracil, and p-p stacking interactions between the uracil molecule and the graphene surface. ZPVE and BSSE corrected interaction energies between the uracil molecule and metal particles range from -8 to -17 kcal/mol and depend significantly on the structure of the particles. It should be noted that the structure of both gold and silver particles in most complexes changes significantly as a result of interaction with both graphene and uracil. The interaction energies of graphene with gold and silver particles also depend significantly on the structure of the particles. The strongest interactions with graphene are observed for planar gold and silver particles. ZPVE and BSSE corrected interaction energies for the complexes are -68.1 kcal/mol for the Gr- Au (planar) complex and -58.9 kcal/mol for the Gr- Ag (planar) complex.

Calculations of harmonic frequencies, IR intensities and Raman activities were performed for all complexes found. It was found that the greatest changes in the vibrational spectra of uracil are caused by the formation of coordination bonds between uracil and metal particles. At the same time, the interaction between uracil and graphene has insignificant spectral manifestations. In this case, the changes in the uracil frequencies do not exceed 10 cm^{-1} .

The authors acknowledge financial support from National Academy of Sciences of Ukraine (Grant № 0123U100628). An allocation of computer time from the Computational Center at Institute for Low Temperature Physics and Engineering and from UA Research High Performance Computing (HPC) and High Throughput Computing (HTC) at the University of Arizona is gratefully acknowledged.

Functionalization of transition metal dichalcogenides by organic polymers studied by mass spectrometry

**V. G. Zobnina¹, V. S. Shelkovsky¹, O. A. Boryak¹, P. O. Kuzema², M. V. Kosevich¹,
V. A. Karachevtsev¹**

¹*B. Verkin Institute for Low Temperature Physics and Engineering of the NAS of Ukraine,
47 Nauky Ave., Kharkiv, 61103, Ukraine*

²*Chuiko Institute of Surface Chemistry of the NAS of Ukraine,
17 General Naumov Str., Kyiv, 03164, Ukraine
e-mail: valezobnina@gmail.com*

It is hard to list all useful applications of organic polymers based on polyethylene glycol (PEG), including food and pharmaceutical industry, medicine, cryoprotection, green chemistry, etc. In nanotechnology, PEGs are applied for so-called pegylation aimed at protection of nanomaterials and enhancing their bioavailability within the tasks of drug delivery and cancer therapy.

The aim of the present work was to apply laser desorption/ionization (LDI) mass spectrometry to study the functionalization of a set transition metal dichalcogenides (TMD) MoS₂, WS₂, MoSe₂ by PEG-600 and the combining of MoS₂ with PEG-4000, PEG-20000, oxyethylated glycerol OEG-5, and polyvinyl alcohol (PVA). The nanocomposites of TMD with the polymers were prepared by sonication of their mixture in aqueous medium using a piezoelectric oscillator generating 1700 kHz frequency. LDI mass spectra of the dried composites were obtained by applying a UV laser operating at 337 nm wavelength.

Positive ion LDI mass spectra of (PEG-600 + TMD) nanocomposites of the polymer with all three TMD consisted of two bell-shaped sets of cationized oligomers [HO-(CH₂-CH₂-O)_n-H]•K⁺, [H-(CH₂-CH₂-O)_n-H]•K⁺ which practically coincided with the mass spectra characteristic of pure PEG-600. No noticeable products of PEG degradation were recorded in the small masses range. However, there were peak groups corresponding to single Mo⁺ or W⁺ ions. At the same time, no clusters of PEG oligomers with molybdenum or tungsten cations were observed. Negative ion LDI mass spectra of (PEG-600 + TMD) nanocomposites contained sets of clusters sputtered from TMD with appropriate isotopic distributions caused by the polyisotopic nature of the atomic constituents of the clusters: Mo_xS_yO_z⁻, Mo_xSe_yO_z⁻, W_xS_yO_z⁻ (oxygen component may appear due to oxidation). In the composites, physical adsorption of PEG at the TMD nanosheets surface caused a “shielding effect” reflected in the decrease of abundances of the sputtered clusters with x>1 as compared with the spectra of pure TMD. The same effects were observed for (OEG-5 + MoS₂) system.

In the case of MoS₂ composites with PEGs of higher molecular weight, PEG-4000 and PEG-20000, three extended sets of regular peaks were recorded in the lower mass range of 200-2000 a.u., which pointed to degradation of these polymers on MoS₂.

Upon mixing of MoS₂ with PVA the two components were rapidly assembled into a dark viscous clot which separated from its aqueous environment. This effect may be accounted for in water purification technology. In the positive ion mode LDI mass spectrum of (PVA+MoS₂) composite a set of ions with enhanced abundances for odd masses was present in the lower mass range. These ions may be tentatively attributed to products of hydrogenolysis of PVA polymeric chains, which can occur due to the catalytic activity of MoS₂.

Thus, low molecular weight PEGs are better suited for the pegylation of TMD, which enhances their dispersibility in water and thus bioavailability for biomedical applications of TMD-based 2-D nanomaterials.

This work was supported by a grant № 0123U100628 of the NAS of Ukraine. LDI mass spectra were obtained using facilities of the Center for collective use of scientific equipment "Mass spectrometry and liquid chromatography" of the NAS of Ukraine.

Fluorescent voltage sensors for neuronal activity monitoring

A. G. Bulova

B.Verkin Institute for Low Temperature Physics and Engineering of NAS of Ukraine,
47 Nauky Ave., Kharkiv, 61103, Ukraine
E-mail: andrii.bulova@gmail.com

Current fluorescent voltage sensors allow monitoring action potentials in individual cultured neurons and generally fall into four main categories: voltage-sensitive dyes, genetically encoded voltage indicators (GEVIs), calcium imaging methods, and genetically encoded calcium indicators (GECIs). Each of these methods has specific strengths, enabling precise tracking of neuronal activity through optical signals. However, they also possess inherent limitations that highlight the necessity of developing more advanced and reliable technologies.

The primary limitations include low signal intensity and nonspecific labeling in voltage-sensitive dyes, lower temporal resolution and significant background noise in GEVIs, variable sensitivity and artifact susceptibility in calcium imaging indicators, and prolonged signal decay in GECIs. Given these challenges, there is growing interest in alternative fluorescent sensors. Quantum dots (QDs), semiconductor nanoparticles with exceptional optical properties, have recently emerged as particularly promising candidates to overcome these limitations.

To address these challenges, semiconductor nanoparticles, specifically highly bright quantum dots (QDs), are being explored as inorganic fluorescent voltage sensors. Computational models indicate that typical neuronal spike electric fields (~ 10 mV/nm) can modulate the electronic structure of QDs, resulting in approximately 5% fluorescence intensity changes and emission wavelength shifts of around 1 nm, depending on QD size, composition, and dielectric environment. Furthermore, specially engineered dual-material QDs can exhibit even more substantial fluorescence intensity variations ($\sim 30\%$) during neuronal spikes. Recent studies employing signal detection theory have demonstrated that conventional QDs can enable millisecond-precision monitoring of voltage dynamics across multiple neurons under diverse optical and neurophysiological conditions.

The present study aims to evaluate the potential of QDs as cellular voltage indicators for in vivo applications, emphasizing key challenges and future perspectives. Current investigations highlight the need for further experimental work to refine sensitivity, labeling efficiency, and optical stability. By addressing these critical factors, this research provides valuable insights for future advancements in neurophysiology and biomedical imaging.

- [1] J. Marshall and M. Schnitzer, Optical Strategies for Sensing Neuronal Voltage Using Quantum Dots and Other Semiconductor Nanocrystals. ACS Nano 7, (2013). <http://dx.doi.org/10.1021/nn401410k>.
- [2] O. Bar-Elli et al., Rapid voltage sensing with single nanorods via the quantum confined stark effect. ACS Photonics 5, (2018). <http://dx.doi.org/10.1021/acspophotonics.8b00206>.
- [3] J. Zhao et al., Recent developments in multimodality fluorescence imaging probes. Acta Pharm. Sin. B 8, 320 (2018). <http://dx.doi.org/10.1016/j.apsb.2018.03.010>.

The effect of mutations on the binding affinity of macrolides with ribosomal proteins: a molecular docking approach

N. V. Khmil^{1,2}, V. G. Kolesnikov¹

¹*O. Ya. Usikov Institute for Radiophysics and Electronics NAS of Ukraine,
12 Acad. Proskura str., Kharkiv, 61085, Ukraine*

²*Kharkiv National University of Radio Electronics, Nauky ave., 14, Kharkiv, 61166, Ukraine
e-mail: khmilnatali@gmail.com*

Staphylococcus aureus (*S. aureus*) is a common human pathogen capable of causing a wide range of infections, from mild skin infections to severe complications, particularly in combat-related injuries. The pathogen's virulence, immune evasion mechanisms, and antibiotic resistance present significant challenges for clinical management and infection control [1]. Resistance to macrolides is primarily associated with mechanisms that reduce the ability of these antibiotics to bind to their targets. This study aimed to investigate the effect of mutations in bacterial ribosomal proteins on the binding affinity of macrolides through a molecular docking approach.

Molecular docking was performed using AutoDock Vina (v1.2.5) software tool [2]. The 3D structures of ribosomal proteins were retrieved from the Protein Data Bank (PDB) (PDB IDs: 4WCE and 6WRU) via the website www.rcsb.org. Water molecules were removed; polar hydrogen atoms were added using the AutoDockTools interface. The structures were protonated at pH 7. Macrolide structures, including erythromycin B, erythromycin C, and oleandomycin, were downloaded from PubChem (<https://pubchem.ncbi.nlm.nih.gov/>) and optimized using Open Babel v3.1.1. Visualization of docking results was carried out in BioVia Discovery Studio.

Selected macrolides were docked into the L6, L22, and L23 proteins of the 50S ribosomal subunit from *S. aureus*. These proteins are part of the peptide exit tunnel in the 50S ribosomal subunit and, together with 23S rRNA, form the macrolide-binding site. Their amino acid residues play a key role in stabilizing the tunnel structure and interacting with macrolide antibiotics. Macrolides inhibit protein synthesis by binding to the antibiotic binding site which alters the translational capacity of the bacterial cell and blocks its growth. Therefore, studying protein mutations may reveal new approaches to combating resistance.

The in silico docking study demonstrated that all macrolides can bind to the target proteins through van der Waals forces, conventional hydrogen bonds, and hydrophobic interactions such as Pi-alkyl, Pi-sigma, and carbon-hydrogen bonds. However, the binding affinity varied, ranging from -6,1 to -7,7 kcal/mol. Oleandomycin exhibited the lowest binding energy of -7,7 kcal/mol in a complex with the unmutated L23 protein, interacting with residues Pro85, Ser88, Asn197, and His200 through hydrogen bonds and with Lys214 and Ile216 through alkyl hydrophobic interactions. A mutation in the C-terminal loop of L23 (Ile87Asp) altered the shape of the tunnel and weakened the binding affinity of oleandomycin, as confirmed by docking results: the binding energy increased to -6,5 kcal/mol. In the mutated L6 and L22 protein structures, a tendency for decreased binding affinity was also observed, regardless of the docked macrolide.

The molecular docking is technique with significant potential for understanding macrolide mechanisms and improving their efficacy. The study of macrolides and their effects on *S. aureus* structures is an area of ongoing research, particularly due to the emergence of antibiotic resistance.

- [1] M. Miklańska-Majdanik, *Antibiotics* (Basel, Switzerland), 10(11), 1406 (2021). <https://doi.org/10.3390/antibiotics10111406>.
- [2] O. Trott, and A. J. Olson, *Journal of computation chemistry*. 31, 2 (2010). <http://doi.org/10.1002/jcc.21334>.

Analysis of low-temperature electron transport in a composite film of reduced graphene oxide with molybdenum disulfide

N. V. Kurnosov, A. M. Plokhotnichenko, V. A. Karachevtsev

*B.Verkin Institute for Low Temperature Physics and Engineering of NAS of Ukraine,
47 Nauky Ave., Kharkiv, 61103, Ukraine
e-mail: nick.kurnosov@gmail.com*

Composite materials that contain two-dimensional nanostructures such as graphene-related materials and transition metal dichalcogenides (TMDs) attract essential research interest due to the unique combination of electrical, optical, and chemical properties. Reduced graphene oxide (rGO) can be obtained from graphite by oxidation followed by controlled chemical or thermal reduction. The properties of this nanomaterial strongly depend on the degree of reduction which is characterized by C/O ratio or the relative content of sp^2 and sp^3 hybridized atoms. Molybdenum disulfide (MoS_2) currently is among the most studied TMDs. Bulk MoS_2 crystals can be exfoliated into few-layered flakes which generally are nanosized semiconductors with a band structure dependent on the number of stacked S-Mo-S layers. The potential applications of these nanomaterials and composites (nanoelectronics, electrochemical sensors, etc.) may require detailed information on charge transport mechanisms, which is the aim of our current work.

The composite material studied in this work was formed by nanoflakes of MoS_2 and rGO. We should note that the rGO used for composite preparation had ~87% fraction of carbon which means a large amount of conductive sp^2 domains. The film was obtained by vacuum filtration from the suspension of rGO- MoS_2 hybrids in methanol. Preparation of the suspension was based on ultrasound treatment (60 min, 22 kHz) with the following centrifugation (3000 g, 15 min) of rGO and MoS_2 with a 1:2 weight ratio.

The analysis of electron transport was performed as follows. The temperature dependence of resistance ($R(T)$) of the composite was measured in the 5–290 K range. In order to assess the transport mechanism, the logarithmic derivative analysis of $R(T)$ has been made. We unambiguously confirm that in the range of 5–166 K transport is governed by Efros-Shklovskii variable-range hopping (ES VRH) mechanism, which relies on electron tunneling between localized states and accounts for Coulomb gap phenomenon [1]. We have also analyzed the higher-temperature range using Mott VRH mechanisms [2] of different dimensionalities as well as power-law dependence. Our data suggests that there is a transition from ES VRH to two-dimensional Mott VRH mechanism at higher temperatures as the thermal energy becomes essentially larger than the Coulomb gap. Namely, Mott VRH is applicable from 166 K and persists up to room temperature. We have also compared the electron transport parameters of rGO- MoS_2 composite, such as Coulomb gap width and localization length values, to those obtained for rGO film. Overall, our study confirms that rGO essentially provides the electronic conductivity in rGO- MoS_2 composite, while the presence of MoS_2 nanoflakes can affect the ordering and local dielectric environment of rGO and thus electron transport parameters. The experimental results have been published recently [3].

- [1] B. I. Shklovskii and A. L. Efros, Electronic Properties of Doped Semiconductors (Springer-Verlag, Berlin 1984).
- [2] N. F. Mott and E. A. Davis, Electronic Processes in Non-Crystalline Materials (Oxford: Clarendon Press, New York 1979).
- [3] N. V. Kurnosov, A. M. Plokhotnichenko, and V. A. Karachevtsev, Appl. Phys. A 131, 190 (2025). <https://doi.org/10.1007/s00339-025-08302-7>.

Mass spectrometry and Raman spectroscopy characterization of the bactericidal nanofiber mats with incorporated antibiotics

**V. A. Pashynska¹, A. M. Plokhotnichenko¹, A. Yu. Glamazda¹, P. O. Kuzema²,
V. A. Karachevtsev¹**

¹*B.Verkin Institute for Low Temperature Physics and Engineering of the NAS of Ukraine,
47 Nauky Ave., Kharkiv, 61103, Ukraine*

²*Chuiko Institute of Surface Chemistry of the NAS of Ukraine, 17 General Naumov Str.,
Kyiv, 03164, Ukraine
e-mail: pashynska@ilt.kharkov.ua*

Polymeric films with incorporated bactericidal agents are promising biomedical materials which are used in the current medical practice for wounds and burns dressing, tissue engineering etc. Among such films, electrospun polymeric nanofiber mats with incorporated antibiotics or other antimicrobial agents are in the focus of nanoscience related research as healing coating and drug delivery platforms. Our recent study of the nanofiber mats prepared from the polyvinylpyrrolidone (PVP) and polymethylmethacrylate (PMMA) mixture with the addition of biologically active compounds confirmed the mats electrospun production technology effectiveness and possibility to extract the bactericidal agents from the mats into saline (0.9% aqueous NaCl solution that models physiological conditions) [1]. The current study is devoted to laser desorption/ionization mass spectrometry (LDI MS) characterization of the extracts from the nanofiber mats prepared from PMMA or from a mixture of PVP+PMMA with incorporated antibiotic levofloxacin (LF), as well as to Raman spectroscopy examining of PVP+LF aqueous solutions.

In the positive ion mass spectrum of the extract from PMMA+LF dry mat the most intensive signals are the peaks of LF molecular ions: the cationized peak LF•Na⁺ with m/z 384.4, relative abundance RA=100%, the protonated antibiotic molecule LF•H⁺ with m/z 362.4, RA=29%, and LF•K⁺ peak with m/z 400.4, RA=8%. The presence of abundant molecular peaks of the drug in the LDI spectrum indicates intensive extraction of LF from the mat into saline and confirms the efficiency of the production technology of the nanofiber films with the antibiotic loading. It is important to note the stability of the composition of the nanofiber mats over time, since before measurements the dry mats were stored for several months at room temperature. The comparison of the spectra of extracts of PMMA+LF and PMMA+PVP+LF films shows the general similarity of the spectra, both of which have abundant molecular peaks of the antibiotic, which indicates the efficiency of incorporation of LF in both type mats: prepared from PMMA or from the mixture of polymers PMMA+PVP. At the same time, some differences in the mass spectra of the samples from different films are observed. Namely, in the spectrum of the extract from PMMA+LF mat, the RA abundance of the antibiotic peaks is higher (they dominate in the spectrum) compared to the RA of the LF signals in the spectrum of the PMMA+PVP+LF film extract (RA - below 60%). The results of the LDI MS probing show that significant amount of LF molecules save their molecular structure within the mat (obviously, they bound to the nanofibers noncovalently), which is very important to provide the antibiotic biological activity after its extraction into the physiological system from the mat. The data of the Raman spectroscopy examining of the PVP+LF aqueous solutions (LF:PVP - 1:3 and 1:6 molar ratios) also testify to the noncovalent interactions of LF with the PVP molecules. The deposition of the aqueous solutions on the substrate for the measurements did not lead to the destruction of the PVP+LF complexes formed in aqueous solutions.

This work was supported by a grant № 0123U100628 of the NAS of Ukraine. LDI mass spectra were obtained using facilities of the Center for collective use of scientific equipment "Mass spectrometry and liquid chromatography" of the NAS of Ukraine.

[1] A. M. Plokhotnichenko, V. A. Karachevtsev, V. A. Pashynska, P. O. Kuzema, Low Temp. Phys. 50, N3, 215-221 (2024). <https://doi.org/10.1063/10.0024959>.

Peculiarities of interaction of the sulfur-containing antiviral drug lamivudine with molybdenum disulfide

T. Piddubnyi¹, S. Stepanian¹, L. Adamowicz²

¹*B.Verkin Institute for Low Temperature Physics and Engineering of the NAS of Ukraine,
47 Nauky Ave., Kharkiv, 61103, Ukraine*

²*Department of Chemistry and Biochemistry, University of Arizona, 85721 Tucson AZ, USA
e-mail: piddubnyi@ilt.kharkov.ua*

The aim of this work is to determine the structure, stability and spectral characteristics of molybdenum disulfide (MoS_2) complexes with lamivudine using the quantum mechanical DFT method.

MoS_2 is considered as a potential platform for drug delivery. Lamivudine (2',3'-dideoxy-3'-thiacytidine) is an antiretroviral drug used to treat HIV/AIDS and hepatitis B. Lamivudine (Fig. 1) is a derivative of the nucleic acid base cytosine to which a 1,3-oxothiolane saturated heterocycle is added. The presence of the oxothiolane heterocycle ensures high conformational lability of the lamivudine molecule. In total, we located 16 conformers of lamivudine using the DFT and MP2 quantum-mechanical methods. The two most stable conformers (denoted as Lam A and Lam B) are stabilized by $\text{OH}\cdots\text{S}$ and $\text{OH}\cdots\text{O}$ intramolecular hydrogen bonds, respectively. Conformer Lam A is the most stable structure of lamivudine while ZPVE corrected relative energy of the conformer Lam B calculated at the MP2/aug-cc-pVDZ level of theory is 0.85 kcal/mol higher. For these two most stable conformers of lamivudine, calculations of the structure, interaction energies, and vibrational spectra of complexes with the pristine MoS_2 fragment were performed in vacuum approach and with accounting for the aqueous environment using the PCM method. This fragment included 27 molybdenum atoms and 54 sulfur atoms. The calculations were performed using the DFT/M06-2X method. Calculations were also carried out for complexes of lamivudine with the MoS_2 fragment having point structural defects (substitutions and vacancies). The results obtained for the lamivudine complexes were compared with ones obtained for cytosine and other nucleic acid bases. A total of 12 stable complexes of lamivudine with pristine MoS_2 and 16 complexes with MoS_2 having point defects were found. We demonstrated that the presence of the sulfur-containing heterocycle leads to an increase in the interaction of lamivudine with MoS_2 as compared to cytosine. This is especially noticeable when interacting with point defects in the MoS_2 structure. The calculated vibrational spectra of all complexes found were analyzed. As a result, spectral (IR and Raman) markers of lamivudine interactions with MoS_2 were identified. The results demonstrate high stability of MoS_2 -lamivudine complexes both in vacuum and in an aqueous environment. This allows us to conclude that MoS_2 can be used as an effective nanoplatform for the delivery of the antiviral drug lamivudine. The results obtained can also be used to analyze the experimental spectra of lamivudine with MoS_2 and determine the structure of the MoS_2 -lamivudine complexes.

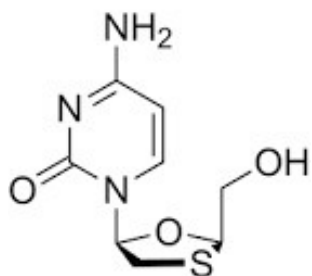


Fig. 1. Structure of lamivudine.

MoS_2 is considered as a potential platform for drug delivery. Lamivudine (2',3'-dideoxy-3'-thiacytidine) is an antiretroviral drug used to treat HIV/AIDS and hepatitis B. Lamivudine (Fig. 1) is a derivative of the nucleic acid base cytosine to which a 1,3-oxothiolane saturated heterocycle is added. The presence of the oxothiolane heterocycle ensures high conformational lability of the lamivudine molecule. In total, we located 16 conformers of lamivudine using the DFT and MP2 quantum-mechanical methods. The two most stable conformers (denoted as Lam A and Lam B) are stabilized by $\text{OH}\cdots\text{S}$ and $\text{OH}\cdots\text{O}$ intramolecular hydrogen bonds, respectively. Conformer Lam A is the most stable structure of lamivudine while ZPVE corrected relative energy of the conformer Lam B calculated at the MP2/aug-cc-pVDZ level of theory is 0.85 kcal/mol higher. For these two most stable conformers of lamivudine, calculations of the structure, interaction energies, and vibrational spectra of complexes with the pristine MoS_2 fragment were performed in vacuum approach and with accounting for the aqueous environment using the PCM method. This fragment included 27 molybdenum atoms and 54 sulfur atoms. The calculations were performed using the DFT/M06-2X method. Calculations were also carried out for complexes of lamivudine with the MoS_2 fragment having point structural defects (substitutions and vacancies). The results obtained for the lamivudine complexes were compared with ones obtained for cytosine and other nucleic acid bases. A total of 12 stable complexes of lamivudine with pristine MoS_2 and 16 complexes with MoS_2 having point defects were found. We demonstrated that the presence of the sulfur-containing heterocycle leads to an increase in the interaction of lamivudine with MoS_2 as compared to cytosine. This is especially noticeable when interacting with point defects in the MoS_2 structure. The calculated vibrational spectra of all complexes found were analyzed. As a result, spectral (IR and Raman) markers of lamivudine interactions with MoS_2 were identified. The results demonstrate high stability of MoS_2 -lamivudine complexes both in vacuum and in an aqueous environment. This allows us to conclude that MoS_2 can be used as an effective nanoplatform for the delivery of the antiviral drug lamivudine. The results obtained can also be used to analyze the experimental spectra of lamivudine with MoS_2 and determine the structure of the MoS_2 -lamivudine complexes.

The authors acknowledge financial support from National Academy of Sciences of Ukraine (Grant № 0123U100628). An allocation of computer time from the Computational Center at Institute for Low Temperature Physics and Engineering and from UA Research High Performance Computing (HPC) and High Throughput Computing (HTC) at the University of Arizona is gratefully acknowledged.

On the features of multi-charged meso-porphyrin binding to nucleic acids

O. A. Ryazanova

B.Verkin Institute for Low Temperature Physics and Engineering of NAS of Ukraine,
47 Nauky Ave., Kharkiv, 61103, Ukraine
e-mail: ryazanova@ilt.kharkov.ua

TMPyP⁴⁺ (Fig. 1) is a well-known *meso*-substituted porphyrin with high biological activity and unique spectroscopic and photophysical properties. This highly symmetric (D_{2h}) fluorescent compound is widely used as a photosensitizer in anticancer photodynamic therapy (PDT), anti-viral and antimicrobial agent, an efficient probe for the nucleic acids structure and dynamics, a carrier of antisense oligonucleotides for their delivery, stabilizer of G-quadruplexes etc. Binding of TMPyP⁴⁺ porphyrin and its tricationic derivative, TMPyP³⁺, to synthetic double-stranded polynucleotides of different base composition and secondary structure including DNA (B-form), RNA (A-form), and DNA-RNA hybrids (A-form) have been comprehensively studied by many authors and us [1, 2] in a wide range of phosphate/dye ratio (P/D) using various spectroscopic methods (absorption spectroscopy, polarized fluorescence, steady state light scattering etc.). It was shown that the way of the porphyrin binding depends on NA base composition and spatial structure, as well as on P/D . An aggregation of both porphyrins on the biopolymers surface at a near-stoichiometric in charge P/D ratio has been revealed for all systems studied. The work is focused on comparison of our data with that of other authors on the spectroscopic features of the porphyrin binding to synthetic nucleic acids, their analysis and generalization.

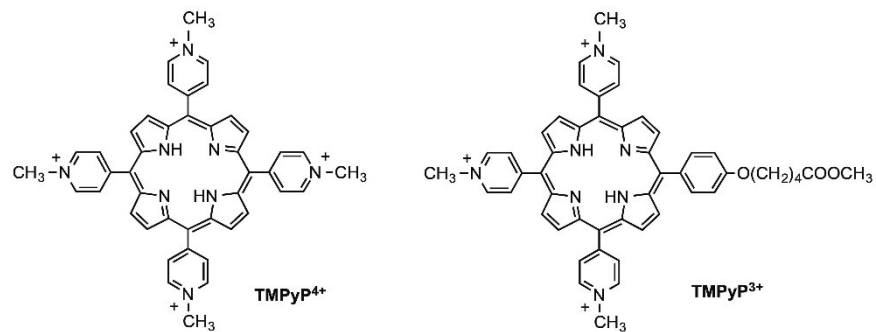


Figure 1 – Molecular structures of tetracationic and tricationic *meso*-substituted porphyrins.

The author acknowledges the National Academy of Sciences of Ukraine for the financial support (Grant No. 0123U100628) and Wolfgang Pauli Institute (Vienna, Austria) for Pauli Postdoc research training scholarships “Data analysis in molecular biophysics” 2021/22.

- [1] O. Ryazanova, I. Voloshin, I. Dubey, L. Dubey, V. Karachevtsev, J. Fluoresc. (2024). <https://doi.org/10.1007/s10895-024-04000-4>.
- [2] O. Ryazanova, V. Zozulya, I. Voloshin, A. Glamazda, I. Dubey, L. Dubey, V. Karachevtsev, Methods Appl. Fluoresc. 4(3), 034005 (2016). doi:10.1088/2050-6120/4/3/034005.

Mass spectrometric probing of C₆₀ with MoS₂ composite produced in aqueous medium

V. S. Shelkovsky¹, M. V. Kosevich¹, O. A. Boryak¹, P. O. Kuzema², A. V. Dolbin¹, N. A. Vinnikov¹, S. V. Cherednichenko¹, V. A. Karachevtsev¹

¹*B. Verkin Institute for Low Temperature Physics and Engineering of the NAS of Ukraine,
47 Nauky Ave., Kharkiv, 61103, Ukraine*

²*Chuiko Institute of Surface Chemistry of the NAS of Ukraine,
17 General Naumov Str., Kyiv, 03164, Ukraine
e-mail: shelkovsky@ilt.kharkov.ua*

Preparation of aqueous dispersions of nanomaterials is required for tests of their biological activity and further biomedical applications. The aim of the present work was to fabricate a nanocomposite of C₆₀ fullerene with molybdenum disulfide 2D nanoflakes in water and to probe it by laser desorption/ionization (LDI) mass spectrometry.

A problem of transfer of hydrophobic C₆₀ to water was solved at the Institute for Low Temperature Physics and Engineering as early as in 1995 [1]. Recently an advanced method of vacuum-sublimation cryogenic deposition for preparation of hydrated fullerenes was proposed [2], which permitted avoiding of traces of organic solvents in aqueous medium. Water solutions of C₆₀ prepared by this method were mixed with water dispersions of MoS₂ for synthesis of (MoS₂ + C₆₀) nanocomposite by ultrasound treatment.

Dried solid (MoS₂ + C₆₀) nanocomposites were studied by LDI technique using an Autoflex II mass spectrometer (Bruker Daltonics, Germany) equipped with a nitrogen laser (337 nm). Variation of laser power permitted to apply laser desorption or ablation modes. Incorporation of C₆₀ into the matrix of exfoliated by sonication MoS₂ nanoflakes was proved by the recording of the C₆₀⁺ and C₆₀⁻ molecular radical cations and anions characteristic of fullerenes in the positive and negative ion modes, applying desorption regime. In the negative ion mode, a set of Mo_xS_yO_z⁻ clusters characteristic of MoS₂ was present.

Evidences of C₆₀ adsorption at the MoS₂ nanosheets in the form of single molecules were obtained applying laser ablation mode. It is known that treatment of solid fullerene samples by high power laser pulses causes degradation and polymerization of fullerenes, which is reflected in the LDI mass spectra in appearance of characteristic fragments of sequential loss of C₂ units [C₆₀ – 2C_n]⁺ and addition of C₂ units [C₆₀ + 2C_n]⁺ [3]. Naturally, fullerene molecules are to be in close contact to provide their binding with each other or with degradation products. Interestingly, in the case of (MoS₂ + C₆₀) composite the spectral pattern characteristic of C₆₀ polymerization was not observed at laser power values which caused this process for crystalline pure C₆₀ samples at the same experimental parameters of the Autoflex instrument. This means, that the distance between single fullerene molecules adsorbed at the surface of MoS₂ is large enough to prevent their interactions in the process of laser desorption. Slight display of polymerization was observed at much higher laser power which provided formation of denser plume of ablated microparticles, where gas-phase ion-molecule interactions became possible. It may be concluded that utilization of hydrated fullerenes permitted to manufacture (MoS₂ + C₆₀) nanocomposite with homogeneous mixing of its components and monomolecular adsorption of C₆₀ on MoS₂ nanosheets.

This work was supported by the Grant 0123U100628 of the NAS of Ukraine.

- [1] G. V. Andrievsky, M. V. Kosevich, O. M. Vovk, V. S. Shelkovsky, and L. A. Vashchenko, J. Chem. Soc. Chem. Commun. 12, 1281 (1995). <https://doi.org/10.1039/C39950001281>.
- [2] N. A. Vinnikov, S. V. Cherednichenko, A. V. Dolbin, V. B. Eselson, V. G. Gavrilko, R. M. Basnukaeva, and A. M. Plokhotnichenko, Low Temp. Phys. 48, 336 (2022). <https://doi.org/10.1063/10.0009739>.
- [3] V. O. Pokrovskiy, et.al., Him. Fiz. Tehnol. Poverhni 4, 78 (2013).

Experimental and theoretical study of the binding of native DNA to MoS₂ nanoflakes

**E. Usenko¹, A. Glamazda^{1,2}, V. Valeev¹, I. Voloshin¹, S. Petrushenko², S. Stepanian¹,
L. Adamowicz³, V. Karachevtsev¹**

¹*B.Verkin Institute for Low Temperature Physics and Engineering of NAS of Ukraine,
47 Nauky Ave., Kharkiv, 61103, Ukraine*

²*V. N. Karazin Kharkiv National University, 4 Svobody Sq., Kharkiv 61022, Ukraine*

³*Department of Chemistry and Biochemistry, University of Arizona, Tucson, AZ 85721, USA
e-mail: usenko@ilt.kharkov.ua*

Currently, the study of the optical and physicochemical properties of 2D materials is of great interest. Such materials include MoS₂, which is currently considered as a promising candidate for use in the field of nanobiosensing (for the development of sensitive nanobiosensors) and nanomedicine (as a theranostic agent) [1].

In the present work, we study whether native DNA would bind to MoS₂ flakes (FLs) at relatively low ionic force (10^{-3} M Na⁺, pH7) using experimental (differential UV spectroscopy and thermal denaturation method) and theoretical (DFT) methods. Based on analysis of the TEM image which showed the adsorption of DNA on MoS₂ FLs and the observation of an increase in the thermal stability of DNA and a decrease in the hyperchromic coefficient at binding with MoS₂ FLs in the thermal denaturation measurements we concluded about the binding of the biopolymer with MoS₂ nanoflakes at these conditions. It was observed, first of all, that the melting curve of DNA in the nanoassemblies has S-like form that indicates keeping the duplex structure of DNA at the conjugation. Observed changes in these DNA characteristics (an increase in melting temperature and a decrease of hyperchromic coefficient) were explained by the electrostatic interaction of the negatively charged oxygen atoms of the phosphate groups of DNA with the MoS₂ FLs.

Consideration of possible complexes of a nucleotide fragment (ribosephosphate group) with MoS₂ nanolayer employing the DFT method showed the forming of the coordination bonds of this nucleotide fragment with Mo atoms located at the edge of the MoS₂ nanolayer and with point structural defects of MoS₂ surface containing the S vacancy. This observation allows us to propose a mechanism of binding of native DNA to MoS₂ FLs, in which their conjugation begins with point contacts of DNA phosphate groups with Mo atoms (at the edge or/and in defects) through the formation of the coordination bond. The results indicate a huge impact of defects and edge atoms of MoS₂ FLs on their biofunctionalization.

The biocompatible MoS₂ FLs are model objects for the development of drug-related products based on transition-metal dichalcogenides. For example, such products can find application in photodynamic therapy, where separation and size control of the acting nanoassemblies are necessary. The results obtained in the present study can also be used to fabricate various hygiene products, as well as products for use in medicine and pharmacology.

The authors acknowledge partial financial support from National Academy of Sciences of Ukraine (Grant № 0123U100628). E.U. acknowledges Wolfgang Pauli Institute, Vienna, Austria for the financial support (Pauli Postdoc research training scholarship in the field of Data analysis in molecular biophysics in the context of the WPI thematic program “Numerical models in Biology and Medicine” (2023/2024)). E.U. and A.G. acknowledge Nanophotonics journal, De Gruyter, Scienwise Publishing, and the Optica Foundation for the financial support (Ukraine Optics and Photonics Researcher Grant 2023). An allocation of computer time from the Computational Center at Institute for Low Temperature Physics and Engineering is gratefully acknowledged.

[1] V. Yadav, S. Roy, P. Singh, Z. Khan, and A. Jaiswal, Small. 15, 1803706 (2019).
<https://doi.org/10.1002/smll.201803706>.

The impact of the outer membrane and general porins on cyanide diffusion in gram-negative bacteria

V. Yakovliev, B. Lev

Bogolyubov Institute for Theoretical Physics of the National Academy of Sciences of Ukraine,
14b Metrolohichna Str., Kyiv 03143, Ukraine
e-mail: vladayakovliev1@gmail.com

The outer membrane (OM) of gram-negative bacteria serves as a permeability barrier, protecting the cell against external aggressive environments. The OM consists of an external lipopolysaccharide monolayer, an internal leaflet of a phospholipid monolayer, and β -barrel proteins such as porins. General porins, including OmpF, OmpC, OmpA, and OprF, form water-filled channels in the OM, allowing the passive diffusion of small hydrophilic molecules, such as nutrients and ions.

In this study, we investigate the diffusion of various cyanide compounds through general porins embedded in the OMs of *E. coli* (OmpF, OmpC, and OmpA porins) and *Pseudomonas* species (OprF porin). The cyanide compounds studied include free cyanide (CN^-), thiocyanate (SCN^-), metal-cyanide complexes such as $[\text{Ag}(\text{CN})_2]^-$, $[\text{Fe}(\text{CN})_6]^{3-4-}$, $[\text{Ni}(\text{CN})_4]^{2-}$, $[\text{Au}(\text{CN})_2]^-$, and several other tetracyano- and hexacyano-metal complexes. The effective diffusion coefficient of a cyanide compound within a general porin D_{eff} is significantly reduced compared to the free diffusion coefficient in water D and can be expressed as $D_{\text{eff},\phi} = D H(\xi) W(\phi)$, where $\xi = r/R$ is the compound-to-porin radius ratio, $H(\xi)$ is the diffusional hindrance factor, and $W(\phi)$ is the correction factor for the effective diffusion coefficient within the porin in the presence of an external potential. The parameter ϕ represents the energy of a charged particle in the external potential, expressed in units of $k_B T$, and is defined as $\phi = \frac{Z e_c V_D}{k_B T}$, where Z is the charge number of the cyanide ion, e_c is the elementary charge, V_D is the Donnan potential (DP) across the OM, k_B is the Boltzmann constant, and T is the temperature of the environment.

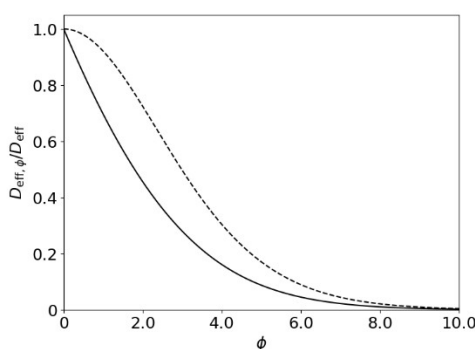


Fig. 1. Dependence of the effective diffusion coefficient on the energy of a charged particle for linear potential (solid line) and periodic potential (dashed line)

prediction of cyanide transport rates through bacterial OMs for developing efficient biological treatment systems for cyanide-contaminated wastewaters.

Our findings reveal that the permeability of cyanide compounds is influenced by several key factors: the compound-to-porin radius ratio, the cyanide ion charge, the number and size of available porins and the fraction of open channels in the OM. Furthermore, the OM of *Pseudomonas* species exhibits greater permeability for larger cyanide compounds compared to *E. coli*, while showing reduced permeability for free cyanide (CN^-) [1]. Quantitatively, the permeability coefficient for free cyanide exceeds that of other cyanide compounds by factors of 3.4-32 in *Pseudomonas* species and 8.6-130-fold in *E. coli* with OmpF-containing membranes.

These insights into bacterial resistance mechanisms have significant implications for optimizing cyanide bioremediation [1,2] as our model enables accurate

[1] V. Yakovliev, B. Lev. Journal of Hazardous Materials, 136117 (2024). <https://doi.org/10.1016/j.jhazmat.2024.136117>.

[2] V. Yakovliev, V. Ermakov, B. Lev. Ukrainian Journal of Physics, 68(2), 113-121 (2023). <https://doi.org/10.15407/ujpe68.2.113>.

MATERIALS SCIENCE

Study of the thermal conductivity of pressed nanocarbon materials at low temperatures

D. Sokolov^{1,2}, K. Vorobieva¹, O. Vorobyova^{1,2}

¹*Al-Farabi Kazakh National University, Al-Farabi av., 71, Almaty, 050040, Kazakhstan*

²*Almaty Technological University, Tole bi av., 100, Almaty, 050012, Kazakhstan*

e-mail: yasnyisokol@gmail.com

In recent years, nanocarbon structures – particularly graphene – have attracted significant interest due to their thermal conductivity properties at low temperatures. These unique properties make graphene a promising material for applications in electronics, especially in heat flow management and efficient heat removal.

The thermal conductivity of carbon allotropes covers an extremely wide range – over five orders of magnitude – from as low as 0.01 W/(m·K) in amorphous carbon to more than 2000 W/(m·K) at room temperature in diamond or graphene. The high thermal conductivity of graphene is due to its two-dimensional structure, high phonon mobility, and low lattice anharmonicity, which makes it attractive for applications in micro- and nanoelectronics. In addition, studies show that the thermal conductivity of graphene at cryogenic temperatures can be significantly modified by dimensionality effects, topological defects, and external influences such as electric or magnetic fields. This makes graphene a promising candidate for low-temperature applications, including cooling systems for quantum computing and superconducting electronics [1].

In this work, the thermal conductivity of graphene powder pressed into tablets was measured. Graphene was pressed into three groups of tablets with different masses and dimensions. The setup for measuring the thermal conductivity of materials uses the relative flat layer method. This method is based on comparing the temperature gradients in a reference plate and the sample under study, while maintaining a constant heat flow, in accordance with Fourier's law [2,3].

Based on the measurements carried out, the temperature dependence of the thermal conductivity coefficient of pressed graphene powder was obtained in the range of 80–300 K. The measured values are consistent with previously reported data for pressed nanocarbon materials, but are significantly inferior to the thermal conductivity of single-crystal graphene.

- [1] A. A. Balandin, Thermal properties of graphene and nanostructured carbon materials, *Nature materials* 10, 569 (2011). <https://doi.org/10.1038/nmat3064>.
- [2] S. Ghosh, I. Calizo, D. Teweldebrhan, E. P. Pokatilov, D. L. Nika, A. A. Balandin, W. Bao, F. Miao, C. N. Lau, Extremely high thermal conductivity of graphene: Prospects for thermal management applications in nanoelectronic circuits, *Applied Physics Letters* 92, 151911 (2008). <https://doi.org/10.1063/1.2907977>.
- [3] A. Shinbayeva, I. Arkharov, A. Aldiyarov, A. Drobyshev, M. Zhubaniyazova, V. Kurnosov, Experimental investigation of thermal conductivity of meat during freezing, *Journal of Low Temperature Physics* 187, 172 (2017). <https://doi.org/10.1007/s10909-017-1754-6>.

Truncated Coulomb potential for planar channeling

M. V. Bondarenko^{1,2}, N. S. Moskvitin^{1,2}

¹*NSC Kharkov Institute of Physics and Technology of NAS of Ukraine,
1 Academic St., Kharkiv, 61108, Ukraine*

²*V.N. Karazin Kharkov National University, 4 Svobody Sq., Kharkiv, 61077, Ukraine
e-mail: bon@kipt.kharkov.ua*

It is shown that if the atomic screening function is described in the Thomas-Fermi approximation, the corresponding continuous potential for planar channeling to a good accuracy reduces to a truncated Coulomb potential (Fig. 1). The sum of two displaced Coulomb potentials also accurately approximates interplanar static continuous potentials for Si, Ge, W crystals in orientation (110), as well as the thermal potential of a Ge crystal in orientation (111), not too close to atomic planes (Fig. 2). Such a possibility can be used to facilitate the description of channeled and quasichanneled particle motions. We illustrate this by calculating classical particle channeling periods, quantum energy levels, and the probability of tunneling of a negatively charged particle through a single atomic plane. Simple scaling laws in dependencies of those quantities on the atomic number Z result this case.

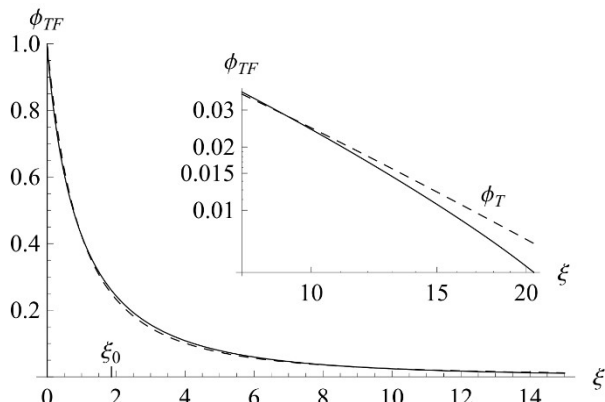


Fig. 1. Thomas-Fermi screening function (solid curve) and its Tietz approximation (dashed curve) vs. the radius ξ in units of the Thomas-Fermi radius.

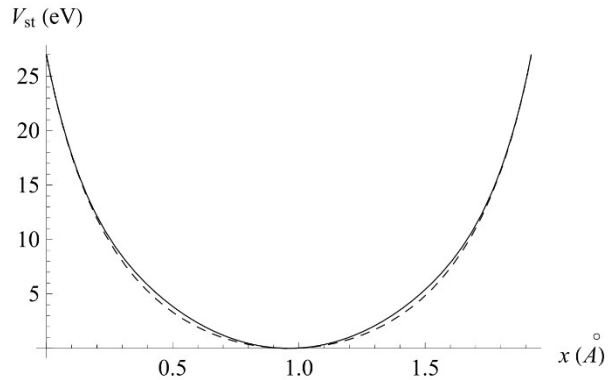


Fig. 2. Static interplanar potential of a silicon crystal in orientation (110). Solid curve, Hartree-Fock parametrization. Dashed, the sum of two truncated Coulomb potentials for the planes limiting the considered interplanar interval.

- [1] M. V. Bondarenko and N. S. Moskvitin. Phys. Rev. B 110, 205205 (2024).
<http://dx.doi.org/10.1103/PhysRevB.110.205205>.

The ordering of defects controlled by the symmetry of the CdI₂ crystal lattice: justification and experimental confirmation

N. Tovstyuk¹, M. Rudka¹, O. Bilenka¹, F. Ivashchyshyn¹, M. Karkuliovsk¹, B. Seredyuk²

¹*Lviv Polytechnic National University, Bandera Str. 12, Lviv, 79013, Ukraine*

²*Hetman Petro Sahaidachnyi National Army Academy,
32 Heroes of Maidan street, Lviv, 79026, Ukraine
e-mail: ntovstyuk@gmail.com*

The low symmetry of layered structure crystals leads to a distinct spatial arrangement of associates of point defects. The process results in the formation of donor–acceptor–donor trimers. Crystals such as CdI₂ serve as ideal model systems for justifying the formation of such defect complexes [1]. The structural features of AB₂-type crystals (such as CdI₂) promote the ordering of local minima in the thermodynamic potential landscape, which are occupied by cations (Cd²⁺). A model of donor-acceptor (DA) defects caused by the aforementioned non-stoichiometric Cd inclusions is considered. The influence of the concentration of these non-stoichiometric Cd inclusions on the electro-optical and photoelectric properties of CdI₂ crystals is studied both experimentally and theoretically. The analysis is performed using the virtual crystal approximation and takes into account the peculiarities of the energy band structure arising from the anisotropic chemical bonding in different crystallographic directions.

In low-dimensional layered crystals and thin films of CdI₂, the dominant luminescence center is a donor-acceptor trimer of the type Cd⁰ – V_Cd²⁺ – Cd⁺, representing a complex of two DA pairs with a common acceptor. The specific orientation of these complexes within the lattice structure allows: a) to apply the virtual crystal approximation to study the electronic spectrum of CdI₂, and b) to take into account structural features associated with bending (flexural) vibrations. The manifestation of a selective absorption band (luminescence excitation) observed exclusively along the direction of light propagation along the main crystallographic axis C₆ is taken into account in the model through the linear concentration dependence of electronic state mixing along this axis. The approach shows a qualitative agreement with the experiment.

- [1] M. Rudka, I. Matviishyn, B. Seredyuk, N. Tovstyuk, M. Karkuliovsk, I. Kravchuk. Luminescence centers in low-dimensional layered cadmium iodide crystals and nanostructures. 2020 IEEE 40th International Conference on Electronics and Nanotechnology, ELNANO 2020 - Proceedings, 2020, pp. 268-271, 9088922. <https://doi.org/10.1109/ELNANO50318.2020.9088922>.

Up-conversion and luminescent properties of SiO₂-CaF₂:Pr³⁺ nanoceramics

O. Bezkrovna^{1,2}, R. Lisiecki¹, P. J. Dereń¹

¹*Institute of Low Temperature and Structure Research, Polish Academy of Sciences,
Okólna 2, Wrocław, 50-422, Poland*

²*Institute for Single Crystals, NAS of Ukraine, Nauky Ave. 60, Kharkiv, 61001, Ukraine
e-mail: o.bezkrovna@intibs.pl*

Droplets that settle on surfaces transmit many infectious diseases (SARS-CoV-2 and others). UVC radiation (100 - 280 nm) destroys these germs but is harmful to humans [1]. Therefore, it is important to create self-sterilizing surfaces, which can be obtained by covering them with phosphors that convert visible light into UVC radiation. In this case, the emission will not be harmful to humans, as it has low intensity while still being sufficient to destroy germs on the surface. Up-conversion phosphors include compounds doped with Pr³⁺ ions due to their characteristic UVC radiation [2]. The CaF₂ crystal has the low phonon energy (466 cm⁻¹) [3] and can be used as a host for Pr³⁺ ions.

In our work, CaF₂:Pr³⁺ nanocrystals were synthesized by the microwave method and incorporated into the SiO₂ xerogel matrix. The structural, optical (luminescence and excitation spectra, absorption, luminescence lifetime, up-conversion emission at excitation in visible spectral range), morphological (TEM) properties of the samples and SEM-EDS mapping were investigated.

The X-ray diffraction analysis of the CaF₂:(1-3%)Pr³⁺ nanocrystalline samples showed the formation of a calcium fluoride pure phase. The introduction of Pr³⁺ ions at concentrations of 1-3% into CaF₂ does not lead to a violation of its crystal structure. The XRD spectra of the SiO₂-CaF₂:3%Pr³⁺ samples were characterized by the presence of a wide halo, which confirms the amorphous structure of the samples. The TEM method showed that the CaF₂:(1-3%)Pr³⁺ nanocrystals have rounded edges, with an average size in the range of 20-40 nm.

The measurement of up-conversion luminescence spectra of the SiO₂-CaF₂:Pr³⁺ composite under the excitation at 444 nm showed that the emission maximum is located in the UVC spectral region. In this case, the intensity was approximately 2.3 times higher than that of the initial CaF₂:Pr³⁺ nanocrystals.

To study the effect of the Pr³⁺ ion concentration on luminescence spectra, the 444 nm excitation was used for CaF₂:Pr³⁺ samples with dopant concentrations of 1, 2 and 3%. An increase in dopant concentration up to 3% led to quenching process of luminescence, likely due to possible cross-relaxation processes dependent on the distance between emitting ions.

Acknowledgements

This research was funded by the National Science Center, grant number 2021/41/B/ST5/03792, which is gratefully acknowledged, by the Program supporting scientists from Ukraine (PAS and NASU), and by the CERIC project (Proposal 20242113).

[1] E. Eadie, W. Hiwar, L. Fletcher, E. Tidswell, P. O'Mahoney, M. Buonanno, D. Welch, C. S. Adamson, D. J. Brenner, C. Noakes and K. Wood, Sci. Rep. 12, 4373 (2022). <https://doi.org/10.1038/s41598-022-08462-z>.

[2] Dace Nilova, Andris Antuzevics, Guna Krieke, Guna Doke, Inga Pudza and Alexei Kuzmin, J. Lumin. 263, 120105 (2023). <https://doi.org/10.1016/j.jlumin.2023.120105>.

[3] N. Pawlik, B. Szpikowska-Sroka, T. Goryczka and Wojciech A. Pisarski, Phys. Status Solidi B. 257, 1900478 (2020). <https://doi.org/10.1002/pssb.201900478>.

Connection of cryogenic pipelines made of different metals by bimetallic adapters

L. M. Lobanov, A. G. Bryzgalin, E. D. Pekar, N. A. Pashin, O. L. Mikhodui, L. M. Malakhova

E. O. Paton Electric Welding Institute, 11 Kazymyr Malevych Str., Kyiv, 03150, Ukraine
e-mail: andreybag60@ukr.net

The International Thermonuclear Experimental Reactor (ITER) has the world's most powerful cryogenic system with kilometers of vacuum lines, Dewar vessels comparable in size to railway tankers, and pipelines carrying liquid helium to cool equipment down to 4 K. The cooling pipelines are made of a special copper alloy, while the supply pipelines carrying liquid helium are made of stainless steel. However, fusion welding of dissimilar metals, such as copper alloys and stainless steel, results in the degradation of joint performance. To address this challenge, bimetallic adapters are required, allowing fusion welding to be performed between homogeneous metals (copper alloy to copper alloy, stainless steel to stainless steel).

The E.O. Paton Electric Welding Institute of the National Academy of Sciences of Ukraine has developed a technology for the fabrication of such bimetallic tubular adapters based on explosion welding. In these adapters, one side of the tube consists of a copper alloy, while the other is made of stainless steel. After explosion welding and subsequent mechanical processing, the adapters undergo heat treatment.

Mechanical testing, including tensile and internal pressure tests, demonstrated that failure occurred within the copper alloy region, confirming the strength of the welded interface. The adapters exhibited high vacuum tightness, with a leak rate no greater than 0.4×10^{-5} Pa. These bimetallic adapters enable the reliable joining of dissimilar pipelines through fusion welding of homogeneous sections. A batch of ten adapters has been delivered to ITER specialists for further research. A schematic cross-section of the adapter is presented in the accompanying figure.

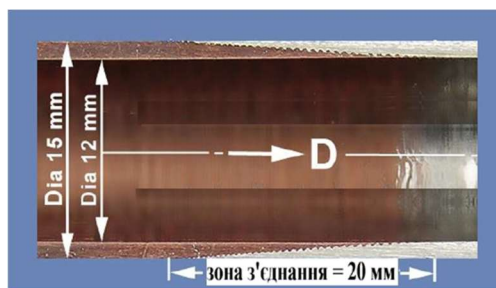


Figure. The cross-section of the bimetallic adapter.

Wave-like structures observed at the interface between the copper alloy and stainless steel indicate the high quality of the resulting joint. These characteristic waves are a hallmark of a well-formed solid-state joint and serve as evidence of effective interfacial mixing without the formation of brittle intermetallic phases. Experimental investigations have also demonstrated the feasibility of fabricating similar bimetallic adapters using various other combinations of metals.

- [1] A. G. Bryzgalin, E. D. Pekar, S. D. Ventsev, M. O. Pashchin, P.S. Shliionskyi, The Paton Welding Journal 6, 38 (2024). <https://doi.org/10.37434/tpwj2024.06.05>.
- [2] Method of manufacturing bimetallic pipe adapters using explosion welding. Application for invention No. 2022 02799 dated 05.08.2022. Industrial Property Bulletin No. 6, 07.02.2024. – Ukrainian version only. (Спосіб виготовлення біметалічних трубних переходників за допомогою зварювання вибухом. Заявка на винахід № 2022 02799 від 05.08.2022. Бюллетень промислової власності №6, 07.02.2024).

Study of structural, electronic, optical, and thermodynamic properties of RbGeI₃ perovskite using DFT

T. Abera

*Wachemo University, P.O. Box 667, Hossana, Ethiopia
e-mail: tejur2785@gmail.com*

In this research, we employ density functional theory (DFT) in combination with the plane-wave pseudopotential (PW-PP) method to study the structural, electronic, optical, and thermodynamic properties of the lead-free cubic perovskite RbGeI₃. To explore its potential as an alternative material for solar cell applications, we studied the RbGeI₃ perovskite. The energy cutoff E_{cutoff} and k-point mesh were set to 65Ry and 7x7x7, respectively. The lattice parameter was found to be 5.95Å, which is in good agreement with available experimental data [1].

The calculated band structure of RbGeI₃ has a semiconductor behavior with a direct band gap of 0.56eV, which lies within the standard range for photo-voltaic, making the material a promising candidate for solar energy conversion. The optical properties of RbGeI₃ were also investigated. The static dielectric constant, $\epsilon_1(0)$, was estimated to be 7.676, while the static refractive index, n(0), was calculated as 2.77. The maximum reflectivity was found to be 0.45 at a photon energy of 2.64 eV. These optical parameters are necessary for the effective utilization of the material in optoelectronic devices.

Regarding the thermodynamic properties of RbGeI₃, at 800 K the maximum entropy was found to be approximately 380 J/(K·mol).

At a lower temperature of 100 K, the Debye specific heat capacity was found to be 112 J/(K·mol), while at 800 K, it increased to 124 J/(K·mol). The Helmholtz free energy gradually decreased with increasing temperature from 0 K to 800 K, reaching its minimum value at 800 K. At T = 0 K, the Debye vibrational energy at constant volume for RbGeI₃ was calculated to be 6.97 kJ/mol. The vibrational energy increased with temperature, and its temperature dependence showed an approximately linear trend at T = 800 K.

- [1] K. Deepthi Jayan, V. Sebastian, Materials Today Communications 28, 102650 (2021). <https://doi.org/10.1016/j.mtcomm.2021.102650>.

Low-temperature ultrasonic investigations of CoCrFeMnNi high-entropy alloy doped with vanadium

V. S. Klochko, A. V. Korniets, V. I. Sokolenko, I. V. Kolodiy, O. O. Kondratov,
I. F. Kislyak, Yu. S. Lipovska, M. A. Tikhonovsky, T. M. Tikhonovska

National Science Center "Kharkiv Institute of Physics and Technology" of NAS of Ukraine,
1 Academicichna St., Kharkiv, 61108, Ukraine
e-mail: korniets@kipt.kharkov.ua

Equiatomic face-centered cubic (fcc) high-entropy alloy (HEA) CoCrFeMnNi, the so-called Cantor alloy, is a model HEA for both materials science and engineering applications [1]. It has high ductility, which is preserved even at cryogenic temperatures. However, the strength characteristics of the alloy need significant improvements. In this regard, an attempt was made to enable it by doping the HEA with vanadium and to further study the doping effect on the microstructure, phase composition, elastic and low-temperature (77-300 K) acoustic properties.

CoCrFeMnNiV_x ($x = 0; 0.25; 0.75; 1.5; 2.0$) ingots were obtained by arc melting the components (purity $\sim 99.9\%$) on a copper water-cooled hearth in a purified argon environment using a tungsten electrode. To improve chemical homogeneity, the resulting ingots were re-melted five times.

According to the structural research, the microstructure of the CoCrFeMnNi alloy had a typical dendritic character, while alloys doped with vanadium had a grain structure. XRD analysis revealed that CoCrFeMnNiV_x ($x = 0; 0.25$) were single-phase with the fcc lattice. In contrary, the two-phase CoCrFeMnNiV_{0.75} alloy consisted of the fcc matrix with $\sim 40\%$ (wt.) tetragonal σ -phase. Further increase in vanadium content ($x = 1.5; 2.0$) led to the formation of single-phase CoCrFeMnNiV_x alloys with tetragonal (σ -phase) crystal structure. The bulk CoCrFeMnNiV_{0.75} specimen has a texture of a preferred crystallographic orientation [001] of the fcc grains along the direction of the ingot crystallization. A weak texture was also found in the σ -phase, the influence of which was not taken into account when studying the ultrasound (US) data.

US studies in the temperature range of 77-300 K were performed using a pulsed phase-sensitive method according to the passage scheme. Excitation and detection of US oscillations were carried out using the broadband (± 2 MHz) LiNbO₃-piezotransducers with a resonant frequency of 50 MHz. Measurements were conducted in the amplitude-independent region of internal friction during heating. Both the velocity (V_L) and the change in attenuation ($\Delta\alpha_L$) of longitudinal US were measured simultaneously. The shear wave velocity was measured only at 300 K.

As a result of US studies of the CoCrFeMnNiV_{0.75} specimen, we detected the characteristic deflections on $V_L(T)$ and the presence of maxima P_1 , P_2 and P_3 on $\Delta\alpha_L(T)$ at temperatures of 106, 154, 294 K, respectively, caused by relaxation resonance of the Hasiguti (P_3) and Bordoni type (P_2). The maximum of acoustic attenuation P_1 is probably due to the transition from the paramagnetic state to the spin glass. The elastic characteristics at 300 K have been determined. In CoCrFeMnNiV_x alloys ($x = 0; 0.25$), maxima on $\Delta\alpha_L(T)$ with localization temperatures of ~ 160 and 115 K, respectively, were found. It is assumed to be due to the relaxation resonance of the Bordoni type (for $x=0$) and the possible transition from the paramagnetic state to the spin glass (for $x = 0.25$), respectively. High attenuation of US waves did not allow determining the values of ultrasound velocities, as well as elastic moduli.

In the CoCrFeMnNiV_x alloys ($x = 1.5; 2.0$), critically high attenuation of both shear and longitudinal US was recorded, which turned out to be incompatible with further acoustic studies.

[1] C. Wagner, A. Ferrari, J. Schreuer, J-P. Couzinié, Yu. Ikeda, F. Körmann, G. Eggeler, E. P. George, G. Laplanche, Acta Materialia 227, 117693 (2022).
<https://doi.org/10.1016/j.actamat.2022.117693>.

Particularity of relaxation of mechanical properties of polyimide films of the Kapton H type at different strain rates after long-term exposure at environmental conditions

V. A. Lototskaya

*B. Verkin Institute for Low Temperature Physics and Engineering of NAS of Ukraine,
47 Nauky Ave., Kharkiv, 61103, Ukraine
e-mail: vallototskaya@gmail.com*

According to [1], polyimide films with a $C_{22}H_{10}N_2O_5$ monomer unit and a non-isotropic oriented structure exhibit a noticeable relaxation of mechanical properties after exposure at room temperature for a time comparable to the time of their stay in outer space. It is of scientific and practical point of view to clarify the effect of strain rate on the degree and direction of change in mechanical properties of exposed films with an amorphous or partially crystalline structure.

We carried out the study of mechanical properties (the limit of forced elasticity, fracture stress, deformation before failure and the values of its components, elasticity moduli and elasticity at different stages of deformation) of $C_{22}H_{10}N_2O_5$ polypyromellitimide films of different thicknesses (25.75 and 125 μm) produced in the People's Republic of China in the initial state and after a long-term exposure. Mechanical properties of "fresh" films and those exposed for several years were studied under conditions of uniaxial tension at room temperature and strain rates varying by two orders of magnitude.

The stages of deformation of amorphous (25 and 75 μm) and partially crystalline films (125 μm) differ both in the initial state and after exposure. The elastic moduli (Young's moduli) at the initial stage and the moduli at the linear stages of forced elasticity of all films, with the exception of the first linear stage of forced elasticity in a film of 125 μm thickness, increase after exposure. The modulus at the first linear stage of forced elasticity in a partially crystalline exposed film with a thickness of 125 μm remains equal to zero at all strain rates. In all films, deformation occurs unevenly at all stages. However, at this stage only in 125- μm films, the deformation front clearly spreads across the working part of the sample.

No noticeable unambiguous changes in the strength characteristics with time of exposition were detected. The limits of forced elasticity and fracture stress of all "fresh" and exposed films increase slightly with increasing strain rate.

After exposure, the relative deformation before fracture of amorphous films decreases, while for partially crystalline films, on the contrary, it increases, maintaining the same trend of change with the strain rate as in fresh films.

The values of the total highly elastic both reversible and delayed deformation decrease after exposure of films. The irreversible deformation shows a noticeable increase (almost twofold in a partially crystalline film with a thickness of 125 μm). After exposure of the films, a change in the nature of the dependences of reversibility values upon removal of the load, as well as the total highly elastic deformation with a change in the strain rate was detected. In the initial state, both characteristics decrease with increasing strain rate, while in exposed films, they vice versa increase. As a result, in a partially crystalline film of 125 μm thickness, the value of highly elastic deformation, reversible when the load is removed, at the highest strain rate turned out to be higher than that in the initial state.

[1] V. A. Lototskaya and L. F. Yakovenko, Low Temp. Phys. 49, 1222 (2023).
<https://doi.org/10.1063/10.0021365>.

Energetics of carbon-related defects in YAG and their role in controlling the concentration of anion and cation vacancies

K. V. Hermash¹, D. V. Fil^{1,2}

¹Institute for Single Crystals of NAS of Ukraine, 60 Nauky Avenue, Kharkiv, 61072, Ukraine

²Karazin Kharkiv National University, 4 Svobody Square, Kharkiv, 61022, Ukraine

e-mail: kostiantyn.hermash@gmail.com

We study point defects in the Yttrium Aluminium Garnet ($\text{Y}_3\text{Al}_5\text{O}_{12}$, YAG) crystal by using the density functional theory (DFT). The formation energies and concentrations of simple (single) and complex (pairs, triples) defects in different charge states are calculated.

The formation energy of the i-th defect is defined by the equation:

$$E_i^{\text{defect-formation}} = E_i^{\text{defect-cell}} - E_{\text{YAG}}^{\text{perfect-cell}} + \mu_i + \mu_e q_i + E_i^M,$$

where $E_i^{\text{defect-cell}}$ is the energy of a unit cell of YAG with a defect, $E_{\text{YAG}}^{\text{perfect-cell}}$ is the energy of a perfect unit cell of YAG (without defects), μ_i is the chemical potential for the i-th defect, μ_e is the chemical potential of electrons, q_i is the charge of a defect (in the units of a positive elementary charge e), E_i^M is the Madelung energy. The chemical potential μ_i is given by the equation $\mu_i = a\mu_X - b\mu_Y$, where a is the number of X-type atoms, which are deleted from the unit cell, and b is the number of Y-type atoms, which are added to the unit cell, μ_X is the chemical potential of X-atom, μ_Y is the chemical potential of Y-atom.

The energies $E_i^{\text{defect-cell}}$ and $E_{\text{YAG}}^{\text{perfect-cell}}$ are calculated by means of the SIESTA computer program [1], involving YAG unit cells (160 atoms) with one simple or complex defect.

The chemical potential of electrons μ_e is calculated using the charge neutrality equation, taking into account all types of defects at the YAG melting temperature: $T_{\text{YAG}}^{\text{melting}} = 2213\text{K}$.

In order to calculate the chemical potentials of atoms, the approach [2] is used. We consider the case, when we have an excess of Al_2O_3 . The oxygen chemical potential varies from the minimal value (reducing limit) to the maximal one (oxidizing limit). The carbon chemical potential is calculated from the energies of CO and CO_2 .

According to calculations, the following carbon-related main defects appear in YAG:

1) substitution of aluminium for carbon $\text{C}_{\text{Al(t)}}^{+1}$ in the tetragonal environment; 2) substitution of oxygen for carbon C_0^0 , C_0^{-1} ; 3) complex defects $[\text{C}_0 - \text{V}_0]^0$, $[\text{C}_0 - \text{V}_0]^{+1}$; 4) complex defects $[\text{C}_{\text{Al(t)}} - \text{V}_0]^{+3}$, $[\text{C}_{\text{Al(t)}} - \text{V}_0]^{+1}$. The concentrations of $\text{C}_{\text{Al(t)}}^{+1} - \text{V}_Y^{-3}$, $\text{C}_{\text{Al(t)}}^{+1} - \text{V}_{\text{Al(t)}}^{-3}$, and $\text{C}_{\text{Al(t)}}^{+1} - \text{V}_Y^{-3} - \text{C}_{\text{Al(t)}}^{+1}$ complex defects increase in the oxidizing limit, but their concentrations remain much smaller than that of isolated $\text{C}_{\text{Al(t)}}^{+1}$.

It is established, that carbon-doping leads to increase of concentrations of:

- 1) charged oxygen vacancies V_0^{+1} , V_0^{+2} in the reducing limit;
- 2) aluminium and yttrium vacancies $\text{V}_{\text{Al(t)}}^{-3}$, V_Y^{-3} under intermediate and oxidizing conditions.

[1] J. M. Soler, E. Artacho, J. D. Gale, A. García, J. Junquera, P. Ordejón, D. Sánchez-Portal, The SIESTA method for ab initio order-N materials simulation, *J. Phys.: Condens. Matter* 14, 2745 (2002). <https://dx.doi.org/10.1088/0953-8984/14/11/302>.

[2] L. Yu. Kravchenko and D. V. Fil, Control of charge state of dopants in insulating crystals: Case study of Ti-doped sapphire, *Phys. Rev. Research* 2, 023135 (2020). <https://doi.org/10.1103/PhysRevResearch.2.023135>.

Investigation of electrophysical properties, phase diagrams and charge carrier transfer in $\text{Bi}_{1-x}\text{Sm}_x\text{FeO}_3$ nanopowders

V. O. Kolupaiev, A. N. Morozovska, V. N. Poroshin, and O. S. Pylypchuk

*Institute of Physics, National Academy of Sciences of Ukraine, 46, pr. Nauky, 03028 Kyiv, Ukraine
e-mail: kolupaiev.v.o@gmail.com*

Nanoscale multiferroics with different sizes and shape parameters are basic model objects for studying polar, antipolar, and magnetic orientation as well as magnetoelectric interaction. Samarium doped bismuth ferrite ($\text{Bi}_{1-x}\text{Sm}_x\text{FeO}_3$) is a classical orthoferrite, whose polar and magnetic properties have been sufficiently studied for the bulk and thin film samples.

However, both theoretically and experimentally, the properties of $\text{Bi}_{1-x}\text{Sm}_x\text{FeO}_3$ nanoparticles have been studied insufficiently [1], despite being an excellent candidate for application in energy harvesting [2] and storage [3], as well as for creating advanced FeRAM devices [4].

In this work we use the Ginzburg-Landau-Devonshire approach to perform phenomenological calculations of polar, dielectric, and magnetoelectric properties of $\text{Bi}_{1-x}\text{Sm}_x\text{FeO}_3$ nanoparticles, and construct phase diagrams in dependence on the nanoparticle sizes and shape parameters, and on the proportion of samarium in solid solution. Calculations of the surface adsorption/desorption influence on dielectric, polar and magnetoelectric properties at different temperatures are performed in the framework of the Stephenson-Highland approach.

Experimental studies of the temperature dependence of the $\text{Bi}_{1-x}\text{Sm}_x\text{FeO}_3$ nanopowders conductivity in the temperature range of 300 - 700 K are carried out in two modes: at fixed values of the current through the sample and at fixed values of the voltage applied to the sample corresponding to different values of the applied field. Current-voltage characteristics of the powder samples are measured at constant temperature.

The results of the study will allow to improve understanding of the physical mechanisms of conductivity and charge transfer in orthoferrite nanopowders, which will further allow us to create new nanocompounds with improved and/or controllable properties, as well as expand the perspectives of their advanced applications in nanoelectronics and energy storage.

Acknowledgements. The work of A.N.M. and O.S.P. are funded by the National Research Foundation of Ukraine (project “Manyfold-degenerated metastable states of spontaneous polarization in nanoferroics: theory, experiment and perspectives for digital nanoelectronics”, grant N 2023.03/0132). V.O.K. and V.N.P. acknowledges the Target Program of the National Academy of Sciences of Ukraine, Project No. 5.8/25-II “Energy-saving and environmentally friendly nanoscale ferroics for the development of sensorics, nanoelectronics and spintronics”.

- [1] A. N. Morozovska, E. A. Eliseev, I. V. Fesych, Y. O. Zagorodniy, O. S. Pylypchuk, E. V. Leonenko, M. V. Raleev, A. D. Yaremkevych, L. P. Yurchenko, L. Demchenko, S. V. Kalinin, O. M. Fesenko, Reentrant polar phase induced by the ferro-ionic coupling in $\text{Bi}_{1-x}\text{Sm}_x\text{FeO}_3$ nanoparticles, *Physical Review B* 110, 224110 (2024), <https://doi.org/10.1103/PhysRevB.110.224110>.
- [2] S. Chaturvedi, S. K. Singh, P. Shyam, M. M. Shirolkar, S. Krishna, R. Boomishankar, S. Ogale, Nanoscale LuFeO_3 : shape dependent ortho/hexa-phase constitution and nanogenerator application, *Nanoscale* 10, 21406 (2018). <https://doi.org/10.1039/c8nr07825d>.
- [3] Z. Fan, S. Gao, Y. Chang, D. Wang, X. Zhang, H. Huang, Yu. He, Q. Zhang, Ultra-superior high-temperature energy storage properties in polymer nanocomposites via rational design of core-shell structured inorganic antiferroelectric fillers, *Journal of Materials Chemistry A* 11, 7227 (2023). <https://doi.org/10.1039/d2ta09658g>.
- [4] L. Baudry, I. Lukyanchuk, V. M. Vinokur, Ferroelectric symmetry-protected multibit memory cell, *Scientific Reports* 7, 42196 (2017). <https://doi.org/10.1038/srep42196>.

Structural and optical study of undoped and Ag-doped Sb₂S₃ polycrystals and thin films

**Y. M. Azhniuk¹, V. V. Lopushansky¹, A. I. Pogodin², M. J. Filep³,
I. M. Voynarovych¹, V. M. Kryshenik¹, A. V. Gomonnai¹**

¹*Institute of Electron Physics, Nat. Acad. Sci. Ukr., 21 Universytetska Str., 88017, Uzhhorod, Ukraine*

²*Uzhhorod National University, 46 Pidhirna Str., 88000, Uzhhorod, Ukraine*

³*Ferenc Rákóczi II Transcarpathian Hungarian Institute, Kossuth Sq. 6, Berehovo 90200, Ukraine*

e-mail: yu.azhniuk@gmail.com

Antimony trisulphide Sb₂S₃ is a promising chalcogenide material with potential applications in solar energy conversion, thermoelectric cooling technologies, and optoelectronics in the infrared spectral range. Doping Sb₂S₃ with silver, in particular, is known to decrease its intrinsic high electric resistivity what is essential for its use as buffer layer in photovoltaics as well as to increase its refractive index, making it attractive for applications in photonics.

Here we present an X-ray diffraction (XRD) and Raman spectroscopic study of polycrystalline Sb₂S₃ and Sb₂S₃:Ag ingots as well as thermally evaporated films of similar compositions. Sb₂S₃ was synthesised from high-purity elemental Sb and S taken in stoichiometric proportions in evacuated quartz ampoules by two-zone synthesis. Polycrystalline Ag_x(Sb₂S₃)_{1-x} alloys with $x \leq 0.1$ were synthesised at 650 °C in evacuated quartz ampoules for 4 h with subsequent rapid quenching down to room temperature in air. Sb₂S₃ and (Sb₂S₃)_{1-x}Ag_x films were prepared by flash evaporation at 1200 °C on cold silicon and silicate glass substrates.

The polycrystalline Sb₂S₃ and (Sb₂S₃)_{1-x}Ag_x samples were studied by X-ray diffraction (XRD) using an AXRD Benchtop diffractometer with Cu K α radiation and a Ni filter. The XRD patterns of the Sb₂S₃ samples clearly show reflections corresponding to the orthorhombic structure while for Ag_x(Sb₂S₃)_{1-x} diffraction peaks characteristic for both orthorhombic Sb₂S₃ (stibnite) and cubic AgSbS₂ are observed, the intensities of the latter increasing with Ag content.

Raman spectra of the polycrystalline and thin-film Sb₂S₃ and (Sb₂S₃)_{1-x}Ag_x samples were measured using an XPlora Plus spectrometer (Horiba) equipped with a 532 nm laser and a cooled CCD camera. At low laser power density $P_{\text{exc}}=4$ kW/cm², the polycrystalline samples exhibited Raman spectra typical for crystalline Sb₂S₃ with most prominent features at 282 and 302 cm⁻¹. Silver-containing polycrystalline samples did not reveal Raman peaks characteristic for cubic AgSbS₂ or any noticeable features which could be related to the vibrations of Ag–S or Ag–Sb bonds. At increased $P_{\text{exc}}=40$ kW/cm², we observed the appearance of new sharp Raman peaks as evidence for the photoinduced crystallisation of elemental Sb (106, 117, and 142 cm⁻¹) as well as Sb₂O₃ (188, 250, 370, and 447 cm⁻¹). Most likely, the photococrystallisation is driven by thermal mechanism (the sample heating due to the absorption of the above-bandgap laser beam), although a contribution of nonthermal mechanism cannot be excluded either (photodeformation of the sample surface in the form of a pit in the laser spot was clearly observed).

Raman spectra of the Ag_x(Sb₂S₃)_{1-x} films measured at $P_{\text{exc}}=4$ kW/cm² exhibited broad features, typical for amorphous Sb₂S₃, namely a less intense maximum near 140 cm⁻¹ and a prominent broad band at 287 cm⁻¹, corresponding to the vibrations of SbS₃ (often denoted as SbS_{3/2}) structural units present in the amorphous Sb₂S₃ structure. Increasing P_{exc} to 40 kW/cm² results in photoinduced crystallisation of Sb₂S₃ in the films, accompanied by the appearance of Raman features of elemental Sb and Sb₂O₃. Interestingly, the Raman features related to Sb₂O₃ appear in the Raman spectra measured at an increased P_{exc} even when the sample during the measurement is immersed in isopropanol to prevent access of oxygen from the air. In our opinion, oxygen might have been contained in the subsurface voids in the film structure.

The study was supported by the "Advanced Science in Ukraine" grant No. 2023.03/0013 by National Research Foundation of Ukraine.

Optical properties and transition temperatures of multiple structures of amorphous ice mixed with CO₂

N. N. Chigambayeva, A. Y. Nurmukan

*Al-Farabi Kazakh National University, al-Farabi ave., 71, Almaty, 050040, Kazakhstan
e-mail: nurgul050490@gmail.com*

Amorphous ice has unique optical properties such as refraction, absorption and scattering of light, which depend on temperature, pressure and density. When mixed with carbon dioxide, the properties change due to its interaction with water molecules, which affects the molecular structure of ice [1]. At low temperatures, amorphous ice exhibits anomalous absorption and scattering spectra. CO₂ alters the thermodynamic behavior of amorphous ice, promoting the formation of denser phases. This, in turn, affects its optical properties and transition temperatures, including the sublimation temperature of both ice and CO₂ [2]. Temperature-induced transitions of amorphous ice mixed with CO₂ include both transformations between different amorphous states and crystallization. The transition temperature varies depending on the mixture's composition and pressure [3]. Experiments are ongoing to study these systems under various conditions, which is important for the development of cryogenic CO₂ storage technologies and for understanding the behavior of ice in planetary environments [4].

In this work, the experiments were conducted using a cryovacuum setup designed to study substances under conditions simulating those of outer space. The setup enables to study infrared spectra, refractive indices, and the density of condensed substances in the temperature range of 11–300 K and at pressures down to 1×10^{-10} Torr. Important physical and optical parameters are determined based on FTIR spectroscopy (the spectral measurement range of 400–7800 cm⁻¹) and laser interferometry [5]. Non-directional deposition of substances from the vapor phase promotes the formation of ice analogous to that found in space, making the setup an effective tool for interpreting astrophysical data and studying the properties of space objects.

During the experimental studies, it was found that gas molecules adsorbed on the material's surface gradually desorb as the temperature increases. These experiments enabled a more in-depth study of the interaction between the substance and various gases, as well as an investigation of how gas molecules bind to the material's surface under varying temperature conditions. The mass spectrometry results showed peaks corresponding to carbon dioxide molecules mixed with water. Additionally, peaks corresponding to the release of CO₂ and H₂O molecules were obtained, along with changes in the intensity of laser radiation recorded during the heating of the film. These data demonstrate the desorption of carbon dioxide from the material's surface during the temperature-induced desorption experiment, in which the gradual increase in temperature causes the gas to be released from the surface.

- [1] E. Korshikov, A. Aldiyarov, A. Nurmukan, O. Vorobyova, D. Sokolov, Solid State Sci. 161, 107830 (2025). <https://doi.org/10.1016/j.solidstatesciences.2025.107830>.
- [2] L. J. Karssemeijer, G. A. de Wijs, H. M. Cuppen, Phys. Chem. Chem. Phys. 16, 15630 (2014). <https://doi.org/10.1039/C4CP01622J>.
- [3] J. N. Stern T. Loerting, Phys. Chem. Chem. Phys. 20, 12589 (2018). <https://doi.org/10.1039/C7CP08595H>.
- [4] K. B. Fard, I. B. Smith, Icarus 410, 115895 (2024). <https://doi.org/10.1016/j.icarus.2023.115895>.
- [5] O. Golikov, D. Yerezhep, A. Akylbayeva, D. Yu. Sokolov, E. Korshikov, A. Nurmukan, A. Aldiyarov, Sci. Rep. 13, 21155 (2023). <https://doi.org/10.1038/s41598-023-48541-3>.

Change of structure of polyimide PM-A after low temperature deformation

V. G. Geidarov

*B.Verkin Institute for Low Temperature Physics and Engineering of NAS of Ukraine,
47 Nauky Ave., Kharkiv, 61103, Ukraine
e-mail: geydarov@ilt.kharkov.ua*

Polyimide polymers are widely used in various fields of modern technology due to their unique physical properties [1, 2]. However, because of the complex molecular structure, some questions still need to be clarified. Thus, there is no information about what happens to the objects mentioned under the influence of low temperatures. In this work, we suggest one explanation for the reaction of the sample processing method. The X-ray studies of these substances give the X-ray scattering pattern, typical for amorphous solids and characterized by a short-range order.

This paper presents the results of the X-ray diffraction study of the PM-A polyimide type (Group V) [1], subject to uniaxial tension (elastic deformation), bulk compression (by means of cooling down to low temperatures) and their joint impact. Samples for the experiments had a shape of strips with dimensions 70 x 5 x 0.08 MM³. The X-ray diffraction studies were performed on a DRON-2.0 facility. Measurements were carried out over a wide range of angles.

All radiographs observed a halo typical for amorphous solids. The halo is symmetrical to the initial film. An external influence (of low temperature and strain nature) results in a substantial redistribution of intensities. The observed asymmetric shape of the halo consists of two peaks: the main one at $2\theta = 17^\circ$ and the satellite one at $2\theta = 23^\circ$. An additional peak indicates the appearance of the area of short-range order with the atom density, which differs from that of the initial sample.

Upon cooling the sample from nitrogen down to helium temperatures, the main peak does not change its position, while the satellite one shifts toward small angles ($2\theta = 5.5^\circ$). During deformation at 77 K (the combined effect of temperature and strain), no qualitative changes appear in comparison with the net cooling regime of the sample. After applying deformation at 4.2 K, the diffraction pattern becomes symmetrical.

We suggest that the behavior of the PM-A polyimide can be explained within different mechanisms of ordering of long molecules under uniaxial and bulk loading.

[1] M. I. Bessonov, M. M. Koton, V. V. Kudryavtsev, L.A. Laius, Polyimides: Thermally Stable Polymers (Macromolecular Compounds, Springer-Verlag, New York 1987). ISBN-13: 978-1461576365.

[2] V. E. Gul, Structure and Properties of Conducting Polymer Composites (New Concepts in Polymer Science, CRC Press, London 1996). <https://doi.org/10.1201/9780429070273>.

Classical and fractal models of chalcogenide glasses viscoelasticity

A. A. Horvat, A. A. Molnar, V. V. Minkovych

*Faculty of Physics, Uzhhorod National University,
A. Voloshin str., 54, 88000 Uzhhorod, Ukraine
e-mail: ahorvat@ukr.net*

This report presents experimental data on the viscoelastic behaviour of chalcogenide glasses in a sufficiently wide time (frequency) domain near the softening temperature and the models used to describe the mechanical relaxation processes.

Chalcogenide glasses have been extensively studied by various methods, however their long-term mechanical relaxation processes have not been investigated. We have therefore studied mechanical stress relaxation and creep on a torsion pendulum observing the time dependence of the torque in response to a step deformation or strain behavior under constant stress.

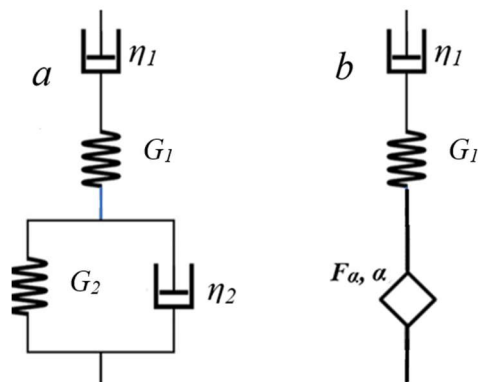


Fig. 1. Classical Burgers (*a*) and partially fractal (*b*) viscoelastic models.

example, for As-Se glass with $T_g \approx 435\text{K}$, in the range of $370 - 430\text{ K}$, G_2 decreases drastically from 150 GPa by more than a hundred times, while G_1 changes only from 6.0 GPa to 3.5 GPa.

Classical rheological models represent a simple combination of Hooke's and Newton's bodies, resulting in exponential stress and strain time dependencies. However, a vast of materials with complex microstructures, such as glasses, are characterized by a power-law dependence of their creep and stress with time. The power-law behaviour can be explained by generalizing the classical models by introducing a fractional derivative of different orders, which leads to the creation of fractal viscoelastic models. In order to reflect the diversity of viscoelastic behavior, it is advisable to use a combination of classical and fractal models; in particular, we proposed to replace the Kelvin-Voigt element by a fractal element in the Burgers model. In this way, purely elastic and plastic properties are reproduced, and the fractal element provides a power law for the behaviour of the mechanical parameters. The constitutive equation for this model is

$$\sigma + \frac{F_\alpha}{\eta} \frac{d^{\alpha-1}\sigma}{dt^{\alpha-1}} + \frac{F_\alpha}{G} \frac{d^\alpha\sigma}{dt^\alpha} = F_\alpha \frac{d^\alpha\varepsilon}{dt^\alpha}, \text{ and its solution is as follows: } \varepsilon(t) = \sigma_0 \left(\frac{1}{G} + \frac{t}{\eta} + \frac{t^\alpha}{F_\alpha \Gamma(1+\alpha)} \right).$$

Even this partially fractal model gives a better correlation between experimental and calculated data than the classical one. The parameter α of the fractal model varies within a small range: $0.25 \leq \alpha \leq 0.20$, while F_α decreases sharply, as expected, when the glass softening point is approached. It should also be noted that the introduction of fractality leads to an increase in the parameter η_1 of 20-25% with an unchanged value of G_1 in comparison with the classical model. It can be assumed that the physical meaning of the fractional derivative order in the description of viscoelasticity is determined by the fractal dimension of the relaxation times set.

As expected, an increase in temperature accelerates the relaxation processes, while the initial value of the mechanical stress σ , needed to achieve the constant strain, decreases with increasing temperature. Even at temperatures far from the glass softening temperature T_g , the strain ε does not disappear after removal of the mechanical load and relaxation for $(6-9) \cdot 10^3$ sec clearly indicates the presence of residual plastic deformation in the studied glasses. Taking the fact into consideration, we firstly considered the four-element Burgers model (Fig. 1 *a*), which consists of Maxwell and Kelvin bodies connected in series. The temperature dependence of these model parameters η_1 , G_1 and η_2 , G_2 were determined using experimental data on the relaxation of mechanical stress with time. For

The microstructure and low-temperature mechanical properties of ultrafine-grained copper: effect of deformation and annealing

T. Hryhorova¹, S. Shumilin¹, P. Zabrodin^{1,2}, D. Drozdenko³

¹*B.Verkin Institute for Low Temperature Physics and Engineering of NAS of Ukraine,
47 Nauky Ave., Kharkiv, 61103, Ukraine*

²*Czech Academy of Sciences, Institute of Theoretical and Applied Mechanics,
Prosecka 809/76, 190 00 Prague, Czech Republic*

³*Charles University, Faculty of Mathematics and Physics, Department of Physics of Materials,
Ke Karlovu 5, Prague, 121 16, Czech Republic
e-mail: grigorova@ilt.kharkov.ua*

In this paper, a comparative analysis of the mechanical properties and microstructure of oxygen-free copper in the ultrafine-grained (UFG) and coarse-grained (CG) states is carried out. The UFG copper structure was obtained as a result of angular hydroextrusion of 5 passes along the B_c route. The coarse-grained state was achieved by high-temperature annealing of UFG samples at a temperature of 600°C for 1 hour in a vacuum.

Electron backscattering spectroscopy (EBSD) and optical microscopy were used to obtain microstructure data. Grain size, high-angle and low-angle boundary ratios, and internal stresses of copper samples were analyzed. The temperature dependence of stress sensitivity and strain rate was studied to obtain information on the plastic deformation mechanisms of the studied polycrystals in different structural states and at different temperatures. The grain size after hydroextrusion was 500 nm. Annealing resulted in recrystallization and grain growth, with an average grain size of 20 μm. Constant-rate strain experiments were conducted at temperatures of 77 K and 295 K. In addition, the stress relaxation method was used to estimate the activation volume V of plastic deformation.

It was found that as a result of annealing, leading to an increase in the grain size, a decrease in the flow stress occurs. In this case, the correspondence according to the classical Hall-Petch relation is fulfilled. With a decrease in temperature, the plasticity of the samples increases due to the suppression of dynamic recovery processes. Analysis of the hardening curves indicates that dynamic recovery has the greatest effect on the parameters of hardening and relaxation of UFG samples at 295 K. At T = 77 K, in CG copper, intensive accumulation of dislocations mainly occurs during plastic deformation, in contrast to UFG copper, where recovery processes are also observed.

Estimation of the activation volume V for CG and UFG copper showed the following. For CG copper at 77 K and 295 K, V is 200b³ and 1200b³, respectively, which is in good agreement with the theory of thermally activated motion of dislocations through local obstacles. Meanwhile, for UFG copper, both at 77 K and at 295 K, the value of the activation volume is about 100b³. The absence of growth V with temperature contradicts the above theory and indicates a change in the mechanism of plastic deformation at 295 K in UFG copper polycrystals.

The low-temperature plasticity and deformation microstructure of SPD Al-Li alloy

T. Hryhorova¹, S. Shumilin¹, P. Zabrodin^{1,2}, D. Drozdenko³

¹*B.Verkin Institute for Low Temperature Physics and Engineering of NAS of Ukraine,
47 Nauky Ave., Kharkiv, 61103, Ukraine*

²*Czech Academy of Sciences, Institute of Theoretical and Applied Mechanics,
Prosecka 809/76, 190 00 Prague, Czech Republic*

³*Charles University, Faculty of Mathematics and Physics, Department of Physics of Materials,
Ke Karlovu 5, Prague, 121 16, Czech Republic
e-mail: grigorova@ilt.kharkov.ua*

The plastic deformation of microgranular polycrystals of Al-Li alloy obtained by severe plastic deformation (SPD) was investigated. The SPD used was an angular hydroextrusion (AHE) method (6 passes, B_c route). A comprehensive analysis of the microstructure was carried out with an emphasis on the evolution of grain size, texture and dislocation structure.

Flat samples of the solid solution Al-3.8 at. % Li alloy cut from AHE-blanks were subjected to tensile deformation in a wide temperature range (from helium to above room temperature) in the active deformation and stress relaxation mode in a helium cryostat equipment. The microstructure evolution was studied using electron backscatter diffraction (EBSD) method, including orientation and mean misorientation (KAM) imaging.

It has been established that hydroextrusion results in grain refinement (average size $d \sim 1 \mu\text{m}$) and the formation of a microstructure characterized by grains with small angles of misorientation and high dislocation density. Grain refinement and an increase in the grain boundary density after hydroextrusion determine the high yield strength observed in the microcrystalline alloy.

It is shown that the microstructure of the samples after tensile deformation at temperatures below 77 K is characterized by high internal deformations and a high density of low-angle grain boundaries, which indicates a high capacity for dislocation accumulation. This ensures an increase in plasticity and strain hardening with a decrease in temperature in the range of 4.2-100 K. In the temperature range of 140-295 K low plasticity (elongation to failure of 3-7 %) of the microcrystalline alloy, which is expressed in the localization of plastic deformation already at small deformations, is due to the low rate of strain hardening due to increased dynamic recovery in micrograins. The microstructure of the sample deformed at 400 K differs from rest of the samples deformed at lower temperatures and characterized by a high density of high-angle grain boundaries and low internal deformations.

The temperature dependences of the yield strength and activation volume of plastic deformation obtained in experiments are discussed within the model of thermally activated intersection of dislocations against the background of significant strengthening of microgranular polycrystals due to the high density of grain boundaries and dislocations.

Peculiarities of the electronic and elastic properties of indium selenide in different structural modifications

O. I. Korolov, L. Yu. Kharkhalis, K. E. Glukhov

*Institute for Physics and Chemistry of Solid State, Uzhhorod National University,
54 Voloshin St., Uzhhorod, 88000, Ukraine
oleh.korolov@uzhnu.edu.ua*

Today, the InSe two-dimensional crystals are considered promising candidates for optoelectronics and alternative energy sources due to their unique optical and transport properties. These materials, owing to the layered structure, are widely used for the formation of nanosheets and heterostructures (β -InSe/graphene, InSe/Si, InSe/InP, and InSe/In₄Se₃, InSe/MoSe₂) for the development of new semiconductor devices so as transistors, photodetectors, and sensors [1, 2]. Indium selenide also possesses various polytypes with different stoichiometry, depending on the arrangements of atoms and the stacking layers. For example, β -InSe and ε -InSe polytypes crystallize in a hexagonal lattice, and γ -InSe features a rhombohedral structure [3]. The differences between the geometry of crystalline polytypes of InSe directly influence their electronic, optical, and mechanical properties. Therefore, the investigation of physical properties of these structural modifications is of great interest. Such a study is significant for constructing novel heterostructures to optimize their electronic properties and promote mechanical stability.

The report compares three modifications of indium selenide (InSe) – β -InSe, ε -InSe, and γ -InSe – focusing on their electronic, mechanical, dielectric, optical, and light absorption properties.

From our first-principles calculations of the band structure, the β -InSe and γ -InSe bulk crystals demonstrate the direct band gap (at the Γ and Z points in the Brillouin zone, respectively). At the same time, the ε -InSe polytype shows the indirect band gap. Mulliken charges analysis supports the distinct variations of their redistribution across the polytypes that can be attributed to the specialty of the crystallographic arrangements and provides a detailed understanding of the electronic distribution and bonding characteristics within β -InSe, ε -InSe, and γ -InSe.

The study also compared dielectric properties, refractive indices, and absorption characteristics of the three InSe modifications. The real and imaginary parts of the dielectric function, refractive indices, and absorption coefficients were calculated for each modification across different polarizations along crystal axes. For β -InSe and ε -InSe modifications, significant variations with anisotropy character in dielectric properties depending on photon energy are observed. At the same time, γ -InSe exhibits isotropic dielectric behavior, making it ideal for applications demanding consistent properties.

Mechanical characteristics (elastic moduli, Young's moduli, Poisson's ratios) were also calculated for the β -InSe, ε -InSe, and γ -InSe bulk crystals. Analysis of these characteristics and the B/G ratio, an indicator of ductility, shows that γ -InSe and β -InSe have closer values than ε -InSe.

Thus, carried-out investigations of electronic, optical, and mechanical properties of indium selenides in different structural polytypes confirm that each modification exhibits unique characteristics and provides valuable insights for specific applications of selected materials in optoelectronics, photonics, and semiconductor devices.

- [1] D. K. Sang, H. Wang, M. Qiu, R. Cao, Z. Guo, J. Zhao, Yu Li, Q. Xiao, D. Fan, H. Zhang, Nanomaterials 9, 82 (2019). <https://doi.org/10.3390/nano9010082>.
- [2] Z. Chen, J. Biscaras, A. Shukla, Nanoscale 7, 5981 (2015). <https://doi.org/10.1039/C5NR00400D>.
- [3] I. Grimaldi, T. Gerace, M. M. Pipita, I. D. Perrotta, F. Ciuchi, H. Berger, M. Papagno, M. Castriota, D. Pacilé, Solid State Communications 311, 113855 (2020). <https://doi.org/10.1016/j.ssc.2020.113855>.

The role of internal stresses in the realisation of dislocation-diffusion viscous flow of eutectic alloys under the conditions of superplasticity

V. F. Korshak¹, Y. O. Shapovalov², P. P. Pal-Val²

¹*V. N. Karazin Kharkiv National University, 4 Svobody Sq., Kharkiv, 61022, Ukraine*

²*B. Verkin Institute for Low Temperature Physics and Engineering of NAS of Ukraine,
47 Nauky Ave., Kharkiv, 61101, Ukraine
e-mail: vera.korshak@gmail.com*

At present, when studying the effect of superplasticity, the opinion has been dominated that there are two types of superplasticity: the structural one, which is observed in ultrafine-grained materials, and superplasticity under special external conditions, associated, in particular, with the occurrence of a distinct phase transformation. In this case, the role of external conditions is to ensure a high level of internal stress in the material. As applied to materials exhibiting structural superplasticity, the issue of internal stresses has practically not been studied.

The eutectic alloys of Sn-38 wt.% Pb and Bi-43 wt.% Sn are considered typical ones exhibiting structural superplasticity. However, the studies conducted by the authors show that the superplastic flow therein is realized against the background of the decomposition of supersaturated solid solutions formed under crystallization conditions. Under superplastic conditions, the determining mechanism of deformation is a diffusion-dislocation viscous flow, but not grain boundary sliding, as reported in the literature. The updated results have actualized an issue of the role of internal stresses in the manifestation of the superplasticity effect in mentioned alloys [1–3].

The authors found that internal stresses arise therein as a result of the preliminary deformation by compression in a press by 70–75%. This is evidenced by the observed decrease in the parameters of the crystal lattice of the $\beta(\text{Sn})$ phase (solid solution of lead in tin) in the Sn-38wt.%Pb alloy and macroscopic cracking of Bi-43wt.%Sn alloy ingots, as well as an increase in the Young's moduli of both alloys as a result of compression. Superplastic flow is accompanied by relaxation of internal stresses, as indicated by an increase in the crystal lattice parameters of the $\beta(\text{Sn})$ phase in the Sn-38 wt.% Pb alloy and a decrease in the Young's moduli of both alloys. Moreover, the performed estimations indicate that the level of the indicated stresses is sufficient to activate the Frank-Read dislocation sources inside the grains and to ensure a significant increase in the dislocation density during the process of superplastic deformation. The reduction in elastic moduli and the formation of a highly dispersed structure of the material, associated with the occurrence of initial stages of decay, also ensure, on the one hand, the activation of additional dislocation sources and diffusion processes in the material, on the another hand. It is shown that the decomposition of supersaturated solid solutions in studied alloys is accompanied by the emergence of internal stresses caused by the volumetric effect of transformation. Such stresses affect the kinetics of decay and the dislocation subsystem in the material. The kinetic correspondence of the processes of deformation and structural-phase transformations, determined by the nonequilibrium of the phase composition and the occurrence and relaxation of internal stresses, ensures the possibility of the active development of dislocation-diffusion viscous flow of eutectic alloys under conditions of superplasticity.

- [1] V. F. Korshak, Yu. O. Shapovalov, P. V. Mateichenko, J. Mater. Sci., 53, 8590 (2018). <https://doi.org/10.1007/s10853-018-2163-1>.
- [2] V. F. Korshak, Yu. A. Shapovalov, A. L. Samsonik, P. V. Mateichenko, Phys. Met. Metallogr. 113, 190 (2012). <https://doi.org/10.1134/S0031918X1202007X>.
- [3] V. F. Korshak, Yu. A. Shapovalov, P. P. Pal'-Val', P. V. Mateichenko, Bull. Russ. Acad. Sci. Phys., 75, 1345 (2011). <https://doi.org/10.3103/S1062873811100200>.

Photo- and thermostimulated phase transformations in $\text{Ge}_2\text{Sb}_2\text{Se}_{5-x}\text{Te}_x$ glasses

V. M. Kryshenik¹, S. M. Hasynets¹, Y. M. Azhniuk¹, M. J. Filep²,
V. V. Lopushansky¹, O. O. Gomonnai³, V. Y. Loya¹, A. V. Gomonnai¹

¹*Institute of Electron Physics of NAS of Ukraine, 21 Universytetska Str., Uzhhorod, 88017, Ukraine*

²*Ferenc Rákóczi II Transcarpathian Hungarian Institute, Kossuth Sq. 6, Berehovo 90200, Ukraine*

³*Uzhhorod National University, 46 Pidhirna Str., Uzhhorod, 88000, Ukraine*

e-mail: kryshenik@gmail.com

Optical phase-change materials are characterised by extraordinary variation of optical parameters under reversible phase transitions between the crystalline and amorphous states. Among them, Ge–Sb–Se–Te compounds are especially important, with high differences of refractive index and reflectivity for the crystalline and amorphous phases combined with low optical loss in a broad spectral range (1–18 μm) for both phases [1]. High glass formation ability of these materials provides stability of their characteristics in highly productive optical switches and modulators [2].

$\text{Ge}_2\text{Sb}_2\text{Se}_{5-x}\text{Te}_x$ glasses with $0 \leq x \leq 1$ were prepared from stoichiometric amounts of elemental components in evacuated quartz ampoules heated to 973 K at a rate of 30 K/h followed by the mixture heating to 1273 K at a rate of 20 K/h with the subsequent aging for 20 h and cooling at 25 K/h down to 873 K and rapid quenching in cold water.

The structure of samples in the whole compositional range obtained was studied by X-ray diffraction (XRD) using an AXRD Benchtop diffractometer with Cu K_α radiation and a Ni filter and confirmed to be completely amorphous without any crystalline inclusions.

Kinetic analysis of the processes of non-isothermal crystallisation in $\text{Ge}_2\text{Sb}_2\text{Se}_{5-x}\text{Te}_x$ was performed using differential thermal analysis data obtained at a fixed set of heating rate values ($\beta = 2, 4, 6, 9, 12$, and 15 K/min). This enabled us to determine the glass-forming temperature T_g , the phase transformation onset temperature T_{ons} , and the exothermic crystallisation peak temperature T_p . For all the samples under study, thermally stimulated crystallisation is shown to be governed by a one-step mechanism. Formation of crystalline inclusions in the amorphous matrix is confirmed by the XRD measurements for the samples heated at $\beta \geq 6$ K/min, the crystalline phase being identified as $\text{Ge}_2\text{Sb}_2\text{Se}_5$ (for $x = 0$) or $\text{Ge}_2\text{Sb}_2\text{Se}_4\text{Te}$ (for $x > 0$), compared to the known data [4].

The activation energy E_c of the amorphous-to-crystalline transformation under study was determined by the Kissinger method [3]. With increasing Se content in $\text{Ge}_2\text{Sb}_2\text{Se}_{5-x}\text{Te}_x$ from 0 to 1, the crystallisation peak temperature T_p at $\beta = 6$ K/min gradually varied from 599 to 622 K with E_c decreasing from 178 to 142 kJ/mole. A similar trend was observed for other heating rate values.

Raman spectroscopic measurements were performed using an XPloRa Plus spectrometer (Horiba) equipped with a 532 nm laser and a cooled CCD camera. Raman spectra measured at a medium power density $P_{\text{exc}}=4$ kW/cm² exhibit a weak compositional dependence with most prominent relatively broad features in the ranges of 150–160 and 190–200 cm⁻¹ rather similar for all sample compositions. Meanwhile, the increase in P_{exc} to 40 kW/cm² results in a drastic change in the Raman spectra with emerging broad maxima at 180–190 and 420–440 cm⁻¹. Possible nonthermal and thermal mechanisms responsible for this photostructural transformations are discussed. No evidence for the separation of elemental tellurium was observed, which is quite typical for telluride-based materials under heating or intense illumination.

- [1] Y. Zhang, J. B. Chou, J. Li et al, Nat. Commun. 10, 4279 (2019). <https://doi.org/10.1038/s41467-019-12196-4>.
- [2] X. Chen, Y. Miao, Y. Zhang, Y. Bai, J. Yao, J. Opt. 27, 025801 (2025). <https://doi.org/10.1088/2040-8986/ada2fc>.
- [3] H. E. Kissinger, J. Res. Natl. Bur. Stan. 57, 217 (1956). <https://doi.org/10.6028/jres.057.026>.
- [4] R. Svoboda, P. Bezdička, J. Gutwirth, J. Málek, Mater. Res. Bull. 61, 207 (2014). <https://doi.org/10.1016/j.materresbull.2014.10.032>.

Study of the sensory response of porous films with fluorescent dyes to microconcentrations of acetone and ammonia

Ya. P. Lazorenko¹, V. P. Mitsai²

¹*G.V. Kurdyumov Institute for Metal Physics of the NAS of Ukraine,
36 Akad. Vernadskogo blvd., Kyiv, 03142, Ukraine*

²*V.G. Baryakhtar Institute of Magnetism of the NAS of Ukraine,
36-b Akad. Vernadskogo blvd., Kyiv, 03142, Ukraine
e-mail: lazorenko85@gmail.com*

Porous film structures with fluorescent dyes represent a promising direction in the development of selective and highly sensitive sensors of volatile compounds [1]. Currently, the materials are actively studied in order to improve their sensor characteristics with further implementation in various fields of application, such as environmental air pollution monitoring, non-invasive medical diagnostics by analyzing biomarker molecules in exhaled air, and more [2]. Organic fluorescent dyes, particularly rhodamine 6G, can be used as fluorophores in films that interact with acetone or ammonia molecules, leading to changes in their fluorescent properties. Of particular interest is the fluorescence enhancement of dye molecules by quantum dots (QDs) through the Förster resonance energy transfer (FRET), which can be utilized to increase the effective fluorescence signal. Porous silicate sorbents have a large specific surface area and are promising for the adsorption of volatile molecules from gaseous environment in gas-sensor materials. This work is devoted to the study of the fluorescent and sensing properties of silicate sorbents with rhodamine 6G films to volatile acetone and ammonia in gas mixtures in the microconcentration range.

Experimental studies have shown a 1.5-fold increase in the fluorescence intensity of rhodamine 6G in an ethanol solution when CdTe/TGA quantum dots are added at a 1:1 ratio. The FRET explains the effect, which occurs due to the overlap between the fluorescence band of QDs and the absorption band of rhodamine 6G.

The spectral-luminescent properties of porous film samples based on adsorption matrices of Aerosil A-180 (specific surface area of 180 m²/g) with rhodamine 6G dye, as well as silica gel-60 (500 m²/g) with rhodamine 6G dye and CdTe/TGA quantum dots were investigated. We obtained absorption, fluorescence excitation, and fluorescence emission spectra of the aforementioned samples. No shift of the fluorescence band was observed when rhodamine 6G interacted with acetone molecules in the Aerosil matrix.

The sensory responses of the fabricated films were investigated upon interaction with acetone or ammonia molecules in an air environment, representing a decrease in the fluorescence intensity of the samples. The fluorescent response of the samples with Aerosil to an acetone concentration of 6.9 ppm was 3.26 %, while that of the samples with silica gel to an ammonia concentration of 5 ppm was 3 %. After purging the cuvette containing a sample with clean air, the fluorescence intensity of each sample type was restored, indicating sensor recovery due to the desorption of analyte molecules from the film surface.

The synthesized sensor materials with rhodamine 6G showed fluorescent sensitivity to acetone and ammonia in air within the concentration range of 1-10 ppm, demonstrating their potential for use in highly sensitive sensors for ambient air pollution monitoring and noninvasive medical diagnosis based on exhaled breath analysis.

[1] Risipandi Mesin, Cheng-Shane Chu, and Zong-Liang Tseng, Opt. Mater. Express 13, 945 (2023). <https://doi.org/10.1364/OME.487332>.

[2] V. P. Mitsai, Ya. P. Lazorenko, A. G. Misura, and S. O. Mamilov, Nanosist. nanomater. nanotehnol. 19, 0941 (2021). <https://doi.org/10.15407/nnn.19.04.941>.

Experimental studies of hydrogen-palladium interaction in the α -region of the Pd-H diagram

O. M. Liubymenko

*State higher education institution "Donetsk National Technical University",
Sambirska st., 76, Drohobych, Lviv region, 82100, Ukraine
e-mail: e.n.lyubimenko@gmail.com*

At the present stage of Ukraine's development, the issue of energy independence is extremely important. One of the most promising areas is the use of hydrogen as an energy source. In order to ensure the safety of energy plants that use and store hydrogen, it is necessary to study in detail the interaction of hydrogen with materials, in particular with palladium. The interaction of hydrogen with palladium in the α -region of the Pd-H system causes hydrogen concentration stresses and changes in its crystal structure. The effect observed is due to the ability of hydrogen to penetrate the octahedral lattice cavities, which can result in equipment breakdowns and changes in the shape of products even at low hydrogen concentrations in the material. Studies of the interaction between palladium and hydrogen are important for the development of new materials for hydrogen storage.

The work presented aims to experimentally study the shape change of cantilevers made of α -PdH_n alloy (where n is the hydrogen concentration in palladium) under additional and sequential hydrogen saturation.

The main focus is on conducting experiments and studying the behaviour of materials under different conditions, which will help solve problems with hydrogen storage and production. The experimental part was devoted to the study of the hydrogen content change on the same value when saturating the α -PdH_n alloy at different rates.

A cantilever made of high-purity palladium (99.99%) was placed in a hydrogen-vacuum apparatus [1], with one end fixed in a holder. The upper side of the cantilever was coated with a copper film, which is impermeable to hydrogen and does not influence the cantilever's deformation. In the chamber at a constant temperature, the pressure was increased to a predetermined value at different rates. Simultaneously, the hydrogen saturation of the cantilever and its shape change were observed, with the cantilever's bending measured using a cathetometer. As a result, alloys with different hydrogen contents, α -PdH_n, α -PdH_{2n}, and α -PdH_{3n}, were obtained. The saturation process was recorded on video. This enabled the acquisition of the time-dependent change in the cantilever's shape during the formation of temporary gradient alloys of palladium with hydrogen. Our studies show that the bending of the cantilever from the α -PdH_n alloy is fully reversible and occurs in two stages:

- 1) the maximum bending is achieved and a plateau is formed (the stage itself is very short);
- 2) the cantilever returns to its original state (the stage is longer than the first one).

Notably that in case of this alloy, the maximum bending value for the cantilever exceeds the bending that pure palladium can withstand, indicating the formation of an alloy with enhanced plastic properties.

Experimental studies have shown that, with the same increase in hydrogen concentration in palladium, the time required to reach the maximum bend (peak) increases with each subsequent infusion. This indicates that the hydrogen accumulation in the palladium structure causes changes in the kinetics of hydrogen diffusion and dilatation of the material's crystal lattice.

For the first time, it has been experimentally documented that the shape of the curves, the rate of reaching the steady state, and the kinetics of the process of returning the cantilever to its initial state for α -PdH_n alloys depend on the rate of hydrogen injection into the chamber, and consequently, on the rate of hydrogen saturation and penetration into the palladium.

[1] O. M. Lyubimenko, Metallofizika i Noveishie Tekhnologii 45, 263 (2023).
<https://doi.org/10.15407/mfint.45.02.0263>.

The influence of hydrogen diffusion on electrical resistivity of amorphous metallic alloys

A. Grib, V. Makharynskyi

*Physics Department, V. N. Karazin Kharkiv National University,
Svobody sq. 4, Kharkiv, 61022, Ukraine
makharynskyi2025fo13@student.karazin.ua*

In the present work, we discuss the determination of the hydrogen diffusion coefficient D_H in amorphous metallic alloys based on changes in the electrical resistivity $\Delta\rho$ of the alloy caused by hydrogen. The method for determining D_H in crystalline metals from $\Delta\rho$ values is based on the proportionality of the residual resistivity to the small concentration of hydrogen, since protons in metal lattices are treated as interstitial impurities. By specifying the initial spatial distribution of hydrogen, one can calculate D_H from the spatial evolution of $\Delta\rho$ over the diffusion time. However, in metallic alloys with an amorphous structure, this approach fails, since the main contribution to the electrical resistivity comes from the structure factor of the alloy at twice the Fermi wave number, $2k_F$, of electrons [1]. In the present work, we modeled hydrogen diffusion in amorphous metals considering changes in the structure factor induced by hydrogen.

We numerically modeled hydrogen diffusion from an infinite thin hydrogenated layer in the middle of an infinite quasi-one-dimensional amorphous rod at a temperature of 300 K. In this model, the hydrogen diffusion coefficient $D_H = 5.0 \cdot 10^{-9} \text{ m}^2/\text{s}$ was initially set. The aim of the work was to calculate this coefficient from the spatial distribution of resistivity changes in the amorphous rod, expressed as $\Delta\rho(x)/\rho_0 = f(x)$, where $\Delta\rho(x) = \rho(x) - \rho_0$, $\rho(x)$ is the resistivity at a given point x in the hydrogen-saturated part, and ρ_0 is the resistivity of the non-saturated rod. In other words, the goal was to model the experimental conditions and expected results.

The amorphous structure of the rod is described by means of the structure factor, calculated based on the well-known solution of the Percus-Yevick equation for the hard-sphere model [2], with the packing-density parameter of 0.525. To calculate the electrical resistivity, we used a model of electron-phonon scattering in amorphous solids [1], based on the Ziman theory of the electrical resistivity of liquid metals. Our estimates of the influence of hydrogen on resistivity suggest that the main change in resistivity arises from modifications to the structure factor, caused by the volume expansion of the amorphous solid due to the presence of hydrogen and the corresponding shift in k_F . Thus, our main assumption is that the resistivity of hydrogenated parts of the rod is proportional to the value of the structure factor at the shifted value of $2k_F$. Using the assumption, spatial distributions of $\Delta\rho(x)/\rho_0 = f(x)$ along the rod were calculated at different times of the diffusion process. The proton diffusion coefficient was obtained from the time dependence of the variance of these distributions $\langle(x-x_0)^2\rangle = f(t)$. The calculations were performed for various positions of $2k_F$ relative to the position k_p of the first maximum of the structure factor. We found that at $2k_F > k_p$, the presence of hydrogen caused an increase in resistivity, thus $\Delta\rho/\rho_0 > 0$, whereas at $2k_F < k_p$, we obtained $\Delta\rho/\rho_0 < 0$. In both cases, we obtained the correct hydrogen diffusion coefficient D from the dependence of the variance on time, $\langle(x-x_0)^2\rangle = f(t)$. We also discussed the special case of $2k_F \sim k_p$, in which the deviation of the calculated diffusion coefficient from the preset value D_H becomes significant. Therefore, in the present work we demonstrated that the hydrogen diffusion coefficient in an amorphous metal or amorphous alloy can be calculated from the spatial distribution of resistivity changes caused by hydrogen, except in the case when $2k_F \sim k_p$.

- [1] S. R. Nagel, Phys. Rev. B 16, 1694 (1977). <https://doi.org/10.1103/PhysRevB.16.1694>
- [2] N. V. Ashcroft, J. Lekner, Phys. Rev. 145, 83 (1966). <https://doi.org/10.1103/PhysRev.145.83>

Modification of electrophysical parameters of CuInP₂S₆ crystals by betta, gamma and neutron irradiation

A. Molnar¹, A. Haysak¹, I. Haysak¹, D. Gál²

¹Uzhhorod National University, Voloshina Str. 54, Uzhhorod, 88000, Ukraine

²HUN-REN WIGNER Research Center for Physics, Po.Box. 49, 1525 Budapest, Hungary

e-mail: alexander.molnar@uzhnu.edu.ua

The modern development of electronics has reached the physical limits imposed by the miniaturization of microchip active elements to just a few nanometers. At such scales, quantum-mechanical and fundamental physical laws become increasingly significant, manifesting, for example, through tunneling effects or limitation of the subthreshold swing. To overcome these limitations, functional 2D materials such as layered ferroelectrics CuInP₂S₆ are becoming increasingly important. The primary benefit of this material is that it retains its ferroelectric properties at thicknesses below 4 nm, with spontaneous polarization directed perpendicular to the structural layers. Negative capacitance transistors and neuromorphic computational elements have been created on their basis. Therefore, optimization and improvement of the parameters of this material, as well as the study of possible limits of its application is an urgent task.

As with many electronic materials, CuInP₂S₆ crystals exhibit certain disadvantages, including a relatively low phase transition temperature ($T_c \approx 315$ K), ionic conductivity, and other limitations. The present study investigates the influence of radiation defects on the electrophysical parameters of CuInP₂S₆ crystals, a subject of particular importance for the further use of devices based on them in the aerospace industry. It is noteworthy that this technique (irradiation of samples) has a long-standing history in the semiconductor industry, particularly in modifying the mobility of charge carriers.

In the present study, we utilized CuInP₂S₆ crystals, grown from the melt using the Bridgman method. The chemical composition of the crystals was confirmed by the EDAX method, and their dimensions were measured to be 5x5x3 mm³. After measuring the temperature dependence of their dielectric constant (as a reference measurement), the sample was divided into three 1 mm thick plates to ensure chemical composition uniformity. The same procedure was then repeated for each of the resulting plates. The samples were then exposed to β and γ particles at the Microtron accelerator (10^{15} cm²). After irradiation, the temperature dependence of the dielectric permittivity was immediately measured again under the same conditions as in the initial reference studies.

It has been established that irradiation of CuInP₂S₆ samples with β and γ particles significantly affects the dielectric constant, both during phase transitions and at ambient temperature. Furthermore, the phase transition temperature and the shape of the $\epsilon(T)$ anomaly remain largely unaltered. It has been demonstrated that an enhancement in the irradiation dose leads to a suppression of the dielectric constant, with the replacement of β with γ particles resulting in a further reduction in ϵ . This phenomenon is attributed to an increase in the defectiveness of the crystal structure, and the observed difference in the efficiency of β and γ particles are attributed to the different penetration depths of these particles. The defect formation is likely to be charged, and the capture of charge carriers in the CuInP₂S₆ crystal is a probable consequence. This is manifested in the reduced electrical conductivity of the samples, which is reflected in the decrease in the high-temperature "tails" $\epsilon^*(T)$ above 330 K, which are caused by the conductivity of the samples.

Neutron irradiation leads to more significant changes resulting in both phase transition blurring, a decrease in the phase transition temperature and the maximum value of the dielectric constant. This is most likely due to the transmutation of some elements in the CuInP₂S₆ crystals.

Estimation of the thermal conductivity of porous silicon using molecular dynamics and machine learning methods

V. V. Kuryliuk, O. Ya. Olikh

*Taras Shevchenko National University of Kyiv, 64/13, Volodymyrska Str., Kyiv, 03028, Ukraine
e-mail: olegolikh@knu.ua*

Porous media are widely used in various applications, such as thermal barriers or thermoelectric materials for enhancing the figure of merit. In particular, porous silicon (p-Si) layers can be effectively utilized in high-efficiency solar-thermal energy storage systems. Efficiently predicting their thermal conductivity (TC) can accelerate the design of porous systems to improve energy efficiency, among other benefits [1]. The accurate TC estimation can be obtained through the molecular dynamics (MD) simulation. However, such calculations require high computational and time costs. One way to reduce expenses and obtain results for a vast number of cases is to use artificial intelligence methods [2].

This study focuses on applying machine learning (ML) techniques to predict the TC of p-Si based on data obtained from MD simulations using the LAMMPS package. TC was determined by computing the ensemble average of the heat current autocorrelation function within the Green-Kubo formalism. The interaction between silicon atoms was described using the Tersoff potential. We calculated the temperature dependence of TS for porosities of 0%, 20%, and 40%, as well as the dependence of TS on porosity at 300 K – about 30 values in total (see Fig).

The ML application involved two distinct approaches. The first one utilized Symbolic Regression (SR), a method capable of generating analytical equations without prior constraints. The resulting expression obtained using the PySR package is as follows:

$$TC = \left(-7.024 + \frac{7.4810658}{p^{0.54849} + (T_n - 0.10475) / (\sin[T_n / (4.48577618 \cdot p - 0.2514)] + 27.089)} \right) \exp(-p), \quad (1)$$

where p is the porosity ($0 \leq p < 1$), $T_n = T / 300$ is the normalized temperature. The mean percentage error for Eq. (1), compared to MD calculations, is less than 3%.

The second approach employed Random Forest (RF), Gradient Boosting (GB), and Support Vector Regression (SVR) algorithms to construct heat current autocorrelation function. The resulting thermal conductivity values, predicted for T and p values not covered by MD calculations, exhibited median percentage errors of 14% for RF, 15% for GB, and 45% for SVR, compared to the values predicted by Eq. (1). Notably, the prediction with a trained ML model takes a split second on a laptop, while the MD calculation takes about a week on a cluster.

The work was supported by National Research Foundation of Ukraine (project No. 2023.05/0024).

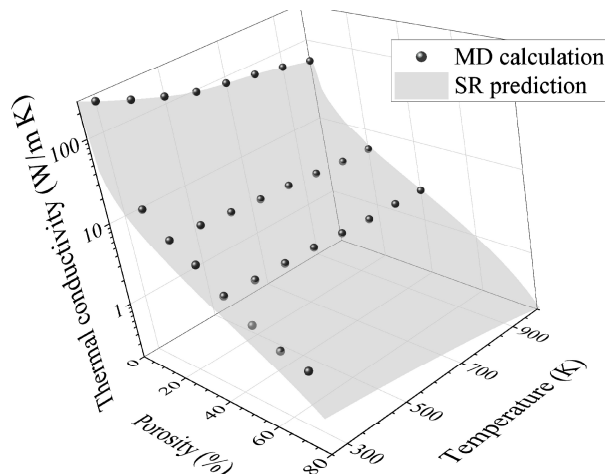


Fig. Dependence of the TC of porous silicon on temperature and porosity. The balls represent the results of MD calculations, while the surface corresponds to Eq. (1).

- [1] J. Xu, H. Wei, and H. Bao, Int. J. Heat Mass Transf. 217, 124671 (2023). <https://doi.org/10.1016/j.ijheatmasstransfer.2023.124671>.
- [2] H.-G. Nguyen, T.-D. Le, H.-G. Nguyen, and T.-H. Fang. Mater. Sci. Eng. R 160, 100833 (2024). <https://doi.org/10.1016/j.mser.2024.100833>.

Prediction of isomorphous substitutions of strontium or barium by sodium and actinides for their immobilization in molybdates with a scheelite-type structure

S. V. Radio, E. I. Get'man

Vasyl' Stus Donetsk National University, Vinnytsia, Ukraine
vul. 600-richchia, 21, Vinnytsia, 21027, Ukraine
e-mail: radio@donnu.edu.ua

Researchers are interested in solid solutions of the form $M^{II}_{1-x}(M^I_{0.5}An_{0.5})_xMoO_4$, where M^{II} is an alkaline earth metal, M^I is an alkali metal, and An is an actinide, due to their potential practical application in the immobilization of radioactive waste. In this study, within the framework of the crystal energy theory of isomorphous substitutions, the mixing energies (interaction parameters), critical decomposition (stability) temperatures, and isomorphous substitution limits were calculated, and the thermodynamic stability of $Sr_{1-x}(Na_{0.5}An_{0.5})_xMoO_4$ solid solutions was evaluated.

It has been shown that with an increase in the actinide atomic number, the mixing energies and critical decomposition temperatures of the solid solutions systematically increase, primarily due to the growing size parameter, which results from the increasing differences in the sizes of the substituting structural units. A thermodynamic stability diagram and decomposition domes of the solid solutions are presented for concentrations ranging from $x = 0$ to $x = 1.0$ in increments of $x = 0.05$. The diagrams allow for graphical determination of the decomposition temperature for a given composition, the equilibrium substitution limit at a given temperature, and the assessment of thermodynamic stability ranges. It has been established that substitution in the $Ba_{1-x}(Na_{0.5}An_{0.5})_xMoO_4$ systems follows our previously formulated second rule of isomorphous substitution polarity: the decomposition temperature is higher for the component with the smaller substituting structural unit.

Under the temperature conditions recommended by the IAEA for radioactive waste disposal (373 K or lower), continuous solid solution series of $Sr_{1-x}(Na_{0.5}An_{0.5})_xMoO_4$ are thermodynamically stable in the case of actinides from the Ac–Pu series. However, these solid solutions will either decompose or become metastable under such conditions for actinides from the Am–No series.

Lanthanides from the La–Gd series can serve as actinide simulants, as the critical decomposition temperatures of their solid solutions differ only slightly (~100–200 K) from those of the corresponding actinide-containing solid solutions. However, their use as simulants is unlikely due to the significantly larger difference (~200–400 K) in the decomposition temperatures of solid solutions involving heavy actinides compared to those with lanthanides (see Fig. 1).

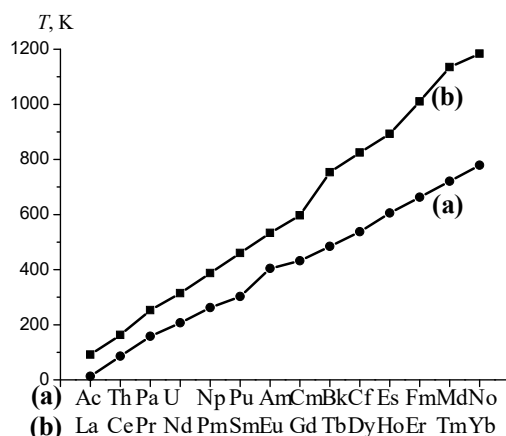


Figure 1 – Dependences of the critical decomposition temperatures of $Sr_{1-x}(Na_{0.5}An_{0.5})_xMoO_4$ (a) and $Sr_{1-x}(Na_{0.5}Ln_{0.5})_xMoO_4$ (b) on the atomic number of actinides and lanthanides.

Low-temperature thermal properties of carbon-based nanomaterials: exploration of graphene oxide and fullerene composites

**O. O. Romantsova^{1,2}, D. Szewczyk², A. Jeżowski², Yu. Horbatenko¹,
M. Vinnikov¹, S. Cherednichenko¹, A. I. Krivchikov^{1,2}**

¹*B.Verkin Institute for Low Temperature Physics and Engineering of NAS of Ukraine,
47 Nauky Ave., Kharkiv, 61103, Ukraine*

²*Institute of Low Temperatures and Structure Research, Polish Academy of Sciences,
2 Okólna str., Wrocław, 50-422, Poland
e-mail: romantsova@ilt.kharkov.ua*

This study investigates the heat capacity of thermally reduced graphene oxide (TRGO) combined with fullerene C60 (HyFn) within the temperature range of 2–300 K, utilizing the Physical Property Measurement System (PPMS) with a Heat Capacity Module. In addition to these materials, reference tests with commercial samples from the Sigma-Aldrich Corporation were performed both for pure fullerene C60 and graphene oxide. The research aims to uncover how the structural disorder influences thermal behaviour by focusing on identifying anomalies such as the boson peak – a feature associated with vibrational density of states in disordered systems, crucial for understanding low-temperature thermal properties in nanostructured materials.

Structural and vibrational characteristics were explored using X-ray diffraction (XRD) and Raman spectroscopy. As a result, we revealed detailed information on phase stability, molecular interactions, and disorder-induced effects on lattice dynamics. Additional transmission electron microscopy (TEM) analysis highlighted structural differences between synthesized TRGO-HyFn composites and commercial samples, emphasizing the impact of synthesis methods on material properties.

The experimental results were analyzed using both phenomenological and theoretical models, such as the soft-potential model and the Debye model in order to establish a correlation between structural disorder and heat capacity behavior. A pronounced boson peak was observed in fullerene and TRGO-HyFn composites, while it is absent in graphene oxide, indicating significant vibrational anomalies tied to the materials' unique structures. This study not only enhances understanding of heat transport mechanisms in carbon-based nanostructures but also provides valuable insights for applications in nanotechnology and cosmic science, where efficient thermal management is vital for performance and material stability. The findings underscore the importance of material synthesis methods in tailoring thermal properties, paving the way for future research on advanced carbon composites in extreme environments.

The publication is based upon work from COST Action “Carbon molecular nanostructures in space (NanoSpace)” CA21126, supported by COST (European Cooperation in Science and Technology).

The effect of the vanadium content on the microhardness of CoCrFeNiMnV_x high-entropy alloys in the temperature range of 77-293 K

H. V. Rusakova¹, L. S. Fomenko¹, S. V. Lubenets¹, M. A. Tikhonovsky², I. F. Kislyak², E. D. Tabachnikova¹, Yi Huang³, and Terence G. Langdon⁴

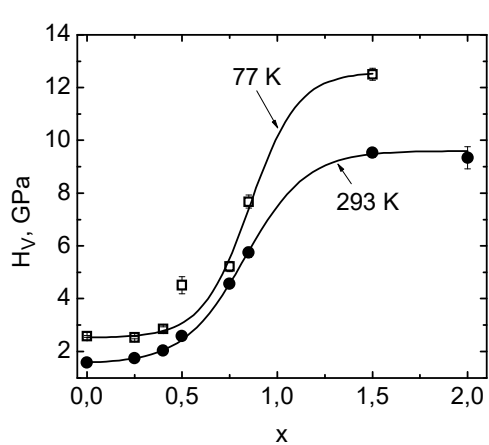
¹B.Verkin Institute for Low Temperature Physics and Engineering of NAS of Ukraine,
 47 Nauky Ave., Kharkiv, 61103, Ukraine

²National Science Center “Kharkiv Institute of Physics and Technology” of NAS of Ukraine,
 1 Akademichna Str., Kharkiv, 61108, Ukraine

³Department of Design and Engineering, Faculty of Science and Technology,
 Bournemouth University, Poole, Dorset BH12 5BB, UK

⁴Materials Research Group, Department of Mechanical Engineering, University of Southampton,
 Southampton SO17 1BJ, UK
 e-mail: rusakova@ilt.kharkov.ua

The main purpose of this work was to investigate the micromechanical properties of CoCrFeNiMnV_x ($x = 0, 0.25, 0.4, 0.5, 0.75, 0.85, 1.5, 2.0$) high-entropy alloys in the coarse-grained state at temperatures of 77-293 K. The as-cast samples were annealed for homogenization at 1050 °C for 3 h. Dependences of Vickers microhardness on temperature $H_V(T)$ were obtained for all mentioned alloys except the alloy with $x = 2$ for the reason of its brittleness. The microhardness data for the alloy with $x = 0$ were taken from [1]. The figure below shows the vanadium content dependences of the microhardness at two boundary temperatures, 77 and 293 K. The microhardness increases significantly with a decrease in temperature down to 77 K: from 1.58 to 2.57 GPa for $x = 0$ and from 9.46 to 12.52 GPa for $x = 1.5$. The microhardness increases with an increase in vanadium content within the range of $x = 0-1.5$ approximately 6 times at room temperature and 5 times at 77 K.



In [2], it was shown that in similar samples, addition of a small amount of vanadium into CoCrFeNiMn alloy does not change its crystal lattice structure. At $x \lesssim 0.25$, the lattice basically retains the fcc type, and the microhardness changes slightly with increase in x . However, with a further increase in the vanadium content, the formation of a new phase, the intermetallic sigma phase with a tetragonal lattice, takes place [2]. The new hard precipitates act as athermal barriers to the motion of dislocations. A sharp increase in the microhardness, starting from $x \sim 0.5$, is due to an increase in the volume fraction of the sigma phase from $\sim 20\%$ up to approximately 100 % in alloys with $x = 1.5 - 2$. The microhardness of the sigma phase itself at 293 and 77 K is about 9.5 and 12.5 GPa, respectively.

The results obtained in this research correlate well with the microhardness measurements of the CoCrFeNiMnV_x ($x = 0, 0.25; 0.5; 0.75; 1.0$) alloys performed at room temperature [2] and with the measurements of temperature dependences of yield strength of the alloys with $x = 0, 0.25, 0.5, 0.75$, performed in the wide range of low temperatures [3].

- [1] H. V. Rusakova, L. S. Fomenko, S. N. Smirnov et al., Mater. Sci. Eng. A 828, 142116 (2021). <http://dx.doi.org/10.1016/j.msea.2021.142116>.
- [2] N. D. Stepanov, D. G. Shaysultanov, G. A. Salishchev et al., J. Alloys and Compounds 628, 170 (2015). <http://dx.doi.org/10.1016/j.jallcom.2014.12.157>.
- [3] E. D. Tabachnikova, A. V. Podolskiy, M. O. Laktionova et al., J. Alloys and Compounds 698, 501 (2017). <http://dx.doi.org/10.1016/j.jallcom.2016.12.154>.

The effect of low temperatures on the rheological properties of amorphous and amorphous-crystalline polymers

V. D. Natsik, H. V. Rusakova, V. A. Lototskaya

B. Verkin Institute for Low Temperature Physics and Engineering of NAS of Ukraine,
47 Nauky Ave., Kharkiv, 61103, Ukraine
e-mail: rusakova@ilt.kharkov.ua

We carried out a comparison and analysis of previously recorded in low-temperature experiments on cooling from 293 down to 77 and 4.2 K tensile diagrams $\sigma(\varepsilon; T, \dot{\varepsilon})$ of amorphous and amorphous-crystalline films of Kapton H type polyimide polymer [1, 2]. It was found that the pronounced effects of low-temperature highly elastic deformation of amorphous polyimide samples at $293 \text{ K} \geq T \geq 4.2 \text{ K}$ [1, 2] are preserved with moderate cooling of amorphous-crystalline samples to 77 K. However, at 4.2 K, they acquire the properties of glassy materials with brittle fracture at the initial stage of elastic deformation. It is shown that the kinetics of highly elastic deformation of polyimide with molecular structures of both types is due to the thermomechanical activation of elaston excitations on molecular chains in the amorphous component of the material and is described by the nonlinear rheological equation derived earlier [3, 4] for the molecular model of an amorphous polymer. By comparing the experimental and theoretical results (Figure 1), empirical estimates for the rheological characteristics of polyimide samples with molecular structures of both types, as well as the parameters of elaston excitations in these structures, were obtained.

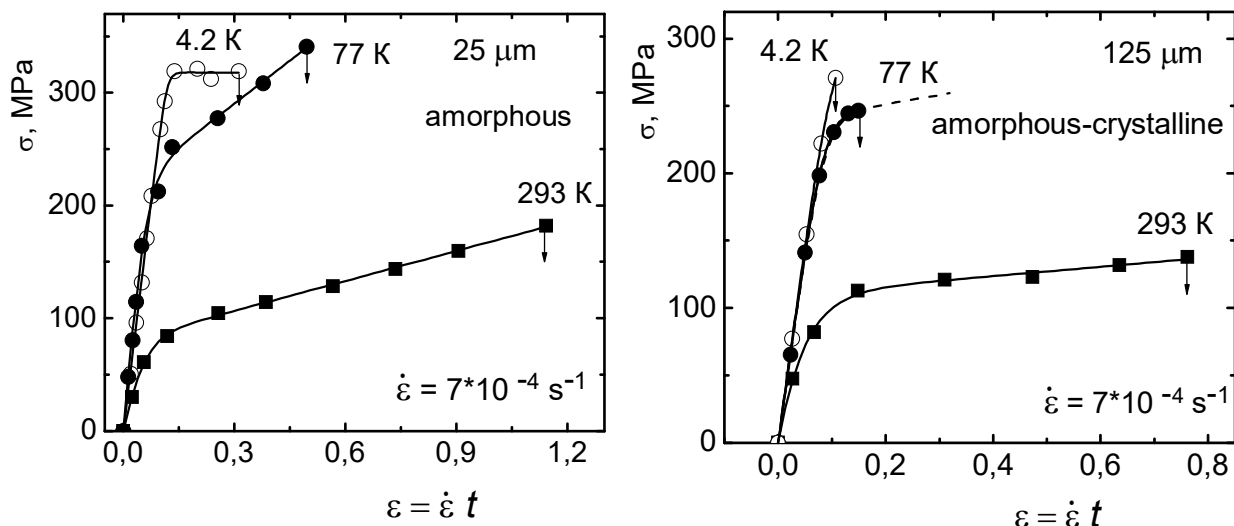


Figure 1. Experimental values (\circ , \bullet , \blacksquare) of the strain stress $\sigma(\varepsilon; T, \dot{\varepsilon})$ and their approximation (—) by the solution of the rheological equation for an amorphous polymer.

- [1] V. A. Lototskaya, L. F. Yakovenko, E. N. Alekseenko, V. V. Abraimov, and W. Z. Shao, East Eur. J. Phys. 4, 144 (2020). <https://dx.doi.org/10.26565/2312-4334-2020-4-18>.
- [2] V. D. Natsik, H. V. Rusakova, S. V. Lubenets, V. A. Lototskaya, and L. F. Yakovenko, Fiz. Nizk. Temp. 49, 569 (2023) [Low Temp. Phys. 49, 521 (2023)]. <https://dx.doi.org/10.1063/10.0017812>.
- [3] V. D. Natsik and H. V. Rusakova, Fiz. Nizk. Temp. 48, 281 (2022) [Low Temp. Phys. 48, 253 (2022)]. <https://dx.doi.org/10.1063/10.0009545>.
- [4] V. D. Natsik and H. V. Rusakova, Fiz. Nizk. Temp. 49, 246 (2023) [Low Temp. Phys. 49, 228 (2023)]. <https://dx.doi.org/10.1063/10.0016875>.

Investigation of low-temperature dislocation structure and dynamics in the high-entropy alloy Al_{0.5}CoCrCuFeNi

**Yu. Semerenko¹, V. Natsik¹, N. Galtsov¹, D. Hurova¹, V. Zoryansky¹, E. Tabachnikova¹,
T. Bednarchuk², Yu. Lipovska³**

¹*B. Verkin Institute for Low Temperature Physics and Engineering of NAS of Ukraine,
47 Nauky Ave., Kharkiv, 61103, Ukraine*

²*Institute of Low Temperature and Structure Research, Polish Academy of Sciences,
P.O. Box 1410, 50-950 Wroclaw, Poland*

³*National Science Center Kharkiv Institute of Physics and Technology,
1 Akademicheskaya St., Kharkiv, 61108, Ukraine
e-mail: semerenko@ilt.kharkov.ua*

Low temperature dynamics and kinetics of dislocation motion in the high entropy alloy Al_{0.5}CoCrCuFeNi were comprehensively studied in a wide range of elastic deformations using two different experimental methods (mechanical resonance spectroscopy and active plastic deformation). A theoretical analysis of the low-temperature processes of plastic deformation and acoustic relaxation in a high-entropy alloy Al_{0.5}CoCrCuFeNi was carried out. A dislocation model [1] is proposed that allows an adequate description of the experimentally observed features of low-temperature plastic deformation and acoustic relaxation in the studied high-entropy alloy. Within the framework of this dislocation model, we have obtained following results: the most important types of dislocation defects in the lattice structure of the alloy; types of barriers that prevent the movement of dislocation lines (strings); mechanisms of thermally activated movement of various elements of dislocation lines through barriers at room and low temperatures. Based on this dislocation model, quantitative estimates have been calculated for the most important characteristics of dislocations and their interaction with barriers (distance of 4.1 nm between local obstacles in the slip plane, the Peierls stress of 4·10⁶ Pa for dislocations in an easy slip system and others). The estimate for speed of sound 3.4·10³ m/s obtained within the framework of our proposed model is in good agreement with the experimental data of [2]. It has been established that the obtained empirical estimates for the energy per unit length of a dislocation are 12.4·10⁻⁹ J/m, and the linear mass density of 1.1·10⁻¹⁵ kg/m do not contradict their estimates in the modern continuum theory of dislocations.

A detailed study of the dislocation structure of the studied high-entropy alloy Al_{0.5}CoCrCuFeNi at room temperature was performed using X-ray structural analysis methods, and a numerical estimate of the dislocation density was obtained. It was found that the value of 4x10¹³ m⁻² of the dislocation density obtained by X-ray structural analysis methods correlates with estimates for the density of dislocation that effectively interacts with elastic vibrations of the sample (the total length of dislocation segments per unit volume), obtained within the framework of the dislocation model proposed by us.

[1] Yu. O. Semerenko, V. D. Natsik, E. D. Tabachnikova, Y. Huang and T.G. Langdon, Metals 14, 778 (2024). <https://doi.org/10.3390/met14070778>.

[2] O. S. Bulatov, V. S. Klochko, A. V. Korniyets, I. V. Kolodiy, O. O. Kondratov, T. M. Tikhonovska, Funct. Mater. 28, 492 (2021). <https://doi.org/10.15407/fm28.03.492>.

**Comparative analysis of mechanical properties and microstructure
of coarse-grained and nanostructured nonequiatomic medium-entropy alloys
 $\text{Fe}_{40}\text{Mn}_{40}\text{Co}_{10}\text{Cr}_{10}$ and $\text{Fe}_{50}\text{Mn}_{30}\text{Co}_{10}\text{Cr}_{10}$
in the temperature range of 4.2–300 K**

**S. E. Shumilin¹, T. V. Hryhorova¹, S. N. Smirnov¹, Yu. O. Semerenko¹, I. V. Kashuba¹,
Yu. O. Shapovalov¹, E. D. Tabachnikova¹, M. A. Tikhonovsky², Y. Huang³, T. G. Langdon⁴**

¹*B.Verkin Institute for Low Temperature Physics and Engineering of NAS of Ukraine,
47 Nauky Ave., Kharkiv, 61103, Ukraine*

²*National Science Center “Kharkiv Institute of Physics and Technology” of NAS of Ukraine,
1 Akademichna Str., Kharkiv, 61108, Ukraine*

³*Department of Design and Engineering, Faculty of Science and Technology,
Bournemouth University, Poole, Dorset BH12 5BB, UK*

⁴*Materials Research Group, Department of Mechanical Engineering, University of Southampton,
Southampton SO17 1BJ, UK
e-mail: grigorova@ilt.kharkov.ua*

At present, the study of the physical and mechanical properties of high-entropy (HEA) and medium-entropy (MEA) alloys is of considerable interest. In this paper, based on the data obtained in [1-3], a comparative analysis of the low-temperature mechanical properties and microstructure of nonequiatomic MEA alloys $\text{Fe}_{40}\text{Mn}_{40}\text{Co}_{10}\text{Cr}_{10}$ and $\text{Fe}_{50}\text{Mn}_{30}\text{Co}_{10}\text{Cr}_{10}$ in the coarse-grained (CG) and nanostructured (NS) states is carried out. During plastic deformation in the $\text{Fe}_{50}\text{Mn}_{30}\text{Co}_{10}\text{Cr}_{10}$ alloy, the fcc – hcp phase transformation (TRIP effect) occurs, and in the $\text{Fe}_{40}\text{Mn}_{40}\text{Co}_{10}\text{Cr}_{10}$ alloy, intense twinning (TWIP effect) is observed, which leads to strengthening of these alloys while maintaining high plasticity. It was found that under tensile deformation at 4.2 K, the CG TRIP alloy exhibits strength values of $\sigma_U \approx 1500$ MPa and ductility values of $\varepsilon_U \approx 47\%$. Under the same conditions, the CG TWIP alloy exhibits $\sigma_U \approx 1800$ MPa and $\varepsilon_U \approx 45\%$. In the initial state, the CG TRIP alloy is two-phase (fcc and hcp phase), and in the deformed state it becomes practically single-phase with an hcp lattice. In the initial state, the CG TWIP alloy is single-phase with an fcc lattice, and in the deformed state, along with the enhancement of the twinning process, a partial fcc – hcp phase transition is observed in this alloy. Studies of the acoustic properties of CG TRIP and CG TWIP alloys have shown that after plastic deformation the temperature dependence of the dynamic Young's modulus changes by 50% and its values decrease in the temperature range of 4.2 – 300 K. In the NS states obtained by severe plastic deformation by high-pressure torsion (HPT) at temperatures of 300 and 77 K, the average grain size decreases from 40 μm to $\approx 40 - 100$ nm. The following main features are observed in TWIP and TRIP alloys [3]: 1) an almost complete phase transition from the fcc phase to the hcp phase occurs and the alloys become almost single-phase; 2) HPT deformation leads to a significant increase in the microhardness HV, and in the TWIP alloy this effect is more pronounced than in the TRIP alloy; 3) the plasticity of the alloys decreases and significant hardening is observed in comparison with the CG state; 4) TWIP alloy retains plasticity under active compression deformation at 300 and 77 K, whereas in TRIP alloy under similar conditions macroscopic plasticity is absent; 5) in TWIP alloy, the thermally activated nature of plastic deformation is retained during the transition from the CG to the NS state.

- [1] E. D. Tabachnikova, T. V. Hryhorova, S. E. Shumilin, et al., Low Temp. Phys. 48, 955 (2022). <https://doi.org/10.1063/10.0014029>.
- [2] T. V. Hryhorova, S. E. Shumilin, Y. O. Shapovalov, et al., J. V. N. Karazin Kh. Nat. Univ. Phys., 32, 41, (2020). <https://doi.org/10.26565/2222-5617-2020-32-05>.
- [3] E. D. Tabachnikova, T. V. Hryhorova, S. N. Smirnov, et al., Low Temp. Phys. 49, 1294 (2023). <https://doi.org/10.1063/10.0021377>.

On the influence of surface roughness of polymer kapton-H on momentum transfer in supersonic flow of atomic oxygen plasma

**V. A. Shuvalov, G. S. Kochubei, Yu. P. Kuchugurnyi,
D. K. Voronovskyi, B. V. Yurkov,**

*Institute of Technical Mechanics of NAS of Ukraine and SSA of Ukraine
15 Leshko-Popel St., Dnipro, 49005, Ukraine
e-mail: vashuvalov@ukr.net*

The environment in ultra-low Earth orbits (at altitudes ranging from 150 to 350 km) is extremely aggressive for polymer materials. The materials are susceptible to erosion, which results in mass loss and a reduction in the thickness of polymer coatings. During prolonged spacecraft operation in orbit, the roughness of polymers increases significantly due to the effect of chemically active atomic oxygen. As a result, the momentum and energy transfer coefficients, as well as the aerodynamic drag coefficients of spacecraft structural elements, change.

This paper presents the results of experimental and theoretical studies of the effect of surface roughness in spacecraft polymeric materials, in particular Kapton-H polyimide, caused by surface degradation in a supersonic flow of atomic oxygen plasma (with ion velocities ranging from 8 to 10 km/s), on the aerodynamic drag of bodies (models) with simple geometric shape (sphere, cylinder, cone).

The experimental studies were conducted using a plasmoelectrodynamic test bench. The drag and tangential forces acting on the surface elements of the polymer-coated model with a given roughness were measured as a function of the angle of attack and the flow rate of the atomic oxygen plasma.

It is shown that for primary smooth surfaces ('mirror scattering'), the drag coefficient of a sphere and a cone increases by up to 40% as the roughness coefficient increases. For the Kapton-H polymer, such an increase corresponds to approximately one year of operation at ~250 km altitude during solar minimum or ~340 km during solar maximum. For a transverse cylinder, the drag coefficient increases by about 8.6%. For predominantly rough surfaces ('diffuse reflection'), the drag coefficient also increases for bodies with simple geometries: by ~11% for a sphere, by ~9% for a transverse cylinder, and between 2% and 11% for a cone, with the increase being greater for cones with smaller apex angles.

Strain rate dependent deformation behavior of Ti-Nb alpha-alloys at low temperatures

V. A. Moskalenko, R. V. Smolianets

*B.Verkin Institute for Low Temperature Physics and Engineering of NAS of Ukraine,
47 Nauky Ave., Kharkiv, 61103, Ukraine
e-mail: smolianets@ilt.kharkov.ua*

When identifying the microscopic mechanisms of dislocation plasticity of crystals, the main interest is in the measurements and analysis of such differential characteristics as the temperature dependences of the critical shear stress and its rate sensitivity. Thus, it is important (specifically, in the case of titanium) to consider effect of the content and type of dissolved impurities/alloying elements with their different effects on the controlling mechanisms. The physical mechanism of low-temperature plasticity by slip in high-purity titanium consists to overcoming of Peierls barriers by dislocations as a process of nucleation, expansion and annihilation of paired kinks [1]. However, the interaction of dissolved elements with these linear defects can affect its dominant role on the strengthening in materials. In this regard, the study effect of impurities which provide the most pronounced changes of mechanical properties has been studied in detail [2, 3]. It was found that the controlling mechanism (at oxygen concentrations above 0.1 at. %) is thermally activated overcoming local barriers by dislocations caused by impurity atoms. In contrast, the effect of substitution atoms on the deformation behaviour and mechanisms of low-temperature plasticity in titanium and other metals of the HCP crystallographic group are not sufficiently studied. However, the very alloying with chemical elements of this type plays an important role in the determination of chemical and physical-mechanical properties in modern titanium alloys.

In this work, the effect of Nb as a substitution alloying element at a change in its concentration (0.25 - 2.1 at. %) on the value and temperature dependence of the shear stress rate sensitivity $\beta = (\Delta\tau/\Delta \ln \dot{\gamma})_T$ in high-purity titanium at the temperature range of 1.7 – 423 K was studied for the aim of identification of the plastic deformation mechanisms. It was found that the

determined values of β for the alloys are approximate to obtained in titanium with an oxygen concentration of less than 0.1 at % [1, 4], where the controlling mechanism is the dislocations overcoming of the Peierls barriers. The observed lack of the effect in the Nb content on the value and temperature dependence of the shear stress rate sensitivity β (see Fig. 1) may indicate the conservation of plasticity mechanism in the alloys inherent high-purity titanium. Found on the basis of the shear stress rate sensitivity β measurements, the activation volume values ($V^*/b^3 \approx 65$) of the plastic deformation process and, most importantly, its independence from the concentration of the alloying element Nb indicate that the possible controlling mechanism is dislocations that overcome the Peierls barriers in the studied Ti-Nb alpha solid solutions.

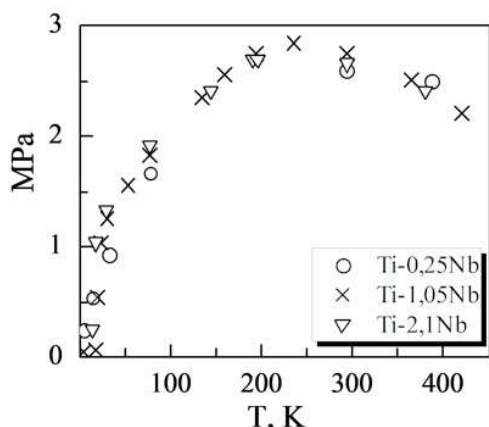


Fig.1. Temperature dependence of the shear stress rate sensitivity β for Ti-Nb alpha-alloys.

- [1] V.A. Moskalenko, V. D. Natsik and V. N. Kovaleva, Low Temp. Phys. 31. 1190 (2005). <https://doi.org/10.1063/1.2126949>.
- [2] V. N. Kovaleva, V. A. Moskalenko and V. D. Natsik, Phil. Mag. 70, 423 (1994). <https://doi.org/10.1080/01418619408242549>.
- [3] H. Conrad, Prog. Mater. Sci. 26, 123 (1981). [https://doi.org/10.1016/0079-6425\(81\)90001-3](https://doi.org/10.1016/0079-6425(81)90001-3).
- [4] E. D. Levine, Trans. Metall. Soc. AIME 236, 1558 (1966).

Study of pore distribution in activated carbon by low-temperature nitrogen adsorption

V. M. Vashchynskyi

Lviv Polytechnic National University, 12 S. Bandery St, Lviv 79013, Ukraine
e-mail: v.vashchynskyi@gmail.com

Gas adsorption plays a crucial role in the characterization of a wide range of porous materials. Among the many gases and vapors that are readily available for use as adsorbates, nitrogen remains universally preeminent. The surface area and pore size distribution of solid catalyst materials can be determined through gas adsorption–desorption measurements at 77 K. For pore structure analysis, nitrogen adsorption–desorption isotherms should be measured over the widest possible range of relative pressures while accounting for slow equilibration and other operational challenges, particularly at very low pressures.

Numerous methods exist for calculating surface area, pore size, pore distribution, and pore volume by fitting isotherm data to different models. For example, the Brunauer–Emmett–Teller (BET) method is commonly used to determine the specific surface area, while the Barrett–Joyner–Halenda (BJH) model [1] is applied for pore size distribution analysis. According to the IUPAC classification proposed by Sing et al., pores are categorized based on their width into four classes: macropores (> 50 nm), mesopores (2–50 nm), micropores (< 2 nm), and ultramicropores (< 0.7 nm) [2].

This study investigates the effect of carbonization temperature on the porosity and surface area of KOH-modified activated carbon samples. Apricot kernel shells were initially carbonized in a closed furnace at temperatures ranging from 300 to 900 °C. Due to the incomplete development of porosity at this stage, additional activation was performed. The obtained carbonized material was mechanically crushed and impregnated with KOH at different mass ratios. The mixture was stirred for 1–2 hours, and heated in an Ar atmosphere to 900 °C, followed by an isothermal exposure. Subsequently, mineral impurities and ash were chemically removed from the samples using hydrochloric acid (HCl). The material was then rinsed with distilled water until a neutral pH was achieved and dried in an oven until a constant mass was obtained.

The low-temperature nitrogen adsorption method (LINAM) was used to detect the mesoporous structure of seven apricot-derived carbon materials, and the experimental results are analyzed in this paper. The minimum pore diameter detectable by LINAM is 0.6 nm, facilitating the study of pore distribution in activated carbon. Ultramicropores and micropores with diameters ranging from 0.6 to 1.5 nm contribute most significantly to the specific surface area across the entire series of samples, compared to pores with diameters of 2 to 50 nm. However, for the sample carbonized at 300 °C, mesopores with diameters of 3–4 nm accounted for approximately 36% of the total pore volume.

- [1] E. P. Barrett, L. G. Joyner, P. P. Halenda, *J. Am. Chem. Soc.* 73, 373 (1951).
<http://dx.doi.org/10.1021/ja01145a126>.
- [2] K. S. W. Sing, D. H. Everett, R. A. W. Haul, L. Moscou, R. A. Pierotti, J. Rouquerol, T. Siemieniewska. *Reporting Physisorption Data for Gas/Solid Systems. Handbook of Heterogeneous Catalysis* (Wiley-VCH: Weinheim, Germany 2008).
<http://dx.doi.org/10.1002/9783527610044.hetcat0065>.

Impact of electromagnetic radiation from spark discharge on the dielectric properties of Cd_{1-x}Zn_xTe crystals within the low-frequency region

O. Chugai, S. Kulish, Yu. Voloshyn, S. Sulyma

*National Aerospace University "Kharkiv Aviation Institute",
17 Chkalova St., Kharkiv, 61070, Ukraine
e-mail y.voloshyn@khai.edu*

The crystalline structures of Cd_{1-x}Zn_xTe (x = 0.10-0.20) crystals grown from the melt under high-pressure argon atmospheres were examined. The experiments were conducted on samples exhibiting low-frequency values of the real and imaginary parts of the complex dielectric permittivity, ranging from 11.5 to 15.5 and from 0.50 to 2.10, respectively.

Long-term changes in these values caused by the influence of electromagnetic radiation from a spark discharge were investigated at constant frequencies of the measuring field. Additionally, the energy spectrum of localized charge carrier states was examined using scanning photodielectric spectroscopy [1].

The investigation revealed that electromagnetic radiation from the spark discharge can induce both positive and negative changes in the measured parameters. However, the mean values of these changes, averaged over all samples, exhibit a systematic dependence on the frequency of the applied field.

The influence of electromagnetic radiation from a spark discharge on the energy spectrum of localized states of charge carriers has been examined.

The observed changes in the dielectric properties of crystals are attributed to the presence of point defect complexes inherent in their crystal structure. Exposure to electromagnetic radiation from the spark discharge induces a transition of these defects into a metastable state, characterized by a distinct polarizability.

This transition is accompanied by a noticeable change in the measured parameters in the low-frequency region.

- [1] O. Chugai, O. Poluboiarov, S. Oliinyk & S. Sulima, Scanning Photodielectric Spectroscopy of CdZnTe Crystals (Advances in Fabrication and Investigation of Nanomaterials for Industrial Applications, Cham: Springer International Publishing 2024).
https://doi.org/10.1007/978-3-031-42700-8_6.
- [2] B. Meng, B. D. B. Klein, J. H. Booske, R. F. Cooper, Microwave absorption in insulating dielectric ionic crystals including the role of point defects, Physical Review B 53, 12777 (1996).
<https://doi.org/10.1103/PhysRevB.53.12777>.

Formation energies of point defects in Ti-doped YAG crystals: first-principles calculations

M. Y. Vovsianiker, D. V. Fil

*Institute for Single Crystals NAS of Ukraine, 60 Nauky Ave., Kharkiv, 61072, Ukraine
e-mail: mark.vovsianiker@gmail.com*

Yttrium aluminum garnet (YAG) is widely used in optics. When doped with various elements, YAG finds application in solid-state lasers and other optical devices, with impurities exerting a significant influence on its physical and optical properties.

One of the less-studied impurities in YAG is titanium. Nevertheless, several experimental studies suggest that Ti-doped YAG holds promise for practical applications. For instance, in work [1], it was found that Ti:YAG ceramics retain high optical quality after annealing in vacuum. Three absorption peaks were observed at wavelengths of 400, 498 and 586 nm, along with intense photoluminescence at 775 and 810 nm. These findings led to the conclusion that this ceramic could be suitable for lasers. Similar results were reported for the YAG crystal [2]. The presence of Ti^{3+} ions increases the gain of Nd:YAG laser crystals, according to [3]. At the same time, the associated increase in losses at 1064 nm is relatively minor compared to the gain. This makes Ti-doped YAG a potential candidate for pulsed laser systems. Furthermore, study [4] revealed that Ti impurities suppress the long-lived transient absorption observed in pure Nd:YAG. This absorption is known to cause thermal deformation of laser rods, which limits output power at higher pump levels. Therefore, Ti doping may also contribute to improved thermal stability in Nd:YAG-based lasers.

According to the experimental data presented above, it is of particular interest to investigate the properties of defects formed in Ti:YAG using the density functional theory (DFT) method. Such studies can provide deeper insight into the nature and behavior of titanium-related defects and may help to clarify the mechanisms through which Ti affects the optical and laser performance of YAG. Furthermore, DFT-based analysis can assist in identifying strategies to enhance the beneficial Ti effects while mitigating its detrimental impact. For instance, co-doping with other elements that can form favorable defect complexes with Ti may lead to improved laser characteristics of the material.

We present the results of a theoretical study of properties of point defects in the Ti:YAG crystal based on DFT calculations performed using the SIESTA software package [5]. Calculations of the formation energies of impurity defects, namely Ti_{Al} substitution defects and interstitial Ti atoms, concentrations of such defects, as well as energy levels in the Ti:YAG band gap associated with such defects, were performed. Corresponding calculations were also performed for some possible complexes of both impurity–impurity and impurity–intrinsic combinations, including vacancies, antisite defects, and native interstitial YAG atoms.

- [1] T. Huang, B. Jiang, Y. Wu, J. Li, Y. Shi, W. Liu, Y. Pan, and J. Guo, Journal of Alloys and Compounds 478, L16 (2009). <https://doi.org/10.1016/j.jallcom.2008.11.157>.
- [2] F. Bantien, P. Albers, and G. Huber, Journal of Luminescence 36, 363 (1987). [https://doi.org/10.1016/0022-2313\(87\)90153-0](https://doi.org/10.1016/0022-2313(87)90153-0).
- [3] J. Kvapil, Jos Kvapil, J. Kubelka, and B. Perner, Czechoslovak Journal of Physics B 32, 817 (1982). <https://doi.org/10.1007/bf01596834>.
- [4] J. Kvapil, Jos Kvapil, B. Perner, J. Kubelka, B. Mánek, and V. Kubeček, Czechoslovak Journal of Physics B 34, 581 (1984). <https://doi.org/10.1007/bf01595714>.
- [5] J. M. Soler, E. Artacho, J. D. Gale, A. García, J. Junquera, P. Ordejón, and D. Sánchez-Portal, J. Phys.: Condens. Matter. 14, 2745 (2002). <https://doi.org/10.1088/0953-8984/14/11/302>.

The temperature dependences of resistivity of spinel-nanocarbon-epoxy composites

**O. Yakovenko¹, L. Matzui¹, L. Vovchenko¹, L. Kaykan²,
J. Mazurenko^{1, 2, 3}, D. Zaiatc¹, K. Dubyk¹, D. Shpylka¹**

¹Taras Shevchenko National University of Kyiv, Volodymyrska 64/13, Kyiv, 01601, Ukraine

²G.V. Kurdyumov Institute for Metal Physics, N.A.S. of Ukraine,

36 Academician Vernadsky Boulevard, Kyiv, 03142, Ukraine

³Institute of Experimental Physics SAS, Watsonova 47, 040 01 Košice, Slovak Republic

e-mail: alenka-ya@ukr.net

The development of modern technologies requires the creation of new materials with changed properties. Significant attention is paid to the production of electrically and thermally conductive polymer composites, which find extensive applications in construction, microelectronics, the aerospace industry, biomedicine, and other fields [1]. The simultaneous incorporation of magnetic fillers and nanocarbon materials has been used to improve the properties of polymer composites.

The aim of this work was to investigate the electrical properties of epoxy composites filled with 20 wt. % of CoFe_2O_4 , CuFe_2O_4 and NiFe_2O_4 nanosized ferrites with a spinel structure, along with addition of 5 wt. % of multiwalled carbon nanotubes (MWCNT) or graphene nanoplatelets (GNP), in the temperature range of 77–293 K, and to reveal how the filler type affects the electrical properties of the prepared materials. CuFe_2O_4 , NiFe_2O_4 , and CoFe_2O_4 were synthesized using the sol-gel autocombustion method. Spinel-nanocarbon-epoxy composites were prepared by solution mixing, and their electrical resistance was measured by the standard four-probe technique.

The temperature dependences of electrical resistivity of the prepared composites at $T = 77 \div 293$ K are presented in Figure 1.

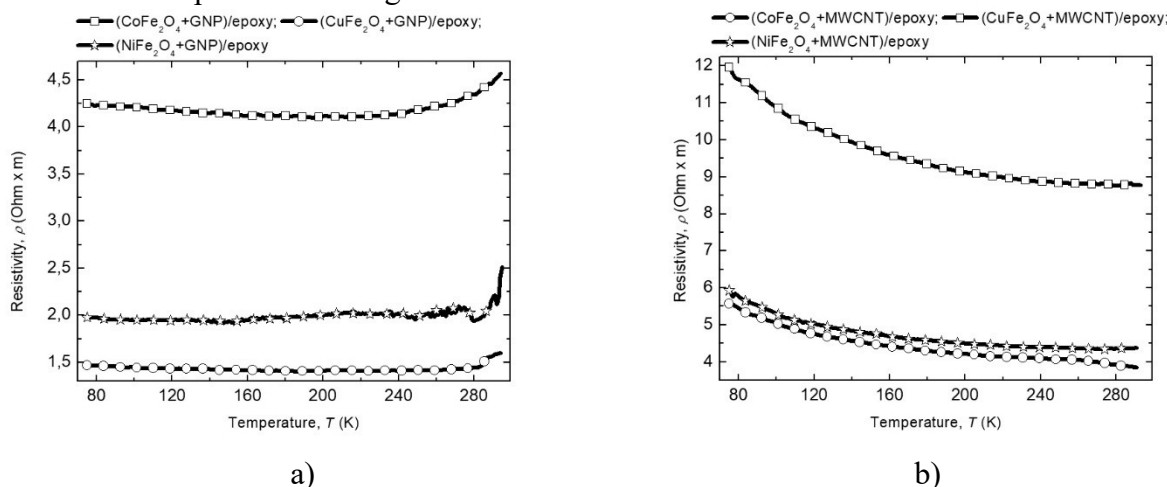


Figure 1. The temperature dependences of the electrical resistivity of spinel-nanocarbon-epoxy composites with 20 wt. % of spinel (CoFe_2O_4 , CuFe_2O_4 , NiFe_2O_4) and 5 wt. % of nanocarbon of different types: GNP (a), MWCNT (b).

The results indicate that, in composites with spinel and disc-shaped nanocarbon particles (GNP), the temperature dependences of electrical resistivity are determined by both contact resistance at direct interparticle junctions and tunneling resistance across narrow gaps between adjacent particles.

In contrast, the temperature dependence of the electrical resistivity of composites with spinel and cylindrical nanocarbon particles (MWCNT) shows that electron transport is predominantly governed by a tunneling mechanism across the entire investigated temperature range.

THEORY OF CONDENSED MATTER PHYSICS

Density of states and differential entropy in graphene in crossed magnetic and in-plane electric fields

Andrii A. Chaika, Yelizaveta Kulynych, D. O. Oriekhov, and Sergei G. Sharapov

*Bogolyubov Institute for Theoretical Physics,
National Academy of Sciences of Ukraine, 03143 Kyiv, Ukraine
sharapov@bitp.kyiv.ua*

The density of states and differential entropy per particle are analyzed for Dirac-like electrons in graphene subjected to a perpendicular magnetic field and an in-plane electric field. The study considers ballistic electrons and also includes the effect of small impurity scattering. In the latter case, the limit of zero magnetic field and the so-called collapse of Landau levels in grapheme are examined analytically. By comparing the results with numerical calculations on graphene ribbons, we demonstrate that the Landau state counting procedure must be modified for Dirac-like electrons, leading to a fields-dependent Landau level degeneracy factor.

[1] A.A. Chaika, Ye. Kulynych, D.O. Oriekhov, and S.G. Sharapov, "Density of states and differential entropy in the Dirac materials in crossed magnetic and in-plane electric fields", Phys. Rev. B 111, 085426 (2025).

On inhomogeneous equilibrium states in single-sublattice high-spin magnets

M. Yu. Kovalevsky

*National Science Center "Kharkov Institute of Physics and Technology" of NAS of Ukraine,
1, Akademicheskaya St., Kharkiv, 61108, Ukraine
e-mail: mik@kipt.kharkov.ua*

A statistical approach to the problem of classifying inhomogeneous equilibrium states of condensed matter with spontaneously broken magnetic symmetry and symmetry with respect to displacements and rotations in the configuration space has been developed. This approach is based on the concept of quasi-averages [1,2] and the idea of residual symmetry of degenerate equilibrium states [3,4]. The form of the residual symmetry generator and spatial symmetry generators in terms of a linear combination of integrals of motion with respect to which the symmetry is broken has been established. Equilibrium states of magnets with spin $s=1/2, 1, 3/2$ and $SU(2s+1)$ symmetry of the exchange magnetic interaction have been investigated.

Classification equations are obtained and their non-uniform solutions for equilibrium values of magnetic degrees of freedom are found. An explicit dependence of these degrees of freedom on the coordinate and parameters of spontaneous magnetic anisotropy for symmetry subgroups $SO(3)$, $SO(3) \times U(1)$, $SO(3) \times SO(3)$, $SO(4)$ is established. It is shown that, along with the solution known as spiral ordering, other non-uniform equilibrium states are possible for the magnets under consideration.

- [1] N.N. Bogolubov, Physica 26 S1 (1960). [https://doi.org/10.1016/0031-8914\(60\)90217-2](https://doi.org/10.1016/0031-8914(60)90217-2).
- [2] M.Y. Kovalevsky, S.V. Peletmibsky, Statistical Mechanics of Quantum Liquids and Crystals, Moscow (2006).
- [3] L. Michel, Rev. Mod. Phys. 52 617 (1980). <https://doi.org/10.1103>
- [4] M.Y. Kovalevsky, A.A. Rozhkov Low Temp. Phys. 51, 88 (2024). <http://dx.doi.org/10.1063/10.0034650>.

Flexo-sensitive ferrons in Van der Waals ferrielectrics at low temperatures

**Oleksii V. Bereznykov¹, Anna N. Morozovska¹, Eugene. A. Eliseev², Mykola Ye. Yelisieiev³,
Guo-Dong Zhao⁴, Yujie Zhu⁵, Venkatraman Gopalan⁴, Long-Qing Chen⁴, Jia-Mian Hu⁵, and
Yulian M. Vysochanskii⁶**

¹*Institute of Physics, National Academy of Sciences of Ukraine,
46, pr. Nauky, 03028 Kyiv, Ukraine*

²*Frantsevich Institute for Problems in Materials Science, National Academy of Sciences of Ukraine,
Omeliana Pritsaka str., 3, Kyiv, 03142, Ukraine*

³*Institute of Semiconductor Physics, National Academy of Sciences of Ukraine,
45, pr. Nauky, 03028 Kyiv, Ukraine*

⁴*Department of Materials Science and Engineering, Pennsylvania State University,
University Park, PA 16802, USA*

⁵*Department of Materials Science and Engineering, University of Wisconsin-Madison,
Madison, WI, 53706, USA*

⁶*Institute of Solid-State Physics and Chemistry, Uzhhorod University, 88000 Uzhhorod, Ukraine
e-mail: alexber36@gmail.com*

The contribution of the flexoelectric coupling to the long-range order parameter fluctuations in the ordered phase of ferroics can be critically important [1, 2]. Our main goal is to extend concept of the “ferron” [1] to the van der Waals (vdW) ferroelectrics and to analyze the dispersion law of soft optic and acoustic “flexo-phonons” and “flexo-ferrons” considering the flexoelectric coupling, damping, and higher elastic gradients in the Landau-Ginzburg-Devonshire free energy functional of the van der Waals uniaxial ferrielectric CuInP₂S₆ at low temperatures [3]. The special attention is paid to the changes in the flexo-phonon and flexo-ferron spectra related with the appearance of spatially modulated phases induced by the flexoelectric coupling [2]. We show that the four-well free energy of CuInP₂S₆ determines the unique features of its phonon spectra and ferron dispersion and analyze the contribution of optic and acoustic flexo-ferrons to the pyroelectric and electrocaloric response of CuInP₂S₆ at low temperatures.

Acknowledgements. O.V.B. and A.N.M. acknowledge the Target Program of the National Academy of Sciences of Ukraine, Project No. 5.8/25-II “Energy-saving and environmentally friendly nanoscale ferroics for the development of sensorics, nanoelectronics and spintronics”. The work of A.N.M., E.A.E., G.-D.Z., Y.Z., V.G., J-M.H., and L.-Q.C. is supported by the DOE Software Project on “Computational Mesoscale Science and Open Software for Quantum Materials”, under Award Number DE-SC0020145 as part of the Computational Materials Sciences Program of US Department of Energy, Office of Science, Basic Energy Sciences. The work of E.A.E. is also funded by the National Research Foundation of Ukraine (grant N 2023.03/0132 “Manyfold-degenerated metastable states of spontaneous polarization in nanoferroics: theory, experiment and perspectives for digital nanoelectronics”).

- [1]. P. Tang, R. Iguchi, K. Uchida, and G. E.W. Bauer. Excitations of the ferroelectric order. Phys. Rev. B 106, L081105 (2022), <https://doi.org/10.1103/PhysRevB.106.L081105>.
- [2]. A. N. Morozovska, M. D. Glinchuk, E. A. Eliseev, and Yu. M. Vysochanskii. Flexocoupling-induced soft acoustic mode and the spatially modulated phases in ferroelectrics. Physical Review B, 96, 094111 (2017) <https://doi.org/10.1103/PhysRevB.96.094111>.
- [3]. A. N. Morozovska, E. A. Eliseev, O. V. Bereznykov, M. Ye. Yelisieiev, G.-D. Zhao, Y. Zhu, V. Gopalan, L.-Q. Chen, J.-M. Hu, and Yu. M. Vysochanskii “Flexo-phonons” and “Flexo-ferrons” in Van der Waals ferroelectrics, to be submitted to Phys. Rev. B, ArXiv (2025).

Measurement-induced phase transitions in the Lipkin-Meshkov-Glick spin model

P. O. Kofman^{1,2}, N. Samos¹, P. Ribeiro^{1,3}

¹*Instituto Superior Técnico, Universidade de Lisboa, Av. Rovisco Pais, 1049-001 Lisbon, Portugal*

²*B.Verkin Institute for Low Temperature Physics and Engineering of NAS of Ukraine,
47 Nauky Ave., Kharkiv, 61103, Ukraine*

³*Beijing Computational Science Research Center, Beijing 100193, China
e-mail: polina.kofman@tecnico.ulisboa.pt*

Measurement-induced phase transitions have recently been identified, characterized by distinct entanglement properties of quantum trajectories of many-body systems [1]. Here, we explore these transitions explicitly within the Lipkin-Meshkov-Glick (LMG) spin model, a paradigmatic example of collective quantum dynamics. Extending recent results [2], we demonstrate that the transition manifests clearly in several measurable observables, each capturing specific aspects of quantum trajectory dynamics. Our analysis provides concrete signatures that enable precise identification and characterization of the measurement-induced phase transition within the LMG model framework.

[1] Xiangyu Cao, Antoine Tilloy, Andrea De Luca, Entanglement in a fermion chain under continuous monitoring, *SciPost Phys.* 7, 024 (2019);

[2] Gianluca Passarelli, Xhek Turkeshi, Angelo Russomanno, Procolo Lucignano, Marco Schirò, and Rosario Fazio, *Phys. Rev. Lett.* 132, 163401 (2024).

Maximization of squeezing and amplification in open quantum systems in the Jaynes-Cummings model by means of Holstein-Primakoff transformations

R. T. Ovsianikov¹, D. I. Bondar², K. Jacobs^{3,4}, A. G. Sotnikov¹

¹*NSC «Kharkiv Institute of Physics and Technology», Kharkiv Ukraine*

²*Tulane University, New Orleans, Louisiana, United States*

³*United States Army Research Laboratory, Adelphi, Maryland 20783, USA*

⁴*Department of Physics, University of Massachusetts at Boston, Boston, Massachusetts 02125, USA*

e-mail: roman.ovsiannikov@student.karazin.ua

The ability of numerous color centers in diamond to transition to the ground state under laser irradiation in the optical range enables the creation of ultra-low-noise or significantly cooled systems. This makes them ideal for processing and transmitting microwave signals.

Multilevel emitters can generate nonlinear interactions for electromagnetic fields. This is achieved by applying external control fields, which can induce effects such as electromagnetically induced transparency. This phenomenon is crucial as it minimizes unwanted absorption, which typically accompanies nonlinearity and leads to the decay of energy levels in the emitters. The issue of energy loss due to absorption is a major concern, but it becomes less significant in the case of color centers. For instance, in nitrogen-vacancy centers, the lowest-energy spin levels, such as the three-level configuration, exhibit exceptionally long lifetimes. As a result, energy losses due to decay are significantly reduced, improving the efficiency of the system. Additionally, using an ensemble of emitters enhances the interaction, as the collective operation of multiple emitters increases the interaction rate.

At this stage of the study, the ensemble of N two-level emitters is replaced by a single N -level emitter, which is described within the framework of the Jaynes-Cummings model. Its interaction with a resonator mode is analyzed in the large- N limit using the Holstein-Primakoff transformation. In this approximation, a system of equations for the second moments of the quadrature operators is derived. Numerical solutions of this system, obtained using adaptive integration methods near double resonance, along with the positivity properties of the second-moment matrix, allowed us to determine the conditions for maximum squeezing and amplification. Damping is also taken into account in the analysis.

The authors acknowledge support by the National Research Foundation of Ukraine under the call “Excellence science in Ukraine” (2024-2026), project No. 0124U004372.

Interaction-induced directional tunneling through asymmetric potential barriers in the Fermi-Hubbard lattice model

S. S. Litvinova¹, A. G. Sotnikov^{1,2}

¹*V.N. Karazin Kharkiv National University, Svobody Square 4, 61022 Kharkiv, Ukraine*

²*Akhiezer Institute for Theoretical Physics, NSC KIPT, Akademichna 1, 61108 Kharkiv, Ukraine*

e-mail: litvinova2022tya11@student.karazin.ua

We study the tunnelling dynamics of fermionic systems in lattices with asymmetric external potentials, which can be realized in experiments with ultracold atoms in optical lattices. It is well known that non-interacting particles have symmetric tunneling probabilities regardless of the barrier orientation. In contrast, we observe a breaking of this symmetry due to interparticle interaction and reproduce the previous results [1] on the dependence of the tunneling behavior on the initial spin configurations and the presence of effects arising from the resonant trapping and resonant tunneling in few-body quantum systems.

Furthermore, we also extend the range of the systems under study and analyze the time dependencies of physical observables on the number of lattice sites and the number of interacting particles. We observe new resonance effects in dependencies on the system size and lattice filling, as well as indications of suppression of tunneling dynamics due to formation of Mott-insulator states. Our results can be applied in designing novel nanoscale devices with diode-like properties.

The authors acknowledge support by the National Research Foundation of Ukraine under the call “Excellence science in Ukraine” (2024-2026), project No. 0124U004372.

[1] Elvira Bilokon, Valeriia Bilokon, Dusty R. Lindberg, Andrii Sotnikov, Lev Kaplan, and Denys I. Bondar, Few-fermion resonant tunneling and underbarrier trapping in asymmetric potentials, arXiv:2412.03495.

Application of Kolmogorov-Arnold-network-based neural quantum states for continuous many-body systems

M. O. Luhanko¹, I. V. Lukin², D. I. Bondar³, A. G. Sotnikov^{1,2}

¹*Karazin Kharkiv National University, 4 Svobody Square, Kharkiv, 61000, Ukraine*

²*Akhiezer Institute for Theoretical Physics, NSC KIPT, Kharkiv, 61108, Ukraine*

³*Department of Physics and Engineering Physics, Tulane University,
6823 St. Charles Ave., New Orleans, LA 70118, USA*

e-mail: a_sotnikov@kipt.kharkov.ua

e-mail: luhanko2021tya11@student.karazin.ua

Solving quantum many-body problems is notoriously difficult, with analytical solutions typically confined to mean-field approximations and a limited number of exactly solvable models, which necessitates the use of variational approximation methods. In this study, we develop a method tailored for bosonic integrals that is applicable to a broad range of nonlocal Hamiltonians. This method is capable of determining the ground state energy and computing expectation values of various physical observables, thereby offering a versatile tool for probing complex quantum many-body systems.

We introduce a novel neural network architecture that analyzes the internal structure and captures the symmetries inherent to bosonic systems. By employing a deep sets framework, our approach achieves a permutation invariance under the bosonic interchange of the wave function—a significant improvement over previous approaches based on fully connected layers. The possibilities afforded by our architecture are scientifically valuable: it enhances interpretability, supports model distillation, and provides explicit accounting of symmetries. Moreover, one of the advantages of using Kolmogorov-Arnold networks (KANs) is their superior expressibility relative to the number of parameters compared to dense layers; however, KANs are also known to be more intricate to train. This study, therefore, lays the groundwork for more effective variational methods, opening new avenues for the study of non-local interactions and complex quantum systems.

The authors acknowledge support by the National Research Foundation of Ukraine under the call “Excellence science in Ukraine” (2024-2026), project No. 0124U004372.

Comparison of viscoelastic properties of fluorosubstituted aliphatic alcohols using an artificial neural network

O. V. Khorolskyi¹, A. M. Hetalo¹, Ye. G. Rudnikov^{2,3}

¹Poltava V. G. Korolenko National Pedagogical University,

2 Ostrogradskogo Str., Poltava, 36003, Ukraine

²Taras Shevchenko National University of Kyiv, 64/13 Volodymyrska Str., Kyiv 01601, Ukraine

³National Technical University of Ukraine "Igor Sikorsky Kyiv Polytechnic Institute",

37 Beresteiskyi Ave., Kyiv 03056, Ukraine

e-mail: khorolskiy.alexey@gmail.com

Fluorinated alcohols have found their application in pharmacology and organic synthesis as specific solvents, as components of high-temperature coolants, lubricants and adhesives, as well as in the manufacture of pesticides and polymeric materials. Fluorinated alcohols continue to master new areas of application, in particular, they are used in biotechnology for stabilizing peptides, biomodifying enzymes, changing the structure of protein macromolecules, modifying the properties of lipid membranes [1], etc. Despite the widespread use of fluorinated alcohols in various industries, their physical properties still remain poorly studied.

For aliphatic alcohols and their fluorinated analogues in the vicinity of the critical point, with increasing number of carbon atoms at a certain same reduced temperature, the kinematic viscosity decreases. For aliphatic alcohols in the vicinity of the freezing point, with an increase in the number of carbon atoms at a certain same reduced temperature, the kinematic viscosity decreases, while for their fluorinated analogues, on the contrary, it increases.

Based on the obtained experimental data on viscoelastic properties for aliphatic alcohols and their fluorinated analogues, with the involvement of artificial neural network simulation of the critical parameters and Van der Waals parameters for fluorinated alcohols, the article shows that the homologous series of aliphatic alcohols and their fluorinated analogues have a number of physical differences. The reduced density of fluorinated aliphatic alcohols, unlike limiting aliphatic alcohols, at a certain reduced temperature decreases less with increasing number of carbon atoms, and then increases. While for non-fluorinated aliphatic alcohols, the reduced density at the same reduced temperature increases first with increasing number of carbon atoms, and then decreases.

The reduced sound velocity, which is inversely proportional to the reduced density, increases due to the fluorination of aliphatic alcohols, which, in our opinion, is associated with a decrease in the density of hydrogen bonds in the liquid. Note that in water, where there is a network of hydrogen bonds, the sound velocity is lower than for limiting aliphatic alcohols.

The adiabatic compressibility coefficient decreases when going from a limiting aliphatic alcohol to its fluorinated analogue, and also decreases for fluorinated and non-fluorinated alcohols with an increase in the number of carbon atoms.

Comparison of the properties of alcohols with the properties of water, which has a continuous network of hydrogen bonds, and the properties of hydrogen peroxide, which has hydrogen bonds but no network, shows that the change in physical properties upon fluorination is related to the number of hydrogen bonds per unit volume.

[1] M. Zhang, T. Peyear, I. Patmanidis, D.V. Greathouse, S.J. Marrink, O.S. Andersen, H.I. Ingólfsson. Fluorinated alcohols' effects on lipid bilayer properties. Biophysical Journal. 115(4), 679 (2018). <https://doi.org/10.1016/j.bpj.2018.07.010>

[2] L. A. Bulavin, Yu. L. Zabulonov, A. M. Hetalo, L. O. Matyash, S. O. Samoilenko, O. V. Khorolskyi, Ye. G. Rudnikov. Comparison between viscoelastic properties of aliphatic alcohols and their fluoro-substituted analogs. Ukr. J. Phys. 70(3), 191 (2025). <https://doi.org/10.15407/ujpe70.3.191>

The effect of inelastic scattering on the resonant peak in a binary alloy type model

D. A. Dobushovskyi, A. M. Shvaika

*Institute for Condensed Matter Physics of the National Academy of Sciences of Ukraine,
1 Svientsitskii Str., 79011 Lviv, Ukraine
e-mail: dobushovskiy@icmp.lviv.ua*

We present results of the investigation on thermoelectric properties and optical conductivity spectra for the binary alloy type system with off-diagonal disorder and additional inelastic scattering processes. We consider the Falicov-Kimball model with correlated hopping — one of the simplest models of strongly correlated electrons, extended by the indirect inclusion of the inelastic scattering. Despite its simplicity, the Falicov-Kimball model has very rich phase diagram and exhibits a metal-insulator transition for large on-site Coulomb repulsion, and, most importantly, is exactly solvable via dynamical mean-field theory (DMFT) in the infinite dimensions.

This study extends our previous works [1-2], which considered an effect of correlated hopping on transport properties, and recent study of the closely related model with large enhancement of the thermoelectric power factor via resonant scattering in a low doping regime [3]. As we found previously for a wide range of the model parameters, the sharp singularities appear in both the single-particle density of states and the transport function (the “quasiparticle” scattering time). Due to these anomalies and violation of the electron-hole symmetry, there is a significant enhancement of the thermoelectric properties, and the optical conductivity exhibits a number of interesting features in the vicinity of these singularities. In paper [3], a resonant peak was also observed, but in a reduced form due to the inclusion of a small inelastic scattering rate. While their results were obtained numerically on a cubic lattice within Chebyshev-polynomial Green’s function method, we demonstrate that similar results can be achieved using a much simpler DMFT approach. Furthermore, we can predict an exact location of the resonant peak and its impact on the optical conductivity spectra.

- [1] D.A. Dobushovskyi, A.M. Shvaika, V. Zlatić, Resonant enhancement of thermoelectric properties by correlated hopping for the Falicov-Kimball model on Bethe lattice. *Phys. Rev. B* 95, 125133 (2017). <https://doi.org/10.1103/PhysRevB.95.125133>.
- [2] D.A. Dobushovskyi, A.M. Shvaika, Nonlocal correlations in the optical conductivity spectra. *Condens. Matter Phys.* 21, 23702 (2018). <https://doi.org/10.5488/CMP.21.23702>.
- [3] S. Thébaud, Ch. Adessi, G. Bouzerar, Large enhancement of the thermoelectric power factor in disordered materials through resonant scattering. *Phys. Rev. B* 99, 245203 (2019). <https://doi.org/10.1103/PhysRevB.99.245203>.

Two-qubit detector of microwave photons

O. A. Ilinskaya, S. N. Shevchenko

*B.Verkin Institute for Low Temperature Physics and Engineering of NAS of Ukraine,
47 Nauky Ave., Kharkiv, 61103, Ukraine
e-mail: ilinskaya@ilt.kharkov.ua*

The advantages of using two qubits coupled to the same cavity instead of a single qubit for the microwave photon detection has been recently discussed [1], and it is noted that the benefit is the suppression of a dark count rate.

In this report, we investigate a detector of a classical microwave signal based on two ZZ-coupled superconducting flux qubits. Such a system, widely studied in different aspects (see, for example, Ref. [2]), is a four-level one, and the external harmonic driving field is resonant with two of these levels. As a first step, we consider such a situation when the external signal affects just one qubit. Then, the problem comes down to an excitation of a two-level system, where, in addition to a numerical solution, analytical results can be obtained within the rotating-wave approximation in the multiphoton excitation regime [3]. We numerically calculate the averaged over time occupation probabilities of the qubit's levels as functions of the driving frequency. The graphs qualitatively differ for different driving amplitudes (see Figure), and we can find the sensitivity of the detector.

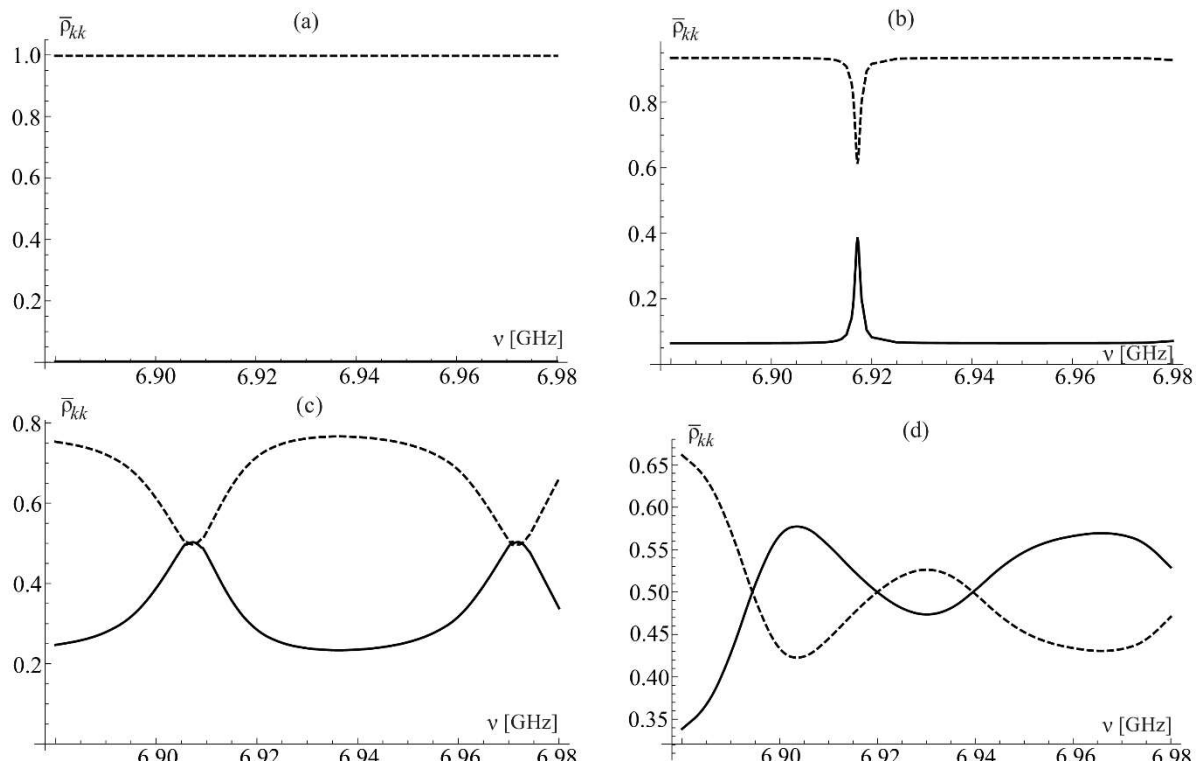


Figure. The averaged over time occupations probabilities (in the physical basis) of the qubit's levels as functions of the driving amplitude, which grows from (a) to (d). The solid (dashed) curve corresponds to the qubit's state with the supercurrent flowing clockwise (counterclockwise). In the panel (a) the external signal is too weak to be detected.

- [1] A. Rettaroli, L. Banchi, H. A. Corti et al., Nucl. Instrum. Methods Phys. Res. A 1070, 170010 (2025). <https://doi.org/10.1016/j.nima.2024.170010>.
- [2] S. H. W. van der Ploeg, A. Izmalkov, A. M. van den Brink et al., Phys. Rev. Lett. 98, 057004 (2007). <https://doi.org/10.1103/PhysRevLett.98.057004>.
- [3] S. N. Shevchenko, Mesoscopic Physics meets Quantum Engineering (World Scientific, 2019). <https://doi.org/10.1142/11310>.

Implementing signal processing algorithms using the adiabatic-impulse model

O. V. Ivakhnenko^{1,2}, D. O. Shendryk^{1,3}, S. N. Shevchenko¹, and F. Nori^{2,4}

¹*B.Verkin Institute for Low Temperature Physics and Engineering of NAS of Ukraine,
 47 Nauky Ave., Kharkiv, 61103, Ukraine*

²*Center for Quantum Computing, RIKEN, Wakoshi, Saitama 351-0198, Japan*
³*Ruhr-Universität Bochum 44780, Germany*

⁴*Physics Department, University of Michigan, Ann Arbor, MI 48109-1040, USA*
 e-mail: login@inbox.com

Quantum signal processing (QSP) is a powerful tool that utilizes single qubit dynamics and allows for performing polynomial function transformations with $O(d)$ elementary unitary operations of the quantum subsystem, where d is the degree of the polynomial function. QSP can be used as part of more complex algorithms such as quantum search, Hamiltonian simulation, quantum phase estimation, enhancing signal in NMR with BB1 algorithm, etc. [1,2]. QSP consists of a combination of adjustable rotation-gates around the z -axis, which leads to a phase gain between energy levels, and fixed x -axis rotations on the Bloch sphere, which can change the occupation of the energy levels. These x - and z -axis rotations are applied one by one, depending on the QSP sequence size.

The adiabatic impulse model (AIM) is a popular method for analytically solving the dynamics of qubits with a small energy gap [3,4]. It consists of adiabatic evolution (when the energy levels occupation is conserved but a phase difference is gained), and diabatic transition, - that leads to interference in the occupation between energy levels. So, the AIM results in a combination of rotations around the z -axis and x -axis, which is the same as in QSP. We found the parameters of AIM that allow to implement a QSP algorithm. Then we found that using double Landau-Zener-Stückelberg-Majorana (LZSM) transitions [4] allows to perform this QSP algorithm using fast non-adiabatic LZSM-gates [4].

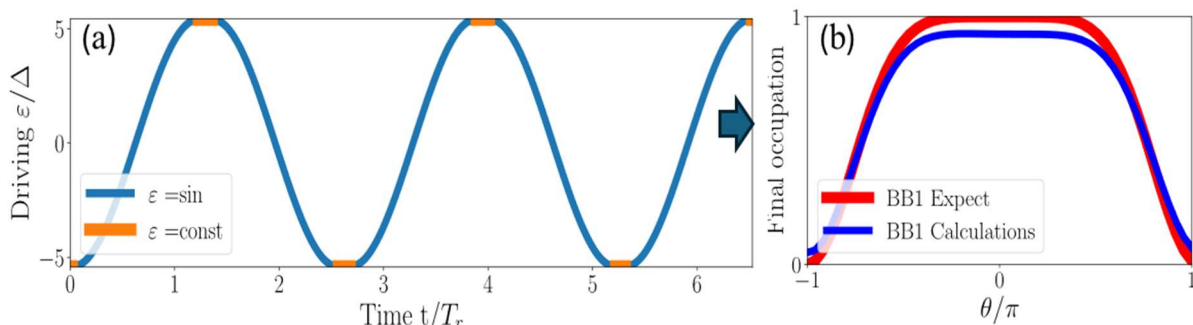


Figure 1: (a) High amplitude non-resonant LZSM-type driving to perform the BB1 QSP algorithm, (b) qubit upper-level occupation result of the BB1 QSP algorithm.

- [1] H. L. Guang, L. C. Isaac, Phys. Rev. Lett. 118, 010501 (2017). <https://doi.org/10.1103/PhysRevLett.118.010501>.
- [2] J. M. Martyn, Z. M. Rossi, A. K. Tan, and I. L. Chuang, PRX Quantum 2, 040203 (2021). <https://doi.org/10.1103/PRXQuantum.2.040203>.
- [3] O. V. Ivakhnenko, S. N. Shevchenko, F. Nori, Phys. Rep. 995, pp. 1-89 (2023). <https://doi.org/10.1016/j.physrep.2022.10.002>.
- [4] A. I. Ryzhov, O. V. Ivakhnenko, S. N. Shevchenko, M. Gonzalez-Zalba, F. Nori, Phys. Rev. Res. 6, 033340 (2024). <https://doi.org/10.1103/PhysRevResearch.6.033340>.

Tunneling transport in semiconductor nanostructures considering the presence of a weak time-dependent electromagnetic field: Lewis-Riesenfeld approach

I. V. Bovko¹, Ju. O. Seti²

¹*Ternopil Ivan Puluj National Technical University, 56 Ruska Str., Ternopil, 46001, Ukraine*

²*Lviv Polytechnic National University, 12 Stepan Bandera Str., Lviv, 79013, Ukraine*

e-mail: boyko.i.theory@gmail.com

Semiconductor nanostructures created on the basis of two- or three-component semiconductor alloys of gallium arsenide or gallium nitride, depending on their geometric shape, according to which such nanosystems can be quantum dots, quantum wires, or planar resonant tunneling nanostructures and others, are of significant interest both from the point of view of theoretical research and from the point of view of their application in electronics, medicine, and high-frequency technology. The standard approach, which is based on the application of the stationary Schrödinger equation, only allows for the determination of the electronic spectrum in such nanostructures. However, no information about the dynamics of electron tunneling transport can be obtained in this case. In particular, resonant-tunneling structures, which are constituent elements of cascade lasers and detectors of electromagnetic waves [1], require a completer and more distinct from the standard approach, since electronic states in these nanostructures are quasistationary.

Due to the quasi-stationary nature of electronic states in resonant tunneling structures and the finite lifetimes τ_n of these states, electronic transitions lead to the emergence of an alternating electromagnetic field. The electric component of this field has a harmonic time dependence, which takes the form: $\xi(t) = \xi_m \cos \omega t$, where ξ_m is its amplitude, and ω is the frequency of the electromagnetic field, which is determined by the magnitude of the quantum transition. In the present work, we consider the process of electron tunneling through an open nanostructure with N layers, alternating between quantum wells and barriers. As a result, the electron tunneling process through the nanostructure in such a problem can be described exclusively by the complete Schrödinger equation in the following form:

$$i\hbar \frac{\partial \Psi(x,t)}{\partial t} = \left\{ -\frac{\hbar^2}{2} \frac{\partial}{\partial x} \frac{1}{m(x)} \frac{\partial}{\partial x} + U(x) - eF \sum_{p=1}^N [\theta(x - x_{p-1}) - \theta(x - x_p)] - \right. \\ \left. - 2e \{x[\theta(x) + \theta(x - x_N)] + x_N \theta(x - x_N)\} \xi \cos \omega t \right\} \Psi(x,t), \quad (1)$$

where $U(x)$ - is the potential profile of a nanostructure in a model with rectangular potentials, F – the intensity of an applied constant electric field, $\theta(x)$ - unit step function. The solutions of the full Schrödinger equation have been obtained by us in exact analytical form using the Lewis-Riesenfeld method. The obtained wave function can be represented in form:

$$\Psi(x,t) = \exp[i\delta(t)]\Phi(x,t), \quad (2)$$

where $\delta(t)$ is obtained from the equation:

$$\hbar \frac{d\delta(t)}{dt} = \langle \Phi(x,t) | i\hbar \frac{\partial}{\partial t} - H(x,t) | \Phi(x,t) \rangle, \quad (3)$$

$\Phi(x,t)$ is an eigenfunction of the invariant: $I(t) = -i\hbar\alpha(t)\partial/\partial x + \beta(t)x + \gamma(t)$.

Using the obtained wave functions, the electronic spectrum in the nanosystem and the features of electronic tunneling transport were investigated.

[1] Rached A., Bhouri A., Sakr S., Lazzari J.-L., Belmabrouk H., Superlattices Microstruct. 91, 3 (2016). <https://doi.org/10.1016/j.spmi.2015.12.035>.

The fluxon interaction with the dipole impurity in the Josephson transmission line

Ivan. O. Starodub, Yaroslav Zolotaryuk

*Bogolyubov Institute for Theoretical Physics of the NAS of Ukraine,
14-b Metrolohichna str., Kviv, 03143, Ukraine
e-mail: starodub@bitp.kyiv.ua*

The fluxon dynamics in a long Josephson transmission line with the presence of a spatial inhomogeneity of variable polarity and taking into account the influence of the medium discreteness is studied. Such an impurity models a qubit inductively coupled to a Josephson transmission line. The influence of discreteness on the qubit state readout process, which is based on measuring the time of fluxon passage through the dipole impurity, is analyzed. The results are compared with the case of a long continuous Josephson junction with a dipole spatial inhomogeneity of finite size [1]. Taking into account the external current and dissipation, the equation of motion of the fluxon and the form of the potential in the field of which it is located are analytically obtained. The threshold current of the fluxon pinning on the impurity is calculated. The dependencies of the threshold current on the discreteness value, the impurity amplitude and dissipation in the system are built. The difference in the times of fluxon passage through the transmission line with the qubit in different states – the delay time – is found. The dependencies of the delay time on the external current, the discreteness coefficient and dissipation were obtained. The influence of the Josephson transmission line size on the delay time is analyzed. It was found that discreteness leads to a decrease of the interval between the threshold current of the fluxon on the qubit in different states, which worsens the sensitivity of the qubit state readout process. On the other hand, discreteness causes an increase in the fluxon delay time on the qubit, which is favorable for the sensitivity of the readout process [2].

- [1] Ivan O. Starodub, Yaroslav Zolotaryuk, Physics Letters A 383, 1419 (2019).
<https://doi.org/10.1016/j.physleta.2019.01.051>.
- [2] Ivan O. Starodub, Yaroslav Zolotaryuk, Physics Letters A 503, 129414 (2024).
<https://doi.org/10.1016/j.physleta.2024.129414>.

Longitudinal Josephson effect in two-layer systems with electron-hole pairing

S. I. Shevchenko, O. M. Konstantynov

*B.Verkin Institute for Low Temperature Physics and Engineering of NAS of Ukraine,
47 Nauky Ave., Kharkiv, 61103, Ukraine
e-mail: akonstantinov@ilt.kharkov.ua*

The study examines the problem of non-dissipative longitudinal current states in bilayer systems with pairing of spatially separated electrons and holes in the presence of a potential barrier that divides the system into two macroscopic subsystems (right and left). The flow of longitudinal currents through the barrier can naturally be referred to as the longitudinal Josephson effect. The flow of current from the electron layer to the hole layer through an insulating interlayer can naturally be called the transverse Josephson current. Under experimental conditions, this current can be made very small; therefore, in the present study, the transverse Josephson current is neglected. It is shown that the dependence of the longitudinal current on the matrix elements of tunneling through the barrier is significantly determined by the degree of system dilution.

In the case of high-density systems, where the size of electron-hole pairs is much larger than the average distance between pairs, the current is proportional to the product of the matrix elements of tunneling through the barrier in the electron and hole layers. This, in particular, means that the emergence of the longitudinal Josephson effect in a high-density bilayer electron-hole system requires the presence of weak coupling in both layers. This result was obtained using two methods: the tunneling Hamiltonian method and the t -representation method.

In low-density systems, the current is proportional to the harmonic mean of these tunneling matrix elements. This result implies that even in the absence of a barrier in one of the layers, the longitudinal Josephson effect will still occur due to the strong coupling of the pair components. In the general case, the coordinates of the potential barriers in the electron and hole layers may not coincide. When coordinates of the barriers coincide, the current, for instance, in the electron layer is given by $j_e = (1/\lambda)\sin\varphi$ where λ^{-1} is the total transparency of the barriers, and φ is the phase drop of the order parameter at the barrier. Hole current $j_h = -j_e$. In the case when the potential barriers in the electron and hole layers are shifted relative to each other by a distance significantly exceeding the coherence length, the current is equal to $j_e = -j_h = \left(1/\sqrt{\lambda_e^2 + \lambda_h^2 + 2\lambda_e\lambda_h \cos\varphi}\right)\sin\varphi$.

Here λ_e^{-1} and λ_h^{-1} are the transparencies of the barriers in the electron and hole layers and $\varphi = \varphi_e + \varphi_h$, where φ_e and φ_h are the phase drops at the barrier in the electron and hole layers, respectively.

The obtained results show that in systems with pairing of spatially separated electrons and holes through a potential barrier separating the left and right sides of the system, a non-dissipative electric current can flow, as in traditional superconductors.

Dynamics of small fluctuations in Boltzmann kinetics

A. I. Sokolovsky, S. F. Lyagushyn

*Oles Honchar Dnipro National University, 72 Nauky Ave. Dnipro, 49045, Ukraine
 e-mail: alexander.i.sokolovsky@gmail.com*

In Boltzmann kinetics, a system of identical particles is described by the average values of the occupancy numbers $n_p \equiv \eta_{1p}$ (p is the set of a particle momentum and its internal quantum numbers). The Hamiltonian operator of the system consists of a main part $\hat{H}_0 = \sum_p \varepsilon_p \hat{n}_p$ and a small interaction \hat{H}_1 ($\hat{\eta}_{1p} \equiv \hat{n}_p = a_p^+ a_p$ is the occupancy number operator). We will describe the fluctuations in the system by the average values η_{2p} of the operator $\hat{\eta}_{2p} \equiv \hat{n}_p^2$. Nonequilibrium states of the system can be investigated using the Bogolyubov reduced description method based on the Peletminkii–Yatsenko model [1]. The non-equilibrium statistical operator (SO) of Boltzmann kinetics $\rho(\eta_1)$ in the basic approximation by interaction \hat{H}_1 is quasi-equilibrium one, i.e. it has the form $\rho_q^0 = e^{\Omega^0 - \sum_p Z_{1p}^0 \hat{n}_p}$. The non-equilibrium SO of Boltzmann kinetics $\rho(\eta_1, \eta_2)$, considering the above fluctuations, is also quasi-equilibrium in the same approximation and has the form $\rho_q = e^{\Omega - \sum_p (Z_{1p} \hat{n}_p + Z_{2p} \hat{n}_p^2)}$. In this case, the exact relations $\text{Sp} \rho_q = 1$, $\text{Sp} \rho_q^0 = 1$, $\text{Sp} \rho_q \hat{\eta}_{2p} = \eta_{2p}$, $\text{Sp} \rho_q \hat{\eta}_{1p} = \eta_{1p}$, $\text{Sp} \rho_q^0 \hat{\eta}_{1p} = \eta_{1p}$, which determine all the quantities in the SO ρ_q^0 , ρ_q are valid. Complete SOs $\rho(\eta_1)$, $\rho(\eta_1, \eta_2)$ are expressed through quasi-equilibrium SOs ρ_q^0 , ρ_q known from the theory of Peletminkii–Yatsenko [1] formulas in the theory of perturbations by interaction \hat{H}_1 . All average values related to Boltzmann kinetics are calculated by ρ_q^0 using the Wick's rules. However, there are no similar rules for ρ_q since its exponent contains a fourth-order form in terms of operators a_p, a_p^+ . To overcome this problem, we propose to limit ourselves to considering Boltzmann kinetics taking into account the dynamics of small fluctuations when the quantities $\eta_{2p} - \text{Sp} \rho_q^0 \hat{\eta}_{2p} = \text{Sp}(\rho_q - \rho_q^0) \hat{\eta}_{2p} \equiv \delta \eta_{2p}$ are small. On this basis, the SO ρ_q is found in the power-law perturbation theory in $\delta \eta_{2p}$. After that, the calculation of averages with the SO ρ_q is reduced to the calculation of averages with the SO ρ_q^0 using Wick's rules. As a result, taking into account the results of Peletminkii–Yatsenko [1] of the small-interaction perturbation theory in \hat{H}_1 , the equation of the dynamics of small fluctuations in Boltzmann kinetics is obtained: $\partial_t \eta_{1p} = L_{1p}(\eta_1, \delta \eta_2)$, $\partial_t \delta \eta_{2p} = L_{2p}(\eta_1, \delta \eta_2)$. This work develops the ideas put forward in our paper [2] in connection with the problem of correlation estimation in spin and quasispin systems, which is relevant for the Dicke superradiance dynamics.

- [1] A. I. Akhiezer, S. V. Peletminkii, Methods of Statistical Physics (Pergamon Press, Oxford, 1981). ISSN 0731-8871.
- [2] A. Sokolovsky and S. Lyagushyn, Low Temp. Phys. 51, 357 (2025). doi: 10.1063/10.0035835.

Modeling of metal strengthening during severe plastic deformation

O. V. Khomenko, A. P. Chopov, K. P. Khomenko, M. S. Holubnycha

*Sumy State University, 116, Kharkivska st., Sumy, 40007, Ukraine
e-mail: o.khomenko@mss.sumdu.edu.ua*

The theory of nonequilibrium evolutionary thermodynamics is applied [1, 2]. Changes in internal energy are represented in the form of a thermodynamic identity, which includes the law of energy conservation, taking into account energy exchange with the external environment and its transformation at the level of internal degrees of freedom during relaxation. Therefore, within the studied method, we considered processes where energy is replenished through the work of external sources of heat and relaxation processes. The relaxation of the system occurs in two ways: on the one hand, through an increase in the number of structural defects, and on the other, through the production of heat (formation of entropy). The study showed that at the initial stage of the process of energy increase, the growth of internal energy dominates due to the intensification of defects. This growth occurs due to the increase in the number and average energy of defects.

In the study, methods for the production of nanostructured materials were also analysed, in particular, methods of severe plastic deformation and approaches of nonequilibrium evolutionary thermodynamics. We consider a model of two-defect approximation, key relations in the context of internal energy and the phasing of the fragmentation process. We investigate how the densities of dislocations and grain boundaries change over time, and also analyse these changes taking into account nonlinear connections. As an example, we show that the density of dislocations transforms from lower to significantly higher levels at the beginning of severe plastic deformation, indicating a structural phase transition. After that, although dislocations stabilize at a steady level, the density of grain boundaries continues to grow and reaches a steady value more slowly, following the dynamics of dislocation density.

The study outlines how external stresses depend on the density of grain boundaries, taking into account nonlinear connections. It has been found that this dependence is generally represented by a monotonically decreasing curve, which does not show pronounced jumps or fluctuations. A change in the slope of the curve can be noticed in the zone of structural phase transition, which can significantly affect the change in the material strengthening law.

- [1] A. V. Khomenko, J. Phys. Stud. 24, No. 2, 2001 (20 p.) (2020).
<https://doi.org/10.30970/jps.24.2001>.
- [2] A. V. Khomenko, D. S. Troshchenko, L. S. Metlov, Phys. Rev. E, 100, 022110 (2019).
<https://doi.org/10.1103/PhysRevE.100.022110>.

Theory of Bose-Einstein condensation with pair correlations within successive iteration method

M. Bulakhov^{1,2}, A.S. Peletminskii^{1,2}

¹*Akhiezer Institute for Theoretical Physics*

²*National Science Center "Kharkiv Institute of Physics and Technology", NAS of Ukraine,
1 Akademichna Str., 61108 Kharkiv, Ukraine
e-mail: aspelet@kipt.kharkov.ua*

We study a many-body system with broken U(1) symmetry, which contains condensates of atoms and their correlated pairs. To derive the equations describing its equilibrium state, we employ a self-consistent non-perturbative approach based on the diagonalization of the non-equilibrium statistical operator and the principle of maximum entropy [1]. This approach is equivalent to the Hartree-Fock-Bogolyubov approximation [2,3]. The interatomic interaction potential, which appears in the coupled equations, is taken to be of a non-contact type with both repulsive and attractive parts. We analyze the system of equations perturbatively by using the condition of slow particle motion (valid at low temperature) and the method of successive approximations. The main thermodynamic characteristics of the system are obtained.

The authors acknowledge support by the National Research Foundation of Ukraine, Grant No. 0124U004372.

- [1] A.I. Akhiezer, V.V. Krasil'nikov, S.V. Peletminskii, A.A. Yatsenko, Phys. Rep. 245, 1 (1994). [https://doi.org/10.1016/0370-1573\(94\)90060-4](https://doi.org/10.1016/0370-1573(94)90060-4).
- [2] Yu.M. Poluektov, Low Temp. Phys. 28, 429 (2002). <https://doi.org/10.1063/1.1491184>.
- [3] J.O. Andersen, Rev. Mod. Phys 76, 599 (2004). <https://doi.org/10.1103/RevModPhys.76.599>.

General collisionless kinetic approach to studying excitations in arbitrary-spin quantum atomic gases

M. Bulakhov¹, A. S. Peletminskii¹, and Yu. V. Slyusarenko^{1,2}

¹*Akhiezer Institute for Theoretical Physics, National Science Center "Kharkiv Institute of Physics and Technology", NAS of Ukraine, 1 Akademichna Str., 61108 Kharkiv, Ukraine*

²*Lviv Polytechnic National University, 79000 Lviv, Ukraine*

e-mail: bulakh@kipt.kharkov.ua

We develop a general kinetic approach to studying high-frequency collective excitations in arbitrary-spin quantum gases. To this end, we formulate a many-body Hamiltonian that includes the multipolar exchange interaction as well as the coupling of a multipolar moment with an external field. By linearizing the respective collisionless kinetic equation, we find a general dispersion equation that allows us to examine the high-frequency collective modes for arbitrary-spin atoms obeying one or another quantum statistics. We analyze some of its particular solutions describing spin waves and zero sound for Bose and Fermi gases. [1]

M. Bulakhov acknowledges support by the National Research Foundation of Ukraine, Grant No. 0124U004372. A.S. Peletminskii and Yu.V. Slyusarenko acknowledge support by STCU under the call “Magnetism for Ukraine 2024/2025”.

[1] Bulakhov M., Peletminskii A.S., Slyusarenko Yu.V. General collisionless kinetic approach to studying excitations in arbitrary-spin quantum atomic gases. Annals of Physics 2025, Vol. 474. P. 169920. DOI: 10.1016/j.aop.2025.169920.

Fluctuation pinning/depinning as a result of transmutation of diffusive gas-fluctuation modes into opposite propagating ones at the formation of two non-Hermitian topological phases originated by gas scattering on impurity center

S. P. Lukyanets, O. V. Kliushnichenko

Institute of Physics of NAS of Ukraine, 46 Nauky Ave., Kyiv, 03028, Ukraine
e-mail: lukyan@iop.kiev.ua, kliushnichenko@iop.kiev.ua

We consider the emergence of spatially separated topological phases, as a formed non-equilibrium steady state, originating from compressible gas scattering on an impurity center [1,2], which corresponds to the non-Hermitian system obeying periodical boundary conditions. The formation of such two distinct bulk phases is accompanied by the transmutation of gas fluctuation diffusive modes into propagating ones [3,4] with opposite directions in the different phases, and by a Liouvillian gap [5] onset for fluctuation spectrum. These result in the pinning of gas fluctuations near the one of inter-phase boundary and their “repulsion” from the other one corresponding to the impurity center. This mechanism leads to the emergence of an adiabatic invariant – the sub-system (impurity-center state or the boundary one) effective protection against perturbations or fluctuations in a gas [1,6]. In the simplified case, such gas fluctuations behavior can be reduced to the Hatano-Nelson model [7] for two different interacting topological phases with the same complex spectrum but opposite winding numbers. Despite the fluctuation eigenspectrum remains complex, the system demonstrates a non-Hermitian skin effect in each phase, and undergoes several spectral transitions, revealing an interesting interplay between non-Hermitian topology and nonequilibrium dynamics of gas fluctuations.

- [1] S.P. Lukyanets, O.V. Kliushnichenko, Phys. Rev. E 109, 054103 (2024).
<https://doi.org/10.1103/PhysRevE.109.054103>
- [2] O.V. Kliushnichenko, S.P. Lukyanets, Phys. Rev. E 98, 020101(R) (2018).
<https://doi.org/10.1103/PhysRevE.98.020101>
- [3] H.C. Fogedby, Eur. Phys. J. B 20, 153 (2001). <https://doi.org/10.1007/PL00011097>
- [4] H.C. Fogedby, Phys. Rev. E 68, 026132 (2003). <https://doi.org/10.1103/PhysRevE.68.026132>
- [5] T. Haga, M. Nakagawa, R. Hamazaki, and M. Ueda, Phys. Rev. Lett. 127, 070402 (2021).
<https://doi.org/10.1103/PhysRevLett.127.070402>.
- [6] S.P. Lukyanets, O.V. Kliushnichenko, Low Temp. Phys. 51, 149 (2025).
<https://doi.org/10.1063/10.0034660>
- [7] N. Hatano, D.R. Nelson, Phys. Rev. Lett. 77, 570 (1996).
<https://doi.org/10.1103/PhysRevLett.77.570>; Phys. Rev. B 56, 8651 (1997).
<https://doi.org/10.1103/PhysRevB.56.8651>; Phys. Rev. B 58, 8384 (1998).
<https://doi.org/10.1103/PhysRevB.58.8384>.

Quasiclassical energy spectra of the Boussinesq breathers in anharmonic crystals

O. V. Charkina, M. M. Bogdan

*B.Verkin Institute for Low Temperature Physics and Engineering of NAS of Ukraine,
47 Nauky Ave., Kharkiv, 61103, Ukraine
e-mail: charkina@ilt.kharkov.ua*

The supersonic nonlinear wave in an anharmonic crystal is an analog of a shock wave [1] like the tsunami wave in the ocean. The wave is described as the one-parametric soliton solution (kink) of the integrable Boussinesq equation for the displacement field or the soliton pulse for the deformation variable. The Boussinesq equation possesses the multisoliton solution, which reproduces completely the interaction process of the shock wave analogs. For a long time, it was generally accepted that the equation had no nonlinear oscillating solution until M. Tajiri and Y. Murakami found such a complex solution, which was called by authors the breather solution [2]. Unfortunately, the cumbersome form of the solution and the absence of this kind of nonlinear waves in the completely integrable continuous Korteweg-de Vries and discrete Toda equations, closely related to the Boussinesq equation, left the found breather solution as an odd duck in the soliton theory.

In the present contribution, we propose a new parameterization of the found breather solution, which significantly simplifies the realization of an analytical approach to research of dynamical characteristics of the breather solution. We find exactly the existence boundary of the breather, previously obtained only numerically. We show explicitly that the complex solution represents the algebraic sum of the kink and the breather expressions. The variability of the solution forms is simply explained by the difference in the amplitudes of these components. However, in the Boussinesq equation the breather part of the solution cannot exist separately from the kink. We found that at the nearest vicinity of the existence boundary on the plane of the dimensionless parameters of the kink inverse length and the carrier wave number, the breather emerges from the *linear localized mode* of the single soliton, and this is the first time when such a birth process is demonstrated analytically. On the plane of the frequency and wave number parameters the breather existence area is restricted by the line of the localized mode frequencies and the high-frequency portion of the continuous wave spectrum. The deviations from these two lines inward the existence area define two different small parameters for independent asymptotic constructions of similar breather solutions in non-integrable equations, in particular, in those bearing topological kinks with the internal modes. In modern terms of the soliton theory, such a kind of composite solution should be attributed to the category of the wobbling kinks [3]. Taking into account its unusual dynamical properties, we single out this complex oscillating solution into a special category and call it the Boussinesq breather.

As a principal result of the contribution, we have exactly obtained the first integrals, the energy and the field momentum, for the Boussinesq breather and explicitly calculated the adiabatic invariant for this complex excitation. Using the found integral characteristics of the Boussinesq breather dynamics, we have carried out the quasiclassical quantization of the nonlinear oscillating solution, obtaining its energy spectrum, i.e., the energy dependence on the momentum and the number of states, and established the Hamiltonian equations for this particle-like excitation.

- [1] A. M. Kosevich, The Crystal Lattice: Phonons, Solitons, Dislocations, Superlattices (2nd Ed., WILEY-VCH, Weinheim, Germany 2005).
- [2] M. Tajiri and Y. Murakami, J. Phys. Soc. Japan, 58, 3585 (1989). DOI: 10.1143/JPSJ.58.3585.
- [3] M. M. Bogdan and O. V. Charkina, Low Temp. Phys. 47, 155 (2021). DOI: 10.1063/10.0003177.

Breathers dumping by extended moving domain walls in highly dispersive nonlinear systems

O. V. Charkina¹, Igor Poltavskyi², Anton Charkin-Gorbulin², M. M. Bogdan¹

¹*B.Verkin Institute for Low Temperature Physics and Engineering of NAS of Ukraine,
47 Nauky Ave., Kharkiv, 61103, Ukraine*

² *University of Luxembourg, L-1511 Luxembourg City, Luxembourg
e-mail: charkina@ilt.kharkov.ua*

The large class of antiferromagnetic and ferromagnetic materials at low temperatures behave as low-dimensional magnets. The known organometallic compounds TMNB, TMNC, TMANC, and FeTAC have been considered as the 1D ferromagnets in the narrow region above the critical temperature of the 3D magnetic ordering. They demonstrate the presence of nonlinear excitations like the 1D domain walls that contribute to the thermodynamic properties of the magnets. The small spin values and closeness to the transition temperature cause quantum and thermal fluctuations leading to deviations from the classical picture. This fact motivates us to elaborate the nonlinear magnetic metamaterials with large classical spins. In the last decades, the progress in the synthesis led to the creation of molecular magnetic clusters known as “magnetic molecules”. Nowadays, there is a great diversity of the “molecules” [1]. In a strong magnetic field, some of them have a total magnetic moment about tens of Bohr magnetons. Arranging the molecules in organic compounds as chains of classical moments, one obtains a 1D metamaterial with desired interactions and structural constants.

In the present contribution, we investigated the dissociation processes in the nonlinear dynamics of the magnetic domain walls and their transformation under the influence of the high dispersion. We started with the analytical description of the evolution of the nonequilibrium moving domain wall in the framework of the integrable SGE for the spin angular variable. We calculated exactly the energy distribution among all the nonlinear and linear excitations as a result of the dissociation process, using the exact solution of the direct scattering problem associated with the SGE [2]. It was shown that the extended domain wall dumped the excess energy by emerging the unmoving breathers and radiating the spin waves. Using the conservation of another first integral, the field momentum, we established the relation between the effective length and the initial velocity of the extended domain wall and the final velocity of the stationary moving domain wall at large times. It was possible in the case of unmoving arising breathers and the absence of radiation.

The effects of the strong dispersion of underlying magnetic systems, coming from their discreteness, were taken into account by introducing the fourth mixed derivative term into the SGE. The nonlinear dynamics of the non-integrable modified equation, known as the regularized sine-Gordon equation, were studied numerically. We revealed the unusual processes of the moving kink dissociation accompanied by the strong breather emission. For the first time, we found a large variety of the reactive motions of all nonlinear excitations with their ahead and backward mutual scattering. Due to the higher dispersion, all resulting breathers began to move. In the simplest case after the one-breather dumping, the domain wall moved ahead and left the breather in its wake. In the case of two- and three-breathers dumping the initially fast domain wall could shoot the large breather ahead and was stopped itself and then moved backward. The rest breathers could move forward or backward as single excitations, but sometimes, they formed the breather molecules [3]. We calculated the frequencies of the single breathers in the reference frames moving with them, analyzed the FFT spectra of oscillations of the breathers and their “molecules”. We also calculated the energy and field moment distributions among all the nonlinear excitations.

[1] D. Gatteschi, R. Sessoli, and J. Villain, Molecular Nanomagnets (OUP, New York, 2006).

[2] M.M. Bogdan and O.V. Charkina, Low Temp. Phys. 47, 155 (2021). DOI: 10.1063/10.0003177.

[3] M. Jia, J. Lin, S. Y. Lou, Nonlin. Dyn., 100, 3745 (2020). DOI: 10.1007/s11071-020-05695-3.

Interface phonon spectrum and electron-phonon interaction in GaN/AlGaN nanostructures

Ju. O. Seti¹, I. V. Boyko²

¹*Lviv Polytechnic National University, 12 Stepan Bandera Str., Lviv, 79013, Ukraine*

²*Ternopil Ivan Puluj National Technical University, 56 Ruska Str., Ternopil, 46001 Ukraine*

e-mail: jseti18@gmail.com, yuliia.o.seti@lpnu.ua

Group III nitride-based heterostructures are promising materials for infrared optoelectronic devices operating on intersubband quantum transitions between quantized electron energy levels [1]. The energy of these transitions is determined by the geometrical parameters of quantum wells and barriers, as well as the physical characteristics of the heterostructures of nanodevice active elements. This flexibility enables the realization of photodetectors of various wavelengths by using the same material system and simply modifying the nanolayers widths and their component composition. In particular, quantum well infrared photodetectors and quantum cascade detectors with various active region designs, based on GaN, AlN, InN, and their ternary compounds, have been developed, covering a broad spectral range from terahertz to near-infrared.

The wurtzite crystal lattice, typical for Group III nitrides, results in the anisotropic physical properties of these materials and the emergence of internal polarization fields in heterostructures. These fields are significant and distort the potential profile of the nanostructure, causing the potential wells and barriers to become triangular. Regarding phonon spectra, wurtzite nanostructures exhibit considerably more complex phonon spectra compared to isotropic GaAs-based materials with a cubic crystal lattice [2, 3].

This paper is dedicated to investigating the energy spectrum properties of interface phonons and the influence of electron-interface-phonon interaction on the spectral characteristics of electron states in $\text{Al}_x\text{Ga}_{1-x}\text{N}/\text{GaN}/\text{Al}_x\text{Ga}_{1-x}\text{N}$ nanostructures as a key element of photodetectors [1]. The study is focused on establishing the dependence of these characteristics on the geometric parameters of the structure and the Al concentration.

To develop the theory of electron-phonon interaction, we first find solutions for the electron and phonon problems independently. Electron energies and wave functions are calculated within the effective mass framework as a self-consistent solution of the Schrödinger and Poisson equations. The energy spectrum and polarization field potentials of interface phonons are determined from electrostatic Maxwell's equations within the anisotropic dielectric continuum Loudon model.

The electron-phonon interaction Hamiltonian is calculated in the second quantization representation with respect to electron and phonon variables [4]. Using the Fermi Golden Rule, the derived electron-phonon coupling functions allow for calculating electron relaxation times for phonon-assisted intersubband transitions.

To obtain the electron spectrum renormalized by interaction with all branches of interface phonons, the Fourier image of the electron Green's function is calculated, which is related to the mass operator through the Dyson equation. The calculation of the mass operator allows us to obtain the shifts and damping of the electron energy levels [4].

- [1] M. Beeler, E. Trichas, E. Monroy, *Semicond. Sci. Technol.* 28, 074022 (2013). <https://doi.org/10.1088/0268-1242/28/7/074022>.
- [2] M.A. Stroscio, M. Dutta, *Phonons in Nanostructures* (Cambridge University Press, Cambridge, 2001), <https://doi.org/10.1017/CBO9780511534898>.
- [3] J. Seti, M. Tkach, O. Voitsekhivska, *Rom. J. Phys.* 63, 607 (2018).
- [4] J. Seti, O. Voitsekhivska, E. Vereshko, M. Tkach, *Appl. Nanosci.* 12, 533 (2022). <https://doi.org/10.1007/s13204-021-01708-8>.

**TECHNOLOGIES AND INSTRUMENTATION FOR
PHYSICAL EXPERIMENTS**

Global perturbations of the ionosphere during the geospace storm on September 11-21, 2024.

L. F. Chernogor, V. O. Bessarabova

V. N. Karazin Kharkiv National University, Kharkiv 61022, Ukraine
e-mail: Leonid.F.Chernogor@gmail.com

Solar storms are accompanied by coronal mass ejections, flashes of electromagnetic and corpuscular radiation, and the generation of high-speed solar wind flows. The disturbed solar wind, reaching the Earth, causes geospace storms. Geospace storms are a complex of magnetospheric, ionospheric, atmospheric storms, and storms in geophysical fields (electric, magnetic, baric, and thermal). Ionospheric storms are the main manifestation of ionospheric weather, which is part of space weather. The state of ionospheric weather significantly affects the propagation of radio waves, the operation of radio navigation, radar and radio communication systems, and radio sounding of the space, and the functioning of space-based and ground-based electronic devices.

It is known that each storm has its own unique properties. This explains the need to study each geospace storm, in particular unique events. The geospace storm on September 11–21, 2024 is one of such storms. The storm lasted about 10 days. It consisted of two main magnetic storms, the maximum K_p-index of which reached 7 and 7+. The first storm, September 11–12, 2024, had a main phase duration of about 10 hours, the D_{st}-index reached a minimum of -121 nT. The second storm, September 16–17, 2024, had a main phase duration of about 9 hours, and the D_{st}-index also reached a minimum of -121 nT. In addition to these two main magnetic storms in the period from September 12–19, 2024, a series of less intense magnetic storms occurred, the K_p-indices of which were from 4 to 7-. The F region of the ionosphere is the main indicator of ionospheric storm manifestations. According to the international GIRO network, the values of the critical f₀F2 frequency of the F2 layer fluctuated quite significantly. Thus, in the eastern hemisphere on the reference day, September 11, 2024, the critical frequency value varied from 9.2 MHz to 12.4 MHz during the day (from 5 MHz to 6.4 MHz at night), and in the western hemisphere it varied from 9.5 MHz to 13.2 MHz during the day (from 3 MHz to 6.1 MHz at night). At the northern stations on September 12, 2024, the value of the critical frequency f₀F2 decreased, and at the middle stations, on the contrary, it increased. In the western hemisphere on this day, an increase in the critical frequency f₀F2 was observed, and at night its decrease. On this day, positive and negative ionospheric storms were observed (in the Eastern Hemisphere, negative minor and positive minor, and in the Western Hemisphere, even negative strong ionospheric storms occurred at night). On September 17, 2024, negative strong and extreme ionospheric storms were observed at night. The value of the critical frequency f₀F2 decreased everywhere, except for stations NI135 and CAJ2M. Thus, the second main storm had a greater intensity than the first. The duration of blackouts during the storm at stations TR169 and CAJ2M was ~70 h and ~120 h, respectively. At station FF051, the disappearance of the reflection from the F2 layer and the appearance of the reflection from the F1 layer (G-condition) were observed. On September 12, 2024, the f₀F1 values varied from ~2 MHz to ~7.5 MHz, and on September 17, 2024 it varied from ~2 MHz to ~4 MHz. In the period from September 11 to 21, 2024, the variations of the critical frequency of the E region were almost the same. During the day, the values of the critical frequency f₀E reached ~3.5–3.9 MHz, at night no values were recorded. The ionospheric storm had no effect on the E region of the ionosphere.

- [1] Chernogor L. F., and Domnin, I. F., Physics of geospace storms (Kharkiv: V. N. Karazin Kharkiv National University Publ. 2014).
- [2] Chernogor L. F., Physics of geospace storms, Space Science and Technology. V. 27, 3–77 (2021). <https://doi.org/10.15407/knit2021.01.003>.
- [3] Chernogor L. F., Bessarabova V. O., Variations of ionospheric weather during geospace storm on May 10–11, 2024. Kinematics and Physics of Celestial Bodies, 41, №4 (in print).

Analysis of total electron content disturbances in the ionosphere on May 10–11, 2024, caused by high solar activity

L. F. Chernogor, R. M. Kovalov, M. B. Shevelev

V. N. Karazin Kharkiv National University, Krarkiv, 61022, Ukraine
e-mail: Leonid.F.Chernogor@gmail.com

The purpose of the report is to present the results of the analysis of the total electron content (TEC) disturbances in the ionosphere, which were observed on a global scale during the geospace superstorm of May 10–11, 2024.

The analysis was based on the primary data presented on the website [<ftp://nfs.kasi.re.kr>]. Measurement data from 6 stations were analyzed using the G06, G09, G11, G12, G17, G20, and G25 satellites.

On May 8, 2024, the activity of the Sun increased. A series of M- and X-class solar flares were observed during May 8–11, 2024. The flares were accompanied by a number of coronal mass ejections that reached Earth on May 10–11, 2024 [<https://www.spaceweatherlive.com/en/archive/2024/05/10.html>].

On May 10–11, the most powerful geospace storm in the 25th solar activity cycle was observed [1]. It led to intense storms in the magnetosphere, ionosphere, atmosphere, lithosphere and geophysical fields (magnetic, electric, pressure, and thermal fields) [2, 3]. The magnetic storm began on May 10, 2024, and continued for about 7 days.

Simultaneously with the magnetic storm, an ionospheric storm was observed. In the Eastern Hemisphere on May 10, 2024, the TEC, N_V , in the ionosphere was practically no different from the TEC on the reference day of May 9, 2024. On May 10, 2024, the highest TEC values were observed at low-latitude stations (22°N , 114°E), where for different satellites $N_{V_0} \approx 92 - 110$ TECU ($1 \text{ TECU} = 10^{16} \text{ m}^{-2}$), and XMIS (10°S , 106°E), where $N_{V_0} \approx 75 - 113$ TECU. Such TEC values are explained by the influence of the equatorial ionization anomaly. With increasing latitude in both the Northern and Southern Hemispheres, the TEC gradually decreased to approximately $39 - 45$ TECU at 52°N and to $46 - 52$ TECU at 29°S .

Thus, for the HKSL and XMIS stations, the TEC was $49 - 92$ TECU and $55 - 65$ TECU, respectively. On May 11, 2024, a negative ionospheric storm with $I_{NIS} = 3 - 4.8$ dB took place [2, 3]. The $I_{NIS} = 2 - 4$ dB corresponds to a moderate storm, and $I_{NIS} = 4 - 6$ dB corresponds to a strong storm. As on May 10, 2024, on May 11, TEC decreased with increasing latitude. At a latitude of 52°N TEC did not exceed $13 - 22$ TECU, and at a latitude of 29°S TEC was within $22 - 25$ TECU.

Solar flares of X3.98 and X5.89 classes occurred on May 10 and 11, 2024, respectively. The temporal variations of TEC were superimposed by the TEC spikes. On May 10, 2024, ΔN_V bursts were equal to $0.6 - 2$ TECU depending on the latitude. On May 11, they reached $0.9 - 6.1$ TECU, that is, they were noticeably larger. The greatest effect was recorded at the HKSL ($\Delta N_V \approx 1.4 - 6.1$ TECU, $\delta N_V = \Delta N_V / N_{V_0} \approx 2.8 - 9.1\%$) and XMIS ($\Delta N_V \approx 3.2 - 7.7$ TECU, $\delta N_V \approx 6 - 12\%$) stations. This was due to the small zenith angle of the Sun and the influence of the equatorial ionization anomaly. On May 10, 2024, δN_V value was $1 - 1.9\%$ and $0.8 - 2.3\%$ for the same stations. No clear dependence of δN_V on latitude was observed.

[1] L. F. Chernogor, Energetics of physical processes operated on May 8–12, 2024: From the solar storm to lithospheric disturbances. *Adv. Space Res.* 75, 6, 4825–4849 (2025). <https://doi.org/10.1016/j.asr.2024.12.069>.

[2] L. F. Chernogor and I. F. Domnin, Physics of Geospace Storms (V. N. Karazin Kharkiv Nat. Univ. Publ., Kharkiv 2014) [in Russian].

Highly informative format for comprehensive analysis of space weather conditions

L. F. Chernogor, D. R. Kulyk

V.N.Karazin Kharkiv National University, 4 Svobody Square, Kharkiv, 61022, Ukraine
e-mail: dmytro.kulyk@karazin.ua

The study demonstrates capabilities of the developed format for a comprehensive analysis of solar activity and space weather, for the geospace storm of September 11-21, 2024 description as an example. The format covers more than 60 time-dependent parameters across the Sun–interplanetary medium–magnetosphere–ionosphere–atmosphere–Earth system. The effects of the solar and geospace storms, as well as their components (magnetospheric, ionospheric, atmospheric, electric, and magnetic storms) are analyzed.

On September 12 and 14, 2024, X1.3 and X4.54 class solar flares occurred, accompanied by coronal mass ejections (CMEs), which upon reaching Earth's magnetosphere, triggered a geospace storm. The flares had power levels near Earth of 16.6 GW and 57.9 GW, transferring 9.5 TJ and 73 TJ of energy, respectively. The CMEs triggered disturbed solar wind flows with speeds near Earth up to 583 km/s, particle density up to $3.9 \times 10^7 \text{ m}^{-3}$ and plasma temperature of $9.7 \times 10^5 \text{ K}$ for the first flare, while the second CME had lower particle density of $1.55 \times 10^7 \text{ m}^{-3}$ and temperature of $6.27 \times 10^5 \text{ K}$, despite a slightly higher speed of 595 km/s. The solar storm was also accompanied by the injection of solar cosmic rays, reaching power of 760 GW and 490 TJ energy for the first burst, and 714 GW and 513 TJ for the second respectively.

The first burst of disturbed solar wind (21-hour duration) subjected the magnetosphere to dynamic, magnetic, and thermal pressures, with power reaching 94 TW, 2.24 TW, and 3.1 TW, and energy values of 2.8 EJ, 74 PJ, and 30 PJ, respectively. The second burst (24-hour duration) produced 53.1 TW, 1.1 TW, and 0.5 TW, with 2.1 EJ, 42.8 PJ, and 14.1 PJ, respectively.

Sudden storm commencements (SSC) and interplanetary magnetic field (IMF) variations were observed in response to significant jumps in dynamic pressure and the SYM-H index: first SSC (September 11, 15:30 UTC) caused a negative jump in B_Y to -8 nT, a positive jump in B_Z to 5 nT, followed by oscillations within $\pm 10 \text{ nT}$. Second SSC (September 12, 03:30 UTC) triggered a sharp southward shift of B_Z , marking the start of the main storm phase with oscillations reaching 25 nT. The second burst was characterized by a third SSC (September 16, 23:20 UTC) with a sharp southward turn of B_Z and a positive jump in B_Y , followed by oscillations up to 17 nT over a 24-hour period, marking the main phase of the second storm and a gradual transition to the recovery phase.

The energy of the magnetospheric storm is described by Akasofu's ε_A parameter, with observed peak values of 0.62 and 0.32 TJ/s, and Dst index values: $Dst^*_{\min} \approx -137 \text{ nT}$, $Dst^*_{\min} \approx -139 \text{ nT}$ for the first and second bursts, respectively. The magnetospheric energy E_{ms} reached 5.48 PJ and 5.58 PJ, respectively.

The ionospheric and atmospheric storms were characterized by significant negative disturbances at high latitudes, peaking on September 14 and 17, with a gradual weakening at lower latitudes. In the mid-latitude European region, a negative ionospheric storm was observed, with an INIS index of up to 6-7.6 dB. The atmospheric storm was marked by a decrease in the $\Sigma O/N_2$ ratio from undisturbed values of 0.6-1.0 to 0.2-0.4 during both bursts, followed by a gradual recovery.

- [1] L. F. Chernogor, Adv. Space Res. 75, 6, 4825–4849 (2025). <https://doi.org/10.1016/j.asr.2024.12.069>
- [2] L. F. Chernogor and I. F. Domnin, Physics of Geospace Storms (V. N. Karazin Kharkiv Nat. Univ. Publ., Kharkiv, 2014).
- [3] L. F. Chernogor, Space Sci. Tech. 27, 3–77 (2021). <https://doi.org/10.15407/knit2021.01.003>

Amorphous $\text{Mo}_{1-x}\text{Si}_x$ films for quantum systems applications

O. O. Leha¹, V. Yu. Lyakhno^{1,2}, I. O. Martynenko², S. V. Bengus¹, O. G. Turutanov^{3,1}

¹*B.Verkin Institute for Low Temperature Physics and Engineering of NAS of Ukraine,
47 Nauky Ave., Kharkiv, 61103, Ukraine*

²*G.V. Kurdyumov Institute for Metal Physics, N.A.S. of Ukraine,
36 Academician Vernadsky Boulevard, 03142 Kyiv, Ukraine*

³*Department of Experimental Physics, Comenius University, 842 48 Bratislava, Slovakia
e-mail: legus96@gmail.com*

We have further developed the technology of deposition of superconducting amorphous $\text{Mo}_{1-x}\text{Si}_x$ thin films with enhanced sheet resistance due to high uniformity at low thicknesses. The films were produced by DC-magnetron sputtering from two separate sources in an argon atmosphere. We present the results of four-point resistance measurements in a cryostat cooled to liquid helium temperature for films with various thicknesses down to 4 nm.

The preparation procedure enables fine-tuning of the normal sheet resistance of $\text{Mo}_{1-x}\text{Si}_x$ superconducting films by controlling their thickness and composition thus making these thin films promising for use in a number of quantum detection devices. Precise resistance control allows us to optimize the Q-factor of resonators to introduce limited pre-set decoherence in quantum detection systems. While in a quantum computer dissipation leads to unacceptable decoherence which destroys the quantum state of the entangled qubits, in single photon detectors the presence of a certain degree of relaxation is principally necessary.

In e.g. bolometric optical photon detectors, high normal sheet resistance of the sensor material provides generation of a high-amplitude voltage pulse during the absorption act [1]. Dissipation in the quantum detector helps to hold the magnetic flux changed after absorption of a single photon in a microwave counter based on a flux qubit [2]. High normal sheet resistance of amorphous superconducting thin films causes their relatively large kinetic inductance even far from T_c . Thin-film elements with high kinetic inductance reduce the geometric sizes of planar resonators in quantum circuits and weaken the coupling to the external dissipative environment [3]. The temperature dependence of the kinetic inductance can be utilized in photon detectors due to a frequency shift in the resonant circuit after absorption of an optical photon [4]. Also, the development of a planar Josephson junction using MoSi_2 [5] as the tailored-proximity barrier layer expands their potential in quantum computing and sensing applications. We can form such a layer *in situ* during deposition process. The superconducting films with the normal sheet resistance close to the quantum one, near metal-insulator transition, can be implemented in the phase-slip qubit [6].

O.G.T. has been funded by the EU NextGenerationEU through the Recovery and Resilience Plan for Slovakia under the project No. 09I03-03-V01-00031.

- [1] Yu. P. Korneeva, et al., Superconductor Science and Technology, 27(9), 095012 (2014). <https://doi.org/10.1088/0953-2048/27/9/095012>.
- [2] V. I. Shnyrkov, et al., Low Temp. Phys. 44 213–20 (2018). <https://doi.org/10.1063/1.5024538>.
- [3] V. I. Shnyrkov, et al., Low Temp. Phys. 41, 867 (2015). <http://dx.doi.org/10.1063/1.4935839>.
- [4] M. Trgala, et al., Appl. Surf. Sci., 312, 216 (2014). <https://doi.org/10.1016/j.apsusc.2014.05.200>.
- [5] Y. Chong, P. Dresselhaus and S. Benz, Appl. Phys. Lett., 232505 (2005). <https://doi.org/10.1063/1.1947386>.
- [6] J. E. Mooij and C. J. P. M. Harmans, New J. Phys. 7, 219 (2005). <https://doi.org/10.1088/1367-2630/7/1/219>.

Method of detonation velocity measuring of the condensed explosives

E. D. Pekar, A. G. Bryzgalin, N. A. Pashin, S. D. Ventsev, L. M. Malakhova

E.O. Paton Electric Welding Institute, 03150, 11, Kazymyr Malevych str., Kyiv, Ukraine
e-mail: svarka2000@ukr.net

The detonation velocity is the main characteristic of an explosive which significantly depends on the detonation conditions. Taking into account these circumstances, a method of detonation velocity measuring was developed, which corresponds to the requirements of DSTU [1].

The measurements are based on determining of the time interval between the triggering of sensors, which are located at a known distance from each other. The sensor is two copper wires with a diameter of 0.1-0.15 mm, covered with insulating material (varnish) and connected to different electrical potentials. At the moment of triggering, a capacitor is discharged through the sensor and this is recorded on a digital oscilloscope.

Due to the fact that the closing of the sensors is accompanied by the so-called "contact rattling", a signal converter was developed that generates a discrete pulse with a duration of 0.2 μ s. This makes it possible to record time intervals with high resolution.

4 sensor placement points are used to measure the speed. According to the proposed method, three measurements of the detonation speed can be made at these four points in one experiment, which meet the requirements of DSTU. In addition, at each measurement point the sensors can be duplicated, which allows to increase the number of measurements on one sample of an explosive device, which increases the accuracy of measurements while reducing the number of experiments.

To register the sensor signals, two-channel oscilloscope with a memory capacity of 640,000 measurements for each channel and a sampling period of 50 ns was used.

The measurement method and the equipment used meet the safety requirements for the use of explosive materials and devices. Practical work has revealed a reduction in material and labor costs for conducting experimental research.

[1]. DSTU EN 13631-14:2005 Explosives. Part 14. Determination of detonation velocity.

System spectral analysis of infrasonic wave disturbances caused by the Tonga supervolcano eruption on January 15, 2022

L. F. Chernogor¹, O. I. Liashchuk², N. M. Tilichenko¹, M. B. Shevelev¹

¹*V. N. Karazin Kharkiv National University, Kharkiv, 61022, Ukraine*

²*Main Center of Special Control, National Center for Control and Testing of Space Means
of the State Space Agency of Ukraine, Horodok, Zhytomyr region, Ukraine
e-mail: alex.liashchukk@gmail.com*

Infrasound, i.e. sound waves with a frequency below 20 Hz, is an important object of research due to its unique properties, such as the ability to propagate over long distances with minimal attenuation. Infrasound phenomena occur during natural processes (volcanic eruptions, earthquakes, lightning, meteoroid falls), as well as due to human activity (rocket launches, aircraft flights, explosions, industrial plants). Studying the generation and propagation of infrasound is necessary to better understand global natural processes, predict disasters and assess the impact on human health.

The main objective of the study is the spectral analysis of infrasound waves caused by the super-powerful explosion of the Tonga volcano, determining their characteristics, such as frequency, amplitude and propagation speed. This allows us to assess the impact of the explosion on the atmosphere and ionosphere, as well as to identify features in the propagation of waves [1- 3].

The object of the study is the infrasound waves generated by the explosion of the Tonga supervolcano and registered at the Ukrainian infrasound network of stations, their spectral characteristics and mechanisms of interaction with other geophysical processes.

The main methods of digital signal processing were used for the analysis: bandpass filtering and system spectral analysis, which is based on a combination of mutually complementary short-time and adaptive Fourier transforms and wavelet transforms. The short-time Fourier transform has better time resolution, adaptive has better frequency resolution, and the wavelet transform based on the Morlet basic function acts as a «mathematical microscope» for studying the thin structure of the signal [4].

As a result of applying the above methods to the initial data at the Akademik Vernadsky Station, stations “Kamenets-Podilsky”, “LUGA” and “MAAG”, “Horodok” and “Balta” (the distances from the infrasound source to the place of registration varied from 8867 km to 16330 km), the following was established [2–4]. The delay time of the arrival of the infrasonic wave was from 465 to 1305 min, the speed varied within 210–318 m/s, the amplitude range was mostly from 110 to 250 Pa, the main periods observed in the spectral composition had values of 4–6, 8–10, 400–600 s. The key feature of the signal recorded at the Akademik Vernadsky Station was that the infrasound packet consisted of three parts, namely a Lamb wave with a delay time of 465 min, periods of 400–600 s, and two infrasound groups with periods ranges from 200 to 300 s and from 500 to 700 s. The signal durations ranged from 8 to 10 min for oscillations in the period range from 1 to 10 s, and from 2 to 3 h in the period range from 100 to 1000 s.

It is confirmed that the unique explosive eruption of the supervolcano caused significant disturbances in the atmosphere and the World Ocean on a global scale. The atmospheric effects of the shock wave, Lamb wave, infrasonic wave, and oceanic tsunami have been identified for the first time, and their parameters have been estimated.

- [1] L. F. Chernogor and M. Yu. Holub, *Kinem. Phys. Celest. Bod.* 39, 247 (2023) <https://doi.org/10.3103/S0884591323050033>.
- [2] L. F. Chernogor, *J. Atmos. Solar-Terr. Phys.* 253, 106157 (2023). <https://doi.org/10.1016/j.jastp.2023.106157>.
- [3] L.F. Chernogor and Y. Luo, Statistical Analysis of Seismic and Tsunami Waves Generated by the 2022 Tonga Volcano’s Eruption. A Comprehensive Study of Volcanic Phenomena. (Ed.: Dr. Károly Németh. IntechOpen, 2024). <https://doi.org/10.5772/intechopen.1006881>.
- [4] L. F. Chernogor, *Geomag. Aeron.* 48, 652 (2008). <https://doi.org/10.1134/S0016793208050101>.

Global response of total electron content of ionosphere during powerful geospace storm on November 4-5, 2023

M. Yu. Tkachenko, L. F. Chernogor

V. N. Karazin Kharkiv National University, Krarkiv, 61022, Ukraine
e-mail: tkachenko.postgrad@gmail.com

Powerful geospace and magnetic storm ($K_p = 8-$) was unique event that caused significant impact on Earth-Atmosphere-Ionosphere-Magnetosphere (EAIM) system [1,2,3,4]. The geospace storm on November 4-5, 2023, eventually reached a G3 level, which is classified by NOAA [<https://www.noaa.gov/>] as a "strong" storm. Such storms can cause disruptions in the operation of various radio systems, create interference that hinders their functioning, and even affect power transmission lines. This storm also triggered rare red auroras, which were observed as far south as regions of Ukraine. The geomagnetic storm began at 18:00 UT on November 4, 2023, and continued until 08:00 UT on November 6, 2023, after which the recovery phase began.

We present the result of analysis of several parameters that describe energy and matter flow from Sun to EAIM system (solar wind particles concentration, speed, temperature, it's dynamic pressure on magnetosphere, Akasofu parameter), interplanetary magnetic field (IMF) within its B_z and B_y projections [<https://omniweb.gsfc.nasa.gov>] and subsystems of EAIM system (Dst -index, K_p -index [<https://wdc.kugi.kyoto-u.ac.jp>], total electron content (TEC) maps)). Also, both amplitude (S4) and phase (SIGMA_PHI) ionospheric scintillation maps were analized [<https://cedar.openmadrigal.org/openmadrigal>]).

Significant disturbances of parameters describing solar wind, IMF and EAIM were detected during the main phase of the storm (November 4-5) and at the beginning of recovery phase (November 6). Also we provided statistical analysis of percentage deviation of mean values of TEC in different latitudes in both hemispheres via bootstrap algorithm [<https://github.com/timofeytkachenko/fastbootstrap/blob/main/fastbootstrap/bootstrap.py>]. During reference pre-storm days (November 2-3) mean values of TEC in equatorial latitudes were equal to 36.2 TECU in Northern hemisphere and 40.9 TECU in Southern hemisphere, 18.66 TECU and 32.17 TECU in mid latitudes and 10.59 TECU and 23.21 TECU in high latitudes in Northern and Southern hemispheres respectively. We have determined the presence of a negative ionospheric storm phase: in high latitudes on November 5 in Southern hemisphere (-33.36% deviation from non-disturbed mean values); high latitudes on November 6 in both hemispheres (-19.1% and -45.24% for the Northern and Southern hemispheres respectively) and mid latitudes in Southern hemisphere this day (-26.28%); and in mid and high latitudes in Southern hemisphere on November 7 (-12.44% and -30.9% respectively). Also, there were positive ionospheric storm phases in: high latitudes in Northern hemisphere on November 4 (+28.6%); mid latitudes in Northern hemisphere on November 5 (+22.4%).

By analyzing both amplitude and phase scintillation indices strong scintillations (over 0.2) were detected during storm day (November 5) and during the start day of recovery phase (November 6) that can be a signal of the presence of ionospheric disturbances and irregularities above the locations of these measurements.

- [1] L. F. Chernogor. Radio Physics and Radio Astronomy, vol. 8, no. 1, pp. 59-106, 2003.
- [2] L. F. Chernogor. Space Science and Technology, vol. 9, no. 5/6, pp. 96-105, 2003.
- [3] L. F. Chernogor. Space Sci. & Technol, vol. 9, no. 1, pp. 03-77, 2021.
<https://doi.org/10.15407/knit2021.01.003>.
- [4] L. F. Chernogor and I. F. Domnin, Physics of Geospace Storms (V. N. Karazin Kharkiv Nat. Univ. Publ., Kharkiv, 2014) [in Russian].

Computer modeling of a nitrogen-cooled cryopanel

O. Vorobyova^{1,2}, D. Sokolov^{1,2}, Ye. Korshikov¹

¹*Al-Farabi Kazakh National University, Al-Farabi av., 71, Almaty, 050040, Kazakhstan*

²*Almaty Technological University, Tole bi av., 100, Almaty, 050012, Kazakhstan*

e-mail: olga.vorobyova842@gmail.com

Cryosurfaces play an important role in cooling and science work with samples in the low temperature range. Computer modeling is one of the most modern and relevant methods for studying the processes of heat transfer of cryopanels when interacting with the environment and materials of various compositions applied to the surface of the substrate. This will solve a number of problems related to:

- 1) the development of an effective heat exchanger and the study of its heat transfer properties;
- 2) the creation of an autonomous system for maintaining temperatures of varying accuracy under conditions of thermal energy balance on the surface of the cryopanel.

Cooling of a cryogenic surfaces is the process of cooling a line for pumping cryogenic liquids in/on surface of panel, which is implemented from room temperature to cryogenic temperature ($T \sim 77$ K). This process is attracting increasing attention as cryogenic liquids play an increasingly important role in modern industries and academic fields [1-2].

One of the biggest challenges when cooling a cryogenic line is understanding the transient heat transfer characteristics and the ability to predict the cooling process [3-4].

In this work, the process of cooling a cryogenic panel to nitrogen temperatures (from 300 to 80 K) is simulated. The results of the distribution of the cryogenic temperature front over the surface and volume of the cryopane are shown. The model was developed using the finite element method (FEM) and flow and heat transfer for cryogens was achieved using experimental correlations, analytical models, and computational fluid dynamics (CFD) models.

When considering the volumetric temperature distribution, the influence of the distribution of cooling tubes and the prefabricated structure over the volume of the cryosurface on the cooling intensity was revealed. The obtained results indicate that adjusting the geometric parameters of heat exchange tubes improves the cooling efficiency, which provides useful information for the design of more efficient cryogenic surfaces.

- [1] D. Y. Sokolov, D. Yerezhep, O. Vorobyova, M. A. Ramos, A. Shinbayeva, Optical Studies of Thin Films of Cryocondensed Mixtures of Water and Admixture of Nitrogen and Argon, Materials 15, 7441 (2022). <https://doi.org/10.3390/ma15217441>.
- [2] B. Wang et al., Potential applications of cryogenic technologies to plant genetic improvement and pathogen eradication, Biotechnology advances 32(3), 583 (2014).
- [3] H. Hu, J. N. Chung, S. H. Amber, An experimental study on flow patterns and heat transfer characteristics during cryogenic chilldown in a vertical pipe, Cryogenics (Guildf) 52, 4-6, 268–27 (2012).
- [4] V.S. Devahdhanush, I. Mudawar, Review of Critical Heat Flux (CHF) in Jet Impingement Boiling, Int. J. Heat Mass Transf. 169, 120893 (2021).

Methodology of multichannel study of cryoeffect *in vitro*

V. Yu. Globa¹, G. O. Kovalov¹, M. O. Chyzh¹, G. V. Shustakova²,
Ed. Yu. Gordienko², Yu. V. Fomenko²

¹*Institute for Problems of Cryobiology and Cryomedicine of the NAS of Ukraine,
23 Pereyaslavskaya str., Kharkiv, 61016, Ukraine*

²*B.Verkin Institute for Low Temperature Physics and Engineering of the NAS of Ukraine,
47 Nauky Ave., Kharkiv, 61103, Ukraine
e-mail: globa.1978@gmail.com*

Cryosurgery is a minimally invasive, effective and safe method, which is intended for targeted and controlled destruction of affected tissues by low temperatures. This method is indicated for the treatment of benign, precancerous and malignant neoplasms. Conducting experimental studies in biological tissues allows us to study the mechanisms of freeze-thawing processes that occur during cryosurgical treatment. The progress of cryosurgery is inextricably linked to understanding the freezing and thawing processes, because they are the main factors in the destruction of biological tissues. Assuming the serious ethical problems when performing the studies in animals, *in vitro* experiments are preferable, the data of which could be extrapolated to biological tissues *in vivo*.

To control the dynamics of the freezing zone parameters in a model system during *in vitro* cryogenic exposure, a technology has been developed that is based on the use of various information-retrieving channels. The technology consists of (i) a special experimental setup [1] and (ii) an appropriate methodology for monitoring *in vitro* cryogenic exposure on this set-up. The methodology has been developed based on the results of 2-year experimental studies on the designed and manufactured setup, supported by theoretical calculations [2]. The methodology is a document, describing the optimal procedure for performing the research (obtaining results) during low-temperature exposure in a model system.

The methodology contains requirements for equipment and facilities as well as a step-by-step description of testing and preparing equipment, measuring using all components of the set-up, quantitative analysis of the results obtained, etc. Due to multi-channeling, the technology can be used for simultaneous and synchronous quantitative monitoring of the dynamics of the ice ball size and shape (three video surveillance channels), measuring temperature dynamics at specified points in the model system volume (up to 8 microthermometers), monitoring the freezing front movement on the surface and quantitative analysis of the dynamics of thermal fields on the model system entire surface (infrared thermal imaging channel), etc.

The methodology can be used for various types of cryotools (application, spraying and penetrating actions) and different types of model systems, but is most specifically focused on the specific case of the impact of a quasi-point cryoapplicator cooled by liquid nitrogen on the surface of a gelatin 5% hydrogel, which in its characteristics is close to biological tissues. The methodology contains the procedure for manufacturing a 5% hydrogel and other useful data and tips, for example, the maximum cryoexposure time is estimated, at which it is permissible to evaluate the freezing depth of an object according to the temperature fields on its surface, the impact of a vessel model with blood flow, influence of adverse factors on thermal fields on the surface and in the system depth, etc.

This work was supported by the National Research Foundation of Ukraine (Grant No. 2022.01/0094).

[1] G. Kovalov, M. Chyzh, V. Globa, G. Shustakova, E. Gordienko, Cryobiology. 117, 105133 (2024). <https://doi.org/10.1016/j.cryobiol.2024.105133>.

[2] O.V. Ivakhnenko, O.F. Todrin, V.Yu. Globa, M.O. Chyzh, G.O. Kovalov, S.N. Shevchenko, bioRxiv 2024.10.19.619201. <https://doi.org/10.1101/2024.10.19.619201>.

Theoretical aspects and engineering approaches to energy-saving liquid atomization technologies

P. E. Trofymenko, O. V. Khomenko, M. V. Naida, D. T. Lohvynenko

*Sumy State University, 2, Rymskogo-Korsakova St., 40007 Sumy, Ukraine
e-mail: maks.nai@ukr.net*

The development of energy-saving liquid atomization technology is one of the most promising areas in the field of engineering and industrial processes. Over the past decades, much attention has been paid to the search and implementation of new atomization methods that not only increase the efficiency of heat and mass transfer and reaction processes, but also reduce energy costs for production. Given the global problems associated with energy resources and environmental challenges, the creation of energy-efficient and environmentally friendly technologies has become an important goal for scientists and engineers in many industrial fields.

In this regard, the need to develop and implement energy-saving technologies for atomizing liquids is becoming increasingly relevant. The search for new approaches that can significantly reduce energy consumption without losing the quality of processes is an important part of modern research. The development of efficient atomizers that use minimal energy costs is becoming an important area in the modernization of existing technologies.

Special attention is drawn to the analysis of the liquid state and its influence on the atomization processes. The liquid phase is very important in many technological processes, since its properties - such as viscosity, surface tension and heat capacity - significantly affect the characteristics of sprayers. Theoretical understanding of these properties makes it possible to optimize the design of sprayers and increase the efficiency of heat and mass transfer in liquid-gas systems.

Increasing energy efficiency in liquid atomization processes is an important step towards reducing energy costs and reducing the environmental impact of industrial production. To do this, it is necessary to introduce the latest technologies that contribute to reducing energy consumption while maintaining high process efficiency. One of such solutions is the use of thin-film technologies, which allow significantly increasing the surface area of the liquid and accelerating the evaporation process. This allows reducing energy costs, while simultaneously increasing atomization efficiency and reducing the time required to achieve the necessary physicochemical changes.

The use of such innovative atomization methods allows to achieve not only economic advantages, but also significantly improve the environmental efficiency of production processes. In the future, the development of energy-saving technologies in the field of liquid atomization will ensure a more sustainable development of industrial processes, allowing to reduce their energy consumption and environmental impact. Research in this direction will undoubtedly contribute to the creation of new, more effective solutions for energy saving and improving productivity in various industries.

The research is based on an analysis of contemporary literature, physical and technical models and experimental data. The importance of considering the specific properties of liquids in the development of new atomizer designs, as well as the necessity of an interdisciplinary approach to optimizing process is emphasized. The obtained results indicate the prospects of further research in the field of energy-saving technologies for liquid atomization. This will ensure that industrial processes are both economically beneficial and environmentally sustainable.

Quantum point-contact sensors for the emotion state detection in real time

**M. Romanov¹, D. Harbuz¹, V. Belan¹, O. Pospelov², L. Kamarchuk³,
V. Gudimenko¹ and G. Kamarchuk¹**

¹*B. Verkin Institute for Low Temperature Physics and Engineering of NAS of Ukraine,
47 Nauky Ave., Kharkiv, 61103, Ukraine*

²*National Technical University “Kharkiv Polytechnic Institute”,
2 Kyrpychov Str., Kharkiv, 61002, Ukraine*

³*SI “Institute for Children and Adolescents Health Care” of NAMS of Ukraine,
52-A Yuvileinyi Ave., Kharkiv, 61153, Ukraine
e-mail: m.d.romanov.1997@gmail.com*

Quantum point-contact sensors have proven to be a highly effective tool for analyzing a variety of human body states. The features of electric current flow through Yanson point contacts provide a unique opportunity to examine a wide range of gas mixture components in real time [1].

Recent studies have shown that, among other things, quantum point-contact sensors can be used to study human hormonal states [1, 2]. It is well known that certain emotional states are closely related to the content of the corresponding hormones. Moreover, emotional self-regulation cannot be achieved without hormones and neuromediators production variation [3]. At the same time, the content of hormones such as serotonin and cortisol in the body is associated with various types of socially aggressive behavior [4]. The introduction of a tool suitable for analyzing human emotional states in real time regime would open up many opportunities, in particular in the field of public safety. This work is devoted to pioneering research aimed at developing such a tool.

Quantum point-contact sensors based on the Cu-TCNQ compound, obtained by combined electrochemical deposition from a saturated solution in acetonitrile, were used for the research. A specially developed device for vacuum zone sublimation was used for the preliminary purification of the gas-sensitive substance. In the study, 30 volunteers took part. The response curves of the point-contact sensor to the action of breath were recorded before and after the emotional impact. The impact was realized by watching a video by a volunteer, which a person found funny, for 10 minutes.

Analysis of the spectral curves of the response of the quantum point-contact sensor to the action of breath made it possible to find an experimental relation between the features of the response curve and the emotional state of a person. Based on the method proposed in our previous works [1, 2], the levels of serotonin and cortisol hormones in the human body were estimated using breath analysis. The results obtained demonstrate a high agreement with previously obtained data, which indicates the high reliability of the method proposed.

Therefore, during this work, an approach to detect human emotional states using point-contact sensors of human breath was proposed. The proposed approach has broad prospects for use in applied purposes – for public safety or lie detectors, which are based on a new physical principle of operation.

- [1]. G. Kamarchuk, A. Pospelov, L. Kamarchuk, et al., Sci Rep., 13, 21432 (2023).
- [2]. L. Kamarchuk, A. Pospelov, D. Harbuz, et al., J. Breath Res., 16, 016002 (2022).
- [3]. M. Butnariu and I. Sarac. Annals of Pharmacovigilance & Drug Safety, 1, 1001 (2019).
- [4]. E. R. Montoya, D. Terburg, P. A. Bos and J. van Honk, Motivation and Emotion, 36, 65 (2011).

Relevance of metrological documentation development for heat flux calculations in ultracold neutron converters

A. K. Sauleyeva¹, Ye. S. Korshikov¹, K. Turlybekuly², V. V. Nesvizhevsky³

¹*Institute of Experimental and Theoretical Physics (IETP), al-Farabi Kazakh National University.*

²*Institute of Nuclear Physics, Ministry of Energy of the Republic of Kazakhstan*

³*European Centre for Neutron Research "Institut Max von Laue – Paul Langevin" (ILL), Grenoble, France*

e-mail: altynaysauleyeva@gmail.com

The development of accurate methodologies for calculating heat fluxes in ultracold neutron (UCN) converters is a critical task requiring rigorous metrological assessment. Modern research in neutron physics highlights the significant influence of temperature factors on the processes of UCN generation and transport. However, despite advancements in numerical methods and improvements in experimental facilities, challenges related to metrological assurance of calculations persist. Key issues include measurement uncertainties in temperature gradients, the complexity of calibrating thermal sensors under cryogenic conditions, and the necessity of accounting for the spectral characteristics of neutron radiation.[1] In the absence of standardized metrological documentation, data interpretation and reproducibility of calculations may be hindered, directly impacting the reliability of obtained results. This study aims to develop a set of metrological standards and methodologies for accurate heat flux calculations in UCN converters. To achieve this goal, the following tasks must be addressed:

Analyze existing approaches to heat flux measurements in cryogenic systems and assess their applicability to UCN converters.

Develop a methodology for metrological calibration of thermal sensors considering the specifics of ultracold temperature regimes.

Identify key sources of uncertainty in calculations and propose methods for their minimization.

Measuring heat fluxes in ultracold neutron environments presents a range of complex metrological challenges. The primary issues involve the high sensitivity of sensors to external factors and the need for precise calibration at extremely low temperatures. On an international level, metrological aspects are regulated by organizations such as the International Bureau of Weights and Measures (BIPM) and the International Organization of Legal Metrology (OIML). In neutron research, standards governing measurement, calibration, and data processing are employed, including:

ISO 21348 – Standards related to radiation fluxes.

GOST 8.586 – Regulatory documents governing thermal measurements in various physical processes.

IAEA Recommendations – Documents of the International Atomic Energy Agency, outlining requirements for metrological assurance in neutron research.

The application of these standards facilitates the unification of measurement methodologies, improves calculation accuracy, and enhances the reproducibility of experiments involving ultracold neutrons.[2]

[1] G. F. Kovalenko et al. Experimental Techniques for Measuring Temperature Gradients in Cryogenic Systems // Journal of Metrology and Thermophysics. – 2020. – Vol. 45, No. 3. – Pp. 112-126.

[2] J. K. Andersen et al. Spectral Composition Influence on Heat Transfer in Ultracold Neutron Converters // Journal of Low-Temperature Physics. – 2019. – Vol. 195, Issue 2. – Pp. 245-260.

AUTHOR INDEX

A

- Abdullayev J. Sh.....178
Abera T.....220
Abramenko L. O.....140
Adamowicz L.....202, 208, 211
Aksanova N. A.....162
Aliev A.....73
Amrit J.....49
Andreev Eu. O.....201
Andriichuk V. L.....141
Anlage S. M.....38
Arciszewska M.....120
Averkov O. Yu.....71
Averkov Yu. O.....71
Azarenkov N. A.....85
Azhniuk Y. M.....225, 233

B

- Baloh P.....121
Bandurin Yu.....136
Barabash Yu. M.....201
Barabashko M. S.....163, 171
Baránek M.....81, 86
Basnukaeva R. M.....65, 179
Bazaliy Ya. B.....39
Bednarchuk T.....243
Belan V.....287
Beliayev E. Yu.....93
Belogolovskii M.....90
Bendelian I. B. G.....69
Bengus S. V.....96, 280
Berezhnyi O. Yu.....142
Bereznykov O. V.....75, 255
Berry M.....37
Bessarabova V. O.....277
Bezkrovna O.....218
Bezkrovnyi O.....41
Biesuz M.....55
Bilenka O.....217
Bilych I. V.....82
Biri S.....48
Bludov M. A.....53
Bludov O.....107
Bludova L. V.....74, 77, 94
Bogdan M. M.....272, 273
Bohachov K. H.....76
Boiko V. V.....41
Boliasova O. O.....101
Bondar D. I.....257, 259
Bondar I. S.....83, 180
Bondareno M. V.....216
Bondarenko S. I.....88
Borisova T. O.....41
Boryak O. A.....197, 199, 203, 210
Boyko I. V.....264, 274
Breslavets O. A.....125
Brinck T.....40
Brodskii R. Ye.....198
Bryzgalin A. G.....219, 281
Büchner B.....97
Bukhanko A. F.....126

- Bukhanko F. N.....159
Bulakhov M.....269, 270
Bulova A. G.....204
Buravtseva L. M.....179
Butch N. P.....38

C

- Carlton-Jones A.....38
Casseta M.....55
Černošek Z.....121
Černošková E.....121
Chagovets V. K.....160
Chaika A. A.....253
Charkina O. V.....272, 273
Charkin-Gorbulin A.....273
Chen Long-Qing.....255
Cherednichenko S. V.....210, 240
Chernogor L. F.....277, 278, 279, 282, 283
Cherpak N. T.....92
Chichibaba I. A.....93
Chigambayeva N. N.....226
Chiorescu I.....60
Chopov A. P.....268
Chugai O.....248
Chyzh M. O.....285
Čížmár E.....103, 108, 121

D

- Danylchenko O. G.....161
Darwich A.....102
Demianenko D. V.....143
Demianyk O.....127, 129
Dereń P. J.....155, 218
Dgebuadze G. N.....69
Dmytrenko V.....84
Dobushovskyi D. A.....261
Dolbin A. V.....179, 210
Doronin Yu. S.....128
Dovbeshko G. I.....41, 171, 201
Drozdenco D.....229, 230
Dryhailo M.....66
Dubyk K.....250
Dudetskaya G.....190
Duma V.-F.....42
Dzhenzherova K. S.....181, 185

E

- Efremov D. V.....97
Eliseev E. A.....75, 255
Erdelyi R.-A.....42
Eremenko Z. E.....125, 138, 186
Esel'son V. B.....179
Ettah E. B.....83
Ezerskaya E. V.....57, 110, 112, 181, 185

F

- Fedorchenko A. V.....108
Feher A.....108, 121
Feia O.....73
Feldii M.....135

- Fertman E. L.....108
 Fesenko P. M.....78
 Fil D. V.....82, 223, 249
 Fil V. D.....82
 Filep M. J.....225, 233
 Finocchio G.....106
 Flachbart K.....117
 Fliahin R. V.....144
 Fomenko L. S.....241
 Fomenko Yu. V.....285
 Frolov V. A.....85
 Futimsky S.....147

G

- Gabáni S.....117
 Gabunia V. M.....69
 Gagor A.....43
 Gál D.....237
 Galtsov N. N.....156, 162, 243
 Gavrilko V. G.....179
 Gedeon S. V.....145
 Gegenwart P.....109
 Geidarov V. G.....227
 General A.....137
 Get'man E. I.....239
 Glamazda A. Yu.....44, 109, 118, 207, 211
 Globa V. Yu.....285
 Glukhov K. E.....107, 231
 Gnatenko Kh. P.....45
 Gnatyuk O. P.....41
 Gnezdilov V. P.....109, 118
 Gomonnai A. V.....225, 233
 Gomonnai O. O.....233
 Gopalan V.....255
 Gordiyenko Ed. Yu.....285
 Grajcar M.....81, 86
 Grankina I. I.....182
 Grechnev G. E.....114
 Grib A.....236
 Grimaldi A.....106
 Gritsak R.....135
 Grygorova G.....190
 Grytsiuk E. M.....179
 Gudimenko V.....287
 Guslisty A. A.....200

H

- Hakonen P.....175
 Hamalii V. O.....183, 184
 Harbuz D.....287
 Harnagea L.....97
 Hasynets S. M.....233
 Haysak A.....237
 Haysak I.....237
 Herasymov S. S.....146
 Herczku P.....48
 Hermash K. V.....223
 Hetalo A. M.....260
 Holub M.....108
 Holubnycha M. S.....268
 Holubová J.....121
 Horbatenko Yu. V.....163, 166, 167, 171, 240
 Horielyi V. A.....93
 Horvat A. A.....228
 Hrankina S. S.....182
 Hrechykha O. S.....70
 Hrinchenko A.....129, 131
 Hryhorova T. V.....229, 230, 244

- Hu Jia-Mian255
 Huang Yi241, 244
 Hubenko K. O174
 Hurova D. E162, 243

I

- Ilinskaya O. A.....262
 Illyashenko L. N.....130, 172
 Ioppolo S.....48
 Ishaje M. E.....83
 Ishchenko L. O.....78
 Ivakhnenko O. V.....263
 Ivanchenko S. E.....75
 Ivanov V. I.....120
 Ivashchyshyn F.....217

J

- Jacobs K.....257
 Jeżowski A.....171, 240
 Jishiashvili D. A.....69
 Juhász Z.....48

K

- Kabanenko M. A.....183, 184
 Kabatova A. O.....110
 Kachur I. S.....119
 Kagalovsky V.....46
 Kalenyuk O.....90, 147
 Kamarchuk G. V.....128, 287
 Kamarchuk L.....287
 Kamenskyi D.....111
 Kaňuchová Z.....48
 Karachevtsev V. A.....44, 197, 199, 203, 206, 207, 210, 211
 Karaseva E. V.....85
 Karkulovska M. S.....193, 217
 Kasatkin A. L.....70
 Kashuba I. V.....244
 Kavok N.....190
 Kaykan L.....250
 Kazakov A. P.....78
 Kazakov V. I.....145
 Kern S.....86
 Khaldeev S. I.....175
 Kharchenko M. F.....115
 Kharchenko Yu. M.....115, 116
 Kharkhalis L. Yu.....231
 Khmil N. V.....205
 Khomenko K. P.....268
 Khomenko O. V.....268, 286
 Khorolskyi O. V.....200, 260
 Khrustalyov V.....111
 Khyzhniy I. V.....53
 Kilanski L.....120
 Kimura S.....111
 Kinzhybalo V.....61, 162
 Kislyak I. F.....221, 241
 Kitsenko O. Y.....80
 Kizilova N. M.....173
 Kliushnichenko O. V.....271
 Klochko V. S.....85, 221
 Klochkov V. K.....174
 Kobets M.....107
 Kobzar I. P.....108
 Kochubei G. S.....245
 Kofman P.O.....256
 Kolchigin N. N.....172

Kolesnichenko Yu. A.	74, 89
Kolesnikov V. G.	205
Kolezhuk O.	105
Kolinko A. E.	95
Kolisnyk A. S.	77, 94
Kolodiy I. V.	221
Kolupaiev V. O.	224
Kondratov O. O.	221
Konenko S. Ye.	112
Konoplyuk S. M.	113
Konotop O. P.	161
Konstantinov V. A.	167
Konstantynov O. M.	266
Kordyuk A. A.	76
Korniets A. V.	85, 221
Korolkov R. Yu.	142, 144, 149, 154
Korolov O. I.	231
Korolyuk O. A.	163, 166, 167
Korotun A. V.	140, 142, 143, 144, 148, 149, 150, 154, 189
Korshak V. F.	232
Korshikov Ye. S.	284, 288
Kosevich M. V.	197, 199, 203, 210
Koshina E. A.	87
Kot Yu.	190
Kotomin E. A.	183
Kovalenko O. Y.	57
Kovalenko V. O.	181, 185
Kovalevsky M. Yu.	254
Kovalov G. O.	285
Kovalov R. M.	278
Koverya V. P.	88
Kozin I.	103
Kozlov I. V.	89
Krainyukova N. V.	183, 184
Kravets A. F.	113
Krevsun A. V.	88
Krivchikov A. I.	163, 166, 167, 171, 240
Krivoruchko V. N.	87, 90, 101
Krupa M. M.	187
Kryshenik V. M.	225, 233
Kuchugurnyi Yu. P.	245
Kulish S. M.	138, 248
Kulyk D. R.	279
Kulynych Y.	253
Kumar J.	104
Kumar M.	175
Kurbatsky V. P.	150, 189
Kurnosov N. V.	206
Kurnosov V. S.	119
Kuryliuk V. V.	238
Kutko K. V.	111, 116
Kuzema P. O.	197, 199, 203, 207, 210
Kuznetsova K. S.	186
Kvitnitskaya O. E.	97

L

Lähderanta E.	74, 94, 191
Lakatos G.	48
Langdon T. G.	241, 244
Lazorenko Ya. P.	234
Lazur V. Yu.	145
Leha O. O.	96, 280
Lemmens P.	109
Len T.	191
Leonov V. O.	188
Lev B.	212
Liashchuk O. I.	282
Lipovska Yu. S.	221, 243
Lisetski L. N.	133, 177, 182

Lisiecki R.	218
Litvinova S. S.	258
Liubymenko O. M.	235
Lobanov L. M.	219
Lobzhanidze T. E.	69
Lohvynenko D. T.	286
Lopushansky V. V.	225, 233
Lototskaya V. A.	222, 242
Loya V. Y.	233
Lubenets S. V.	241
Luhanko M. O.	259
Lukin I. V.	259
Lukyanets S. P.	271
Lupan M. I.	174
Lyagushyn S. F.	267
Lyakhno V. Yu.	96, 280
Lykah V. O.	176
Lyogenkaya A.A.	114

M

Makharynskyi V.	236
Mäkinen J. T.	175
Maksimchuk P. O.	174, 190
Malakhova L. M.	219, 281
Malysh R. O.	149
Manca D.	81
Maniuk M. S.	189
Mankovska O.	131
Mantena V.	175
Martynenko I. O.	90, 147, 280
Maslov V. V.	132
Mason N. J.	48
Mastrikov Y. A.	183
Matiushyn V. M.	140, 144
Matzui L.	191, 250
Mazurenko J.	250
Meisel M. W.	47
Melnyk S. I.	91, 92
Menelaou Melita	69
Menesenko D.	73
Menshykova S. I.	175
Metskhvarishvili I. R.	69
Metskhvarishvili M. R.	69
Mifsud D. V.	48
Mikhailov M. Yu.	96
Mikhaylovskiy R. V.	57
Mikhodui O. L.	219
Minakova K. A.	83, 180
Minajluk-Gawel N.	155
Minkovych V. V.	228
Minya A.	135
Mirzoiev I. G.	93, 180, 191
Mitsai V. P.	234
Molnar A. A.	134, 228, 237
Moroz H. V.	150
Morozovska A. N.	75, 224, 255
Moskalenko V. A.	246
Moskvitin N. S.	216
Mykytiuk O. Y.	193
Myloslavskva O. V.	115

N

Naida M. V.	286
Naidyuk Yu. G.	97
Natsik V. D.	242, 243
Neilinger P.	81, 86
Nemchenko K.	49, 139
Nemchenko Ye.	49

- Nerukh O. G. 130, 172
 Nesterenko N. M. 116
 Nesvizhevsky V. V. 288
 Neuhodov Ye. 190
 Nikolaenko V. A. 164
 Nojiri H. 111
 Nori F. 263
 Nurmukan A. Y. 226

O

- Odarenko E. N. 71
 Ohloblia M.O. 72
 Ohta H. 111
 Okovit V. S. 85
 Olenchuk M. V. 201
 Olikh O. Ya. 238
 Onishchenko A. 190
 Onufriienko O. 117
 Orendáč M. 102, 103, 121
 Orendáčová A. 102, 103, 121
Oriekhov D. O. 253
 Ovcharenko A. 139
 Ovsiannikov R. T. 257
 Ovsiienko I. 191

P

- Paglione J. 38
 Pal-Val P. P. 232
 Panfilov A. S. 114
 Parra A. 73
 Pashchenko V. A. 107, 114
 Pashin N. A. 219, 281
 Pashkevich Yu. G. 108
 Pashynska V. A. 186, 199, 207
 Pavlyshche N. I. 151
 Pekar E. D. 219, 281
 Peletminskii A. S. 269, 270
 Pershin Yu. V. 54
 Peschanskii A. V. 118
 Petrenko E. V. 74, 77, 94
 Petrov E. G. 188
 Petrushenko S. 211
 Piddubnyi T. 202, 208
 Piryatinskaya V. G. 119
 Plecenik T. 86
 Plokhotnichenko A. M. 206, 207
 Pogodin A. I. 225
 Poida A. V. 85
 Pokhila A. S. 95
 Poláčková M. 86
 Polevoy S. 127, 129, 139
 Poltavskyi I. 273
 Pop M. 135
 Poroshin V. N. 224
 Pospelov O. 287
 Postolnyi B. O. 65
 Pristáš G. 117
 Pritula I. M. 132
 Prokeš K. 117
 Pustovit Yu. V. 72
 Pylypchuk O. S. 75, 224

R

- Rácz R. 48
 Radio S. V. 239
 Ratner M. 165

- Reva V. I. 143, 149
 Ribeiro P. 50, 256
 Roch T. 86
 Rogacki K. 74, 77, 79
 Rogova S. 49
 Romanov M. 287
 Romantsova O. O. 166, 171, 240
 Ropakova I. Yu. 133
 Roushan P. 51
 Rudka M. 152, 217
 Rudnikov Ye. G. 260
 Rusakova H. V. 241, 242
 Ryazanova O. A. 209

S

- Sagan V. V. 166, 167
 Sakurai T. 111
 Salak A. N. 108
 Samoilov O. M. 133, 182
 Samos N. 256
 Sapaev I. B. 178
 Sauleyeva A. K. 288
 Savchenko E. V. 53
 Savin Yu. N. 153
 Savina Yu. 107
 Sedda A. 74, 94, 191
 Seidel P. 84
 Sementsov Yu. 171
 Semerenko Yu. O. 156, 243, 244
 Seminko V. V. 174, 190
 Seredyuk B. O. 193, 217
 Seti Ju. O. 264, 274
 Shapovalov A. P. 73, 90, 147, 192
 Shapovalov Yu. O. 232, 244
 Sharapov S. G. 253
 Shaternik V. E. 192
 Shelkovsky V. S. 197, 203, 210
 Shendryk D. O. 263
 Shevchenko S. I. 266
 Shevchenko S. N. 80, 262, 263
 Shevchenko Ye. V. 188
 Shevelev M. B. 278, 282
 Shitsevalova N. 117
 Shmat'ko A. A. 71
 Shpylka D. 191, 250
 Shudra T. 131
 Shumilin S. E. 229, 230, 244
 Shustakova G. V. 285
 Shuvalov V. A. 245
 Shvaika A. M. 261
 Shvydkyi M. A. 154
 Shytov M. V. 74, 77
 Siemensmeyer K. 117
 Sirenko V. A. 83, 180
 Sivakov A. G. 95
 Slavin A. N. 122
 Slavin V. V. 119
 Slipko V. A. 54
 Slobodianuk D. V. 106
 Slyanko V. E. 120
 Slyusarenko Yu. V. 270
 Smirnov S. N. 244
 Smolianets R. V. 246
 Sofronov D. S. 177
 Sokolenko V. I. 85, 155, 221
 Sokolov A. M. 141
 Sokolov D. 215, 284
 Sokolov S. S. 160
 Sokolovsky A. I. 267

Solovjov A. L.	74, 77, 79, 94, 191
Sorokin O. V.	133, 182
Sotnikov A. G.	257, 258, 259
Stadnyk V.	121
Starodub I. O.	265
Stegantsev E.V.	143
Stepanian S.	202, 208, 211
Stetsenko D. O.	75
Stoliaryk O. D.	200
Stolyarov E. V.	141
Strek W.	41
Sulik B.	48
Sulyma S.	248
Surmanidze D. L.	69
Svitlichnyi E.	134, 135, 136, 137
Syrkin E. S.	176
Syvokon V. E.	160
Szewczyk D.	55, 155, 171, 240

T

Tabachnikova E. D.	241, 243, 244
Tarasenko R.	102, 103, 108, 121
Tarenkov V.	90
Tchankvetadze A. D.	69
Terekhov A. V.	77, 78, 79, 93, 191
Terekhov R. S.	138
Teslenko V. I.	188
Teslia R.	105
Tikhonovska T. M.	221
Tikhonovsky M. A.	221, 241, 244
Tilichenko N. M.	282
Titov I. M.	149, 154
Tkáč V.	103, 108, 121
Tkachenko A. A.	128
Tkachenko M. Yu.	283
Tokarčík M.	121
Tolochko A. S.	41
Tonkonozhenko A.	49
Tovstolytkin O.I.	113
Tovstyuk N. K.	193, 217
Trofymenko P. E.	286
Trotsky Y. M.	176
Tsvitkovskyi V. P.	70
Turlybekuly K.	288
Turutanov O. G.	81, 280
Tuz V.	127, 139

U

Usenko E.	211
Ushii L. I.	122
Uyutnov S. A.	53

V

Vakula V. L.	128
--------------	-----

Valeev V.	211
van Ruitenbeek J. M.	52
Vashchenko O. V.	198
Vashchenko P. V.	177
Vashchynskyi V. M.	247
Ventsev S. D.	281
Verba R. V.	106, 122
Vikhtinskaya T.	49
Vinnikov N. A.	179, 210, 240
Volavka D.	117
Volobuev V. V.	56
Voloshin I. M.	199, 211
Voloshyn Yu.	248
Vorobieva K.	215
Vorobyova O.	215, 284
Voronovskyi D. K.	245
Vovchenko L.	250
Vovk N. R.	57
Vovk R. V.	74, 94
Vovsianiker M. Y.	249
Voynarovich I. M.	225
Vysochanskii Y. M.	107, 255

W

Wu Y.-J.	58
----------	----

Y

Yakovenko O.	250
Yakovliev V.	212
Yampol'skii V. A.	71
Yanovsky V. V.	165
Yarovyi V. M.	78, 79
Yefimova S. L.	133, 174, 182, 190
Yelisieiev M. Ye.	255
Yermakov O.	127, 129, 131, 139
Yurkov B. V.	245

Z

Zabrodin P.	229, 230
Zaiatc D.	250
Zhao Guo-Dong	255
Zhekov K. R.	82
Zhitlukhina E.	84, 90
Zhu Y.	255
Zinoviev P. V.	156
Zobnina V. G.	203
Zolochevskii I. V.	78
Zolotaryuk Y.	59, 265
Zoryansky V. N.	156, 243
Zraichenko O. V.	96
Zvyagina G. A.	82

**V International Conference
Condensed Matter and Low Temperature Physics
CM<P 2025**

**Book
of
abstracts**

Kharkiv, B. Verkin ILTPE of NASU, 2025

Електронне видання, ум. друк. арк. 5.2.
Свідоцтво про внесення суб'єкта видавничої справи
до Державного реєстру видавців, виготовників
і розповсюджувачів видавничої продукції
від 07.06.2002 р., серія ДК № 941.
Видавництво ФТІНТ ім. Б. І. Вєркіна НАН України
просп. Науки, 47, Харків, 61103, Україна
<https://www.ilt.kharkiv.ua>